CONF-900280--Vol.2

DE91 015775

Volume 2
Technical Summary

International Magnetic Pulse Compression Workshop

H. C. Kirbie
M. A. Newton
P. D. Siemens

Manuscript date: April 1991

LAWRENCE LIVERMORE NATIONAL LABORATORY
University of California • Livermore, California • 94550

Disclaimer

Work performed under the auspices of the U.S. Department of Energy by Lawrence Livermore National Laboratory under Contract W-7405-Eng-48.

Acknowledgments

The Workshop at Granlibakken was made possible by the contributions, time, and enthusiasm of many dedicated people. We on the editorial staff gratefully acknowledge the hard work of all who participated by recognizing the following groups in which they served. Thank you one and all for making the International Magnetic Pulse Compression Workshop a successful enterprise.

Organizing Committee Members: Chairmen, Cochairmen, and LLNL Representatives

The 15-member Organizing Committee selected the five working groups as an organizational structure and developed the technical scope and goals for each group over a 9-month period. During the workshop, these same people served as the leaders for each of the working group sessions. After the workshop, the chairmen of each working group wrote the group summaries and reports contained in the proceedings. Clearly, the workshop was forged from the dedication and leadership of these people and we thank you.

The Organizing Committee membership represented four private industries: Allied Signal Corp., Beta Development Corp., British Aerospace, and Spectra Technology; as well as two national laboratories: Sandia National Laboratory and Lawrence Livermore National Laboratory (LLNL). Each parent organization supported the participation of their employees in the workshop preparation process. We gratefully acknowledge the support and interest of the various parent companies in the professional development of their employees and in magnetic pulse compression technology.

Special recognition also goes to Mark Newton, Committee Chairman, who united the contributions of the committee members located in several cities with the central membership located at LLNL in Livermore, CA. Mark and the LLNL representatives helped ensure that distance did not diminish the influence of any committee member.

Workshop Staff Members: Secretaries, Administrators, Coordinators, and Editors

The Workshop Staff supported the activities of the Organizing Committee and played a vital role in the preparation of the workshop. In key staff positions, the secretaries and administrators handled the great volume of workshop correspondence and tracked the financial and institutional business generated by the workshop. The coordinators provided the detailed work that gave the workshop its highly professional appearance and smoothly run services. They arranged the artwork and printing of the various workshop materials, organized the library, and gathered and transported to Granlibakken the office equipment and computers. Generally, the workshop editors reviewed the plans of the Organizing Committee and suggested ways for the working group discussions to end with a specific end product that was suitable for publication.

Two special staff positions were created to fill two specific jobs: William Niven served as Student Awards Judge and selected the six students who received scholarships to attend the workshop. Cheri Johnson served as Soviet Liaison and attended to the complex travel and financial arrangements for the five visiting Soviet scientists.

To all the staff members, we acknowledge your hard work and vital contributions. Each staff member worked diligently to help shape the workshop during the months of preparation. At Granlibakken, the same hard work continued behind the scenes to keep the library, office, communication, and publication services working smoothly. Thank you for your personal dedication. The workshop would not have been possible without you.

Executive Advisors

The workshop greatly benefited by the advice and counsel of its three Executive Advisors: Dr. Art Guenther from Los Alamos, Dr. Magne Kristiansen from Texas Tech University, and Dr. Gennadi Mesyats from the Soviet Academy of Sciences. Dr. Mesyats represented the Organizing Committee in the Soviet Union by selecting the scientists who attended the workshop as invited guests. Drs. Guenther and Kristiansen helped shape the workshop and its organization by drawing from their previous experiences with many other workshops and conferences. At Granlibakken, they all provided valuable advice to the committee and staff members, which helped keep the sessions well-focused. We gratefully acknowledge and appreciate the advice and guidance you gave us.

Invited Speakers

The five working groups were each represented by a keynote speaker who shared their valuable technical experience and put into perspective the issues each group addressed in the private sessions that followed. We acknowledge the unique contributions from the speakers and appreciate the preparation each lecture required. Thank you for your leadership and expertise.

Invited Authors

The five working groups also were represented by three invited authors, each of whom prepared a presentation for their respective working group sessions and a publication for this proceedings. The papers and presentations addressed specific technical issues that were shared with working group members and used as initial discussion topics. Thank you for your contributions to the workshop discussions and to these proceedings.

Granlibakken Staff

A special thanks also goes to Bill Parson and his staff at Granlibakken for their very professional help during the workshop preparation. In all our pre-workshop business dealings, the Granlibakken staff was always informative, cooperative, very skilled, and willing to assist with any problem, large or small. During the workshop, the staff handled our unforeseen difficulties with polish and style. Thank you Bill and Norma. You were the perfect hosts.

Special Recognition

The Editorial Staff also recognizes the contributions of four very special individuals: William Abraham, Gloria Davalos, Sally Twisselmann, and Sue Winkler. In their respective roles, Sally Twiselmann was the Workshop Secretary and Gloria Davalos was her assistant. Sue Winkler and Bill Abraham were both Workshop Coordinators. Each of these four people helped to secure a successful meeting by giving long work hours, creative ideas, and dedication to an effort that was full of new and trying experiences. We on the Editorial Staff salute your contributions and recognize that great things are accomplished only when caring people are involved. Thank You.

Preface

Although pulsed-power engineering traditionally has been practiced by a fairly small, close community in the areas of defense and energy research, it is becoming more common in high-power, high-energy commercial pursuits such as material processing and lasers. The relatively small cadre of pulse-power practitioners and experts has depended primarily on personal contacts, organizational focus, and select workshops or conferences for information exchange. In the last decade, efforts have begun to document research and development activities in the pulsed-power field through activities such as Tamarron workshops, IEEE Pulsed-Power Conferences, the well-established IEEE Modulator Symposium, and, more recently, endeavors like the series of books on Advances in Pulsed-Power Technology and the Laser and Particle Beam Journal. Over the past 15–20 years, a few dedicated university-based pulsed-power education and research programs also have emerged. Recently, there has been a noticeable warming trend in the relationship and interaction between eastern and western organizations in the pulsed-power field and in science in general. This was exemplified by the invitation and participation of several Soviet scientists in this workshop.

The aspect of pulsed-power engineering that constrains design or limits performance is switching: the controlled initiation, transmission, or termination of power flow. The switching limit is, therefore, the subject of numerous and diverse research efforts and approaches, each of which attempts to address some application-driven switching characteristic such as delay, jitter, risetime, lifetime, reliability, reproducibility, power-handling capability, repetition rate, charge transfer, or voltage-handling range, etc.

As indicated, a few individuals have tried to broaden the understanding of specific and salient pulsed-power topics. One such attempt is this documentation of a workshop on magnetic switching as it applies primarily to pulse compression (power transformation), affording a truly international perspective by its participants under the initiative and leadership of Hugh Kirbie and Mark Newton of the Lawrence Livermore National Laboratory (LLNL) and supported by other interested organizations.

During the course of the Workshop at Granlibakken, a great deal of information was amassed and a keen insight into both the problems and opportunities as to the use of this switching approach was developed. The segmented workshop format proved ideal for identifying key aspects affecting optimum performance in a variety of applications. Individual groups of experts addressed network and system modeling, magnetic materials, power conditioning, core cooling and dielectrics, and finally circuits and application. At the end, they came together to consolidate their input and formulate the workshop's conclusions, identifying roadblocks or suggesting research projects, particularly as they apply to magnetic switching's trump card—its high-average-power-handling capability (at least on a burst-mode basis).

The workshop was especially productive both in the quality and quantity of information transfer in an environment conducive to a free and open exchange of ideas. We will not delve into the organization proper of this meeting, rather we wish to commend to the interested reader this volume, which provides the definitive and most up-to-date compilation on the subject of magnetic pulse compression from underlying principles to current state of the art as well as the prognosis for the future of magnetic pulse compression as a consensus of the workshop's organizers and participants. The serene but awe-inspiring ambiance of the conference venue, Granlibakken at Lake Tahoe, California, and its always helpful staff, in no small manner catalyzed our productivity.

A. H. Guenther
Los Alamos National Laboratory

M. Kristiansen
Texas Tech University

Conference Advisors

Staff and Organizing Committee

Workshop Executive Staff

Hugh Kirbie	Workshop Director	Lawrence Livermore National Lab
Sally Twisselmann	Workshop Secretary	Lawrence Livermore National Lab
Arthur Guenther	Executive Advisor	Los Alamos National Lab
Magne Kristiansen	Executive Advisor	Texas Tech University
Gennadi Mesyats	Executive Advisor	Soviet Academy of Sciences
Phillip Siemens	Executive Editor	Lawrence Livermore National Lab
William Niven	Student Awards Judge	Lawrence Livermore National Lab

Organizing Committee Staff

Mark Newton	Committee Chairman	Lawrence Livermore National Lab
Sally Twisselmann	Committee Administrator	Lawrence Livermore National Lab
Gloria Davalos	Assistant Administrator	Lawrence Livermore National Lab
Sue Winkler	Coordinator	Lawrence Livermore National Lab
William Abraham	Coordinator	Lawrence Livermore National Lab
Phillip Siemens	Senior Proceedings Editor	Lawrence Livermore National Lab
Ron Kihara	Reference Editor	Lawrence Livermore National Lab

Organizing Committee Working Group Members

Network and Systems Modeling Group

Anthony Payne	Working Group Chairman	Lawrence Livermore National Lab
Steve Sampayan	Group Cochairman	Lawrence Livermore National Lab
John DeFord	LLNL Representative	Lawrence Livermore National Lab

Magnetic Materials Group

Gordon Fish	Working Group Chairman	Allied Signal Corporation
Ken Avery	Group Cochairman	British Aerospace

Power Conditioning Group

Chris Young	Working Group Chairman	Spectra Technology
David Barrett	Group Cochairman	Lawrence Livermore National Lab
Ron Kihara	LLNL Representative	Lawrence Livermore National Lab

Core Cooling and Dielectrics Group

Kim Reed	Working Group Chairman	Sandia National Lab
Henry Harjes	Group Cochairman	Sandia National Lab
Sally Bahowick	LLNL Representative	Lawrence Livermore National Lab

Circuits and Applications Group

James Swingle	Working Group Chairman	Lawrence Livermore National Lab
Ken Whitham	Group Cochairman	Lawrence Livermore National Lab
Roger Stone	LLNL Representative	Lawrence Livermore National Lab

Sponsors

This workshop was made possible by contributions from the following sponsors:

- Allied Signal Corporation
- English Electric Valve
- Lawrence Livermore National Laboratory
- Los Alamos National Laboratory
- National Magnetics Corporation
- Office of Naval Research
- Pulse Sciences Incorporated
- Sandia National Laboratory
- TRW Corporation

Contents

Introduction

Background

Magnetic pulse compression has captured the imagination of researchers in the pulsed-power field since Melville first summarized the technique in 1951.[1] It is based on the simple and fascinating idea that a high-power switch can be constructed from only a magnetic core and a few turns of insulated wire. Each generation of researchers with a repetitive switching problem rediscovers magnetic switching because of its seductive properties. The magnetic switch is free of wear, moving parts, and the sparks and discharges that are present in other switches. It does not require triggering, filament supplies, or sophisticated support systems. The magnetic switch is rugged, very reliable, and simple in construction and function. It is free from electromagnetic interference and the prefires that plague other switch styles. This versatile switch also has the intrinsic ability to quickly repeat its operation and thereby compress one pulse after another at a very high rate. It is this high average power capability, more than any other property, that repeatedly draws us away from conventional switching techniques and into the world of magnetic pulse compression.

By the mid-1960s, several books had been written about the design and construction of various magnetic pulse generators.[2–4] The literature of the time also contains numerous articles that describe the Melville network and its applications. Despite the many published examples, magnetic pulse compression technology has never been as widely used as spark gaps, thyratrons, or solid-state circuits. The technique was routinely discarded as a serious switching alternative because of poor timing control, a limited optimum operating range, and the lossy magnetic materials of the day. Since then, two developments have increased the popularity of magnetic pulse compression: the production of low-loss amorphous magnetic alloys in the mid-1970s[5] and the recent demand for high-average-power lasers and accelerators. The new magnetic alloys aid magnetic pulse compression technology because they consume less energy and have a greater saturation flux density than silicon steel. In addition, the power needs for certain lasers and accelerators are well served by magnetic pulse compressors because the output pulses are all of a constant amplitude and recur at a high rate. For the first time since Melville's day, magnetic pulse compression technology has found a problem to solve and inherited the means to compete with other switching techniques.

Researchers at the Lawrence Livermore National Laboratory (LLNL) have long been interested in magnetic pulse compression technology and its continued development. Over the years, LLNL programs have applied the technique to power large copper-vapor lasers and a high-average-power linear induction accelerator (ETA II). Both of these applications represent a significant investment in magnetic pulse compression technology and a general desire to explore new methods of generating high-average-power pulses.

The Laboratory served as host and cosponsor for the International Magnetic Pulse Compression Workshop in an effort to assess recent advances in magnetic pulse compression technology and to seek new applications that will help advance the field.

Our library research indicates that the Special Technical Conference on Nonlinear Magnetics and Magnetic Amplifiers was the last U.S. conference devoted to magnetic pulse compression technology and magnetic networks. It was held in Washington, D.C., on September 23–25, 1959. Since then, there have been many new developments in the areas of magnetic materials and computational modeling. After 30 years, we thought it was time to review the field once again.

Workshop Structure and Services

The Workshop was organized around five working groups who examined magnetic pulse compressors from five different aspects. The technical domain of each working group slightly overlapped the domains of other groups to stimulate discussions and interactions. A list of the

working groups is shown below with a brief description of the topics discussed:

The Network and System Modeling Group set out to establish the state of the art in modeling magnetic pulse compressors and to recommend future research and development efforts in this area. The group surveyed the many magnetic switch models available in the literature and concluded that none of them was the clear model of choice. The group also discussed the features that an ideal model would contain for accurate system studies.

The Magnetic Materials Group concentrated on the topics of materials production, pulsed testing methods, and recent magnetization modeling techniques. Core manufacturing considerations were also discussed, including annealing, insulation, thermal management, and core-winding methods.

The Power Conditioning Group identified and discussed the key issues in the design of a power-conditioning system to drive a magnetic pulse compressor. After reviewing popular circuit topologies, the group distilled their discussions to three critical areas: voltage regulation techniques, component limitations for high average power, and advanced power conditioning systems that may some day eliminate the need for magnetic pulse compression stages between the source and the load.

The Core Cooling and Dielectrics Group surveyed the state of the art in dielectric materials and core-cooling techniques and identified research topics and experiments that would enhance the field. This working group divided into three subgroups to discuss the technology from three perspectives: commercial power industry experience, liquid and solid dielectric materials, and cooling techniques for tape-wound cores.

The Circuits and Applications Group surveyed the wide range of potential applications for magnetic switching technology and derived from that the research topics that would be most productive over the next several years. The survey was divided into three applied areas: electrical discharge devices and plasma sources, ultra-high-current applications, and induction accelerators.

Each group was assigned a chairman, cochairman, and LLNL representative to serve as group discussion leaders during the workshop. Months before the workshop convened, these same individuals served on the Organizing Committee to help plan the technical scope and content for their respective groups. Each group hosted an invited speaker to represent them by presenting a key technical issue to the Workshop membership during the opening plenary session. Each group also hosted three invited authors who presented their papers to their own working group members during private group sessions. The invited author presentations addressed specific technical issues and stimulated the initial group discussions. The group reports and summaries from each chairman, combined with the invited papers, make up the bulk of the Workshop Proceedings.

Generally, the three meeting days had similar schedules; each day contained a morning and an evening session. Each afternoon was free for the members to continue their morning discussions, review the poster papers, or just relax. During the morning and evening sessions, the five working groups were supported by a fully equipped office facility and six staff members. The office contained eight computers (for calculations or word processing), copy machines, viewgraph production facilities, FAX and binding machines, and a large library of books and articles to aid the groups in their discussions. These services were provided to create a working environment that was vigorous and supportive.

Workshop Highlights

The morning session of the first day was devoted to the five invited speaker presentations and to the poster presentations by student scholarship recipients and visiting Soviet scientists.

The following list identifies the Invited Speakers and their presentations:

Network and System Modeling Group
Jan-Mark Zentler, *Modeling Magnetic Pulse Compression Networks,*
Lawrence Livermore National Laboratory

Magnetic Materials Group
Carl Smith, *Magnetic Materials in Magnetic Pulse Compression,*
Allied Signal Corporation

Power Conditioning Group
David Barrett, *Power Conditioning Networks for High Average Power Magnetic Pulse Compression Systems,*
Lawrence Livermore National Laboratory

Core Cooling and Dielectrics Group
Gerry Rohwein, *Insulation of Dense Windings,*
Sandia National Laboratory

Circuits and Applications Group
James Swingle, *Cost Scaling Large Systems that Use Magnetic Pulse Compressors,*
Lawrence Livermore National Laboratory

Posters from the Soviet scientists and students were hung on the walls of the main meeting room to be viewed by the workshop members during scheduled breaks and free afternoons. Poster authors were available to discuss their work during this first morning session. The invited speaker presentations, listed above, are not included in the proceedings, but the student posters and some Soviet poster papers are published in the Technical Summary.

The evening session of the first day began with a plenary meeting where the working groups were charged with their mission and responsibilities. After questions and a discussion of schedules, the membership broke up into their working groups. At this point, the Chairmen took charge of their groups and introduced their objectives for the next two days. Most of the groups elected to hear presentations from their three Invited Authors. These invited technical papers are also included in the Technical Summary.

The morning session of the second day commenced with a brief plenary meeting to answer questions and to dispense news items. The membership then retired to their working groups for the remainder of the morning. The evening session of the same day began with a brief progress report from each Chairman. Following these reports, the membership again broke up into their working groups for the evening.

The morning session of the last day began with a very brief plenary meeting to answer any questions. Afterward, the membership broke into working groups to finalize their discussions and conclusions. The evening session was split into two main events: a presentation from our last invited speaker and the final group reports from each chairman. The featured speaker was Vitalii Bystritskii from the High-Current Electronics Institute in Tomsk, U.S.S.R., who elected to present some recent opening-switch results. His presentation, entitled *Experimental Investigation on the Conduction Phase of the Microsecond Plasma Opening Switch* was a welcome break from three days of magnetic pulse compression discussions. Following Bystritskii's presentation, the group Chairmen reported on the findings and conclusions of the group members. A detailed report by each Chairman is included in the Technical Summary. A brief working-group summary from each Chairman also appears in the Executive Summary.

Demographics

The workshop was attended by researchers from five countries outside the U.S. (the number in parentheses indicates the number of delegates from each country): France (1), Japan (2), Soviet Union (5), United Kingdom (5), and West Germany (1).

The U.S. organizations at the workshop can roughly be divided into three categories: private companies, universities, and national laboratories. The table shown below identifies the organizations in each category.

Companies (20)	*Universities (10)*	*Laboratories (41)*
Allied Signal	Auburn University	Idaho Ntl. Eng. Lab
Berkeley Research Assoc.	Old Dominion University	Lawrence Berkeley Lab
Beta Development	Texas Tech University	Lawrence Lvmr. Ntl. Lab
L. Schlitt Consulting	U. of South Carolina	Los Alamos Ntl. Lab
Maxwell Laboratories	U. of Southern California	Sandia Ntl. Lab
McDonald Douglas	U. of Texas at Arlington	Stanford Lin. Accel. Cntr.
National Magnetics	U. of Texas at Austin	
North Star Research		
Physics International		
Power Spectra		
Pulse Sciences		
Spectra Technology		
Vacuumschmelze (USA)		
Westinghouse		

The total number of representatives for each category is given in parentheses at the top of each column. The greatest variety of participating organizations was provided by companies while the total workshop population was dominated by U.S. laboratories.

The Organizing Committee awarded six scholarships to qualified graduate students working in the general area of repetitive switching. The scholarship fund was provided by Sandia National Laboratory and covered the workshop registration fee and accommodation expenses for each student. The scholarship program was designed to bring the pulsed-power students in contact with the professional community in an interactive workshop atmosphere. Six universities were represented: five from the U.S. and one from the U.K. We have included in the proceedings a copy of each student's poster presentation.

Comments

The Organizing Committee intended that this workshop would unite a growing interest in magnetic pulse compression, as expressed by the growing number of related papers presented at recent conferences. We structured the working groups and the daily schedules to promote three beneficial activities:

- A sharing of information and techniques gained by recent experiments using modern magnetic materials.
- Discussions in the technical areas where information is sparse, such as switch modeling, material data, and component behavior at a high pulse-repetition frequency.
- An exploration into the future of magnetic pulse compression, including ideas for new applications and critical areas requiring continued research.

The two-volume set of proceedings is designed to document the workshop events and to serve as a lasting reference for further work. The two volumes have been made available to recap the information in a detailed format for technical readers and in summary form for technical program managers.

In our opinion, the membership found the unique office services very helpful in preparing presentations and reports. In some cases, the technical library enhanced

the working group discussions, but generally the resource was under-utilized because of the limited time available. The working groups were very active and covered the technology with some overlap; however, the time was too short to explore the full interests of each group or to interact with other groups on related topics. The invited speaker presentations were well received and helped to orient the membership on key technical issues. The invited author presentations were insightful and of interest to each working group, but each presentation reduced the time available for group discussions. Some groups faired with this tradeoff better than others. Generally, the isolated winter surroundings were an excellent backdrop for huddled, contemplative discussions. The accommodations, organized activities, and food services provided by Granlibakken were very well done.

References

1. W. S. Melville, "The Use of Saturable Reactors as Discharge Devices," *IEE Proceedings (London), Part 3; Radio and Communication*, **98**, p. 185 (1951).
2. G. T. Coate and L. R. Swain, Jr., "High-Power Semiconductor-Magnetic Pulse Generators," *Research Monograph* **39**, (The M. I. T. Press, Cambridge, MA, 1966).
3. I. S. Garber, *Magnetic Pulse Modulators*, Sovietskoye Radio, Moscow (1964).
4. I. G. Katayev, *Electromagnetic Shock Waves*, Sovietskoye Radio, Moscow (1963). Translation by Scripta Technica Ltd., Edited by D. L. Jones (Ph.D.), and Published by London Iliffe Books Ltd. (1966).
5. P. Chaudhari, B. Giessen, and D. Turnbull, "Metallic Glasses," *Scientific American* **242**,(4), pp. 98–117.

'90

Invited Papers

Network and System Modeling Group

MAGNETIC MODULATOR SYSTEM ISSUES

Edmond Y. Chu
Maxwell Laboratories, Inc.
8888 Balboa Ave
San Diego, Ca 92123

Abstract

Magnetic pulse compression techniques are used to improve the performance of conventional switches. Because these pulse compression stages involve a multiple set of capacitors and saturable inductors, they add a significant amount to the size, weight, cost, and complexity to the system. In this paper, we examine the possibility of minimizing the size and weight of the magnetic modulator by reducing the saturation times of the saturable inductors and choosing the optimum number of pulse compression stages. Other design issues such as core reset and bias, prepulses, and reflected energy from the load are also discussed.

I. INTRODUCTION

Magnetic pulse compression techniques are often adopted to extend the performance envelope of pulse power systems using conventional switches (e.g. Silicon Controlled Rectifiers (SCR), thyratrons, spark gaps, etc.). Through the use of saturable inductors and additional energy storage elements, magnetic modulators can provide significantly higher output dI/dt, peak current, voltage, repetition rate, shot life and overall system reliability.

The basic operation and design of magnetic modulators were first discussed in detail by W. S. Melville[1] and later by R. A. Mathias, et al[2] and D. L. Birx, et al[3]. The principles of operation for the magnetic modulators can be understood by considering the series switching, cascade discharge circuit as shown in Figure 1.

In the series switching, cascade discharge circuit, the capacitors usually have equal capacitances whereas the saturable inductors have successively lower inductances (i.e. the i^{th} inductor has lower inductance than the $(i-1)^{th}$ inductor). Initially, the first capacitor C_0 is charged to a desired voltage V_0. Upon closure of switch S_1, C_0 begins to discharge through L_0. If the saturable reactor L_1 has a high unsaturated inductance when compared to that of L_0, then most of the energy initially stored in C_0 will be resonantly transferred to C_1 in a time period given by:

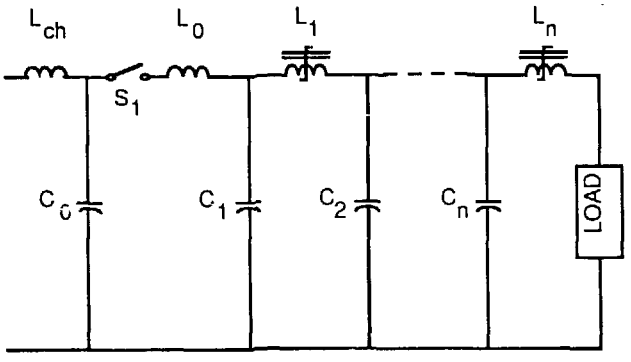

Figure 1. A simple series switching, cascade discharge circuit.

$$\tau = \pi \sqrt{\frac{L_0 C_0}{2}} \qquad (1)$$

provided L_1 will remain unsaturated during the transfer process. Saturation of L_1 will then transfer the energy from C_1 to C_2 at a faster rate determined by the saturated inductance of L_1. By careful selection of the saturable inductor saturation times, this process can be repeated efficiently through the successive stages until C_n discharges into the load. Power amplification is thus obtained through the reduction in series discharge inductance in each successive stage.

Because the magnetic pulse compression stages are physically between the initial energy storage capacitor and the load, the design of the magnetic modulator is dependent on the characteristics of the start switch (S_1) and the load requirements. To design a magnetic modulator to meet a given set of input and output electrical requirements is generally straightforward. However, if optimum design is required to minimize system size, weight, cost, or to maximize the system efficiency (as these parameters can vary by a factor of 2 between optimized and unoptimized designs), then the following system design issues must be addressed:

- Magnetic switch saturation times
- Number of pulse compression stages

- Magnetic switch reset and bias
- Output prepulses
- Reflected energy

II. DESIGN ISSUES

A. *Switch Saturation Times*

The design parameters of the saturable inductors in a magnetic modulator are related to their saturation times by the Faraday's law:

$$\int_0^{(\tau_{sat})_i} V dt = \langle V \rangle_i (\tau_{sat})_i = N_i (A_m)_i (\Delta B)_i \qquad (2)$$

where $\langle V \rangle_i$ = average voltage across the saturable inductor
N_i = number of turns on the winding
$(A_m)_i$ = core cross-sectional area
$(\Delta B)_i$ = available saturation magnetization

Because of the diode-like properties of saturable inductors (i.e. the inductor will have a large inductance for current in the reverse direction immediately after forward conduction), *magnetic modulators are generally very tolerant of excessive* saturation times of the saturable inductors. Since the core volume of each saturable inductor, $(Vol)_i$, is strongly dependent on its saturation time, as shown by the following equation:

$$(Vol)_i \approx \frac{(\mu_{sat})_i}{(L_{sat})_i} (N_i (A_m)_i)^2$$

$$= \frac{(\mu_{sat})_i}{(L_{sat})_i} \left(\frac{\int_0^{(\tau_{sat})_i} V dt}{(\Delta B)_i} \right)^2 \qquad (3)$$

where

$(L_{sat})_i$ = saturated inductance of the saturable inductor
$(\mu_{sat})_i$ = the saturated permeability of the core material

it is important to minimize the saturation time without compromising the efficiency of the pulse compression process.

Energy transfer efficiency as a function of the saturation time can be investigated using the simple two mesh cascade discharge circuit shown in Figure 2. If we assume that the saturated inductance of L_1 is approximately $25L_2$ (a reasonable approximation for many applications), we can calculate the energy transfer efficiency from C_1 to C_3 as we vary the saturation times of L_2. The result of this calculation is depicted in Figure 3. As shown in the plot, energy transfer efficiencies of >0.9 can be achieved at saturation times as short as 0.75 times the nominal resonance transfer time. In general, it has been found that satisfactory performance can be achieved using a saturation time given by:

$$(\tau_{sat})_i = \pi\sqrt{L_{i-1}C_{i-1}/2} - \pi\sqrt{L_iC_i/2} \qquad (4)$$

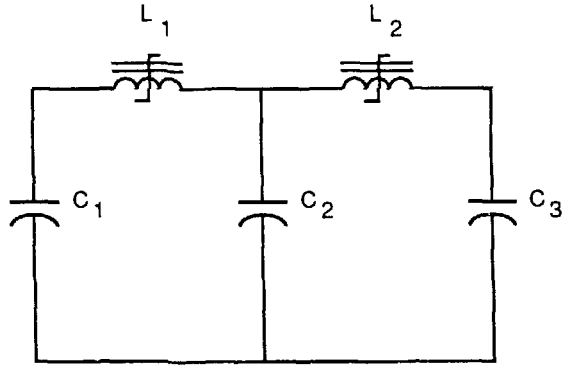

Figure 2 A two mesh cascade discharge circuit. $C_1 = C_2 = C_3$

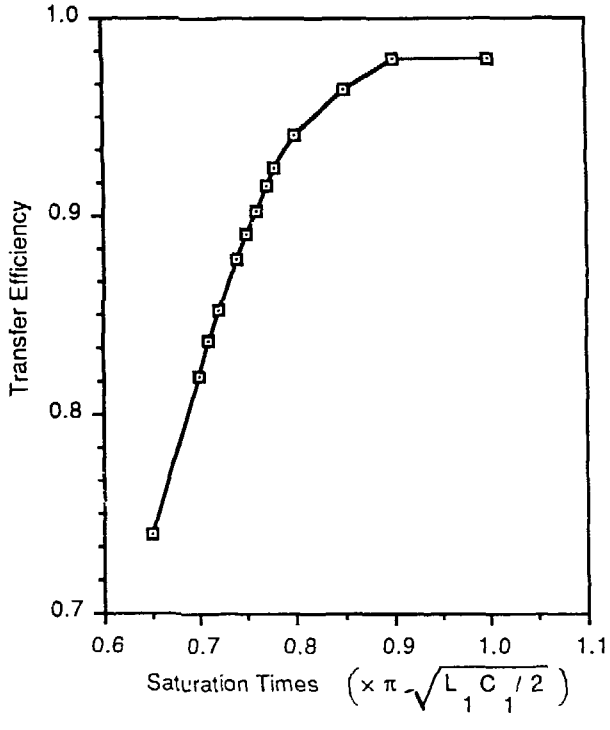

Figure 3 Energy transfer efficiencies as a function of saturation times of L_2

B. *Number of Stages*

The size, weight, efficiency, and cost of a magnetic switching modulator is strongly dependent on the number of stages of pulse compression chosen to satisfy the requirements.

If one defines the overall gain of the magnetic pulse compression stages as:

$$G = \left(\frac{L_0}{L_n}\right)^{0.5} \approx \frac{\tau_0}{\tau_n} \tag{5}$$

which is approximately the ratio of the start switch conduction time to the characteristic time associated with energy transfer to the load, then G can be expressed as:

$$G = \prod_{i=1}^{n}\left(\frac{L_{i-1}}{L_i}\right)^{0.5} = \prod_{i=1}^{n} G_i \tag{6}$$

where G_i, the individual stage gain is defined as:

$$G_i = \left(\frac{L_{i-1}}{L_i}\right)^{0.5} \tag{7}$$

It can be shown that (by using Eq (3)) the volume of magnetic switch core in each stage, $(Vol)_i$, can be related to its stage gain, G_i, by the following equation:

$$(Vol)_i = G_i^2 \frac{E_i \pi^2 (\mu_{sat})_i}{4 \Delta B_i^2} \tag{8}$$

where E_i = the energy stored in C_i,

The total magnetic modulator core volume is then equal to:

$$(Vol)_{core} = \sum_{i=1}^{n} (Vol)_i$$

$$= \sum_{i=1}^{n} G_i^2 \frac{E_i \pi^2 (\mu_{sat})_i}{4 \Delta B_i^2} \tag{9}$$

If G_i, E_i, $(\mu_{sat})_i$, and ΔB_i are identical for all stages, then

$$(Vol)_{core} = n\, G^{2/n} \frac{E \pi^2 \mu_{sat}}{4 \Delta B^2} \tag{10}$$

A plot of the total volume of core materials as a function of the number of pulse compression stages for various overall system gains is shown in Figure 4.

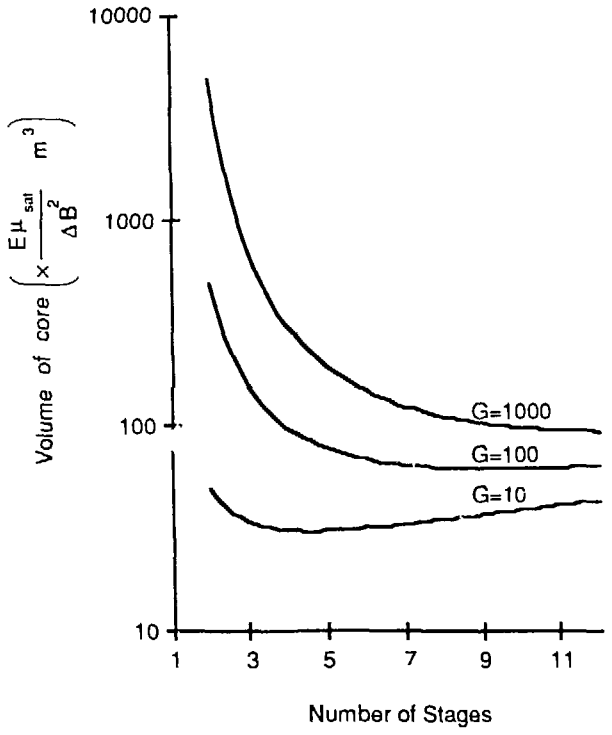

Figure 4 Plot of total core volume versus the number of pulse compression stages

Since there is one capacitive energy store for each pulse compression stage, the total volume of capacitors in the magnetic modulator can therefore be written as:

$$(Vol)_{cap} = (n+1)\frac{E}{\xi} \tag{11}$$

where ξ = capacitor energy density in J/m^3.

In most applications, it is desirable to minimize the weighted sum:

$$\alpha\,(Vol)_{core} + \beta\,(Vol)_{cap} \tag{12}$$

by varying the total number of stages. If α and β are densities of the core and capacitor respectively, then the weighted sum becomes the total weight of the system. Generally, because of the contributions from the capacitors, the minimum tends to occur at a value of n less than that depicted in Figure 4.

C. *Reset and Bias*

Because of the inverse square dependence of core volume on ΔB (see Eq (3)), it is important to pulse reset or dc bias the core to obtain as much flux swing as possible. The choice of pulse reset versus dc bias depends largely on the

specific application. In general, pulse reset will be preferred if the pulse repetition rate is low and the saturable core material has a square B-H loop. This is because at high repetition rate, the power requirements for pulse resetting can approach the output power of the magnetic modulator. A material having a low residual induction (B_r) will not provide a large ΔB after the reset pulse. For magnetic modulators that employ command resonant charging techniques for the charging of the initial energy storage capacitor, a self-reset approach as shown in Figure 5 can be used to simply the system design. To ensure proper core reset, the peak charging current must provide the required magnetization to saturate the core in the reverse direction. Because charging is usually achieved at a much longer time period compared to the discharge time period, the reset process will follow a lower frequency hysterisis loop which requires a relatively low magnetization for saturation. At the end of the charging current pulse, the cores will then acquire a negative residual induction B_r. If the core materials have a square B-H loop, then $B_r \approx B_{sat}$. Consequently, the available magnetization, ΔB, for the core will be approximately equal to 2 B_{sat}.

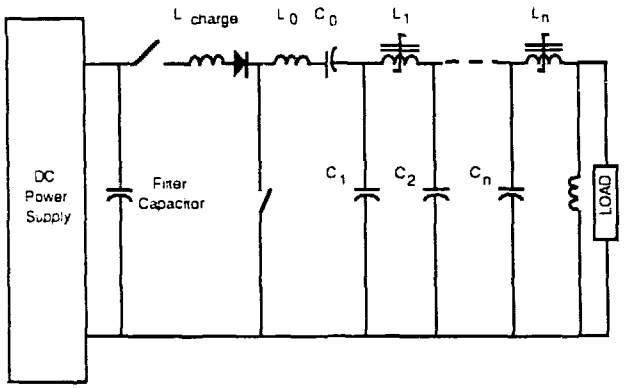

Figure 5 Circuit showing the use of charging current to reset saturable reactor cores

Figures 6 and 7 show two of the common approaches for providing core bias using dc power supplies. If maximum output efficiency is required for a large range of operating voltages, the core material should have a low residual induction. Moreover, using the bias scheme shown in Figure 6 will allow fine tuning of the saturation times of the saturation inductors. Trade-offs between induced voltage and reset/bias current can also be made if separate windings are used for the reset/bias process.

D. Output Prepulses

Because leakage currents are required for saturation of the saturable inductors, output prepulses are almost inevitable with magnetic modulators. There are many approaches to reduce the level of pre-pulses at the load. A common approach is to use a shunting impedance (e.g. inductor, capacitor, etc.) placed in parallel with the load. A low shunt impedance will result in a low prepulse amplitude. However, a low shunt impedance also reduces the energy delivered to the load, increases the output risetime, and distorts the output pulse shape. If the load has a well defined impedance characteristics, an output transmission line between the output saturable inductor and the load will produce a low prepulse amplitude without the drawbacks of the shunt impedances. Prepulse amplitude can also be suppressed if the gain of the output stage is reduced. This can usually be done by allowing a faster charge time for the output energy storage capacitor.

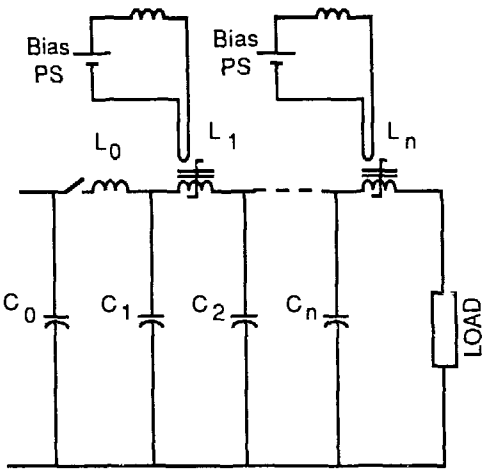

Figure 6 DC core bias using separate windings

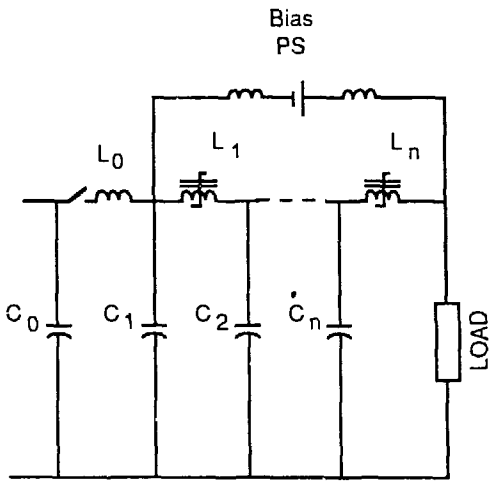

Figure 7 DC core bias using a single bias power supply

For applications involving a line type pulse forming network or pulse forming line as the final energy store in the pulse compression circuit, prepulse can essentially be eliminated using a symmetrically charged Blumlein[4] arrangement as shown in Figure 8. This is because the leakage associated with the output saturable inductor is a small perturbation to the total energy stored in each pulse forming line resulting in nearly identical charging voltage on both pulse forming lines. Since the prepulse across the load is the difference between the charging voltage of the pulse forming lines, the amplitude is significantly smaller than other approaches.

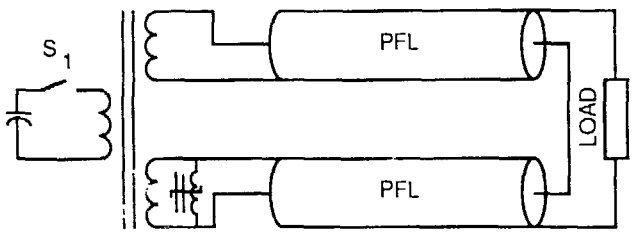

Figure 8 Prepulse is virtually eliminated using the symmetrically charged Blumlein

E. Reflected Energy

In applications where the load is inductive, a large voltage reversal will develop across the output stage capacitance following saturation of the output saturable inductor. Because of the diode nature of the saturable inductors, energy reflected from the load will be propagated towards the initial energy storage capacitor rather than resulting in high frequency ringing across the load. If this energy is not removed at the start energy, it will be reflected again towards the load. In high repetition rate operations, the energy reflected back and forth between the load and the start circuit can interfere with the subsequent pulses resulting in varying output voltage amplitude. Figure 9 shows an approach that would remove the reflected energy from the pulse compression circuit by recycling some of the reflected energy to the power source.

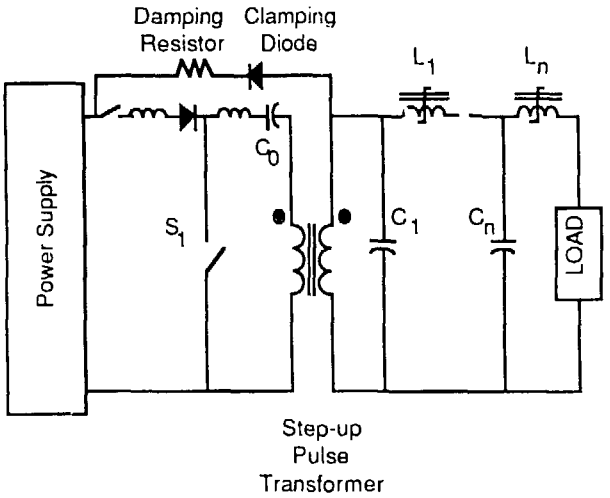

Figure 9 Clamping diode recovers reflected energy and prevents energy from oscillating between load and start circuit

III. REFERENCES

[1] W. S. Melville, "The Use of Saturable Reactors as Discharge Devices for Pulse Generators," *Proceedings Institute of Electrical Engineers*, London, England, Vol. 98, Part 3 (Radio and Communication), No. 53, 1951, pp.185-207.

[2] R. A. Mathias and E. M. Williams, "Economic Design of Saturating Reactor Magnetic Pulsers," *Transactions of the American Institute of Electrical Engineers*, Vol. 74, Part I, 1955, p.169.

[3] D. L. Birx, et al, "Basic Principles Governing the Design of Magnetic Switches," Lawrence Livermore National Laboratory, Livermore, CA UCID 18831, 1980.

[4] Symmetrically charged Blumlein is a Maxwell Laboratories, Inc. patented concept.

Critical System Issues and Modeling Requirements—the Problem of Beam Energy Sweep in an Electron Linear Induction Accelerator*

W.C. Turner, D.M. Barrett, S.E. Sampayan
Lawrence Livermore National Laboratory
Livermore, California 94550

Introduction

In this paper we discuss system issues and modeling requirements within the context of energy sweep in an electron linear induction accelerator. When needed, particular parameter values are taken from the ETA-II linear induction accelerator[1] at Lawrence Livermore National Laboratory. A diagram of the major systems for this type of accelerator is given in Fig. 1, and parameter values for ETA-II are summarized in Table 1. The ETA-II accelerator parameters are determined by the desired applications of the electron beam—a driver for a megawatt average power microwave free-electron laser (FEL) and a demonstration of front-end accelerator technology for a shorter wavelength FEL. Nominal parameters are beam current 3 kA, beam energy 6 MeV, and pulse flattop 50 ns. Up to the present time, ETA-II has been operated at 1- to 10-Hz pulse repetition frequency. Within the next year we hope to begin operating ETA-II for 10-ms bursts at 5 kHz and eventually extend the burst length to 0.5 s. For this paper, the most important parameter in Table 1 is energy sweep during a pulse. It is important to have low energy sweep to satisfy the FEL resonance condition and to limit the beam corkscrew motion. It is desired to achieve $\Delta E/E = \pm 1\%$ for a 50-ns flattop whereas the present level of performance is $\Delta E/E = \pm 1\%$ in 10 ns. To improve this situation

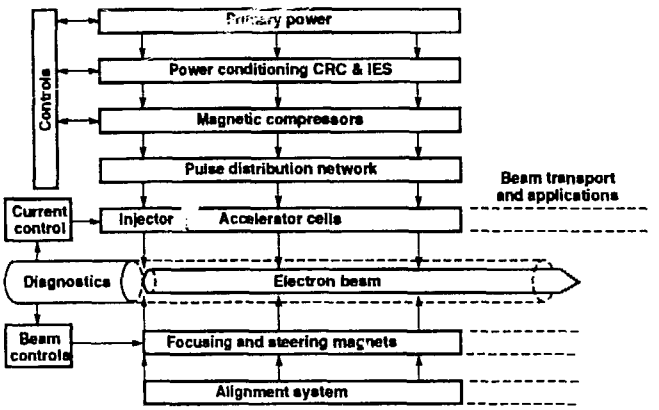

Fig. 1. Diagram of linear induction accelerator systems.

we will identify a number of areas in which modeling could help increase understanding and improve our ability to design linear induction accelerators.

In general two types of modeling questions can be asked: component and system. A component question is: Can a magnetic pulse compressor be built that delivers a well-defined pulse shape into a specified load impedance at given pulse repetition frequency (PRF)? A system question is: What is the optimum number of accelerator cells driven by a single magnetic compression modulator (e.g., the number that minimizes the total cost of the accelerator or FEL)? For the most part, I will be concerned with problems of performance that arise at the component level defined by the boxes in Fig. 1.

* Work performed jointly under the auspices of the U.S. Department of Energy by Lawrence Livermore National Laboratory under contract W-7405-ENG-48, for the Strategic Defense Initiative Organization and the U.S. Army Strategic Defense Command in support of SDIO/SDC MIPR No. W31RPD-0-D4074.

Table 1. ETA-II parameters.

Parameter	Goal	Current status (12/89)
Brightness (A/rad-cm)^2	$>2 \times 10^9$	6×10^8
Current (kA)	3.0	>3
Beam energy (MeV)	6, 7.5, 10	6
Energy sweep (head to tail)	±1%, 50 ns	±1%, 10 ns
Energy stability (pulse to pulse)	±0.1%	—
Flux line alignment (μm)	±100	±3000
Centroid displacement (mm)	<1, 50 ns	10, 10 ns
Angular sweep (mrad)	<10, 50 ns	6, 10 ns
Rep rate (kHz)	5	0.01
Duration (sec)	0.01, 0.5	—

Energy Sweep

Energy sweep combined with misalignment of the magnetic axis with respect to the beam propagation direction leads to an undesirable differential rotation between the head and tail of the pulse known as corkscrew.[2,3] The differential phase advance is cumulative as the beam propagates down the accelerator. An example of this corkscrew motion at the end of ETA-II is shown in Fig. 2.[4] The data are shown for a time interval of approximately 50 ns during which the beam current exceeds half its maximum value of 1.7 kA. The radius of the transverse motion is about 1 cm, ten times the desired goal of 1 mm, and this is our primary motivation for wanting to control the energy sweep. Improvement of magnetic axis alignment is also being pursued but will not be discussed in this paper.

If we want to limit the energy sweep $\Delta E/E$ to a certain value for a time interval t, the voltage pulse on the acceleration gaps must satisfy this same constraint—$\Delta V/V = \pm 1\%$ for 50 ns. If we refer to the component subsystems shown in Fig. 1, there are a large number of effects that are listed in Table 2 that can influence $\Delta V/V$ applied to the acceleration gap. Because the time delay through a magnetic pulse compressor (MAG) is voltage dependent, there is an intimate connection between the voltage and timing of the output pulse. In addition, core reset defines the available flux swing in each magnetic switch and is therefore also related to the voltage and timing of the output pulse. Relative timing error between the beam current load and the voltage pulse applied to the acceleration cells can affect the shape of the pulse and therefore the energy sweep. The shape of acceleration pulse is also obviously affected by the MAG pulse shape and the behavior of the various loads at the acceleration cell—cell capacitance, cell ferrite, and the electron beam current. In some cases the effects listed in Table 2 can be used in a compensating way. For example, the output pulse of the MAG can be deliberately distorted to account for change in load impedance during the pulse caused by cell capacitance and ferrite. In addition, the dependence of acceleration pulse shape on the beam current load can also be used to advantage by programming the beam current to offset slowly drifting pulse-to-pulse voltage variations due to effects such as thermal variation of ferrite loading in the acceleration cells.

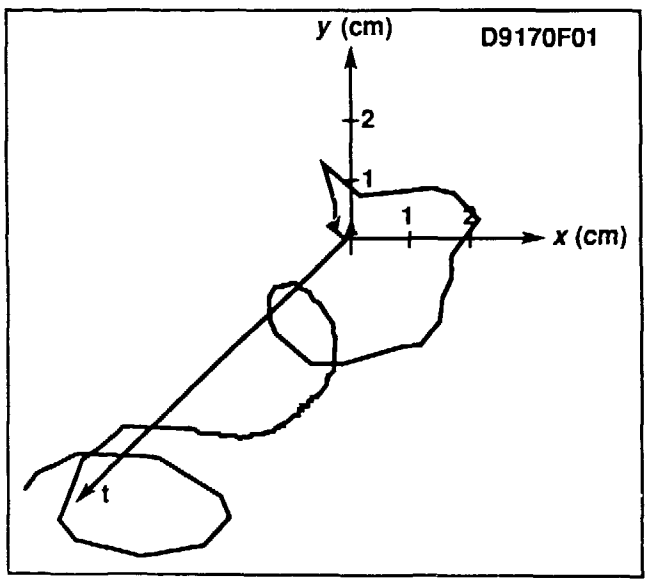

Fig. 2. An example of corkscrew motion of the beam at the exit of ETA-II for I = 1.7 kA and W = 6 MeV. Data are shown for the 50 ns that the beam current exceeds half its maximum value.

Table 2. Factors that influence energy sweep.

1. **IES voltage regulation**
2. **Core reset stability**
3. **MAG output pulse timing jitter**
4. **Thermal drift in ΔB_{sat} of the MAG cores**
5. **MAG output pulse shape**
6. **Impedance mismatch in the pulse distribution network**
7. **Cell capacitance**
8. **Ferrite loading**
9. **Beam loading**

Our strategy for dealing with the effects listed in Table 2 consists of the following four components:

- Voltage regulation
  DeQ circuit regulates the intermediate energy storage (IES) voltage input to the MAG to ±0.04%.
- Jitter control
  Feedback and feedforward circuits control the IES switch trigger time, holding MAG output jitter to <1 ns.
- Passive compensation
  Pulse distribution network and tapered MAG PFL compensate for cell ferrite and capacitance loading at low PRF;
  $\Delta V/V = \pm 1\%$, 50 ns, 1 Hz.
- Delayed feedback current control
  Feedback control of injector current is used to compensate thermal drift in cell ferrite loading at high PRF;
  $\Delta E/E = \pm 1\%$, 50 ns, 5 kHz.

In this paper we will concentrate on passive compensation issues and delayed feedback current control where modeling can have a significant impact. Voltage regulation and jitter control have been discussed in a previous paper.[5]

The Magnetic Compression Modulator

A schematic of the MAG I-D three-stage modulator used on ETA-II is shown in Fig. 3. Points where the voltage can be measured are labeled A through E, and a typical set of waveforms

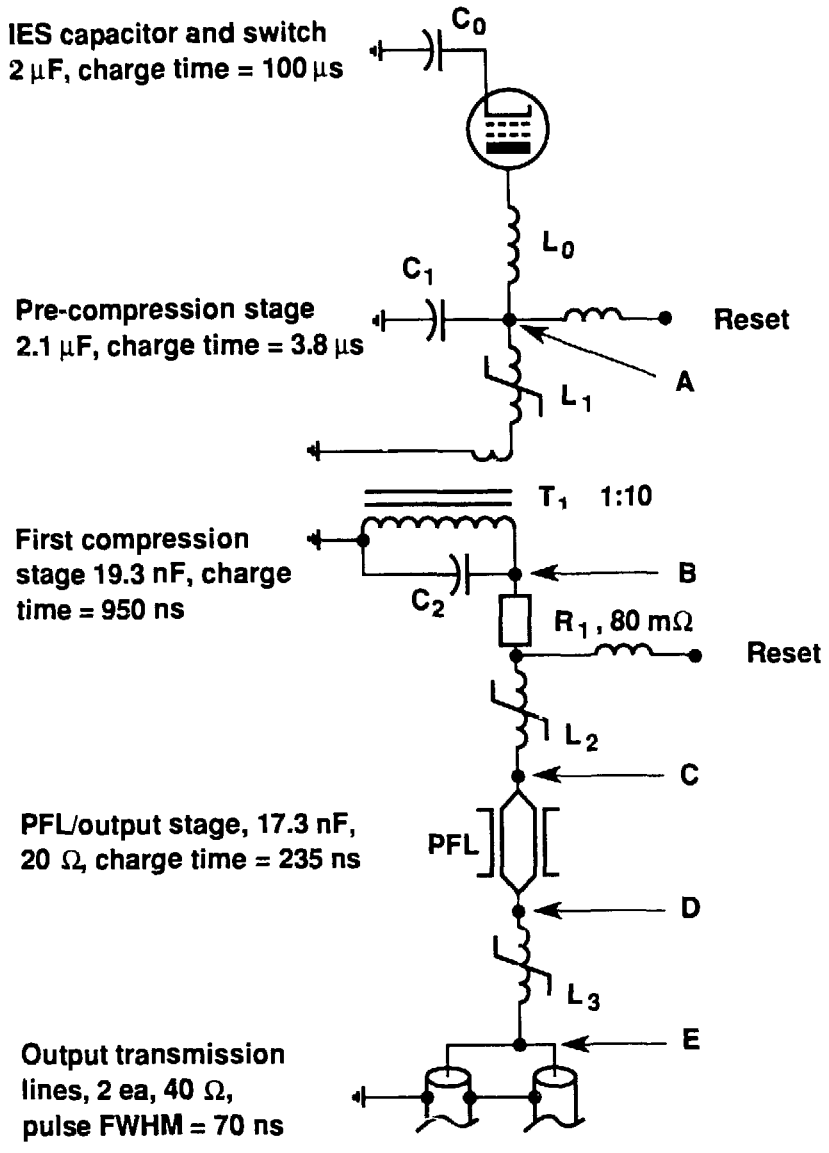

Fig. 3. Schematic of a MAG I-D magnetic compression modulator.

are shown in Fig. 4. The stage-to-stage cumulative efficiency is also indicated in Fig. 4. The energy for each stage has been calculated from the peak voltage. The MAG I-D output energy in Fig. 4d exceeds that listed for the PFL in Fig. 4c because the voltage is not uniform along the PFL, and the the PFL continues to charge after the output reactor saturates. Although these modulators have been used to successfully operate ETA-II to obtain the parameters in Table 1, there are some improvements that can be made. First, one notices that the interstage voltages switch before reaching the peak of a 1-cos(ωt) waveshape. This can occur for two reasons: too-small volt-second products stored in the switches or saturated inductances that are too large. If the saturated inductances are too large, this raises the question, What is the effective saturated permeability of the Metglas in these switches? Second, the overall efficiency of the MAG I-D for the data shown in Fig. 4 is 58%, and it is desirable to know if this can be improved. The largest loss (236 J) occurs in energy transfer between the first compression stage capacitor and the PFL. Further experiments have shown that most of this loss is due to the output magnetic switch, which has the highest *dB/dt* (~15T μs while the PFL is being charged). It would be of interest to know how much of the hysteresis loss is intrinsic small-sample loss and how much is due to saturation wave effects because of the large core area and early saturation of the inner radius material. Another interesting point is that because of the low output impedance of the MAG I-D, the saturated magnetization current in the output switch reaches very high values—in excess of 50 kA. Non-squareness of the *B–H* hysteresis curve could result in significant loss occurring during the switching time. If this is the case, it would be interesting to consider a larger number

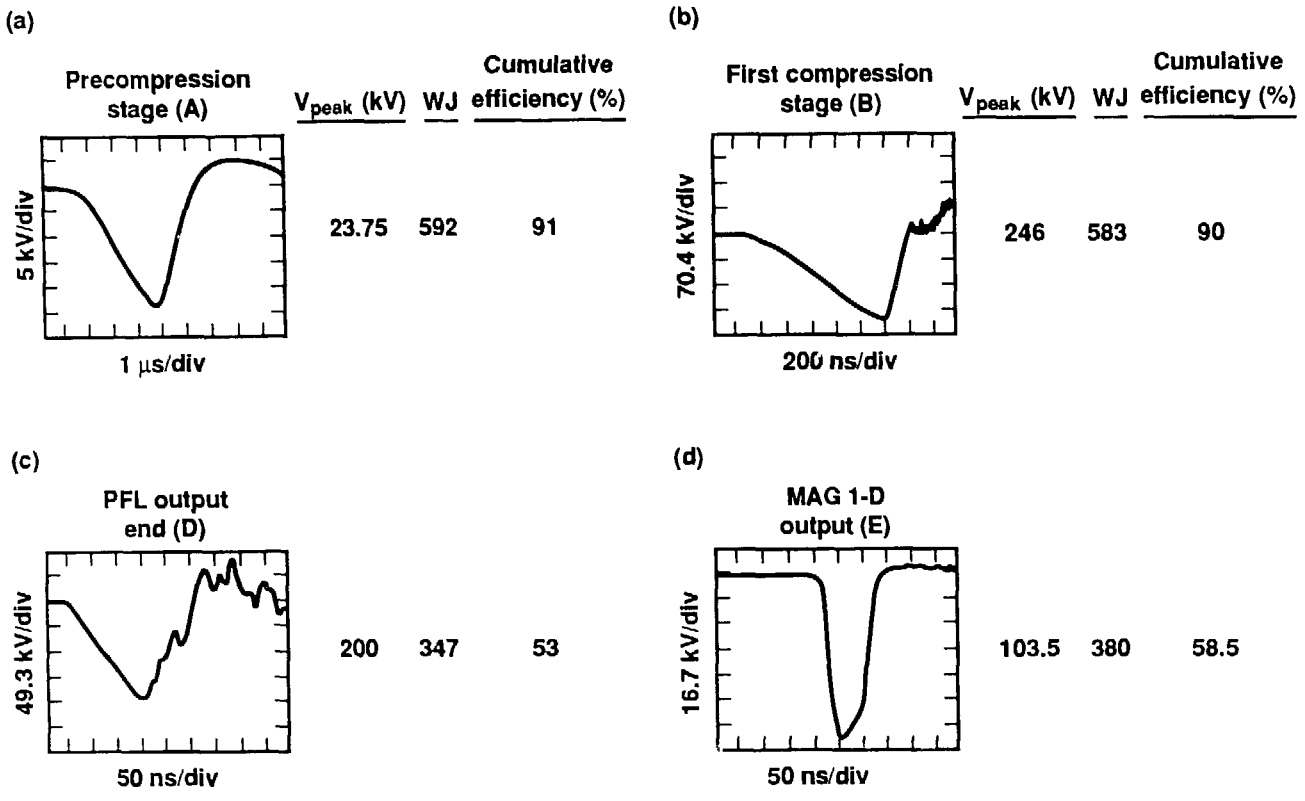

Fig. 4. Typical set of MAG I-D voltage waveforms. See Fig. 3 for the location of the pickoff points A, B, D, and E.

of higher impedance magnetic compression modulators to increase efficiency.

Figure 5 illustrates another important feature of MAG I-D operation that must be taken into account when we are concerned about energy sweep—namely that the shape of the output pulse is amplitude dependent. In Fig. 5 the MAG I-D output voltage is shown for several values of voltage on the command resonant charging circuit (CRC) that drives the MAG I-D. The variable output pulse shape has been modeled with the SPICE code[6] and is explained by the presence of traveling waves on the PFL that are excited during its 235-ns charge time. Achieving low energy sweep will require operation at a single point or consideration of a variable compensation scheme if it is desired to operate over a range of output voltages.

A primary issue for a magnetic modulator is preservation of output waveform quality at high PRF since these devices are usually of interest for high average power applications. For example, on ETA-II we would like to demonstrate pulse-to-pulse stability of 0.1%, an order of magnitude better than the pulse flatness requirement, in order to ensure the stability of delayed feedback current control discussed below. An example of the type of difficulty that can occur at high PRF is shown in Fig. 6 where the amplitude of the MAG I-D precompression capacitor voltage is shown for the first 60 pulses of 5-kHz and 3-kHz pulse bursts. The amplitude appears to have more than one quasi-stable value with number of transitions increasing as the frequency is raised. The behavior is reminiscent of mode-jumping behavior that occurs in periodically driven non-linear systems. We do not have a detailed understanding of the process that is occurring here, but it seems likely that it is caused by reflected energy from the previous pulse not being completely dissipated before the arrival of the succeeding pulse so that the switch cores are not precisely reset to their initial conditions.

In this section we have given some indication of non-ideal behavior that can occur in a real-life magnetic compressor to stimulate thought about where modeling could help increase our understanding. As often happens in the development of science and technology, the experimental development of the high-power magnetic compression modulator has led the modeling capability. There is not much experience with models that can calculate waveforms and compare them with precision to the type of data given in Figs. 4 to 6. The non-trivial problem here is of course modeling the behavior of the non-linear magnetic switch elements, a problem that also occurs with the induction accelerator cell. There is also the numerical problem of dealing with the four-order-of-magnitude variation in time scales of interest from the hundreds of microseconds between pulses to the tens of nanoseconds duration of output pulse. In the development of a magnetic modulator model it is important to build in predictive capability for devices not yet built or only imagined as well as to replicate the data from an existing device. For example, it should be easy to change the core geometry and size, magnetic material, specific magnetization model, and number of compression stages. In this way a number of devices could be modeled with a common tool, and the possibility of doing system optimization studies would exist.

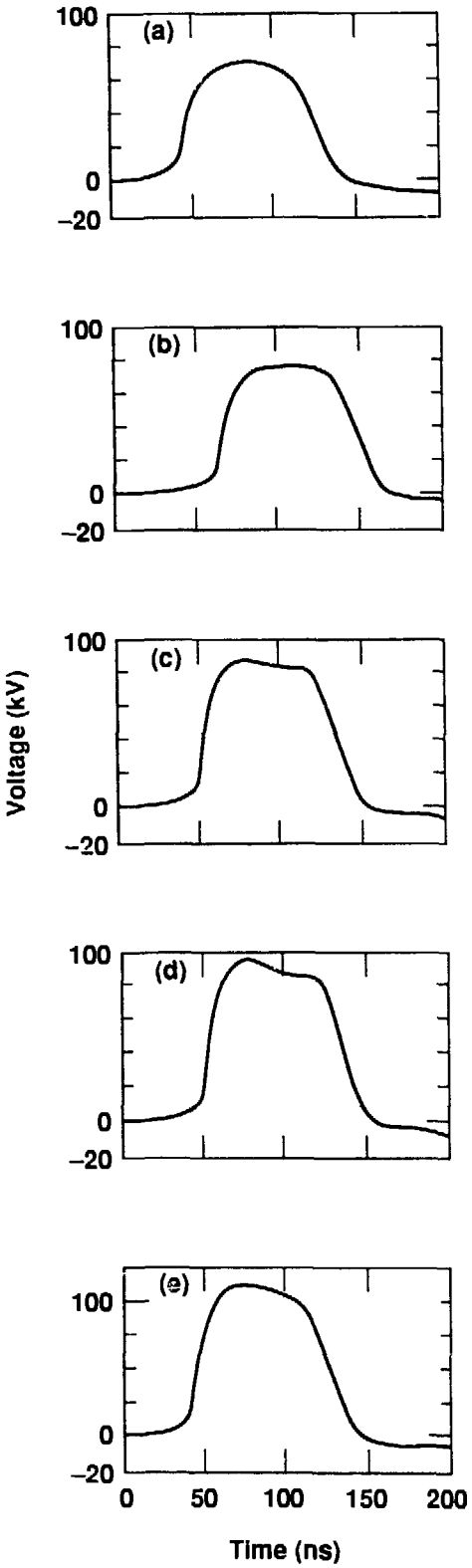

Fig. 5. Illustration of the changing shape of the output pulse of the MAG I-D as the command resonant charging (CRC) voltage is varied, (a) CRC = 10 kV, (b) CRC = 11 kV, (c) CRC = 12 kV, (d) CRC = 13 kV, (e) CRC = 15 kV.

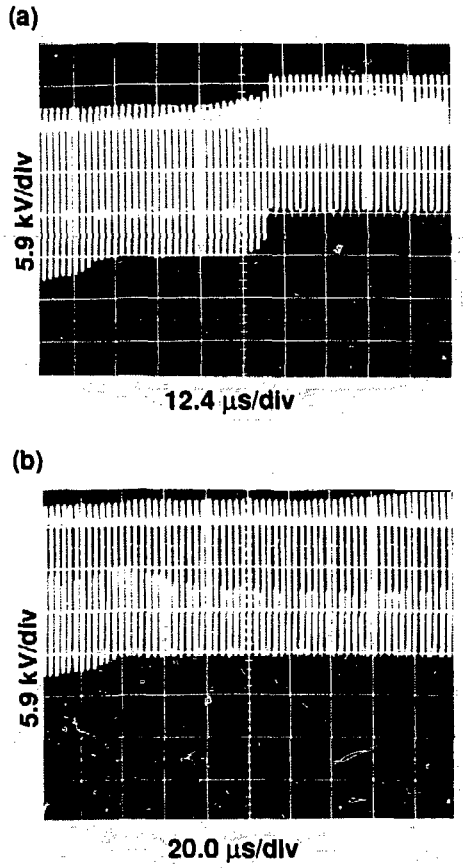

Fig. 6. Illustration of an amplitude instability of a MAG I-D at high rep rate, (a) f = 5000 Hz, (b) f = 3000 Hz. In each case the first 62 pulses of the pre-compression stage capacitor voltage are shown.

The Induction Accelerator Cell

A cross section view of an ETA-II acceleration cell is shown in Fig. 7. The cell contains a two-sided high voltage feed across a nominal 0.75-cm gap, a solenoidal coil for focusing the electron beam and ferrite toroids (8 ea. i.d. = 20.3 cm, o.d. = 35.6 cm, thickness = 2.54 cm) for high voltage isolation. A simplified schematic of the cell and drive circuitry is shown in Fig. 8. The drive circuitry is represented by a voltage source $2V_0$ in series with an impedance Z_0. The cell is represented by the parallel combination of gap capacitance C_0, ferrite impedance Z_f, and a beam current source I_0. Because of the dominant lossy nature of the ferrite, we approximate the ferrite as a non-linear resistor with a value equal to the instantaneous ratio of voltage to current rather than as an inductor represented by a non-linear permeability. The acceleration voltage across the gap is then simply

$$V_b = 2V_0 - (I_c + I_f + I_b) Z_0 \qquad (1)$$

and the variation of acceleration voltage is related to variation of ferrite impedance by

$$\delta V_b/V_b = (Z_0/Z_f)\,(\delta Z_f/Z_f) \ . \qquad (2)$$

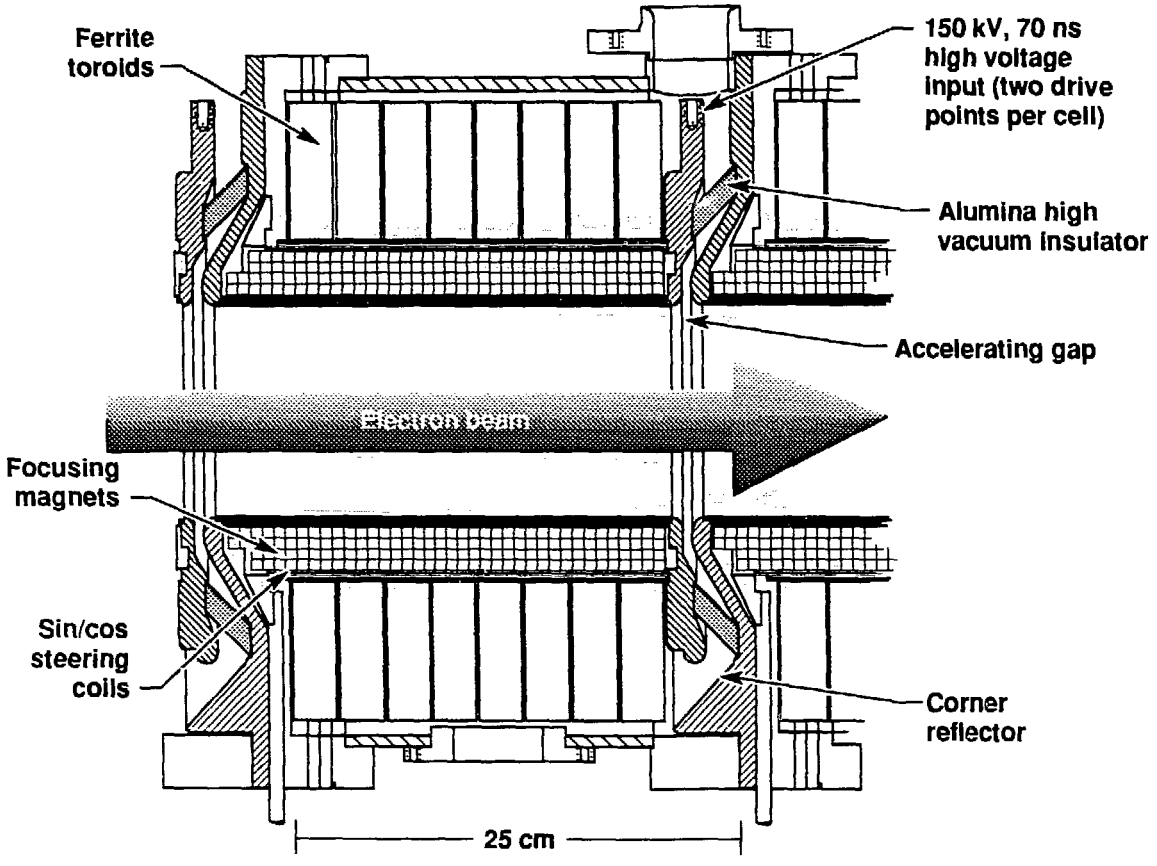

Fig. 7. Cross section view of an ETA-II accelerator cell.

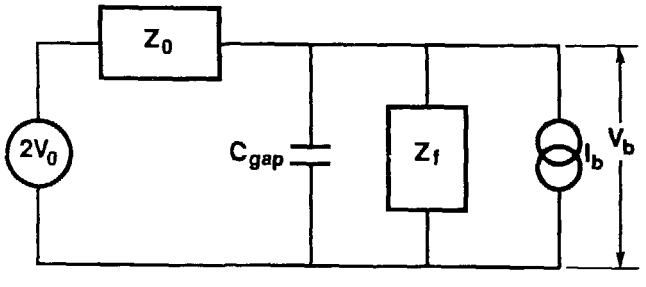

Fig. 8. Simplified circuit schematic of an accelerator cell.

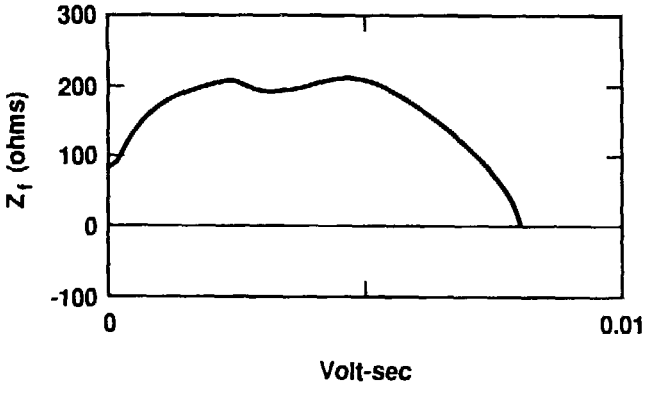

Fig. 9. Impedance of the ferrite in an ETA-II cell as a function of the applied volt-seconds for a drive voltage V = 108 kV.

The impedance Z_f of the ferrite in an ETA-II cell has been measured. A typical result is shown in Fig. 9 where Z_f is plotted as a function of the volt seconds applied to the cell for a drive voltage pulse of 108 kV.[7] Although the impedance is near 200 Ω for a large fraction of the volt-seconds, it is far from constant. A fractional impedance variation may be easily calculated as a function of the fraction of volt-seconds utilized. Calculating from the center of the pulse for volt-second utilization fractions of 0.5, 0.75 and 0.90, the fractional impedance variations are $\delta Z_f/Z_f$ = 0.10, 0.31 and 0.60. For ETA-II the nominal ratio of drive impedance per cell to ferrite impedance is Z_0/Z_f = 40/200 = 0.2, giving from Eq. 2 acceleration gap voltage variations $\delta V_b/V_b$ = 0.02, 0.06, and 0.12. Clearly some compensation of the ferrite impedance variation will be required to achieve ±1.0% beam energy flatness for 50 ns. For a practical system there will be some tradeoff between utilization of the ferrite volt-seconds and complexity of compensation of the impedance variation. Eq. 1 suggests two ways to compensate for variation of Z_f: vary the drive impedance Z_0 and/or the beam current I_b.

Up to now ETA-II has been driven with 4 Ω cables feeding pairs of transmission lines that run along a group of ten acceleration cells—shown schematically in Fig. 10a. Because of impedance matching problems with this type of distribution, the shape of acceleration voltage pulse varies considerably from cell to cell. An example of voltage waveforms measured at the first and tenth cell of a ten-cell set is given in Fig. 11. To eliminate this undesirable effect, the distribution system is being modified so each pair of cells is driven by a pair of 40 Ω cables as shown in Fig. 10b. The individual pairs of cells are transit-time isolated, and symmetry, shorter bus length and greater care taken in impedance matching have eliminated the cell-to-cell distortion observed in Fig. 11.

The pulse distribution networks shown in Fig. 10 have been thoroughly modeled with SCEPTRE to predict the acceleration gap voltage including the effects of beam and ferrite loading. The beam is treated as a current source equal to the measured output current pulse of the ETA-II injector. The ferrite load is taken directly from impedance measurements like those shown in Fig. 9. The results of some of these calculations are shown in Fig. 12a where the width of pulse having a given fractional energy variation is plotted for the existing transmission line feed, for the 40 Ω multi-cable feed and for the 40 Ω multi-cable feed and tapered PFL. For these calculations the beam current was 2.2 kA, and the peak amplitude of the MAG I-D output pulse was 110 kV. The calculations predict that the existing transmission line feed will achieve ±1% energy flatness over only 13 ns of the pulse, and this is in excellent agreement with the beam energy sweep measured on ETA-II.[4] From Fig. 12a the calculations further predict that ±1% energy flatness will be achieved for

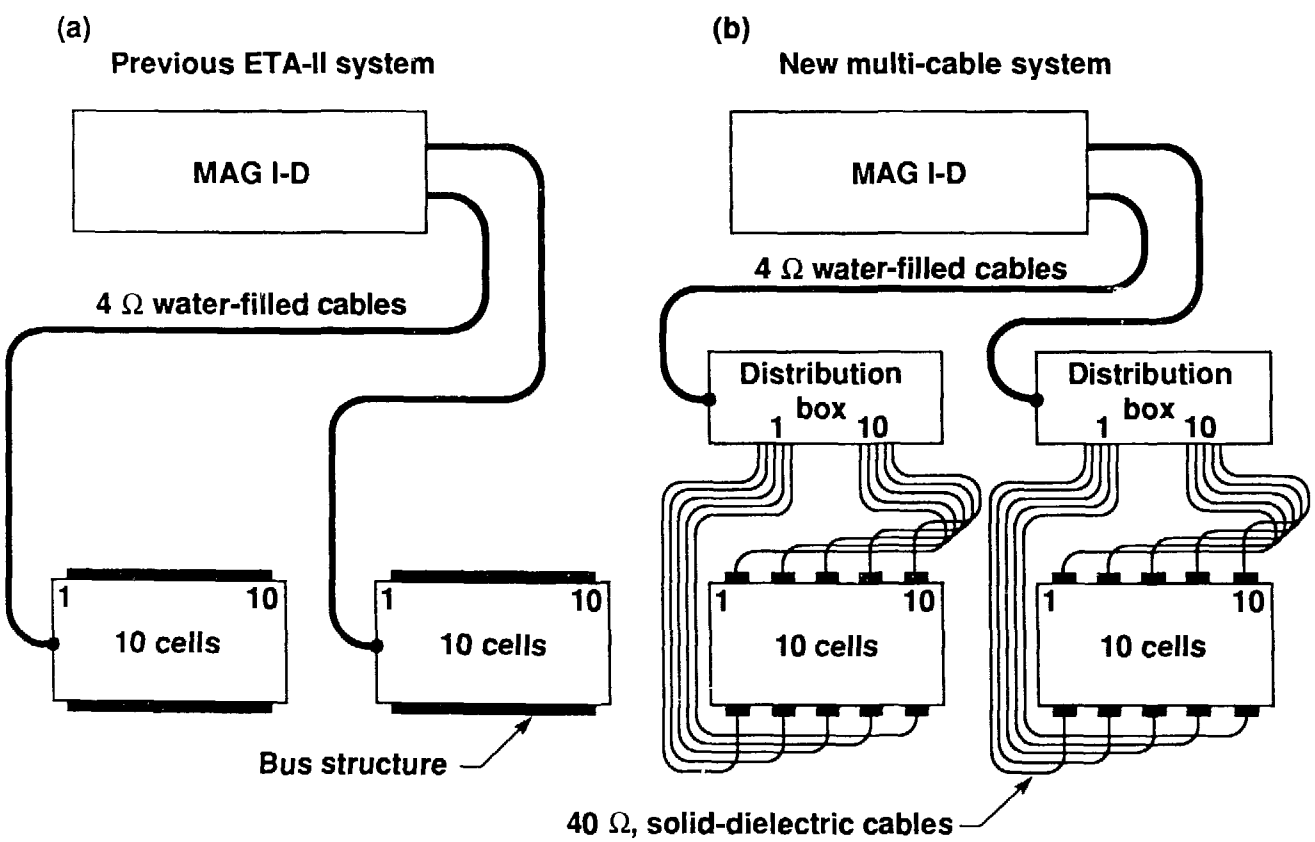

Fig. 10. Schematic of pulse power distributions to the accelerator cells of ETA-II, (a) ten-cell transmission line feed, (b) multi-cable feed; each pair of cells is driven by a pair of 40 Ω cables.

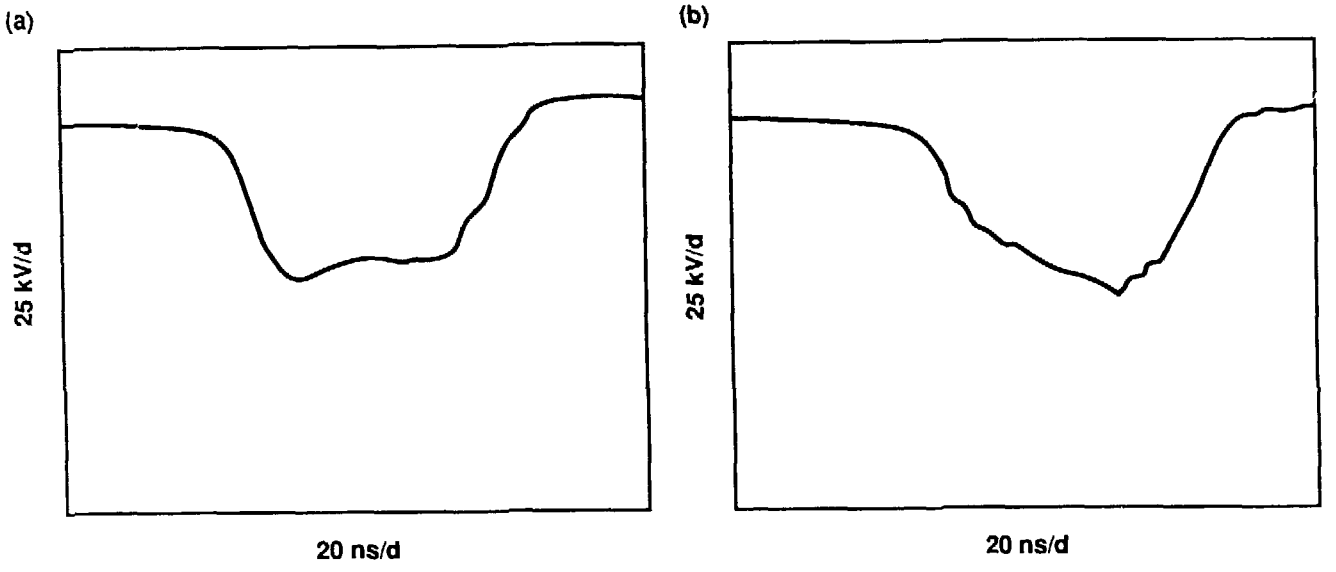

Fig. 11. Voltage waveforms measured at (a) the first and (b) the tenth cell of a ten cell set driven with the transmission line feed of Fig. 10a.

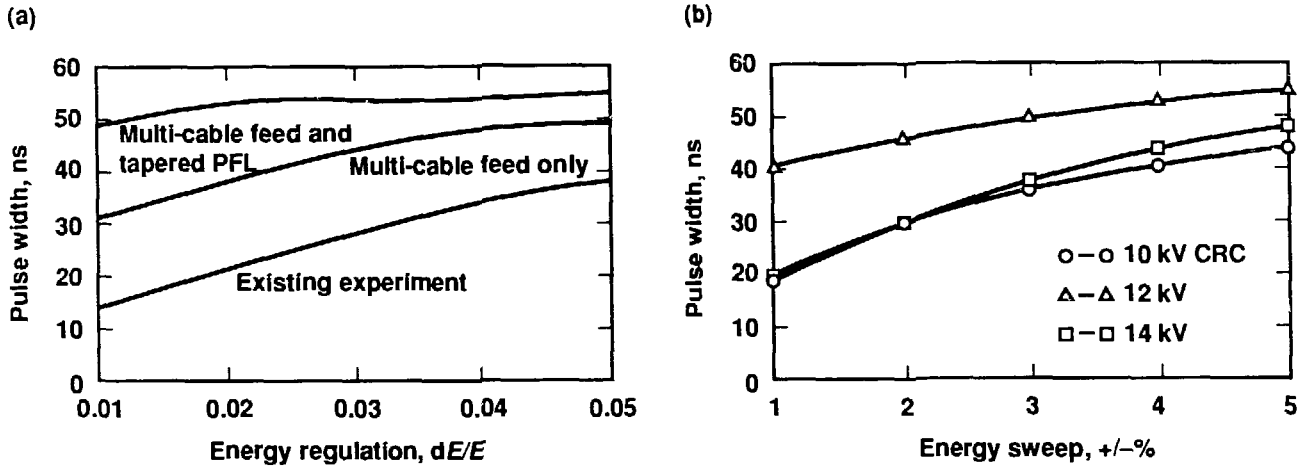

Fig. 12. (a) Results of circuit calculations showing the width of the pulse flattop as a function of flattop energy regulation ΔE/E for a transmission line feed as in Fig. 10a, a multi-cable feed as in Fig. 10b and multi-cable feed and tapered pulse forming line on the output stage of the MAG I-D. (b) Measurements of flattop pulse widths on the prototype multi-cable feed system as a function of ΔE/E for CRC voltages of 10, 12, and 14 kV.

31-ns pulse width with the multi-cable feed and for 49 ns with the tapered PFL addition. The impedance of the PFL varies by ±12%. The ±1% pulse width achievable has a rather hard upper bound of 50 ns because of the 70-ns transit time on the PFL and 20-ns rise and fall times. So far we have prototype-tested the 40 Ω multi-cable feed with a fixed 38.5 Ω resistive load per cell to simulate beam loading. Pulse width versus energy sweep is given in Fig. 12b for three values of the CRC voltage. With a CRC voltage of 12 kV, the duration of ±1% flattop is 28 ns, in reasonable agreement with the predictions in Fig. 12a. For CRC voltages above and below 12 kV, the duration of flattop is reduced because of the charging phenomenon noted in Fig. 5.

From the modeling perspective, the problem of the ferrite response of an accelerator cell is similar to modeling a magnetic switch in the pulse compressor except that the switching material is ferrite instead of Metglas. Clearly, from the component design viewpoint, it is desirable to have a cell model that includes the ferrite response. At the present time a cell model does not exist that allows one to model component design to the level of the ±1% energy sweep that we desire to achieve. In the immediately preceding discussion the modeling calculations presented in Fig. 12a are somewhat of a cheat since the cell response was taken directly from experimental measurements. In fact it may be unrealistic—no one has developed a complete model of accel-

erator pulse shape that calculates everything from material properties and geometry and correctly predicts energy sweep to ±1% accuracy. So we are left with the present approach that combines modeling, experimental measurement and component design that allows some degree of tunability. For example, the tapered PFL discussed above has been designed as a parallel plate structure with variable spacing to allow for uncertainty of cell loading and the amplitude dependence of MAG 1-D pulse shape illustrated in Fig. 5. In any case, it still seems desirable to develop a model of the acceleration cell that attempts to push back the level at which experimental data enter the calculations. To that end we initiated a program of experiment and modeling magnetization reversal in small samples of ferrite where propagation effects and spatial variation of field strength could be neglected. These results are then to be used to describe local reversal of magnetization in transmission line models and field solving codes for large ferrite cores and accelerator cells where propagation effects are important. So far we have only made progress with the small sample part of this program. Small ferrite toroids (o.d. = 31 mm, i.d. = 19 mm, l = 40 mm) have been driven with a coaxial pulser and the current and voltage measured for magnetization reversal rates that are similar to a full-scale accelerator cell. It is particularly important to have a model that accurately describes the dependence of magnetization current on the rate of magnetization reversal (proportional to applied voltage) and the instantaneous magnetization (proportional to the time integral of the applied voltage). Figure 13 shows the results of measurements on TDK PE11B and comparison with a simple model based on collapsing spherical domains and a domain wall velocity that depends linearly on the applied magnetic field.[8] The model predicts the following equation for magnetization reversal:

$$(V/(I-I_1))^{3/2} = R_0^{3/2}(Q - \int_0^t V dt/\phi_s) \qquad (3)$$

where V and I are the voltage and current, I_1 is the sum of the effects of the applied dc reset current and coercivity, ϕ_s is the saturation flux and R_0 and Q are fitted parameters. The fit of the model to experimental data shown in Fig. 13b is reasonably good except at low values of the integrated volt-seconds where the model is expected to break down due to merging of domain walls during the initial stage of flux reversal. This model has not yet been used in transmission line and field equation models to compare to large ferrite cores and accelerator cells.

Delayed Feedback Current Control

From Eq. 1 it is apparent that variation of electron beam current I_b can be exploited as a way of controlling the acceleration gap voltage. Figure 14 illustrates schematically the idea of delayed feedback current control and a practical way of doing this.[9] Two special-purpose cells driven by programmable high voltage vacuum tube modulators are added to the series stack of ordinary cells that comprise an induction linac injector. The ordinary cells are driven by magnetic pulse compression modulators with fixed pulse-to-pulse shape. Since the injector is ordinarily operated in the space charge-limited regime, the beam current is related to the cathode-to-anode voltage V_b by the Child-Langmuir relation

$$I_b = A\, V_b^{3/2}/d^2 \qquad (4)$$

and controlling the voltage provides the means to control I_b (relativistic corrections to Eq. 4 are not important for this discussion). The triodes are connected in parallel with a resistor and operate in a shunt regulator mode with the voltage drop across the tubes generated by the beam return current. Generally one is interested in controlling approximately the top 10% of the current pulse to avoid beam transport problems and large variations of beam power during the energy flattop. Total injector voltages are of the order of a megavolt, and triode modulator voltages of interest fall in the range 25–100 kV. Compact high current tubes of this voltage and with band widths extending to 1 GHz are readily available commercially. An error signal derived from an energy analyzer at the end of the accelerator is

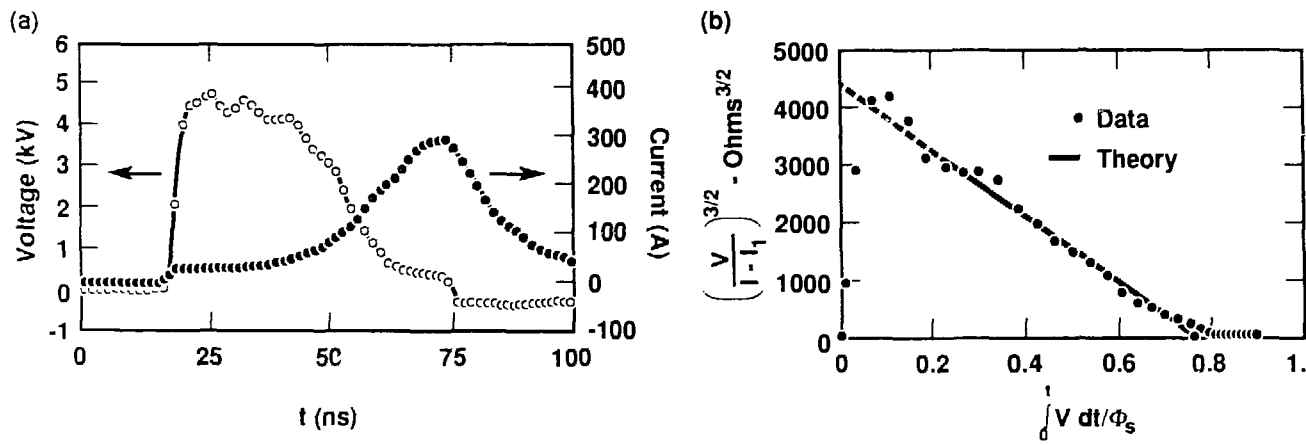

Fig. 13. (a) Measurements of voltage and current driving a small toroidal core of PE11B ferrite, i.d. = 19 mm, o.d. = 31 mm, l = 40 mm. (b) Fit of the collapsing domain model of flux reversal to the data in (a).

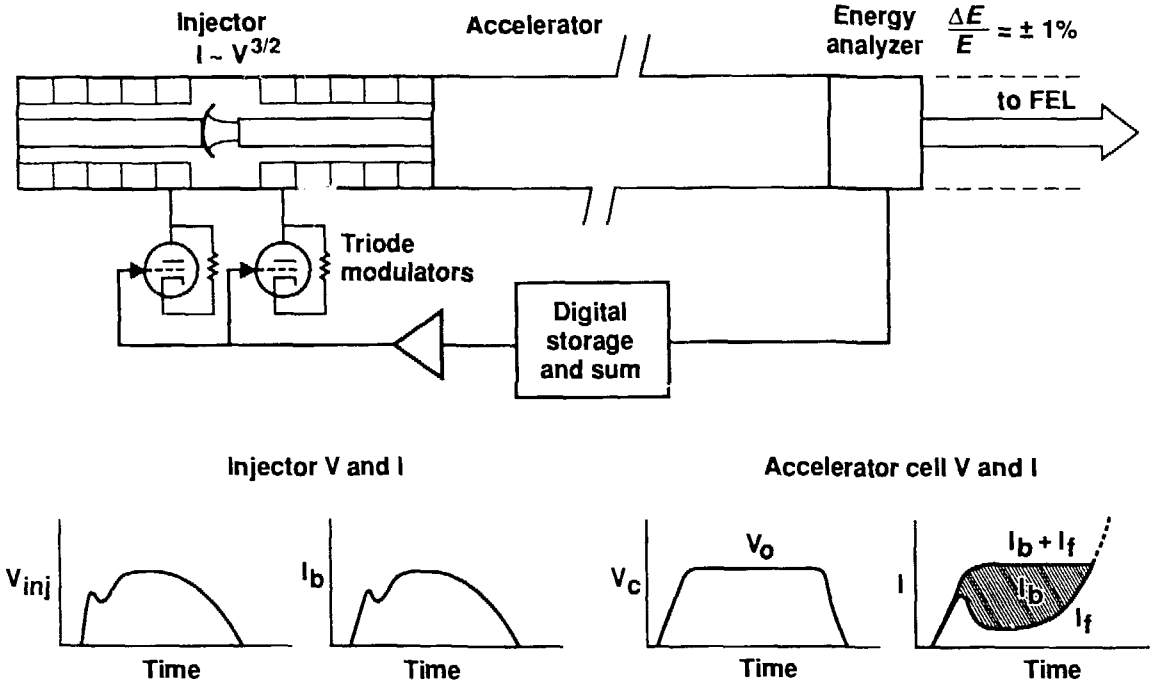

Fig. 14. Schematic of delayed feedback current control of beam energy variation.

summed over previous pulses and used to drive the triodes to maintain constant energy.

The scheme in Fig. 14 is envisioned as a means of correcting slow thermal drifts during a long pulse burst at high PRF but can also obviously be used to provide the same type of correction as the tapered PFL of the MAG I-D discussed above. Although using the vacuum tube modulator approach on every cell of an induction linac would be prohibitively expensive, it is reasonable with the injector where it only has to be done once. It is also a very powerful approach because it provides the accelerator with an adjustable knob so that everything does not have to be understood in complete detail to get a satisfactory energy flattop.

So far an electron injector and accelerator experiment demonstrating the principle of Fig. 14 has not been done. However some simple experiments illustrating the performance of a triode modulator have been done.[9,10] Figure 15 shows a schematic of an experiment utilizing two induction cells. The first cell is driven by a spark gap-triggered Blumlein pulse line, and the voltage induced across the second cell is regulated by a triode modulator (in this case consisting of 32 Varian YU-114 triodes in parallel). A 35 Ω resistor passes through the axis of both cells and simulates the beam current load. Waveforms from this experiment are shown in Fig. 16. The uncorrected voltage across the second cell with the triodes turned off is given in Fig. 16a and fully corrected with the triodes turned on to generate a flattop pulse in Fig. 16c. Figure 16d shows the function generator pulse applied to the modulator circuit for the fully corrected pulse.

The technique presented in this section illustrates a method that would provide some insulation from having to model and build everything correctly to get the desired energy sweep; however, it also suggests some areas where modeling would be useful. Although considerable work has been done on modeling electron optics of an injector, there does not appear to be experience modeling the shape of the current pulse from existing injectors. It would also be informative to model the dynamics of current modulation with an equivalent circuit model of the injector and the interaction of the injector current with an accelerator cell.

Summary

In this paper we have attempted to motivate the development of modeling tools for linear induction accelerator components by giving examples of performance limitations related to energy sweep. The most pressing issue is the

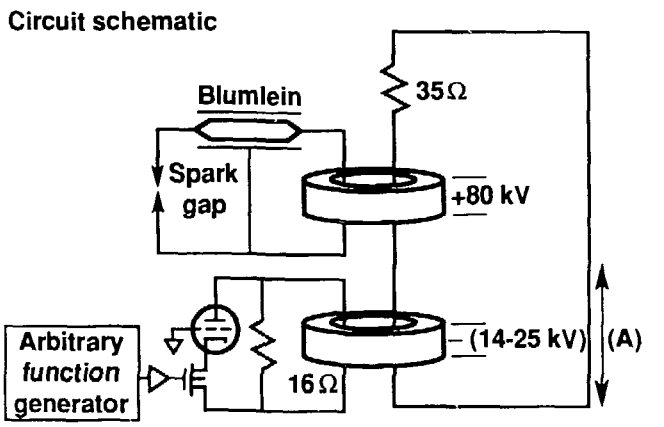

Fig. 15. Schematic of a two-cell experiment demonstrating performance of the vacuum tube modulator for feedback current control.

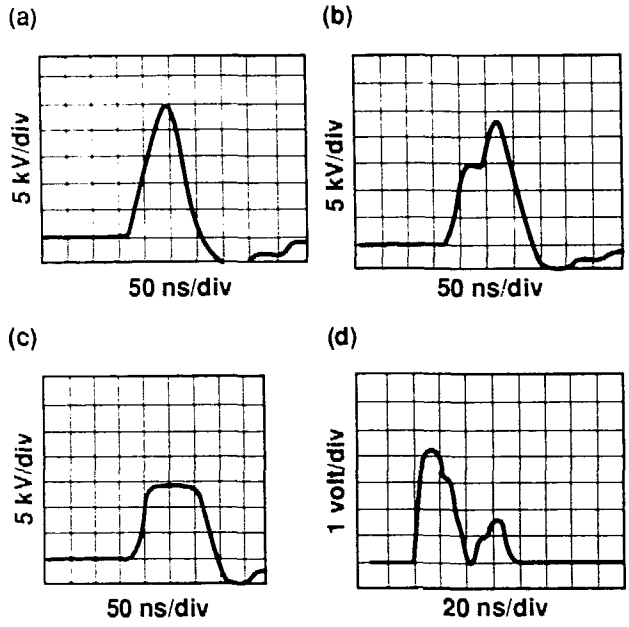

Fig. 16. Results of an experiment demonstrating compensation of cell voltage waveform with a vacuum tube modulator, (a) the uncorrected waveform, (b) partially corrected waveform, (c) fully corrected waveform, and (d) the pulse from the function generator driving the vacuum tube modulator.

development of an accurate model of the switching behavior of large magnetic cores at high dB/dt in the accelerator and magnetic compression modulators. Ideally one would like to have a model with as few parameters as possible that allows the user to choose the core geometry and magnetic material and perhaps a few parameters characterizing the switch model. Beyond this, the critical modeling tasks are: simulation of a magnetic compression modulator, modeling the reset dynamics of a magnetic compression modulator, modeling the loading characteristics of a linear induction accelerator cell, and modeling the electron injector current including the dynamics of feedback modulation and beam loading in an accelerator cell. Of course in the development of these models care should be given to benchmarking them against data from experimental systems. Beyond that one should aim for tools that have predictive power so that they can be used as design tools and not merely to replicate existing data.

References

[1] J.C. Clark, F.E. Coffield, F.J. Deadrick, M.A. Newton, D.S. Prono, D.S. Ravenscroft, A.L. Throop, W.C. Turner, and K. Whitham, "Design and Initial Operation of ETA-II Induction Accelerator," in *1988 Linear Accelerator Conference Proceedings*, Williamsburg, VA, Oct. 3–7, 1988, pp. 19–23. Also UCRL-99201, Lawrence Livermore National Laboratory, Livermore, CA.

[2] G.J. Caporaso, W.A. Barletta, D.L. Birx, R.J. Briggs, Y.P. Chong, A.G. Cole, T.J. Fessenden, R.E. Hester, E.J. Lauer, V.K. Neil, A.C. Paul, D.S. Prono, K.W. Struve, "Beam Dynamics in the Advanced Test Accelerator(ATA)", in *Proc. of the 5th Intl. Conf. on High Power Particle Beams*, San Francisco, CA., Sept. 12–14, 1983. p. 427.

[3] Y.-J. Chen, "Corkscrew Modes in Linear Accelerators," to be published in *Nuclear Instruments and Methods in Physics Research A*. Also UCRL-102325, Lawrence Livermore National Laboratory, Livermore, CA.

[4] W.E. Nexsen, D.P. Atkinson, D.M. Barrett, Y.-J. Chen, J.C. Clark, L.V. Griffith, H.C. Kirbie, M.A. Newton, A.C. Paul, S.E. Sampayan, A.L. Throop, and W.C. Turner, "The ETA-II Induction Linac as a High Average Power FEL Driver," in *Proceedings of 11th International Conference on Free-Electron Lasers*, Naples, FL, Aug. 28–Sept. 1, 1989. Also UCRL-101154, Lawrence Livermore National Laboratory, Livermore, CA.

[5] M.A. Newton and J.A. Watson, "Timing and Voltage Control for Magnetic Modulators on ETA-II," in *Proceedings of 7th IEEE Pulsed Power Conference*, Monterey, CA, June 11–14, 1989. Also UCRL-100322, Lawrence Livermore National Laboratory, Livermore, CA.

[6] D.M. Barrett, "Modeling the Characteristics of a Magnetically Switched Pulse Forming Line," *Proceedings of 7th IEEE Pulsed Power Conference*, Monterey, CA, June 11–14, 1989. Also UCRL-100317, Lawrence Livermore National Laboratory, Livermore, CA.

[7] W.C. Turner, G.L. Caporaso, G.D. Craig, J.F. DeFord, L.L. Reginato, S.E. Sampayan, R.W. Kuenning, I.D. Smith, in *Proc. of 7th Intl. Conf. on High Power Particle Beams*, Karlsruhe, Germany, July 4–8, 1990, p.845. Also UCRL-97738, Lawrence Livermore National Laboratory, Livermore, CA.

[8] R.K. Avery, J.F. DeFord, G. Kamin, W.C. Turner and J.M. Zentler, "A Simple Domain Model of Flux Reversal in Ferrites," in *Proceedings of 34th Annual Conference on Magnetism and Magnetic Materials*, Boston, MA, Nov. 28–Dec. 1, 1989. Also UCRL-101299, Lawrence Livermore National Laboratory, Livermore, CA.

[9] E.E. Bowles and W.C. Turner, "Induction Linac Energy Regulation", To appear in the Proc. of 1990 Nineteenth Power Modulator Symposium, June 1990, San Diego, CA. Also UCRL-102623, Lawrence Livermore National Laboratory, Livermore, CA.

[10] E.E. Bowles and W.C. Turner, "50 MHz, 12 MW Induction Linac Current Modulator", *Proceedings of 7th IEEE Pulsed Power Conference*, Monterey, CA, June 11–14, 1989. Also UCRL-100316, Lawrence Livermore National Laboratory, Livermore, CA.

Present Circuit Simulation Tools

Wayne N. Weseloh
Power Spectra, Incorporated
42660 Christy Street
Fremont, California 94538

and

Robert J. Kares
Berkeley Research Associates
P.O. Box 241
Berkeley, California 94701

ABSTRACT

There are many circuit and network analysis codes which exist in the pulsed power community. This paper is a select survey of a few of the most popular and interesting of these codes.

INTRODUCTION

We will discuss the following software: SCEPTRE, NET2, SPICE and its offspring, MICROCAP, TLCODE, SCREAMER, and SCIMATH. The list is intended to be representative of the software which can be used for circuit analysis. It is not exhaustive or complete. Rather it should be considered a resource for the researcher in the choice and selection of a circuit analysis tool.

SCEPTRE is a mainframe circuit analysis code which has its origins more than 20 years ago. It is still one of the most powerful and flexible circuits codes available in the pulsed power community. NET2 is a code of a similar vintage to SCEPTRE and has shown many of the same successes and failures as SCEPTRE. SPICE is a generic name given to a set of circuit analysis codes which are derived from the U. C. Berkeley SPICE 2 program. MICROCAP is a graphics based microcomputer circuit program. TLCODE and SCREAMER are "home grown" circuit analysis programs developed as an alternative to the other circuit analysis programs. Finally, SCIMATH is a numerical mathematics language which can be used for circuit simulations. It represents a departure from the traditional circuit analysis software to a more general integrated approach.

SCEPTRE

SCEPTRE is a circuit analysis program which has been used extensively for many years by many pulsed power houses [1]. In recent years it has been updated, expanded and ported to several new computer systems. The Beam Research Group at the Lawrence Livermore National Laboratory, for example, is currently running a Cray version of SCEPTRE converted from the Control Data Cyber 175/176 version by Waldo Magnusson [2].

Although SCEPTRE is one of the older circuit simulation codes in use today, it has a number of very powerful features which are still not available in most of the newer, more modern tools which we will discuss later. Two of these features are particularly worthy of note. The first is the ability to define the temporal behavior of an element value by a user supplied function coded in FORTRAN. There is no restriction on the complexity of such a function which may be many lines of FORTRAN code long. Further, such functions may depend explicitly upon time, the currents and voltages across other circuit elements, or other auxiliary parameters called DEFINED PARAMETERS which may be computed in parallel with the circuit solution. The ability to use FORTRAN functions to define element behavior makes it possible to construct a usable element model for almost any device using SCEPTRE.

The second powerful SCEPTRE feature worthy of note is the program's ability to easily compute the behavior of auxiliary parameters defined by differential equations. For example, one way to compute the behavior of one of these DEFINED PARAMETERS is to specify its initial value together with a differential equation which determines its time evolution. SCEPTRE will then solve the simultaneous coupled system of differential equations for the circuit quantities

and the DEFINED PARAMETER to obtain a fully self consistent solution for both. In general, the ordinary differential equation for a given DEFINED PARAMETER may depend explicitly upon time, the currents and voltages across circuit elements and the value of the given DEFINED PARAMETER or any other. It is even possible to easily construct a coupled system of differential equations for many different DEFINED PARAMETERS which may be solved simultaneously with the circuit equations.

When the two SCEPTRE features discussed above are combined, some very powerful circuit modeling can be done in a straightforward fashion. To illustrate this point we consider the problem of the example circuit consisting of a simple MARX generator connected to a lossless transmission line which is in turn coupled to an imploding plasma load. This load consists of a cylindrical plasma column of radius R inside of a metal shell of radius RW, which provides a return current. The imploding plasma column acts as a time varying inductor which controls the current through the load. The load current and column radius R in turn control the radial acceleration of the column surface. The following fragment from the corresponding SCEPTRE input deck illustrates how SCEPTRE may be used to obtain a self-consistent solution for the load current as well as the radius and radial velocity of the plasma column's surface as a function of time.

```
SUBPROGRAM
C
C THESE USER DEFINED ROUTINES MODEL THE IMPLODING LOAD
C PARAMETERS ARE AS FOLLOWS:
C R - RADIUS OF PLASMA COLUMN (METERS)
C V - IMPLOSION VELOCITY (METERS/NS)
C CUR - LOAD CURRENT (MA)
C FL - LOAD INDUCTANCE (NH)
C FLDOT - DL/DT OF LOAD (NH/NS)
C DVEL - ACCELERATION OF PLASMA COLUMN (METERS/NS**2)
C PLENG - LENGTH OF PLASMA COLUMN (METERS)
C RW - RADIUS OF LOAD WALL (METERS)
C DENS - DENSITY OF PLASMA COLUMN (KG/METER)

    FUNCTION FLDOT(R,V)
    DATA PLENG/4.0E-02/
    FLDOT = -2.0E+02*PLENG*V/R
    IF (FLDOT .EQ. 0.) FLDOT = 1.0E-06
    RETURN
    END

    FUNCTION DVEL(CUR,R)
    DATA DENS/8.0E-08/
    DVEL = -(1.0E-13/DENS)*((CUR*CUR)/R)
    RETURN
    END

    FUNCTION FL(R)
    DATA PLENG,RW/4.0E-02,4.285E-02/
    FL = 2.0E+02*PLENG*ALOG(RW/R)
    RETURN
    END

CIRCUIT DESCRIPTION
IMPLODING LOAD TEST
$ UNITS ARE NH,NF,OHMS,MV,MA,TW,KJ

ELEMENTS
C1MX,0-1=97.8
R1MX,1-2=2.9
L1MX,2-4=10000.0
T1,4-5-0=MODEL TLINE(PERM,CHANGE PT=20.0,PZ=15.0,PN=1.)
LTB,5-6=1.0
LD,6-7=Q1(PR)
RLD,7-0=Q2(PR,PV)

DEFINED PARAMETERS
$ PR IN METERS, PV IN METERS/NS
PR = 2.0E-02
PV = 0.0
DPR = PV
DPV = Q3(ILTB,PR)

FUNCTIONS
Q1(A) = (FL(A))
Q2(A,B) = (FLDOT(A,B))
Q3(A,B) = (DVEL(A,B))
```

The load is a variable inductance representing the imploding plasma column. In SCEPTRE language this variable inductance is represented by the inductance LD connected in series with the resistance RLD. LD represents the inductance of the load and RLD the corresponding dL/dt. The value of LD is given by the function Q1 which is defined under the FUNCTIONS subheading by the user supplied function FL. Similarly, RLD is given by Q2 which is the user supplied function FLDOT. FL returns the inductance of the load as a function of the radius of the plasma column and FLDOT returns dL/dt as a function of column radius and implosion velocity. The DEFINED PARAMETERS PR and PV represent the radius and implosion velocity of the column.

The values of PR and PV are found as a function of time by giving their initial values and differential equations for their time derivatives denoted by DPR and DPV under the DEFINED PARAMETERS subheading. DPV, the acceleration of the plasma column, is given as a function of the load current and column radius by the user supplied function DVEL. SCEPTRE automatically integrates the differential equations for PR and PV with the given initial conditions together with the circuit equations. The result is a fully self consistent solution for the behavior of the generator and load.

SCEPTRE is one of the oldest simulation programs discussed in this paper. Over the years users have identified several deficiencies with SCEPTRE. Some of these have been addressed and solved and some have not. One problem has been that no ideal transmission lines or switch models are included in the seminal version of the program. However, in the years since its release, several transmission line models have been created to remedy this particular omission [3,4]. But, since SCEPTRE was not designed with transmission lines in mind, numerical difficulties can arise when pulses emerge from a transmission line and encounter lumped circuit elements. The circuit must respond to an impulse every time a new reflection emerges from a transmission line. This usually has the effect of driving the internally calculated time step to an extremely small value. Also, the maximum allowable time step has to be limited to a fraction of the smallest length transmission line in the circuit. Otherwise, the individual reflections and transmissions cannot be accounted for properly.

A general switch model was developed by one of the authors (Weseloh) for the SCEPTRE code. The details of the implementation are shown below. The previously described DEFINED PARAMETERS statement is used to set the necessary switching parameters.

```
CIRCUIT  DESCRIPTION
SMOOTH  SWITCH  TEST
$ UNITS  ARE  SI

ELEMENTS
RS1,4-0 = 455.0E + 03
LSW,4-5 = 250.0E-09
RSW,5-6 = QSW(PRF,PRI,PSIG,PTAU,TIME)
CSW,4-6 = 817.0E-12
RS2,6-0 = 455.0E + 03

DEFINED  PARAMETERS
$  PRF  -  FINAL  IMPEDANCE    (OHMS)
$  PRI  -  INITIAL  IMPEDANCE   (OHMS)
$  PSIG  -  SWITCHING  RATE  (SECONDS)
$  PTAU  -  SWITCHING  TIME  (SECONDS)
PRF = 25.0E-03
PRI = 100.0E + 03
PSIG = 1.25E-08
PTAU = 75.0E-09

FUNCTIONS
QSW(A,B,C,D,E) = (A + 0.5*B*(1.0-TANH((ED)/C)))
```

The switch impedance profile is described by a function based on a hyperbolic tangent. The choice reflects no special insight into the physics of switching, rather it is simply a conveniently smooth function. This is an important point for the numerics of the solution of the differential equations (ODEs). The algorithms employed by SCEPTRE have a difficult time when the element values are not smooth (differentiable). The time and rate of impedance collapse can be precisely controlled by the values of PRI, PRF, PSIG, and PTAU. The constants PRI and PRF are the initial and final values of the switch impedance, respectively. The values of PSIG and PTAU are related to the rate and time of switching.

In addition to its sophisticated treatment of user defined functions and auxiliary differential equations SCEPTRE has some other interesting features. One of these is the ability to select the integration method to be used in computing the circuit solution from a choice of four different methods. In addition to the standard Runge-Kutta algorithm and simple Trapezoidal method there is also a Predictor-Corrector algorithm, and an exponential integration method, XPO. For a given circuit problem it is usually possible to get one of these three algorithms to run the solution, even if the others fail providing added flexibility to the code. Another advantage of SCEPTRE is the ability to create stored models of complicated elements which can be utilized by name in the definition of more complicated circuits. We have already exhibited an example of the use of such a stored model in the first SCEPTRE deck above. TLINE is the name of a stored model which represents a lossless transmission line with one way transit time PT and characteristic impedance PZ. Such models typically consist of an internal circuit definition for the modeled device together with the functions which define the behavior of the internal elements. These functions may again be supplied in terms of FORTRAN code so that it is possible to create rather complicated device models and then to package them up for use by name in larger circuits. Further, a permanent library of such named models can be created to make the process of using them even more convenient. Finally, we would like to mention another advantage of SCEPTRE, namely maintainability. The internal documentation of the source code is excellent making bug fixes and modifications possible with a reasonable effort.

Unfortunately, SCEPTRE has some shortcomings as well. Current versions of the code are limited to a maximum of 300 elements allowed in the circuit definition including all the elements in any stored models which are utilized. This still represents a substantial sized circuit but users designing large pulseforming networks should be aware of this limitation. A similar hard dimension exists with the implementation of mutual inductances; the number of mutual inductances is limited to 50. Another shortcoming of the basic SCEPTRE code is the crude printer graphics which it generates. Although several good graphics postprocessors have been written to improve this situation these processors are not available to the general public and so quality graphics remains a problem with SCEPTRE.

NET-2

While SCEPTRE is probably the most widely used mainframe circuit code used in high voltage/current simulations, there is another worth mentioning. The program is called NET-2.

NET-2 is a general purpose network analysis program which solves nonlinear time domain circuit problems. It has been used by many institutions including Physics International Company (PI), Los Alamos National Laboratories (LANL), and Pulse Sciences Incorporated (PSI). NET2 contains element models for magnetic cores, lossless transmission lines, ideal switches, as well as many semiconductor elements.

While NET-2 is undeniably one of the major circuit design tools currently utilized on mainframe systems its use presents some very frustrating problems for anyone uninitiated in its quirks. In particular, NET-2 has a tendency to crash on problems for no apparent reason, and it seems fair to say that running NET-2 is something of an art form. There appears to be some internal problems in the way NET-2 manages its transmission line buffers and fixing such problems is next to impossible because of the extremely poor internal documentation of the NET-2 source code. (In fact the NET-2 source code is completely unreadable since the author has adopted an extremely obscure method of naming program variables. This coupled with a complete absence of internal documentation in the program makes it impossible to alter.) NET-2 also provides an ability to solve auxiliary differential equations using the so-called X variables in a manner somewhat reminiscent of SCEPTRE. However, this capability is extremely limited compared to that of SCEPTRE which is by far the superior code in this respect. NET-2 does have one significant advantage

over SCEPTRE in that there are no hard wired limitations on the size of the network which can be simulated with NET-2. The user is limited only by the available resources of the machine.

THE SPICE CIRCUIT CODES

The SPICE family of circuit codes all derive from the SPICE2 circuit simulation program [5] developed at the University of California, Berkeley, during the mid 1970s. SPICE3 is the newest implementation of the SPICE2 program that integrates circuit simulation into U. C. Berkeley's computer aided design (CAD) research effort. Neither version of the program is supported by U. C. Berkeley. This is a major reason for the many commercial versions of the SPICE program.

The commercially available personal computer versions of the SPICE program can be placed into two categories. The first group includes AllSpice from AcoTech, HSpice from MetaSoftware, Is-Spice from IntuSoft, and Z-Spice from Z-Tech. These commercial programs are strictly based on SPICE2 and have the same features found in the original version. The second group contains rewritten versions of the SPICE programs with many additions and minor improvements. This group includes SPICE-Plus from Analog Design Tools, DSpice from Daisy Systems, and PSpice from MicroSim. In this paper we will discuss the PSpice program.

PSpice

PSpice [6] is a circuit simulation program developed by the MicroSim corporation and based on the original Berkeley SPICE circuit simulation code. The PSpice program, however, does contains many features not contained in the Berkeley version of SPICE. For example, the PSpice package contains integrated graphics, preprocessing and post-processing software. The ability to display raw and user derived quantities interactively is a significant achievement. A researcher can easily calculate the total energy deposited in a magnetic core by simply integrating the product of the voltage drop across the core and the instantaneous current in the core - a one step process in PSpice.

Another significant advance over the original SPICE is the inclusion of a nonlinear magnetic model. The device model, based on the Jiles-Atherton magnetic model [7], accounts for the following nonlinear effects: initial permeability, saturation of magnetization, hysteresis (including coercivity and remanence), and dynamic core losses. An example of these features is shown in Figure 1.

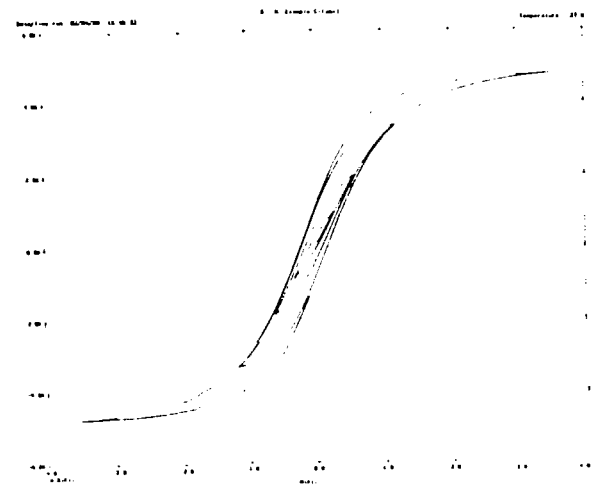

Figure 1. Post-processing output display of a typical B-H curve of 3C8 ferrite (Ferroxcube Corporation).

It is often necessary to introduce user derived equations and models into a circuit simulation. Until recently, SCEPTRE was one of the only circuit simulation codes which allowed these additions. PSpice allows a significant amount of user control of the governing equations of an element. As an example, a simple linearly varying resistance can be modeled with the following input fragment:

```
GSW   16 17  VALUE = {V(16,17)/(RI-(RI-RF)*V(99))}

VCON  99 0   PWL(0.0E-09   0  45.0E-09   0  50.0E-09   1)
RCON  99 0   1.0
.PARAM   RI = 10.0E+03,RF = 10.0E-03
```

The element GSW is a voltage controlled current source connected between nodes 16 and 17 of the circuit. The controlling voltage source (VCON) is contained in a separate and distinct circuit. The parameters RI and RF are the initial and the final values of the resistance, respectively. The effective impedance of the element is 10 kilohms until 45 nsec, when it linearly falls to a value of 10 milliohms at 55 nsec and remains at that final value. The VALUE and .PARAM statements are added features within PSpice and not standard in the Berkeley SPICE statement syntax.

A difficult and important component to model is the voltage controlled inductor and capacitor. Paul Tuinenga has described a subcircuit definition which satisfies many of these necessary requirements [8]. However, the modeling of capacitors which are controlled by arbitrary equations involving time, current, and voltage is beyond the capabilities of PSpice. However, the authors do feel that many of the circuits now being performed with SCEPTRE, NET2, and SCREAMER can easily be run with PSpice.

As with all simulations the researcher must exercise care and judgment with the results. For example, consider the simple LC simulation show in Figure 2, [9]. The input and output are shown in Figure 2. The voltage amplitude envelope decays to a fraction of its initial value in only a few periods. The circuit should oscillate without any losses. The problem is obviously numerical and is due to the particular choice of convergence constants. Without knowing a user can be led to an erroneous solution.

Input:

```
L C Example Circuit
L 0 1 1.0E-06
C 1 0 1.0E-09 IC = 1.0
.PROBE
.TRAN 5.0E-09 2.5E-06 UIC
.END
```

Output:

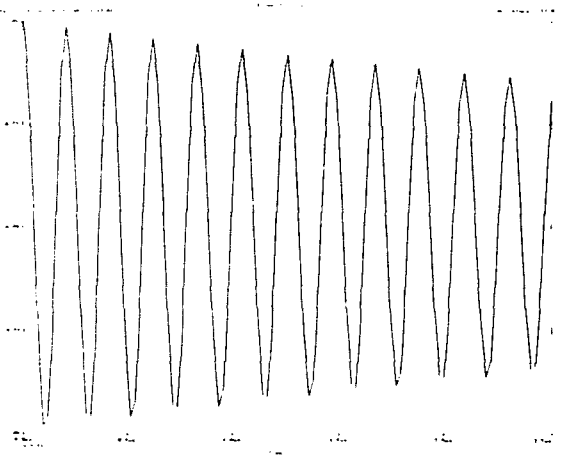

Figure 2. PSpice LC Example circuit showing numerical convergence effects.

A specific remedy to the numerical malady is to either to place a limit on the maximum allowable time step

```
.TRAN 5.0E-09 2.5E-06 0.0E-09 2.5E-09 UIC
```

in this case the maximum step is 2.5 nsec, or by reducing the solution convergence criteria to a lower value

```
.OPTIONS RELTOL = 1.0E-04
```

which is ten times smaller than the default value. There are four convergence factors ABSTOL (absolute current tolerance), CHGTOL (absolute charge tolerance), RELTOL (relative current/voltage tolerance), and VNTOL (absolute voltage tolerance). When it becomes necessary to modify these factors, always begin with the RELTOL factor.

The post-processing, as mentioned earlier, is a simple and powerful portion of the PSpice software. In fact, the graphics post-processor, called PROBE, can perform integrations, scalings, and discrete Fourier transforms on waveforms. Once a simulation has been performed the user can interrogate the data at will. This process is diametrically opposite to the procedure in most mainframe codes in which the user must specify all the outputs and calculated quantities desired at the time the simulation is performed. The ability to visualize and manipulate the data can only lead to greater understanding and insight into the physical problems we are trying to model.

One final comment is warranted about the distribution of PSpice. The MicroSim corporation currently sells an IBM / DOS evaluation version of the software for only $75.00, and they encourage the copying and distribution of this version. This evaluation version is a fully functional circuit simulation code. Recently one of the authors simulated a network with over forty ideal transmission lines using the evaluation copy of PSpice. The authors consider the existence and support of a low cost evaluation version of this code an enlightened attitude and commend MicroSim for their policy.

MICROCAP

MicroCap is a graphically oriented circuit analysis code [10]. It main strength is that circuits can be constructed interactively and graphically on the personal computer monitor.

The newest version of the software includes a simple non-linear magnetic model, as well as rudimentary analog behavior modeling capabilities. The software developers seem to be driven by the successes of the newer versions of SPICE. All the newest features in MicroCap are identical to those features previously developed in many SPICE versions.

There are several major deficiencies with the MicroCap software. The transmission line model in MicroCap is wholly inadequate for pulsed power applications. The transmission and reflections do not conform to any known theory and the element does not seem to be able to store energy. The equation solution algorithms are no where discussed or referenced. The user can enter a minimum accuracy of the simulation, but, the meaning and interpretation of this value is vague. Also, the code has many numerical difficulties in solving even moderately complex pulsed power circuits.

TLCODE

TLCODE is a special purpose microcomputer circuit code developed at Pulse Sciences Incorporated [11]. The software has been used extensively for the design of many pulsed power systems including the Hermes III Inductor Linac [12] and the Spiral Line Inductor Accelerator [13]. The code was developed exclusively for the design and analysis of pulsed power circuits.

The fundamental circuit element in this software is the transmission line, and the fundamental concept is the impedance mismatch. Capacitors and inductors are modeled as spatially distributed impedances. That is, all physical capacitances and inductances have a characteristic transit time. The software assures that the proper reflections, transmissions and transit times occur properly in a simulation.

This circuit simulation code is different in many respects from the other codes previously described. It does not construct nor solve any differential equations. The code, instead, solves algebraic equations based on Kirchhoff's laws. In fact, this is one of the major advantages of the software. All the numerical difficulties associated with the solution of systems of ordinary differential equations are eliminated. In addition, new element models can very easily be incorporated into the code.

But, as with all the other home grown software packages, the plotting and post-processing is idiosyncratic and site dependent.

There are a few other notable transmission line codes used in pulsed power research. Several codes based on the original Lupton [14] transmission line calculation exist today. In 1982 a new (completely rewritten) version of the code was created at the Harry Diamond Laboratories (HDL) in Maryland [15]. This software has been used extensively at the Harry Diamond Laboratories Aurora facility in there study of several pulsed power machines. Recently, Dr. L. G. Schlitt has created a transmission line code which runs on IBM type microcomputers [16]. Given the power and simplicity of its approach, transmission line based circuit codes will continue to have a significant role in circuit simulations.

SCREAMER

SCREAMER is a circuit simulation code developed at Sandia National Laboratories primarily for the study of single module accelerators [17]. Circuits for simulation are constructed from individual building blocks. Each different building block element contains a particular number and specific connection of capacitors, inductors, resistors, and sources. By the proper choice of values, a single building block can behave like an pure inductance, resistance, or a ladder network.

SCREAMER contains many models routinely used in pulsed power systems including triggered gas switches, magnetically insulated transmission lines, and a magnetic switch model of a saturable core inductor [18]. Also, the code accepts user-defined routines for defining element values. This inclusion makes the code extremely flexible, powerful, and capable of handling new models.

One of the conclusions of the authors of SCREAMER is that specialized software running on microcomputers or workstations can provide useful, fast, and accurate simulation results at a fraction of the cost and time of conventional mainframe codes. There are, however, hidden cost involved with in-house codes. The cost of the software development, verification, and maintenance is not inconsequential. Often significant time is spent just in the care and maintenance of the software. This is of course balanced by the fact that users have access to the author of the software as well as the source code itself. Any minor software bugs or coding problems can be resolved simply and immediately.

CIRCUIT CODE ALTERNATIVES

SciMath

The codes discussed up to this point are designed primarily for the analysis of relatively large networks. In smaller problems for which it is practical to write down the loop differential equations by hand an interesting and powerful alternative to traditional methods of solution using conventional circuit codes is provided by the software package called SciMath [19]. SciMath is a very high level command driven numerical mathematics language which is easy to learn and is available for most of the MS-DOS family of personal computers. Using SciMath it is simple to define and solve a system of up to 20 coupled nonlinear differential equations. However, this is only one of the program's many capabilities of interest to the circuit simulator. Another is the ability to easily express very complex functional relationships which is of considerable benefit in the construction of new models. In particular the program provides a large collection of built-in functions including Bessel functions, elliptic functions and variety of other special functions which are not found in other simulation languages. These make the expression of very sophisticated device models possible. In addition the program contains an integrated set of extremely powerful two and three dimensional graphics features which make the production of publication quality laser printer graphics a simple exercise. We should also mention that it is easy to import experimental data into SciMath and manipulate it so that direct comparison between simulated and measured waveforms can be conveniently

done. SciMath is currently in use at many institutions including Physics International Co., Pulse Sciences, Inc., Los Alamos and Livermore National Laboratories and a number of different universities to perform a variety of analysis and simulation tasks.

As an example of a simple application of SciMath to problems in circuit simulation we consider the system illustrated in Figure 3. It consists of a magnetic store of inductance L0 coupled to a railgun with inductance per unit length L'. In parallel with the railgun is a load with constant impedance R and a small inductance L2. The system begins at t = 0 with the magnetic store charged with current and the projectile of mass m at rest at x = 0. As the projectile is accelerated down the track it acts as an dL/dt transfer switch which shunts the store current into the parallel load. While railguns clearly do not make very practical opening switches this problem is of some interest because it represents perhaps the simplest explicit example of an dL/dt transfer switch whose operation can be calculated in detail, and it captures many of the essential physical features of such switches. The aim of our discussion here is not to review the rather interesting behavior of this system. Rather, we would instead like to focus on how SciMath may be applied to easily solve this problem.

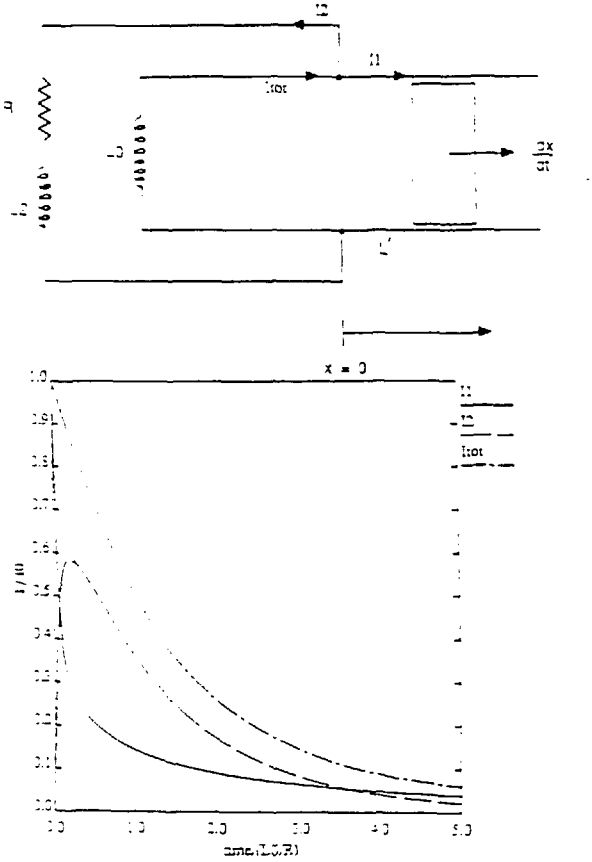

Figure 3. The railgun circuit and its corresponding normalized circuit solutions.

The description of the railgun switch system of Figure 3 consists of two 1st order ordinary differential equations (ODE's) for the 2 circuit loops and one 2nd order equation for the motion of the projectile. This 2nd order equation can be reduced to two first order equations in the usual manner so that the complete description of the system consists of 4 coupled 1st order nonlinear ODE's. This system can easily be rewritten in dimensionless form by normalizing all currents to I0, the initial current in the magnetic store, time to L0/R and projectile position to L0/L', the characteristic length associated with the store inductance L0. The resulting dimensionless system of ODE's depends on only 2 dimensionless parameters, the ratio of inductances L2/L0 and a 2nd parameter called GAMMA defined by,

```
GAMMA = 0.5*m*(R/L')**2/(0.5*L0*I0**2)
```

which is the ratio of the kinetic energy of the projectile when dL/dt = R to the initial energy of the magnetic store. This system of ODE's can be defined and solved using the following short SciMath procedure,

```
L2L0 = .05
GAMMA = 0.01
F1(y1,y2,y3,y4) = (-(1+L2L0)*y1*y4 + y2)/(L2L0 + (1+L2L0)*y3)
F2(y1,y2,y3,y4) = (y1*y4 - y2*(1+y3))/(L2L0 + (1+L2L0)*y3)
F3(y4) = y4
F4(y1) = y1*y1/(2*GAMMA)
ode railsw
y1' = F1(y1,y2,y3,y4)
y2' = F2(y1,y2,y3,y4)
y3' = F3(y4)
y4' = F4(y1)

ivp railsw
0.0  5.0  0.01
I1 = 1.0
I2 = 0.0
eta = 0
eta' = 0

Itot(t) = I1(t) + I2(t)
```

Here we have chosen L2/L0 = 0.05 and GAMMA = 0.01. The above short SciMath language program symbolically defines the system of 4 coupled ODE's called *railsw* and then solves this named system using the SciMath *ivp* (initial value problem) command. *ivp* creates 4 numerically defined solution functions over the normalized time interval from 0 to 5 with the given names I1, I2, eta and eta' which are the solutions of *railsw* for the specified initial values I1 = 1, I2 = eta = eta' = 0 at t = 0. I1 is the current through the projectile normalized to I0, I2 is the normalized current switched into the parallel load, eta and eta' are the dimensionless position and velocity of the projectile. Once these numerically defined functions have been created using *ivp* they may used freely in any subsequent SciMath command or expression. For example, they may be plotted, manipulated or even used to symbolically define other new functions. For instance, in the above code fragment we have defined the total current in the magnetic store Itot symbolically as the sum of I1 and I2. Figure 3 shows a SciMath plot of I1, I2 and Itot as a function of the normalized time for the above case. For this choice of GAMMA rapid current transfer to the load takes place as Figure 3 demonstrates.

The full power of the SciMath approach becomes more readily apparent when we realize that the above code fragment may easily be included in a larger SciMath procedure. For example, if we wished to calculate how the fraction of the initial stored energy which is lost in the railgun switch varies with GAMMA the above fragment could be used in a larger procedure to resolve the system as the value of GAMMA is varied over the desired range.

Circuit simulation using the ODE solver is only one of the many modeling tasks possible with SciMath. We illustrate this point with an elementary example in high current accelerator design generous provided by Vern Bailey of Pulse Sciences, Inc. The problem is to compute the total B field across a cylindrical beam pipe which contains a uniform Bz field upon which is superimposed the quadrupole focussing field due to 4 linear current elements that are oriented along the Z axis and are equispaced in azimuth about the outer radius of the pipe. The fields of the linear elements can be expressed in closed form as elliptic integrals of the 1st and 2nd kind. Since elliptic integrals are provided as built-in functions in SciMath it is a simple matter to symbolically define and plot the variation in the magnitude of the total B across the X-Y cross-section of the pipe. Figure 4 shows a 3D surface plot of the magnitude of the total B(x,y) with the equal B contour lines projected beneath on the X-Y plane which has been generated using SciMath's laser printer graphics. The fourfold rotational symmetry of the field is readily apparent.

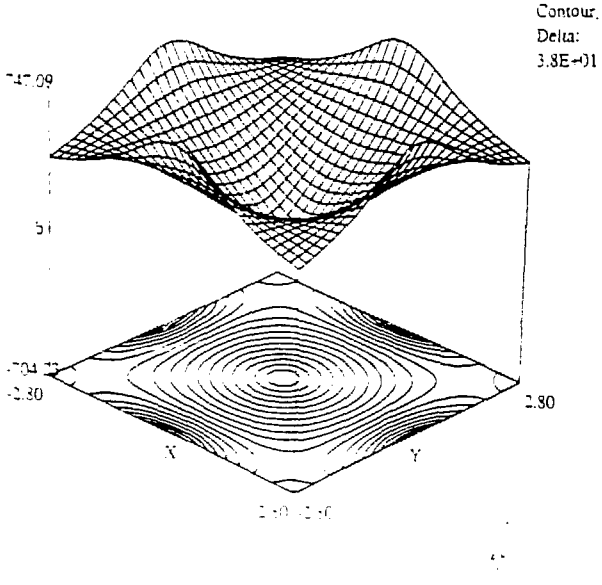

Figure 4. 3D surface plot of the total B field in a cross section of a beam pipe.

Many members of the community are not yet aware that tools such as SciMath exist. We hope that these alternative methods of solving circuit and network problems will gain wider acceptance and use. In fact with the increasing complexity of magnetic models and simulations, we expect that eventually researchers will be forced to accept alternative methods of circuit simulation. The models and equations involved will be of such a complexity that more traditional circuit codes will be unable to effectively deal with these problems.

CONCLUSIONS

At present, SCEPTRE is the most full featured and flexible code which is generally in use. However, PSPICE is continually being expanded and upgraded. Soon PSPICE could outdistance SCEPTRE. The development of a SCEPTRE featured Spice or a Personal Computer version of SCEPTRE are both well within the realm of possibility.

No single circuit simulation program can provide a good solution to every circuit. It is hoped that the preceding discussion will in some way aid researchers in the selection, use and development of circuit simulation tools.

References

[1] J. C. Bowers and S. R. Sedore, SCEPTRE: A Computer Program for Circuit and System Analysis. Englewood Cliffs, NJ, Prentice Hall, 1971.

[2] W. Magnusson, Lawrence Livermore National Laboratories, Livermore, CA, (private communication). SCEPTRE 3 program.

[3] D. B. Seidel, Sandia National Laboratories, Albuquerque, NM, (private communication). The TXLO Tline Subprogram/.c.

[4] S. J. Garrett, "Transmission Line Models for Transient Analysis", Proceedings of the 11th Design Automation Workshop, Denver, CO, June 1974, p. 209.

[5] L. W. Nagel, "SPICE2: A Computer Program to Simulate Semiconductor Circuits", University of California Berkeley Electronics Research Laboratory Memo ERL-M520, 1975.

[6] PSpice, MicroSim Corporation, 20 Fairbanks Ave., Irvine, CA 92718, (714) 770-3022, $75 for an evaluation version.

[7] D. C. Jiles and D. L. Atherton, "Theory of Ferromagnetic Hysteresis", Journal of Magnetism and Magnetic Materials, 61, September 1986, p. 48.

[8] P. W. Tuinenga, SPICE: A Guide to Circuit Simulation and Analysis Using PSpice (R), Englewood Cliffs, NJ, Prentice Hall, 1988, p. 189.

[9] D. Wake, Pulse Sciences Inc., San Leandro, CA, (private communication).

[10] Micro-Cap III: Microcomputer Circuit Analysis Program, Spectrum Software, 1021 S. Wolfe Road, Sunnyvale, CA 94086, (408) 738-4387, $150 for an evaluation version.

[11] W. N. Weseloh, "TLCODE- A Transmission Line Code for Pulsed Power Design", Proceedings of the 7th IEEE International Pulsed Power Conference, Monterey, CA, June 1989.

[12] L. Schlitt, W. Weseloh, I. Smith, V. Bailey, D. Garafalo, and D. Battilana, "Hermes III Induction Cavity Design", PSI report PSI-FR-234-3, July 1986.

[13] V. Bailey, Pulse Sciences Inc., San Leandro, CA, (private communication).

[14] J. K. Burton, J. J. Condon, M. D. Jevnager, W. H. Lupton, and T. J. O'Connell, The TRITON Electron Beam Accelerator Proceedings, The 5th Symposium on Engineering Problems of Fusion Research, Princeton, NJ, 1973, p. 613.

[15] G. A. Huttlin and A. J. Lelis, TLINES: A Computer Program for Circuits of Transmission Lines, Harry Diamond Laboratory Technical Memo HDL-TM-83-22, 1983.

[16] L. G. Schlitt, Livermore, CA, (private communication).

[17] M. L. Kiefer and M. W. Widner, "SCREAMER - A Single Line Pulse Power Design Tool", Proceedings of the Fifth IEEE International Pulsed Power Conference, Arlington, VA, June 1985, p. 685.

[18] M. Stockton, E. L. Neau, and J. P. VanDevender, "Pulsed Power Switching Using Saturable Core Inductors", Journal of Applied Physics, 53, 1982, p. 2765.

[19] SciMath, Spindrift Software, Inc., 11 Totterdell Ct., Orinda, CA 94563, (415) 376-4647, $350 per copy for a full implementation.

Magnetic Materials Group

MODELING PULSED MAGNETIZATION

R. K. Avery
British Aerospace Inc, 13873 Park Center Road, Herndon, VA22071

Abstract

This paper considers dynamic magnetization equations for use in the design of saturable inductor cores for pulse compression circuits. The main approaches to modeling pulsed magnetization in materials of interest for magnetic pulse compression are summarized. The derivation of magnetization equations from considerations of domain wall motion in these materials is then discussed and constitutive relations characteristic of a number of simple domain configurations are given. The way in which core characteristic electrical equations are related to the local magnetic quantities is outlined. Finally, some refinements which help to bring these models into closer agreement with experimental data are mentioned.

I. INTRODUCTION

The design of saturable inductor cores which will perform as expected in devices such as magnetic pulse compressors and linear induction accelerator cells relies on an accurate description of the magnetic behavior of the core material when pulsed under appropriate conditions. The aim of magnetic materials modeling work relevant to the design of these devices is therefore to provide dynamic magnetization equations in the form of constitutive relations linking the magnetic field H, flux density swing ΔB, and rate of change of flux density dB/dt which accurately describe the pulsed reversal of soft magnetic cores. The reversal usually starts from a reverse bias state defined by the initial flux density $-B_r$ and proceeds to saturation in the direction of the applied field in times ranging typically from ~10μs to less than ~100ns. Under these conditions, the materials of interest are metallic glasses (field-annealed Fe- and Co-based alloys), traditional steels such as grain-oriented Si-Fe, and ferrites (particularly Ni-Zn ferrites). A review of magnetic materials for pulse compression was given by Smith in the plenary session of this workshop.

Once a dynamic magnetization equation has been obtained, the characteristic electrical equation linking the windings current I, voltage V and flux density swing $\Delta\Phi=\int V dt$ can be derived, as well as the specific quantities used in the design of pulse compression cores such as the core loss per unit volume U', "saturated" permeability μ_S, and flux density swing to "saturation" ΔB_S[1,2]. Also, knowledge of the detailed form of the magnetization equation allows the effect of the radial distribution of magnetic field on the core switching properties to be calculated. In addition, the availability of accurate magnetization equations for different candidate core materials enables the materials to be evaluated and compared for use in a particular pulse compression stage.

There are a number of different approaches to modeling the pulsed magnetization process. The simplest involves characterizing test cores under approximately the drive conditions of interest and then using the data as a basis for predicting magnetization behavior of pulse compression cores. This procedure is satisfactory if the conditions do not change but it has the disadvantage that it involves no real understanding of the influences of the materials, core construction and drive circuit parameters, or the complex way in which they are interrelated. If the conditions are changed, such as using a core of different dimensions, the measurements have to be repeated with the new core and the drive waveform of interest if the data are to be used with confidence. In the case of large cores such a procedure is impractical if a particular performance specification is to be met.

Another type of approach to modeling involves postulating magnetization equations based on mathematical considerations of the required form of the constitutive relation linking the magnetic quantities. The equations contain free parameters whose values are determined by comparison with experimental data. A review of such approaches was given by Zentler in the plenary session. In particular, Hodgdon has developed a mathematical approach which has been successful in describing d.c. hysteresis loops[3] and which has been extended to the case of dynamic magnetization[4]. This has the advantage that it provides a magnetization equation and the model can be refined in the light of new data. However, like the first approach, it suffers from the disadvantage that there is no real confidence that the magnetization equation is valid, except under the conditions in which it was fitted to experimental data.

A third approach, which will be considered in more detail here, begins by identifying the physical mechanisms dominating the magnetization process on the microscopic scale and then derives magnetization equations based on an analysis of these mechanisms. Comparison with experimental data allows fitting of materials parameters, such as the distance between neighboring domain wall nucleating sites, which may be difficult to specify accurately. There have been many papers describing work of this type. Those relating to metallic tapes have been reviewed by Smith[5] and some of the work on ferrites has been referred to by Avery *et*

al[6]. Like the mathematical models, the physical approach has the advantages that it leads to magnetization equations and can be refined by a more detailed description of the physical mechanisms. In addition, this approach provides a basis for understanding the significance of the experimental parameters involved. The shortcomings of existing physical models can be either a lack of accuracy under some conditions due to oversimplification of the problem[7], or, in the case of more detailed analyses which account for experimental data more accurately with a more precise description of the magnetization process, that they do not lead to magnetization equations that lend themselves readily to circuit analysis[8].

II. MAGNETIZATION EQUATIONS FROM DOMAIN WALL MOTION

A. General Approach

While the detailed magnetization processes taking place within a pulse compression core during magnetization reversal are complex, the magnetization mechanisms are usually dominated either by domain wall motion or spin rotation. During spin rotation, the dipole moment of the material rotates towards the direction of the applied field, therefore changing the direction of magnetization of the sample. In domain wall motion, an applied field causes the boundary between domains magnetized in different directions to move, thus changing the net magnetization of the sample. Magnetization by domain wall motion is in fact a special case of magnetization by spin rotation in which the rotation only takes place within the domain walls. In the materials of interest, and at the reversal rates of interest, domain wall motion is expected to be the dominant magnetization mechanism during most of the reversal and it alone will be considered here.

The general method for deriving dynamic magnetization equations for thin toroidal samples from considerations of domain wall motion will now be outlined before going on to consider some specific cases. Firstly, a simple domain configuration is assumed to be established early in the reversal. The geometry of the domain walls moving through the material is largely responsible for determining the form of the magnetization equation. On the basis of this domain configuration, the net ΔB and dB/dt can be expressed in terms of the position and velocity of the domain walls. Next, the applied field H needed to drive the walls is calculated as a function of their position and velocity. For thin cores in which eddy currents do not play a significant role, the applied field is the same as the field driving the domain wall. When eddy currents are important, there may be significant shielding of the domain walls from the applied field and this effect must be taken into account when deriving the expression for H. Finally, the position and velocity of the domain walls must be eliminated between the two expressions to obtain the required magnetization equation linking H, ΔB and dB/dt.

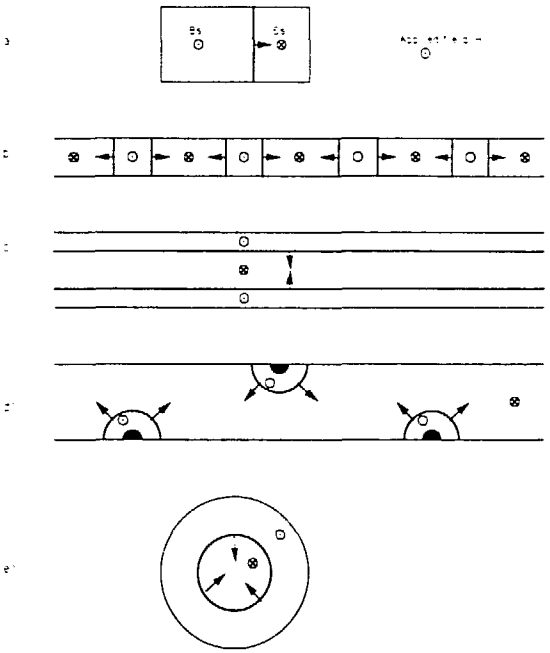

Fig. 1. Some frequently-considered domain configurations

B. Domain Configurations

Some of the most frequently-considered domain geometries are shown in Fig.1. In each of these figures both the easy direction of magnetization and the applied field are normal to the page and the sample is assumed to be toroidal or infinitely long in the direction normal to the page. Figure 1(a) shows a single plane domain wall moving through a sample of rectangular cross section in which eddy currents are negligible. This configuration applies for example in the case of single crystal "picture frame" samples assembled with the easy axis of magnetization parallel to the frame sides[9]. It has also been applied to magnetization of individual ferrite grains within a polycrystalline sample[10]. Figure 1(b) shows the case of "bar domains"[5]: this is the appropriate domain geometry for relatively slow reversal in metal tapes and is relevant to design calculations for transformers and saturable inductor cores situated early in a pulse compression line. Figure 1(c) shows "sandwich domains"[5] in which plane domain walls move inwards parallel to the sample surface effectively enclosing the entire unreversed portion of the material. This geometry approximates the magnetization of metallic tapes undergoing very fast reversal. In Fig.1(d), hemicylindrical domains are shown expanding on the sample surface. This is an example of "surface domains" which are responsible for the initial stages of magnetization of metal tapes when the domain walls are expanding around nucleating sites[8]. As a result of the difference in shape between the domain walls and the sample, this mechanism cannot account for the whole of the magnetization reversal and merging of the doman walls to form some other domain configuration must take place at some stage. This may lead to a similar

configuration in which cylindrical domains are collapsing. Figure 1(e) shows a spherical domain wall collapsing within a spherical region. This geometry has been used to account for pulsed magnetization reversal in individual grains of polycrystalline ferrites[6]. If the collapsing domain wall is not driven all the way to annihilation, resetting of the sample may take place by expansion of the central spherical domain.

A number of factors influence the domain geometry which is established in a particular core material driven under given conditions. The type of core material and the shape of the core have a strong influence on domain structure because they determine the easy directions of magnetization within the material and the representative volume of the core material which must be considered in calculating the magnetization equation. For example, toroidal cores of "square-loop" metallic glass or traditional steel ribbons wound with interlaminar insulation have the easy direction of magnetization lying along the tape length almost everywhere in the material: this coincides with the direction of H for a circumferential field produced by toroidal windings. The tape cross section is then a natural region to use in determining the magnetization behavior of the core. On the other hand, in polycrystalline ferrite toroids in which the grains are randomly oriented, the easy direction of magnetization lies in general between the core circumference direction and the easy axes of magnetization of the individual grains, and so varies from grain to grain. The applied field direction does not therefore necessarily coincide with the easy direction of magnetization in ferrites and the magnetization properties of the individual grains must be considered in order to derive a magnetization equation.

The initial magnetization state of the material is another important factor related to the domain wall geometry. Pulse compression cores are usually reset by a d.c. field, and it is generally assumed that this corresponds to a well-defined initial magnetic state. Although this is expected to be close to complete saturation in the reverse-biased direction, the distribution of the regions of the material which are not reverse biased at reset is very important in determining the domain structure occurring during the magnetization reversal process since these regions act as domain wall nucleating sites. The distribution of nucleating sites also affects the representative region which must be considered in determining the magnetization equation. Nucleating sites occur for example at crystal defects and surface features such as bumps and scratches and may be the sites at which domain walls are created or at which existing walls can be unpinned by providing the required magnetostatic energy. Domain walls can then expand around these sites as shown for example in Fig. 1(d) and may merge before establishing the domain configuration of interest.

Loss mechanisms can be an important factor in determining the domain wall geometry. These can be divided into static and dynamic losses. Static or d.c. hysteresis loss represents the work needed to overcome domain wall pinning and can affect the domain geometry via the distribution of domain pinning sites in the material. Hysteresis loss is not important in "square loop" metal tape-wound cores at reversal rates of interest in pulse compression but can be important in ferrites. The main dynamic loss mechanisms are eddy current loss, the dominant effect in metals, in which eddy currents circulate in regions of changing flux leading to resistive loss and eddy current shielding, and spin relaxation damping loss, a phenomenological loss process associated with spin rotation, which can dominate in ferrites at high reversal rates. Of these, eddy current shielding plays the most important role in determining domain wall geometry because it reduces the local field at the wall below the applied field value. Another loss mechanism, associated only with magnetostrictive materials, is magnetomechanical loss. This can become important when there is a match between drive frequencies and resonant mechanical frequencies of the core[11]. Since these resonant frequencies are typically a few kHz, certain pulse repetition rates may lead to increased losses.

C. Simple Magnetization Equations

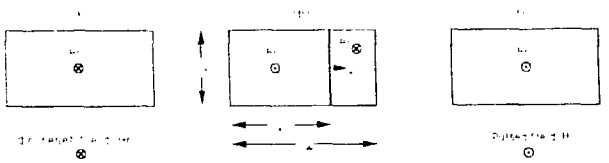

Fig.2. Three stages in magnetization reversal by a single plane wall

As an example of the derivation of a magnetization equation, consider a homogeneous uniaxial toroidal sample shown in cross section in Fig.2. The easy direction of magnetization, the d.c. reset field $-H_r$, and the pulsed field H are all parallel to the core circumference. The flux density in the direction of the pulsed field can therefore take values B_S or $-B_S$. If the reversal takes place fairly slowly, magnetization may be caused by the motion of a single domain wall moving from the inside to the outside of the core as in the case of picture frame samples. Figure 2(a) shows the initial reset state where, neglecting the volume of any domains pinned at nucleating sites, the initial net flux density of the core in the direction of the pulsed field is $B(0)=-B_S$. Figure 2(b) shows an intermediate state at time t during the reversal. The domain wall has moved distance x from the inside of the core (left side of the figure) and the experimentally-deduced flux density $B(x)$ is the volume-averaged value

$$B(x) = B_s\left[xd-(w-x)d\right] / wd \qquad (1)$$

The flux density swing from the reset state at time t is therefore

$$\Delta B(t) = B(x) + B_s = \frac{2x}{w} B_s \qquad (2)$$

Differentiating this gives the experimentally-deduced rate of change of flux density

$$\dot{B} = \frac{2\dot{x}}{w} B_s \tag{3}$$

As long as the reversal rate is not too high, the domain wall velocity is simply related to the field driving it[9]:

$$v=\dot{x}=C(H-H_r-H_o) \tag{4}$$

where C is the domain wall mobility, H-H_r is the net applied field and H_O is approximately equal to the d.c. coercivity. Eliminating dx/dt between Eq. (3) and (4) yields the required magnetization equation:

$$H=H_O+H_r+\frac{w}{\Delta B_S C}\dot{B} \tag{5}$$

where $\Delta B_S=2B_S$. If the initial net flux density characteristic of the reset state is $-B_r$ rather than $-B_S$, then $\Delta B_S=B_r+B_S$.

Table 1 gives magnetization equations derived using the same general approach for the domain configurations shown in Fig.1. In the case of reversal by bar domains, the distance *between domain wall nucleating sites is proportional to* $(dB/dt)^{-1/2}$ and this must be included in the calculation to arrive at the dependence of H on $(dB/dt)^{1/2}$ [5]. The parameter K_{bar} depends on materials parameters including resistivity and domain wall spacing. In the sandwich domain calculation, the field driving the domain walls inward is less than the applied field H, due to shielding by eddy currents circulating in the outer, reversed domains and this gives rise to the dependence of H on ΔB. d is the ribbon thickness and ρ the resistivity, and so there are no free parameters to be fitted in the sandwich domain model. In the equation for magnetization reversal by collapsing cylindrical domain walls, the - signs apply in the denominator and the 1/2 power results from the geometry of the domains. K_{cyl} is a materials parameter involving ΔB_S, the grain size and the domain wall mobility. ΔB_{-cyl} is a measure of the maximum net flux density swing which can result from domain wall motion. In the case of reversal by expanding cylindrical domains, the + signs apply in the denominator. It is noted that ΔB_{+cyl} and ΔB_{-cyl} are not generally equal. Similarly, in the equation for magnetization reversal by spherical domain walls, the - signs in the denominator apply to collapsing domains and the + signs to expanding domains. The 2/3 power is a consequence of the domain wall geometry[6]. K_{sph}, ΔB_{+sph} and ΔB_{-sph} are materials parameters with similar significance to the parameters for cylinders and it is noted that ΔB_{+sph} and ΔB_{-sph} are not equal. In fact, the various parameters ΔB_S, K_{bar}, K_{cyl}, ΔB_{+cyl}, ΔB_{-cyl}, K_{sph}, ΔB_{+sph} and ΔB_{-sph} depend in general not only on materials parameters such as domain wall mobility and average grain size, but also on the magnetic history of the sample.

Table 1. Magnetization equations for frequently-encountered domain geometries

DOMAIN WALL GEOMETRY	MAGNETIZATION EQUATION	MAGNETIZATION REVERSAL DIAGRAM
Single plane wall	$H = H_o + H_r + \frac{w}{\Delta B_s C}\dot{B}$	
Bar domains	$H = H_o + H_r + K_{Bar}\sqrt{\dot{B}}$	
Sandwich domains	$H = H_o + H_r + \left(\frac{d^2}{4\rho}\right)\dot{B}\frac{\Delta B}{\Delta B_s}$	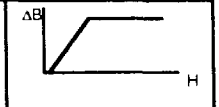
Expanding/ collapsing cylinders	$H = H_o + H_r + \frac{K_{Cyl}\dot{B}}{(\Delta B_{\pm Cyl} \pm \Delta B)^{1/2}}$	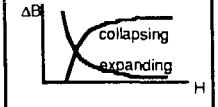
Expanding/ collapsing spheres	$H = H_o + H_r + \frac{K_{Sph}\dot{B}}{(\Delta B_{\pm Sph} \pm \Delta B)^{2/3}}$	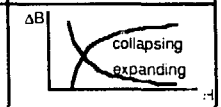

Table 1 also gives sketch magnetization diagrams for reversal by each of the domain configurations under conditions of constant net dB/dt. Single plane wall and bar domain geometries both lead to "square loop" behavior, although the field required to cause reversal depends differently on dB/dt for these two geometries. The diagram for sandwich domain reversal is not "square" and has a slope which decreases with increasing dB/dt. Collapsing cylinder and sphere geometries show a continuous transition from the unsaturated to the saturated state. Expanding cylindrical and spherical domain walls require a high field initially but become easier to drive as the reversal proceeds. These sketches are intended as a reminder of the relationship between domain geometry and particular features of the reversal diagram. For example, reversal diagrams derived from pulsed core current and voltage waveforms often exhibit a sharp initial increase in field followed by a reduction in field to a value which then remains fairly constant until saturation. The sketch diagrams suggest that domain walls, initially created or unpinned during the sharp rise in field, expand while the field is falling, before merging to form a bar domain structure driven by a constant field until saturation. It is important to note, however, that the shape of the magnetization diagram depends on dB/dt and this may not be constant. Of particular importance is the "$1-\cos\omega t$" waveform which normally drives the cores in a pulse compression line.

III. CHARACTERISTIC ELECTRICAL EQUATIONS

The electrical quantities I, V and $\Delta\Phi$ are related to the magnetic quantities by Ampere's and Faraday's laws:

$$I = 2\pi r_m \underline{H} = 2\pi r \underline{H} \tag{6}$$

$$V = SA\dot{B} = S\int w\,dr\,\underline{\dot{B}} \tag{7}$$

$$\Delta\Phi = SA\Delta B = S\int w\,dr\,\Delta\underline{B} \tag{8}$$

where H, dB/dt and ΔB are core-averaged values which assume the core thickness to be small compared to its mean radius r_m. A is the core cross section and S, the fraction of the core occupied by magnetic material, is a stack factor which allows for the presence of interlaminar insulation in tape-wound cores and the space occupied by any cooling channels. If the core is not of negligible thickness, these quantities H, dB/dt and ΔB are still employed in the design of pulse compression cores but they now describe magnetic behavior averaged over the core thickness. The local magnetic behavior can vary strongly with radial position[12], the basic reason being that the local azimuthal field is a function of radial position r. This is indicated by $\underline{H}$ in Eq. (6). As a result of this radially-varying field, the local value of flux density swing and its time derivative are also functions of r as indicated by $\Delta\underline{B}$ and $d\underline{B}/dt$ in Eq. (7) and (8). The magnetization equations listed in Table 1 describe the reversal of thin cores. When used to describe thick cores, they link the local quantities $\underline{H}$, $d\underline{B}/dt$ and $\Delta\underline{B}$ at a particular radius r. It is therefore necessary to carry out the integrations in Eq. (7) and (8) in order to relate H, dB/dt and ΔB and so derive the characteristic electrical equations linking I, V and $\Delta\Phi$. As an example, for thin cores in the sandwich domain regime, the magnetization equation given in Table 1 leads to the following characteristic electrical equation:

$$I = I_1 + \left(\frac{d^2}{4\rho}\right)\frac{V}{Sv_{core}}\frac{\Delta\Phi}{\Delta\Phi_S} \tag{9}$$

where $I_1 = 2\pi r_m(H_0 + H_r)$, $v_{core} = 2\pi r_m A$ is the core volume, and $\Delta\Phi_S = SA\Delta B_S$, is the saturated flux swing. An analysis of reversal by sandwich domains in thick cores has been given by Winter *et al*[13]. It shows that there are two regimes separated by saturation of the inner wrap of the core. Prior to inner-wrap saturation, the core characteristic equation is similar to Eq.(9). After the inner wrap has saturated, a saturation wave moves outwards through the core and the field required rises more rapidly than for a thin core.

IV. CONCLUSION

Taking into account the effect of core thickness is one of several refinements which can improve the accuracy of these models. For example, in metallic tapes the shape of the initial expanding domains depends on dB/dt due to domain wall shielding. At relatively low dB/dt the domains expand without significant change of shape to merge across the tape and form bar domains. At very high dB/dt eddy current shielding causes severe bowing of domain walls with rapid movement along the tape surfaces leading to the formation of sandwich domains. The intermediate stages have been treated numerically by Bishop and Williams[8]. Possible improvements to the domain models of reversal in ferrites include statistical treatments of grain sizes and realistic grain shapes, domain sizes and realistic domain shapes, and distributions of the easy directions of magnetization and nucleating sites. The influences of core manufacture on the magnetic properties of the core materials need to be quantified in order to be included in core models. The effects that must be considered include: stresses, which couple with the magnetic properties via magnetostriction; winding geometries and their effectiveness in linking changes in the core flux with the external circuit; interlaminar insulation, particularly with respect to annealability and resistance to breakdown; cooling schemes.

It is important to work closely with experimental data in the form of voltage and current waveforms and experimentally-derived magnetization diagrams when developing magnetization models. Also, it should be borne in mind that the simpler the magnetization equation, the more useful it is for engineering design purposes. Conversely, when designing pulse compression cores it must be remembered that magnetization reversal is a complex physical process and so the simpler the magnetization equation employed, the poorer its accuracy is likely to be and the more constraints must be placed on the conditions under which it is valid.

REFERENCES

[1] H.C. Kirbie, "Magnetic switching", Proceedings of the High Gradient Accelerator Workshop, Shelter Island, NY, October 1988.

[2] R.W. Kuenning, "Design of large magnetic pulse compressors", Proceedings of the International Magnetic Pulse Compression Workshop, Granlibakken, CA, February 1990.

[3] B.D. Coleman and M.L. Hodgdon, "A constitutive relation for rate-independent hysteresis in ferromagnetically soft materials", Int. J. Engng. Sci., vol. 24, pp. 897-919, 1986

[4] M.L. Hodgdon, "Applications of a theory of ferromagnetic hysteresis", IEEE Trans. Magn., vol. MAG-24, pp 218-221, 1988.

[5] C.H. Smith, "Application of amorphous magnetic materials at very high magnetization rates", J. Appl. Phys., vol. 67, pp. 5556-5561, 1990.

[6] R.K. Avery, J.F. DeFord, G. Kamin, W.C. Turner and J.M. Zentler, "A simple domain model of flux reversal in Ferrites", J. Appl. Phys., vol. 67, pp. 5562-5564, 1990.

[7] C.H. Smith, "Magnetic pulse compression by metallic glasses", J. Appl. Phys., vol. 64, pp. 6032-6034, 1988.

[8] J.E.L. Bishop and P. Williams, "A comparison of rapid surface and volume magnetization measurements on 50% NiFe tape with models of eddy-current-limited domain wall motion", J. Phys. D: Appl. Phys., vol. 10, pp. 225-241, 1977.

[9] H.J. Williams, W. Shockley and C. Kittel, "Studies of the propagation velocity of a ferromagnetic domain boundary", Phys. Rev., vol. 80, pp. 1090-1094, 1950.

[10] J.E. Knowles, "Some observations of Bitter patterns on polycrystalline 'square loop' ferrites, and a theoretical explanation of the loop shape and pulse characteristics of the material", Proc. Phys. Soc., vol. 75, pp. 885-897, 1960.

[11] V.J. Thottuvelil, T.G. Wilson and H.A. Owen Jr, "Unusual high-frequency behavior of some amorphous metallic-alloy tape-wound magnetic cores" IEEE Trans. Magn., vol. MAG-20, pp. 570-578, 1984.

[12] R.M. Jones "Step dB/dt magnetization losses in toroidal amorphous ribbon and polycrystalline cores", IEEE Trans. Magn., vol. MAG-18, pp. 1559-1561, 1982.

[13] S.D. Winter, R.W. Kuenning and G.G. Berg, "Pulse properties of large 50-50 NiFe tape cores" IEEE Trans. Magn., vol. MAG-6, pp. 41-45, 1970.

MATERIALS PROPERTIES AND PULSED MAGNETIC CHARACTERISATION

Ralf Wengerter, Giselher Herzer, Friedrich Lenhard
Vacuumschmelze GmbH, D-6450 Hanau, FRG

Abstract

Core losses of Fe- and Co-based amorphous alloys were measured at magnetization rates dB/dt of 0.1 T/µs to 100 T/µs. A comparison with existing dynamic domain models indicates that the induced magnetic anisotropy determines core losses in the low dB/dt region. Strip thickness dominates core losses at high dB/dt-rates, but the amount due to the anisotropy is only negligible for low anisotropy values. A three stage compression circuit was calculated for a low and high anisotropy material respectively. The best overall result could be achieved when using different materials in the compression stages.

Introduction

Saturable reactors for the pulse compression technique require materials with a high flux density swing, a rectangular hysteresis loop and low core losses. A high flux density swing reduces the volume of the core which is important not only for economical reasons but determines mainly the saturated inductance of the saturable reactor due to core size. A rectangular hysteresis loop enables resetting by means of current pulses. Since the cores are subject to high magnetization rates and increasing repetition frequencies core losses play a decisive role in the application. The demands on magnetic properties are summarized in table I.

Ferromagnetic amprphous metrals ribbons are considered as a most promising core material [1,2]. The particular versatility of amorphous metals hereby is based on the absence of crystalline anisotropy and of structural defects, which yields high permeability, extremely low coercivities and low hysteresis losses. The additional advantage of amorphous metals is their high electrical resistivity combined with a production-inherent low thickness which both limit the eddy current losses[3].

Looking at the high magnetization rates which correspond to frequencies in the MHz-range, thin crystalline Fe-50%Ni strips can hardly compete and moreover provide problems with the core construction due to their extreme sensitivity to plastic strain. Due to their low losses ferrites are also under discussion as magnetic switche materials in linear acceleration inductors. But the general advantage of amorphous metals is their high bipolar induction swing which is up to 4 times higher than in ferrites. This enables smaller core sizes or a decisive reduction of the required acceleration length for the particle beam.

Table I. Demands on magnetic properties for pulse compression

Property	Demand	Constituent for
Saturation flux density	high	Volume,saturated inductance
Core losses	low	Temperature raise, cooling, dynamic permeability
Remanence	high	Enables reset with current pulse
Saturation behaviour	good	Saturated inductance, compression factor

Basically there are two groups of amorphous alloys. On the one hand the Fe-rich magnetic alloys which exhibit the highest saturation flux densities among the amorphous metals and which are based on inexpensive raw materials. However the relatively high saturation magnetostriction limits the magnetic properties. The Co-base metallic glasses, on the other hand, are distinguished by their low or vanishing magnetostriction leading to highest permeabilities and lowest core losses[4-7].

The Fe-base amorphous alloys which attain saturation flux densities of 1.8 T allow a compact and cost-effective design. High magnetization rise rates and/or high repetition frequencies however could complicate the application due to core losses. Deterioration of the pulse due to magnetoelastic resonance effects or due to a too slow approach to saturation could be a further problem[8]. In such cases Co-base alloys exhibiting significantly lower core losses even at high magnetization rates can be an alternative.

Experimental

Aim of the investigations was the measurement of magnetic swichting cores made of different amorphous alloys at high magnetization rates as they occur in pulse compression devices. Toroidal strip-wound cores, annealed to a rectangular hysteresis loop before or after winding, were pulse-magnetized from the remanence to the opposite saturation with a near rectangular voltage. The iron cross-section of the samples was about 2 to 5 cm^2.

To achieve sufficiently high magnetization rates pulse compression was used to create the driving voltage. Fig. 1 shows schematically circuit and construction of the equipment. A thyristor was selected as a primary switch. By using a saturable protection choke it is possible to achieve a current rise rate of 6 kA/µs[9]. Next to the primary circuit follows a setup-transformer and two compression stages (parallel technique). A coaxial design minimizes the discharge time of the capacitors C_2 and C_3. To avoid creeping discharge, the voltage at the capacitors was limited to about 20 kV.

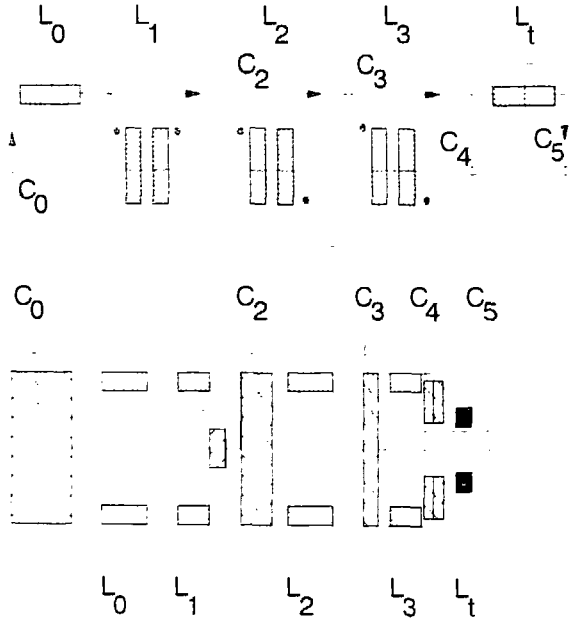

Fig. 1 Circuit and construction of measuring equipment

Depending on the core size magnetization rates up to 100 T/µs could be achieved. The maximum current is about 6 kA. Resetting is realized by a seperate winding, using a choke for decoupling.

The pulse current is measured with a coaxial shunt design for 200MHz and 20 kA peak value.The voltage is measured with a high-voltage "measuring head" with a limiting frequency of 75 MHz. For both current and voltage measurement capacitive noise is damped by magnetic cores. The measuring results are digitalisized to enable further evaluation with an Digital Oszilloscope. Sampling technique was used to achieve a sufficiently high digitisation rate[10].

Core losses at high dB/dt

Fig. 2 shows the measured core losses for two Co-base alloys (VITROVAC 6030Z, 6150Z) and one Fe-base alloy (VITROVAC 7600Z). Devious from the common pulse losses versus magnetization rate characteristic we have normalized the pulse losses by deviding them through the actual flux density swing and plotted this value versus the switching time, e.g. the time for which the core has to withstand the voltage. Comparing alloys this way seems to be quite fair with respect to the application which requires the core to withstand a certain time-voltage area. The characterisation takes into account that materials with higher flux density swing are subject to higher magnetization rates due to their smaller iron cross-section, and considers at the same time the actual volume of the material.

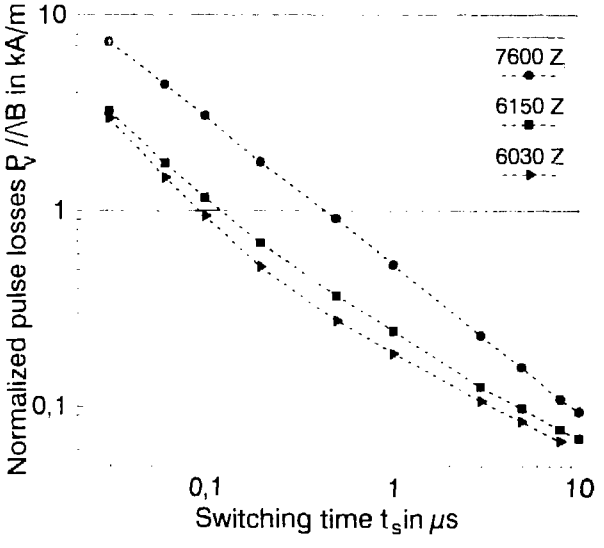

Fig. 2 Pulse losses P_v//\B normalized to /\B (≈ $2B_s$) vs magnetization time t_s for VITROVAC 6030Z, 6150Z and 7600Z (strip thickness ≈ 23 µm)

Although the Fe-base material requires only about half of the core volume of the Co-based alloys, the losses of a core designed for the same time voltage area are significantly higher in the whole plotted magnetization time range. This difference in losses can only partly be explained by the difference in the magnetization rate indicating that besides strip thickness and electrical resistivity other material parameters play a role[8]. Both Co-base alloys show a dB/dt-behaviour at longer switching times and a dB/dt-behaviour at short switching times. This is not recognizable for the Fe-base alloy in the plotted range.

Following the common dynamic magnetic domain models three different regions can be distinguished before the material is saturated. Fig. 3 shows the schematic hysteresis loop according to this model.

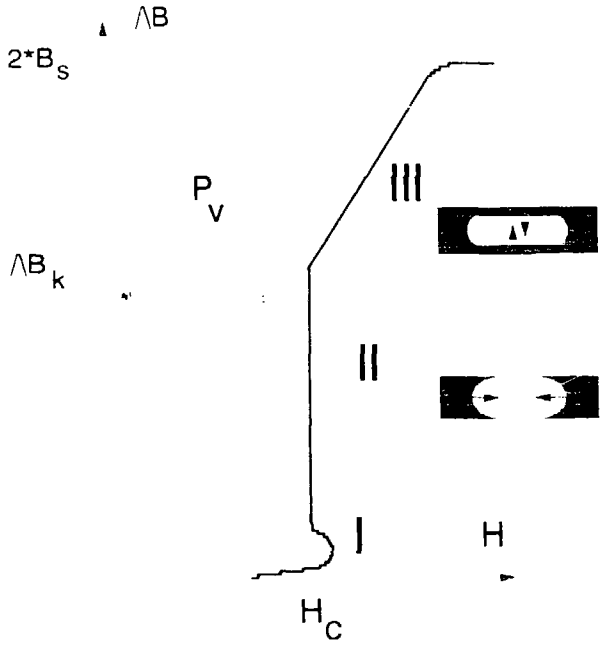

Fig. 3 Schematic hysteresis loop for bar domain and sandwich domain model

In region I very often a fast rise of the magnetic field is found returning to a smaller value again thus forming some kind of nose. This region is definite especially for very rectangular hysteresis loops and can be understood as the nucleation of bar domains across the whole strip thickness[11].

In region II the material is further magnetised by the motion of the bar domains. At high magnetization rates the mobility in the surface-near regions is remarkably higher than in the middle of the strip due to induced eddy currents leading to a strong bending of the domain walls. The driving field for bent domain walls can be described according to Bishop as[11,12]:

$$H_c \approx 0.7 * \sqrt{\mathring{B} * \gamma * L / (B * \rho)} \qquad (1)$$

where ρ is the electrical resistivity, $\gamma = 4\sqrt{A*K}$ is the the specific Bloch wall energy with the anisotropy K and the exchange energy A, and L is the mean domain width. As the driving field does not depend on the flux density swing /\B the hystersis loop has a rectangular shape in this region.

In region III two domain walls moving together have closed at the surface and a sandwich-like domain is formed around the strip. The magnetization front now moves from the surface into the bulk. Following this model the driving field can be described as[13]:

$$H = \mathring{B} * d^2 * /\B / (\gamma * \rho * B_s) \qquad (2)$$

where d is the strip thickness. In this region the driving field is proportional to /\B.

The transition from the bar domain model to the sandwich domain model occurs when the surface is fully magnetized. According to Fig. 3 this point can be estimated as:

$$/\B_k \approx 1.4 / d^2 * \sqrt{\gamma * L * B_s * \rho / \mathring{B}} \qquad (3)$$

According to equation (3), for $/\B_k > 2B_s$ the domain walls cannot close the sandwich domains and the magnetization process is based upon the movement of relatively weak bent domains transverse to the strip (bar-domains). The dynamic hysteresis loop has a rectangular shape and pulse losses can be described by:

$$V_p = 2 * H_c * B_s \qquad (4a)$$

$$\approx 1.4 * \sqrt{B_s * \mathring{B} * \gamma * L / \rho} \qquad (4b)$$

Equation (3) is valid for slow magnetization rates and small strip thickness as well as for high specific wall energies and big domain wall distances L (which corresponds to an extremly rectangular loop with only a few nucleation centres). Pulse losses do not depend on strip thickness and increase with the square root of the magnetization rate.

At $/\B_k < 2B_s$ the whole near-surface region is fully magnetized and a sandwich-like domain is formed. Following Fig. 3 the pulse losses can now be estimated as:

$$V_p = B_s * H + 0.5 * H_c * /\B_k \qquad (5a)$$

$$\approx \mathring{B} * d^2 * B_s / (4 * \rho) + 1.9 * \gamma * L / d^2 \qquad (5b)$$

where the first term describes the amount of the magnetization front coming from the surface and the second term considers the density of nucleation centres (domain width L) and the wall energy γ or the anisotropy parallel to the ribbon respectively. For sufficiently high magnetization rates the second term is typically very small, but it can reach significant values for extremly

thin strips with highly rectangular hysteresis loop and high anisotropy.

Fig. 4 shows a comparison of measured pulse-loss values versus dB/dt with theory using equation (4b) and (5b) for a Fe-base alloy and a Co-base alloy respectively. The theoretical lines clearly distinguish two regions. At low dB/dt pulse losses follow equation (4b), e.g. they are determined by the motion of laminar bar domains and independant from strip thickness in this region. Important parameters are the wall energy and the domain width which both depend on the anisotropy energy.

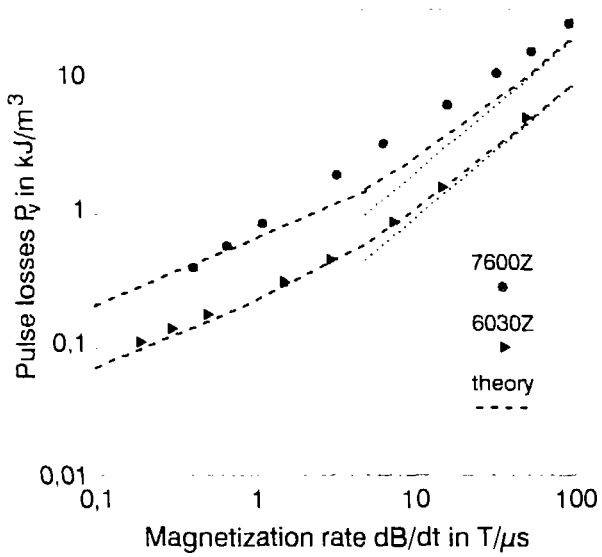

Fig. 4 Pulse losses of an Fe- and Co-base alloy and comparison with theory

For very high dB/dt pulse losses approach the sandwich-domain model (first term of equation (5b)) which is derived from the classical eddy current theory and describes the lower physical limit. Details of the domain structure like wall energy or domain width play no role in this region and strip thickness is the most important parameter.

For medium magnetization rates, e.g in the transition zone between the two domain models, pulse loses are described by equation (5b).

For the Co-base alloy theory fits well with the experimentell results. In the low dB/dt region theory is not precise enough to allow a quantitative comparison but the $\sqrt{dB/dt}$-characteristic is obvious. Even for very high dB/dt the measured values are slightly higher than calculated with the sandwich domain model. For practical reasons due to the process inherent tolerance of the strip thickness this additional amount seems to be neglectible for Co-base alloys.

The Fe-rich alloy shows significant higher losses in the faster dB/dt-region than predicted by theory. The transition zone from bar domain to the sandwich domain model can not be recognized in the plotted dB/dt-range. The main difference besides saturation flux density and magnetostriction to the Co-base alloy is the value of the induced anisotropy which is about 10 times higher. Therefore the domain walls are much stiffer and the anomalous eddy current losses are significantly higher which yields remarkable exess losses up to high dB/dt.

As a result the induced anisotropy along the ribbon axis, necessary to establish a rectangular loop, turns out as an important material parameter for excess losses. This applies especially to Fe-base alloys where relatively high values of anisotropy are necessary to overcome magnetoelastic anisotropies due to internal or winding stresses. As a consequence alloys with rather high anisotropy values ($\approx$ 1000 J/m^3) have to be selected out of the group of Fe-base alloys.

In near-zero magnetostrictive Co-base alloys on the other hand a rectangular loop can be achieved with longitudinal anisotropies of only some 10 J/m^3. Thus Co-base amorphous alloys come close to the physical minimum, which is described by the sandwich model, at significant lower dB/dt. As a consequence gauge reduction is much more effective for loss reduction. Table II lists the magnetic properties of some typical amorphous alloys.

Table II. Magnetic properties of amorphous alloys for pulse compression.

	Co - based		Fe - based	
Anisotropy (J/m^3)	50-100	250-550	100	900
Saturation (T)	0.7-0.8	1.0-1.2	1.4-1.6	1.75
Magneto-striction ($*10^{-6}$)	<0.2	<0.2	24-30	35
Products:				
VITROVAC^R	6030	6150	7505	7600
Metglas^R	2705M	2705MN	2605SC	2605CO

For low magnetization rates losses can be even more reduced decreasing the induced anisotropy by more sophisticated heat treatments [14]. However the long term stability of the properties after such optimizing heat treatments at present remains still unclear.

Optimization of a pulse compression circuit with respect to the core material

For high energy pulse compression the most popular materials are Fe-based amorphous alloys such as Metglas 2605CO or VITROVAC 7600, which have the highest saturation flux density and thus require the smallest volume. At high dB/dt rates and/or high repetition frequencies cooling of the system could be a serious problem. The question is, whether the use of "low-loss" Co-base materials can improve the loss situation significantly and what would be the effect with respect to core volume.

We calculated a series pulse compression circuits with three stages using Fe-base VITROVAC 7600 (B_s = 1.75 T, /\B = 3.3 T) and/or VITROVAC 6150 (B_s = 1.0 T, /\B = 1.9 T) as core materials. The calculation was done for a low inductivity coaxial design taking into account the actual core losses and their influence on the time constant of each stage, the saturated inductance of the cores due to size and winding design, and additional inductances of the circuit. Further it was considered, that the optimum switching time is not reached when the next capacitor is fully loaded, but at a somewhat lower voltage which saves core volume and losses[15]. The core volume of each stage is optimized numerically[16].

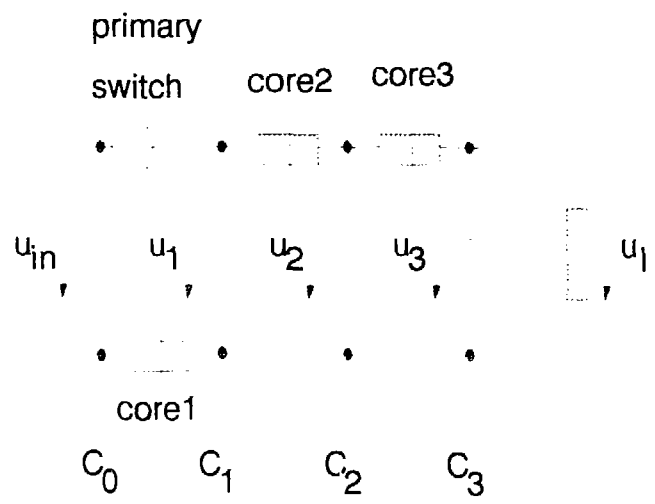

Fig. 5 Principle three-stage series pulse compression circuit.

Fig. 5 shows the principle features of the compression circuit used for the calculation. The voltage at the load was assumed to be 40 kV, the pulse energy 25 Ws and the pulse width 50 ns. The primary switch should be able to handle a pulse current of 2kA. The rate of current change should be limited to about 6kA/µs.

The result of the calculation is listed in table III. Using Fe-base VITROVAC 7600 Z in all three stages requires a minimum core weight, but losses are highest. Using Co-base VITROVAC 6150 Z reduces the core losses significantly, but this solution requires more than twice the core volume.

Table III. Calculation of total core volume and losses for a three-stage compression circuit using Fe-and Co-base alloys only or a combination of them.

	solution I	solution II	solution III
stage 1	7600 Z	6150 Z	7600 Z
core size (mm)	100*50*50	137*81*50	100*53*50
turns	20	20	20
core weight (kg)	1,57	3,93	1,74
core losses (Ws)	0,269	0,125	0,299
stage 2	7600 Z	6150 Z	7600 Z
core size	162*99*50	249*143*50	163*103*50
turns	5	5	5
core weight	3,42	8,99	3,34
core losses	0,91	0,573	0,882
stage 3	7600 Z	6150 Z	6150 Z
core size	147*89*50	221*123*50	221*123*50
turns	1	1	1
core weight	2,82	7,27	7,27
core losses	2,98	1,85	1,85
Σ weight	7,81	20,2	12,13
Σ losses	4,16	2,55	2,99

Solution III is proposed as a compromise. The Fe-base alloy is used in the first and second stages, the Co-base alloy in the third and fastest stage. Compared to solution II the core weight is reduced by about 40%, and compared to solution I the core losses are reduced by about 30%.

The calculation does not consider a possible deterioration of the pulse form due to magnetoelastic resonance effects or a saturated permeability >1 which would increase the core volumes and losses of solution I.

Conclusions

Soft magnetic materials for saturable reactors in pulse compression technique have to combine high flux density with extremly low core losses. This demand can be best fullfilled with amorphous metals featuring almost as high saturation flux densities as the crystalline soft magnetic metals and core losses almost as low as soft magnetic ferrites. A further optimization of the compression device can be achieved by taking into acount the specific advantages of Fe-based and Co-based amorphous alloys respectively.

References

[1] R. Hiramatsu, K. Harada and I. Sasada. IEEE Trans. on Magn. MAG-18, 1764 (1982)

[2] S.E. Ball and T.R. Burkes, Int. Pulse Power Conf., Albuquerque (1981)

[3] G. Herzer and H.R. Hilzinger, "Recent Developments in Soft Magnetic Materials," Physica Scripta T24 (1988) p.22

[4] T. Egami, Rep. Prog. Phys. 62 (1984) p. 1601–1725

[5] R.C. O'Handley, J. Appl. Phys. 62 (1987) R15–R49

[6] H. Warlimont, Materials, Science and Eng. 99 (1988) p.1

[7] G. Herzer and H.R. Hilzinger, in: Proc. Symposium on Magnetic Properties of Amorphous Metals, Benalmådena 25.–29.5.87, North Holland, p. 354

[8] V.R.V. Ramanan, C.H. Smith and L. Barberi, J. Appl. Phys. 57, 329 (Blackpool 1985)

[9] J.L. Steiner, A. Schweizer and J. Vitins, "Fast Switching Thyristors Replace Thyratrons in High-Current Pulse Applications," Power Semiconductor Department ABB Ltd, Switzerland

[10] F. Lenhard, "Cores and Chokes for Magnetic Swithces," BMFT-Report No. FB-13N53366

[11] J.E.L. Bishop and P. Williams, J. Phys. D 10

[12] J.E.L. Bishop, IEEE Trans. on Magn. MAG 10 (1974) p.1132

[13] C. H. Smith, D. Natasingh and H.H. Liebermann, IEEE Trans. on Magn. MAG 20 (1984) p. 1320

[14] S.M. Sheard, M.R.J. Gibbs and R.K. Avery, J. Appl. Phys. 64 (1988) p. 6035–6037

[15] G.L. Bredenkamp and P.H. Swart, "A Theoretical Basis for the Optimization of Electromagnetic Pulse Compressors using Saturable Ferromagnetic Cores," Systems Laboratory, Rand Afrikaans University, Republic of South Africa

[16] F. Lenhard, to be published

MAKING A WORKABLE CORE

Richard H. Wood
National Magnetics Corp
15925 Piuma Street
Cerritos CA 90701
(800) 877-7641

Abstract

This paper is dedicated to pulse design engineers who have spent many a sleepless night analyzing and testing pulse compression or magnetic modulator designs only to find out the fix was changing the CORE! A poorly constructed magnetic core WILL NOT WORK PROPERLY! We will investigate and present experimental results of newly developed construction and manufacturing procedures which result in much improved switching times and reduction of high frequency losses.

Introduction

Early in 1980 we started investigations of 50% and 80% nickel-iron tape wound toroidal and "C" core products for magnetic modulator applications. These devices act as transformers to charge the pulse forming network and then saturate to discharge it into the magnetron load. The rise time of the output pulse across the magnetron, which is the fall time of the voltage pulse across the switching core, was in the order of 1 to 3 microseconds. This is much slower than the required 200 to 300 nanoseconds. Excessive droop and poor shape at the end of the pulse in some of the units tested was related to bad cores. In the next six years the following experimental results were obtained which lead to the manufacturing processes now used at National Magnetics for all types of high power pulse cores of nickel-irons and metallic glasses.

Experimental

We first investigated the internal resistance measured from the outside lamination to the inside lamination. This resistance (commonly called the stack resistance), must support the operating VOLTS PER TURN of the device which can be hundreds to thousands of volts per turn. Slitting procedures using carbide slitting knives resulted in shorts at the edges of the tape. The edge of the tape was shaped into a 1/2 circle and coated with 3 to 12 coats of a magnesium methylate high temperature coating. This resulted in laminations that can support well over a 100 volts per lamination prior to the heat treating process. These coatings are typically 20 to 25 millionth of an inch thick and are pure crystalline magnesium oxide(MgO).

The skin effect of the tape used to wind the core was next investigated. A 200 foot long piece of 1 mil thick, 1/2 inch wide, 50% nickel tape was laid out in a U shape. AC resistance measurements were taken at 100hz, 1000hz, and 10khz on a HP4262A bridge. The resistance varied from 100 ohms at 100 hz to 112 ohms at 10khz or about 12 % from 100hz to 10khz. Next the tape was wound tightly into a core and the test repeated. The resistance increased by a factor of 2 (see figure 1) at 1000hz and a factor of 4 at 10khz. This effect, which I call proximity effect, increases the effective resistivity of the metal from 75 micro-ohms/cm to approximately 150 micro-ohms/cm. It is caused by adjacent laminations pulling eddy currents to the surface more than skin effect would explain. This effect did not occur when adjacent laminations were SHORTED to each other! Even a short every 3 or 4 laminations will destroy this effect.

Figure 1

CONDITION	100HZ	1KHZ	10KHZ	UNITS
U shape	100	102	112	ohms
wound 3 coats Mgo	100	205	420	ohms
wound 12 coats Mgo	100	260	620	ohms
U shape	.04	.03	.025	uh
wound 3 coats MgO	14.2	13.3	5.6	mh
wound 12coats MgO	19.5	17.7	6.25	mh

There are two ways to measure this effect in an uncut core. One is to measure the AC resistance from 100hz to 10khz and observe the increased resistance at the higher frequency as we did in the previous example. The second way is to measure the AC inductance at 100hz to 10khz and observe the DECREASE in inductance at the higher frequency. The low frequency inductance of the core when measured from the inside turn to the outside turn is increased by this proximity effect. The high frequency inductance is a measure of how many turns of the core are NOT shorted. The above tests indicate how important it is to get the laminations perfectly insulated with extremely thin coatings. The proximity effect is reduced in metallic glass tapes due to the irregular surface on one side of the strip. This side, opposite the chilled casting plate, has little sharp pointed bumps. These are due to the spray casting procedure used in the manufacturing of these metallic glasses.

The field penetration and voltage distribution in nickel switching cores was next investigated. A core with a 5 inch OD, 3 inch ID, and 1 inch strip width was wound with seven single turn pickup coils. Each coil sampled 1/8 of an inch of the cores build up from the inside turn to the outside turn of the core as shown in figure 2.

FIGURE 2

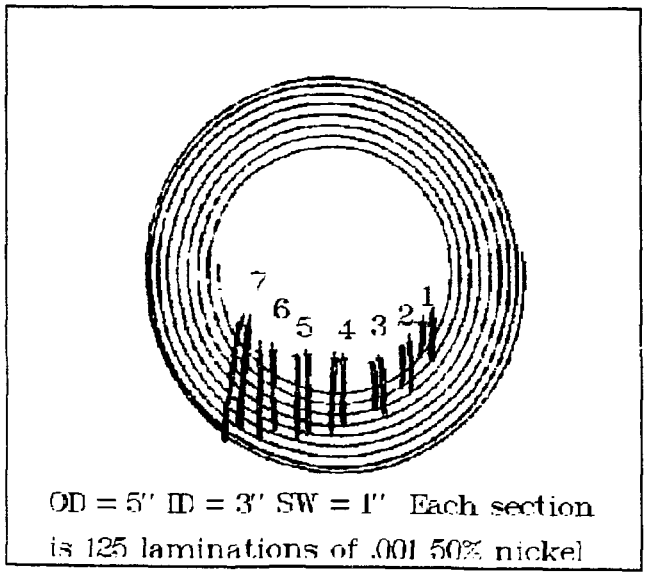

The core was operated in a switching mode circuit. Waveforms were recorded and plotted for each of the seven single turn pickup coils. The voltages across each winding and the whole core are shown in figure 3. The inside diameter section #1 saturated first as might be expected. Sections #2 and #3 saturated next in that order. Section #4, the center section, supported very little voltage until all of the other sections had saturated. Sections #5 and #6 saturated more toward the end of the pulse due to longer magnetic path length as expected. Section #7, the very outside, saturated last (neglecting #4) and had a great effect on the fall time of the output waveform. It was next decided to make 2 cores up from 1/2 inch tape and stack them side by side. This was done in a attempt to get better penetration of fields and to try to make the center section #4 carry its share of the voltage. This split core configuration reduced the turnoff switching time from 1.5 microseconds to 400 nanoseconds and improved the trailing edge shape substantially.

FIGURE 3

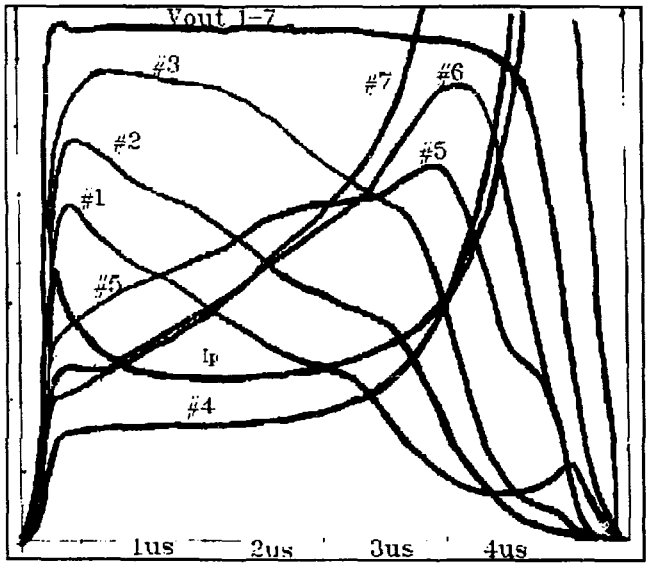

We have manufactured many types of composite cores. These cores are made out of two or more types of magnetic material. A core was constructed with supermendur (Bs=22KG) for sections #1 and #2, 50% nickel/iron (Bs=16KG) for sections #3 and #4, and 80% nickel/iron (Bs=8KG) for sections #5, #6, and #7. By putting high flux material where it had saturated too soon and low flux material where it had saturated too late, it was hoped that, all parts of the core would saturate at the same time. It was NOT TO BE! These tests indicated that the split core, properly constructed with 50% nickel/iron only, was much better in overall performance than the composite core. The reason why the SPLIT core preforms so well is easily understood when one considers it to be made up of seven little concentric cores. If for example, section #7 in one core

is partially shorted, the waveforms shown in figure 3 for section #7 will tend to be supported by the other cores section #7. This sharing of the problems from one section or another between cores allows Mother Nature to have the voltage distribution she requires for fast switching! In effect, what ever is bad in one core, is handled in the good part of the other core. The actual voltage distributions in the two cores will modify itself to still make the TOTAL output voltage look like Vout in figure 3.

The voltage across the cores laminations was next studied. The core has a voltage measured across its laminations from the inside turn to the outside turn. This voltage is equal to the volts/turn that the core is being operated at. It can be hundreds to thousands of volts and must be supported by the cores laminations without arc over or catastrophic breakdown. Taking this volts/turn and dividing it by the number of laminations in the stack, yields the volts per lamination. Volts per lamination of 1 to 100 volts can be supported in well designed cores.

There is an ADDITIONAL core loss associated with this stack resistance. The laminations in an ideal core are perfectly insulated resulting in a very high stack resistance. Most cores will have a stack resistance less then ideal. This results in an additional loss. Take for example, a value of 100 volts per turn across a SHORTED core of 2 ohms. The additional watt loss is V^2/R or 10,000/2 which works out to be 5000 watts! In practice you can expect up to 50% of that value. Low stack resistance cores are characterized by high droop and an exciting current Ip which lacks the negative resistance effect as shown in figure 3. You will notice the current first ramps up to a peak in 20 to 30 nanoseconds. Next, it DROPS back to 60% of the peak 1.5 microseconds later and stays relatively flat to 3 microseconds. It then increases very abruptly at saturation. The correct shape of this current waveform improves the output voltage Vo in three ways. First, the front higher current peak reduces the leading edge voltage overshoot. Second, the current is REDUCING in the middle of the pulse, which reduces droop. Third, the current gets a flying run at saturation (the top of the page) so it can switch very abruptly. Further studies of the shape of this current Ip led to the next experiments on how to heat treat the magnetic material.

It was discovered that various temperatures and times in the heat treat processes led to the results shown in figure 4. Slight secondary recrystalization of the 50% nickel materials allows control of the shape of the B-H loop. The IDEAL B-H loop shown on the left in figure 4 has the negative resistance effect in Ip. Notice how the loop necks in and is narrower near the origin as compared to the POOR one on the right. This IDEAL loop is what we're looking for! The POOR one on the right has a pronounced step at about 80% of saturation flux and also lacks the negative resistance effect. Its output voltage Vo has a front spike on it and the back half of the upper waveform is missing. This effect is caused by the last 20% of the magnetic domains which are not aligned correctly. These domains require more energy to saturate.

FIGURE 4

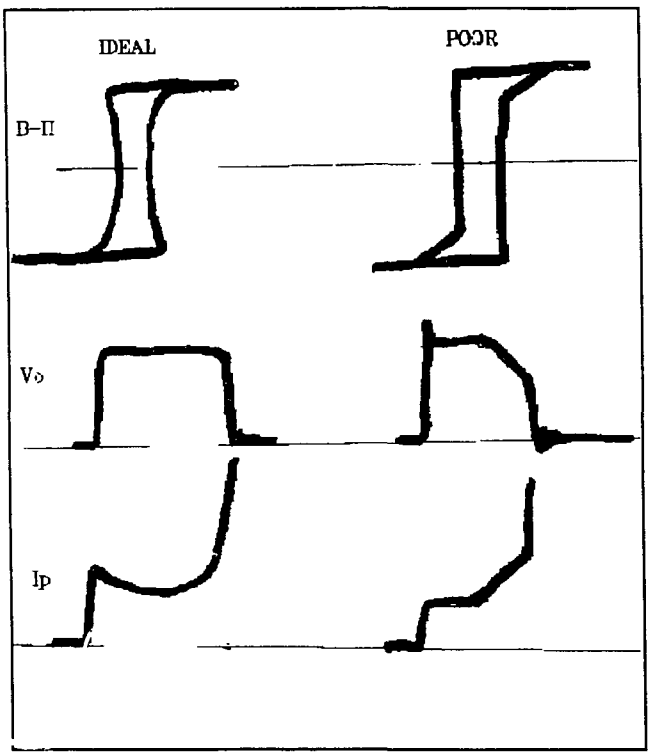

By careful attention to the correct heat treat temperatures and time, it is possible to custom shape nickel-iron and metallic glass cores for pulse applications. We have obtained better switching characteristics from metallic glasses after special heat treat. First, the glass is slit to size and both edges are shaped to a 1/2 circle. Next, 3 to 12 coats of Mgo are applied and cured. Care must be exercised in the curing of the Mgo on the glass strip so that the metallic glass does NOT recrystallize. Next, either AC or DC field annealing is used to change the shape of the dynamic loop. AC field annealing, with an extra integrating single turn pickup winding, allows you to look at the dynamic B-H loop at 60 Hz while you are annealing the core. This is done by cooling the core down to below its curie temperature, observing the B-H loop, and if not the proper shape, elevating the temperature back to the recommended annealing temperature for some more annealing time. After the proper time and temperature have been established, DC annealing can then be used for slightly improved performance. If one is compelled to use 0.3 mil Kapton or Mylar as additional insulation, Kapton will withstand the 675°F required for the annealing. Also, the 3 to 12 coats of Mgo covers up the little sharp points on the side opposite the casting plate on metallic glasses and reduces the possibility for the glass to cut through the Kapton insulation!

Core Losses

Core loss can be calculated in a number of different ways. We have developed a computer program called COMPCORE which is a core simulation program for the IBM computer and compatible. One of its output screens is shown in figure 5. The program is capable of accurate projections of core losses and other properties of the core from .06 khz to 100 khz.

FIGURE 5

```
Tech Support Phone                * 1 PHASE *                        VER 1.01
 (213) 924-7541          NATIONAL MAGNETICS CORPORATION              F1 = HELP

                  *MOD*    *** C O M P C O R E ***                  *HOT*
 A) N.M. Part # :CH-16      N) MAT    :5181        B) GapcoRe  :   0.00075
 D) D dimension :  1.125    SF        :  0.830     V) Volts    :  334.438
 E) E dimension :  0.625    An in²    :  0.584     T) Turns    :  1
 F) F dimension :  0.625    AwAc      :  0.787     Q) FreQ     :  200.000
 G) G dimension :  1.937    MIL       :  0.001     *B) Bac_req :  10.000
    Weight      :  1.212    Gaptot    :  0.00075   S) AMPS dc  :  0.000
    MGL         :  6.979                          U) WIREcm/a :  750.000
 P) Prefix+Awac :CH-0000.7660                      A) Amb T°C  :  20.000

Enter letter to modify, <C>alc, <FGDM> or <Esc> twice

 1) Watts     :7335.236    2) L Hy    :7.62E-06    3) Gap Watts:  42.231
 4) Iex       :  33.133    5) L'Hy    :7.64E-06    6) Gap Req  :  0.000
 7) Bac       :  10.000    8) F flux  :  1.000     9) Bdc      :  0.000
10) Bac+B'dc  :  10.000   11) VA mat  :8182.048   12) B'dc     :  0.000
13) Pmat      :4.12E+03   14) VA gap  :2978.958   15) Watts/# :6851.271
16) Peff      :2.86E+03   17) Bsat    :  15.000   18) VA/#    :6683.853
19) V/T       :  334.438  20) Hdc     :  0.000    21) P@Ic/Ig :9.31E+03
22) BQ10uts/# :  0.298    23) B expo  :  1.888    24) LI ²    :  0.000
```

The core loss is calculated by the equation:

$$W/lb = a_0 f^{a_1 + a_2 \log f} B^{a_3 + a_4 \log f + a_5 \log B}$$

where:

f = frequency in khz
B = flux density in kilogauss
A0 = .046520
A1 = 1.222690
A2 = .092990
A3 = 1.972270
A4 = -0.022580
A5 = -0.111910

This equation will produce watts per pound for 1 mil 50% nickel impregnated toroids. The values for A0 through A5 vary for each type of material and are available from National Magnetics upon request. A output file from the curve plotter in COMPCORE is shown in figure 6.

FIGURE 6

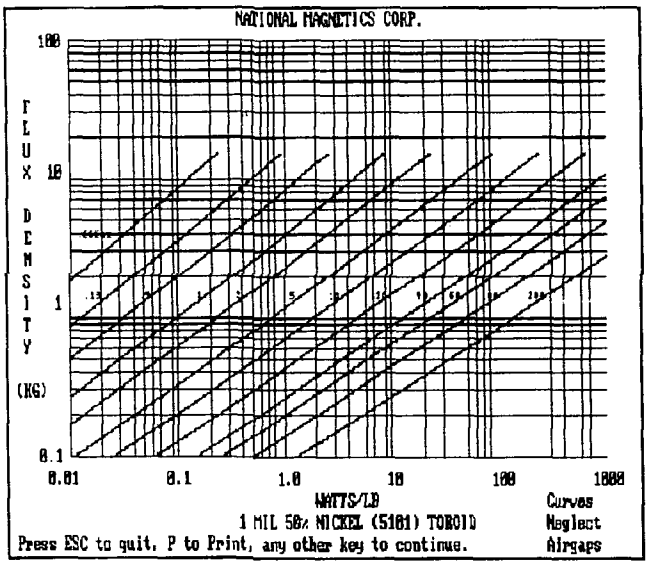

Using this equation a estimate can be made of the pulse excitation losses as follows. Take a pulse of 2.5 microseconds at 1000 pulses per second and the core operating under DC bias reset conditions.

frequency of on time = 1/(2*2.5*10^-6) = 200khz
frequency of off time = 1/(2*997.5*10^-6) = .501khz
duty cycle = on time/off time = 2.5/997.5 = .002506

Watts = W/lb * lb * 1/2 of the loops losses at the operation flux and frequency(200khz) * Duty cycle.
We use 1/2 of the ac losses that compcore gives us at 200khz since the pulse is unidirectional and we only need the area of the right hand side of the B-H loop.
Using a 1.212 pound 50% 1 mil nickel core operating at 10 KG(ΔB=20KG) and 200khz COMPCORE gives us 6051 watts/# or 7335 watts! One half of this times duty cycle = 7335/2 * .0025 or 9.168 watts average loss. Next we need to do the same calculation for the OFF time frequency, again using 1/2 of the left side of the B-H loop and add this to the ON time losses for the total losses. At .501khz at 10 KG COMPCORE gives us 1.50 watts/# or 1.818 watts. Off time losses are 1.818/2 = 0.909 watts. Adding the on and off time losses we arrive at 9.168 + 0.909 or 10.077 watts total.

Conclusions

Nickel and metallic glass core systems can be constructed to operate down to 50 nanosecond in pulse switching and compression circuits with careful construction techniques and the losses can be estimated with computer assisted programs.

Power Conditioning Group

Switching Devices for High Average Power Magnetic Pulse Compressors

Glen McDuff and T. R. Burkes
Pulse Power Engineering
P.O. Box 16577
Lubbock, Texas 79490

W. M. Portnoy
Texas Tech University
Lubbock, Texas 79409

INTRODUCTION

Numerous devices, "trons and tors" have been developed over the years but in todays world of high power high repetition rate pulse generation, these numbers have dwindled to essentially three; the thyratron, the thyristor, and the spark gap. Although, many other devices exist (many of which will be described below) and are currently under development, only these three have the manufacturing base to be available in large and consistent quantities. There are many switches capable of operation at repetition rates in the multi-kiloHertz realm. The most common triggered, high power switches are spark gaps and thyratrons. A non-triggered "switch," in which operation is based on the nonlinear properties of magnetic materials, also falls into this class. A "magnetic" switch is better described as a pulse compressor or pulse sharpener. Being a passive element, the "magnetic" switch experiences an impedance change determined by the nonlinear characteristics of the ferromagnetic core material. It is not a switch in the general definition of the term, but the use of magnetic material in the generation of very short high energy pulses is an important technique in high repetition rate modulator design. Solid state devices, despite the potential for use in high power pulse generation have not been widely used. This in part is due to the relatively small market for high power pulse switches and the astronomical cost of development associated with advanced semiconductors. However, there is considerable basic research work in the area of solid state switching as will be reviewed later.

The quality of a high power switch may be judged by its ability to hold-off high voltage, conduct rapidly when triggered, recover its hold-off properties after conduction, and maintain a proper operating temperature. Recovery characteristics determine the upper bound at which a switch can operate repetitively. In plasma and arc discharge switches, the rate in which the arc products can be cleared from the switch determines the recovery time. In a magnetic switch, the recovery is determined by how fast the core magnetization can be reset to its initial starting value. A solid state switch may be limited by recombination time and the level of impurities added to the base material to derive a certain performance. In all high power switches, the most critical issues are mechanical design and fabrication techniques. Where circuit power levels are exceeding Megawatts, even the most efficient switches will require a substantial amount of heat removal. A proposed switching technology may possess all the attributes to solve the worlds switching problems but if it can not be manufactured in a thermally acceptable and cost effective package then the need will never manifest. With these thoughts in mind, lets examine the current devices and capabilities of high power switches.

SPARK GAPS

Spark gaps are by far the most versatile of all high power switches. They can be designed to operate in gases or liquids at voltages from a few hundred volts to many Megavolts and switch currents from milliamperes to Megamperes. Even though spark gaps can be designed to operate over enormous electrical ranges, any one particular design is usually limited to a very narrow dynamic range. That is to say, a spark gap designed to operate at 50 kV will probably not perform with equal electrical and life characteristics (if at all) at 40 kV in the same circuit. Because spark gaps are designed on an "as needed" basis, it is practically impossible to develop a testing procedure to establish a data base on performance and design techniques. Electrode materials, flow rates, and dielectric

media such as gas mixes and liquids, further complicate a systematic analysis of spark gap technology. This along with the wide variety of geometries, i.e. point-plane, rail, coaxial, etc, make it impossible to form an organized comparison of spark gap technology with any other switching technique. For these reasons, a spark gap evaluation is only good for the specific parameters at which the gap was designed to operate. The wide diversity of high power spark gaps could not possibly be addressed with any sort of continuity in this report. Instead, a brief history of high power sparks gaps is presented.

Theory of spark gap design and breakdown phenomena have been investigated for well over one hundred years in all parts of the world. J.C. "Charlie" Martin, of the Atomic Weapons Research Establishment in Aldermaston, England, is considered by many as the first researcher to derive basic concepts of high power switching that in many areas are still considered the standard in the field. Spark gaps for repetitive modulators date back to the late 1800's. Early repetitive switches took the form of rotary spark gaps. The first non-experimental applications of repetitive spark gap modulators were for lighting, medical, and radio applications [1-3]. In the pre-radar period of the M.I.T. Radiation Laboratory, the first systematic development of repetitive spark gaps for short pulse applications had its beginning. Rotary gaps [4], and multi-electrode quenched spark gaps were developed for use in kilohertz modulators. J.D. Craggs of the Metropolitan-Vickers Electric Company, Ltd. announced the invention of the "trigatron", the first three electrode sealed spark gap in 1942 [5]. The trigatron is still the most common type of spark gap used today.

The main concern of a repetitive spark gap design is clearing the metallic vapor from the gap after conduction. Sealed repetitive gaps either operate at extremely low powers or in very short bursts because of the concentration of residual metallic vapor. To achieve long duration of operation a flow system is added to the gap to force the clearing of residues.

Spark gap erosion has been investigated more than any other parameter in high power switching. This is partly due to the fact that each spark gap application usually has a unique spark gap that was designed specifically for that job and life information is desired for some logistic reason. The other reason is that erosion measurements are fairly simple to obtain. Spark gap erosion is a complex function of many variables and is not completely understood [6]. Surveys of repetitive spark gap characteristics [7,8] revealed one very interesting fact with regard to erosion. Regardless of the electrode material or electrical operating conditions, at best, electrode material is eroded at an average rate of 50 micrograms per coulomb of charge transfer through the gap. This means that if a particular application requires a switch to transfer 100 Megacoulombs (not unreasonable in a high repetition rate modulator) the electrodes would have to have some 5 kg of material available for erosion.

Summary

Due to the nature of spark gaps, it is difficult to summarize their performance. It should suffice to say that a spark gap can probably fill any high power switching requirement. If the need is Megavolts and Megamperes with di/dt of $>10^{13}$ A/s, the spark gap is the only alternative. The only real drawback to spark gaps is in repetitive circuits. Due to the erosion limitations, losses, low gain, and the complexity of a flushing system to remove the metallic residue after conduction, spark gaps are often not cost effective in continuously operated repetitive circuits. However, in single shot and very low rep-rates, a spark gap may well be the switch of choice.

SOLID STATE SWITCHES

Thyristors

Thyristors have long been used in low frequency long pulse applications. Only recently has substantial interest been focused on their uses in short pulse operation. Most user results are in general undocumented but there are instances where conventional thyristors will exceed their stated ratings. Recent reports have indicated that under special conditions, there is a strong possibility that more-or-less conventional thyristors can be used in some applications normally fulfilled by thyratrons; these conditions involve either the insertion of saturable inductors [9,10] or gating

modifications [11-16]. This combination has been used successfully [9] to switch a Reverse Conducting Thyristor, a RCT, which delivered a 2 μs (half-width) sinusoidal pulse with a peak current of 3.3 kA with a forward conduction drop of 50 V. Likewise, a Gate Turn-off thyristor, GTO, delivered a similar pulse with a peak current of 2.4 kA with a forward conduction drop of 100 V. Both of the above were conventional gated devices and the circuits included snubbers. These currents translate to a di/dt level of around $7 \cdot 10^9$ A/s for the RCT and $4 \cdot 10^9$ A/s for the GTO.

Enhanced performance can also be obtained by the use of a large gate drive in interdigitated devices, particularly if the amplifying gate is disabled. Interdigitated thyristors have switched, single shot, 10 μs pulses at $1.4 \cdot 10^{10}$ A/s at the 800 V level and $1 \cdot 10^{10}$ at 800 Hz [13]. Although the forward voltage drop in the later case was over 50 V, the case temperature increased to 58°C by the end of an hour's operation. The gate drive was an 8 μs wide pulse with a leading edge current of 12 Amperes. Other measurements [14] have indicated that only the gate pulse current affects the anode current di/dt and neither pulse width (>30 ns) nor pulse shape have significant effect. Another case of a highly interdigitated (involute) gate thyristor switched a 13 kA, 10 μs pulse at a peak anode voltage of 2 kV when triggered by a 100 A, 500 ns gate pulse [15,16]. In this case the amplifying gate was shorted to the main gate. In devices with unshorted gates, a maximum of only 8.5 kA from a 1.7 kV charge has been obtained before failing. It was observed that the amplifying gate slowed the rate of anode current rise.

Avalanche Injection Switches

If the electric field created by a voltage across a high resistivity semiconductor bar is increased, avalanche breakdown will occur. Holes produced by the avalanche will drift toward the negative terminal increasing the conductivity and decreasing the electric field. This results in an enhanced field at the positive end and the avalanche generation rate will increase. In the limit, the electric field will be concentrated in a narrow region at the positive end, producing large numbers of holes that are injected into the low field region. This results in a conductivity that is so great, high currents can flow even with very low applied potentials. This effect is known as "avalanche injection [17].

Reversed bias diodes (avalanche injection diodes) [18-22] have been used to implement this phenomenon and to obtain very fast high power switching. For example, a 1600 V pin diode, driven with a reverse voltage, was used to deliver a 1.8 kV pulse to a 50 Ω load with a risetime of 200 ps. Even though the di/dt was $1.8 \cdot 10^{11}$ A/s, the peak current was only 35 Amperes and the forward conduction drop was over 500 volts. A large sustaining voltage (10-20 V) [17,18, 23-31] is characteristic of silicon avalanche diodes. Injection stimulated avalanche has also been used to obtain high repetition rates in transistor devices at low power levels [32] but the most pronounced effect is in thyristor devices [23,33-37].

Avalanche injection in thyristors provides uniform carrier distribution over the entire cross section of the device. This results in the minimization of local charge injection which takes place at the emitter-base periphery during conventional triggering. One type of device that utilizes avalanche injection is the reverse connected, or reverse turn-on, dynistor. Gating is performed with a very short high reverse voltage (cathode-anode) pulse which is decoupled from the load and the bias networks. Anode current of 25 kA with a di/dt of $2 \cdot 10^{10}$ A/s have been demonstrated with a forward conduction drop of about 15 volts. A modified version [37] of the above mentioned device has obtained switched currents of 30 kA at $7 \cdot 10^9$ A/s di/dt with a conduction drop of about 20 volts.

Laser Triggered Switches

The first type of light triggered switches to be described are the intrinsic silicon switches. These are basically a conductivity modulated high resistive silicon device. Because photoconductivity is a bulk phenomenon, a single device has the potential to be scaled to large voltage and current ranges. Optical control has the most obvious advantage of high voltage isolation and very fast switching due the relative large amount of energy available for triggering in a short wavelength laser pulse. Blocking voltages of these devices are limited by surface breakdown and the peak current is restrained by

thermal runaway. These switches have demonstrated peak currents of 1.8 kA, 200 ns pulse with a 5 ns risetime with a 100 kV holdoff voltage [38]. Repetitive operation of 100 Hz has been demonstrated at low temperatures (77°K) [39] at 15 kV, 1.2 kA with a 500 ns wide pulse. This performance approaches that of some small thyratrons. However, the electrical conduction time can be increased only by increasing the optical pulse width which can present formidable task and reduce the overall gain of the system to less than unity. Also, large photoconductors (which are difficult to fabricate) must be illuminated over large areas, requiring large optical energies that are not readily obtainable.

Photoconductive switches have also been fabricated in gallium arsenide [40-50]. Surface flashover voltages in gallium arsenide are somewhat greater than in silicon [41], but the principle interest in this material is its large resistivity. Along with greater carrier mobility (i.e. larger peak currents), and its short carrier lifetime (higher repetition rates) make these the most attractive of light triggered switches. In the photoconductive mode, these devices have switched 800 Amperes from a 46 kV source turning off in a few nanoseconds [48]. Currents as great as 4 kA from 3 kV sources have also been obtained [42]. In LEC gallium arsenide devices pulse risetimes of 200-300 ps and fall times of 1-2 ns have been demonstrated in the 10-30 kV range [45].

Silicon and gallium arsenide photoconductive switches have the same dependence on optical energy; and an intrinsic low gain, thus making fairly inefficient switches. However, gallium arsenide exhibits a negative resistance behavior, termed "lock-on" [42, 44-48] which can greatly enhance the gain and permit switching with relatively low energy levels. The conduction voltage drop during lock-on is as large as 10% of the switch voltage. Lock-on switching has been used to generate 60 Ampere pulses at 30 kV [41, 46].

Another type of laser triggered switch is the reversed biased silicon p-i-n diode [51-54]. A p-i-n structure has several advantages over bulk photoconductive silicon switch. Reverse leakage current in a junction is significantly less than a bulk switch allowing for DC operation rather than pulse charging. Also, it is much easier to form ohmic contacts to the low resistivity p- and n- regions than it is to the high resistivity bulk silicon. However, to avoid transit time effects, the i-region must be relatively narrow (<50 μm) [53]. Discrete devices of this type have switched 56 A at a 1 kV blocking voltage [54].

The last laser triggered switch to be profiled is the thyristor. When properly illuminated, a laser triggered thyristor will turn on much more rapidly than conventionally triggered devices [23,24,33,51,55-64]. It is important to emphasize that this type of illumination is different than that used for "optical gating"; the later is simply an alternative to conventional electrical triggering where turn-on is still dependent on comparatively slow drift and diffusion to establish and spread conducting plasma throughout the device. Laser triggering refers to the spatially distributed illumination of a large area of the device. The rate of anode current rise and amplitude will depend on various device operation parameters. Such as: the energy of the laser pulse, the area and perimeter of the illuminated region, and the thermal characteristics of the device and its mounting assembly. Such a switch fired by the output of a Nd:YAG laser has delivered a 10 kA pulse (1 kV anode voltage) at $7.5 \cdot 10^8$ A/s with a 200 V forward drop [59]. Other examples are: 1.7 kV anode voltage, 40 μs pulse width with a di/dt of $4 \cdot 10^{10}$ A/s and peak amplitude of 2.4 kA; 1 kV anode voltage, 10 kA with a 100 ns pulse width and a di/dt of $1.1 \cdot 10^{12}$ A/s [60]. High conduction drops are associated with the pulse currents [59, 64]. Several energy sources can be used for this type of triggering. A flashlamp triggered device was tested at 2.4 kV passing a 10 kA pulse with several microsecond risetime [25]. In another case microwaves were used to obtain a 4 kA pulse from a two device stack [26]. A 600 V optically triggered gallium arsenide thyristor has recently been described [27] which passed 140 Amperes at a rate of $1.7 \cdot 10^9$ A/s.

MOS Controlled Thyristor

The MOS controlled thyristor, MCT, is a relatively new device in the high power switching world and little is known about the ultimate capability of this technology. To date single device characteristics are limited to a few kilovolt holdoff and can pass a few hundred amperes. Risetimes on the order of

microseconds are typical for both turn-on and turn-off [65]. Where GTOs exhibit turn-off gains on the order of 4-10, the MCT can approach several thousand. The highly efficient turn-off characteristics makes the MCT a promising candidate for high power opening switch applications. Development work on the MCT is continuing as this technology possesses all the attributes to be the "switching device" in the next millennium.

Summary

Solid state switches offer several advantages over all other high power switches. First, they require no standby, and support power other than cooling. Semiconductor devices have a good track record in some applications of long reliable performance. However, the major drawback to semiconductor technology is the limited single device voltage capability. Experimental devices have approached the 4 kV hold-off but about 1 kV is all that should be expected in an off-the-shelf component. This requires series connections of many expensive devices to achieve the high voltage hold-offs which in itself is not a real tough technological challenge but when adding in the complexity of mounting, cooling, insulation, inductance, etc., often is not a viable economic option. Below is listed (Table 1) a summary of single pulse capabilities of the above mentioned semiconductor switches. The relative small market for high power switches, and the high cost of semiconductor manufacturing has severely limited the device availability. The commercial demand has not provided the market incentive to invest in research and development of solid state devices for high power switching applications so most of the development is centered in the university sector.

Switch	Voltage	Pulse Width	Peak Current	di/dt A/s
LTIS	100 kV	200 ns	1.8 kA	$3.6 \cdot 10^{11}$
LTIGaAs	30 kV		200 A	
LTSD	1 kV		56 A	
LTST	1 kV	100 ns	10 kA	$1.1 \cdot 10^{12}$
AIT			25 kA	$2 \cdot 10^{10}$
Thyristor	2 kV	10μs	13 kA	$1 \cdot 10^{11}$

LTIS...Laser triggered intrinsic silicon
LTIGaAs...Laser triggered intrinsic GaAs
LTSD...Laser triggered silicon diode
AIT...Avalanche injection thyristor

Table 1. Single pulse switching capabilities of solid state devices.

THYRATRONS

Since its patent in 1918 [66], the hydrogen thyratron has become the most used switch in high power pulse generation. State-of-the-art thyratrons can have a dynamic switching range of over 100 in voltage and 100,000 in pulse current in a single device. Lifetimes of thyratrons in radar type modulator circuits have been demonstrated to exceed 50,000 hours [67], a total charge transfer of over 300 Megacoulombs [68], and 10^{10} shot lifetimes at current rates of rise of over $3 \cdot 10^{11}$ A/s [69]. With documented lifetimes of these magnitudes, the thyratron is often the best candidate for repetitive switching tasks.

Basic principles of thyratron operation have been published in three volumes of "Research Study on Hydrogen Thyratrons" [70] and in two books from the Soviet Union [71,72]. A comprehensive study into the ultimate limits of peak current and di/dt capabilities of a hydrogen thyratron was performed at E.G.&G. about 7 years ago [73]. These collections, along with over 500 hundred published research reports and numerous theses, provide a good foundation in the understanding of the hydrogen thyratron. The huge amount of research conducted toward the development and use of hydrogen thyratrons is a good indication of the importance of this switch.

By far the most important aspect of thyratron technology, that has been overlooked in practically all the publications, is device construction. Plasma physics, electron dynamics, and electric field related phenomenon comprise only a small part of today's high power thyratrons. Materials compatibility, sealing, electrode processing, and thermal design constitute the major aspects of new device development. These "non-glamorous" issues in hydrogen thyratron technology have been addressed solely by the manufacturers of this device. Because of the great investment of time and money by the manufacturers in the development of construction techniques, much of this information is closely guarded.

At last count there are over 150 different glass and ceramic thyratrons and a two dozen or so metal envelope thyratrons available commercially. Thyratrons have operational ranges (in single devices) from: a few hundred to over 100 kV, a few amperes to over 100 kA, repetition rates from single shot to >180 kHz, and repetitive di/dt capability of greater than $3 \cdot 10^{11}$ A/s. Obviously, a detailed analysis is well beyond the scope of this report. These large dynamic ranges also make it difficult to define a "quality" factor to describe a thyratrons performance in general. Rather, a brief description and review of electrical characteristics of high power thyratron devices will be given followed by a review of the current state-of-the-art in "super power" devices available today.

Modern hydrogen thyratrons come in two basic types, the oxide coated cathode/ceramic or glass envelope and the dispenser cathode/metal envelope. The glass envelope thyratron, illustrated in Figure 1, is the oldest type of tube.

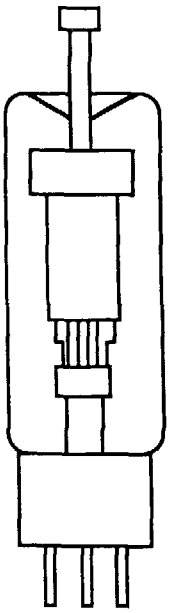

Figure 1. Outline drawing of a glass envelope thyratron.

In the 1920's glass thyratrons were filled with mercury vapor or an inert gas such as Xenon. Mercury and inert gas thyratrons have been superseded by hydrogen filled devices because of the shorter recovery time and the ease of hydrogen storage in titanium hydrides. Even with a higher forward conduction voltage drop in hydrogen, i.e. 100-200 volts, compared to 30

volts for mercury, the advantages of hydrogen with respect to device lifetimes and safety considerations have driven the heavy gas thyratrons to extinction.

Glass envelopes thyratrons are manufactured in two basic styles. The electrode structure is the same in both styles, the difference in how much of the glass envelope is filled by the structure. Both styles behave the same electrically but they require different cooling requirements. For the type that has a large gas volume between the electrode structure and the glass envelope wall, only natural convection is needed for cooling the tube envelope. If forced air is directed on this type of tube, the gas density will increase near the glass wall resulting in a rarification in the electrode structure. If the entire envelope is filled with the electrode structure then forced air cooling on the envelope is acceptable. In either case, air should be directed at the base (as with all thyratron) and the anode connection of either type of tube. Of course, the best environment for any thyratron is oil. Glass tubes, by consequence of construction, are low average power devices although substantial power can be achieved in burst mode and in single shot applications.[74-78].

A typical oxide cathode/ceramic envelope thyratron for use in a short pulse circuit is illustrated in Figure 2.

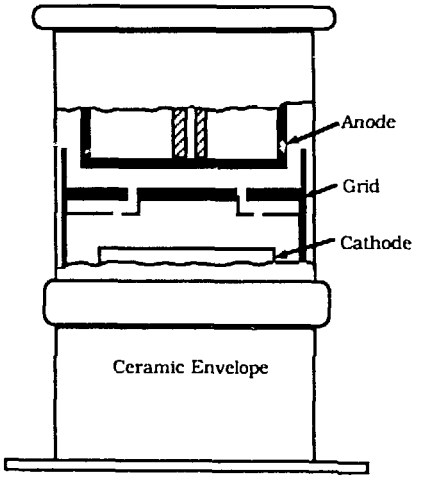

Figure 2. Outline drawing of a ceramic envelope thyratron.

The tube consists of a cathode coated with a mix of calcium, strontium, and barium oxides, a grid(s), and an anode. The basic thyratron is essentially a gridded diode that can conduct in only one direction. In 1978, a new type of thyratron was introduced designed specifically for pulsed lasers [79-81]. This new thyratron , illustrated in Figure 3, incorporated a "hollow anode" which allows the tube to conduct in the reverse direction without arcing. The cavity

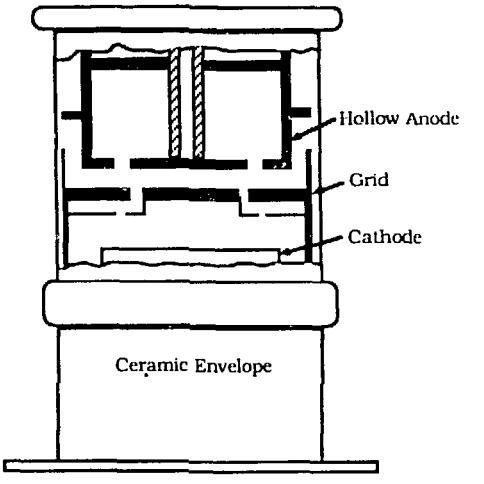

Figure 3. "Hollow Anode" ceramic envelope thyratron.

anode provides a source of electrons to support conduction in the reverse direction. Because of the time varying and extremely low impedance of a laser discharge, efficient matching of the impedance of the energy store to the load is practically impossible. It was proposed that is would be far easier and more economical to develop a switch that will operate in a mismatched circuit, than to attempt to develop nonlinear circuitry to match the load. For this reason, a large development effort was undertaken to advance the hollow anode thyratron [80-82]. Successes with oxide cathode designs were excellent. However the superior power handling capability dispenser cathode/metal envelope thyratrons opened the possibility of making very compact high power modulators. For example, an 11.4 cm diameter, 30 cm long ceramic hollow anode thyratron can switch about 10 kW of average power in a short pulse laser circuit. A dispenser cathode/metal envelope thyratron of the same physical size, can switch approximately three to five times as much power.

This is an ever important consideration as modulators extend into the Megawatt average power range. Higher average power can be switched in a metal envelope thyratron because

of the greater emission properties of the dispenser cathode and the construction methods. A detailed examination of this type of thyratron is given by Cook [83,84]. While the ceramic thyratron is constructed of cup shaped electrodes supported by ceramic tubes, the metal-envelope tube is somewhat more complex. A typical dispenser cathode/metal envelope thyratron is depicted in Figure 4.

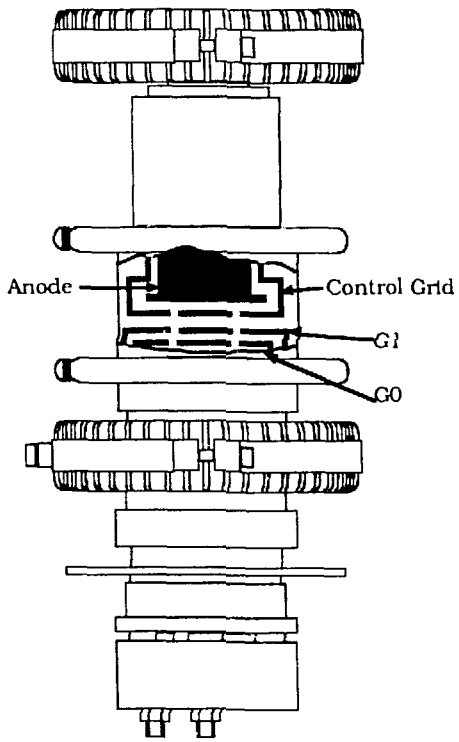

Figure 4 Diagram of a typical dispenser cathode metal-envelope thyratron.

An important feature of this design is the manner in which the massive anode is completely enclosed by the grid structure. This enhances the cooling of the anode and the high voltage recovery of the tube [84]. Also, by increasing the amount of surface area of the electrode structures, namely the grids, exposed to the external environment, the thermal resistant of the envelope is as much as a factor of 10 lower than with the standard cup type electrode design.

Several variations of glass, ceramic, and metal envelope tubes have been developed over the years for particular applications. The "double-ended" thyratron, is a tube that essentially has a cathode on both ends thus it can conduct current equally well in either direction [85,86]. Placing an electron source at both ends of the thyratron greatly increases the recovery time and requires close attention to the circuit design. These types of tubes are of great importance in crowbars and pulsed accelerator magnet circuits [87]. Operation in the tens of kiloampere range at over 100 kV have been demonstrated with double-ended devices.

A thyratron of special importance to high repetition rate circuits is the screen grid version of a pentode thyratron. The addition of a screen grid which is connected to ground via a small impedance, reduces the recovery time thus allowing much high pulse repetition rates. Screen grid thyratrons have demonstrated operation to 180 kpps [88,89].

Another type of pentode thyratron is the triple grid. With this device the third grid is the control grid and the other two are for preionizing the grid cathode volume. This special design allows a line of sight path from the cathode to anode thus reduce anode falltime, higher di/dt operation without excessive heating and arcing and reduced drive power for minimal jitter. Triple grid thyratrons have demonstrated lifetimes of 10^{10} pulses at di/dt rates of $>3 \cdot 10^{11}$ Amperes/second, 500 pps, with a grid aperture current density of 10 kA/cm^2 [69].

Addition of extra grids is also used to increase the level of the applied anode voltage. These grids grade the electric field between the anode and the control grid (which is essentially at ground potential) and are referred to as gradient grids. There are two types of gradient grid designs, the planar and cavity grid [90]. Planar gradient grid tubes should be used when high repetition rates are required. Cavity grids are detrimental to the recovery time, thus limit the upper bound on pulse repetition frequency but allow a higher voltage per gap than the planar counter part.

Hollow Cathodes, Pseudosparks, and Back-Lighted Thyratrons

These devices consist of a very old phenomena that has come of age in the 1980's. Nearly, simultaneously in the U. S. and Germany, an entirely new breed of high power switches was born. All of these technologies have electrical characteristics approaching that of the spark gap but in a diffuse discharge

conduction medium. Current densities of greater than 50 kA/cm^2 [91] have been demonstrated in single devices. Single gap hollow cathode switches have demonstrated >60 kV hold-off and switched >40 kA [92]. Recently, a multigap device [93] was operated at an anode voltage of 100 kV and passed >80 kA in a 100 ns pulse with di/dt in excess 10^{11} A/s. Both of the above cases were at single shot. Research in this technology is very active and promises to deliver, light weight, high gain, low cost switches for the pulse power community in the coming decade. Currently, being a relatively young technology, there are only experimental devices available. For systems now in the final design stages, this, as with the MCT, is most likely not a viable option. But, for systems in the research and development stages, the entire class of hollow cathode switches should be a consideration.

Summary

There are several parameters of interest when discussing high power thyratrons: anode voltage, e_{py}, peak current, i_b, average and RMS currents, di/dt, and pulse repetition rate, prr. In recent years, several major advances have been made in all of these areas. Development is currently underway at various places throughout the U. S. and the U. K. A list of these values for some of the most recent advances in thyratron technology is seen in Table 2 below.

epy	ib	iavg	di/dt A/s	prr Hz	τp	Pavg*	Ref
40kV		30A	small	70	250μs	500kW	95
9kV	18kA	80A	small	10	800μs	{1}	100
60kV	3.5kA		$7 \cdot 10^{11}$	4500	200ns	100kW	90
50kV	50kA -25kA	9A	$3 \cdot 10^{11}$	1000	250ns	500kW	98
25kV	6.5kA	30A	small	1000	6.5μs	360kW	99
40kV	3kA		small	6000	6μs	600kW	97{3}
25kV	7kA	50A	small	1500	5μs	700kW	99
60kV	10kA-5kA	.5A	$3 \cdot 10^{11}$	250	250ns	40kW{2}	69
80kV	80kA	small	$6 \cdot 10^{11}$	5	1μs	small	96

* Continuous duty unless otherwise noted.

{1} 8 Coulombs per pulse, 10 second burst

{2} 10^{10} shot lifetime

{3} Consecutive 100 second burst

Table 2. State-of-the-art in high power thyratron technology.

CONCLUSIONS

We have reviewed just a few of the technologies in the area of high power switching. Choosing the proper switch is a complex quandary of lifetime, performance, cost, system interaction, power, myths, and superstitions. But, with the wide variety of technologies available, there is most likely a switch to fill most every need. The graphs in Figures 5 and 6 are a compilation of switch performance of documented systems [7,8]. These plots display both peak current and charge per pulse versus pulse repetition rate for spark gaps, SCR/thyristors , and thyratrons. This data does not take into account the lifetime or mean-time-to-failure of the switch in question rather, only successful operational experience. All of these cases are from modulators programs that meet the design goal whether it be burst mode of continuous operation. These two graphs are not intended to state the ultimate performance or limits of the technologies but where particular devices have completing the required mission. As one examines Figures 5 and 6 it becomes clear that the operation of a switch can be manipulated to show advantage in one or more particular parameters, a trick often used to promote one particular technology of interest. Because of the wide variety of electrical parameters, a fair comparison of competing switch technologies is difficult at best. One of the better comparisons for "pulse power" switches, is shown in Figure 6. This graph defines the general areas with regard to energy transfer per pulse versus times (pulsewidths) at which the energy is delivered. This data holds true for all cases as long as the average power of the device (and other thermal limitations) are considered. Figure 6 is based on actual commercial available "off-the-shelf" devices for thyratrons and solid state, and the actual performance of custom built spark gaps [94].

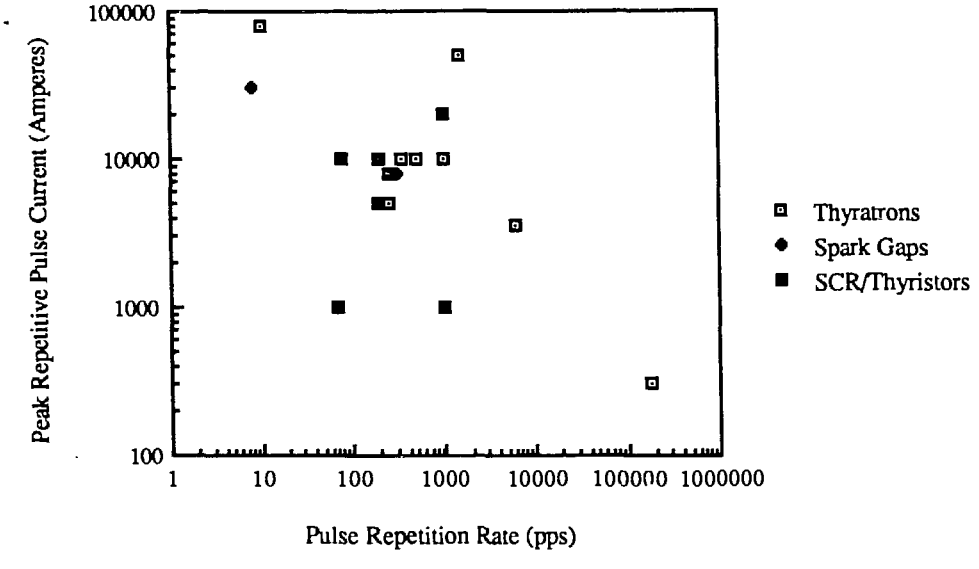

Figure 5. Peak Repetitive Pulse Current vs. Pulse Repetition Rate for Commercial Switches

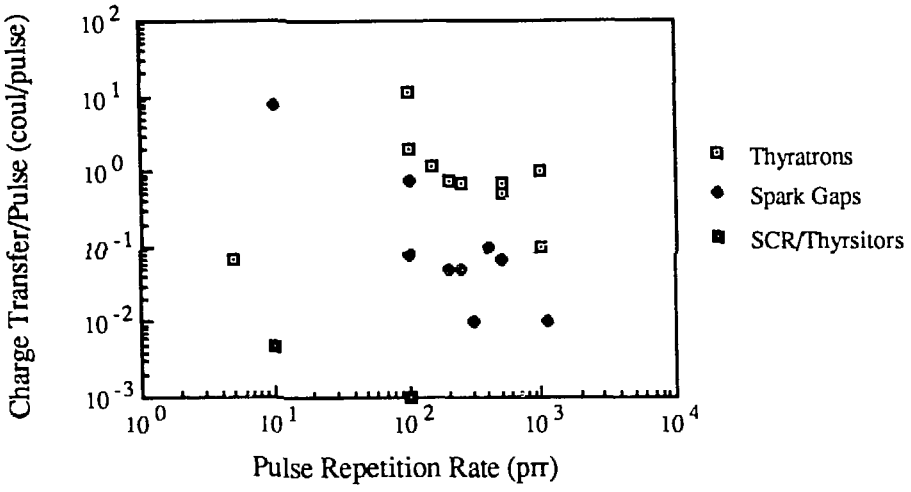

Figure 6. Charge Transfer per Pulse vs. Pulse Repetition Rate for Commercially Available Switches

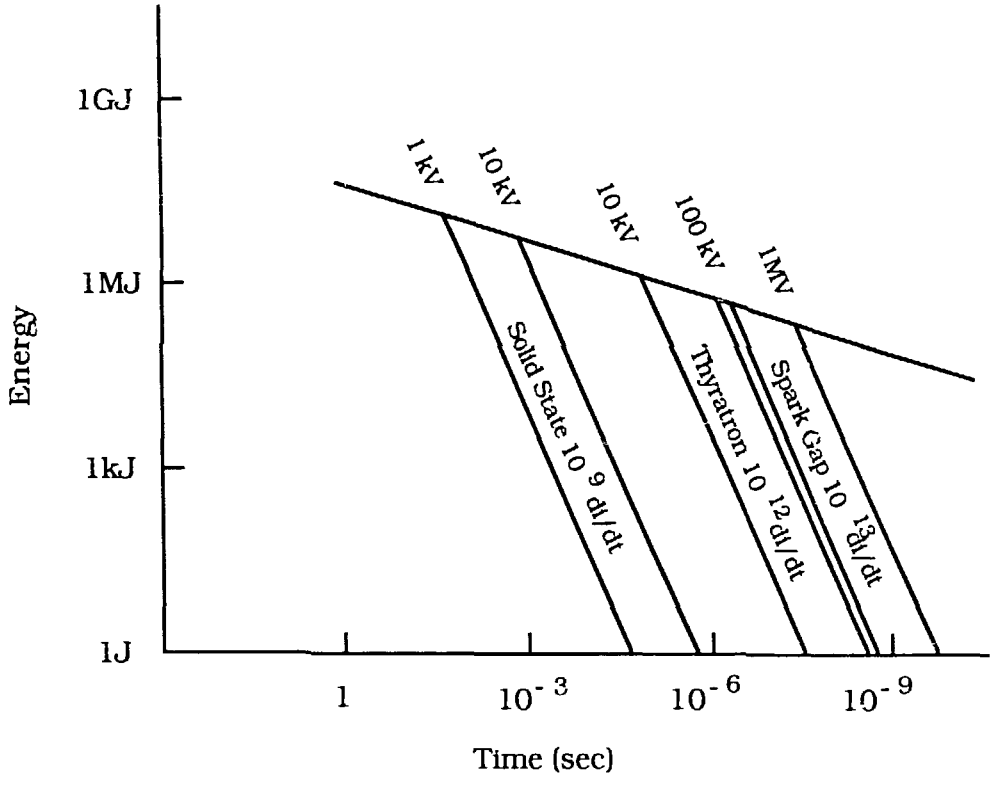

Figure 7. Switch Energy/Power Areas of Repetitive Pulse Operation

The most effective approach in selecting the switch for your particular application is to contact the manufacturer (contrary to popular belief). It is not in the best interest of the manufacturer to sell a potential customer the wrong technology. Most everyone in the high power switch industry is fairly well up to date on current technologies and will recommend the best device for your particular application. All technologies have a place in high power switching, but no one device can meet ever requirement, there is no "ideal switch".

BIBLIOGRAPHY

1. N. Tesla, "Alternating Electric Current Generator," U.S. Patent 447,921 March 10, 1891 and "Method of Operating Arc Lamps," U.S. Patent 447,920, March 10, 1891.

2. N. Tesla, "High Frequency Oscillators for Electro-Therapeutic and other Purposes," American Electro-Therapeutic Association, Buffalo, New York, Sept, 1898.

3. N. Tesla, "Apparatus for Utilizing Effects Transmitted from a Distance to a Receiving Device Through Natural Media," U.S. Patent 685,955, Sept. 8, 1899.

4. J. V. Lebacqz and H. J. White, "The Rotary Spark Gap," from Pulse Generators, McGraw-Hill Book Co., 1946, ch. 8, pp.273-289.

5. J. D. Craggs, M. E. Haine, J. M. Meek, "The Development of Triggered Spark Gaps with a Particular Reference to Sealed Gaps," Metropolitan-Vickers Electric Co., Ltd., Report C-331, Sept. 1942.

6. M. Kristiansen and M. Hagler, "Spark Gaps" from A Critical Assessment of High Power Switches, T. R. Burkes Principle *Investigator, Naval Surface Weapons Center* Report # NP30/78, 1978, ch. 4, pp.176-278.

7. T. R. Burkes, "A Critical Assessment of High Power Switches," Naval Surface Weapons Center, Dahlgren, Virginia, 1976.

8. T. R.Burkes, "A Critical Assessment of High Power Switches Revised Edition," Naval Surface Weapons Center, Dahlgren, Virginia, 1987.

9. J. Vitins, J.L. Steiner, A. Sweitzer, and H. Lawatsch, "Power Semiconductor Devices for Submicrosecond Laser Pulse Generation," IEEE Power Modulator Symposium, Hilton Head Island, SC, June 1988.

10. J.L. Steiner and J. Vitins, "Semiconductor Devices for High Power Pulse Switching," 1989 EPE Conference, Aachen. FRG, October 1989.

11. J. L. Hudgins and W.M. Portnoy, "Fast Transient Behavior of Thyristors Switches," IEEE PESC Record, Toulouse, France, June 1985.

12. J. L. Hudgins and W.M. Portnoy, "Gating of Thyristors for Laser Power Supplies," SPIE Pulse Power for Lasers, Los Angeles, CA January 1987.

13. J. L. Hudgins and W.M. Portnoy, "High di/dt Switching of Thyristors," IEEE Transactions on Power Electronics, vol. PE-2, no.2, April 1987.

14. J. L. Hudgins and W.M. Portnoy, "Gating Effects on Thyristor Anode Current di/dt," IEEE Transactions on Power Electronics, vol. PE-2, no. 2, April 1987.

15. J. L. Hudgins, V. A. Sankaran, W. M. Portnoy, and K. M. Marks, "High di/dt Switching with Thyristors," IEEE Power Modulator Symposium, Hilton Head Island, SC, June 1988.

16. V. A. Sakaran, J. L. Hudgins, and W. M. Portnoy, "Role of Amplifying Gate in the Turn-on Process of Involute Structure Thyristors," IEEE Transactions on Power Electronics, in press.

17. J. B. Gunn, "Avalanche injection in semiconductors," Proc. Phys. Soc., London, vol. B-69, no. 440B, pp. 781-790, August, 1956.

18. A. F. Gibson and J. R. Morgan, "Avalanche injection diodes," Solid-State Elect., vol. 1, no. 1, pp. 54-69, January, 1960.

19. I. V. Grekhov, and A. F. Kardo-Sysoev, and L. S. Kostina, "Breakdown delay and excitation of ionization waves in pn junctions," Sov. Phys. Tech. Lett., vol. 5, no. 8, pp. 399-400, August, 1979.

20. I. V. Grekhov, and A. F. Kardo-Sysoev, L. S. Kostina, and S. V. Shenderei, "High power subnanosecond switch," IEDM Technical Digest, Washington, DC, December 1980, pp. 662-663.

21. I. V. Grekhov, and A. F. Kardo-Sysoev, L. S. Kostina, and S. V. Shenderei, "Initiation of breakdown of pn junctions subject to

overvoltage," Sov. Phys. Tech. Phys., vol. 26, no. 8, pp. 984-985, August, 1981.

22. Y. D. Belinko, et al., "Computer model study of the process of switching of a reverse biased pn junction to a high conductivity state," Sov. Phys. Semicond., vol. 17, no. 10, pp. 1156-1158, October, 1983.

23. A. F. Kardo-Sysoev, V. P. Reshetin, I. G. Tschashnikov, and V. B. Shuman, "Avalanche injection in high speed thyristors," IEEE Trans. El. Dev., vol. ED-23, no. 11, pp. 1208-1211, November, 1976.

24. T. J. Pickens and W. C. Nunnally, "Investigation of optically gated silicon controlled rectifiers operating at 77 K, " IEEE Pulsed Power Conf., Monterey, CA, June 1989.

25. V. M. Volle, V. B. Voronkov, I. V. Grekhov, and V. A. Kozlov, "High current thyristor switched by microsecond light pulses," Sov. Phys. Tech. Phys., vol. 30, no. 8, pp. 909-912, August, 1985.

26. I. V. Grekhov, A. F. Kardo-Sysoev, and A. V. Kriklenko, "Control of high power semiconductor switches by microwave radiation," Sov. Phys, Tech. Phys., vol. 16, no. 10, pp. 1109-1112, October, 1982.

27. J. H. Hur, et al., "GaAs based opto-thyristor for pulsed power applications," IEDM Tech. Dig., Washington, DC, December, 1989, pp.15.5.1-15.5.4.

28. D. Meyerhofer, A. S. Keizer, and H. Nelson, "A light activated semiconductor switch," J. Appl. Phys., vol. 38, no. 1, pp. 111-123, January, 1967.

29. I. V. Grekhov, and A. F. Kardo-Sysoev, "Subnanosecond current drops in delayed breakdown of silicon pn junctions, " Sov. Phys. Tech. Lett., vol. 5, no. 8, pp. 395-396, August, 1979.

30. H. Egawa, "Avalanche characteristics and failure mechanism of high voltage diodes," IEEE Trans. El. Dev., vol. ED-13, no. 11, pp. 754-758, November, 1966.

31. P. L. Hower and V. G. K. Reddi, "Avalanche injection and second breakdown in transistor," IEEE Trans. El. Dev., vol. ED-17, no. 4, pp. 320-335, Aprils, 1970.

32. Y. Mizushima and Y. Okamoto, "Properties of avalanche injection and its application to fast pulse generation," IEEE Trans. El. Dev., vol. ED-14, no. 3, pp. 146-157. March, 1967.

33. I. V. Grekhov, M. E. Levinshtein, and V. G. Sergeev,"Some new possibilities of fast switching of large area pnpn structures," Sov. Phys. Semicond., vol. 10, no. 2, pp. 206-208, February, 1976.

34. A. F. Kardo-Sysoev, "Distribution of the potential in pnpn structures during switching transients," Sov. Phys. Semicond., vol. 5, no. 12 pp. 2039-2040, June, 1972.

35. A. F. Kardo-Sysoev, I. G. Chashnikov, and V. B. Shuman, "Avalanche injection in thyristors," Sov. Phys. Semicond., vol. 8, no. 6, pp. 718-720, December, 1974.

36. A. V. Gorbatyuk, I. V. Grekhov, S. V. Korotkov, L. S. Kostina, and N. S. Yakovchuk, "New possibilities for rapid high power switching by devices of the thyristor type," Sov. Tech. Phys. Lett., vol. 8, no. 6, pp. 298-299, June 1982.

37. I. V. Grekhov, A. V. Gorbatyuk, L. S. Kostina, S. V. Korotkov, and N. S. Yakovchuk, "Superpower switch of microsecond range," Solid-State Electron., vol. 26, no. 11, pp. 1132, November, 1983.

38. W. C. Nunnally and R. B. Hammond, "80 MW photoconductor power switch," Appl.Phys. Lett., vol. 44, no. 10 pp.980-982, May, 1984.

39. R. A. Petr, W. C. Nunnally, and C. V. Smith Jr., "Switching performance of a cryogenic silicon photoconductive switch," J. Appl. Phys., vol. 63, no. 8, pp 2839-2847, April, 1988.

40. B. L. Thomas and W. C. Nunnally, " Recent developments in the investigation of surface flashover on silicon photoconductive power switches," IEEE Pulsed Power Conf., Monterey, CA, June, 1989

41. G. M. Loubriel, M. W. O'Malley, and F. J. Zutavern, "Toward pulsed power uses for photoconductive semiconductor switches," IEEE Pulsed Power Conf., Arlington, VA, June, 1987, pp. 145-148.

42. G. M. Lobriel et al., "High current photoconductive semiconductor switches," IEEE Power Mod. Sym., Hilton Head Island, SC, June, 1988, pp, 312-317

43. C. H. Lee, "Picosecond optoelectronic switching in GaAs," Appl. Phys. Lett., vol 30, no. 2, pp. 84-86, January, 1977.

44. S. Williamson, G. F. Albrecht, and G. Mourou, "Laser triggered Cr:GaAs HV sparkgap with high trigger sensitivity," Rev. Sci. Instrum., vol. 53, no. 6, pp. 867-870, June, 1982.

45. R. L. Druce, M. D. Pocha, K. L. Griffin, and W. W. Hofer, "Subnanosecond linear GaAs photoconductive switching," IEEE Pulsed Power Conf., Monterey, CA, June, 1989.

46. A. Kim, et al., "Bulk GaAs photonic devices with two opposite gridded electrodes," IEEE Pulsed Power Conf., Monterey, CA, June, 1989.

47. G. M. Loubriel, F. J. Zutavern, H. P. Hjalmarson, and M. W. O'Malley, "Closing photoconductive semiconductor switches," IEEE Pulsed Power Conf. Monterey, CA, June, 1989.

48. F. J. Zutavern, et al., "Photoconductive semiconductor switch recovery," IEEE Pulsed Power Conf. Monterey, CA, June, 1989.

49. A. Yamashita and Y. Osada, "A new switching effect in semi-insulating GaAs and its use for deep level spectroscopy," Japan. J. Appl. Phys., vol. 25, no. 11, pp. 1684-1690, November, 1986.

50. J. B. Gunn, "Instabilities of current in III-V semiconductors," IBM J. Res. and Devel., vol. 8, no. 2, pp. 141-159, April, 1964.

51. I. V. Grekhov, M. E. Levinshtein, V. G. Sergeev, and I. M. Yassievich, "Switching characteristics of a laser stimulated semiconductor switch," Sov. Phys. Tech. Phys., vol. 24, no. 5, pp 597-601, May, 1979.

52. I. V. Grekhov and I. M. Yassievich, "Theory of an optoelectronic diode power switch," Sov. Phys. Semicond., vol;. 13, no. 9, pp. 996-1002, September, 1979.

53. A. Rosen, P. J. Stabile, D. W. Bechtle, et al., "Optically achieved pin diode switch utilizing a two-dimensional laser array at 808 nm as an optical source," IEEE Trans. El. Dev., vol. 36, no. 2, pp. 367-374, February, 1989.

54. A. Rosen, et al., "100 kW DC biased all semiconductor switch using Si pin diodes and GaAs 2d laser arrays," IEEE Photonics Tech. Lett., vol. 1, no. 6, pp. 132-134, June, 1989.

55. I. V. Grekhov, M. E. Levinshtein, and V. G. Sergeev, "Homogeneous optical switching of large area semiconductor structures," Sov. Phys. Semicond., vol. 8, no. 4, pp. 431-434, October, 1974.

56. J. R. Davis, "A theoretical model of light fired thyristors," IEEE PESC Record, Culver City, CA June, 1975, pp. 305-312.

57. O. S. F. Zucker et al., "High power semiconductor switching in the nanosecond regime," IEEE Power Mod. Sym., New York, NY, February, 1976, pp. 1253-1256.

58. J. R. Davis and J. S. Roberts, "Ultra-fast high power laser activated switches," IEEE PESC Record, Cleveland, OH, June, 1976.

59. O. S. F. Zucker, J. R. Long, V. L. Smith, D. J. Page, and P. L. Hower, "Experimental demonstration of high power, fast risetime switching in silicon junction semiconductors," Appl. Phys. Lett., vol. 29, no. 4, pp. 261-263, August, 1976.

60. L. R. Lowry and D. J. Page, "Light Activated semiconductor switches," NAECON Record, Dayton, OH, May, 1977, pp. 616-622.

61. L. R. Lowry, "Optically activated switch," Westinghouse R&D Center Technical Report AFAPL-TR-78-17, Pittsburgh, PA, April, 1978.

62. P. G. McMullin and L. R. Lowry, "Optical drive requirements for laser activated semiconductor switches," IEEE Power Modulator Sym., Buffalo, NY, June, 1978, pp. 159-162.

63. I. V. Grekhov and I. N. Yassievich, "Theory of high power thyristor optoelectronic switch," Sov. Phys. Tech. Phys., vol. 14, no. 9, pp. 1038-1043, September, 1980.

64. V. M. Volle, et al., "High power nanosecond thyristor switch controlled by a light pulse," Sov. Phys. Tech. Phys., vol. 26, no. 2, pp. 225-228, February, 1981.

65. Conversations with Sol Schnieder, 1989.

66. I. Langmuir, "Electric Discharge Controlling Device and Method of Operating the Same," U.S. Patent 1,289,823, Dec. 31, 1918.

67. Los Alamos National Laboratory, Operating Log for the WNR Fast Extraction Kicker Magnet, Group P-9.

68. Stanford Linear Accelerator Center, Operation Log of the Beam Line Thyratron Modulators, 1974.

69. G. McDuff and K. Rust, "Life extension of thyratrons in short pulse circuits with the use of saturable magnetic sharpeners," IEEE Power Modulator Symposium, San Diego, CA, 1990. (Submitted)

70. K. J. Germeshausen,, S. Goldberg, D. F. Riley, "Research Study on Hydrogen Thyratrons...Volumes I,II, & III," Edgerton, Germeshausen, & Grier, Inc. Boston, Massachusetts, 1953, 1956, & 1957.

71. T. B. Fogel'son, L. N. Vagin, L. N. Breusova, "Impulse Hydrogen Thyratrons," Soviet Radio, Moscow, 1974.

72. T. A. Voronchev, "Impulse Thyratrons," Soviet Radio, Moscow, 1958.

73. D. Turnquist, S. Friedman, R. Caristi, S. Merz, "The effects of inductance and plasma growth on the current rise rate in ultra-fast high power hydrogen thyratrons," Advanced Copy to be Published, 1980.

74. L. L. Reginato and R. E. Hester, "Overview of the ETA/ATA Pulse Power," IEEE Fourteenth Pulse Power Modulator Symposium, June, 1980.

75. E. G. Cook and L. L. Reginato, "Off-resonance transformer charging for 250 kV water Blumlien," IEEE Tran. Elec. Dev., vol. ED-26, no. 10, October, 1979.

76. L. L. Reginato, "Advanced test accelerator (ATA) pulse power technology development," IEEE Tran. Nuc. Science, vol. NS-28, no. 3, June, 1981.

77. M. A. Newton, D. L. Birx, C. W. Ollis, L. L. Reginato, M. E. Smith, and J. A. Watson, "Design and testing of the 5 kHz, 3 MW thyratron modulators for the ETA II," IEEE Power Modulator Symposium, Hilton Head Island, SC, June 1988.

78. R. L. Snelling, B. P. Newton, A. Andrews, and I. Littlewood, "High rate of rise of current pulse generation using low cost glass envelope thyratrons," International Pulse Power Conf., Lubbock, Texas, November, 1976.

79. H. Menown, and C. V. Neale, "Thyratrons for short pulse laser circuits," IEEE Thirteenth Pulse Power Modulator Symposium, June, 1978.

80. G. McDuff, "Test and Evaluation of the CX-1574 Thyratron," EEV Technical Reprint, EEV Co. Ltd., Chelmsford, Essex, England, CM1 2QU, 1983.

81. G. McDuff and K. Rust, "Evaluation of bidirectionally conducting thyratrons for pulsed excimer lasers," IEEE Sixteenth Power Modulator Symposium, June 1984.

82. G. McDuff and K. Rust, "A Short Note on Hollow Anode Metal Envelope Thyratrons for High-Power High Repetition-Rate Lasers," EEV Technical Reprint 159, EEV Co. Ltd. Chelmsford, Essex, England, CM1 2QU, 1985.

83. K. G. Cook, "A high power metal envelope deuterium thyratron," Sixth Symposium on Hydrogen Thyratrons, 1960.

84. K. G. Cook, "A compact metal-ceramic deuterium thyratron," Seventh Symposium on Hydrogen Thyratrons and Modulators, 1962.

85. H. Menown and B. P. Newton," A multigap, double ended hydrogen thyratron," IEEE Eleventh Modulator Sym., September, 1973.

86 N. S. Nicholls, H. Menown, and R. J. Wheldon, "Double-ended hydrogen thyratrons for crowbar protection of high power TWT systems," Thirteenth Power Modulator Sym., Buffalo, NY, June, 1980.

87. W. E. Hannant, C. Rowe, and H. Menown," The use of a double-ended hydrogen thyratron for crowbar applications," IEEE Twelfth Modulator Symposium, New York, NY, February, 1976.

88. L. J. Kettle and R. J. Wheldon, "A triple grid thyratron," IEEE Twelfth Modulator Sym., February, 1978.

89. G. A. Hill and T. R. Burkes," High frequency thyratron evaluation," International Pulse Power Conf., Lubbock, Texas, October, 1976.

90. C. A. Pirrie, P. D. Culling, H. Menown, and N. S. Nicholls, "Performance of a compact four gap thyratron in a high voltage high repetition rate circuit," IEEE Power Mod. Sym., Hilton Head Island, SC, June, 1988, pp. 141-146.

91. G. Kirkman, T. Y. Hsu, R. L. Liou, and M. A. Gundersen, "Recent experimental studies of the BLT switch," IEEE Pulse Power Conf., Monterey, CA June, 1989.

92. J. Bernardes and T. Houghton, presented at the 1989 NATO Advanced Research Workshop on Physics and Applications of High Power Hollow Cathode Glw Switches, Lillehammer, Norway, July, 1989.

93. T. Y. Hsu, G. Kirkman, R. L. Liou, H. Figeroa, and M. A. Gundersen," Multigap BLT's for high power applications," IEEE Pulse Power Conf., Monterey, CA June, 1989.

94. T. R. Burkes, "Scaling pulse generators for lasers," Proc. Pulse Power for Lasers, SPIE, vol. 735, pp. 99-100, Los Angeles, CA, January, 1987.

95. R. Legg, T. Russel, and D. Turnquist, "Design and test of a 600 kW, 25 Ampere average, long pulse modulator," IEEE Power Mod. Sym., Hilton Head Island, SC, June, 1988, pp. 75-79.

96. K. Rust, "1 MV repetition rated modulator," IEEE Power Mod. Sym., Hilton Head Island, SC, June, 1988, pp.52-53.

97. IT&T, F-266 Performance Data

98. EEV, CX1700HA Performance Data

99. EEV, CX-1700 Performance Data

100. EEV, CX-1710 Performance Data

Prime Power Systems and Charging Circuits

W. C. Nunnally
Applied Physical Electronics Research Center
The University of Texas at Arlington

Introduction

Magnetic switches[1] in pulse compression circuits can be used to obtain peak power gain and provide load voltages, load currents, and load pulse rates not obtainable with other technologies. However, magnetic switches will not sustain dc voltages and thus an input pulse to the magnetically switched pulse compression system must be provided using conventional means. The two major methods of generating the input pulse to a magnetic pulse compression system are 1) capacitor discharge, inductor circuits using conventional switches such as thyratrons, BLT's, spark gaps, etc. or 2) repetitive sinusoidal and quasi-sinusoidal generators such as the common alternator and the compulsator, respectively.

The average power delivered to the load plus the average power dissipated in losses in the system must be provided by the prime power source through the charging system. This paper discusses the methods used to provide the average power required in repetitive pulse, magnetic pulse compression systems.

II. Switched Pulse Generation Circuits

The generation of an input pulse for a magnetic pulse compression circuit is dependent upon the capabilities of the switch and the resonant circuit response. The most common method of generating an input pulse is to discharge a capacitor through an inductor to charge the first capacitor section of the pulse compression network as illustrated in Fig. 1. Note that the procedure is the same if a series or parallel pulse compression system is used. Once the system voltage and the stored energy are specified, the output capacitance, C_2, is determined. The voltage on the output capacitor is given by

$$V_{c2}(t) = \frac{V_o \cdot C_1}{C_1 + C_2} \cdot (1 - \cos\omega t) \quad (1)$$

where the charge time, T_c, is equal to one half the resonant period or

$$T_c = \frac{T}{2} = \pi \left| L \cdot \frac{C_1 \cdot C_2}{C_1 + C_2} \right|^{1/2} \quad (2)$$

and L is the inductance of the series inductor. In this common circuit, the value of C_1 is chosen

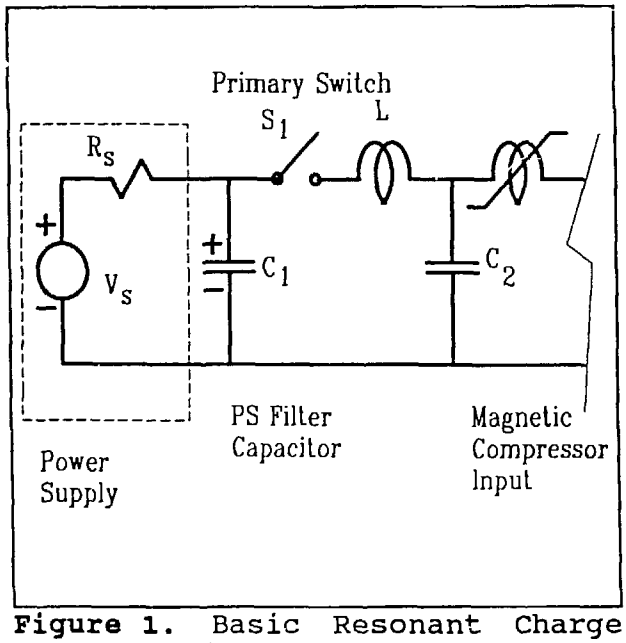

Figure 1. Basic Resonant Charge Circuit

in light of the following considerations. Usually, the value of C_1 is chosen to be much larger than the value of C_2 such that the peak voltage on capacitor C_2 is equal to twice the charge voltage on C_1. In this case, capacitor C_1 is the filter capacitor of the power supply and charging C_2 from C_1 removes only a portion of the energy stored in C_1 and the load voltage has been increased by a factor of two. Note that the value of C_1 can be chosen equal to C_2 such that the peak voltage on C_2 will be equal to the charge voltage on C_1 and all of the energy stored in C_1 will be transferred to C_2. This arrangement is used when faults are perceived to be a problem, but results in another charging stage to recharge C_1 between pulses.

The next component of concern is the inductor through which the energy must be transferred. In the case that C_1 is much larger than C_2, the inductance can be related to the charge time and the energy transferred, E_T, through

$$L = \left| \frac{V_o \cdot T_c}{2 \cdot \pi} \right|^2 \left| \frac{1}{E_T} \right| \qquad (3)$$

The switch current, and the inductor current, is given by

$$I_s(t) = V_o \cdot \left| \frac{C_T}{L} \right|^{1/2} \cdot \sin\omega t \qquad (4)$$

where C_T is the series combination of C_1 and C_2 and the resistance in the circuit, R_s, is such that

$$R_s << \left| \frac{L}{C} \right|^{1/2} \qquad (5)$$

The input current pulse to the magnetic pulse compression circuit

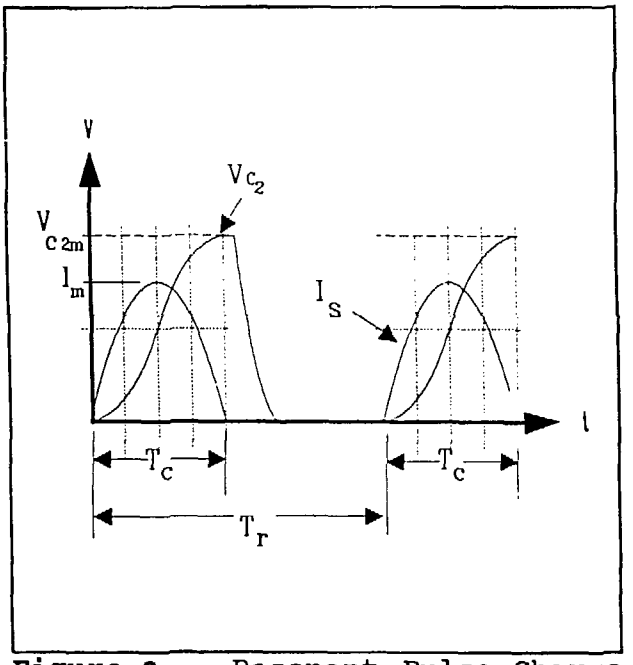

Figure 2. Resonant Pulse Charge Waveforms

is sinusoidal as shown in Fig. 2. In a resonant pulse charge system, the switch illustrated in Fig. 1, is not used such that the capacitor C_2 is connected directly to the power supply filter capacitor, C_1. In this case, capacitor C_2 begins to recharge immediately after the pulse has been injected into the magnetic pulse compression line. For a repetitive system, this arrangement produces a constant pulse rate. A second alternative is to add a charge switch, S_c, between the power supply filter capacitor, C_1 and load capacitor, C_2 such that the pulse rate can be varied on command. This use of a charging switch arrangement is termed a command charge system.

The charging inductor, L, shown in Fig. 1, is assumed to be a linear inductor without magnetic material. However, the use of a magnetic switch in this location has the following specific advantages: 1) the rise of the switch current is delayed until the switch voltage has dropped to a small value which reduces switching losses, and 2) the

voltage applied to the switch after switching is reduced because of the large, unsaturated switch inductance.

If the pulse is repeated with a pulse separation of T_r, the average and rms values of the charging current, in the absence of resistance are given by

$$I_{avg} = V_o \cdot \left| \frac{C_T}{L} \right|^{1/2} \cdot \frac{T_p}{\pi \cdot T_r} \qquad (6)$$

and

$$I_{rms} = V_o \cdot \left| \frac{C_T \cdot T_p}{2 \cdot L \cdot T_r} \right|^{1/2} . \qquad (7)$$

The average and rms values are important in determining the specifications for the switching devices, the energy dissipated in the inductor resistance, and the power supplied by the power supply. The average power of an pulse generation system is dependent upon the average power capabilities of the primary switches used

Magnetic pulse compressors require extreme repeatability in the time integral of the input voltage pulse. Since the saturation time of the first magnetic switch is dependent upon the time integral of the input voltage pulse, the pulse to pulse regulation of the capacitor charge voltage is of prime importance. Conventional power supplies voltage regulation can be specified as 0.1 percent while maintaining reasonable costs.

However, magnetic pulse compression systems can require pulse to pulse voltage regulation or consistencies of up to $^{2}0.01$ percent or one part in 10^{-4}. This requirement can be met using the common de-Q circuit approach, illustrated in Fig. 3, in which the voltage across the capacitor is monitored during the resonant charge process. A second winding on the charging inductor and a "De-Q" switch are added to the resonant pulse charge system, as illustrated in Fig. 3. When the voltage on capacitor C_2 reaches the desired value, the "De-Q" switch is closed and the remaining energy stored in the charging inductor is diverted to the resistor. Other circuit arrangements can be used to reroute the excess energy back to the power supply filter capacitor. This arrangement is termed a "De-Q" circuit because closing the "De-Q" switch places the De-Q resistor, effectively, in series with the charging circuit and thus reduces the circuit Q.

The second method of generating an input pulse for a magnetic pulse compression system is through the use of a transformer. Specifically, this paper discusses 1) a common pulse transformer with a high coupling coefficient ($k \approx 0.99$) and 2) a dual resonant pulse transformer with a relatively low coupling coefficient ($k \approx 0.6$). The advantages of using a pulse transformer are dc isolation of primary and secondary, voltage or

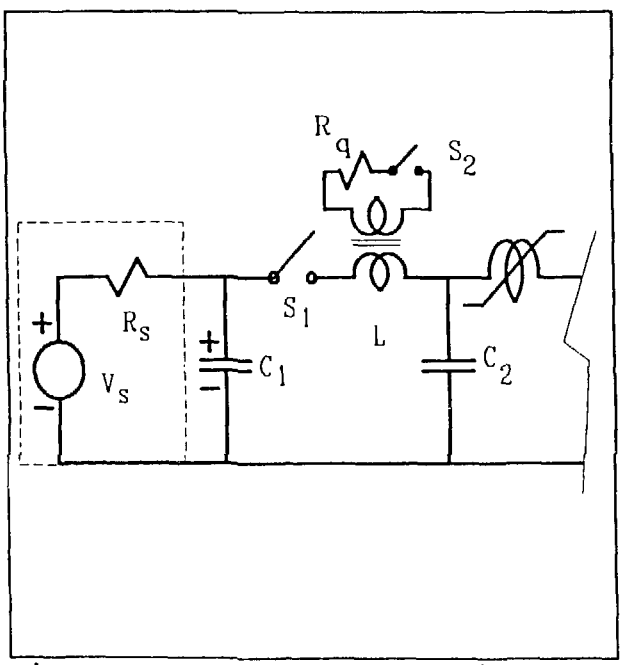

Figure 3. Resonant Charging De-Q Circuit

current scaling, and in the case of the resonant transformer, unique switch and voltage characteristics. Two arrangements using a high coupling coefficient transformer pulse generation circuit are shown in Fig. 4. The capacitor to be

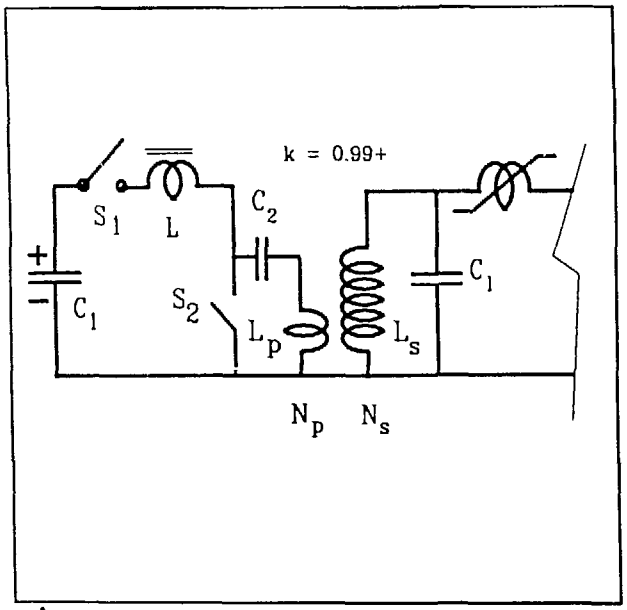

Figure 4. Transformer Pulse Generation Circuit

discharged through the transformer primary is first pulse charged as previously discussed. The choice of circuit arrangement of the capacitor and switch relative to the transformer determines the system operation. In Fig. 4a. the capacitor is charged independent of the transformer and then switched into the transformer. In Fig. 4b, the capacitor is charged through the transformer primary. When the switch is closed, the capacitor discharge current flows in the opposite direction through the transformer so that the charge current can be used to reset the transformer magnetic system (if used). The transformer can be modeled using the equivalent circuit shown in Fig. 5.. The primary leakage inductance, L_{pl}, the secondary leakage inductance, L_{sl}, and the magnetizing inductance, L_m, on the primary side of the transformer are related to the

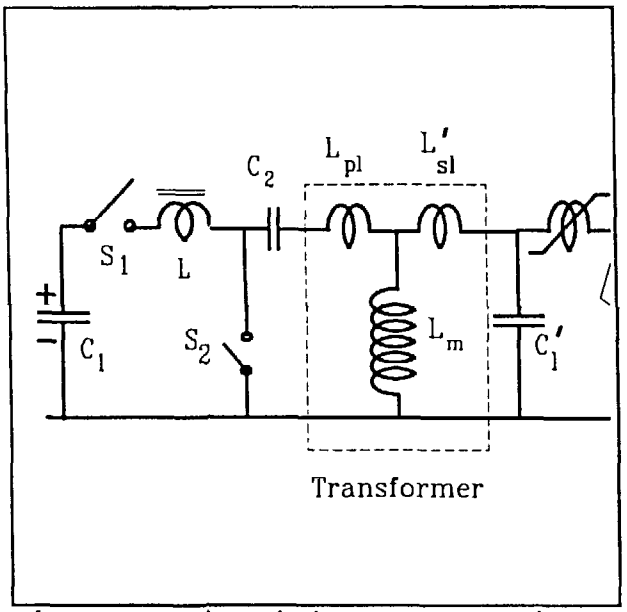

Figure 5. Simplified Capacitor-transformer Pulse Generation Circuit

transformer primary inductance, L_p, and secondary inductance, L_s, by

$$L_{pl} = (1-k)\cdot L_p \qquad (8)$$

$$L_{sl} = (1-k)\cdot L_s\cdot (N_p/N_s)^2 \qquad (9)$$

$$L_m = k\cdot L_p \qquad (10)$$

where N_p and N_s are the number of primary and secondary turns, respectively. In addition, the load capacitance, C_l, and inductance L_l, of the first stage of the magnetic pulse compressor can also be reflected to the primary as

$$C_l' = (N_s/N_p)^2\cdot C_l \qquad (11)$$

$$L_l' = (N_p/N_s)^2\cdot L_l \qquad (12)$$

where C_l' and L_l' are the inductance values seen in the transformer primary.

Thus the simplified circuit for the capacitor discharge through the transformer primary is shown in Fig.5. In a high coupling

coefficient transformer, the magnetizing inductance is usually much larger than the leakage inductances so that it can be neglected in Fig. 5. In this case, the current and voltage waveforms are identical to those for the resonant pulse charge circuit discussed previously. Thus the switch current has the form $I_o \cdot \sin\omega t$ and the output capacitor voltage has the form of $(1-\cos\omega t)$. Ideally, the current through the pulse generation switch and the voltage through the switch would go to zero and remain thus after the output pulse has been generated until the capacitor must be resonantly recharged. However, the ideal conditions do not exist because the rate of current change is large at the current zero and the small current through the transformer magnetizing inductance is sufficient to make switch recovery difficult.

This problem can be reduced by placing a small magnetic switch or saturable inductor in series with the primary switch. This arrangement has the following advantages: 1) the current rise is delayed until the switch voltage drops which reduces switching losses and 2) the saturable inductor delays the voltage applied to the switch after switching during recovery.

The coupling coefficient of high voltage step-up transformers is rarely close to unity because of the insulation and thus spacing required between primary and secondary due to the voltage differential. When the coupling coefficient much less than unity (0.6-0.9), a dual resonance transformer circuit, illustrated in Fig. 6., in which the resonant frequency of the primary and the secondary are made equal or $L_p \cdot C_{p_3} = L_s \cdot C_s$, can be used. Earlier work

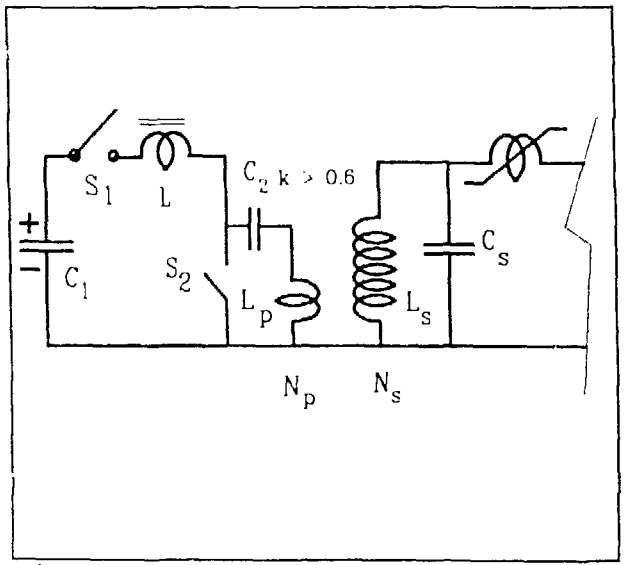

Figure 6. Dual Resonant Transformer Pulse Generation Circuit

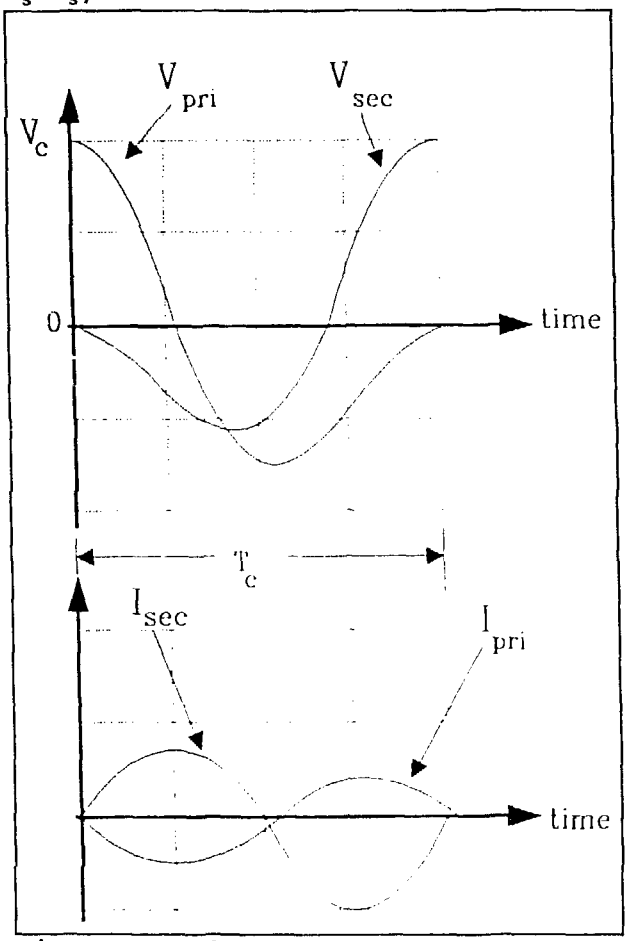

Figure 7. Off-Resonance Transformer Charging Waveforms

determined that when the coupling coefficient is 0.6 and the primary and secondary have equal resonant frequencies, the current and voltage waveforms illustrated in Fig. 7. result. Figure 6 indicates that the primary capacitor voltage, the primary current, and the secondary current all go to zero with minimum slope and that the secondary capacitor voltage reaches its peak value at the same time. For these conditions, the energy transfer efficiency of the circuit is near unity, even with a non-unity coupling coefficient that exists in high voltage transformers.

In addition, transformers with a coupling coefficient less than unity, but not equal to 0.6 may be used. Note from Fig. 4, the "T" model of the transformer, that a smaller value of the coupling coefficient, k, increases the leakage inductance. Thus, the effective coupling coefficient of any transformer can be modified by adding series inductances to the primary and secondary of the transformer.

One further component must be added to transformer pulse generation circuits to reduce the voltage transients produced by the energy stored in stray inductances and capacitances. These components are best designed using circuit analysis codes and accurate placement and values of stray capacitances and inductances.

III. Power Supply Circuits

The power supply must provide the average load power and the average loss power to the filter capacitor. In magnetic pulse compression systems, the power supply voltage regulation has a major role in determining the output pulse temporal reproducability. Therefore, the power supply output voltage regulation should be sufficient to result in a output pulse time deviation that is compatible with the range of dynamic, magnetic switch biasing systems. Usually, the output voltage regulation and ripple can be minimized by using multiple phase rectifier circuits and a minimum power supply series impedance. These concepts are discussed very thoroughly in manufacturers handbooks and power supply design manuals. Conventional power supply designs can provide regulation to within 0.1 percent at reasonable cost.

IV. Alternator Power Systems

The most common method of producing repetitive, sinusoidal input pulses to magnetic pulse compression systems is the common alternator.[1,4] Several advantages of the common alternator include: 1) an intermediate dc power supply is not required, 2) pulse generating switches are not required, 3) bipolar pulse generation is possible and/ or the magnetic switches do not require resetting, and 4) relatively large average powers are possible.

However, the average power and the peak power from an alternator are roughly equal and the maximum pulse rate is limited by the frequency of the alternator output.

In general, the average power available from a simple, single phase alternator is given by

$$P_o = V_{rms}^2/(\omega \cdot L_s + R_s) \qquad (13)$$

where V_{rms} is the rms voltage, L_s is the series inductance, and R_s is the series resistance, which can generally be neglected. The inductance of the generator is given by

$$L_s = \frac{\mu_o \cdot N_w^2 \cdot l_w \cdot \pi \cdot r_r}{l_g \cdot N_p} \qquad (14)$$

where μ_o is the permeability of free space (air gap), N_w is the number of winding turns, l_w is the length of the winding, l_g is the length of the

air gap, and N_p is the number of magnetic poles around the circumference of the machine rotor with radius r_r. The basic dimensions and winding arrangement for a simple, single phase alternator are illustrated in Fig.8. The rms voltage induced in the output windings is given by

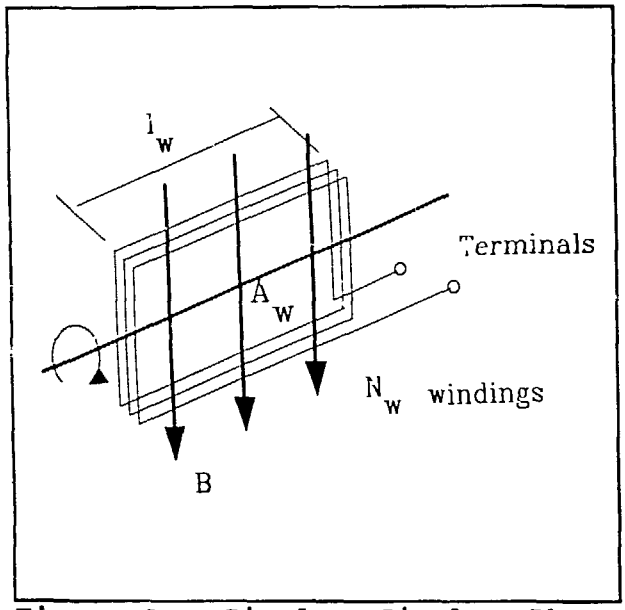

Figure 8. Simple Single Phase Alternator

$$V_{rms} = \pi \cdot N_w \cdot B_{rms} \cdot l_w \cdot \omega \cdot r_r \cdot N_p^{-1} \quad (15)$$

where B_{rms} is the rms value of the magnetic field around the machine circumference. Since the maximum value of the magnetic field is about 1.5 Tesla, the rms field is about 1 Tesla. If the maximum rotor tip velocity is defined by $v_{max} = \omega \cdot r_r$, then, using the above equations, the maximum output power from an alternator, per unit winding length, l_w, is given by

$$P_o/l_w = \frac{B_{rms}^2 \cdot v_{max} \cdot l_g}{\mu_o \cdot N_p} \quad (16)$$

For a maximum tip velocity of 500 m/s, the maximum average power available from a single phase alternator is about 4 MW. Alternators have been developed for use in systems similar to that shown in Fig. 9. In the circuit of Fig. 9, one cycle of the alternator output is used to charge the first or load capacitor, C_2. When the capacitor reaches full voltage, the first magnetic switch, S_1, saturates to transfer the pulse forward for further compression. Note that the full cycle charge from the inductive source impedance alternator is very similar to the dual resonance transformer charge of the load capacitor discussed earlier. In the case that a full cycle is used to charge the first stage capacitor, the magnetic switches must be reset between pulses.

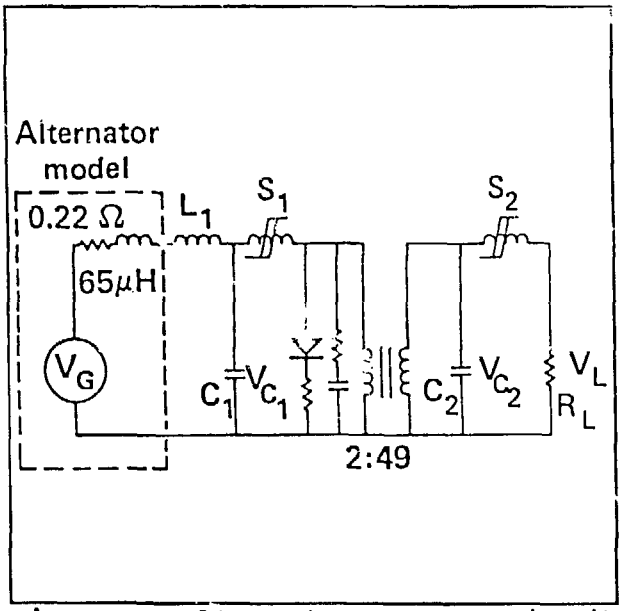

Figure 9. Alternator Source Circuit for Magnetic Pulse Compression

V. Conclusions

This survey has emphasized that magnetic pulse compressors require the generation of an input pulse that is then compressed and amplified by the magnetic system. The two major methods of generating the input pulses are 1) capacitor

discharge-charge, either directly or through a transformer, and 2) rotating machines such as the alternator. Capacitor discharge techniques are limited by the average and rms power and current parameters of the switches used. Transformer systems provide voltage gain as well as pulse generation and impedance scaling. Magnetic switches in series with the electronic switches reduce switching losses by delaying the current rise until the switch voltage has dropped to its conduction voltage.

Alternator input pulse generators provide naturally repetitive input pulses without intermediate dc power supplies and primary switches which greatly reduces the complexity of the system. However, peak and average powers from single phase alternators are limited at high frequencies by the series inductance of the machine.

Both of the above methods of generating input pulses for magnetic pulse compression systems can be operated at multi-megawatts. Improvements in primary switches such as back lighted thyratrons will increase the average power performance parameters of present day systems. Improvements in alternators such as the compensated pulsed alternator with minimal series inductance will increase the average power level from rotating machines.

VI. References

1. W. S. Melville, "The Use of Saturable Reactors as Discharge Switches for Pulse Generators," Proceedings of Electrical Engineers, Radio and Communication, Volume 98, Part 3, No. 53., p. 185, 1951.

2. M. A. Newton and J. A. Watson, "Timing and Voltage Control of Magnetic Modulators on ETA II," Proceedings of the 7th IEEE International Pulse Power Conference, Monterrey, CA, p. 175, June 1989.

3. E. G. Cook and L. Reginado, "Off Resonance Transformer Charging for 250 kV Water Blumlein," IEEE Transactions on Electron Devices, Vol. ED-26, P. 1512, Oct. 1979.

4. R. Kihara and H. C. Kirbie, "An Alternator-Driven, Magnetically Switched Modulator," Proceedings of the 6th IEEE International Pulse Power Conference, Arlington, VA, p. 246, June 1987.

FLUX COMPRESSORS FOR SUBMILLISECOND PULSES

W. F. Weldon, M. L. Spann, and S. B. Pratap
Center for Electromechanics
The University of Texas at Austin
10100 Burnet Road, Bldg. 133
Austin, TX 78756-4497
(512) 471-4496

Abstract

The Center for Electromechanics at The University of Texas at Austin (CEM-UT) has been developing specialized pulsed power supplies for a variety of applications. The compensated pulsed alternator (compulsator) was invented [1] at CEM-UT in 1978. At that time, it was developed as a power supply to drive laser flashlamps. Since then, due to its tremendous potential, it has been applied to diverse fields such as fusion, directed energy weapons, low frequency sound sources, electromagnetic (EM) launcher, and a variety of industrial applications. Several of these machines have been built and tested, successfully demonstrating the principle of operation. This paper provides an overview of short (< 1 ms) pulse-width compulsators. A brief background is presented first followed by a discussion of the state of the art air-core compulsators and their capabilities. Some insight into the means of further reducing the pulse width is also provided.

INTRODUCTION

The compulsator is a specialized alternator in which primary consideration has been given to maximizing the power generating capability. Several techniques are employed to reduce the internal impedance of the device and increase its terminal voltage. As in a conventional alternator, voltage is produced by the relative motion of a multipole armature and field. Higher voltages can be generated by increasing the excitation field strength, the relative speed of the two components, or by increasing the length of the armature. The tip speed of the rotor is generally limited by material strength or dynamic issues. Field strength is dependent on the saturation level of ferromagnetic material or by the allowable current density of the excitation conductors. The third alternative is practically achieved by using a multiturn winding. However, since the internal impedance increases with the square of the number of turns, a gain in output current is not achieved.

The main difference between compulsators and conventional alternators is achieved through the use of compensation. This term refers to a method of reducing armature inductance through compensating currents which limit the volume occupied by the armature current fields. The total magnetic flux produced by the armature is reduced, and the field is contained between the armature and the compensating conductors. Compensation can be provided by a variety of methods. Depending upon the method of compensation, the inductance of the machine can be made to vary with the relative position of armature and compensating conductors or it can be made constant at a low value. Manipulation of the inductance variation is the primary method of achieving a desired pulse shape and increasing power through flux compression. Three basic methods of providing compensation have been explored.

Passive compensation is achieved when the compensating currents are induced in response to the transient armature field produced during discharge. The simplest form of this machine involves the use of a continuous conductive shield (fig. 1a). Since the shield is continuous, equal compensation is obtained in all rotor positions resulting in a constant low inductance. The passive compulsator generates essentially sinusoidal current pulse shapes.

Compensation can also be provided by a second winding which is connected in series with the armature winding (fig. 1b). This is referred to as active compensation and forces the compensating currents to flow in a defined sense. When the magnetic axes of the compensating and armature windings are aligned and aiding, maximum inductance is obtained. When the two axes are *aligned and opposing, minimum inductance is* obtained. Compression ratios (Lmax/Lmin) as high as 46 have been measured in a relatively small device. The *actively compensated machine* generates a narrow pulse of very high peak power. Power is enhanced in this device since additional voltage related to the changing inductance is generated under load.

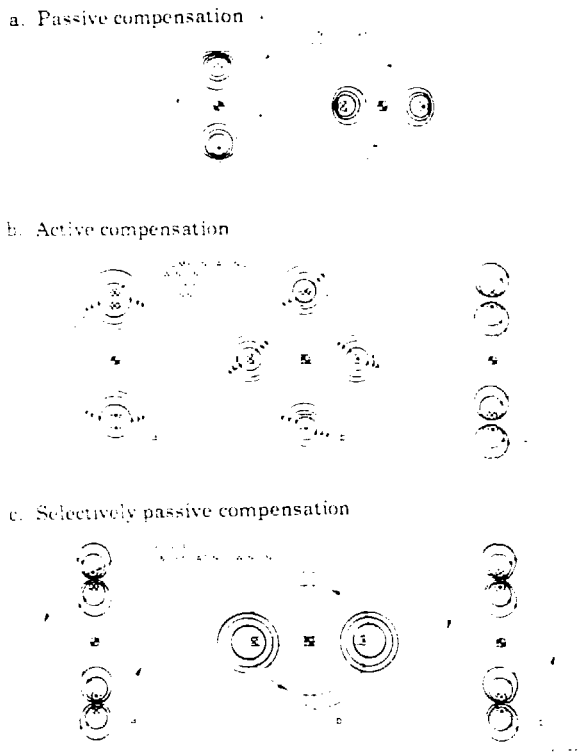

Figure 1. Compensation methods

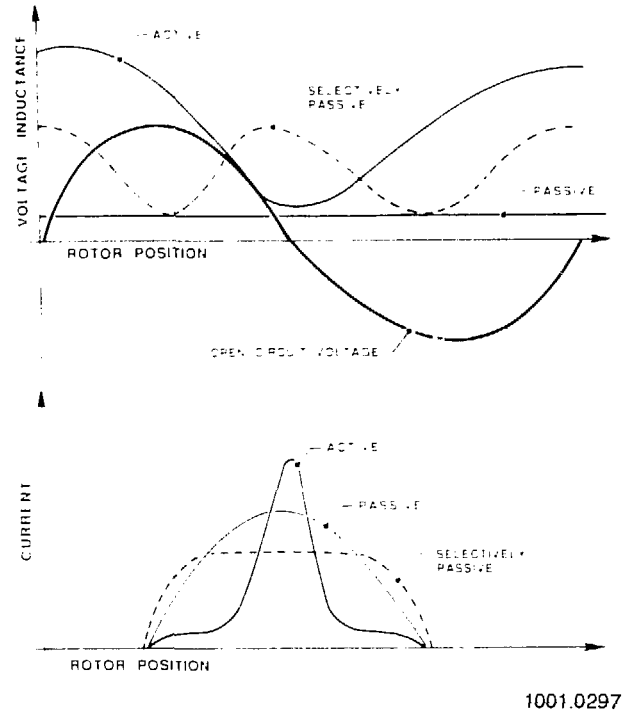

Figure 2. Inductance variation and current waveshapes

Another form of compensation, selective passive compensation (fig. 1c), results in a square pulse shape. This technique is dubbed selectively passive compensation since the currents are induced but compensation is not provided equally in all rotor positions. This can be implemented in several ways, including nonuniform shielding or shorted compensating windings. The currents induced in the compensating component are never in phase with the armature currents and therefore this machine has a lower compression ratio than the active machine. Also, the frequency of the inductance variation is twice the machine electrical frequency.

Inductance variation and typical output current pulses are presented for the three types of machines in figure 2. The active machine uses inductance variation to increase the peak power and decrease the pulse width. The selective passive machine uses inductance variation to produce a square-shaped pulse at the expense of peak power. The passive design has an inductance which is constant at the lower value.

In most applications requiring short pulse widths, the actively compensated machine is employed. As the base frequency of the compulsator is increased, the volt-seconds per pulse supplied by the excitation field decrease. This drastically limits the output power available from the original compulsator concept for pulse times below 100 μs. In order to overcome this limitation, the required volt-seconds are supplied initially by an external source such as a capacitor or even another compulsator. Such a machine would not have a field winding and is referred to as the rotary-flux compressor.

HISTORICAL BACKGROUND

During the 1970's, Lawrence Livermore National Laboratory (LLNL) was developing a laser fusion facility and had a need for high power, short duration electrical pulses. LLNL had steadily increased the peak power of the device using capacitor banks as the primary pulsed power source. However, it was soon realized that capacitors could not supply the series of repetitive pulses which were ultimately required.

The Engineering Prototype Compulsator

Since short pulses of very high power were desired, an actively compensated machine was chosen for development. The prototype shown in figure 3 is a vertical shaft, rotating armature machine. It was designed to generate an open-circuit voltage of 6 kV at a maximum speed of 5,400 rpm and deliver approximately 70 kA, 600-μs pulses into a flashlamp load. At the design speed the machine stored 3.4 MJ and the single phase, four-pole winding operates at an open-circuit frequency of 180 Hz.

The prototype machine was discharged into the flashlamp load a total of 27 times and successfully demonstrated the principle of operation. On the most successful run (from 4,800 rpm), the machine delivered 140 kJ to the load at a peak current of 30 kA and a pulse width of 1.3 ms.[2] On the first attempted discharge from full speed, a short circuit developed in the rotating armature. The armature insulation was composed of fiberglass tape which had been preimpregnated with epoxy. This system had adequate mechanical and dielectric strength but left many voids in the insulation. It is theorized that these voids compromised the dielectric strength resulting in the failure. The prototype machine did however indicate areas of necessary improvements for the following machines.

Active Rotary Flux Compressor (ARFC)

In order to develop new insulation techniques and prove that higher compression ratios were possible, the active rotary flux compressor was fabricated. The ARFC has an overall diameter of 0.51 m (20 in.), a rotor diameter of 0.20 m (8 in.), and weighs approximately 450 kg (1,000 lb). The machine (fig. 4) is an actively compensated, four-pole device with a laminated rotor and stator. The device produced a compression ratio of 46:1 and a current gain of 15:1 into a resistive load. The pulse width obtained from this machine was less than 600 μs (full width half maximum [FWHM]) at a peak current of 17 kA. Table 1 shows some of the short circuit test results of this machine and figure 5 shows the current pulse obtained from this machine.

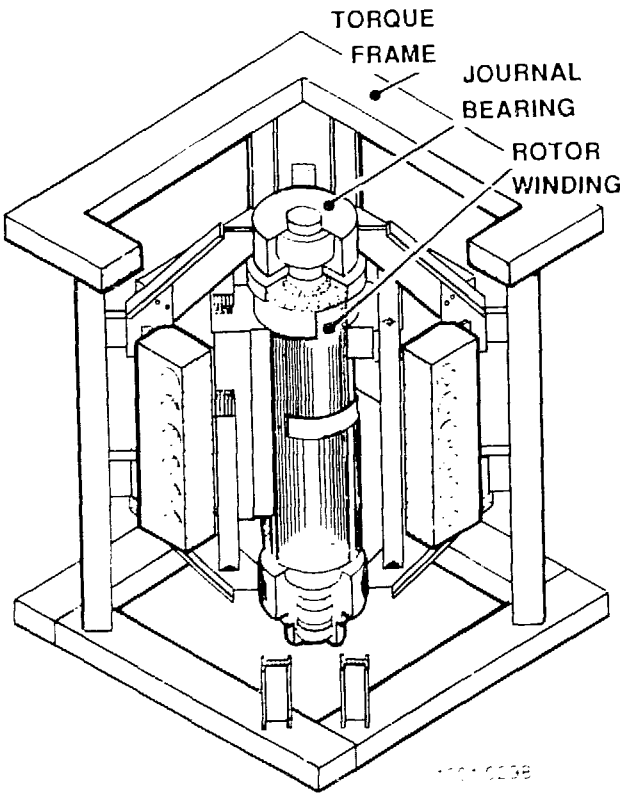

Figure 3. Prototype compulsator

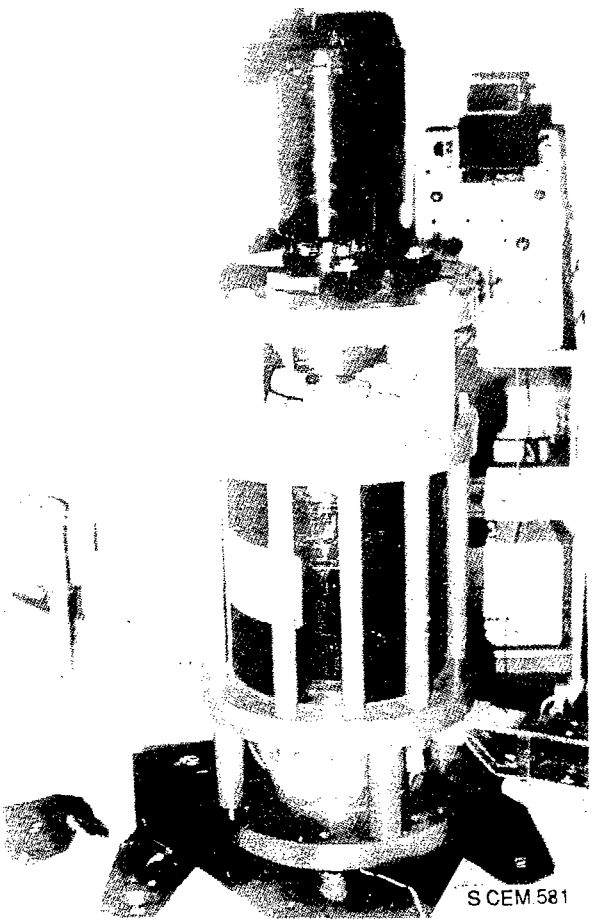

Figure 4. Active rotary flux compressor

Table 1. Short circuit test results of the ARFC

Circuit Parameter	Run #34 Minimum Pulse Width	Run #36 Maximum Pulse Width
Rotor Inertia ($J\text{-}s^2$)	0.39	0.39
Rotor Speed (rpm)	5,600	5,680
Bank Capacitance (μF)	182	369
Bank Voltage (kV)	2.5	3.0
Injection Current (kA)	1.01	1.81
Peak Current (kA)	17.1	25.6
Pulse Width (FWHM) (μs)	590	791

Figure 5. Machine current for run no. 36

Several design studies were conducted in order to use the active device for various applications. Typical applications along with corresponding machine characteristics are discussed below.

10 MJ Active Rotary Flux Compressor for Driving Xenon Flashlamps

An eight pole, drum type active rotary flux compressor was designed to replace an 85% efficient 10 MJ (stored) capacitor bank for driving xenon flashlamps for solid-state lasers.[3] The conceptual machine had a rotor diameter of 1.1 m and would have delivered 8.5 MJ at 18 kV from a speed of 2,648 rpm. The peak current was 750 kA at a pulse width of 670 μs (FWHM). An 800 kJ, 22 kV startup capacitor bank was required to establish the initial magnetic flux in the machine. Figure 6 shows the cross section of the 10-MJ ARFC. Tables 2 and 3 give the physical and performance parameters of the machine. The peak output power of this machine would have been 13 GW. The conclusion of this

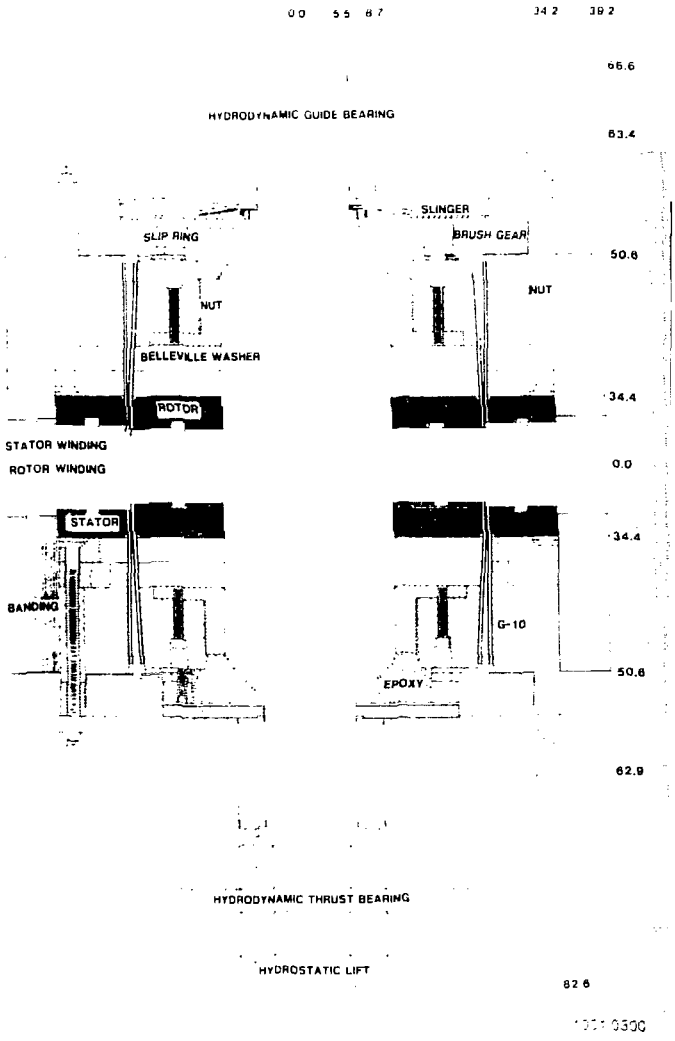

Figure 6. 10 MJ ARFC cross section

study was that the active rotary flux compressor appears to have the best potential of any device for repetition rated short bursts (50 to 100 Hz) or continuous pulsed power (1 to 10 Hz) applications.

Application of the ARFC for Prime Energy Stores for Particle Beam Accelerators

The particle beam fusion accelerators (PBFA I and II) developed by Sandia National Laboratories are equipped with 36 Marx generator modules. These generators provide power to the accelerator through an intermediate storage capacitor, two pulse-forming lines, and a converging magnetically insulated transmission line for each sector. The

Table 2. Physical parameters of the 10 MJ ARFC

Number of Poles	8	
Number of Conductors per Pole	3	
Rotor Speed	2,680	rpm
Laminated Rotor Diameter	1.067	m
Lamination Tip Speed	150	m/s
Laminated Rotor L/D	1.64	
Overall L/D	2.25	
Shaft Length	3.0	m
Shaft Diameter	0.52	m
Outer Winding Diameter	1.090	m
Mechanical Clearance	0.32	cm
Rotor Inertia	2,120	kg-m^2
Total Rotor Mass	15,650	kg
Inner Stator Diameter	1.096	m
Outer Stator Lamination Diameter	1.532	m
Stator Stack Length	1.750	m
Stator Mass (laminations & winding)	11,800	kg
Maximum Stator Diameter	2.10	m
Total Stator Length	2.58	m
Total Stator Mass with Housing	20,500	kg
TOTAL MASS	36,000	kg

Table 3. Performance parameters under load of the 10 MJ ARFC

Peak Current	754	kA
Peak Terminal Voltage	17.8	kV
Peak Output Power	13.4	GW
Peak Torque	61.9	MN-m
Peak Mechanical Power	16.6	GW
Initial Speed	2,680	rpm
Final Speed	2,500	rpm
Polar Moment of Inertia	2,120	kg-m^2
Inertial Energy Stored	84	MJ
Discharge Efficiency, η_l *	76	%
Peak Armature mmf	2.26	MA-t/pole
Peak Air Gap Flux Density	8.5	T
Maximum Magnetic Pressure	28.7	MPa
	(4,170)	(psi)
Armature Temperature Rise	14	°C
Effective Mechanical Shear Area	4.6	m^2
Maximum Average Shear Stress	25.1	MPa
	(3,640)	(psi)

same approach has also been used in the preliminary conceptual design of a light ion target development facility. The complexity and relatively high cost of Marx generators make it worthwhile to pursue alternate, potentially less expensive methods to provide pulsed power for future accelerators. Active rotary flux compressors were evaluated to charge capacitors for both single shot and short-burst duty. The basic load voltage of a single unit was 600 kV when the terminal voltage is boosted by a step-up pulse transformer. Therefore two rotary flux compressors connected in series to the primary of a 2:60 pulse transformer obtain 1 to 2 MV depending on the load impedance. Figure 7 shows the circuit schematic of the proposed system. Tables 4 and 5 give the physical and performance parameters of one unit required for this application. A total of 12 machines would be required for the target development facility.

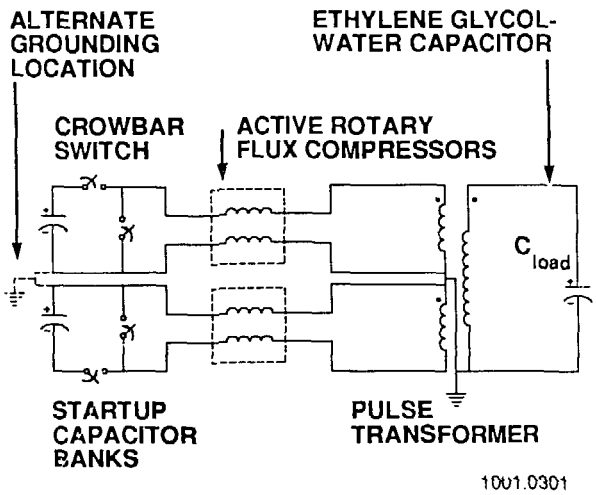

Figure 7. Active rotary flux compressor system

Other Applications

Around 1982, EM launchers received great attention. The compulsator once again proved to be an appropriate power supply for these launchers due to its single element pulse-conditioning capability. Typically, these applications require pulse widths greater than 1 ms; however, they drove the continued development of compulsator technology. The first machine built and tested for these EM launchers was iron-cored and utilized passive compensation since there was no constraint on the pulse shape. As the demands on the performance of these machines increased, it was necessary to go to air-core machines. Air-core machines (which use

Table 4. Physical parameters of the ARFC for particle beam accelerator

Number of Poles	8	
Number of Conductors per Pole	3	
Rotor Speed	3,520	rpm
Laminated Rotor Diameter	0.813	m
Lamination Tip Speed	150	m/s
Laminated Rotor L/D	1.64	
Overall L/D	2.25	
Shaft Length	2.34	m
Shaft Diameter	0.49	m
Outer Winding Diameter	0.83	m
Mechanical Clearance	0.32	cm
Rotor Inertia	550	kg-m^2
Total Rotor Mass	8,700	kg
Inner Stator Diameter	0.84	m
Outer Stator Lamination Diameter	1.17	m
Stator Stack Length	1.33	m
Stator Mass (laminations & winding)	5,324	kg
Maximum Stator Diameter	1.53	m
Total Stator Length	1.9	m
Total Stator Mass with Housing	11,400	kg
TOTAL MASS	20,100	kg

Table 5. ARFC performance of the ARFC for particle beam accelerators

Peak Current	618	kA
Peak Load Voltage	20.9	kV
Delivered Energy	3.85	MJ
Pulse Width (FWHM)	496	μs
Current Gain	11.9	
Energy Gain	21.8	
Maximum Air-Gap Flux Density - B_0	30.5	T
Maximum torque (τ = 4,000 psi)	3.07×10^7	N-M
C_{load}	17.6	mF
C_{start}	1.5	mF
V_{start}	15.0	kV
θ_{mo}	-0.908	rad

fiber reinforced epoxy composite structures) helped to raise some of the constraints on tip speed and excitation flux density, thus greatly enhancing the power density of the machines.

These air-core machines are being developed under two separate projects at present. The power capability of these machines when tested will be 16 GW and 650 MW at a power density of 727 kW/kg and 900 kW/kg, respectively.

Air-Core Machines

A characteristic of these new machines is the absence of ferromagnetic material in the magnetic circuit and they are therefore referred to as "air-core" compulsators. The gains in power density cited above have been made possible by applying fiber/epoxy composite technology to rotating electrical machinery. Fiber/epoxy composites have greater strength and modulus-to-density ratios. This combination allows them to be spun at high tip speeds. High rotational speeds have made it possible to alleviate some of the limitations due to the bond strength of epoxy and also increased the energy density of the machine. Simultaneously research has increased the bond shear strength of the epoxy from 24 MPa (3,800 psi) to 55 MPa (8,000 psi).

Iron-core machines are attractive because they reduce the excitation power requirements but they are therefore limited by the saturation flux density in iron. Air-core machines by their very nature require higher excitation currents. Therefore, it is not an advantage to limit the excitation field strength to 2 T as with iron-core machines. The limitation on excitation field strength in air-core machines is determined by thermal considerations or mechanical strength and deflection consideration for the field-coil conductors. These limitations are generally higher than the saturation field strength in steel. The thermal limit can be made a secondary consideration by pulse charging the field so that the field coil is on only for a short time prior to and during the main discharge pulse. The excitation field strength then is only limited by mechanical considerations.

Tip Speeds

Flywheels for applications other than electrical machinery have been built which can attain tip speeds in excess of 1,200 m/s. Two internal rotor air-core compulsators have been designed at tip speeds in the 500 to 600 m/s range. Using an external

wheel type rotor and radially thin windings, the tip speeds can potentially be raised up to 1,200 m/s.

Voltage and Current Capabilities

The peak voltage generated per unit length per pass of the machine is given by

$$\overline{E} = \overline{v} \times \overline{B}$$

where

v = tangential velocity of the winding
B = peak radial component of the excitation field

Table 6 gives a comparison of these values for iron-core and air-core compulsators. This clearly shows an increase in generated voltage of over five times per unit length as compared to iron-core machines.

Table 6. Comparison of voltage capabilities

TYPE	VELOCITY (m/s)	RADIAL FIELD (T)	E (V/m)
Iron Core	200.0	2.0	400.0
Air Core	550.0	4.0	2,200.0

Since the same generator voltage can be obtained with a shorter machine or fewer number of turns, the machine inductance is also lower. This combination helps to enhance the peak current and therefore the power capability of the machine, especially while driving low impedance loads.

Compression Ratio

For the same physical disposition of the windings, the minimum inductance of an air-core and iron-core compulsator is about the same. However, the maximum inductance is significantly different for the two cases, especially when considering the unsaturated inductance of the iron-core machine. The result is that the compression ratio obtained for identical winding geometries could be lower by an order of magnitude in the case of the air-core machines, compared to iron-core machines. The compression ratio is of importance to the extent that it affects the pulse width (full width half maximum). The minimum short circuit pulse width is given in seconds by:

$$\Delta t_{\frac{1}{2}} = \frac{2}{p\omega_m} \cos\left(\frac{CR-3}{CR-1}\right)$$

where

ω_m = mechanical speed of the rotor
p = number of pole pairs
CR = compression ratio

Figure 8 shows the change in pulse width with the tip speed for an air-core compulsator. Also shown on the same plot is the pulse width obtained from an identical iron-core machine at a tip speed of 150 m/s, which is the maximum tip speed possible for a laminated rotor. This plot shows that for the same geometry an air-core machine must have a tip speed in excess of 600 m/s in order to reduce the pulse width below the saturated-iron case. This tip speed is not only possible but is at the bottom range of the tip speed possible for air-core machines.

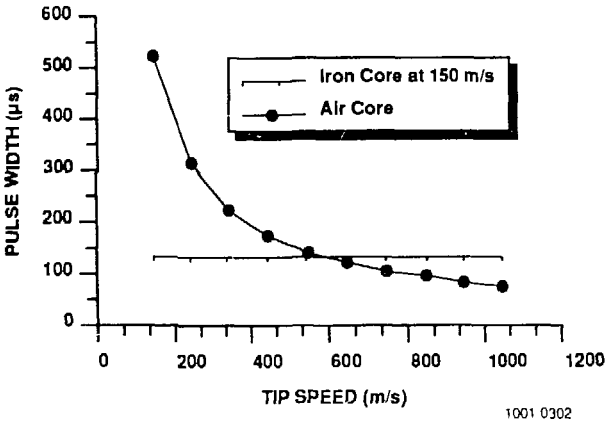

Figure 8. Pulse width as a function of tip speed for air-core machines

The compression ratio of an air-core machine varies as

$$\frac{t}{g} + 1$$

whereas the compression ratio of an iron-core machine varies as

$$\left(\frac{t}{g}\right)^2$$

where

t = pole pitch of the winding
g = effective gap of the armature and compensating winding

Thus the air-core machines have a lower compression ratio but are less sensitive to the ratio of the pole pitch to effective gap.[4]

CURRENT STATUS

Using the knowledge gained from the design of large pulse width air-core, fiber-composite machines, a conceptual design was undertaken for a short pulse width capacitor driver. This machine was required to drive a recirculating linear accelerator. The compulsator/ARFC would charge dielectric cavities through a pulse transformer to 1.5 MV. The desired pulse length was about 25 μs and a repetition frequency of about 5,000 rep/s. The pulse energy required to be stored in each cavity was 50.6 kJ with a total of 36 cavities.

The total energy required to be delivered per pulse was 1.82 MJ. This was more than what could be delivered by a single machine in a period of 25 to 30 μs. It was therefore decided that nine machines would be used, each charging four cavities.

Each machine would have counterrotating rotors and store 106 MJ inertially. The estimated mass is 2,000 kg. The physical and performance parameters would be as indicated in tables 7 and 8, respectively.

CONCLUSION

The use of air-core, composite filament wound machines have raised the design constraints considerably. This has enabled the development of compact high power density machines. New pulse shaping methods have been invented. These are currently being implemented in the development of high power machines which deliver large amounts of energy in times greater than a millisecond.

Table 7. Machine parameters for the recirculating linear accelerator

Number of Poles	14	
Outer Rotor Diameter	0.64	m
Tip Speed of Outer Rotor	760	m/s
Inner Rotor Diameter	0.5	m
Tip Speed of Inner Rotor	600	m/s
Active Length of Machine	1.0	m
Inertially Stored Energy	106	MJ
Maximum Machine Inductance	48.5	μH
Minimum Machine Inductance	2.89	μH
Compression Ratio	16.8	
Number of Conductors per Pole	2	
Peak Open Circuit Machine Voltage	40.0	kV
Winding Thickness	1.0	mm
Winding Resistance	22.0	mΩ
Maximum Excitation Field	1.2	T
Near Armature Winding Angular Frequency (Mechanical) of Both Rotors	2,400	r/s
Electrical Frequency	5,350	Hz

Table 8. Performance parameters for the recirculating linear accelerator

Peak Current	542	kA
Current Half Width (FWHM)	33	μs
Energy Delivered	202.5	kJ
Energy from rotors	350.0	kJ
Efficiency	58	%
Energy from Rotors/Energy Stored	0.33	%
Peak Discharge Torque	6.0×10^6	N-m
Peak Shear Stress	3,000.0	psi
Peak Radial Pressure	2,500	psi
Peak Power	28.0	GW
Armature Conductor Temperature Rise	9.5/pulse	°C

These new concepts can be applied to develop machines with pulse widths much smaller than a millisecond.

BIBLIOGRAPHY

[1] M.L. Spann, S.B. Pratap, M.D. Werst, W.A. Walls, and W.G. Fulcher, "Compulsator Research at The University of Texas at Austin — an Overview," *IEEE Transactions on Magnetics*, vol 25, no. 1, Jan 1989, pp 529-537.

[2] S.B. Pratap, M.L. Spann, and W.A. Walls, "Air-Core Compensated Pulsed Alternators," presented at the 7th IEEE Pulsed Power Conference, Monterey, CA, June 11-14, 1989.

[3] M.L. Spann, W.L. Bird, W.F. Weldon, and H.H. Woodson, "The Design, Assembly, and Testing of an Active Rotary Flux Compressor," presented at the 3rd IEEE International Pulsed Power Conference, Albuquerque, NM, June 1-3, 1981.

[4] S.B. Pratap, W.L. Bird, G.L. Godwin, and W.F. Weldon, "A Compulsator Driven Rapid-Fire EM Gun," presented at the 2nd IEEE Symposium on Electromagnetic Launch Technology, Boston, MA, October 11-14, 1983.

REFERENCES

[1] W.F. Weldon, H.H. Woodson, M.D. Driga, U.S. Patent 4,200,831, April 29, 1980.

[2] B.M. Carter, B.T. Merritt, and W.L. Gagnon (LLNL), W.L. Bird, W.F. Weldon, and R.C. Zowarka, "Driving Parallel Flashlamps with a Compensated Pulsed Alternator," presented at the 14th Pulsed Power Modulation Symposium, Orlando, FL, June 6, 1980.

[3] C.A. Morgan, W.L. Bird, and W.F. Weldon, "A 10 MJ Active Rotary Flux Compressor for Driving Xenon Flashlamps," presented at at the 4th IEEE International Pulsed Power Conference, Albuquerque, NJ, June 6-8, 1983.

[4] W.F. Weldon, W.L. Bird, M.D. Driga, K.M. Tolk, H.H. Woodson, and H.G. Rylander, "Fundamental Limitations and Design Considerations for Compensated Pulsed Alternators," *Proceedings of the 2nd IEEE Pulsed Power Conference*, June 12-14, 1979, Lubbock, TX.

Core Cooling and Dielectrics Group

COATING POSSIBILITIES FOR MAGNETIC SWITCHES

D.J. Sharp, H.C. Harjes, G.A. Mann, and F.A. Morgan
Sandia National Laboratories Division 1841
Albuquerque, N.M. 87185.

ABSTRACT

High average power magnetic pulse compression systems are now being considered for use in several applications. Such systems will require high reliability magnetic switches (saturable inductors) that are very efficient and have long lifetimes. One of the weakest components in magnetic switches is their interlaminar insulation. Considerations related to dielectric breakdown, thermal management of compact designs, and economical approaches for achieving these needs must be addressed. Various dielectric insulation and coating materials have been applied to Metglas foil in an attempt to solve the complex technical and practical problems associated with large magnetic switch structures. This work reports various needs, studies, results, and proposals in selecting and evaluating continuous coating approaches for magnetic foil. Techniques such as electrophoretic polymer deposition and surface chemical oxidation are discussed. We also propose continuous photofabrication processes for applying dielectric ribs or spacers to the foil which permit circulation of dielectric liquids for cooling during repetitive operation.

INTRODUCTION.

In order for a magnetic switch to meet the requirements of high average power applications, its insulation must satisfy several needs. The insulation must have sufficient dielectric strength to endure the voltages which develop between laminations and have a long lifetime in the operating environment (i.e., at elevated temperatures, in a liquid dielectric such as oil, etc.) and not significantly degrade the magnetic properties of the laminations. In addition to these requirements, there are several additional characteristics that would be desirable in the insulation.

A minimum insulation thickness is desirable so that the cores packing factor (fraction of core crossectional area occupied by magnetic material) is maximized. It would also be desirable to have an insulator with a high thermal conductivity. This would aid in the thermal management of core losses. In most applications the width of the insulation extends beyond the width of the magnetic material so that a margin is formed on both sides of the core. If the thermal conductivity of the insulation is low, the margins will form substantial thermal barriers making thermal management in the core more difficult. It is therefore desirable to minimize the length of the margins.

Conventional insulating materials, (lacquers, SiO_2, MgO_2, etc.) used in electric motor and AC power transformer cores, are good insulation choices for low speed magnetic switches (i.e. for switching times on the order of 100μs or more when the interlaminar voltages are a few volts or less). However, in many applications, switching speeds are much faster, approaching a few tens of ns, and the interlaminar voltages can approach 1kV. For these applications, thin dielectic films such as Mylar, polycarbonate, Kapton, Kraft paper, etc. must be used, and, as in the case of capacitors, substantial margins are required. There have been many demonstrations of the successful operation of switches with these types of insulation. The switches in ATA & ETA [1] use 6μm thick Mylar insulation and have operated for 10^7 shots (at 625 J/pulse) with peak interlamina voltages of approximately 50 V. However, the second stage switch in the Comet accelerator [2] (250 kJ/pulse), had a lifetime under 100 shots due to dielectric breakdown of the 12 μm Mylar insulation at peak potentials of about 500 V per turn. This served to demonstrated how fragile the insulation in a magnetic switch can be as the energy/pulse and interlamina voltages are increased. The peak interlamina electric field (240 kV/cm) in these switches was a factor of 20 below the expected breakdown field of the insulation. For the past three years we have been

studying this failure problem to gain an understanding of it and propose appropriate solutions. In the course of this work we have developed magnetic foil coating techniques that seem to solve the low level failure problem. We have also identified, and are now beginning to investigate, several other coating approaches that may yield insulation schemes with more desirable characteristics than presently available insulation processes.

PLANARIZING COATINGS.

Several experiments, described in detail elsewhere [3,4], were conducted to identify the primary cause of the Comet switch failures. The magnetic material in the Comet switch was 2605-SC Metglas (Allied Corporation trademark), and the insulation was two layers of 6μm Mylar film. Since Metglas is a cast material it has a relatively rough surface as shown in the SEM micrograph in Fig. 1a. An example of the largest type of surface protruberance, a pip, is shown. Pips are found on the dull (casting wheel) side of Metglas and result from the replication of craters which develop in the wheel surface during the manufacture of Metglas. The craters continue to erode during the casting process leaving a pip on the Metglas surface with each revolution of the wheel. When Metglas is wound with thin dielectric films, the films are degraded (torn or punctured) during the winding process. Since Metglas is the best magnetic material for certain high frequency switching applications, our efforts were directed toward finding better ways to insulate Metglas laminations. We found that the degradation of these films can be prevented by applying a planarizing coating to the Metglas surface before winding.

The first coating which was tried, Electrodag 154, was applied by a simple dip and dry process. The resulting surface, Fig. 1b., still appears rough but the coating was found to effectively mask pips so that a thin dielectric film could be wound against Metglas without significant degradation.

This coating has been tested in small, 1 inch diameter, wound capacitors and in two 18 inch diameter, 5 kg magnetic switches. The coated Metglas switches were tested to failure at 1.6 MV/cm, an improvement by a factor of two, and six standard deviations above the mean failure level of 30 uncoated Metglas switches.

Fig. 1a. Metglas is a cast material and has a relatively rough surface. An example of large surface protruberances, pips, are shown here. The pips are replications of craters in the casting wheel.

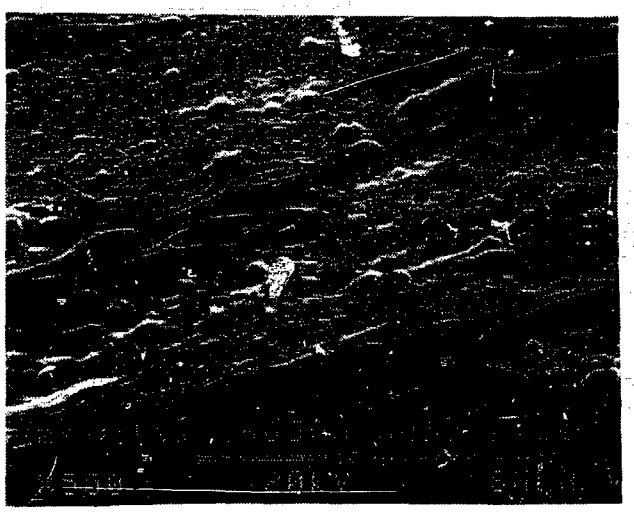

Fig. 1b. Electrodag 154, was applied in a simple dip and dry process. The resulting surface still appears somewhat rough, but the coating was found to effectively mask pips and a thin dielectric film can be wound against the Metglas without significant degradation.

This result clearly demonstrates how modifying the Metglas surface can improve the performance of the insulation in a magnetic switch. However, a conductive coating like Electrodag is not an optimal approach to the problem because it reduces the cores' packing factor. The next coating evaluated was an electrophoretically applied styrene-acrylate

dielectric film [5]. The SEM micrograph in Fig. 1c. shows a rare surface feature on the very smooth coated surface.

Fig. 1c. Electrophoratically applied coatings of Styrene-acrylate were evaluated. The SEM micrograph above illustrates the significantly smoother surface obtained.

This coating approach was selected because it had been extensively studied at SNL and successfully applied in a variety of dielectric coating applications. The electrophoretic process also provides a simple approach for achieving thin uniform, high quality coatings with excellent thickness control. In our prototype continuous coating machine, however, a long, 20 minute, curing time at 200° C was needed. Consequently, the throughput rate only provided us with enough coated foil for small capacitor tests. Another limitation was observed in that the original conformal coating was observed to soften during the initial phases of thermal curing and planarize or flow away from the edges and high points. For our experiments, a coating of 6μm nominal thickness (not sufficient to completely cover the largest surface protuberances) was applied to field-annealed 2605-CO Metglas. After coating, the BH characteristics of the material were measured by Allied Corp., and no significant degradation was detected. Fourteen composite capacitors with coated Metglas conductors and 12μm Mylar insulation were then wound. The DC breakdown distribution on these capacitors was found to be at least as good as the distribution for comparable aluminum conductor test capacitors. The aluminum conductor capacitor distribution was obtained as a reference and should indicate the capability of non-degraded insulation.

ELECTROPHORETIC COATING CONSIDERATIONS.

Electrophoresis is used in a variety of techniques by chemists and biologists as a technique for separation and analysis for gene-typing. It is also used in coating technology. Our major interests and applications at SNL lie within this latter area. Since the 1920s, a large number of patented and generic techniques for applying organic, inorganic, and mixed coatings from aqueous and non-aqueous electrolytes have been developed. A large number of patented and generic techniques for electrophoretic deposition of organic or polymer coatings from a liquid bath are available [6,7,8]. Systems employing aqueous colloidal dispersions of acrylic oligomers have been extensivley investigated at SNL and applied in a variety of dielectric coating applications. The dielectric coating materials considered in our foil coating studies must posess a high degree of dielectric perfection, be stable during extended immersion in dielectric oils at elevated temperatures, have good adhesion, and scale economically for manufacture.

A schematic illustration of a typical electrophoresis cell is shown in Fig. 2 .

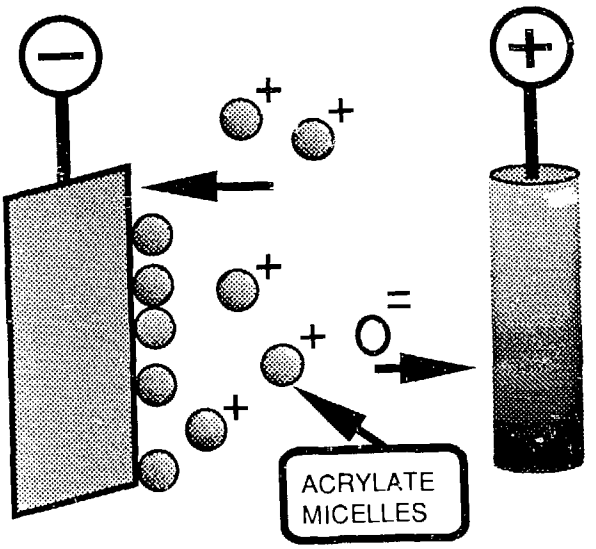

Fig. 2. The positively charged particles (i.e. amine groups) are attracted to the negative cathode where they coalesce as a tacky coating. Thickness uniformity is insured due to the self-limiting effect produced by the insulation resistance of the coating.

Electrophoresis is a phenomena in which electrically charged particles, sufficiently small to remain suspended in a liquid, migrate to and coalesce on an oppositely charged electrode. The coating process is driven by the electric field, hence, the thickness will increase until the field is extinguished by the dielectric coating. In principle, any charged material which can be dispersed in a liquid can also be electrophoretically deposited onto an electrically conductive substrate.

There are many useful advantages associated with electrophoretic deposition that are directly and ideally applicable to coating Metglas foil.

(1) The technique is economical for applying uniform coatings on rough surfaces and also on edges of unusual shaped parts.

(2) The coating is deposited at a relatively high rate (0.5 um per second).

(3) Minimal operator skills are required.

The coating process is relatively simple and only requires processing tanks, a power supply capable of providing piece part current densities on the order of 1 mA/cm^2 at 50 - 600 V, and a drying or curing station.

There are also identifiable limitations which must be provided for. Before drying and curing, the as-deposited coatings may be soft, poorly adherent, and vulnerable to mechanical damage. A drying period is typically required to evaporate entrained solvents or liquids and to establish adhesion and cohesion. Furthermore substrate oxidation or contamination may necessitate pretreatments or the coatings can exhibit flaws or pinholes. In practice, electrophoretic coating baths typically contain a mixture of components such as thermal or photo crosslinking catalysts and other additives. These components must be used in such a way as to provide control of deposition rates, dielectric strength, elasticity, adhesion, and cohesion.

For many electrophoretic deposition processes, there is a practical upper limit on the thickness of the coating which can be deposited. Above approximately 50µm, the as-deposited coatings may run, drip, delaminate, or crack during curing. At this thickness the electric field strength needed to drive the reaction also begins to exacerbate small flaws during the coating formation.

PRESENT DIELECTRIC FOIL COATING EFFORT.

The results of our initial effort to electrophoretically coat Metglas were encouraging in that the degradation problem was solved, and the magnetic properties were unaffected. However, the long thermal curing cycle not only limited our coating speed, it also tended to soften and planarize the initially conformal electrophoretic coating. It seems reasonable that such a coating might be able to serve as the primary dielectric in some regime between a few volts per lamination, where conventional coatings exist, and 1000 V per lamination. This would eliminate the need for the dielectric film insulation with its associated margin and provide a more desirable insulation scheme for that regime. Currently we are investigating an alternate electrophoretically active, aqueous dispersed, acrylic polymer which may be rapidly cured by ultraviolet irradiation. This deposited polymer does not soften or flow and retains its desirable edge coverage attributes throughout the curing step. The feature of thicker dielectric coatings on sharp edges, or other features which emanate higher fields, is a desirable attribute.

Fig. 3 schematically illustrates a coater which is now under development at SNL. The coater is designed to operate at speeds up to 3-4 feet per minute or more and uses an electrodeless microwave excited mercury vapor plasma ultra violet source for photocuring the electrophoretically deposited dielectric. The foil admittance gland at the bottom of the coating cell is allowed to leak solution into a catch reservoir whereupon it is filtered and pumped back to the coating cell. This avoids the use of a roller at the bottom of the tank which could accumulate tacky deposits of the non-polymerized coating. Air knives are used to remove excess electrolyte from the emerging foil thereby eliminating the need of a water rinse step. In order to reduce particulate contamination, the entire system was constructed in an enclosure and pressurized with HEPA filtered air. The coating deposits cathodically on Metglas foil at a current density of 1 mA/cm^2 at 100 volts.

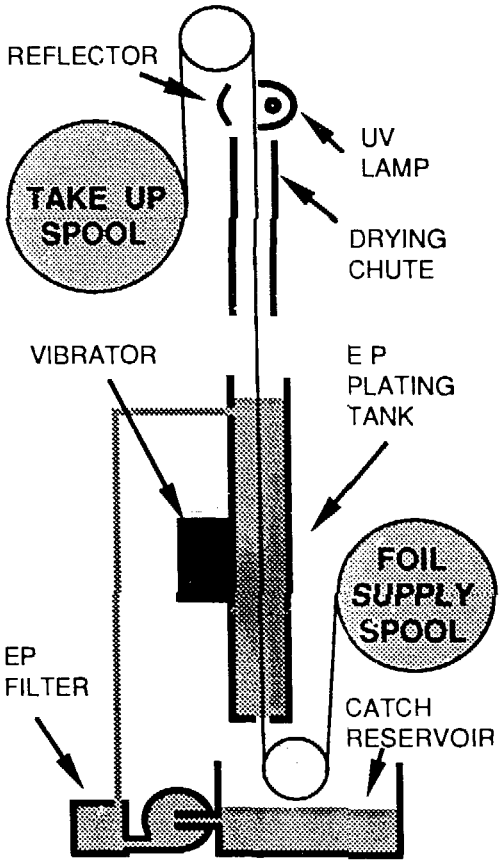

Fig. 3. Schematic illustration of an electrphoretic coating machine used to deposit an acrylic polymer on *Metglas foil. Rapid crosslinking is accomplished with* the use of an intense ultra violet source.

The aqueous based electrophoretic bath which contains acrylic oligomers, detergents, photocatalysts, and pH buffers, is sold by the Shippley Co, Irvine CA as an experimental photoresist emulsion (XP5001). Ultraviolet curing is performed in the 250-350 nm wavelength range at a dose of approximately 250 mJ/cm^2. Fig. 4, illustrates a typical rough edge observed on *as-received Metglas foil at 200X* magnification. Fig. 5 illustrates the edge after coating. A smooth or bead-like thicker polymeric coating of dielectric results. This bead is deposited in proportion to the intensity of the electric field.

One of the early problems that we have observed when using this coating is the formation of occassional hydrogen bubbles(Fig 6a.). We are exploring several process modifications to eliminate them.

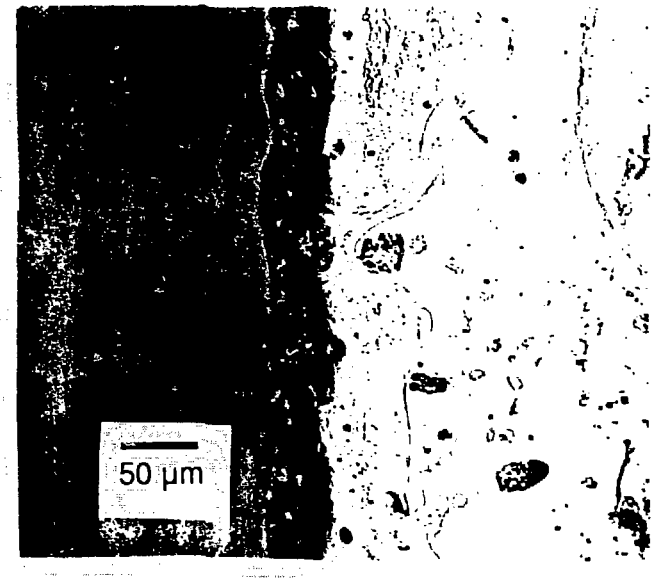

Fig. 4. The rough edge of as-received Metglas foil (middle) shown at 200X. Intense electric fields are produced at the edge of the foil. Foil is on right side.

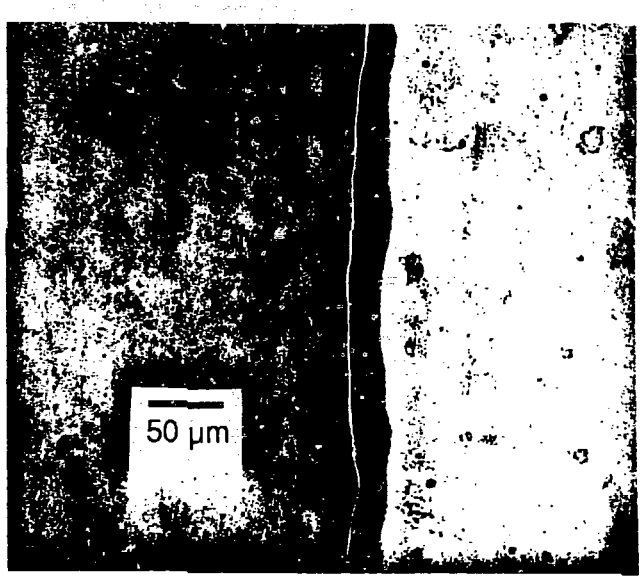

Fig. 5. The higher field common to edges and edge protuberances produce a thicker deposit at the foil edges. The bead of dielectric shown here appears to be on the order of 50 µm thick as opposed to a measured thickness of approximately 12 µm on the foil surface.

For example trace amounts of metals deposited on the foil surface, by the addition of copper sulfate for example, may prevent local accumulation of hydrogen by reducing the cathode cell potential.

However, when large quantities of any material are produced, occasional flaws are inevitable. If nothing is done to control insulation flaws, they will dominate the breakdown characteristics of any large magnetic switch. Here, we have another potential advantage over conventional insulation. They can be reapplied at higher voltages. At 450 V, for example, selective deposition or filling will occur in flawed areas of the coating, which breakdown, as shown schematically in Fig. 6b. Fig. 6c. illustrates a hole in a previously flawed area that resulted from electrical breakdown testing. Fig 6d. illustrates the selectivity of the second electrophoretic coating at higher voltages.

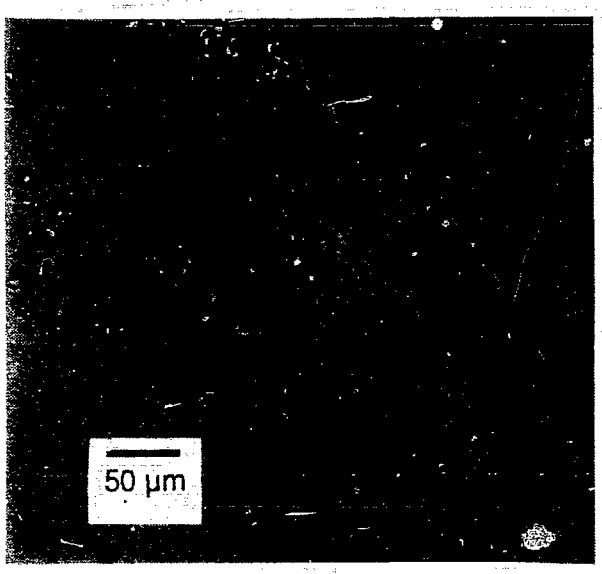

Fig. 6a. Bubbles which become entrained in the coating represent areas of lower dielectric strength.

Preliminary experimental data is being obtained using the higher voltage electrophoretic recoating technique. Electrical breakdown values of the Metglas foil having a single dielectric coating were measured and compared to foil which was processed with an additional coat at higher voltages(i.e. 450 V). The measurements were obtained by gently placing a rounded probe on the planar surface of the electrophoretic coating and ramping the voltage, at a rate of about 100 volts per second, until a current in excess of ten microamps was observed. The analysis of fifteen comparative breakdown values are shown in Table 1. The values obtained were rounded to one hundred volts and listed in ascending order. No meaningful differences were observed with either cathodic or anodic biasing of the foil during the dielectric breakdown voltage testing.

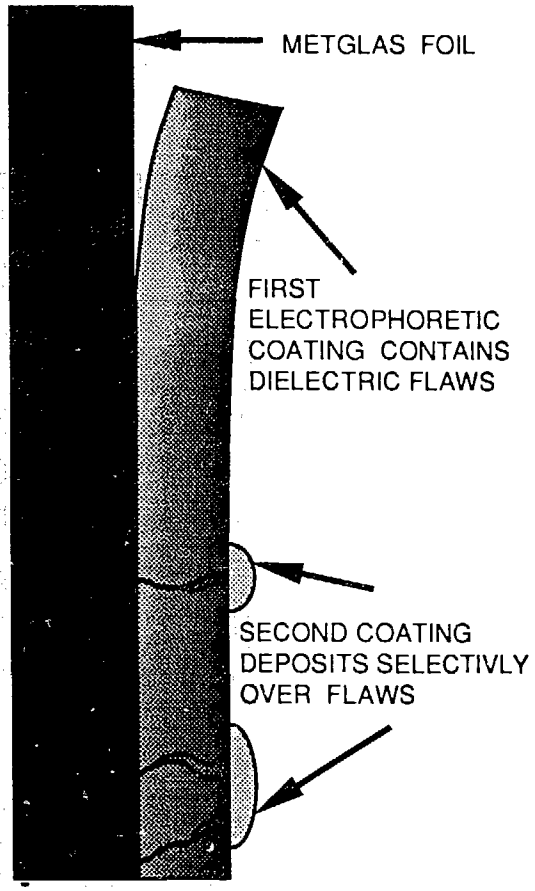

Fig.6b. Electric fields which project through dielectric flaws result in selective deposition of additional dielectric when reprocessed at higher voltages.

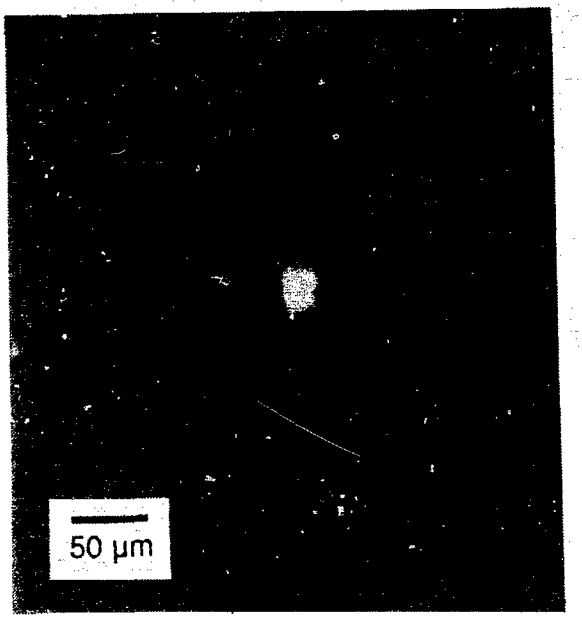

Fig. 6c. Dielectric breakdown occurs at somewhat lower voltages in flawed areas. Here, a hole resulting from high voltage breakdown, can be observed.

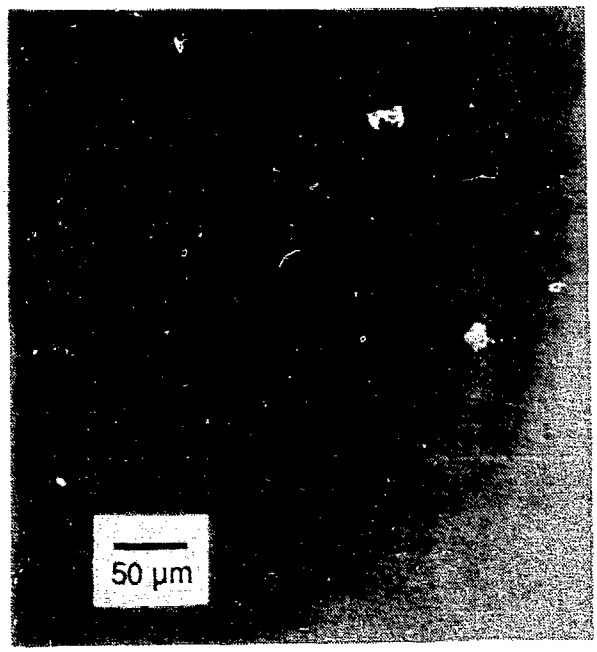

Fig. 6d. Selective deposition of additional electrophoretically deposited dielectric can be observed in the center of a small bubble-like flaw. This results in a net improvement in the breakdown voltage of the dielectric coated foil and a large increase in the minimum breakdown strength.

TABLE 1 (Bulk Breakdown Voltages)

Single Coat	Double Coat
500	1200
500	1400
900	1900
1200	1900
1700	2100
1700	2100
1800	2300
1800	2300
1800	2400
1800	2400
1900	2500
2000	2600
2400	2600
2500	2600
2600	2700
Low Value 500	1200
High Value 2600	2700
Average 1673	2200
Median 1800	2300

OTHER FOIL COATING APPROACHES.

1. Composite Coatings.

There are many insulating composites that can be electrophoretically applied. We are now investigating coatings that contain mica, fluorocarbons, and aliphatics such as polyethylene or polypropylene. A mica loaded composite might, for example, provide insulation with a higher thermal conductivity than present coatings.

2. Chemical Conversion Coatings.

Dielectric coatings comprising silicates, chromates, molybdates, borides, titanates, and phosphates are well documented. [9,10,11] Thermal or chemical decomposition, diffusion, and electrochemical techniques are used to deposit these coatings. The temperatures permitted for producing a chemical conversion coating, and diffusion bonding it to the Metglas foil surface, must be restricted by the temperature limitations of the foil, i.e. a few hundred degrees centigrade.

Electrochemical surface conversion coatings are typically less than a few µm in thickness, are brittle, and have significantly lower breakdown strength as compared to thicker, 12 - 25 µm, polymer films deposited by electrophoretic processes. These coatings, however, do not use curing or baking, are harder than most polymers, and permit compact saturable inductor designs.

We have anodically deposited uniform, thin, adherent coatings of molybdates on Metglas foil at room temperature, from an ammonium molybdate solution using a current density of 5 mA/cm^2. These coatings display a dielectric strength in the order of 20-40 volts. Additional anodic electrochemical reactions which deposit useful dielectric films are being explored.

3. Photofabrication of Spacers or Ribs.

Future magnetic pulse compressor repetition rates require provisions for cooling Metglas inductors. We have proposed using photoengraved ribs or spacers (Fig. 7) which permit circulation of dielectric liquids through the Metglas windings. Here, Metglas foil is shown to pass onto a grooved ultraviolet transparent exposure wheel which has grooves on its surface. The photopolymer, which is encapsulated by flowing into the grooves

becomes photocrosslinked and emerges from the bath as a rib bonded to the foil surface. A variety of photo-polymers with excellent photosensitivity are readily available commercially. Acrylic ribs have been photoengraved in the laboratory on Metglas foil, and Fig. 8 envisions how such a process might be scaled as a continuous processor.

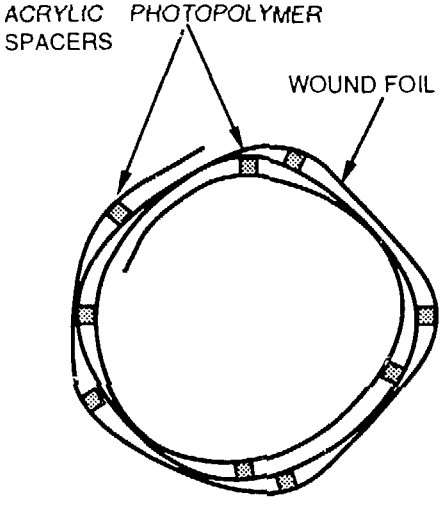

Fig. 7. Photoengraved ribs or spacers permit circulation of dielectric liquids through the Metglas foil windings and may assist in providing thermal management during repetitive pulsed operation.

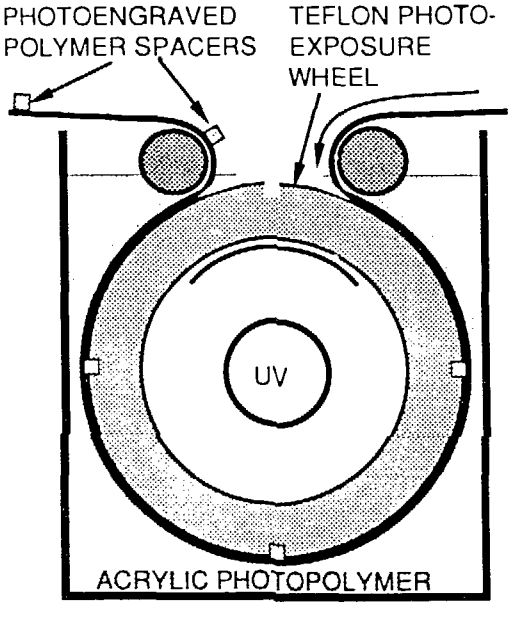

Fig. 8. An ultraviolet transparent wheel with grooves permits photopolymerization of ribs on foil which passes over the photoexposure wheel surface.

SUMMARY

This study has demonstrated the use of electrophoretic deposition for applying a thin, uniform polymer dielectric. With the encouraging early results, we expect that these techniques will have some regime of application in systems requiring an insulation to withstand a few volts to 1000 V per lamination. Once these regimes are identified, the question of economic feasibility can be addressed. The electrophoretic coating processor constructed for this study is capable of additional scale-up and may be run continuously for coating large quantities of Metglas foil. An effort is being made to optimize the process for producing near-perfect dielectric films for Metglas foils. Parallel efforts are underway to adapt these processes to practical large-scale foil coating machines. These dielectric coating techniques may find additional use in coating foils for use in other capacitor-like structures.

We have also electrochemically deposited thin adherent dielectric films of molybdates on Metglas foils for use as a low voltage insulating film. Other electrochemically deposited thin film coatings are being explored.

We have shown that rib-like dielectric spacing structures, derived from liquid, photopolymers can be deposited on Metglas foil which may assist circulation of dielectric liquids for removal of heat. Additional studies are needed to determine the practical aspects of scale-up and subsequent manufacture of these structures.

REFERENCES.

[1] D. L. Birx, E. Cook, S. Hawkins, S. Poor, L. Reginato, J. Schmidt, and M. Smith, "Magnetic Switching", in Proceedings 4th Pulsed Power Conf., Albuquerque, NM, pp. 231-235 (1983).

[2] E. L. Neau, T. L. Woolston, and K. J. Penn, "Comet-II, A Two Stage, Magnetically Switched Pulsed-Power Module", in Conference Record of the Sixteenth Power Modulator Symp., P. 292 (1984).

[3] H. C. Harjes, K. J. Penn, G. A. Mann, and E. L. Neau, "Investigations into the Design of Multi-Terawatt Magnetic Switches", in Proceedings 6th IEEE Pulsed Power Conference, Arlington, Va., pp. 540-543 (1987).

[4] H.C. Harjes, G.A. Mann, F.A. Morgan, and E.L. Neau, "Improved Insulation Schemes for Multi Terewatt Magnetic Switches", in IEEE Pulsed Power Conference, Monterey, CA (1987).

[5] D.J. Sharp, H.C. Harjes, and G.A. Mann, "Electrophoretically Applied Dielectrics for PBFA-Type Amorphous Metal Foil Saturable Inductors", in Conference Record of the Spring Materials Research Society meeting in San Diego, CA. (1989).

[6] Willibald Machu, Handbook of Electro-plating Technology, Electro-chemical Publications Ltd., Bell and Bain Ltd., Glasgow, Scotland, Great Britain (1978).

[7] Robert F. Gould, editor, Electro-deposition of Coatings, Adv. Chem Series 119, American Chemical Society, Washington, DC (1973).

[8] Milan Bier, editor, Electrophoresis Theory, Methods and Applications, Academic Press, New York, NY 10003, Vol I, (1959) and Vol II (1967).

[9] G.V. Samsonov, editor, Protective Coatings on Metals, Kiev, 1972 Translated for National Bureau of Standards, U S Dept. of Commerce and N. S. F., Washington, D.C., by Amerind Pub. Co. Pvt., New Delhi, India (1984).

[10] G.V. Samsonov, editor, Protective Coatings on Metals, Kiev, Translated for National Bureau of Standards, U S Dept. of Commerce and N. S. F., Washington, D.C., by Amerind Pub. Co. Pvt., New Delhi, India (1987).

[11] Wilhelm Wiederholt, The Chemical Surface Treatment of Metals, Robert Draper Ltd. Teddington, G. B. (1965).

CORE COOLING STUDIES AT LLNL AND SANDIA

R. Stone, J. VanSant, and S. Bahowick (Lawrence Livermore National Laboratory, P.O. Box 808, Livermore, CA 94551)
K. Reed and S. Kempka (Sandia National Laboratory, P.O. Box 5800, Albuquerque, NM 87185)

ABSTRACT

We are conducting numerical studies and experimental tests at Lawrence Livermore National Laboratory (LLNL) and Sandia National Laboratory (SNL) to determine a method of cooling pulse compression cores that use saturating magnetic material. We anticipate that for high average power throughput compressors, cores will have cooling channels wound at intervals to maintain the maximum temperature below 125°C. We have calculated, for a range of volumetric heating rates, the expected distance between channels using bulk core properties and laminar flow for the cooling fluid. We have completed Freon-113 flow tests on possible cooling-channel materials. We have found that, in tests using ohmically heated cores without cooling channels, we can achieve good agreement between calculated and measured performance by use of the bulk ore properties and assumed film coefficients. A two-dimensional code has been developed to determine core performance using both edge and channel cooling.

We are planning additional ohmic heating tests of wound cores to further investigate the performance of the cores, both with and without cooling channels. We will then compare the measured values of temperature, flow rate, and pressure drop with code results.

INTRODUCTION

For many years we have used magnetic material for pulse compression in pulse-power units (PPUs) that drive induction accelerators[1]. Typically, the magnetic material and insulator are wound around a bobbin and are then surrounded by a one-turn conductor. A PPU has two or three of these compressor stages. Because of short run times or low pulse-repetition frequencies (PRFs), we have not been concerned with the heat generation from hysteresis losses in these wound cores. For future applications involving high average power throughput, however, a means must be devised to limit the temperature of the wound cores. We at LLNL and SNL have undertaken to assess and find a solution to this problem. This report summarizes the results to date of this effort.

AVERAGE CORE THERMAL PROPERTIES

Figure 1 shows a typical core configuration used in one stage of a magnetic compressor. We fixed the amount of magnetic material (METGLAS) in the core by specifying the number of turns N of thickness t_1 and tape width H.

We measured the build of the core b after winding. A stacking factor SF can be calculated by:

$$SF = (Nt_1)/b \ . \qquad (1)$$

We can determine the average thickness per winding of the cooling fluid by:

$$t_3 = b/N - (t_1 + t_2) \ , \qquad (2)$$

where t_2 is the insulator thickness. The average thickness per winding t_w, therefore, is $t_1 + t_2 + t_3$.

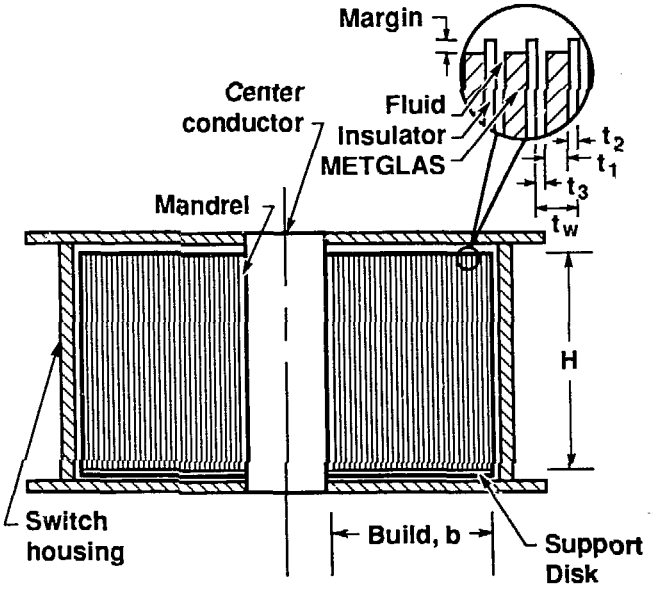

Figure 1. Simplified layout of a wound core showing the magnetic material (METGLAS), insulator, and fluid.

The average properties of the core (including its average density D_C, average specific heat C_C, and average thermal conductivity k_C) can be found by:

$$D_C = \frac{\Sigma \rho_i t_i}{\Sigma t_i} \ , \qquad (3)$$

where ρ_i is the density, and i = 1 to 3;

$$C_C = \frac{\Sigma C_i \rho_i t_i}{\Sigma \rho_i t_i} \ , \qquad (4)$$

where C_i is the specific heat; and

$$k_c = \frac{\Sigma t_i}{\Sigma t_i / k_i}, \qquad (5)$$

where k_i is the radial thermal conductivity.

Figure 2 shows the predicted core thermal conductivity vs SF of layers composed of 25-μm (1-mil) METGLAS, 6.4-μm (0.25-mil) Mylar, and Freon-113 of variable thickness. Also shown on Fig. 2 are experimental thermal conductivity measurements of a stackup of 300 layers, composed of 25-μm METGLAS, 6-μm Mylar, and Freon, placed between two heating plates. We changed the distance between the plates to approximate differing SFs. The measured k_c, 0.275 W/m °C, did not change as the plates were moved. We concluded that the stackup may have obtained a maximum SF during assembly.

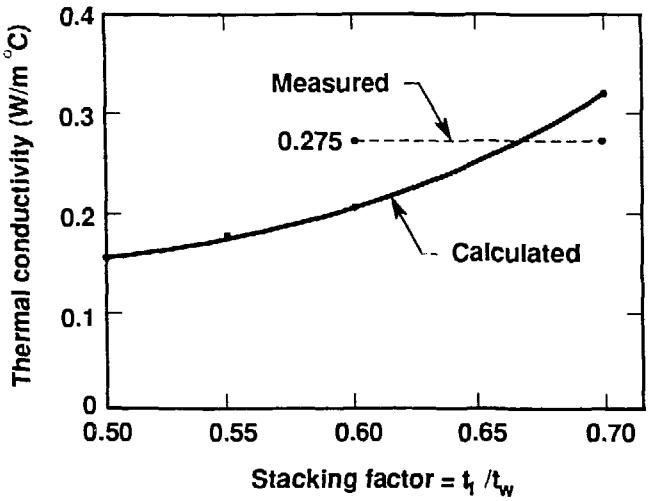

Figure 2. The calculated thermal conductivity vs stacking factor (SF) for 25-μm METGLAS, 6-μm Mylar, and Freon-113. Also shown is a measured value for an SF range of 0.6 to 0.7.

The 2605CO METGLAS volumetric loss rate per pulse q_m as a function of tape thickness and rate of flux change for a rectangular charging voltage is shown on Fig. 3[2]. These values must be modified to account for the effect of an imperfect square-wave charging voltage. The core volumetric loss rate per pulse is $q_c = q_m SF$. If this result is multiplied by the PRF, we obtain the core volumetric heating rate Q_c.

CORE RESPONSE WITHOUT COOLING

If there is no external cooling of the core, the temperature rise per second is given by:

$$\dot{T} = Q_c/(D_c C_c). \qquad (6)$$

We also wound cores with 15.2-μm (0.6-mil) METGLAS, 6.4-μm (0.25-mil) Mylar, an average Freon thickness per winding of 3.8 μm (0.15 mil), and 50-mm (2-in.) tape width. The SF for this configuration was 0.6. The maximum operating temperature for both METGLAS and Mylar is about 125°C. Assuming the initial temperature of the Freon to be 20°C, we can therefore allow a rise of 80°C. Figure 4 shows the time for an 80°C increase in core temperature vs PRF for a METGLAS loss rate per pulse of 1700 J/m^3 for this winding configuration. We took the loss rate for a 1-μs pulse from Fig. 3 and increased it by 50% to account for a nonrectangular charging voltage profile. Changing the METGLAS thickness to 25 μm (1 mil) did not affect the curve significantly. For low PRF, the curve is conservative, as the effect of edge cooling may increase the calculated times.

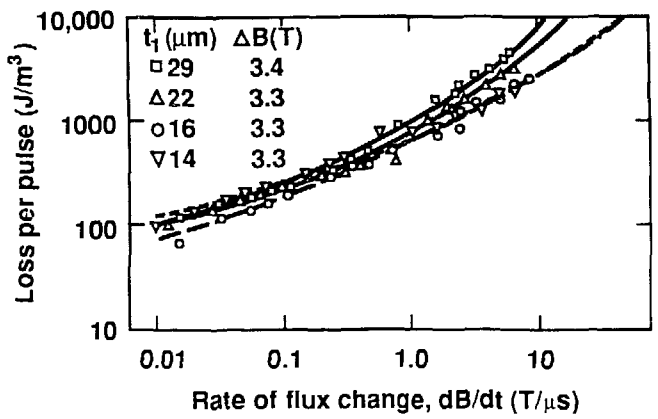

Figure 3. The rectangular-charging-voltage volumetric loss rate per pulse vs rate of flux change and tape thickness for 2605CO METGLAS.

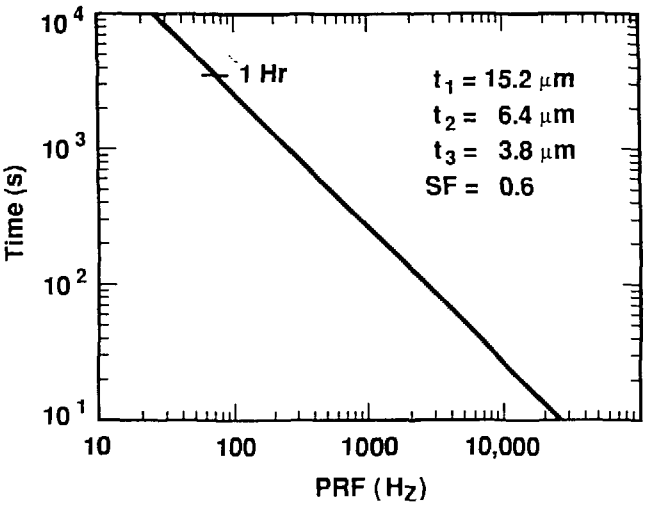

Figure 4. Time for an 80°C core temperature rise vs PRF, with the METGLAS loss assumed to be 50% greater than that with a rectangular 1-μs charging voltage.

CORE RESPONSE WITH COOLING

One-Dimensional Constant Properties

If we assume one-dimensional heat flow and a constant cooling fluid temperature, the cores are either cooled axially at the tape edge or radially at channels wound at intervals. Assuming planar heat flow, the maximum temperature can be approximated by:

$$T_{max} = T_f + (Q_c L/2h_f) + (Q_c L^2/8k) , \qquad (7)$$

where L is the height of tape for edge cooling or the distance between cooling channels, T_f is the temperature of cooling fluid, h_f is the film coefficient, and thermal conductivity is k_m for METGLAS (for edge cooling) or k_c (for channel cooling).

For laminar flow, h_f is a constant, equal to 8.24 k_f/d, where k_f is the fluid thermal conductivity and d is a characteristic length[3].

The cooling fluid must satisfy both electrical and mechanical requirements. At LLNL, we are currently using Freon-113 for magnetic switches, and it has performed satisfactorily. For future applications, the heating rate will increase, which will require active cooling for maintaining the proper core temperature. To minimize the number of cooling channels, the temperature in the core must be allowed to go to the 125°C limit. Because Freon-113 at 1 atm will boil at about 48°C, it must be pressurized to about 6.9×10^5 Pa (100 psi) to reach the required temperature. A pressurized Freon system may not be desirable for environmental, safety, and cost reasons, however; therefore, other fluids must be considered. We are able to compare the performance of Freon-cooled cores and cores cooled by other fluids by means of the heat transfer relationships and flow equations given above.

Radial Heat Flow Only. By rearranging Eq. (7), we can estimate the maximum allowed distance between cooling channels vs volumetric heat generation rate for a given h_f and temperature increase. If we assume an inlet temperature of the cooling fluid of 20°C and a maximum core temperature of 100°C, we obtain the results shown on Fig. 5, which also shows that the number of cooling channels required decreases as the thermal conductivity of the cooling fluid increases. For the cases shown, mineral oil is a better choice than Freon-113, but its viscosity is much higher than that of Freon; therefore, the pressure drop across the core must be considered.

Axial Heat Flow Only. Figure 6 shows the temperature rise at the center of a core vs various tape widths and heat generation rates for axial edge cooling. Because of the high thermal conductivity of METGLAS, edge cooling will be possible if a coating can be developed that can be applied directly to the METGLAS. This will eliminate the region of stagnant fluid due to the insulator margin.

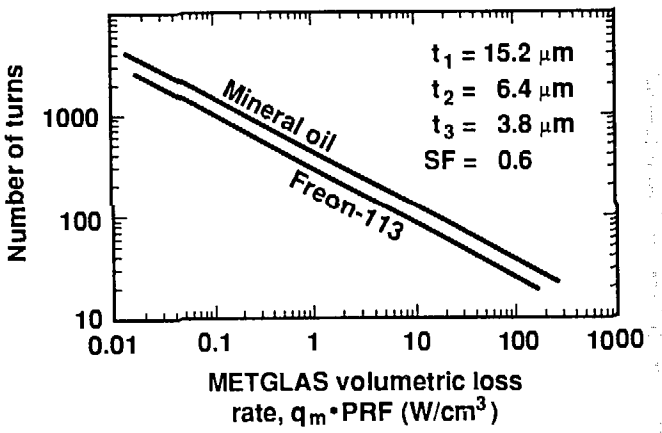

Figure 5. The number of turns per cooling channel vs METGLAS volumetric heating rate, shown for both mineral oil and Freon-113.

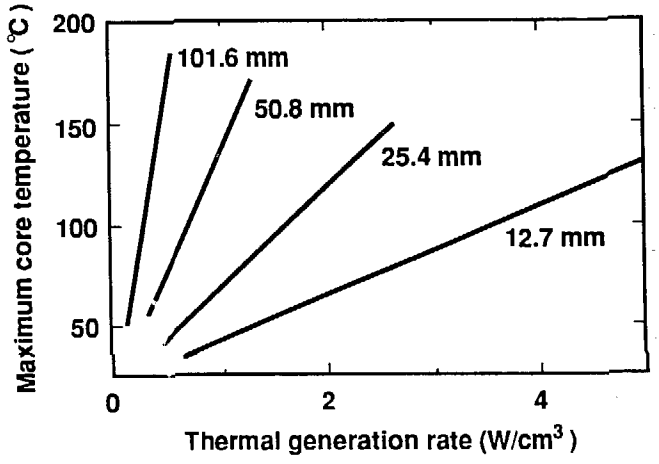

Figure 6. Maximum core temperature vs thermal generation rate and 12.7- to 101.6-mm tape widths H for axial edge cooling.

Two-Dimensional Model of Core

We have developed a two-dimensional model of the wound core (Fig. 1) that assumes the following:

- Neglect of margins.
- Neglect of the support disk under the winding.
- Treatment of the windings as a single material with anisotropic thermal conductivity.
- Uniformity of volumetric heat generation.
- Spatial uniformity of the surface temperature of the disk.

The margins consist of protrusions of insulator outside the METGLAS, with coolant trapped between layers. Since the coolant has low thermal conductivity, it will insulate the edges of the metal from the flowing coolant, while the support disk insulates the bottom of the disk and inhibits heat removal. Neglecting these two effects will cause predicted to be less than actual temperatures. Figure 7 shows the results of one two-dimensional calculation. The temperatures calculated for the selected case far exceed the maximum allowed for the magnetic material, which illustrates the need for interlaced cooling channels. With this model, we can predict the maximum temperature in the core as a function of the materials used, the distance between cooling channels, tape height, and heating rates.

FLOW EXPERIMENTS ON SMALL SAMPLES

We envision a cooling channel in the wound core made up of a material that keeps adjacent turns separated without restricting the flow of coolant. We have considered the cooling-channel materials shown in Fig. 8. These materials were chosen because they can be fabricated in 0.25-mm-or-less thickness and require little or no development. We have completed flow tests using Freon-113 on 50-mm-wide samples, with results shown in Figs. 9 and 10. As expected, comparisons between the various configurations show that the maximum flow was obtained with straight-sided channels (Tab 02, Fig. 8). When Mylar was placed on both sides of the 0.25-mm-thick sample, flow was reduced considerably. We assume that the Mylar margin blocked the entrance to the straight slots.

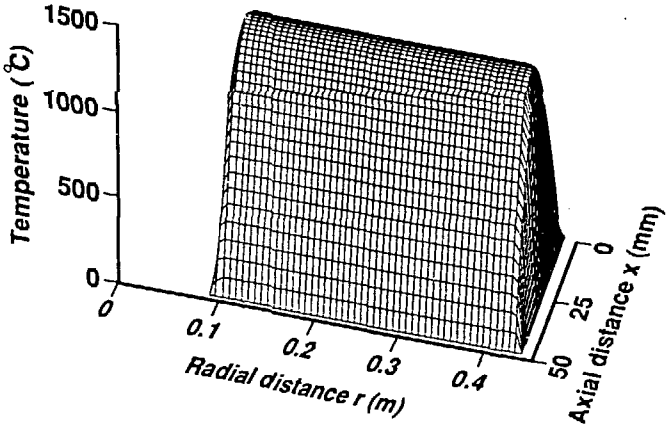

Figure 7. Calculated temperatures in an $x-r$ plane of a wound core. A core volumetric heating rate of 14 W/cm^3 was used.

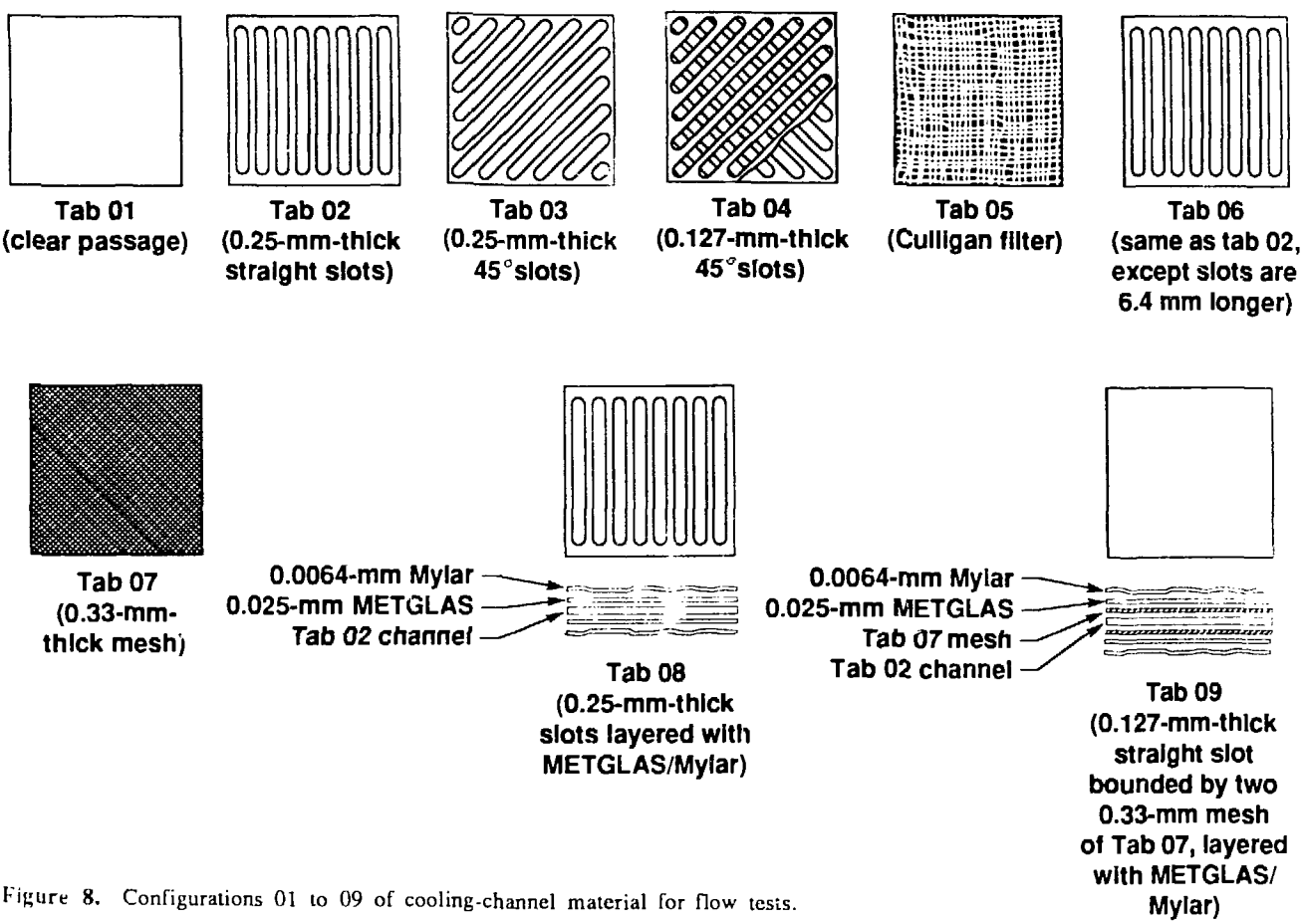

Figure 8. Configurations 01 to 09 of cooling-channel material for flow tests.

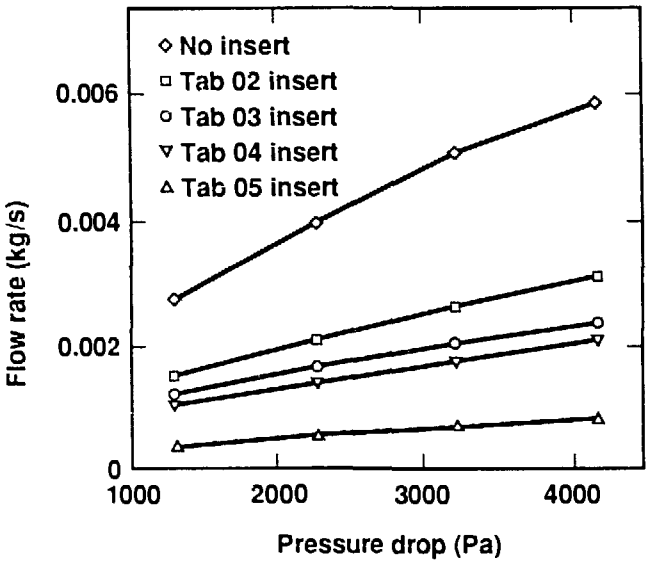

Figure 9. Freon-113 flow rate vs pressure drop for Tabs 01 to 05 (see Fig. 8).

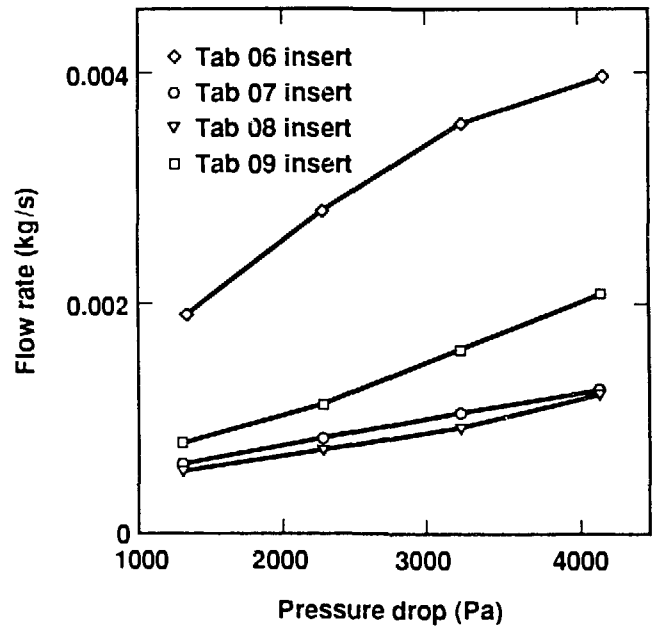

Figure 10. Freon-113 flow rate vs pressure drop for Tabs 06 to 09 (see Fig. 8).

ELECTRICALLY HEATED CORE EXPERIMENTS

Without Cooling Channels

We have wound cores and inserted thermocouples at various locations to measure temperature profiles for a variety of configurations. Ohmic heating simulates the volumetric heat generation due to METGLAS hysteresis loss. Figure 11 is a schematic of an experimental setup at SNL for determining core properties and performance. One test compared the maximum temperature obtained with and without oil circulation. These results (Fig. 12) show that circulating the oil has a minimal effect on the center temperature. We conducted another experiment in which the cooling oil pulsed so the fluid would not be stagnant at the margins. We can see from Fig. 13 that little gain was realized using this complex setup. No further tests of this concept are planned.

We can obtain the accuracy of the calculated average thermal properties of the core using the setup shown in Fig. 11. Figure 14 shows a comparison of measured temperatures with those obtained by calculation. Using bulk core properties, calculated temperatures were consistently higher than measured temperatures by about 4°C. Nonuniform heating or uncertainties in the film coefficients may explain this difference. Table 1 lists the measured core thermal values obtained from this ohmic heating experiment.

Table 1. Measured core thermal parameters.

Parameter	Core (W/m °C)	Margin & gap (W/m °C)	Surface (W/m^2 °C)
k_c (radial)	0.409	0.134	N/A
k (axial)	5.86	0.137	N/A
h_f (vert.)	N/A	N/A	50
h_f (horiz.)	N/A	N/A	40

The effective k_c determined by this experiment using a polycarbonate insulator compares well with 0.407 W/m °C, determined by Eq. (5). Results of this experiment also indicate that the two-dimensional model accurately models the wound core.

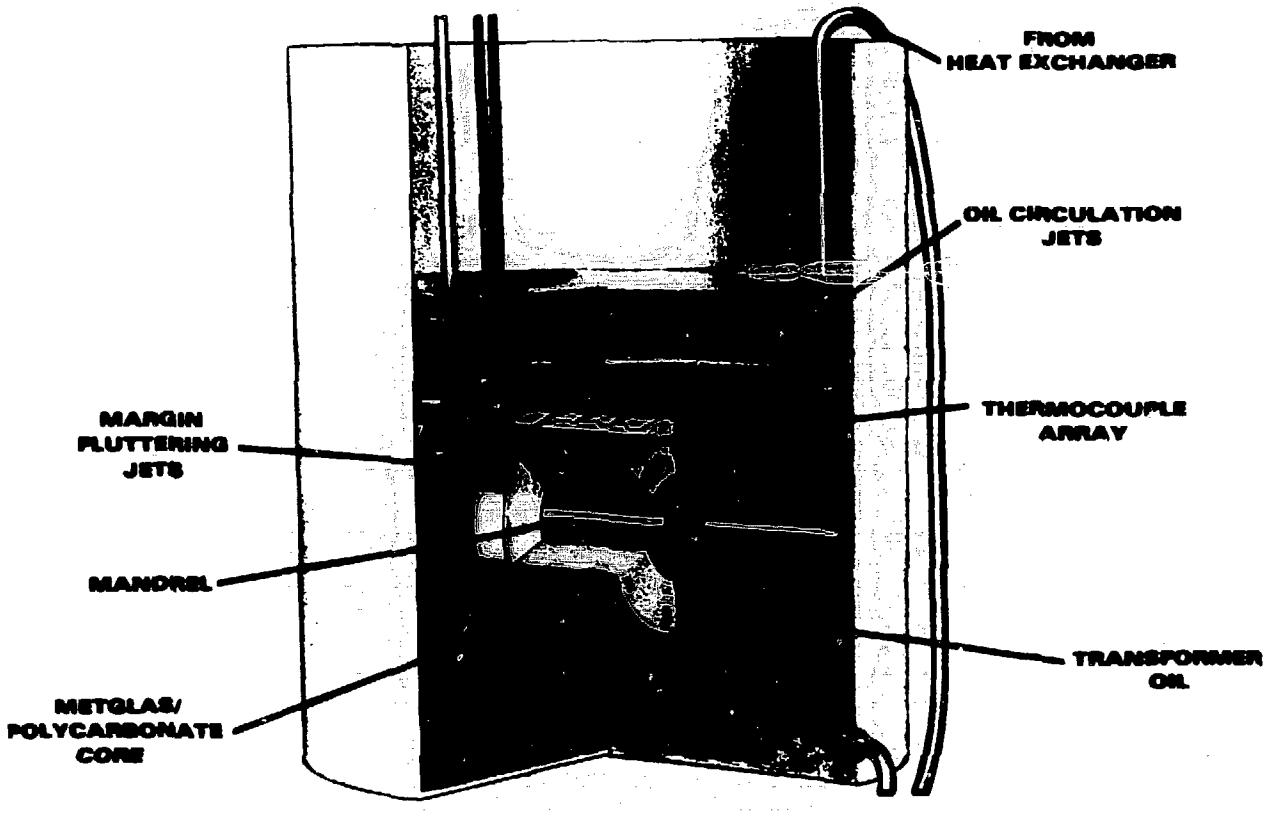

Figure 11. Experimental setup for ohmically heated core with an installed capability for circulating or pulsating the cooling oil.

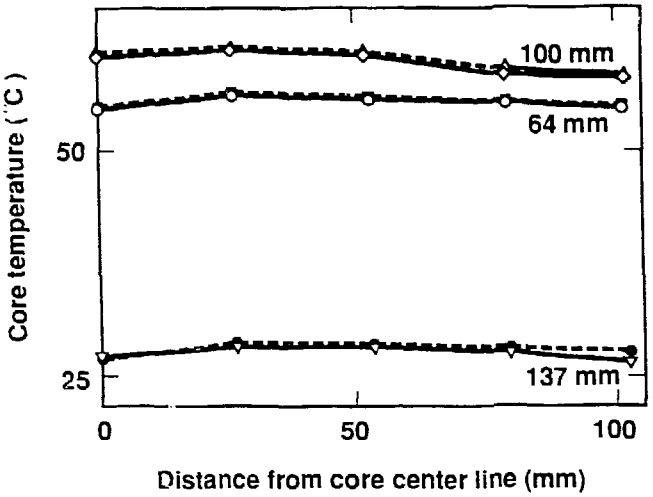

Figure 12. A comparison of measured temperatures inside an ohmically heated core with circulating oil (solid line) and without circulating oil (dashed line). Radial distances from the core of 64, 100, and 137 mm are indicated. Symbols indicate actual data points.

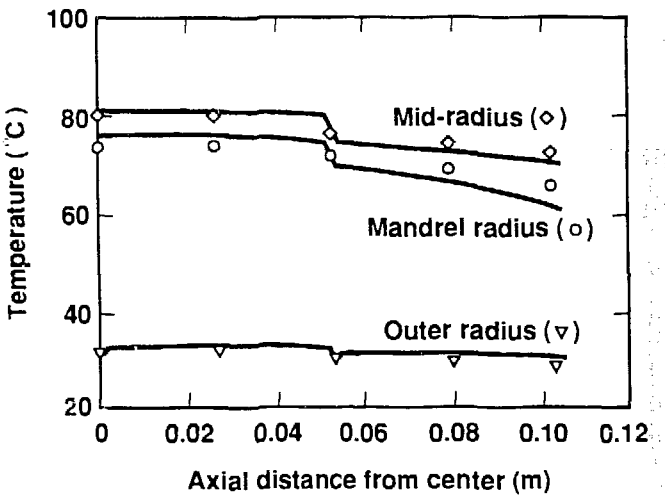

Figure 14. A comparison of calculated temperatures (solid lines) and measured temperatures (at symbols) for radial and axial variations in the electrically heated core experiment shown in Fig. 11. Measured temperatures have been decreased by 4°C.

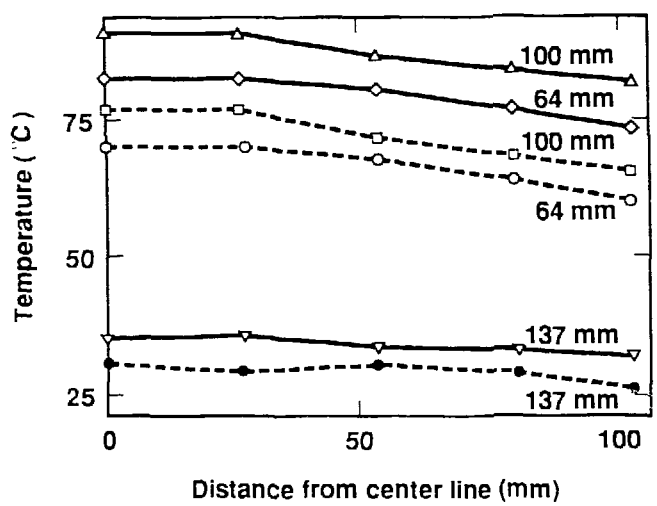

Figure 13. A comparison of measured temperatures inside an ohmically heated core with margin fluttering due to pulsing oil (solid line) and without margin fluttering (dashed line). Radial distances from the core of 64, 100, and 137 mm are indicated. Symbols indicate actual data points.

With Cooling Channels

Although we determined the average thermal properties of the wound core by the experiment described above, the effectiveness of cooling channels can only be determined by experiments with specific channels wound within the core. At SNL, two experiments are planned for studying the capability of specific cooling channels. The first experiment, the "coffee filter" setup shown in Fig. 15, has no internal cooling channels. Coolant will be forced between the METGLAS/Mylar/Freon layers, and the flow rate vs pressure will be determined. An optical fiberscope will be installed to allow observation of the margin. We anticipate a prohibitively large pressure drop for this configuration.

The second experiment will use an ohmically heated core with a mesh interlaced every 73 turns of METGLAS/Mylar. The wound core with cooling channels is inserted into the same holder as that shown on Fig. 15. Thermocouples are dispersed throughout the core so we can determine the maximum temperature and the various gradients. Using this configuration, we can determine both the capacity of the mesh channel and the required coolant flow and pressure drop. A third electrically heated core experiment (Fig. 16) will be conducted to characterize cooling channel performance in lower-power switches. This experiment consists of four

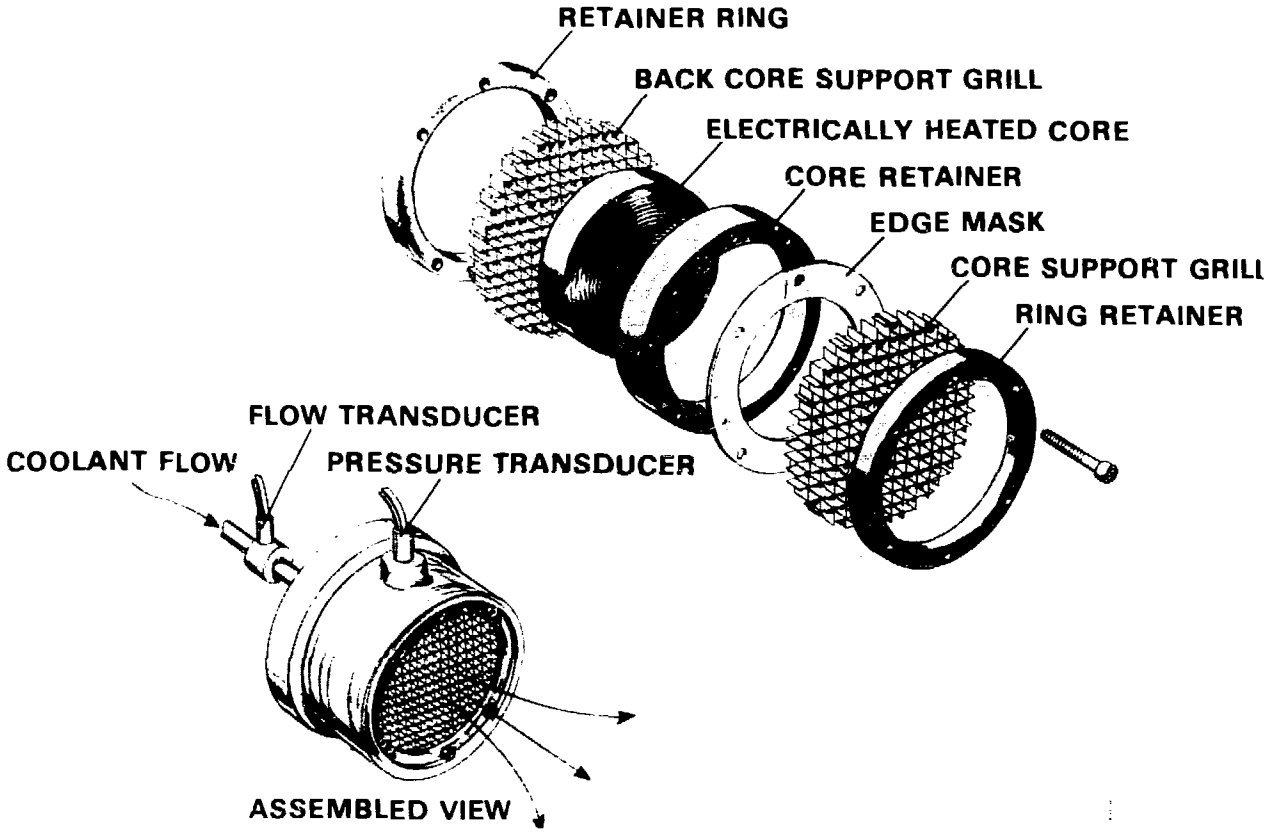

Figure 15. A "coffee filter" experimental setup to determine flow and pressure drop through a core without cooling channels. Cores with channels can also be tested with this arrangement.

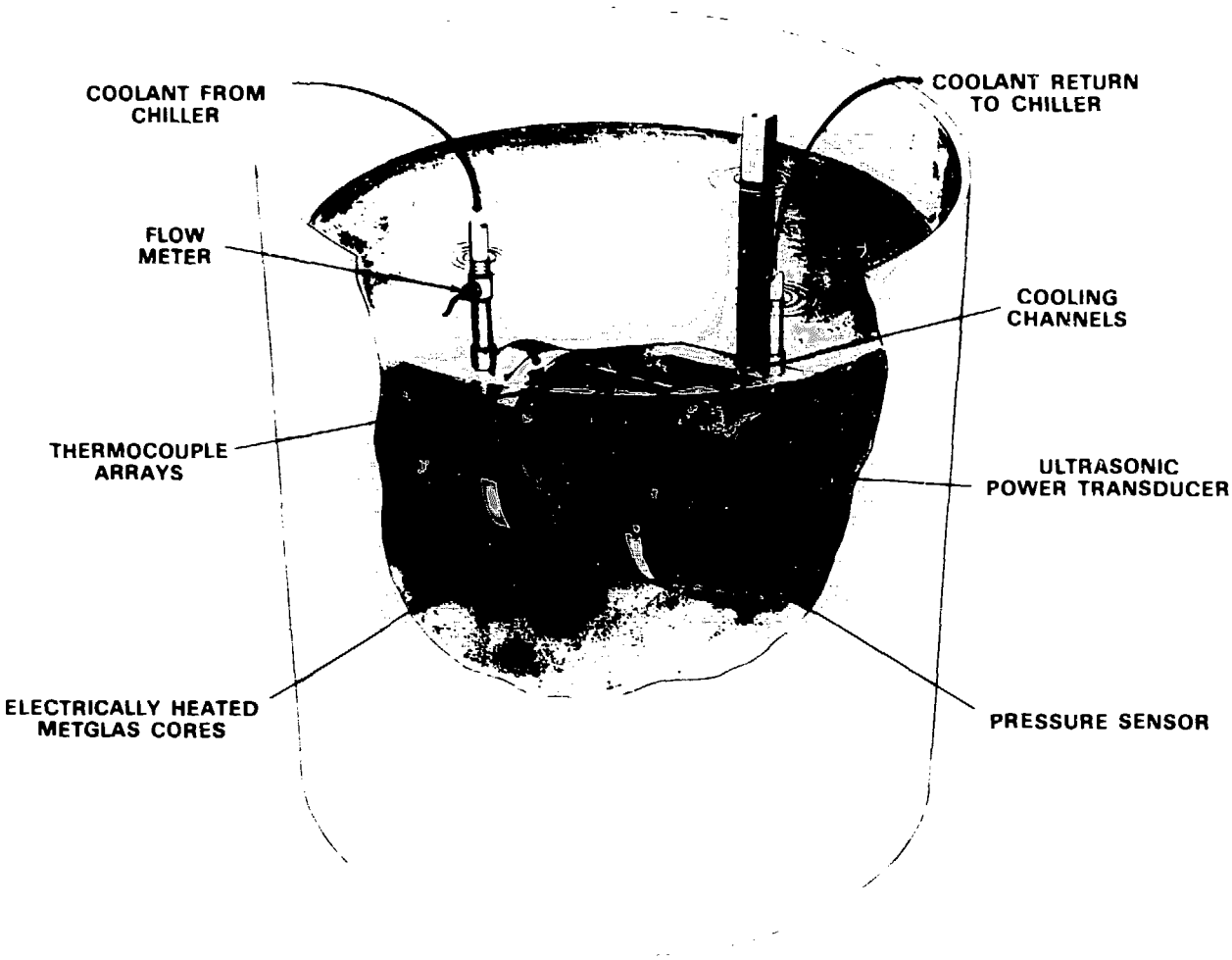

Figure 16. Layout of the experiment for ohmically heated cores with cooling channels. An ultrasonic transducer is provided to determine the effect on performance of induced turbulences.

adjacent 50-mm-wide METGLAS cores with 5-mm-high polycarbonate cooling channels spaced at 25.4-mm intervals radially within the build. The coolant in the channels will be ultrasonically excited to determine whether the induced turbulence will improve channel performance.

CONCLUSION

The studies and experiments we have completed indicate that credible core designs can be made using average core properties that are simple to calculate. We have planned further experiments to determine the effectiveness of cooling channels wound within the core. These results will contribute to designs of magnetic compressor cores that can have a high average power throughput for future applications. Further work is required to determine optimal core cooling-channel materials.

ACKNOWLEGMENTS

This work was performed jointly under the auspices of the U.S. Department of Energy by Lawrence Livermore National Laboratory under contract W-7405-ENG-48, for the Strategic Defense Initiative Organization and the U.S. Army Strategic Defense Command in support of SDIO/SDC MIPR No. W43-GBL-0-5007.

REFERENCES

[1] D. Birx, E Cook, S. Hawkins, L. Reginato, J. Schmidt, and M. Smith, "Magnetic Switching," in Technical Papers of the 4th IEEE Pulsed Power Conference, Albuquerque, NM, June 6–8, 1983.

[2] C. Smith, Allied, Inc., private communication, 1988.

[3] W. Rohsenow and J. Hartnett, eds., *Handbook of Heat Transfer* (McGraw Hill, 1972), p. 7-74.

MAGNETIC COMPRESSOR STUDIES FOR F.E.L. APPLICATIONS AT THE "CENTRE D'ETUDES SCIENTIFIQUES ET TECHNIQUES D'AQUITAINE"

M. Thévenot, P.Eyl, P. Anthouard
CEA CESTA BP N° 2 33114 Le Barp FRANCE

Abstract

A F.E.L. (Free Electron Laser) program based on a linear induction accelerator (LINAC) is currently being developped at CESTA (Aquitaine Center of Scientific and technical Research). This technology requires the development of high power electric pulse generators (150 kV- 2 Ω) able to work at high repetition rates (≥ 1 kHz).

Limitations of conventionnal power components (solid-state circuit, high pressure gas blown switches,...) have led us to design pulse generators using magnetic switches. A prototype has been built and different magnetic cores were tested in single-shot mode.

I - INTRODUCTION

The induction cells used in the LINAC [1] are designed to be driven by rectangular voltage pulse with a 150 kV amplitude and a 80 ns width. The rise time must be less than 20 ns.

Following these parameters, a first pulse generator has been developed at CESTA laboratories. The synoptic is shown in figure 1.

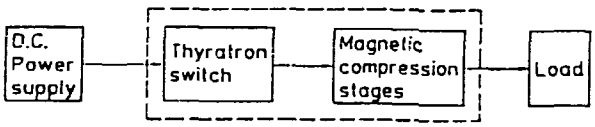

Fig. 1 : *Synoptic of the pulse generator*

It consits of two parts:

- a Command Resonant Charging System (CRCS)

- a pulse forming and compression device (MAG)

The CRCS transforms the DC supply into a low power sinusoidal pulse generator. It is mainly composed of thyratrons (EEV CX 1536), self-inductances and capacitors. The output signal is then applied to the MAG device in order to be amplified (magnetic pulse compression) and temporally formed (transformation of the sinusoidal pulse into a rectangular pulse).

II. MAG DESIGN

The MAG module is built using a coaxial water filled pulse-forming line and magnetic switches operating as magnetic pulse compressors [2] . The first stage consists of a *step-up transformer (1/10)* . The *coaxial structure* of the module makes a good coupling between the line and the other components (figure 2) .

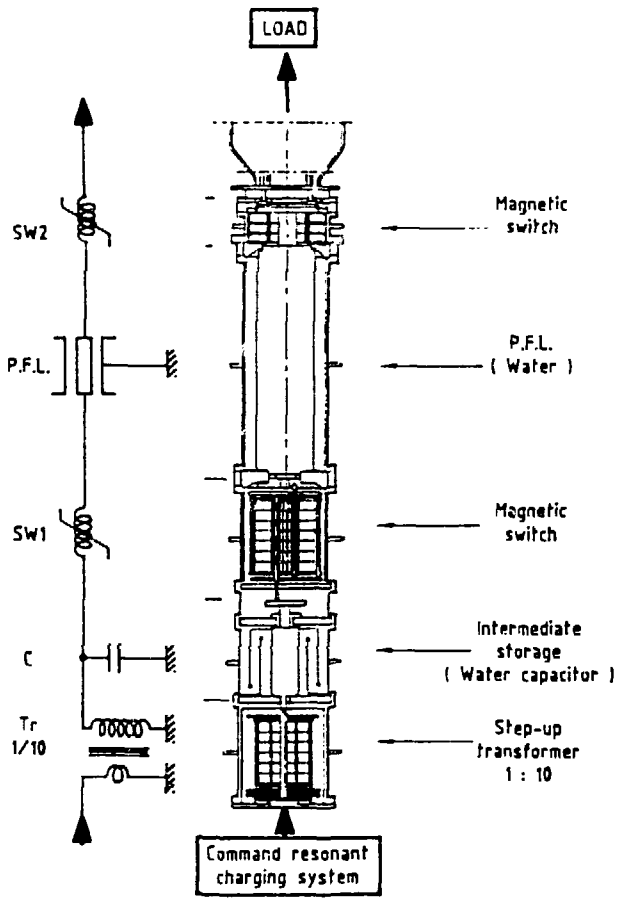

Fig. 2 : *Electrical and mechanical MAG structure*

III. MAGNETIC MATERIAL CONSIDERATIONS

A. *General points*

The materials which can be used to make the cores of the switches must meet the following requirements [3] [4] :

- low losses

- high saturation induction (Bs)

$$\frac{\mu_r^{unsat}}{\mu_r^{sat}} > 400$$

(where μ_r^{unsat} and μ_r^{sat} are respectively the relative permeabilities of the magnetic material before saturation and after saturation).

The amorphous materials (e.g. : metal-glass alloy) are quite adapted to this type of use. Nevertheless their very low resistivity involves a laminated structure. So the core consists of a winding of a small thickness ribbon and each lamination is separated from the others with an insulating material.

There are two types of insulators:

- oxides coating (SiO_2 or MgO)

- MYLAR strip (thickness of a few microns)

The choice of the insulator is very important because it may be subjected to a high voltage during the saturation process. Indeed, when a voltage change is applied to a magnetic switch (saturable inductance), a flux change appears in the core giving an induced voltage ΔV between each magnetic material lamination (figure 3).

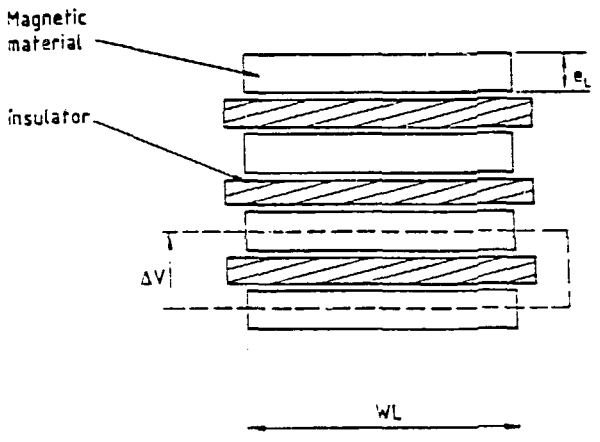

Fig. 3 : *Voltage induced between core laminations*

B. *Interlamination voltage*

The magnetic switch behavior is governed by the equation of flux conservation [2]:

$$\int_0^{\tau} V(t)\, dt = N\, \Delta B\, Sm \qquad (1)$$

where Sm is the area of magnetic material , N the number of turns around the core and $\Delta B = Br + Bs$ with Br (Bs) the remanent (saturating) magnetic field.

Our device works as a resonant energy transfer system [2], so V(t) is given by:

$$V(t) = V_{max} / 2\, (1 - \cos wt) \qquad w = 2\pi / T \qquad (2)$$

with T = period

Saturation occuring at $\tau = T / 2$, Eq.(1) and Eq.(2) yield :

$$V_{max}\, T / 2 = N\, \Delta B\, Sm \qquad (3)$$

resulting in :

$$Sm = V_{max}\, T / (4\, N\, \Delta B) \qquad (4)$$

In addition :

$$Sm = N_L\, e_L\, W_L \qquad (5)$$

where N_L is the number of laminations, e_L and W_L are respectively the thickness and the width of the laminations.

The flux change phenomena induce on the core a voltage which is equal to the single-turn voltage V_{max} / N.

If all the laminations have approximately the same length, this voltage is evenly distributed among N_L laminations, so the interlamination insulation must withstand a voltage ΔV given by :

$$\Delta V = V_{max} / N N_L = 4\, e_L\, W_L\, \Delta B / T \qquad (6)$$

Small values of T may give high interlamination voltage.

If the insulator voltage hold-off is lower than the induced voltage ΔV, leakage may occur in the insulating material giving an increase of the magnetic material thickness and consecutively an increase of losses. Despite a high magnetic field applied to the core, the material may be unable to saturate and the magnetic switch to work correctly.

IV. TESTING

The MAG device shown in figure 2 has been built and tested in our laboratories.

The core of the first magnetic compressor is made of 25 µm METGLAS 2605 Co insulated with MgO.

The last switch, which is submitted to short-pulse (T / 2 < 300 ns) , was used to test two types of cores :

Test 1 : 2605 Co (25 µm) insulated with MgO

Test 2 : 2605 Co (25 µm) insulated with MYLAR (6µm)

Waveforms measured before and after the last switch are shown in figures 4 and 5.

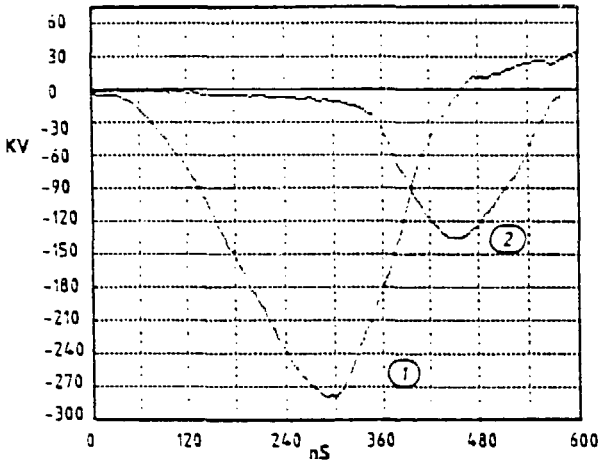

Fig. 4 : *Test of 2605 Co / 25 µm insulated with MgO*

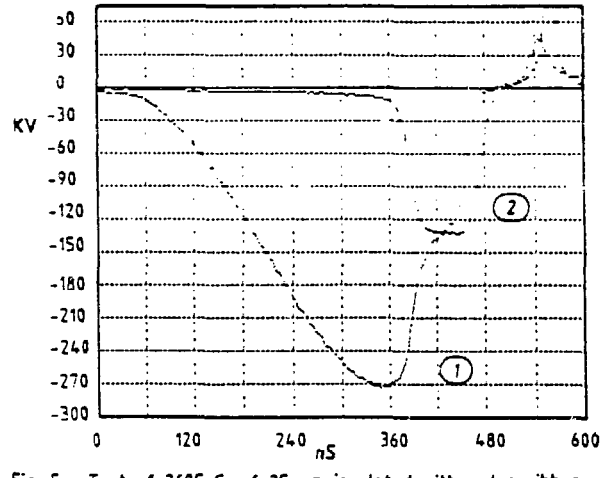

Fig. 5 : *Test of 2605 Co / 25 µm insulated with mylar ribbon*

(1) : *Voltage at the end of line*

(2) : *Voltage on the load*

The output-pulse (10 % - 90 %) rise-time (tr) is given by the following equations [5] :

$$tr = 1.1\ L^{min} / Z_c \qquad (7)$$

$$L^{min} = k\ \mu_r^{min} \qquad (8)$$

where L^{min} is the saturated residual self-inductance of the last magnetic switch , μ_r^{min} the saturated relative permeability of the magnetic material, k a factor which depends on the dimensional features of the core ($k = 24\ 10^{-9}$) and Z_c the line caracteristic impedance (2 Ω).

Theoretically $\mu_r^{min} = 1$ and tr = 13 ns, the experimental results are given by the table 1.

Insulating material	t_r	μ_r^{min}
MgO	90 ns	7
MYLAR	30 ns	2.5

Table 1 : Experimental results

The results obtained with MYLAR are close to the theoretical values, the difference may be due to the parasitic inductance of the load.

When the insulating material is MgO the difference is due to the quality of the insulator. The voltage hold-off given by the manufacturer is equal to 20 V in oil and the voltage applied during the saturation process is greater than 100 V.

V. CONCLUSION

To design short-pulse (T / 2 < 200 ns) high voltage (> 200 kV) magnetic switches , the choice of interlamination insulation is quite as important as that of magnetic material.

The oxides, which give good mechanical qualities to the cores and allow them to be annealed, are totally unusable because of their too low dielectric strength Other tests have been performed with SiO_2 and the results are not better than those obtained with MgO.

VI. REFERENCES

[1] LEISS J.E ., NORRIS N.J., WILSON M.A;

The design and performance of a long pulse high current linear induction accelerator at the National Bureau of Standards. articules Accelerators, 10, 1980, pp. 223-234.

[2] Nunnally, W.C.

Magnetic switches and circuits
Los Alamos National Laboratory Report LA-8862-MS-Rev.2, 1984

[3] BIRX D.L., LAUER E.J., REGINATO L.L., SCHMIDT J., SMITH M.
- Basic principles governing the design of magnetic switches, Lawrence Livermore National Laboratory, UCID - 18831, 1980

[4] MELVILLE W.S.
- The use of saturable reactors as discharge devices for pulse generators
Proceedings Institution of Electrical Engineers (London), 98, Part (3) n° 53, 1951, pp. 185-207

[5] THEVENOT M.
Etude d'intégration des commutateurs magnétiques dans les montages générateurs d'impulsions haute puissance pour accélérateur à induction.
CNAM, DIJON - FRANCE, Mémoire d'ingénieur CNAM, 1989.

ACKNOWLEDGMENTS

We acknowledge the expert technical assistance provided by P. Baudoin, B. Rablade, J.P. Thunot.

Circuits and Applications Group

DESIGN OF LARGE MAGNETIC PULSE COMPRESSORS

Patrick Corcoran and Robert Kuenning

Pulse Sciences, Inc.
600 McCormick Street
San Leandro, CA 94577

Abstract

This paper addresses the design of multi-stage series Melville line magnetic pulse compressors (MPC) in coaxial configuration, with liquid dielectric intermediate stage capacitors and pulse-forming line (PFL) as generally required by high voltage, high energy or short pulses.

Introduction

The basic circuit of a three-stage MPC is shown in Figure 1. It is assumed that the reader has a basic understanding of the operation of MPC's.[1,2] Since an MPC is costly, heavy, and bulky, it is generally used only when there are no other switches suitable for the application. Other switches are generally limited in voltage, peak current, di/dt, and/or repetition rate, compared with an MPC. The simple scaling relations no longer hold very well for large MPC's, since a large MPC will usually have a substantial part of its volume taken up by high voltage insulation or will have the connections between sections providing a significant part of the stage inductance. The high voltage insulation space increases the stage inductance.

There are two fundamental relations that must be satisfied simultaneously in the design of an MPC: the inductor volt-second requirement and its saturated inductance requirement. *In addition, there are auxiliary design considerations to be* addressed: (1) early switchout of the stage before the peak of the (1-cos) charge voltage; (2) large ratios of outer to inner radius of the cores increase the core losses and may increase the core insulation requirements near the outer radius; (3) there is flexibility in the choice of the compression ratio of the individual stages, constrained only by achieving the desired overall compression ratio; (4) relatively short charging times of the output stage pulseforming line (PFL) are possible; (5) the impedance of the pulseforming line can be varied along its length in order to achieve the desired output pulse shape; (6) frequently, a voltage step-up is required from input to output, so there is the choice of where to locate the transformer; and (7) the design must also keep the electric fields at a safe operating level, both inside the cores and in the external spaces.

Because there are so many variables, substantial iteration is required in order to get an optimum design. It is the purpose of this paper to help systematize the design process as much as possible. The emphasis will be on design principles rather than detailed calculations. Rationalized MKS units are used.

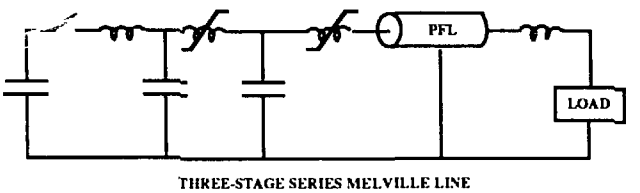

Figure 1. Three-stage MPC.

Design Principles

Before discussing the specific design process, there are several general design principles worth mentioning.

- Early switchout before full charge gives a substantial saving in core weight and cost, with only a small penalty in lost energy, as discussed in Appendix D.

- A one-turn inductor is more space efficient than one with multiple turns at high voltage. Multiple turns require insulation space to both the core and the enclosure, whereas one turn construction can put the full voltage across the core and extra insulation space may not be required. A one-turn design is not always possible, however.

- There are discrete ratios of PFL charging time to output pulse length which inherently give a better output pulse shape, especially lower ripple, as discussed in Appendix G.

- In multi-turn saturable reactors, it is useful to tie the core to the center of the winding, thus reducing both the insulation space required and the saturated inductance.

- Compression ratios in the approximate range of 2.5 to 4.5 seem to work out reasonably well. The first choice for the number of stages can be made by using equal compression ratios in the range of 3 to 4 for all stages. The output stage should be adjusted to the nearest half-integer value, as discussed in Appendix G.

- Transformers are generally easier to design into the earlier stages rather than the later stages, because the leakage inductance requirements are easier to meet.

There are conflicting considerations involved, however. It is desirable to put the transformer further upstream because intermediate stage capacitors using a dielectric fluid are easier to design at higher voltage. At low voltage, the spacing between coaxial electrodes is small, so multiple electrodes are required to keep the length down. This is mechanically complicated and expensive. On the other hand, it is desirable to put the transformer further downstream, because the higher the voltage on a multi-turn core, the more space is required for insulation, which translates to higher saturated inductance. So the choice of transformer location involves compromises and sometimes several iterations.

- A transformer goes ahead of the stage capacitor rather than behind it since a higher leakage inductance is then allowed, without changing the volt-seconds.

- Liquid dielectric PFL's and intermediate stage capacitors work out well for short pulse lengths with a choice of dielectric constants giving design flexibility in Z_o and pulse lengths.

- Avoid large changes in radii between stages, which would require costly flanges and add stray inductance.

Design

In order to start the design, choices for core material and its thickness, fluid insulation and impregnating medium, core insulation material and thickness, pulseforming line dielectric, and intermediate capacitor dielectric need to be made. Once chosen, subsequent iterations may show the need to modify them.

Since the output is usually specified, and the losses must be calculated to determine the input, the design starts at the output stage. From the specified load risetime, the allowable inductance of the output stage can be calculated, making allowance for the stray L's and C's of the load, and estimating a value for the stray inductance at the input and output of the output stage reactor.

The volt-seconds are picked from the early switchout criteria in Appendix D, modified if necessary by a short PFL charge time as discussed in Appendix G. A one-turn output stage is assumed and an allowable E-field calculated from standard formulas at whatever percent of breakdown is appropriate. Calculation of output stage dimensions are then made per Appendix A.

The length of the PFL in the output stage is determined by the output pulse length, including an allowance for risetime. The characteristic impedance of the PFL is determined by the output voltage divided by the output current (plus additional current to account for the losses in the output reactor, calculated so the energies match). An allowable E-field is determined from standard formulas at whatever percent of breakdown is appropriate. Then the dimensions of the PFL are calculated per Appendix E.

It is desirable to keep a running cross-sectional layout sketch to scale, and update it with each significant iteration. This shows up any large differences in the radii of adjacent sections and allows sketching of the transition geometry between sections. Then the stray inductance and field enhancement in the transition sections can be calculated. It also gives guidance for the next iteration.

After preliminary calculations on the output stage look reanable, it should be modelled to profile the impedance, per Appendix H, to get the desired waveshape with early switchout, stray L's and C's, and short PFL charge time (per Appendix G, if used).

Next, the volt-second requirement of the preceding stage is calculated from the compression ratio and the early switchout volt-second ratio that gives a tolerable loss, from Appendix D.

Assuming a multi-turn core, the space required for insulation is estimated, with due regard for field enhancement.

The allowable inductance of the stage (L_{sat}) is calculated from

$$L_{sat} = \frac{(\tau_{dis})^2}{\pi^2 \, C_s} \qquad (1)$$

where τ_{dis} is the discharge time and C_s is the series combination of the connected capacitors.

This stage inductance includes the entrance and exit stray inductance of the core plus 1/3 the inductance of the PFL and the preceding liquid capacitor, obtained from $\tau \, Z_o/3$, where τ is the one-way transit time. From these, K_{SL} (defined in Appendix A) can be estimated and the dimensions of the core determined per Appendix A.

The core and capacitor losses are calculated per Appendices C and E and used to calculate the increased capacitance of the stage per Appendix F. This completes the design of the stage preceding the output stage.

Earlier stages are designed in the same way. The transformer calculations are done for the stage where it occurs, per Appendix B.

Appendix A. Saturable Reactor Inductance, Volt-Seconds, and Core E-field

This analysis will be for a single turn core with the inner and outer conductors tight against the core. If there are gaps between core and conductors, the expressions get somewhat more complicated.

We will combine the expressions for core volt-seconds and stage inductance in order to solve for the average radius. Then we will use the electric field expression and show that *there is a minimum pulse length that is useable to meet the* requirements. For longer pulse lengths, Δr can then be calculated.

The required core volt-seconds can be equated to the flux change:

$$\frac{V}{2}\,\tau_c\,K_{es} = w\,\Delta r\,\Delta B_s\,S\,N \qquad (A1)$$

where V is the peak voltage, τ_c is the full (1-cos) charge transfer time, K_{es} is the ratio of volt-seconds at early switch-out to the volt-seconds at full charge, w is the core length, ΔB_s is the total flux swing, S is the core space factor including the space between individual cores, and N is the number of turns.

The stage inductance is given by

$$L = K_{SL}\,N^2\,200 \times 10^{-9}\,w \log_e \frac{r_o}{r_i} = 2 \times 10^{-7}\,N^2\,K_{SL}\,w\,\frac{\Delta r}{r_{ave}} \qquad (A2)$$

using the $\log_e$ approximation from Appendix J, where K_{SL} is the ratio of stage inductance to core saturated inductance. This has to be estimated initially and refined as calculations proceed. The stray inductance at input and output of the reactor is handled this way rather than as an additive term, in order to simplify the equations. Since w Δr is constant for a given number of core volt-seconds, the saturated inductance is only a function of r_{ave}, for the given core volt-seconds.

We solve Equation (A2) for Δr and substitute it into Equation (A1)

$$\Delta r = \frac{L\,r_{ave}}{2 \times 10^{-7}\,N^2\,K_{SL}\,w} \qquad (A3)$$

$$\frac{V\tau_c K_{es}}{2} = \frac{w\,L\,r_{ave}\,\Delta B_s\,SN}{2 \times 10^{-7}\,N^2\,K_{SL}\,w} \qquad (A4)$$

$$r_{ave} = \frac{10^{-7}\,N\,K_{SL}\,V\tau_c K_{es}}{L\,\Delta B_s\,S}$$

For one-turn cores and the output stage core, the field inside the core at the inner radius may be a limiting factor in the design. Multi-turn cores have less voltage across the core Δr, and the core electric field is usually not a problem.

In a coaxial geometry the electric field at the inner radius is given by

$$E_{ci} = \frac{K_{FE}\,V}{N\,r_i \log_e r_o / r_i} = \frac{K_{FE}\,V}{N\,(r_{ave} - \Delta r/2)\,\Delta r/r_{ave}} = \frac{2K_{FE}\,V\,r_{ave}}{(2r_{ave}\,\Delta r - \Delta r^2)\,N} \qquad (A5)$$

K_{FE} is the field enhancement factor giving the actual core insulation field with respect to the gross field. V appears across the Δr of the core.

$$\Delta r^2 - 2r_{ave}\,\Delta r - \frac{2K_{FE}\,V\,r_{ave}}{N\,E_{ci}} = 0 \qquad (A6)$$

This quadratic equation can be solved for Δr, since r_{ave} and the other terms are known or estimated.

$$\Delta r = r_{ave} \pm 1/2\left[4r_{ave}^2 - \frac{8\,K_{FE}\,V\,r_{ave}}{N\,E_{ci}}\right]^{1/2} \qquad (A7)$$

The quantity inside the brackets must be positive, so

$$4\,r_{ave} > \frac{8\,K_{FE}\,V}{N\,E_{ci}} \qquad (A8)$$

Substituting for r_{ave} from Equation (A7) into Equation (A4),

$$\frac{10^{-7}\,N\,K_{SL}\,V\tau_c\,K_{es}}{L\,\Delta B_s\,S} > \frac{2\,K_{FE}\,V}{N\,E_{ci}}$$

$$\tau_c > \frac{2 \times 10^7\,K_{FE}\,L\,\Delta B_s\,S}{N^2\,K_{SL}\,K_{es}\,E_{ci}} \qquad (A9)$$

which says that there is a minimum charge time for the stage being considered.

Note that at the minimum charge time, the quantity in the brackets in Equation (A7) will be zero, and Δr will equal r_{ave}. This gives $r_o/r_i = 3$. With the accurate $\log_e$ expressions, the ratio would be e, which is not surprising.

When the minimum charge time is exceeded, Δr can be calculated from Equation (A7), using the negative sign. Now w can be calculated from Equation (A1)

$$w = \frac{V \tau_c K_{es}}{2\Delta r \, \Delta B_s \, SN} \qquad (A10)$$

This is for the cores where the E-field in the insulation at the inner radius is limiting.

For cores where the E-field is not limiting, usually multi-turn cores and earlier stages, Δr and w can be chosen more freely.

Appendix B: Transformer Leakage Inductance Calculations

The leakage inductance of a transformer adds directly to the inductance of the preceding stage in determining the charge transfer time. Leakage inductance comes from magnetic flux that links one winding and not the other. In coaxial geometry, this is flux in the region between the primary and the secondary. Inductance calculations in this region can be split into several sections of coaxial line using the coaxial inductance formula for non-magnetic materials

$$L = 2x10^{-7} \log_e r_o/r_i \qquad (B1)$$

The inductance of all sections are added to get the leakage inductance. There will be some added inductance from the three-dimensional aspects of the turns, but this requires an estimating process that is beyond the scope of this paper.

Inductance transforms from one side of the transformer to the other by the square of the turns ratio.

For a first try at calculating the transformer leakage inductance, it is frequently useful to use an approximation. For the trial design, it is assumed that the core and inner winding take up negligible cross-section and the air core inductance of the outer winding is calculated. This gives a high value, but frequently the transformer inductance is not a large fraction of the total stage inductance. It is especially useful for high voltage transformers where the insulation takes a large part of the space.

In a high voltage coaxial transformer, the leakage inductance comes from the insulation space between primary and secondary, which is only weakly dependent on the core cross-section. The volt-seconds, however, are proportional to the cross-sectional area of the core. For a given secondary voltage, the core cross-section is proportional to the pulse length, the leakage inductance is nearly constant, but the allowed leakage inductance is proportional to the square of the pulse length. Therefore, it is much easier to design for the allowable transformer leakage inductance, the longer the charge time of the stage.

Appendix C: Core Losses

For large MPC's it is generally desirable to use a core with the highest flux density swing. Since volt-seconds are proportional to $\Delta B_s \, \Delta r$, and core saturated inductance is proportional to $\log_e \Delta r/r_{ave}$, a reduction in ΔB_s requires a corresponding increase in r_{ave} to keep the same core saturated inductance. Thus the core volume goes as the inverse square of the flux density swing.

This is a major reason for the frequent choice of 2605CO Metglas*, which has a high ΔB_s and comes in thin enough ribbons to keep the losses down at the short pulse lengths commonly used in MPC's.

Allied Signal supplies core loss curves taken with rectangular pulse voltage excitation as shown in Figure C1. Core losses are higher with (1-cos) excitation[11], and with the ratio of core outer to inner radii appreciably greater than one. The inner wraps of the core saturate first, with a higher dB/dt than average thus forcing a higher dB/dt on the outer wraps, later in the pulse, with consequent higher losses.

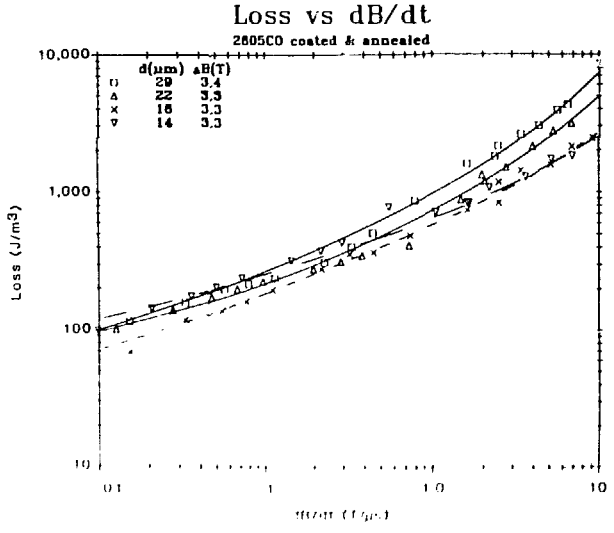

Figure C1. Metglas core loss for square wave excitation.

Ken Avery[6] has derived the combined cases, and the curves for extra loss are shown in Figure C2. One curve is for bar domain behavior and one is for sandwich domain behavior[12] (saturating wave)[13]. For intermediate behavior,

it is necessary to pick the points on the Allied Signal loss curves where the slope is one-half for bar domain behavior and one for sandwich domain behavior. Then the location of the operating point on the Allied signal loss curves gives a clue as to where to interpolate for the extra loss between Avery's curves.

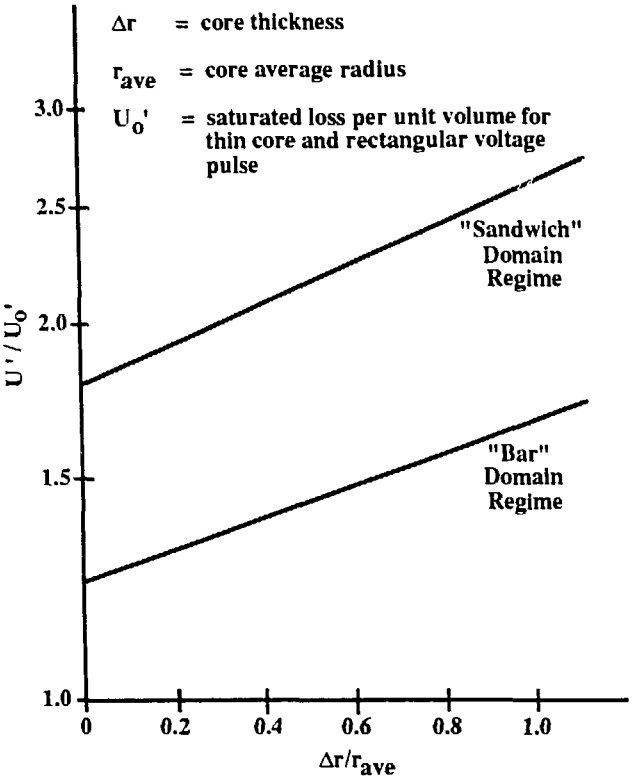

Figure C2. Calculated Mag core loss per unit volume for "1-cos" voltage waveform as a function of core thickness in "bar" and "sandwich" domain regimes.

As a consequence of the few outside wraps of the core saturating last, they have very high dB/dt and thus very high voltage per wrap. This may require thicker insulation between the outer wraps. The very high dB/dt gives a very high loss current, and thus a very high di/dt. This will be limited by circuit impedance, so the voltage per wrap does not get infinite, but the details have not been worked out yet, as far as we know.

*Registered Trademark of Allied Signal.

Appendix D: Early Switchout

Early switchout has been defined as switching out one stage while the preceding stage is still transferring charge.[3,4] Ian Smith has pointed out that the optimum switching time ought to be that which puts the peak of the switched-out current at the time of full charge from the preceding stage.[22] This is not contradicted by the earlier references, and is verified by the simulations given here. Switchout later than this is theoretically 100% efficient, since the preceding stage core prevents the capacitor from discharging backwards. However, there will be additional core losses so it is undesirable to switch later.

Switchout earlier than this optimum will result in some extra loss, but with substantial decrease in core volume. The decrease in core volume results in lower core loss, so that the maximum efficiency including core losses may be at early switchout.

For switchout giving the peak of the discharge current at the time of full charge,

$$\tau_{sw} = \tau_{ch} - \tau_{dis}/2 \qquad (D1)$$

where τ_{sw} is the switching time, τ_{ch} is the full charge time, and τ_{dis} is the discharge time. The compression ratio, C is given by

$$C = \tau_{ch}/\tau_{dis}$$

$$\tau_{sw} = \tau_{ch} - \tau_{ch}/2C$$

$$\tau_{sw}/\tau_{ch} = 1 - 1/2C \qquad (D2)$$

Where V_F is the final full charge voltage, the core volt-seconds up to the switchout time are

$$\int_0^{\tau_{sw}} v\,dt = \frac{V_F\,\tau_{ch}}{2} \int_0^{\tau_{sw}/\tau_{ch}} [1 - \cos(\pi t)]\,dt$$

$$= \frac{V_F\,\tau_{ch}}{2} \left[t - \frac{\sin(\pi t)}{\pi} \right]_0^{\tau_{sw}/\tau_{ch}}$$

$$= \frac{V_F\,\tau_{ch}}{2} \left[\frac{\tau_{sw}}{\tau_{ch}} - \frac{\sin(\pi\,\tau_{sw}/\tau_{ch})}{\pi} \right] \qquad (D3)$$

For optimum, the ratio of switchout volt-seconds to full charge volt-seconds is, using Equation (D3),

$$1 - 1/2C - \frac{\sin\pi}{\pi}(1 - 1/2C) \qquad (D4)$$

Figure D1 shows this expression plotted as the 100% efficiency curve, as well as the results of a computer simulation for earlier switchout times (fewer volt-seconds at switchout). The simulation confirms that expression (D4) is correct for 100% efficiency.

Since the core cross-section is proportional to the volt-seconds, it is apparent that a small reduction in efficiency results in a substantial reduction in core cross-section. In addition, the reduction in core cross-section allows a reduc-

tion in average radius for the same saturated inductance. Thus the core volume savings can be large.

This analysis holds for all stages but only approximately for the output stage. Here it is desirable to model the output stage behavior, since early switchout while the PFL is still charging will modify the output pulse shape. The impedance profile of the PFL can be chosen to compensate for this effect.

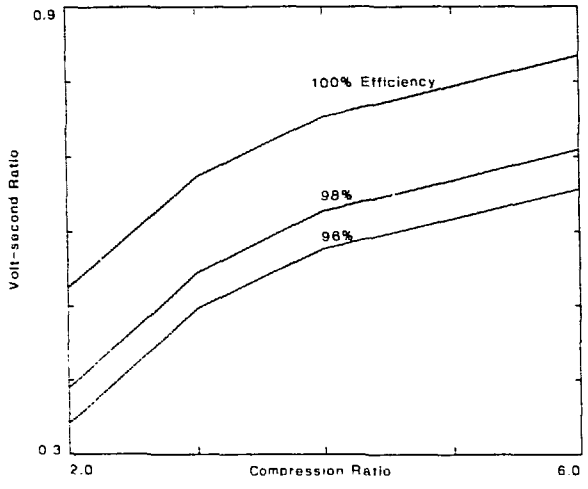

Figure D1. Efficiency of early switchout.

Appendix E: PFL and Liquid Capacitor Calculations

The characteristic impedance of a coaxial PFL is given by

$$Z_0 = \frac{60}{\sqrt{\varepsilon}} \log_e \frac{r_0}{r_i} \qquad \text{(E1)}$$

The E-field is given by

$$E = \frac{V}{r \log_e (r_0/r_i)} \qquad \text{(E2)}$$

The high dielectric constant liquids will stand higher negative fields than positive, by about a 2:1 ratio, so the inner conductor is preferably the negative one. If the ratio of outer to inner conductor radii is greater than the ratio of negative to positive dielectric strengths, the field on the inner conductor will be limiting. Z_0's greater than

$$Z_{LIM} = \frac{60}{\sqrt{\varepsilon}} \log_e F_-/F_+ \qquad \text{(E3)}$$

will have the field at the inner conductor limiting, where F_- and F_+ are the negative and positive breakdown fields, respectively.

We can solve for $\log_e r_0/r_i$ in Equation (E1) and substitute it into Equation (E2)

$$E = \frac{V\ 60}{r\ Z_0 \sqrt{\varepsilon}}$$

$$r = \frac{V\ 60}{E\ Z_0 \sqrt{\varepsilon}} \qquad \text{(E4)}$$

After choosing an allowable E with due regard for field enhancement, we can solve for r, either outer or inner, depending on which has the limiting field. The other radius can be determined from Equation (E1).

It is sometimes desirable to increase the radii of the PFL to better match the radii of the adjacent magnetic components.

The length of the PFL can be determined from

$$\tau_{out} = \frac{w \sqrt{\varepsilon}}{3 \times 10^8}$$

$$w = \frac{3 \times 10^8\ w}{\sqrt{\varepsilon}} \qquad \text{(E5)}$$

High dielectric constant liquid capacitors are limited to a few microseconds charging time at room temperature, as the shunt resistive losses begin to get excessive at longer times.[14]

Liquid capacitors have the same field design criteria as liquid PFL's. At lower voltages, a two electrode coaxial geometry can get rather long because the spacing is small and a definite active fluid volume is needed to store the required energy. Three or four electrode coaxial arrangements or interdigitated radial disks can be used to shorten the length at the expense of mechanical complexity and cost.

One of the most troublesome questions is what electric field stress to use in liquid dielectric at repetition rates. The field strength formulas are based on single-shot data, where advantage can be taken of limited lifetime requirements or streamer propagation time to achieve high fields for short pulses. At repetition rate, ionization, bubbles, and charge injection may not decay before the next pulse and may have a cumulative effect. This is likely to be detrimental. It would seem prudent to stay below the partial discharge inception voltage, however.[7,8,9,10]

APPENDIX F: Energy Storage Increase To Compensate For Reactor And Capacitor Losses

As the design progresses from output to input, the energy storage for each stage has to be increased to cover the downstream stage saturable reactor, water capacitor, PFL, and/or conductor losses. This could be done by increasing the charging voltage with the same capacitance, or by increasing the capacitance with the same charging voltage. The latter is preferable, but calculations using an equivalent series resistance for the losses show the former has less energy left in the upstream capacitor.[15]

The equivalent charge transfer circuit for a saturable inductor is shown in Figure F1, with C1 = C2. The inductance is the saturated inductance including strays, and the

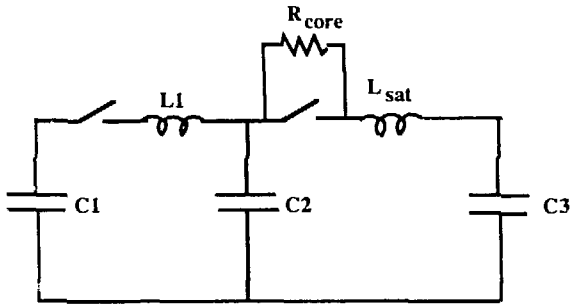

Figure F1. Circuit for loss compensation simulation.

resistor gives the leakage or magnetizing current, and is in general nonlinear. Since we are dealing with low loss ratios, and the core leakage current gets integrated by the downstream capacitor, the exact representation of the nonlinear resistor is of secondary importance. The important factor is the loss, which can be modeled accurately enough with a constant resistance. Note that there is no unsaturated inductance shown, since it is a meaningless term in large MPC's.[16] The leakage or magnetizing current all leads to loss and not stored energy as would be expected of an inductance.

The results of simulations using the equivalent circuit of Figure F1, with larger upstream capacitor, C2, are shown in Figure F2. The upstream capacitor value is chosen to have an energy storage equal to the downstream capacitor energy plus the stage losses, for several ratios of loss to storage. The energy left in the upstream capacitor is plotted versus the loss ratio. The conclusion is that the extra loss is quite low for moderate loss ratios.

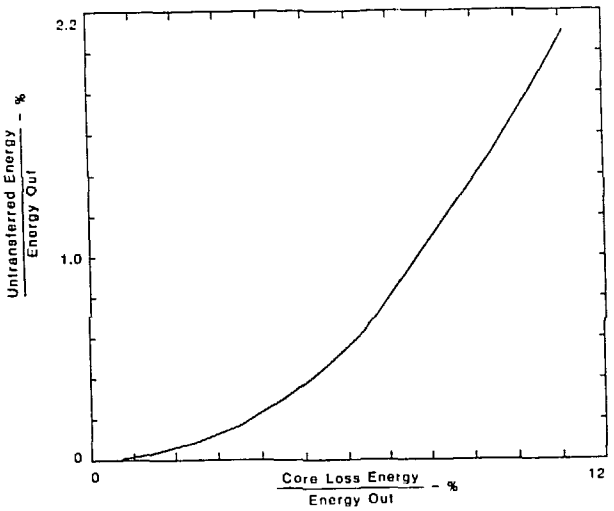

Figure F2. Extra loss due to larger upstream capacitors.

Appendix G: PFL Charge Time

Simulations have been made to determine the preferred charging times for the PFL. The simulations were done using a transmission line code, TLCODE,[17] which has proven very useful for problems of this type.

The circuit is shown in Figure G1, and consists of a capacitor charging a uniform PFL through an inductance. The PFL is open circuited at the output end, and thus the output is the open circuit voltage driving the load, valid for the double transit time of the PFL. The advantage of plotting the open circuit voltage is that the ouptut core switching time can be placed anywhere and the wave shape for the following double transit time of the PFL will give the open circuit voltage applied to the load. The PFL is 100 nsec long one way. The driving capacitor is matched to the PFL capacitance, and the inductance is varied to change the charge time. Minimum ripple conditions were found at approximately half integer and maximums at integer ratios of the PFL charge time to the double transit time of the PFL. Wave shapes for the driving capacitor current and the output voltage of the PFL are shown for these conditions in Figure G2.

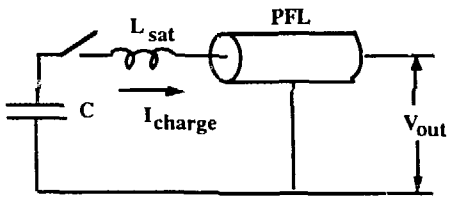

Figure G1. Circuit for PFL charge time simulation.

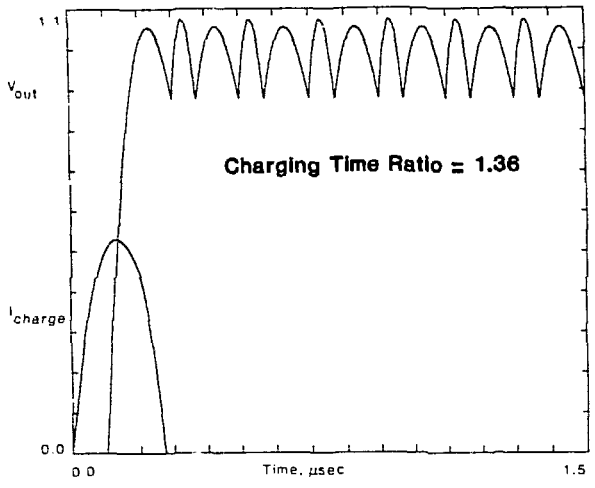

Figure G2(a).

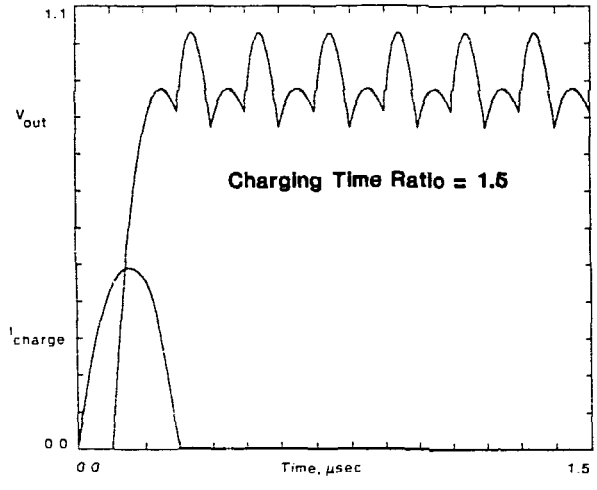

Figure G2(b).

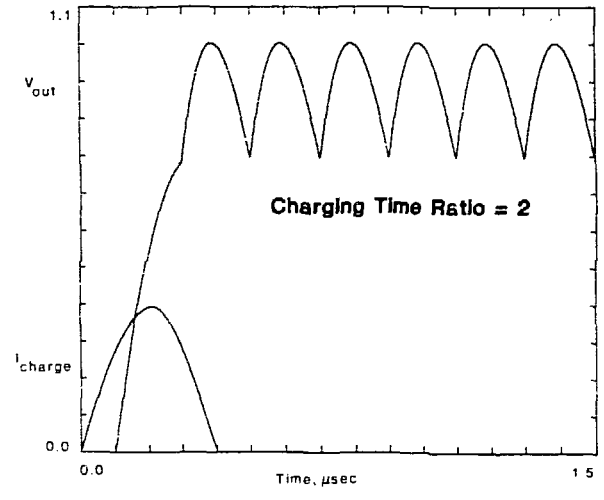

Figure G2(c).

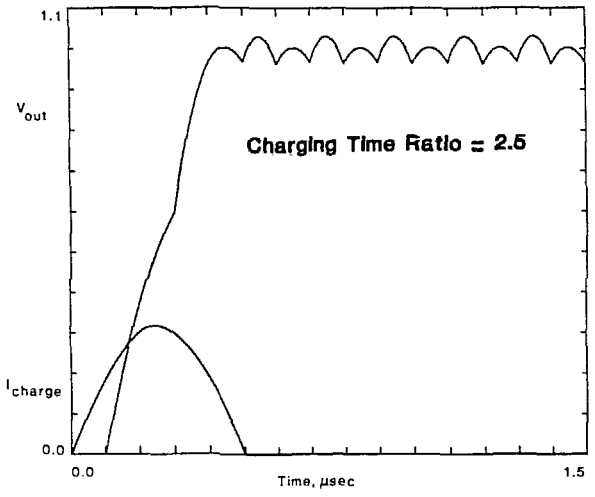

Figure G2(d)

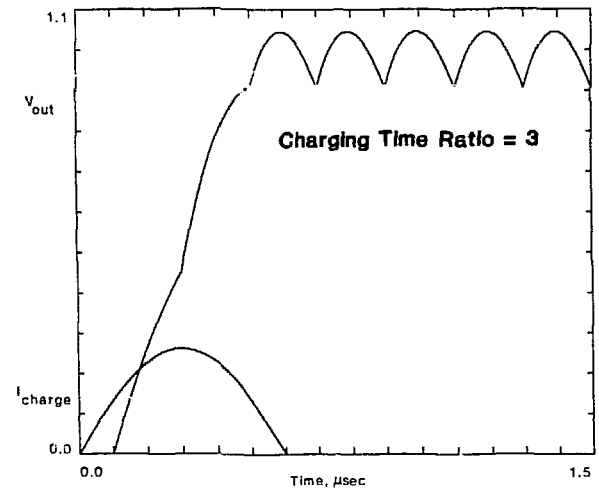

Figure G2(e)

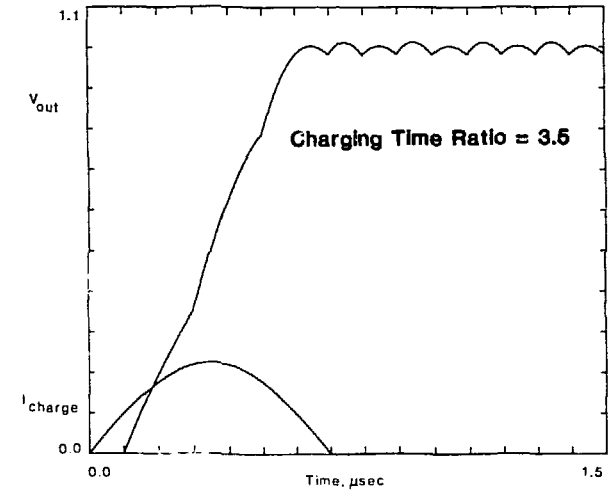

Figure G2(f)

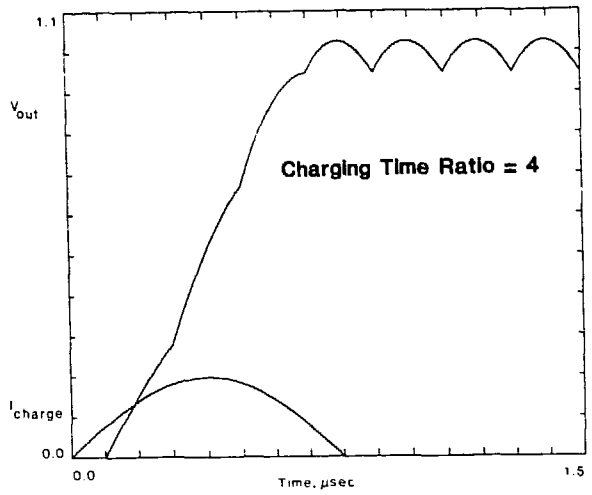

Figure G2(g). PFL open circuit output voltage and charging current.

Figure G3 plots the ripple minimums and maximums versus the ratio of charge time to the PFL double transit time. Note that the minimums are very narrow with respect to the time ratios. Also note that the ripple frequency at half integer time ratios tends to be twice that at integer ratios.

Intermediate time ratios have unequal ripple peaks as shown on the curve for 1.5 time ratio.

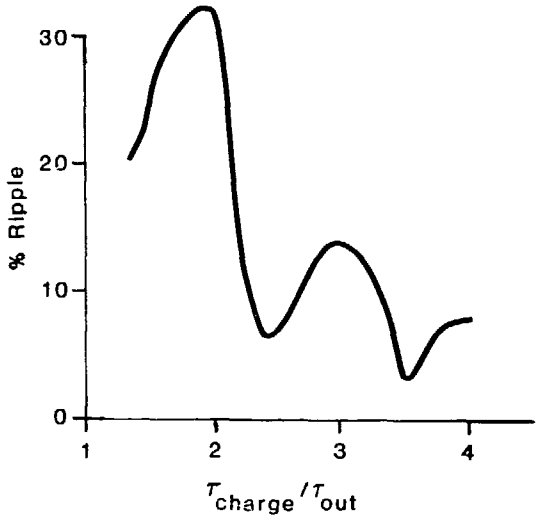

Figure G3. PFL ripple as a function of charging time.

Appendix H: PFL Impedance Profiling

It is possible to vary the impedance of the PFL along its length in order to achieve any reasonable desired output pulse waveshape. This is most conveniently done with a transmission line code, such as AUTOPFL.[23] Extremely flat output pulses can be achieved even with appreciable stray L's and C's, nonlinear loads, and early switchout.

Pulse shaping reduces the efficiency, as all the stored energy cannot be transferred to the output.

An example of a ramped-up output waveshape to achieve a flat output voltage pulse across a load with a trapezoidal current will be described. The trapezoidal current pulse comes from a linear induction accelerator with a constant beam load and a highly ramped accelerator core leakage current load. Since the MPC and accelerator were connected with cables long enough to give time delay isolation, the approach was to provide a ramped voltage pulse that gave the desired load current into the constant cable impedance as a load. This then would give the required flat voltage pulse at the load.

Figure H1 shows the starting output waveshape before impedance profiling. It has the beginnings of a ramp which was achieved by early switchout. Figure H2 shows the open circuit charging voltage of the PFL at the output end. Figure H3 shows the final output waveshape obtained from the impe-dance profile shown in Figure H4. (The impedance profiling could be carried further to get a slightly better output wave- shape.) The steps in impedance would be smoothed out before fabrication.

In order to physically achieve the desired impedance profiles, the changes in PFL radial dimensions should be very small compared with the PFL length, and slowly varying along the length. A short, fat PFL is thus difficult to profile.

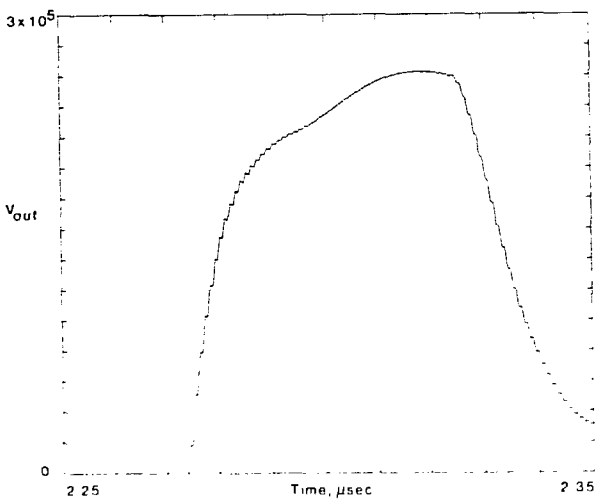

Figure H1. Starting output voltage.

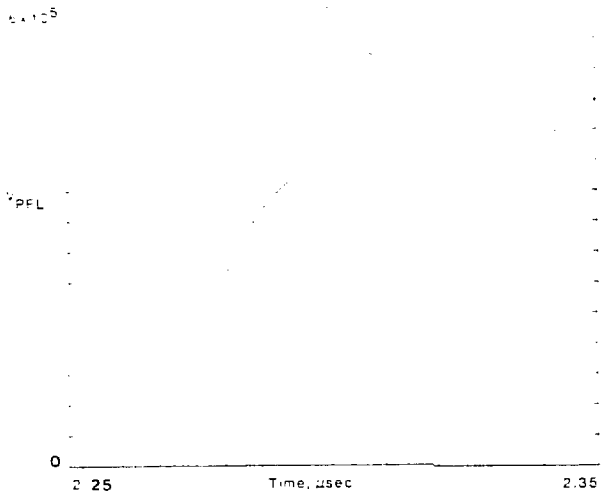

Figure H2. Output end charge voltage on PFL.

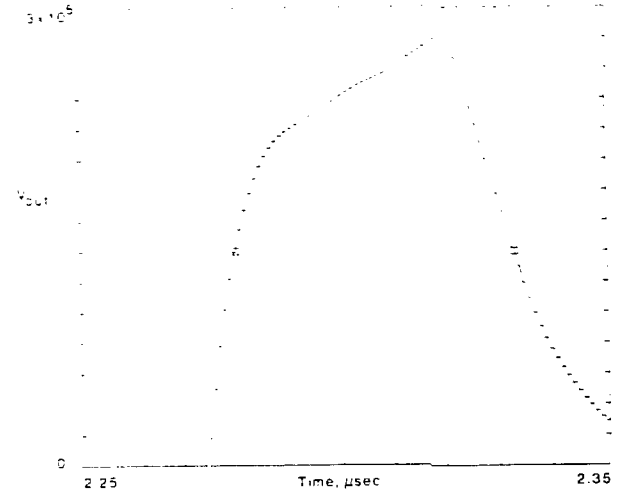

Figure H3. Ending output voltage.

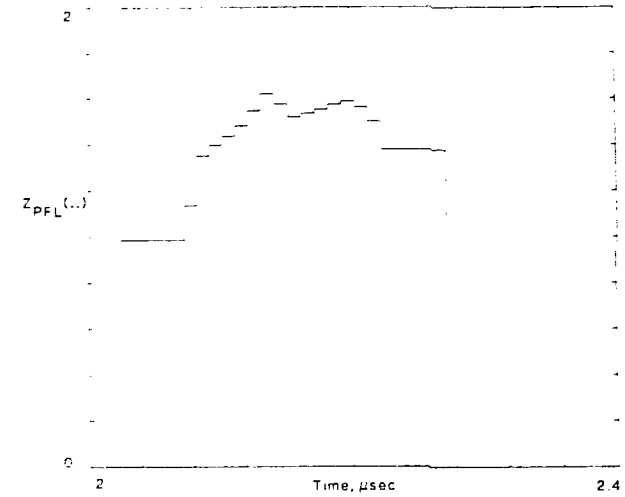

Figure H4. PFL impedance profile.

Appendix I: Core Insulation And Cooling

This is an area where more information is needed. It is expected that some will be presented at this workshop.[20]

Space in the core devoted to insulation has the effect of reducing the average flux density, so the desire is to minimize it Usually, one or two layers of thin flim or paper are used for the core insulation, impregnated with a dielectric fluid. To prevent solid insulation breakdown, the fluid must not break down, as thin film fluid breakdown induces breakdown in the solid insulation. The solid is generally stronger than the liquid.

To determine he actual stress in the fluid and solid film, it necessary to compute the stress distribution in the two-dielectric system according to the relation:

$$E_1 = \frac{V_o}{d_1 + d_2\,(\varepsilon_1/\varepsilon_2)} \qquad (I1)$$

$$E_2 = \frac{V_o}{d_1\,(\varepsilon_1/\varepsilon_2) + d_2} \qquad (I2)$$

where V_o equals the total voltage between magnetic layers, E_1 and E_2 are the voltage stresses in materials 1 and 2, ε_1 and ε_2 are the dielectric constants of materials 1 and 2, and d_1 and d_2 are the thicknesses of materials 1 and 2.

Since the core is loosely wrapped, there will be locations where the local fluid film thickness is nearly zero, even though the average thickness is finite. If 1 represents the fluid, then use $d_1 = 0$ in Equation (I1) to get the maximum fluid stress.

For a core the field enhancement factor for use in Appendix A for the fluid is

$$K_{FE} = \frac{d_1 + d_2}{S\,d_2(\varepsilon_1/\varepsilon_2)} \qquad (I3)$$

where S is the core space factor.

The standard breakdown formulas with area dependence, designed for single pulse breakdown, may be questionable because a few wrap-to-wrap breakdowns can be tolerated without catastrophic core failure.

Some amorphous magnetic ribbons have small projections resulting from pits being etched in the chilling wheels after some time of use.[18,19] Besides making voltage breakdown more likely, the projections can mechanically tear thin film insulation if adjacent magnetic layers slide with

respect to each other. This is a bigger problem on larger cores.

Six μm Mylar* in Freon worked for the LLNL Mag 1D MPC, where the cores were about 0.38 meter OD. The larger 1.7 meter OD Comet cores insulated with two layers of 6 μm Mylar in Fluorinert had unacceptably short life.[18]

Plastic coatings are being developed to cover the projections.[21]

Large, high repetition rate cores require forced cooling.[20] For the highest repetition rates, axial cooling channels are required, spaced throughout the core, with fluid barriers placed to channel the flow. These channels reduce the core space factor, and thus the average flux density in the core.

Appendix J: Logarithmic Approximation

The expression $\log_e r_o/r_i$ appears in inductance and electric field expressions, where r_o and r_i are outer and inner radii respectively. A linear approximation will be developed, to simplify the calculations:

$$\log_e \frac{r_o}{r_i} = \log_e \frac{r_{ave} + \Delta r/2}{r_{ave} - \Delta r/2} = \log_e \frac{1 + \Delta r/2\, r_{ave}}{1 - \Delta r/2\, r_{ave}} \qquad (J1)$$

where r_{ave} is the average radius and $\Delta r = r_o - r_i$. Use the approximation

$$\log_e \frac{1+x}{1-x} = 2x \qquad (J2)$$

where x is small compared to 1

$$\log_e \frac{r_o}{r_i} = \frac{\Delta r}{r_{ave}} \qquad (J3)$$

For $r_o/r_i = 3$, the approximation is only 10% low, so it is adequate for the usual geometries, but the $\log_e$ expression should be used for large aspect ratios.

REFERENCES

[1] W.S. Melville, "The Use of Saturable Reactors as Discharge Devices for Pulse Generators," IEEE Proc. (London), Vol. 98, Part 3, (Radio and Communication) No. 53, 1951, p. 185.

[2] D.L. Birx, et al., "Basic Principles Governing The Design of Magnetic Switches", Lawrence Livermore National Laboratory UCID 18831, November 18, 1980.

[3] S.E. Ball, "Optimum Switching Time for Magnetic Switches," IEEE 18th Power Modulator Symposium, South Carolina, 1988.

[4] G.L. Bredenkamp, J.J. Nel, "A Simultaneous Transfer Electromagnetic Pulse Compressor With Reduced Core Volume," IEEE 7th Pulsed Power Conference, 12-14 June 1989, Monterey, CA.

[5] K. Avery, "Modeling Pulsed Magnetization," to be presented at 1990 International Workshop on Magnetic Pulse Compression.

[6] K. Avery, Private communication.

[7] G.J. Rohwein, "Design of Repetitively Pulsed Megavolt Pulse Transformer Systems," 1984 Sixteenth Power Modulator Symposium, p. 165.

[8] G.J. Rohwein, "Partial Discharge Testing of Bulk Transformer Oil," Proceedings of 3rd International Pulsed Power Conference, Albuquerque, NM, June 1981, p. 420.

[9] G.J. Rohwein, "Partial Discharge Formation and Breakdown in Deionized Water Under Repetitive Stressing," p. 339.

[10] G.J. Rohwein, "Insulation of Dense Windings," to be presented at 1990 Magnetic Pulse Compression Conference.

[11] C.H. Smith, "Permeabilities of Metallic Glasses at High Magnetization Rates," 1988 Eighteenth Power Modulator Symposium, p. 336.

[12] C.H. Smith, "Metallic Glasses in High Energy, Pulsed Power Systems," in Glass....Current Issues, A.F. Wright and J. Dupuy eds., Martinus Nijhoff, Dordrecht, Holland, 1985, p. 188.

[13] S.D. Winter, R.W. Kuenning, and G.G. Berg, "Pulse Properties of Large 50-50 NiFe Tape Cores," IEEE Trans. on Magnetics, MAG-6, No. 1, March 1970, p. 41.

[14] D.B. Fenneman and R.J. Gripshover, "The Electrical Performance of Water Under Long Duration Stress," 1980 Fourteenth Pulse Power Modulator Symposium, p. 150-3.

[15] P.H. Swart, G.L. Bredenkamp, H.M. von Bergmann, "Computer Spreadsheet Design, Numerical Simulation and Practical Evaluation of a Lossy Series Pulse Compressor," 6th IEEE Pulsed Power Conference, Virginia 1987.

[16] R.W. Kuenning, "Unsaturated Permability and Unsaturated Inductance - Fact or Fiction," to be pre- at 1990 International Workshop on Magnetic Pulse Compression.

[17] W.N. Weseloh, "TLCODE - A Transmission Line Code for Pulsed Power Design," IEEE Seventh Pulsed Power Conference, 12-14 June 1989, Monterey, CA.

[18] H.C. Harjes, K.J. Penn, G.A. Mann, and E.L. Neau, "Investigations Into The Design of Multi-terawatt Magnetic Switches.

[19] H.C. Harjes, G.A. Mann, E.L. Neau, and F.A. Morgan, "Improved Core Insulation Schemes for Multi-terawatt Magnetic Switches," IEEE Seventh Pulsed Power Conference, 12-14 June 1989, Monterey, CA.

[20] R. Stone, "Core Cooling Studies at LLNL and Sandia," to be presented at 1990 International Workship on Magnetic Pulsed Compression.

[21] D. Sharp, "Coating Possibilities for Magnetic Switches," to be presented at 1990 International Workshop on Magnetic Pulse Compression.

[22] Ian Smith, Private communication.

[23] P. Corcoran, I. Smith and D. Wake, "Three Reverse Engineering Codes for Pulse Power System Design", IEEE Seventh Pulsed Power Conference, 12-14 June 1989, Monterey, CA.

Possible Applications of Induction Linacs Driven by Magnetic Pulse Compressors

James C. Swingle
Beam Research Program
Lawrence Livermore National Laboratory
Livermore, CA 94551

ABSTRACT

In the 25 years since induction accelerators were first proposed, they have been used extensively as research accelerators for investigation of a range of particle beam and radiation sources. While the technology has been applied in flash radiography, extensive use of these devices in commercial and military applications has not occurred. Over the last decade, increased understanding of the physics of beam transport and the invention of novel pulse-power designs aimed at high-repetition-rate operation have produced the technical possibility of using the technology as the power source for optical and millimeter-wave free-electron lasers (FELs), relativistic klystrons, heavy-ion accelerators, x-ray sources, CARMs, and electron beam (e-beam) waste/pollutant processors. Magnetic switching has been an important element in many of the concepts intended for these applications. We provide a brief summary of the possible applications of induction linacs driven by magnetic switches and technical issues that must be resolved.

INTRODUCTION

The induction accelerator[1], depicted schematically in Fig. 1, produces high-peak-current, high-energy particle beams by sequentially exposing the particles to the accelerating fields produced in gaps in the beamline driven by pulse power sources. The concept was introduced by Christofilos and coworkers[2] in 1964. The azimuthal time-varying magnetic flux produced by a current loop enclosing a toroid made of ferrimagnetic material results in an axial accelerating field in the gap. The concept is often described simplistically as a series of one-turn transformers, with the particle beam performing the role of the secondary circuit. Furthermore, the nonresonant coupling between the particles and the accelerating fields in adjacent gaps is often cited as an important difference between induction linacs and radio frequency (rf) linacs. In fact, the induction accelerator is rich in phenomena that unfold in both time and space, rendering useless the simplistic descriptions of the concept for those seeking a thorough understanding of the design principles for these devices. The goal of producing a mono-energetic particle beam pulse at high peak current, lasting from tens to hundreds of nanoseconds, is made challenging by a number of real-world effects.

The Time-Varying Electromagnetic Field

The energy and the transverse motion imparted to particles in various slices of the beam pulse are affected by variation of the current pulse applied to each accelerator cell. However, even for an ideal current source, the ferrimagnetic core responds to the propagation of a saturation wave through the material. This produces a nonlinear variation of magnetic flux in space and time and a corresponding variation of the electromagnetic field in the gap. There is also the self-induced variation of the field seen by the particles in the accelerating gap if the beam current varies in time, changing the load applied to the drive circuit.

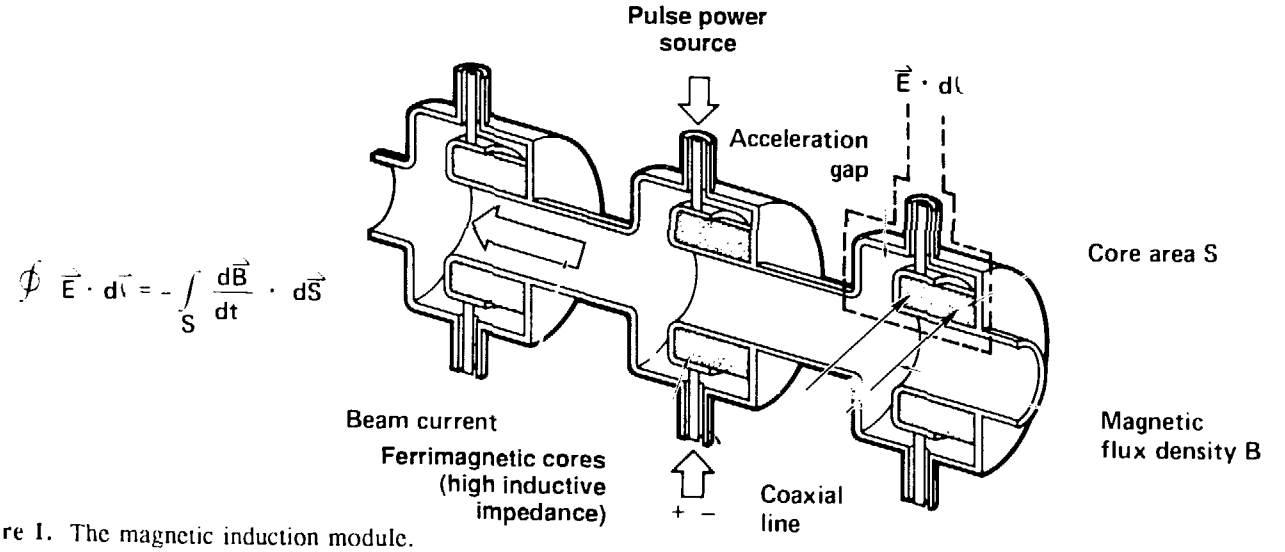

Figure 1. The magnetic induction module.

Non-Ideal Beam Transport

The system of magnets often used to transport the particle beam through the accelerator is usually chromatic to some degree and is subject to errors in the magnitude and location of the magnetic field the beam experiences. The result is that the beam transverse motion from head to tail is directly affected by energy variation during the pulse, often resulting in a "corkscrew" phenomenon that can severely degrade beam quality. Induction accelerators that must meet requirements for high beam quality must be designed for accurate magnetic alignment and precise control of energy sweep during the pulse.

Beam Interaction with Its Own Radiation

Microwave noise radiated by the beam in the transverse direction produces transverse fields that kick the beam off-axis. Sequential kicks to the particles during acceleration lead to the well-known "beam breakup instability" (BBU), where the transverse displacement of the beam grows exponentially along the axial dimension of the accelerator. The design of accelerator cells must include features that minimize the transverse Q for microwaves and optimize the magnet parameters and cell dimensions to control BBU.

Time-Dependent Circuit Parameters at High Repetition Rate

The properties of components change as a function of time when the accelerator is operated at very high repetition rates (particularly in the ferrimagnetic elements of the circuit) due to increases in the temperature. At sufficiently high pulse rates, mismatched elements in the circuit may not have enough time for complete damping, resulting in off-nominal performance.

Over the last several years, each of these phenomena has been studied in a piecemeal fashion in order to gain understanding of the underlying physics. Detailed simulation tools have been developed to study some of these effects with sufficient resolution to allow comparisons with experiment. In the future, it may be possible to integrate pulse power, induction cell, and transport models to produce a simulation tool capable of following all the important processes that affect the beams observed at the output of a high-energy induction machine. Then the scientific validation of the induction accelerator concept can be brought to a close, and detailed design and application of the technology can begin.

The remainder of this article briefly describes some of the radiation and e-beam sources that can be devised using induction accelerators with magnetic switches as power sources. We discuss a series of radiation sources ranging in wavelength from the microwave regime to the x-ray regime, and we discuss the two-beam accelerator concepts, where low-energy induction machines are used to produce high-power, high-frequency microwaves to drive high-gradient rf beamlines. Finally, we mention the possible commercial applications of low-energy induction machines to address environmental problems.

MICROWAVE AND MILLIMETER-WAVE FELS

From the standpoint of research devices, the microwave and mm-wave FELs have achieved great success in validating the physics of single-pass amplification of an input master oscillator signal by the coherent radiation from a suitably bunched relativistic e-beam. The familiar conceptual layout is shown in Fig. 2. Pulses from an induction machine operating in the regime 1–10 MeV, 1–3 kA, 10–100 ns, 1–1000 Hz enter a magnetic wiggler (peak field ~2–5 kG) in conjunction with pulses from a master oscillator operating at the resonant frequency of the wiggler (peak power ~10–1000 W). The e-beam begins to bunch spatially in the axial dimension in response to the undulatory motion of the particles in the periodic wiggler field and the field imposed by the electromagnetic wave of the master oscillator. Electrons that are trapped in this ponderomotive well begin to radiate coherently into the radiation field. The high peak current of the e-beam results in exponential gain of tens of dB/m in the front end of the wiggler. Saturation of the gain begins to occur when the trapped electrons lose sufficient energy to fall out of resonance with the wave. At this point, typically a few percent of the electron energy has been converted to radiation. Additional extraction can be obtained by tapering the wiggler parameters beyond the point of saturation to restore resonance at the appropriate frequency. An impressive demonstration of this technique was obtained on the Electron Laser Facility (ELF) experiment at LLNL[3]. Figure 3 shows the peak power obtained at 35 and 140 GHz on the ELF device. It is noteworthy that the particle simulation code FRED was able to calculate amplifier performance in good agreement with the experiment. The instantaneous bandwidth and mode quality of the ELF amplifier were also shown to be excellent, as shown in Fig. 4.

The ELF experiments were performed at low PRF (~1/2 Hz). When combined with induction accelerator technology capable of kHz operation, these high-peak-power, high-instantaneous-bandwidth microwave and mm-wave devices will provide interesting drive sources for electron-cyclotron heating in tokamaks[4], space power beaming[5], and high-gradient rf linacs for linear colliders[6].

Electron-Cyclotron Heating

FELs in the 140–600 GHz range are needed for this application. Multimegawatt average power levels at high frequency drive the energy requirements up to the range 5–20 MeV at high peak current (~3 kA). Breakthroughs in magnetic switching that would make possible repetition rates in the range 10–50 kHz with good efficiency could significantly affect this field. The key technical issue affecting

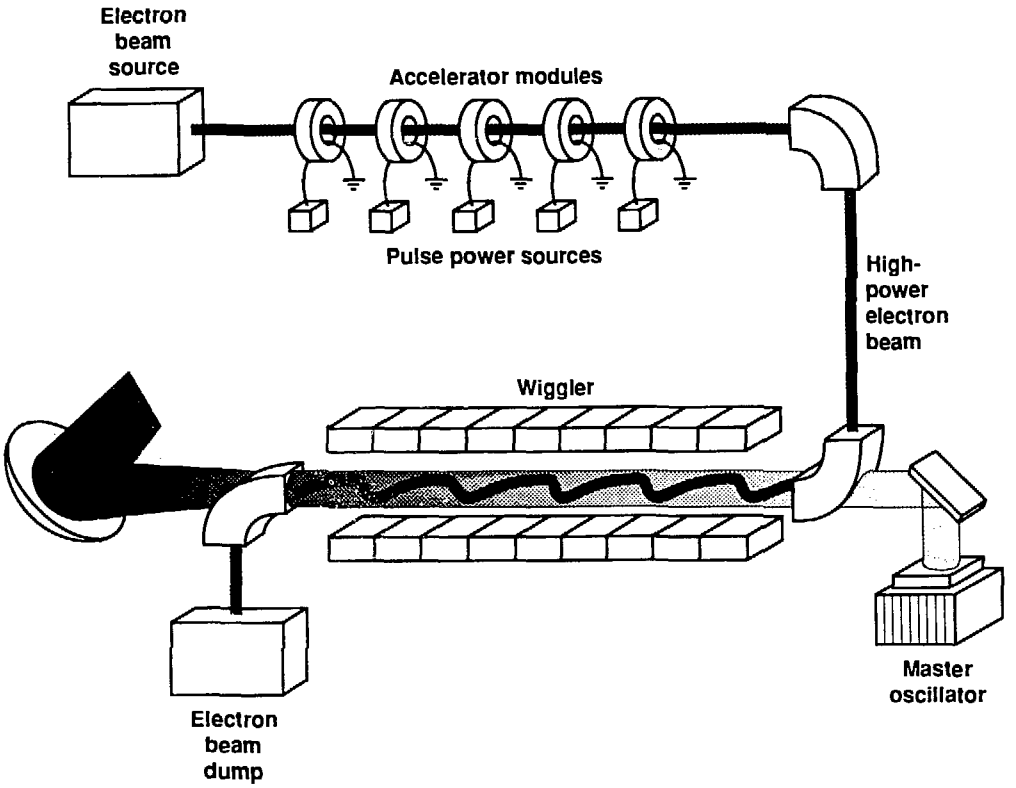

Figure 2. Component technologies for a high-power FEL.

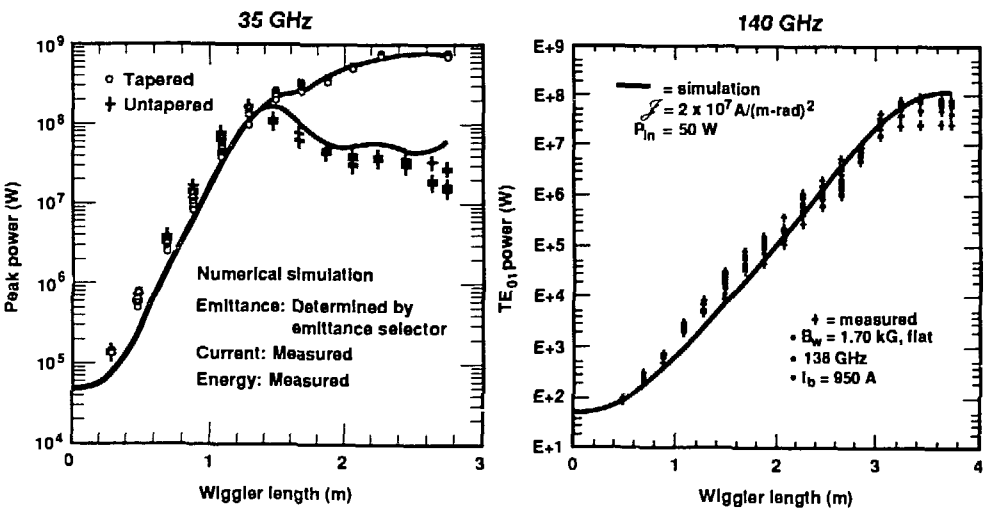

Figure 3. Peak power achieved with the ELF amplifier at 35 GHz and at 140 GHz.

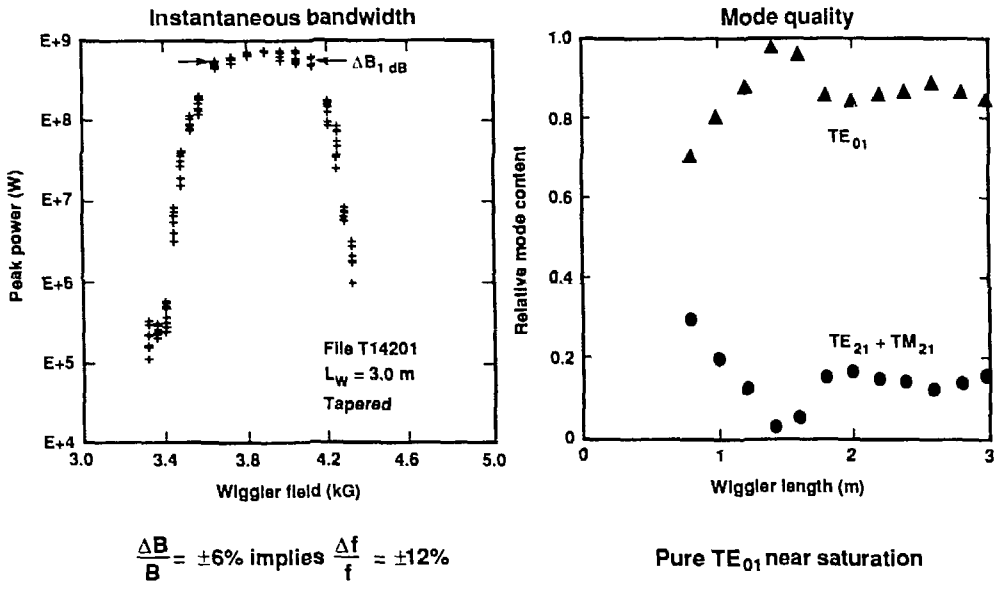

Figure 4. Instantaneous bandwidth and mode quality of the ELF amplifier.

the choice of induction FELs for this application involves the demonstration of benefits due to the use of a limited number of high-peak-power, high-frequency FELs to drive the tokamak as compared to a large number of CW gyrotrons. Issues of cost and reliability will affect the outcome[7]. Computational models for predicting amplifier performance have been developed extensively[8,9]. Characterization of the effects of high-average-power operation has received only preliminary analysis[10].

Space Power Beaming

FELs operating in the regime 35–1000 GHz with megawatts of average power can be considered for powering space platforms or lunar/planetary bases and for providing energy for propulsion. High-power microwave and mm-wave radiation can potentially be converted to electrical power using rectennas or other novel schemes[11].

Linear Colliders

FELs operating in the regime 15–35 GHz could potentially be used to drive rf accelerators with gradients in the range 100–200 MeV/m (see Fig. 5). Microwave drive sources of this type may be needed for the next generation of linear colliders with center-of-mass electron/positron energy in the TeV range.

OPTICAL FELS

Much of the component technology development for induction FELs over the last several years has been directed toward near infrared lasers. In general, the short wavelength of these devices requires tight control on e-beam energy sweep during the pulse and beam brightness.

Inertial fusion power plants driven by lasers may require large quantities of optical excitation power for solid-state storage media (e.g., crystalline host media doped with rare-earth ions). This optical power could potentially be delivered by flashlamps, diode lasers, or FELs. These pump sources will be required to deliver tens of MJ of optical energy per pulse at a rate of 1–10 Hz to drive the power plant. Furthermore, the pump power must be delivered at a cost of <$1 per average watt. There are no existing sources that can simultaneously meet all of the requirements. If FELs are to have an effect on this problem, they will need to operate in the long pulse regime (microseconds)[12] and must re-use the core material of the accelerator in a recirculating fashion[13] to develop the appropriate electron energy (as illustrated in Fig. 6). The pulse-power technology to drive such an accelerator does not exist. There are many issues associated with efficiency, reset, and thermal management that have not been addressed. However, due to the high leverage and possibility of development time for this application, new concepts and new materials can be considered under the assumption that research programs can be formed to pursue them over the next decade.

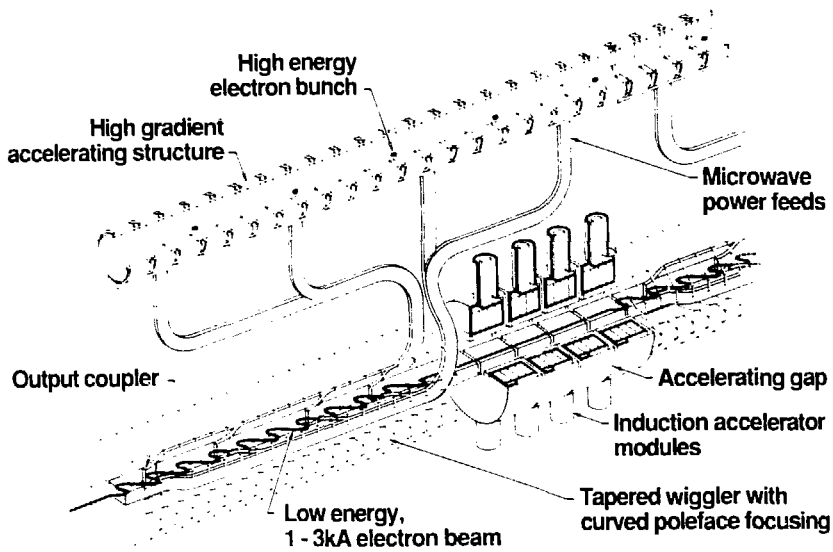

Figure 5. FEL-driven accelerator concept. The two-beam accelerator (TBA) consists of a high-power microwave FEL and a high-gradient linac.

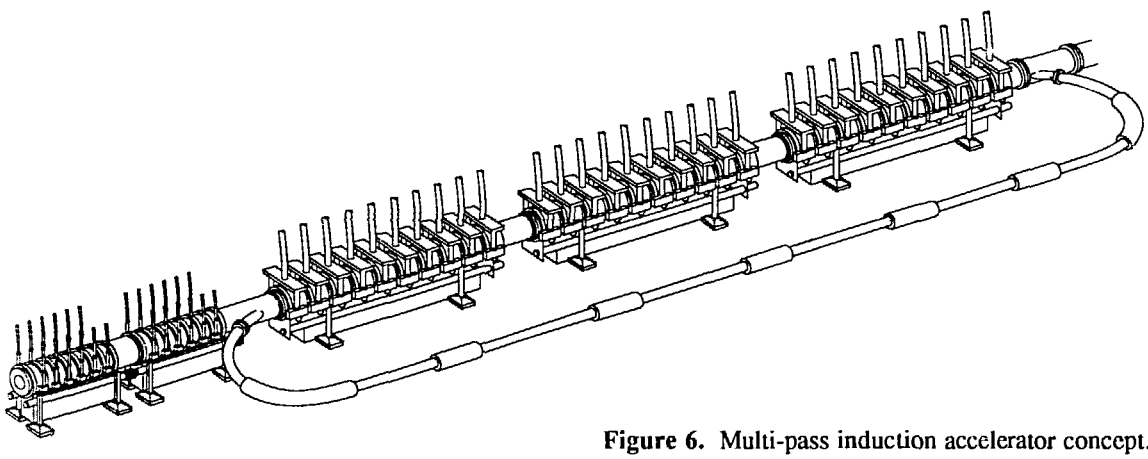

Figure 6. Multi-pass induction accelerator concept.

RELATIVISTIC KLYSTRON-DRIVEN RF LINACS FOR VUV AND X-RAY SOURCES

Low-energy induction linacs (1–3 MeV) driven by magnetic switches can be considered as drive sources for relativistic klystrons[14]. These high-peak-power microwave sources can be used to drive high-gradient rf beamlines in a way similar to that described earlier for the microwave FEL (see Fig. 7). The resulting high-energy, compact rf beamline can be used to produce VUV and x-ray emission when passed through a suitable wiggler. Non-resonant systems producing incoherent radiation may be suitable for semiconductor lithography[15]. Resonant systems producing coherent radiation may be useful for holography, high-resolution spectroscopy, and surface science. Operation of the induction machine at kHz rates could produce enough average power at these short wavelengths to allow commercial uses. The compactness of these designs may imply acceptable costs.

E-BEAM PROCESSING OF FOOD, WASTE, AND STACK GASES

High-repetition-rate, low-energy induction machines can potentially be used to address nutritional and environmental issues. E-beams with characteristics in the regime 1 MeV, 1–3 kA, 50 ns, 1 kHz can be converted to gamma rays and x-rays. These sources can be used to sterilize food[16] or municipal waste[17,18]. For these applications, tens of kW of average beam power is required. Electron beams can also be considered for removal of NO_x and SO_2 constituents from stack gases produced at fossil fuel power plants[19,20,21]. Some demonstration units making use of DC electron beams entering the flow through large foil windows have shown the capability to produce useful fertilizers that precipitate out of the flow when stoichiometric amounts of NH_3 are added to the stack gases upstream of the e-beam system. In order to process the effluent from an entire coal-fired plant, megawatts of e-beam power are required. The capital cost of various e-beam systems is the key issue affecting the ultimate utility of this scheme when compared to chemical separation systems. Induction accelerators have been proposed[22] as one of the possible solutions to these kinds of industrial applications.

SUMMARY

Widespread practical application of the induction accelerator awaits the development of low-cost, reliable components and the experimental validation of end-to-end design tools that follow the nonlinear interaction of the electron beam, the induction cells, the magnetic transport, and the pulse-power system. The range of potential applications for the technology is large; however, the current cost, size, and complexity of these devices stand as obstacles to further development. Innovations in the areas of pulse power and materials research could significantly affect the application of the technology.

This work was performed jointly under the auspices of the U.S. Department of Energy by Lawrence Livermore National Laboratory under contract W-7405-ENG-48, for the Strategic Defense Initiative Organization and the U.S. Army Strategic Defense Command in support of SDIO/SDC MIPR No. W43-GBL-0-5007.

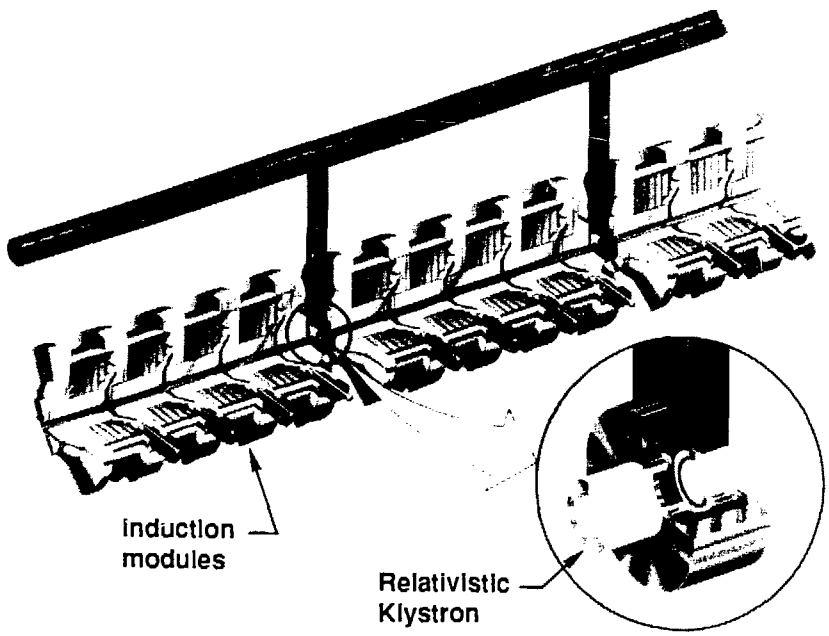

Figure 7. Relativistic klystron version of the two-beam accelerator.

REFERENCES

[1] R.J. Briggs, "Linear Induction Accelerators," Proc. 1986 Linear Accelerator Conf., Stanford Linear Accelerator Center, SLAC-Report-303, 10, September 1986.

[2] N.C. Christofilos, R.E. Hestor, W.A.S. Lamb, D.D. Reagan, W.A. Sherwood, and R.E. Wright, "High Current Linear Induction Accelerator for Electrons," *Rev. Sci. Instr.* 35, 886 (1964).

[3] T.J. Orzechowski, B.R. Anderson, J.C. Clark, W.M. Fawley, A.C. Paul, D. Prosnitz, E.T. Scharlemann, S.M. Yarema, D.B. Hopkins, A.M.Sessler, and J.S. Wurtele, "High Efficiency Extraction of Microwave Radiation from a Tapered Wiggler Free Electron Laser," *Phys. Rev. Lett.* 57, 2172 (1986).

[4] D.W. Ignat, D.R. Cohn, and P.P. Woskov, "The Compact Ignition Tokamak and Electron Cyclotron Heating: Description of Need; Assessment of Prospects," Princeton University Report AA-881018-PPL-05, October 1988.

[5] J.C. Swingle, "Technical Options for High Average Power Free Electron Millimeter-Wave and Laser Devices," Second Beamed Space-Power Workshop, NASA Langley Research Center, Hampton, VA, February 28–March 2, 1989, NASA Conf. Publication 3037, p. 191.

[6] A.M. Sessler and D.B. Hopkins, "The Two-Beam Accelerator," 1986 Linear Accelerator Conf., June 2–6, 1986.

[7] R.A. Jong and R.R. Stone, *Preliminary Design of an Induction-Linac Based Free-Electron Laser Amplifier for Plasma Heating in CIT/ITER*, LLNL Report UCRL-99595, September 1988.

[8] R.A. Jong, W.M. Fawley, and E.T. Scharlemann, "Modeling of induction linac based free-electron laser amplifiers," in "Modeling and Simulation of Laser Systems," *SPIE* 1045, 18 (1989).

[9] R.A. Jong et al., *IMP, A Free Electron Laser Amplifier for Plasma Heating in the Microwave Tokamak Experiment*, LLNL Report UCRL-99368 (1988).

[10] R.A. Jong and R.R. Stone, *Induction-Linac Based Free-Electron Laser Amplifier for Fusion Applications*, LLNL Report UCRL-98675 (1988).

[11] G.A. Askaryan, G.M. Batanov, and I.A. Kossyi, "Plasma-burst conversion of intense microwave radiation and supplying power to space stations," *Sov. Tech. Phys. Lett.* 15, 294 (1989).

[12] J.E. Leiss, N.J. Norris, and M.A. Wilson, "The Design and Performance of a Long-pulse High-current Linear Induction Accelerator at the National Bureau of Standards," *Particle Accelerators* 10, 223 (1980).

[13] M.A. Wilson, "Recirculation Acceleration of High Current Relativistic Electron Beams- A Feasibility Study," IEEE Trans. Nuc. Sci. NS-28, 3375 (1981).

[14] A.M. Sessler and S.S. Yu, "Relativistic Klystron Version of the Two-Beam Accelerator," *Phys. Rev. Lett.* 58, 2439 (1987).

[15] M. Crawford, "The Silicon Chip Race Advances into X-rays," *Science* 246, 1382 (15 December 1989).

[16] M.C. Lagunas-Solar and S.M. Matthews, "Radionuclide and Electric Accelerator Sources for Food Irradiation," *Rad. Phys. Chem.* 25, 691 (1985).

[17] S.B. Ahlstrom, "Irradiation of Municipal Sludge for Pathogen Control," *Rad. Phys. Chem.* 31, 131 (1988).

[18] J.G. Trump, E.W. Merrill and K.A. Wright, "Disinfection of Sewage Wastewater and Sludge by Electron Treatment," *Rad. Phys. Chem.* 24, 55 (1984).

[19] P. Fuchs, B. Roth, U. Schwing, H. Angele, and J. Gottstein, "Removal of NO_x and SO_2 by the Electron Beam Process," *Rad. Phys. Chem.* 31, 45 (1988).

[20] K. Williams, W.A. Frutiger, J. Hiley, and S.V. Nablo, "Requirements for Very High Power Electron Beam Systems for Utility Stack Gas Treatment," *Rad. Phys. Chem.* 31, 29 (1988).

[21] S. Jordan, "Progress in the Electron Beam Treatment of Stack Gases," *Rad. Phys. Chem.* 31, 21 (1988).

[22] J.R. Bayless and R.J. Adler, "Linear Induction Accelerators for Radiation Processing," *Rad. Phys. Chem.* 31, 327 (1988).

'90

Working Group Reports

Network and System Modeling Group

Anthony N. Payne, Chairman
Stephen E. Sampayan, Cochairman

Working Group Members

G. Bowden
J. DeFord
R. Dougal
D. L. Johnson
R. J. Kares
J.-A. Kishiro
W. Niven
A. Payne
S. Sampayan
P. Siemens
B. Turner
T. Warren
W. N. Weseloh

Introduction

The objective of the Network and System Modeling Group was to assess the state of the art in magnetic pulse compressor modeling and to recommend future research and development efforts in this critical area. It was generally felt that this objective was crucial to the overall goal of the workshop which was to explore our ability to design and build high-average-power magnetic pulse compressors that operate continuously. Indeed, significant advances in the design of magnetic pulse compressors of this class will depend to a large degree upon the ability to do high-fidelity modeling.

A primary aim of our group, therefore, was to explore the modeling technology base required both to enhance the efficiency and accuracy of the design cycle and to foster innovative compressor design concepts. To this end, we endeavored to review and summarize the important aspects of the general modeling problem. In particular, we sought to identify the available models of critical network components, to review the current methodology for network and system modeling, to assess the capabilities of existing modeling tools, and finally to identify what we considered to be the most important research areas both in modeling and in the development of analysis and design tools.

In this report, we present the results of the working group's efforts. First, we briefly review the invited presentation representing our group in the plenary session of the workshop as well as the three technical presentations given in our working group. We identify the main points of each presentation and the important comments made in the ensuing discussion. Next, we outline the framework that we constructed to guide our efforts as a group. The remaining sections then summarize our findings and recommendations as they relate to this framework. Specifically, we discuss the modeling of important compressor network components. Most of our effort there is devoted to magnetic switches and transmission lines. We then turn our attention to the modeling of the system aspects of the problem. Here we are concerned with the issue of modeling the design requirements and using such models in the design process. Finally, we consider the subject of modeling, analysis, and design tools. We first review a number of computer programs that are in use in the pulsed power community and critique their applicability to the magnetic pulse compressor problem. We then specify the important features of an ideal tool for compressor problems.

Technical Presentations

Jan-Mark Zentler of LLNL represented the Network and System Modeling Group in the opening plenary session with a presentation entitled "Modeling Magnetic Pulse Compression Networks." Jan reviewed the basic reasons for modeling: models are needed to study such issues as the energy transfer within the network, the interaction between compressor and load, pulse shaping, the switch reset process, and thermal management. Most of the address focused on the challenge of modeling of magnetic switches—a challenge presented by the complex nonlinear nature of the core materials and the effects of factors such as mechanical stress, temperature, and annealing history, that are difficult to quantify. It was noted that numerous magnetic material models have been proposed over the past four decades, ranging from crude circuit models to detailed domain wall and micromagnetic models. It was felt that empirical models, though perhaps lacking in solid theoretical basis, can give reasonable fits to data and tend at present to have the greater applicability.

Following the plenary session, the working group convened during the first session to hear three invited papers. William C. Turner of LLNL addressed critical systems issues arising with the problem of beam-energy sweep in an electron linear-induction accelerator driven by magnetic pulse compressors.[1] This problem typifies the challenges arising in the design of high-average-power, high-repetition-rate magnetic pulse compressors. It is an especially difficult problem from the modeling viewpoint because the extremely stringent system performance requirements necessitate very accurate models. Also, the magnetic pulse compressors must be considered as part of the larger, highly coupled, overall system. The development of system models that are truly predictive of system performance will require accurate models both of large core magnetic switches operating at high dB/dt and of the reset dynamics at high pulse repetition frequency.

In the second invited paper, Edmund Y. Chu of Maxwell Laboratories shared his experiences in designing magnetic pulse compressors and outlined the important design issues that must be addressed to optimize designs with respect to size, weight, cost and efficiency.[2] He discussed the major issues of magnetic-switch saturation times, number of pulse-compression stages, switch reset and bias, output prepulse and reflected energy from the load. The problems associated with reset, prepulses, and reflected energy can often be handled by the proper circuit topology, but design is often performed without adequate models. For example, predicting energy reflected from the load or energy left behind in the compressor can be very difficult. Thus, he emphasized the importance of developing models with good predictive capability to study these major design issues.

In the discussion following these first two papers, the importance of constructing models that are accurate predictors was confirmed. A crucial need is the ability to build parametric models that are applicable over a large region of the design parameter space and that are capable of predicting the performance for compressors before they are built. This is a very different matter and a more difficult task than merely fitting a model to an existing point design and replicating the measured performance data.

Wayne N. Weseloh of Power Spectra presented the final invited paper, in which he gave an overview of three simulation tools that might be of use in modeling magnetic pulse compressors.[3] These were SCEPTRE, PSpice, and SCIMATH. He introduced the group to the relative advantages and disadvantages of each. This analysis set the stage for the group's assessment of modeling tools, which we discuss later.

Framework for Technical Discussions

After the presentation and the discussion of the invited papers, we sought to establish a comprehensive framework to

guide our work in the remaining sessions. We first agreed on a taxonomy of the various aspects of the magnetic pulse compressor modeling problem.

The problem of modeling magnetic pulse compression systems involves two primary considerations. The first consideration relates to the network proper. In this case, we require two pieces of information. First, we need a description of the topology of the network, that is, a description of how the various components are interconnected to achieve magnetic pulse compression. Included in the description of the topology are the pulse-compression scheme (e.g., a Melville series line[4] or a parallel saturating transformer line[5]) and the magnetic switch reset and bias circuitry. Second, we require an accurate description or model of each individual component making up the network.

The second important consideration in pulse compressor modeling relates to the systems aspects of the problem. In particular, we generally desire a model of the compressor not only to simulate accurately its dynamical response but also to evaluate its response as measured against design requirements. Therefore, we require mathematical descriptions of the performance specifications of the overall system as well as of individual network components. Specifically, we are interested in the design parameters of problem, the constraints these parameters must satisfy, and the relevant design objectives or performance measures (e.g., cost, efficiency, output waveform characteristics, etc.) for evaluating the merit of a given design.

To analyze or design a magnetic pulse compressor, we require modeling tools to help with developing models of both the network and the systems aspects of the problem. The modeling tools help us to build overall network and system models and permit us to exercise these models to simulate system performance and to evaluate and compare designs.

We identified, therefore, the following four areas as those in which it seemed most important both to assess the state of the art and to define areas of future research and development.

- The modeling of critical network components: Which of the components used in magnetic pulse compressor systems are most critical to high fidelity modeling?
- The modeling of system design problems: What are the important design parameters, objectives and constraints typically of concern in the design of a magnetic pulse compressor? What are the model-based methods or algorithms available for ascertaining necessary design tradeoffs and finding acceptable designs?
- An assessment of existing modeling tools: What tools are available to do simulations of magnetic pulse compressors? What tools are available to perform system tradeoff studies? How helpful are they for this class of problems and what are their deficiencies?
- The anatomy of an ideal analysis and design tool: What specific requirements does the magnetic pulse compression problem place upon the tool? What type of tool would be most useful in analyzing and designing high-average-power magnetic pulse compressors that operate in a burst mode or continuously?

Note that we did not address the specific modeling issues arising with network topology. Topology, of course, can be an important design "parameter." However, a truly versatile modeling tool should be able to handle all topologies equally well, and our design methodology should be sufficiently general to be independent of specific topology.

Modeling of Critical Network Components

We first considered the problem of modeling the critical network components necessary to do high-fidelity modeling of compressor systems. Besides circuit components that can be adequately represented as lumped resistors, inductors, or capacitors, or other conventional lumped circuit devices, four main classes of components are found in magnetic pulse compressors that require modeling: (1) saturable reactors, or magnetic switches; (2) transmission lines and pulse forming lines; (3) conventional (opening and closing) switches; and (4) loads.

Because of the limited time available to the working group, however, we decided that we should concentrate our attention on a study of only two of these classes of components, namely, magnetic switches and transmission lines.

The modeling of conventional switches can be very important, for example, in a study of timing jitter in magnetic pulse compressor systems. From a computational point of view also, conventional switch models can present difficulties to simulation codes. Therefore, it is important to develop accurate and computationally viable switch models for network and system studies.

The load driven by a magnetic pulse compressor is of course application dependent. In fact, there are many loads that are of interest in the application of magnetic pulse compression technology, including lasers, electrical discharge devices and plasma sources, and the ferrite cells and beam current loads in linear induction accelerators. Loads are rarely simply resistive in nature, nor are they linear and time-invariant. In some applications, the load is transit-time-isolated from the magnetic pulse compressor while in others this may not be possible. In high-repetition-rate applications, however, reflections of energy back from the load can adversely affect the performance of the magnetic pulse compressor. This problem can affect particularly the reset of magnetic switches. It is very important, therefore, to have good models of the load to gain a good understanding of the coupling. These models will generally be nonlinear and time varying, and thus we require modeling tools that effectively cope with the highly coupled nonlinear problem.

Modeling of Magnetic Switches

It was generally agreed that a good model of the magnetic switch is the most critical requirement for high-accuracy network and system modeling. Furthermore, the magnetic switch is perhaps the most difficult element to model. Consequently, we spent a considerable portion of our time discussing magnetic switch modeling and, in particular, several magnetic switch models that have appeared in the literature.

A considerable number of models have been proposed for magnetic switching phenomena.[6–29] As J. Zentler indicated in his plenary address, these models range from simple circuit models, or empirical engineering models, to complex physical models based on domain wall motion or micromagnetics theory. The physical models, while giving insight, do not always necessarily give a good fit to the data and tend to have limited operating regimes. Some of the circuit-based models or empirical models,[16–21,24] can be made to fit data reasonably well over large operating ranges but then give virtually no physical understanding of the device.

Only two models appear to have been implemented in general circuit analysis programs. The first is a model developed by Nitzan[10–13] and is found, for example, in the NET-2 code.[30] This model was developed originally to simulate square-loop ferrite cores for computer memory applications and is also applicable to slowly switched tape-wound cores. It is a semi-empirical model based on the concept of domain wall motion. The model is quite complicated and cumbersome to use because it has a large number of parameters that must be determined by a fit to data. Moreover, the model is of limited utility as it really only models the transition of a core from its remanent state to saturation when a step current input is applied.

The Jiles-Atherton model[27–29] is the second model that has been implemented in a commercially available code. Specifically, the PSpice program[31,32] incorporates a simplified Jiles-Atherton model. This model is also based on domain wall motion but is considerably more simple than the Nitzan model. The model does not, however, include dynamic dependencies that can properly replicate the type of dynamic B-H loops that occur in magnetic cores driven at high dB/dt.

Many models suffer from the deficiency that they are only strictly valid for "thin" cores. For toroidal cores for which the ratio of the outside radius to inside radius is not close to unity, the H field is not uniform

across the core cross section. For this reason, the simple semi-empirical models, such as those of Nitzan and Jiles-Atherton, do not yield a sufficiently accurate representation of the dynamic behavior of the core. In this case, it is necessary to account for the nonuniformity or spatial variation of the fields by zoning the core and assuming some particular point model of the B-H characteristic that holds locally in each zone. This approach has been considered by some researchers.[5,33–37] Unfortunately, the resulting model may comprise a large number of equations and may not always be well suited for use in large system studies.

Much work remains to be done in the area of magnetic-switch modeling before we can say that we are capable of high-fidelity representation of actual switches. There has been no systematic and definitive attempt to evaluate which of the extant models are useful in modeling the materials of interest used in large cores at high magnetization rates and high pulse-repetition rates. Furthermore, no existing model is clearly the model of choice for either ferrite or metallic tape-wound cores. While it is sometimes sufficient, and indeed beneficial, for the purpose of gaining insight into system performance to use a very simple model such as the Chua-Stromsmoe model[17,18] or the Chua-Bass model,[19] this approach is often not adequate if high accuracy over wide operating ranges is required.

At present, there seem to be two major hindrances both to evaluating available magnetic switch models and to developing and validating new models. First, the very nature of some of the mathematical models themselves makes them very difficult to implement in present simulation or circuit analysis codes. Second, there is a lack of magnetization data for the materials of interest in the operating regimes of interest (e.g., at high magnetization rates, high repetition rates). The first hindrance calls for the development of new modeling tools sufficient for the task, while the second requires the careful and systematic construction of a data base in which all experimental conditions are well documented.

For reliable system studies, a concerted effort must be made to develop and validate with experimental data highly accurate magnetic switch models. What are the features that we desire in such models to perform system studies? We may put these under a number of heads:

Hysteresis Effects. Models must be capable of representing major hysteresis loops as well as asymmetrical minor loops. The ability to model minor loops is particularly important in the study of core reset stability, a critical issue for magnetic pulse compressors operating in long burst or continuously. Models must also replicate accurately observed rate-dependent loop-widening effects.

Loss Mechanisms. Models should provide some insight into the loss mechanisms of the device. This is necessary if we are to accurately assess the energy flow in magnetic pulse compressors and reliably predict system efficiency.

Geometric Effects. The important geometric parameters, such as inner radius and outer radius of a toroidal core, packing factor, magnetic material and insulation thicknesses (in the case of tape-wound cores), etc., should be reflected in the model. A good model should permit the user to understand not only the two-terminal characteristics of the device but also the effects of the spatial variation of the fields in thick cores.

Temperature Effects. Ideally, models should include the dependence of magnetic properties upon temperature. This is a crucial feature in the study of thermal stability and thermal management issues for high-average-power continuously operating magnetic pulse compression systems.

Parsimony. It is highly desirable that the model be defined in terms of a minimal number of parameters that are physically meaningful. A parametric model will permit sensitivity studies to be performed. For example, if a model has parameters

that define the squareness of the B-H loop and the saturated flux density B_S, then the sensitivity of compressor performance to these parameters can be calculated. Parametric models are clearly preferable to representing switch models with multidimensional tables obtained from experimental waveforms. In the latter case, scaling the model for different materials or operating conditions is intractable or impossible.

Material Dependency. Ideally, one would like to have a parametric model of the device in which some of the parameters specify the core material type. These parameters would distinguish, for example, a core made of Metglas 2605CO from one constructed of Metglas 2605SC. In addition, it is extremely desirable that tolerance bands for model parameters be established for magnetic materials of interest. This feature would permit us to perform compressor performance sensitivity studies with a view toward developing designs that are robust to material uncertainties.

Defined Region of Validity. It is quite important to define the parameter and dynamic ranges over which models are valid. Then, when such a model is used in system studies, care can be taken to ensure that it is not exercised outside its valid operating region. Many existing models may give a good fit to data for one particular set of operating conditions, but be totally inadequate if other conditions hold. Hopefully, we can construct models that have large regions of validity.

Modeling of Transmission Lines

Transmission lines are also an important component in magnetic pulse compression networks. They come into play, for example, in the distribution network coupling the magnetic pulse compressor to its load, in pulse-forming lines in the output stage of a series Melville line, and generally, at any place in a compressor where it is is not sufficient to treat capacitance or inductance in a lumped element fashion.

There are presently two basic and well-established approaches to the numerical modeling of transmission lines for time-domain network and systems analyses. The first approach represents a line in terms of Thévenin or Norton equivalent circuits at the input and output ports of the line. (This approach is described in some detail in Ref. 38.) This technique is particularly well-suited to the modeling of ideal, loss-less transmission lines and has been employed for this purpose in general-purpose circuit codes. The approach has also been extended to some classes of lossy lines.[39]

One disadvantage of this particular method of modeling transmission lines is that it places a severe restriction on the time-step used to integrate the differential equations describing the entire system. The time-step must be constrained to be no greater than the smallest one-way transit time of any transmission line in the network. For example, the PSpice code restricts the step-size to be no more than one-half of the shortest transit time.[31] In practice, the time step must usually be very much smaller than the smallest transit time.

This fact has particularly severe effects on the simulation of magnetic pulse compression systems. The reason is as follows. By its very design, a magnetic pulse compressor is meant to exhibit several orders-of-magnitude difference in the time scales between the input stage and the output stage (e.g., from a few microseconds at the input to tens of nanoseconds at the output). A short transmission line at the output of the compressor or in the load circuit forces a small time-step to be used and results in a long run time to simulate one pulse through the system. Further, the problem is multiplied many times over if it is necessary to simulate a burst of multiple pulses though the system.

The second approach for modeling transmission lines represents a line in term of an approximate lumped equivalent circuit consisting of a cascade of sections comprised of series inductance and resistance elements and shunt capacitance and conductance elements. In this way, one

can approximate lossy transmission lines. Such an approach is used in the NET-2 program for its model of dispersive transmission lines.

This method also has its disadvantages. First, it is not always an easy matter to determine how many sections are needed to represent the line to a given level of accuracy in a transient analysis of a compressor. In fact, a large number of sections may be required, and this means that a large number of differential equations representing the transmission line are added to what may already be a large overall system model. Second, in pulsed applications, this approach introduces "Gibbs phenomena" or oscillations throughout the pulse, especially on its leading and trailing edges. If we are interested in highly accurate representations of voltage waveforms, as for example in Ref. 1, this imperfection in the model is unacceptable.

Further research is clearly needed in the area of transmission line modeling for pulsed power applications such as magnetic pulse compressors. This research could proceed along a number of avenues. First, a definitive comparison of the two approaches mentioned above in terms of computational efficiency and accuracy for pulse compressor applications would be helpful. Second, attention should also be given to developing models that can be efficiently implemented into system models that inherently possess multiple disparate time-scales, as is the case in magnetic pulse compression systems. Third, the ability to model efficiently nonideal cases, such as lossy, nonlinear, discontinuous, or nonuniform lines, could permit higher fidelity systems modeling and also introduce new degrees of freedom into compressor design. Fourth, an efficient method for modeling and optimizing pulse forming networks and tapered pulse forming lines could lead to significantly improved magnetic pulse compressor designs. Finally, further work is required on modeling problems where some geometrical asymmetry prohibits a simple one-dimensional analysis and the need arises for two- and three-dimensional models of transmission lines to model realistic problem geometries. One possible approach to this particular problem is the transmission line matrix method.[40]

Modeling System Design Problems

In considering the network aspects of the modeling problem, we are primarily interested in a faithful representation of the dynamical response of the compressor circuit. It is, however, rarely sufficient merely to have a network model of a proposed compressor design. There must also be some means of quantifying its performance attributes and characteristics and of evaluating them against design requirements. Thus, we must also model the system design problem itself by formulating quantitative figures of merit or performance measures against which we can evaluate or score alternative designs.

The advantage of building highly accurate system models as an aid to compressor design is clear. These models can help us predict the expected performance of a compressor design before it is built. Indeed, in the absence of such modeling, we are more likely to build compressors that fail to meet some or all of the design specifications. Furthermore, having a system performance model, we can explore the design parameter space much more efficiently and quickly than by a purely experimental approach of prototype construction. Such system models can help us to define the best prototypes to build and to determine the experiments that should be performed. Moreover, they can enable us to determine the performance limitations in an existing prototype. Therefore, high fidelity systems modeling will eliminate costly design mistakes, ensure better designs and ultimately reduce the time, effort and cost of the overall design process.

Model Formulation. Very simply, a mathematical model of the system design problem consists of a mathematical representation of the design variables and requirements of the problem. In particular,

we are concerned with identifying three main sets of entities: (1) design parameters; (2) design constraints; (3) design objectives.

The design parameters are those problem variables that we consider to be adjustable in the design under consideration and that we are free to adjust to satisfy the design constraints and reach the design objectives. For example, the design parameters for a given problem might include, among other variables, the number of magnetic compression stages, the geometry of the magnetic switch cores, the core materials, and the amplitude of the core reset currents.

The design constraints and objectives are really two alternative forms of specifying the design requirements. A constraint may be thought of as a "hard" limit that must not be exceeded. For instance, the application of the compressor may impose a design requirement that the output voltage pulse have a flattop of at least 50 ns duration with no more than a 1% variation in the amplitude (see Ref. 1). These requirements impose constraints on the vector of design parameters $\mathbf{p}$ of the form:

$$50 \text{ ns} \leq W(\mathbf{p})$$

$$|\Delta V(\mathbf{p})/V(\mathbf{p})| \leq 0.01$$

A design objective, on the other hand, may viewed as a "soft" constraint or as some design measure that we wish to maximize or minimize. For example, one important design objective for a compressor operating continuously might be to select the design parameter values so as to maximize the energy efficiency of the compressor. This objective would be expressed as:

$$\max_{\mathbf{p}} \eta(\mathbf{p}),$$

where η is the function defining efficiency and the maximum is taken over all feasible design vector values. Admittedly, the difference between a constraint function and an objective function may be subtle and is somewhat subjective, but possible tradeoffs may be more apparent if some design requirements are considered as design objectives rather than as hard constraints.

The design objectives and constraint functions are defined in terms of the design parameters and quantify mathematically various attributes of the compressor. These attributes may be many and varied, but some that we specifically identified include the following:

- System cost.
- Physical size.
- Weight.
- Energy efficiency.
- Materials and component limitations (e.g., capacitor operating limits).
- Constraints imposed by the interface with the power conditioning system.
- Constraints imposed by the load.
- Output waveform requirements (e.g., pulse flatness, pulse width, rise time, pulse amplitude).
- Pulse repetition rate.
- Pulse-to-pulse stability (e.g., timing jitter, pulse amplitude variation).
- Reliability.
- Lifetime.
- Flexibility in compressor operating range to various load impedances and output voltage requirements.
- Sensitivity to material and component tolerances.
- Robustness to thermal effects.

Some of the attributes may be of more concern than others, depending on the particular application. In any case, problems of this class usually possess multiple constraints and objectives. Furthermore, these constraints and objectives are frequently in conflict, and thus tradeoffs must be made to achieve an acceptable design. Therfore, the main impetus behind the effort to develop a good model of the system design problem is the assessment of the critical design tradeoffs and the selection of an "optimal" or "best" compromise design.

In reviewing the state of the art in systems modeling for magnetic pulse compressors, the general concensus of the working group was that insufficient research has been done and that little experience exists with the formulation of detailed system design models.

Historically, systems studies have emphasized economic considerations only and put stress upon optimizing the core volumes.[41-43] Scant attention has been given to performance issues. Furthermore, most system studies have concentrated on the analysis of the series Melville topology, have employed rather primitive magnetic switch models, and have made overly simplistic assumptions about the energy transfer between compression stages. Such results have consequently possessed limited validity and applicability. What is needed is a more thorough and systematic approach, as outlined above. We are unable to cite a single effort where this has been done and this, therefore, is a recommended area for future research effort.

Solution Techniques

We sought to identify model-based techniques or methodologies for performing design tradeoffs and arriving at optimal designs. We are assuming now, of course, that one has a good network and system model of the compressor design in parametric form and can evaluate the design objective functions and constraints as functions of the design parameters. The issue then is how to exercise or use these models to arrive at an acceptable design. We discussed three main approaches: trial and error, sensitivity analysis, and optimization.

The trial and error approach consists of using the network and system model of the compressor to simulate repeatedly its performance for differing design parameter values. The process continues until acceptable performance is achieved (or the patience of the designer is exhausted). This approach seems to be the most commonly used one at present, if a model-based approach to system design is used at all.

The second and more systematic method is to calculate the sensitivity of each of the important design objective and constraint functions to changes in parameters at some nominal design point. Based upon this sensitivity information, the most critical design parameters can be determined. A gradient to improve incrementally a selected objective function can be calculated also. The critical design parameters can then be tuned in an attempt to improve upon the nominal design.

The third and most efficient technique attempts to use optimization methods to find the value of the design parameters that optimize a figure of merit for the problem subject to the design constraints. This figure of merit may be an objective function, if there is only a single design objective, or the weighted sum of objectives, if there are multiple design objectives.

The pulsed-power community seems to have made little use of these last two approaches. Again, we are not able to cite a single paper where these methods have been used to design magnetic pulse compressors. The lack of capable and suitable computational tools is partly responsible for this situation, and we will comment further upon this fact in the next section. Nevertheless, sensitivity analysis and optimization could lead to significantly improved compressors designs, and thus the application of these methods constitutes a promising area of future research and development in compressor design.

Modeling, Analysis and Design Tools

An Assessment of Existing Tools

We reviewed the capabilities of existing modeling, analysis, and design tools with a view to evaluating their various advantages and disadvantages for magnetic pulse compressor problems. Three classes of codes used by the pulsed-power community are applicable to the modeling, analysis, and design of magnetic pulse compressors: general circuit analysis programs, special transmission-line-based codes, and general ordinary-differential-equation (ODE) or state-space solvers. We considered codes in each of these classes, and our assessment is summarized below. Further discussion of these codes can also be found in Ref. 3.

General circuit analysis codes provide the capability for modeling and simulating

circuits with very general topologies and many types of circuit elements or components. At present, there are three programs of this class that are widely used in the pulsed power community: NET-2, SCEPTRE, and the SPICE family of codes.

NET-2 has a large number of built-in circuit elements including loss-less and dispersive transmission lines, ideal switches, and the Nitzan magnetic core model.[30] It also has a large number of systems elements that give the user a language by which he or she can model analog and digital systems. This feature, however, is not so useful or easy to use as would be a user-defined subprogram capability, such as possessed by SCEPTRE. The program also has some limited capability for performing network optimization with least-squares objective functions. The user is permitted to define nonlinear circuit elements, and there is the capability for defining auxiliary differential equation through the code's X variable feature or through its system elements. NET-2 employs a variable step implicit trapezoidal method as its integration technique.

SCEPTRE[44,45] is the oldest of the three general circuit analysis codes, but has gone through several upgrades, one of the more recent upgrades being its implementation on the CRAY computers at LLNL.[46] SCEPTRE has several very nice advantages but also some disadvantages. On the credit side, the code offers considerable flexibility in circuit element definition by permitting the user to define general nonlinear and time-varying elements. Another very strong feature is its subprogram capability. This permits the user to define element models via FORTRAN function subroutines. Furthermore, the DEFINED PARAMETER feature allows one to define system components in terms of auxilliary ordinary differential equations. SCEPTRE offers the user a choice of several integration routines, including Gear's method for the stiff differential equations. All of these features permit the user to model, in principle, very complicated circuits and systems and thus are very helpful for modeling magnetic pulse compressors.

On the debit side, SCEPTRE has firm limits on the number of circuit elements and nodes, user-defined differential equations, and mutual inductances. Also the code lacks built-in models for two components important for pulsed power modeling: transmission lines and switches. Although models for user-defined elements can be added via the subprogram capability, the structure of the code is such that these elements can drive the integration-time-step to extremely small values and force long run times.

Both NET-2 and SCEPTRE are large codes designed to run in batch mode on mainframe computers. Their original built-in graphics capabilities are archaic and poor, making some form of in-house site-dependent graphics necessary.

The SPICE program was orginally developed for semiconductor and integrated circuit modeling.[47] There are many versions and derivatives of SPICE, so many in fact, that it is not possible here to evaluate the advantages and disadvantages of all of them. Generally speaking, however, the SPICE family of codes does not as yet possess the same flexibility and generality that SCEPTRE, or even NET-2, does in modeling very general and complex systems. The strong point of the recent SPICE-based codes, however, has been their user-interface. For example, the microcomputer-based PSpice[31,32] is interactive, with excellent graphics and post-processing capabilities.

Special transmission-line-based codes are built around the basic circuit element of the transmission line. The programs of this genre include SCREAMER,[48] TLINES,[49] and TLCODE.[50] The basic building block or element in SCREAMER consist of a series inductance and resistance and a shunt capacitance and conductance, as in a single section of the lumped element transmission line model. Networks are built up from this basic element and the solutions are obtained by discretizing the differential equations by a fixed time-step method that is second-order accurate in the chosen time-step. The advertised advantage of SCREAMER is its speed of solution. The program permits some forms of nonlinear

resistors, inductors and capacitors. It also has a provision for implementing user-written subroutines.

The basic circuit element for the TLCODE is the Thévenin equivalent formulation of the ideal transmission line. By modeling capacitors and inductors as spatially distributed transmission lines, the differential equations that would ordinarily be used to model the circuit are reduced to purely algebraic equations that can be stepped forward in time. TLCODE has a subprogram capability for user-defined elements and there exists a driver for circuit optimization.[51]

These two codes are not without their disadvantages. First, there are limits on the circuit topologies and components that they can readily accommodate. For example, SCREAMER must limit the class of element interconnections to ensure computational efficiency, and TLCODE is not well suited to handling mutual inductance; both codes may have difficulty with very general forms of nonlinear, time-varying elements. Second, since the codes employ a fixed time-step (e.g., implicitly set by the shortest transmission line), they may experience difficulty in simulating the multiple time-scale magnetic pulse compressor circuit over many pulses.

In using general ODE or state-space solvers to model magnetic pulse compressors, we write the loop or node equations of the circuit and reduce them to a system of first order ordinary differential equations. This is a viable approach if the compressor system is not too complex, but can be very unwieldy for large systems. The approach will also break down if the magnetic switch model is such that the circuit equations cannot be reduced to a set of ordinary differential equations. In fact, for some proposed forms of magnetic switch models this can actually happen (see Ref. 19). This approach is also at a disadvantage if a change in circuit topology must be made because then the state equations must be reformulated. Two programs of this class, SCIMATH and ACSL, were mentioned in the course of our discussions, but we did not give them detailed treatment. The software package SCIMATH is a general numerical modeling program and is discussed in Ref. 3. ACSL (*A*dvanced *C*ontinuous *S*imulation *L*anguage)[52] is a very powerful state-space modeling program, and it has been used by Rhinehart[36] to model magnetic switches.

We concluded that no existing code seems to possess all the features that would be helpful for magnetic pulse compressor problems. All the existing codes have inadequate magnetic core modeling capabilities. At present, in terms of flexibility, SCEPTRE appears to be the most versatile and to offer the greatest possibility for magnetic pulse compressor network modeling. But when it comes to modeling system design problems, none of the generally available codes offers much substantive help with system sensitivity analysis, or optimization and tradeoff studies, such as those previously described.

Features of an Ideal Code

On the basis of the assessment of existing codes reported above, we may formulate a number of requirements for an "ideal" modeling, analysis and design tool for magnetic pulse compressor problems.

Nonlinear Elements. At the simplest level, the ideal code should permit circuit modeling with very general nonlinear resistors, capacitors and inductors.

Built-In Pulsed-Power Models. The code should have a library of frequently used and important components for modeling pulsed-power systems. Specifically, the library should include loss-less and lossy transmission line models, models for arbitrarily tapered pulse-forming lines and general pulse-forming networks, magnetic hysteresis models, models for gas switches, etc. The model formulation and solver algorithms should be designed to accommodate these kinds of elements with maximal computational efficiency.

User-Defined Models. The ideal code should provide for easy implementation of user-defined models. This is especially important as an aid to evaluating possible magnetic switch models that are suitable

for high-fidelity system modeling. Because there is not at currently a "model of choice" for magnetic switches, the ideal modeling tool is one that provides a sufficiently general framework to permit the most general form that such a model might take. Moreover, the loads driven by magnetic compressors may have very special characteristics that may not be easily defined in terms of the code's stock repertoire of circuit elements. The requirement for implementing user-defined models can be met in at least two ways. First, there should be the provision for models to be defined through user-written subprograms. Second, the code should permit the user to define models through differential equations and couple these to rest of his network model.

Stiffly Stable Solver. Models of magnetic pulse compressor circuits are inherently stiff numerically. This occurs for two reasons. First, as mentioned previously, the dynamics of a magnetic pulse compressor by design evolve over multiple time scales, which may differ by several orders of magnitude from the input stage to the output stage. Second, the magnetic switches in each stage are highly nonlinear and make each stage itself stiff numerically. The stiffness of the compressor circuit model can acutely affect simulation run times, especially when we desire to study the circuit performance at high repetition rate. Therefore, the ideal code should have integration routines that are stable for stiff equations and adaptive in order and time-step size. To enhance the robustness of the code, it is desirable that the user have the option of selecting from several alternative solvers, such as Runge-Kutta methods or methods based upon backward differentiation formulae.

***Sensitivity Analysis and Optimization* Algorithms.** To facilitate the design of magnetic pulse compression systems, it is essential that the code have methods for performing parameter sensitivity and optimization studies. Thus, there must be means of defining design parameters, design constraints, and design objectives and algorithms for searching the parameter space efficiently. The capability to construct performance tradeoff curves for given design objectives would be very helpful.

User-Friendly Interface. As a design tool, the code should have good interactive graphics and post-processing capabilities. The ability to perform and display design tradeoffs interactively is also highly desirable.

Platform. Versions of the code should be available for platforms ranging from personal computers to the large mainframes.

Support. In contrast to codes like SCEPTRE and NET-2, the ideal code is one which either is fully supported by a commerical vendor or is easily maintainable in-house. This latter option necessitates thorough documentation internal to the code, comprehensive user's guides, and supporting external documentation.

Conclusions

We have attempted to review the state of the art in magnetic pulse compressor network and system modeling. We have also sought to suggest crucial areas where further research and development efforts are needed. Generally speaking, the current modeling technology-base is rather weak. Much work remains to be done in modeling important network components, especially magnetic switches, and in developing suitable computational tools to aid the design task. A good model of the magnetic switch that is validated against experimental data is critical to development of high-fidelity system models. A tool, or set of tools, capable of modeling highly coupled, nonlinear, and stiff magnetic compressor systems and of providing help with system optimization is also a critical need. It is hoped that the recommendations of this report

will motivate future work that will significantly advance the art of designing high-average-power magnetic pulse compressors that operate continuously.

References

1. W. C. Turner, D. M. Barrett, and S. E. Sampayan, "Critical System Issues and Modeling Requirements—The Problem of Beam Energy Sweep in an Electrom Linear Induction Accelerator," these proceedings.
2. E. Y. Chu, "Magnetic Modulator System Issues," these proceedings.
3. W. N. Weseloh and R. J. Kares, "Present Circuit Simulation Tools," these proceedings.
4. W. S. Melville, "The Use of Saturable Reactors as Discharge Devices for Pulse Generators," *IEE Proc.* **98**, pt. 3, pp. 185-207 (Feb. 1951).
5. W. C. Nunnally, *Magnetic Switches and Circuits*, Los Alamos National Laboratory, Los Alamos, NM, LA-8862-MS (Revised), (1982).
6. F. Preisach, "Uber die Magnetische Nachwirkung," *Zeitschrift für Physik* **94**, pp. 277-302, 1935.
7. E. M. Gyorgy, "Rotational Model of Flux Reversal in Square Loop Ferrites," *J. Appl. Phys.* **28**, pp. 1011–1015 (Sept. 1957).
8. J. E. L. Bishop, "Modeling Domain Wall Motion in Soft Magnetic Alloys," *J. Magn. Magn. Mat.* **41**, pp. 261–271 (1984).
9. T. C. Chen and A. Papoulis, "Terminal Properties of Magnetic Cores," *Proc. IRE* **46**, pp. 839–849 (May 1958).
10. D. Nitzan, "Computation of Flux-Switching in Magnetic Circuits," *IEEE Trans. Magn.* **MAG-1**(3), pp. 222–233 (Sept. 1965).
11. D. Nitzan, "Models for Elastic and Inelastic Flux Switching," *IEEE Trans. Magn.* **MAG-2**(4), pp. 751–760 (Dec. 1966).
12. D. Nitzan, "MTRAC: Computer Program for Transient Analysis of Circuits Including Magnetic Cores," *IEEE Trans. Magn.* **MAG-5**(3), pp. 524–533 (Sept. 1969).
13. D. Nitzan, "Computation and Modeling of Eddy Currents in Tape-Wound Square-Loop Cores," *IEEE Trans. Magn.* **MAG-7**(1), pp. 185–197 (Mar. 1971).
14. S. D. Winter, R. W. Kuenning, and G. G. Berg, "Pulse Properties of Large 50-50 NiFe Tape Cores," *IEEE Trans. Magn.* **MAG-6**(1), pp. 41–45 (Mar. 1970).
15. R. Bouc, "Modèle Mathématique d'Hystérésis," *Acustica* **24**, pp. 16–25 (1971).
16. J. G. Santesmases, J. Ayala, and A. H. Cachero, "Analytical Approximation of Dynamic HysteresisLoop and its Application to a Series Ferroresonant Circuit," *IEE Proc.* **117**(1), pp. 234–240 (Jan. 1970).
17. L. O. Chua and K. A. Stromsmoe, "Lumped Circuit Models for Nonlinear Inductors Exhibiting Hysteresis Loops," *IEEE Trans. Circuit Theory* **CT-17**(4), pp. 564–574 (Nov. 1970).
18. L. O. Chua and K. A. Stromsmoe, "Mathematical Model for Dynamic Hysteresis Loops," *Int. J. Eng. Sci.* **9**, pp. 435–450 (1971).
19. L. O. Chua and S. C. Bass, "A Generalized Hysteresis Model," *IEEE Trans. Circuit Theory* **CT-19**(1), pp.36–48 (Jan. 1972).
20. S. H. Charap, "Magnetic Hysteresis Model," *IEEE Trans. Magn.* **MAG-10**(4), pp. 1091–1096 (Dec. 1974).
21. A. Y. Hannalla and D. C. Macdonald, "Representation of Soft Magnetic Materials," *IEE Proc.* **127**(6), Pt. A, pp. 386–391 (July 1980).
22. Y. Saito, H. Saotome, and T. Yamamura, "A Lumped Circuit Model for a Nonlinear Inductor Exhibiting Dynamic Hysteresis Loops and its Application to the Electric Circuits," *Comp. Meth. Appl. Mech. Eng.* **38**, pp. 185-202 (1983).
23. Y. Saito, S. Hayano, T. Yamamura, and N. Tsuya, "A Representation of Magnetic Hysteresis," *IEEE Trans. Magn.* **MAG-20**(5), pp. 1434–1436 (Sept. 1984).
24. D. Pei and P. O. Lauritzen, "A computer model of magnetic saturation and hysteresis for use on SPICE2," *IEEE Trans. Power Electronics*, Vol. PE-1, No. 2, pp. 101-110, April 1986.

25. M. L. Hodgdon, "Applications of a Theory of Ferromagnetic Hysteresis," *IEEE Trans. Magn.* **MAG-24**(1), pp. 218-221 (Jan. 1988).
26. M. L. Hodgdon, "Mathematical Theory and Calculation of Magnetic Hysteresis Curve," *IEEE Trans. Magn.* **MAG-24**(6), pp. 3120-3122 (Nov. 1988).
27. D. C. Jiles and D. L. Atherton, "Ferromagnetic Hysteresis," *IEEE Trans. Magn.* **MAG-19**(5), pp. 2183–2185 (Sept. 1983).
28. D. C. Jiles and D. L. Atherton, "Theory of Ferromagnetic Hysteresis," *J. Appl. Phys.* **55**(6), pp. 2115–2120 (Mar. 1984).
29. D. C. Jiles and D. L. Atherton, "Theory of Ferromagnetic Hysteresis," *J. Magn. Magn. Mat.* **61**, pp. 48–60 (1986).
30. A. F. Malmberg, *User's Manual: NET-2 Network Analysis Program (Release 9)*, Braddock, Dunn, and MacDonald, Inc., Harry Diamond Laboratory Report HDL-050-1 (Sept. 1973).
31. *PSpice* (MicroSim Corporation: Laguna Hills, CA, 1987).
32. P. W. Tuinenga, *SPICE: A Guide to Circuit Simulation and Analysis Using PSpice* (Prentice-Hall: Englewood Cliffs, NJ, 1988).
33. Y. Saito, "Three-Dimensional Analysis of Nonlinear Magnetodynamic Fields in a Saturable Reactor," *Comp. Meth. Appl. Mech. Eng.* **22**, pp. 289–308 (1980).
34. Y. Saito, "Three-Dimensional Analysis of Magnetodynamic Fields in Electromagnetic Devices Taking into Account the Dynamic Hysteresis Loops," *IEEE Trans. Magn.* **MAG-18**(2), pp. 546–551 (Mar. 1982).
35. J. P. Karidis and S. R. Turns, "A Comparison of Lumped and Distributed Solution of Nonlinear, Transient, Magnetic Field Problems," *IEEE Trans. Magn.* **MAG-19**(6), pp. 2715–2722 (Nov. 1983).
36. H. E. Rhinehart, *Computer Simulation of Magnetic Switching Circuits and Magnetic Energy Losses*, Ph.D. dissertation, Department of Electrical Engineering, Univ. South Carolina, Columbia, SC (1989).
37. C. D. Boley and M. L. Hodgdon, "Model and Simulations of Hysteresis in Magnetic Cores," *IEEE Trans. Magn.* **25**(5), pp. 3922–3924 (Sept. 1989).
38. F. H. Branin, Jr., "Transient Analysis of Lossless Transmission Lines," *Proc. IEEE* **55**, pp. 2012–2013 (Nov. 1967).
39. F. H. Branin, Jr., "Transient Analysis of Lossy Transmission Lines," *Proc. Sixth Allerton Conf.*, Monticello, IL, pp. 276–286 (1968).
40. W. J. R. Hoefer, "The Transmission Line Matrix Method," in *Numerical Techniques for Microwave and Millimeter Wave Passive Structures*, Tatsuo Itoh, Ed. (John Wiley and Sons, New York, pp. 496–512, 1989).
41. R. A. Mathias and E. M. Williams, "Economic Design of Saturating Reactor Magnetic Pulsers," *AIEE Trans.* **74**, Pt. 1, pp. 169–171 (May 1955).
42. D. L. Birx, E. J. Lauer, L. L. Reginato, J. Schmidt, and M. Smith, *Basic Principles Governing the Design of Magnetic Switches*, Lawrence Livermore National Laboratory, Livermore, CA, UCID-18831 (Nov. 1980).
43. G. Bredenkamp and P. Swart, "A Theoretical Basis for the Optimization of Electromagnetic Pulse Compressors using Saturable Ferromagnetic Cores," *Proc. Eighteenth IEEE Power Modulator Symp.*, pp. 90–94 (June 1988).
44. J. C. Bowers and S. R. Sedore, *SCEPTRE: A Computer Program for Circuit and Systems Analysis* (Prentice Hall, Englewood Cliffs, NJ, 1971).
45. D. Becker, *Extended Sceptre*, Air Force Weapons Laboratory Report AFWL-TR-73-75, Vols. 1 and 2 (Dec. 1974).
46. W. Magnuson, *SCEPTRE-2 User's Manual*, Lawrence Livermore National Laboratory, Livermore, CA, Report M184 (April 1986).
47. L. Nagel, *SPICE2: A Computer Program to Simulate Semiconductor Circuits*, University of California, Berkeley, Electronics Research Laboratory, Memo ERL-M520 (1975).
48. M. L. Kiefer and M. M. Widner, "SCREAMER - a single line pulse power design tool," *Proc. Fifth IEEE Pulsed Power Conf.*, Arlington, VA, pp. 685-688, June 1985.

49. G. A. Huttlin and A. J. Lelis, *TLINES: A Computer Program for Circuits of Transmission Lines*, Harry Diamond Laboratories Technical Memorandum HDL-TM-83-22 (1983).
50. W. N. Weseloh, "TLCODE - A Transmission Line Code for Pulsed Power Design," *Proc. Seventh IEEE Pulsed Power Conf.*, Monterey, CA, June 11–17, 1989, pp. 989–992.
51. P. Corcoran, I. Smith, and D. Wake, "Three Reverse Engineering Codes for Pulse Power System Design," *Proc. Seventh IEEE Pulsed Power Conf.*, Monterey, CA, June 11–17, 1989, pp. 465–467.
52. *Advanced Continuous Simulation Language (ACSL) Reference Manual* (Mitchell and Gauthier Associates, Concord, MA, 1986).

Magnetic Materials Group

Gordon E. Fish, Chairman
Ken Avery, Cochairman

Working Group Members

K. Avery
O. Buchert
G. Fish
C. Fong
M. Greenwood
M. Hodgdon
S. A. Merryman
L. A. Ostrovsky
M. Parsons
M. Shiho
C. Smith
R. Wengerter
R. Wood
J.-M. Zentler

Abstract

The ultimate performance limits for magnetic switching and pulse compression systems are determined by the properties of their magnetic cores. In simplest terms, a pulse compression system has as its underlying purpose the ability to acquire power from a source over a long time scale and then to transfer that power to a load on a shorter time scale. The goal is the maximum possible efficiency in that transfer apparatus, measured in terms of energy as well as in cost, complexity, and reliability. Magnetic switching is a well recognized and proven method of accomplishing that end, especially for repetitively driven systems.

The challenges in constructing working magnetic systems with the best possible characteristics and performance occur at several levels:

- Selection and optimization of soft ferromagnetic core materials.
- Manufacture of actual cores so as to take full advantage of the properties of available material.
- System integration issues such as mounting, cooling, and electrical interconnection.

The Magnetic Materials Working Group surveyed issues at each of these levels to determine present capabilities and identify key limitations which might realistically be overcome in the near to medium term.

A wide variety of properties of soft ferromagnetic core materials are of importance in pulse power. Some (e.g., saturation induction B_s, Curie temperature T_c saturation magnetostriction λ_s and electrical resistivity ρ) are essentially intrinsic for a given composition of material. In contrast, important extrinsic properties such as B-H loop shape, relative permeability μ ($\mu = B/\mu_0 H$), coercivity H_c, magnetic anisotropy energy density K, and core losses are tailored to a great degree by processing which exploits the full apparatus of the modern materials industry.

A second level of complexity is encountered in being able to realize the extrinsic soft magnetic properties measured for a material in a controlled, idealized test environment in a core of the scale and geometry needed for actual devices.

Finally, a magnetic core is never an end in itself; rather, it is a component of a total system. The success of a core is measured by the limitations it imposes on the functioning of a system, whether in performance or in cost. Future developments should have as their ultimate targets:

- Increasing the range of accessible performance parameters (switching times, peak powers, repetition, rates, reliability, etc.).
- Reducing the weight and/or volume of the core for a given requirement.
- Reducing the cost of the core and related systems such as cooling.

• Making practical an expanded repertoire of applications.

The group also considered the state of the art in modeling core performance. Because many pulse-power applications involve unique and costly large-scale devices, it is important to have accurate mathematical and numerical models of core performance to guide systems designers.

Introduction

The Magnetic Materials Working Group was represented in the opening plenary session by Carl Smith (Allied-Signal) who gave an overview of the issues involved in magnetic materials for pulse compression. This talk set the scope of the working group session.

The first working group session began with introductions by the group members. Their interests ranged from materials production, pulsed testing, and magnetization modeling through core manufacture and saturable inductor component users. There were representatives from the U.S., U.K., West Germany, Japan, and the Soviet Union. The major portion of this first session was devoted to three technical presentations on key aspects of magnetic materials for pulse compression. In the first of these Ralf Wengerter (Vacuumschmelze) described material properties and techniques of pulsed magnetic characterization. The next presentation by Ken Avery (British Aerospace) was a description of methods of modeling pulsed magnetization with emphasis on physics-based approaches. The third technical presentation by Richard Wood of National Magnetics was entitled "Making a Workable Core" and discussed many of the technical and practical problems associated with core construction.

The remaining three working group sessions each took one of the technical presentation subjects as its major theme. The second session, therefore, consisted mainly of round-table discussions on materials choices and testing. During this session, Leo Ostrovsky (Soviet Union Institute of Applied Physics) gave a presentation on the use of ferrites in pulse sharpeners. His work addressed both materials properties and nonlinear wave propagation phenomena. The progress of the working group at the end of the second session was reported to the whole workshop by the group's chairman, Gordon Fish (Allied-Signal), in the second plenary session. He called for input from other working groups and summarized the group's conclusions on applications requirements, materials properties and choices, and future material trends. A list of institutes having pulsed characterization capabilities was started during the second working group session and the call was made for other groups to contribute to this list.

The third working group session began with a description of available core-testing facilities known to the group members and indications of the types and ranges of tests available. The main theme for this session was material modeling. Marion Hodgdon (Los Alamos National Laboratory) gave an informal presentation on her approach to magnetization modeling. In contrast to models described by Avery, which start from domain wall motion considerations, Hodgdon employs a continuum approach to develop a phenomenological magnetization equation. Good ability to describe dc and pulsed data was reported as well as a request for more magnetization data. Software based on this model was made available on a personal computer in the Workshop Library. The unexpectedly long duration of the second plenary session limited the time available for discussion of modeling issues during the third working group session.

The final session had as its main theme core manufacturing considerations. After discussions on the various aspects of core manufacture including annealing, insulation, thermal questions, and core winding, the group returned to discussions of materials and core modeling. The group concluded by identifying the following key research topics that were felt to offer significant opportunities for applications in pulse power:

• Magnetization modeling with improved numerical accuracy and better physical insight into loss mechanisms.

• Data on the temperature dependence of relevant pulse magnetization properties

and the need to incorporate these data into testing and modeling.

- Better and more effective interlaminar insulation techniques.
- The need for more pulse magnetization data, especially a better understanding of reset phenomena.

The group chairman presented the progress of the working group and its conclusions in the final plenary session.

Materials

One of the group's first endeavors was to enumerate and quantify the magnetic parameters of importance in current and future pulse-power systems. Table 1 lists some of these characteristics, separating the static or dc parameters from the rate-dependent ac properties. The dc properties of pulse core materials that define the B-H loop (especially remanent and saturation inductions) are important in pulse power. A majority of applications involve a flux change (ΔB) from negative remanence to positive saturation. In this circumstance, the required core volume to switch a given energy is inversely proportional to packing fraction times $(\Delta B)^2$, and the field H needed to reset the core back to $-B_r$ following each pulse is governed by the loop shape. The ac characteristics determine the output waveform of a switched or compressed pulse and the amount of energy lost per pulse to core loss.

Table 1. Magnetic and physical parameters characterizing pulse power cores and systems.

Static (dc) properties		
Coercivity	H_c	
Remanence	B_r	
Saturation magnetization	B_s	
Saturation magnetostriction	λ_s	
Saturated permeability	μ_{sat}	
Squareness ratio	B_r/B_s	
Curie temperature	T_c	
Resistivity	ρ	
Dynamic (ac) properties		
Peak applied field	H_{peak}	10–50 kA/m (laser drivers) 50–75 kA/m (accelerators)
Switching field	H_{switch}	
Switching ratio	H_{peak}/H_{switch}	
Magnetization rate	dB/dt	0.1–1.0 T/μs
Minimum time to saturation	Δt	100 ns (available) 10 ns (desirable)
Core losses	L	

Any change in the magnetization of a ferromagnetic material results in the dissipation of energy as heat as an inevitable consequence of the hysteretic character of the magnetization process. The heat thus produced (generally known as core loss [1]) has significant impact for pulse power, both in its potential for altering the magnetic properties of the core material itself and in the thermal management and cooling requirements imposed on the system design. The minimization of waste heat is thus an overarching concern for pulse systems and, *a fortiori*, for high repetition rate applications.

In the simplest view, total core loss is made up of a quasi-static loss and of eddy-current loss. The hysteresis contribution per magnetization cycle is a constant; the eddy current contribution per cycle is more

difficult to calculate but has a dependence on the magnetization rate, dB/dt, in the range $(dB/dt)^{0.5-1}$.[2] For metallic materials in the usual pulse power dB/dt regime, eddy current losses dominate. They increase with both the material's conductivity and the strip thickness, suggesting two obvious routes to improvement.

Table 2 lists families of materials of current importance in pulse power—polycrystalline metals, amorphous metals, and ferrites—along with representative properties. Each of these materials finds use where appropriate in pulse cores. Designers must balance the diversity of required circuit properties with cores that can be realized in practice. Consideration is given to the forms of material available and to the costs of the raw magnetic material, insulation, and core manufacture.[3]

Table 2. Magnetic materials.

Material 25-mm ribbons	B_s (T)	B_r (T)	H_c (A/m)	T_c (°C)	ρ (μΩm)	ΔB (T)	λ_s (ppm)
METGLAS 2605CO	1.8	1.7	3.2	415	1.23	3.5	3.5
METGLAS 2605SC	1.6	1.5	2.4	370	1.35	3.1	30
METGLAS 2705M	0.7	0.7	0.8	365	1.36	1.4	<1
METGLAS 2714A	0.55	0.5	0.2	205	1.30	1.05	<1
Supermendur	2.35	1.5	90	940	0.35	3.8	80
3.2% Si-Fe	1.97	1.4	50	730	0.50	3.4	5
50% Ni-Fe	1.6	1.5	8	480	0.45	3.1	25
80% Ni-Fe	0.8	0.7	2.2	460	0.55	1.5	1.5
Ni-Zn Ferrite	0.33	0.25	80	>280	10^{12}	0.58	–10
Ni-Zn Ferrite	0.51	0.12	12	>230	10^{7}	0.63	–2

Today's polycrystalline metals applicable to pulse power represent the fruits of over 50 years of development. These materials are widely used in electrical and electronic devices in the form of sheet or tape (ribbon) and are available in large quantity and in a variety of thicknesses. For high dB/dt applications, the comparatively high losses of polycrystalline metals are of concern. Their resistivities are unavoidably low, as delineated in Table 2, and the thermomechanical processing (usually a cycle of rolling and annealing steps) needed to reduce thickness is expensive. Furthermore, the thinning frequently degrades dc properties while not enhancing the ac properties to the degree anticipated. Although the high induction metals (Fe-Co Permendurs and lowers cost Fe-3%Si) are essential for applications with volume and mass constraints, the properties of Fe-50%Ni and Fe-80%Ni alloys have been seriously challenged by the advent of metallic glasses.

In the past decade, metallic glasses have become available in industrially significant quantities and at competitive prices.[4] These materials are manufactured on a commercial scale by quenching suitable alloy melts at rates of 10^{6}°K/s or more into highly ductile ribbons up to some 20 cm wide and on the order of 25 μm thick. Their thin gage results directly from the quenching process without the necessity of further rolling, and their resistivities are high owing to the solute contents needed for glass formation. The inference of attractive properties has indeed been realized in large-scale cores. Iron-based alloys with $B_s \sim 1.5$–1.8 T are most widely used. For certain specialized applications, and despite their lower B_s, the use of more expensive Co-based alloys with near-zero

magnetostriction is justified by their lower losses and higher permeabilities as well as the insensitivity of their properties to stresses. Much of the resurgence of interest in magnetic switching for pulse power applications is thus directly attributable to metallic glasses.

The principal challenges in using metallic glasses in large-scale pulse-power cores have been annealing, insulation, and ribbon geometry (thickness and packing fraction). It is widely recognized that annealing can be used to tailor the B-H loop shape and other magnetic properties of metallic glasses. Annealing is most beneficial for magnetostrictive materials. In them, stresses arising from the casting and core fabrication processes that result in sheared B-H loops and increased losses can be redistributed or eliminated. In addition, regardless of magnetostriction, an anisotropy direction can be established and loop-shape controlled by imposing a magnetic field during annealing. A longitudinal field improves squareness, though sometimes at the cost of marginally increased losses. Transverse annealing results in a flat loop with low core losses but also low remanence and, if $\lambda_s \neq 0$, susceptibility to loss-producing magnetomechanical resonances.[5] It is generally found that the extrinsic properties of annealed materials (especially the magnetostrictive alloys) are generally more consistent and predictable than those of as-cast materials.

There is a close relationship among annealing, insulation, and core fabrication in pulse power applications involving metallic glasses. As detailed below, insulation materials which can withstand the requisite annealing temperatures are expensive and tend to impart undesirable stresses to the metallic glasses. The alternative of insulating cores after annealing is applicable principally to near zero magnetostriction glasses or to high anisotropy materials like METGLAS® 2605CO. Finally, core fabrication procedures for annealed metallic glasses must take into account their reduced bend ductility.

The reduction of thickness has been a route to lower losses in metallic glasses as well as in polycrystalline metals. Fortunately, the casting process for metallic glasses inherently results in a thin product (20–25 μm is typical); however, their high mechanical hardness makes it difficult or impossible to use rolling as a routine thinning method. Furthermore, packing fraction tends to degrade for both polycrystalline and amorphous metals at thicknesses well below 25 μm, as surface imperfections become more dominant.[7] For the usual single-roller cast amorphous metals, there is a substantial qualitative difference between the profiles of two surfaces of the ribbon. The wheel side is characterized by micrometer-sized pockets resulting from air trapped during solidification from the boundary layer associated with the rapidly spinning wheel. The free side also has variations, but on a much longer distance scale. By careful process control it is now routinely possible to realize packing fractions of 80% or more on ribbon of standard thickness. One other class of imperfections is now being recognized as of significance for pulse power properties, so-called "pips", or sharp local asperities as tall as several μm. These pips, with low local radii of curvature, concentrate electric fields leading to dielectric breakdown and the attendant interlaminar eddy current losses, as discussed in detail below. Recent data on vacuum-cast, 5-mm-wide Co-based glasses as thin as 4 μm hold out great hope for improved cores, assuming that cost-effective, industrially viable processing can be developed.[8]

Ferrites are an essential class of magnetic materials for many high-frequency magnetic applications, including pulse power. Although ferrites have undesirably low B_s and T_c, their extremely high electrical resistivities give rise to attractively low eddy current losses, notwithstanding higher hysteresis losses. Ferrites are fabricated by common ceramic processing techniques comprising synthesis of suitable powder, pressing to shape, and sintering. The properties of the cores are strongly influenced by their chemical compositions and microstructures.

The usefulness of ferrites for pulse power would be enhanced greatly by the availability of cores with larger dimensions.

Whereas polycrystalline and amorphous metal cores are fabricated from essentially continuous lengths of tape or sheet, ferrite cores are generally made as integral shapes. The scale-up of tape winding equipment is far easier and less expensive than the acquisition of the presses or related apparatus needed to process larger solid ferrite pieces. For the ferrites it is generally harder to hold stable dimensions since the traditional processing necessitates an operation for densification. The market for the large cores needed for pulse power is small enough that domestic manufacturers have not had sufficient incentive to produce cores 20 cm in diameter or larger. Hence, such cores would likely become available only through targeted government support of the ferrite industry or through novel processing that eliminates the need for large capital equipment. Nonetheless, many of the strides in processing of structural and electronic ceramics have not been extended to ferrites, opening significant possibilities for the future.

The recent development of nanocrystalline materials like Hitachi's FINEMET may open additional options.[9] Nanocrystalline alloys are produced by first making suitable metallic glasses with conventional rapid-quenching techniques. The metallic glasses are then heat-treated to substantially devitrify them. The resulting microstructures are characterized by grain sizes of 10–100 nm, far smaller than those reported heretofore in ingot metals or in conventionally recrystallized metallic glasses. Although few data on pulse magnetization properties are reported for these materials, sinusoidal losses at 10–200 kHz are comparable to those of Co-base amorphous metals. Near-zero magnetostriction has been obtained, along with $B_s \sim 1.2$ T and with T_c's of order 550°C, higher than the T_c's of most metallic glasses. Questions remain as to whether embrittlement will be a problem. Hitachi has recently announced the commercial availability of these materials.

Measurements

The group recognized the importance of reliable measurement techniques in the pulse power endeavor. The paper of Wengerter outlines many of the difficulties and obstacles in obtaining good data, many of which were confirmed anecdotally by group members. The group compiled (see Table 3) a number of laboratories with various measurement capabilities. Most characterization work falls into two classes, using either constant voltage (hence, constant dB/dt) excitation or (1 - cos ωt) voltage waveform. Constant voltage is easier to accomplish, requiring only the discharge of a large capacitor through the inductor under test, but (1 - cos ωt) is preferred, as it simulates the resonant discharge waveform typical in pulse compression networks. However, (1 - cos ωt) tests are normally much more involved, requiring use of a capacitor and a resonant inductor, one of which must be changed to vary the time-to-saturation for the saturable inductor under test.

The various labs are in general agreement on the data being openly reported for dynamic B-H loops and losses. Group members were unaware of any round-robin test comparisons, so that detailed comparisons are rather difficult. The total data base is quite modest, and different labs routinely have reported different ΔB's, times to saturation, waveforms, and sample compositions and treatment conditions. Because of the differences in test apparatus, a simple round-robin is not trivially arranged. The group agreed that state-of-the-art oscilloscopes and digitizers with excellent dynamic range and transient responses are essential to obtain the desired data. For example, in constant voltage data, the instantaneous current (proportional to H) varies by as much as 1:100 between excitation and saturation. Also, careful attention to integration offsets is needed to obtain accurate losses. Despite the general consensus on loops and losses, some significant gaps in our knowledge are recognized. Saturated permeability is an important property for circuit and systems designers but is difficult to measure. The techniques for measurement and analysis must be carefully specified for meaningful comparisons to be made. There is also pressing need to know the temperature dependence of many of the extrinsic magnetic properties.

Table 3. Laboratories doing experimental pulse magnetization characterization.

Institution	Waveform	Max. dB/dt (T/μs)	Max. core size	Contact
Allied-Signal, Inc. (U.S.A.)	const. dB/dt	30 limited	2–3 cm dia. 20 cm dia.	C. H. Smith
National Magnetics (U.S.A.)	const. dB/dt	30	0.1–200 kg	R. Wood
British Aerospace (U.K.)	const. dB/dt 1 – cos	0.1–1	3 cm dia.	N. Seddon
University of Bristol (U.K.)	const. dB/dt 1 – cos)	0.1–10	20 cm dia.	M. Greenwood
Vacuumschmelze (F.R.G.)				R. Wengerter

Temperature Effects

An increase in a magnetic core material's temperature during either processing or operation can have both reversible and irreversible effects on properties. Reversible changes of importance include:

- Decreasing B_s as T approaches T_c, following closely the Brillouin function of statistical physics.
- For magnetostrictive materials, degradation of properties by magnetoelastic coupling to strains arising from differential thermal expansion between the magnetic material and insulation or supporting structures.
- Extrinsic changes in magnetic properties in ways not fully quantifiable *a priori*.

Irreversible changes can include:

- Magnetic aging.
- Microstructural changes.
- Devitrification of amorphous metals.

Table 4 highlights which of these concerns is paramount for various materials and indicates approximate steady-state temperature limits for present materials.

Table 4. Service temperature limits for magnetic materials used in pulse power.

Material	Limit (°C)	Reason
Polycrystalline metals		
FeSi	500	T_c
50Ni-Fe	350	T_c
80Ni-Fe	350	T_c
50Co-Fe	500	T_c
Amorphous metals		
Fe-base	150–175	Aging
Co-base	100-150	Aging
Ferrites	150–200	Low T_c, strong temperature dependence of properties, so materials are carefully optimized at desired use temperature

It is important to note that the materials of prime interest for pulse power—amorphous metals and ferrites—both have temperature limits that fall in the same range as the service temperature limits of many common insulation materials. It thus appears that present device operating temperatures are limited both by their magnetic core materials and, to a lesser degree, by insulation schemes. The chief limit on ferrites (low T_c) is unlikely to be overcome, but there is a moderately high probability that limits set by insulation and concerns about aging of metallic glasses can be mitigated.

The group considered the relevance to pulse power of magnetic aging—various changes in soft magnetic properties due to operation at elevated temperatures. The magnetic aging of crystalline materials has long been studied. Several mechanism are recognized. For metals other than permalloy, magnetocrystalline anisotropy is dominant and the principal aging mechanism is the segregation of impurities (notably C) to grain boundaries. In permalloy, a much weaker induced anisotropy arising from pair ordering during fabrication and annealing is dominant. As discussed below, the formation and stability of this anisotropy can be understood in light of the Neel–Taniguchi theory.[10]

The aging of metallic glasses has been studied extensively, though not in the context of pulse power.[11] Although bulk devitrification has been shown to be of no concern under ordinary conditions, magnetic aging has been reported to make certain first generation materials unsuitable for extended use. Fortunately, current materials are fully adequate within service temperature limits of 100°–150°C. Once again, the Neel–Taniguchi picture provides a conceptual framework for understanding anisotropy and aging. However, the underlying atomic mechanisms are more difficult to elucidate in amorphous structures in which processes with a spectrum of activation energies are operative. An improved understanding of these mechanisms might lead to a better quantification of long-term device behavior and to choice of alloys and annealing conditions with more robust specifications.

In addition to its direct effect on the properties of materials themselves, a temperature rise from core losses has systems implications for thermal management. Suitable means are needed to extract heat generated within the core by transferring it to a cooling medium, whether ambient atmosphere, gas, or a dielectric liquid. A coolant must be chemically compatible with the magnetic material, any insulation, and with other system components. If cooling passages are needed in the core, packing fraction is inevitably reduced.

Insulation

Improved materials and processing for interlaminar insulation are perhaps the single most important issue in pulse core designs comprising metallic materials. Faraday's law dictates that an interlaminar voltage appears between layers of a tape-wound core with a magnitude proportional to the magnetization rate dB/dt times the tape's cross-sectional area. For a typical core with 50-mm × 20-μm metallic glass and dB/dt = 10 T/μs, the voltage is of order 10 V. To limit degradation of packing fraction, any insulation must be much thinner than the material thickness, typically 10–25 μm. Yet the insulation must have sufficient dielectric strength to hold off the local interlaminar voltage. Asperities such as pips present a particular problem in their tendencies both to concentrate the electric field and to puncture the dielectric.

Table 5 lists some characteristics of an ideal insulation material identified by the group. Clearly, no single material can be expected to fulfill perfectly all these requirements. In Table 6 a number of currently used insulation schemes are evaluated against these criteria.

Table 5. Properties of an ideal insulating material.

Thinness
Good dielectric breakdown
High mechanical strength (not compromised by surface imperfections of magnetic material)
Thermal stability (withstands annealing and operating temperatures)
Compliant (does not stick and imparts no stress to magnetic material)
Compatible with dielectric cooling fluid or gas
Adequate edge coverage
Low susceptibility to radiation damage
Low dielectric loss
Inhibition of corrosion
Inexpensive

Table 6. Currently used installation schemes.

Vapor deposited films
Evaporated
Sputtered
Chemical vapor deposition (CVD, especially plasma-enhanced)
Coatings from liquid
MgO — deposited from Mg methylate by evaporation of alcohol; established method for NiFe; more difficult for amorphous metal since high heat needed to eliminate all waters of hydration which cause corrosion.
SiO_2 — deposited from colloidal solution in alcohol
Electrophoretic deposition
Also used to reduce surface roughness
Interwound films
Polyester (MYLAR)
Polyimide (KAPTON)
Polysulfone
Polycarbonate
Transformer paper
Fluids
Transformer oil
Fluorinated hydrocarbons (may be limited by environmental regulations)

Figures of Merit

The group discussed at length the desirability of figures of merit (FOMs) as a means for comparing core materials. Two candidate FOMs have been suggested:

$$FOM_1 = p/\Delta B)^2/t \quad (1)$$

$$FOM_2 = p/\Delta B)^2/E_L \quad (2)$$

FOM_1 is believed to have been suggested originally by C. Cline; it reflects both the energy and volumetric efficiencies of an idealized pulse core. More specifically:

$$FOM_1 \alpha (E_L/E_c)(\text{volume}/E_c) \quad (3)$$

where E_c is the energy compressed per pulse and E_L is the energy lost per pulse. The two

factors in Eq. (3) are the reciprocals of the energy and volumetric efficiencies, respectively. The form of FOM_1 shown above as Eq. (1) may be derived by assuming the predictions of saturation wave theory to infer E_L and discarding all geometrical and systems design factors. All the materials constants are retained to yield Eq. (1).

In practice, observed losses are intermediate between the predictions of saturation wave and bar domain models that predict t^2 and t dependences, respectively. In contrast to the saturation wave model (which assumes only a single encircling, sandwich-like domain wall), the bar domain model depends on extrinsic properties of the magnetic material (viz., domain wall spacing). Hence, it is not possible *a priori* to write a general bar domain expression analogous to Eq. (1). That expression thus may be useful at high dB/dt, but is somewhat limited in its overall predictive value.

Greenwood et al have suggested the experimentally determined value of $E_L/(\Delta B)^2$ as a criterion. As a FOM, the reciprocal is required, as shown in Eq. (2). FOM_2 has the advantage over FOM_1 of not containing any assumptions of loss mechanisms, but requires an actual measurement of E_L. Since $E_c \alpha (\Delta B)^2$ apart from geometrical factors, FOM_2 reduces to an actual measured energy efficiency.

Neither of these FOMs is entirely satisfactory. Ultimately, any FOM must reflect the constraints set by the system in which a given magnetic core is to be used. It is particularly difficult to formulate a single FOM which compares disparate materials well, especially the comparison between ferrites and metallic materials. For a given application, the relative importance of system volume (and mass, its corollary), losses, and price must be specified in formulating a FOM. The group felt that the diversity of pulse applications thus renders it futile to develop and agree on an universal FOM.

Furthermore, none of the FOMs takes into account the system requirements for cooling. The problem of extracting a given amount of heat from a tape wound core with moderately high metallic thermal conductivity is entirely different from that of extracting the same heat from a poorly conducting solid ferrite core. In general, rep-rated applications are most sensitive to these systems constraints for cooling.

Modeling and Theory

The group recommended that a significant effort be devoted to improving the capability for modeling the behavior of magnetic cores. The modeling needed for magnetic switching is inherently demanding because the hysteresis of magnetic materials that any model must be nonlinear and must account for instantaneous properties as a function of the material's past magnetic history.

The modeling of pulse core performance can be approached from many viewpoints on a spectrum. At one extreme of pure physics, the core can be regarded as an ensemble of magnetic atoms whose properties can be calculated from first principles using the apparatus of quantum mechanics. Remarkable progress in this approach has enabled many intrinsic properties (e.g., magnetization) to be calculated with reasonable accuracy. However, extrinsic properties, many varying over even wider ranges than do the intrinsic properties, play a crucial role in ultimate device operation. The magnetic interactions that underlie the extrinsic properties are governed by a much finer energy scale than that addressed for the quantum effects, which determine the ground-state intrinsic properties. The demonstrated effect of microstructure on properties is but one indication that essentially atomic-level calculations are likely at best to have influence only on basic alloy design for the foreseeable future.

For the near term, useful modeling is likely to arise from a more operational approach that takes as its goal an accurate description of the nonlinear electrical circuit properties of the core. Modeling then serves to extend limited empirical data to predict device performance over a wide range of conditions of magnetization rate and traversal of both major and minor B-H loops.

Within this engineering orientation, the requirements of physics may be imposed to varying degrees. The greatest numerical

accuracy is achieved by a purely mathematical approach which uses empirical data to generate functional forms which describe the dynamic B-H loop and the quantities implicit therein (e.g., permeability and core loss). It is obviously not possible to know *a priori* the limits in parameter space at which such models break down, nor is there any obvious connection linking fitting parameters to the choice of material composition and processing. Numerical models thus may be highly useful for the engineer seeking to simulate an operating circuit, but on their face they provide little guidance for the design and processing of materials.

An intermediate approach imposes Maxwell's equations with the relevant boundary conditions and incorporates such concepts as domain structure and magnetostatic energy balance to give prediction of, and theoretical basis for, functional relations between quantities such as loss, flux change, and magnetization rate. Furthermore, these approaches also can tie parameters of the purely numerical models to observable magnetic and microstructural factors. Perhaps the most obvious example is the Pry and Bean model of core loss, which has been enormously useful in the development of present-day electrical steels.[12] This model makes a simple connection between the eddy current component of loss and an easily measured characteristic, mean-domain wall spacing. The model has been predictive, in that wall spoacing can be controlled by varying microstructure; the resulting losses are in reasonable agreement with theoretical prediction. Unfortunately, extending such approaches to the regimes of flux swing and magnetization rate encountered in pulse power is far from trivial.

One of the unique requirements for modeling cores in magnetic switching systems is the need for an adequate description of the magnetic behavior in the regime of technical saturation. The transition fundamentally alters the character of the magnetization process which is dominated by wall motion (giving rise to high mu) below saturation and by magnetization rotation (low mu) above, with the creation and annihilation of walls signaling the transition. These wall processes present a formidable problem: the resulting domain structure is often being strongly frequency dependent, indicating the subtlety of the underlying physics. Anisotropy energy is the central issue.

The Pry and Bean model, for example, is most successful at low frequencies and for small flux changes not involving significant wall creation/annihilation. The model's prediction that core losses under sinusoidal flux conditions vary as $(B_{max}f)^2$ is generally accurate. However, it is widely recognized that the breakdown of these dependences outside the low f, low B_{max} regime reflects the limitations inherent in Pry and Bean's simplified view of wall dynamics.

These limitations have a direct analog under pulse magnetization, as the bar domain model incorporates precisely the same picture of wall structure as does Pry and Bean. As the magnetization rate increases, the bar domain model ultimately gives way to the saturation wave picture of a single encircling domain. The cost in anisotropy energy to create walls must play a key role in this transition, yet this thesis is still not satisfactorily incorporated in modeling or in theory.

The formation of anisotropy is reasonably well understood (at least qualitatively) in crystalline soft magnetic materials. For Fe-Si and Fe-Co alloys, magnetocrystalline effects are dominant. In permalloys, compositions are adjusted to minimize or eliminate magnetocrystalline anisotropy, so that induced anisotropy comes to the fore, in accord with the Neel-Taniguchi directional ordering mechanism. The analysis is facilitated by the very high site symmetry at the magnetic atoms' positions, such as the cubic point symmetry of bcc Fe or fcc Ni-Fe and Fe-Co alloys.

However, for amorphous metals, our understanding is far less comprehensive. The highly noncubic local symmetry at most of the metal atom sites favors a strong anisotropy. However, in the soft magnetic metallic glasses of interest, even stronger exchange coupling dominates this local anisotropy, forcing the global anisotropy to be nearly zero because of spherical

averaging. The marked effect of magnetic annealing on the residual anisotropy and the properties controlled thereby strongly argues for the existence of an ordering mechanism akin to the Neel-Taniguchi picture. One apparent consequence of the competing anisotropies is the notable discrepancy between anisotropy energy values determined from nominally saturated B–H loops and by torque magnetometry in the more fully saturated state. The difference also is manifested in a surprisingly large high field susceptibility which apparently reflects the energy needed to align fully all the magnetic moments whose local easy axes are not collinear. A much more comprehensive understanding of the formation and stability of anisotropy in disordered and amorphous structures would likely lead to more accurate modeling of saturation in these materials of technological importance.

Principal targets for improving pulse models include:

- Generation of a broader base of empirical data to (1) improve the accuracy of numerical models and (2) facilitate the evaluation of physical models.
- A better understanding of the physical significance of parameters generated in mathematical and numerical approaches.
- An understanding of the correlation between materials (microstructure and processing) and the measured or fitted parameters describing their magnetic properties.
- Incorporation of temperature dependence of properties.
- Better description of reset phenomena,

In parallel, better theory needs to be developed to explain:

- The formation and stability of magnetic anisotropy in amorphous and disordered systems.
- The creation and annihilation of domain walls under high dB/dt magnetization and the resulting effect on core losses.
- The dynamic resetting of cores to remanence.

Conclusions and Future Directions

The group recognized that great strides had been made in the development and application of magnetic materials in pulse compression systems. The process has benefited most prominently from the advent of metallic glass technology.

However, pulse power by itself is not a sufficiently large market to exert dominant influence on materials development. Accordingly, it is important for pulse-power designers to take advantage of progress in related applications that may generate technological spinoffs. For example, the increasing use of switch-mode power supplies whose operating frequencies have increased to 1 MHz and beyond has prompted a resurgence of interest in materials, phenomena, and theory applicable at the dB/dt rates of interest in pulse power. Many of these developments are easily transferable.

On the other hand, there are aspects of pulse power which are sufficiently unique that market forces alone are unlikely to drive easily envisioned improvements. For most high frequency devices, cores are inherently small. Hence, raw materials costs are low enough to enable use of high performance materials. In contrast, pulse power devices operating at comparable dB/dt can rival in size large 60–Hz devices—industrial motors and transformers in the electric power grid. Yet the requirements for the pulse power system in magnetic properties, interlaminar insulation, and core construction and cooling may be vastly more demanding. A principal challenge is thus the goal of building pulse power devices using materials such as Fe-based metallic glasses originally designed to replace commodity eletrical steels costing less than $12/kg.

The group identified the following as the most pressing of the requirements for magnetic pulse compression systems for which there is a realistic prospect of advances in the near to medium term:

- Improvement in the physical properties and forms of ferrites and rapidly quenched metals, principally metallic glasses.

- An improved understanding of anisotropy and aging phenomena in disordered and amorphous systems.
- Better interlaminar insulation methods or materials.
- Improvement in the accuracy and theoretical basis for modeling magnetic pulse-power system performance.

References

1. This core loss is often loosely termed "hysteresis loss." More properly, the term "hysteresis loss" is reserved for the limit of loss as the magnetization rate tends to zero. This loss per cycle is equivalent to the area contained within the dc B-H loop. In the modern view, it is recognized that all core losses, even those in the dc hysteresis limit, reflect the dissipation of ohmic currents induced by the changing flux implicit in the discontinuous motion of magnetic domain walls.
2. The magnetization rate (dB/dt) is analogous in the context of pulse power to frequency (f) in the more conventional sinusoidal flux excitation. In the latter case, it is conventional to consider power dissipation, i.e., loss per cycle times f. Thus, the hysteresis and eddy current components of loss vary as f and $f^{1.5-2}$, respectively. Pulse losses are discussed in some detail in C. H. Smith, *J. Appl. Phys.* **67**, p. 5556 (1990).
3. Soft magnetic materials are extensively reviewed in G. E. Fish, Proc. IEEE **78**, 947 (1990).
4. G. E. Fish and C. H. Smith, *Soft and Hard Magnetic Materials with Applications*, Metals Park: ASM, 1986, p. 7.
5. V. R. V. Ramanan, C. H. Smith, and L. Barberi, *J. Appl. Phys.* **57**, p. 3493 (1985).
6. METGLAS is a registered trademark of Allied-Signal, Inc., for alloys of metals.
7. A high packing fraction is important in that the magnetic energy stored in a core is proportional to the square of magnetic induction averaged over the core's entire cross section and thus to $(B_s \times P.F.)$.[2] Equivalently, the switching efficiency varies as the ratio of the inductances of the core in the unsaturated and saturated states, μ_{unsat}/μ_{sat}. A low packing fraction reduces μ_{unsat} but not μ_{sat}.
8. M. Yamaguchi and K. Murakami, EIII Trans. Magn. **MAG-24**, p. 1770 (1988) and M. Yagi and T. Sawa, Intermag Conference, Brighton, England, 1990, paper AD-04, to be published in IEEE Trans. Magn.
9. Y. Yoshizawa, S. Oguma, and K. Yamauchi, *J. Appl. Phys.* **64**, p. 6044 (1988); Y. Yoshizawa and K. Yamauchi, *IEEE Trans. Mag.* **MAG-25**, p. 3324 (1989); and G. Herzer, Intermag Conference, Brighton, England, 1990, paper AD-01, to be published in *IEEE Trans. Mag.*
10. S. Chikazumi and S. H. Charap, *Physics of Magnetism* (Krieger, Huntington, NY), pp. 128–130.
11. G. E. Fish, *IEEE Trans. Mag.* **MAG-21**, p. 1996 (1985).
12. R. H. Pry and C. P. Bean, *J. Appl. Phys.* **29**, p. 532 (1958).

Power Conditioning Group

Chris Young, Chairman
David Barrett, Cochairman

Working Group Members

C. Burkhart
R. Curry
J. Gower
M. Gunderson
R. Kihara
G. Kirkman
M. Mazzola
G. McDuff
H. Menown
G. Neil
C. Pirrie
S. Pratap
F. von Haaften
G. Westenskow

Abstract

The generation of pulses at very high average power levels is often limited by the capabilities of active switching components such as thyratrons and thyristors. A magnetic pulse compression (MPC) network can be employed to extend the performance of a modulator system while enabling the active switch to operate within its capabilities. The use of a MPC network may place special constraints on the power conditioning network. For example, the use of a compression network may significantly reduce the overall efficiency of the modulator system. As a result, the power conditioning system must be capable of delivering additional power to the modulator to compensate for the inefficiencies introduced by the magnetic pulse compressor. The difficulty of obtaining precise timing control of the output pulse is increased when a MPC network is used. Because the switching time of each saturable inductor within the network is dependent on voltage, power supply voltage variations results in output pulse timing jitter. For systems which require low output pulse jitter, it is necessary to compensate for this effect. There are at least three methods which may be used to reduce the effect of power supply voltage variation on the output timing of a MPC network. First, the power supply voltage can be precisely regulated by a number of techniques, thereby eliminating any output pulse timing jitter due to voltage variations. Another method is to make the timing of the pulse compression network less sensitive to power supply voltage variations by charging the first stage of the compression network with a dual-resonant voltage waveform. The integral of such a waveform over the charging period is independent of power supply voltage. As a result, the switching time of the first stage saturable inductor is independent of voltage. Although the switching times of the following stages are dependent on the input voltage, the overall delay of the pulse compressor is less sensitive to the input voltage because the largest portion of the delay is in the first stage.

Finally, a delay compensation circuit can be used to compensate the delay through the MPC network in the face of input voltage variations. The goal of such a circuit is to keep the sum of the compensation circuit delay and the pulse compression network throughput delay constant over a range of power supply voltages. This type of circuit has been shown to be effective in maintaining low output jitter by compensating for variations in the supply voltage.

Although MPC networks have been successful in relaxing the requirements of active switching devices, use of such networks has introduced new problems which must be addressed in the design of

the power conditioning network. For MPC technology to continue its evolution to higher average powers while attaining reliability and cost goals, it will be necessary to invest additional effort in the development of power conditioning networks which are capable of driving high average power magnetic modulator systems.

Introduction

The purpose of the Power Conditioning Working Group was to define the critical issues related to electrical power conditioning systems for repetitively pulsed, high-average-power, MPC systems. The group accomplished this task by first defining the parameter space that characterizes a high-average-power, repetitive, power-conditioning system as shown in Table 1.

Table 1. Power conditioning parameter space.

Average Power	500 kW < P < 5 MW
Pulse Width	1 μs < t < 30 μs
Pulse Repetition Rate	1 kHz < PRR < 5 kHz
Voltage	50 kV < V < 100 kV
Energy	10 J < E < 5 kJ

The group then defined the key issues and divided them into critical and noncritical issues. Three of these key issues were determined to be critical issues and were addressed in detail by the group. The first issue relates to voltage regulation in the power conditioning system which results in timing variations in the MPC system. The second critical issue relates to the components used in the power conditioning system and their effect on general system performance and reliability. If ideal components were available, then magnetic pulse compressors would not be needed. Finally, the third critical issue relates to the requirement that a MPC stage be placed between the load and the power conditioning system. In other words, how can we make power-conditioners better and, possibly, get rid of the requirement for MPC stages?

For each critical issue, the working group divided into three small subgroups. Each group addressed one of the critical issues. The approach that each group took in addressing these issues included four basic steps: (1) determine the effect of the critical issue on system performance, (2) identify the source of the problems, (3) identify technical approaches to overcome these problems, and (4) propose future research and development directions to resolve these critical issues.

Voltage Regulation

Effects

Voltage regulation was determined to be a critical issue because of its impact on both the magnetic pulse compressor and the overall system performance. Voltage variations in the power conditioning system lead to three basic problems: timing jitter, energy variations, and efficiency degradation. Timing jitter induced in the MPC system by voltage variations is directly proportional to the fractional variation in the nominal power conditioner voltage. This timing jitter can lead to problems in synchronization of timing events (or other parallel compressor systems) and reflections within the magnetic pulse compressor stages. Variations in the energy delivered to the load is proportional to the magnitude of the voltage variations squared plus twice the product of the voltage variation times the nominal voltage. Energy delivery variations can have a dramatic effect on the load performance. Voltage variations in the power conditioning system also can directly impact system efficiency because these variations can result in reflections in the magnetic pulse compressor, load mismatching, and possibly decrease the efficiency of the load itself.

Sources

Several sources can contribute to voltage variations within the power conditioning system. Variations (brownouts

r surges) in the prime power source are a ey concern for power conditioner designers. 'rime power variations outside of the lesign parameters can result in significant utput voltage variations. The power upply itself has a small amount of ripple n the output voltage. Ripple can be ninimized at the expense of added iltering or active high-speed control ircuitry. Because the power conditioner resents a finite source impedance to the oad (magnetic pulse compressor), "normal" hanges in the MPC characteristics inductance variations, residual voltages, tc.) can have an impact on the magnitude f the output voltage. Variations in the oad itself can cause reflections in the magnetic pulse compressors which can lead to voltage regulation problems. Feedback errors in the regulation and control circuitry can cause voltage variations. Feedback errors are caused, usually, by spurious noise sources i.e., electromagnetic interference (EMI). Mechanical factors may also lead to output voltage variations. Thermal or mechanical drift of structural or circuit elements or packages can lead to changes in component values (discrete or stray). Mechanical vibrations also can contribute to component variations. All these sources can simultaneously contribute to voltage variations which make specific problem diagnosis rather difficult.

Technical Approaches

There are two basic methods for addressing the problem of voltage variations. One obvious method is to try to regulate the voltage. That is, use some method to adjust the power conditioner on an adequate time scale to reduce or eliminate the voltage variations. The second method is to compensate for or reduce the effects of the variations by adjusting the control circuitry, the magnetic pulse compressor, or the effective load. These methods may be used separately or together, depending on the amount of regulation needed for a particular application.

Many techniques exist which can be used to regulate the output voltage of the power conditioner. One technique is to use a de-Qing circuit to spoil the quality factor or remove the excess energy from a current limiting inductor in the power conditioner. The inductor limits the current by storing energy in a magnetic field and regulation can be accomplished by externally modifying the stored energy. This energy can be dissipated as heat in a resistor or can be removed from the inductor and reused by the power supply. Another technique for regulation is to use switching or linear regulator techniques within the dc supply itself. Boost, buck, or buck/boost techniques can be used to control the output voltage of a power supply. Linear devices may be used in series or shunt modes to limit or divert current as needed to regulate the voltage. Finally, post-regulation techniques can be used to modify the output voltage of the power conditioner which is optimized for precise voltage regulation.

Voltage variations also can be handled by compensating for their effects. As mentioned earlier, three important effects of voltage variations are: timing variations or jitter, delivered energy variations, and efficiency degradation.

Timing variations can be compensated by three basic methods. The first is to monitor the output voltage and vary the primary switch trigger signal in proportion to the voltage variation which reduces the apparent timing jitter in the system. The second is to vary the reset bias on the magnetic switches as a function of the output voltage. By increasing or decreasing the bias current through the MPC stages, the voltage-time product of those stages can be varied to reduce the apparent timing jitter. The third is to use an ac charging technique for the first compression stage. Symmetric ac charging or resonant-transformer charging of the first capacitor can be used. Both techniques ensure that the integrated cycle (set and reset) voltage-time product for the first stage of magnetic compression is a constant relative to voltage variations. This ensures a constant timing sequence for the first stage of magnetics.

Variations in the shunt energy delivered to the load as a result of power conditioner voltage variations can be compensated by using a shunt regulator at

the load. The system can be designed to deliver in excess of the required energy and a linear shunt regulator can be used to divert the excess energy from the load. The diversion of energy can be adjusted so the voltage variations do not result in energy variations at the load.

Voltage variations can decrease system efficiency by causing reflections within the MPC assembly. The reflections represent energy that is not delivered to the load and must be removed from the magnetic pulse compressor before the next shot. Usually, the energy is dissipated as heat in resistive loss mechanisms. Reactive energy recovery techniques can be used to recover and reuse the reflected energy. This recovery process can increase the overall system efficiency.

Future Research

Although we identified some technical approaches, significant research is necessary to develop the technology base to allow implementation of these techniques. Future research should include methods of reactive linear regulation. That is, linear regulators should be developed which can recover the energy of regulation instead of dissipating it in resistors. Capacitors and transformers can be combined in networks which will regulate without degrading system efficiency. Networks of these components should be optimized for series and shunt regulation.

Improvements are needed in the area of diagnostic and control circuitry. High speed power electronic devices are needed in several of the technical approaches identified above. Gigahertz (and beyond) logic and linear integrated circuits are needed to make real-time corrections in the control circuitry to allow accurate voltage regulation. Also, research must be pursued in the area of high precision measurements in adverse pulsed power environments. Precision measurements are needed of high voltages (>100 kV) and high currents with bandwidths ranging from dc to several gigahertz. Research also is needed in the area of regulation components such as opening and closing switches, resonant transformers, and high frequency high-power ac sources. Switch technology directly impacts the power conditioner performance (this will be addressed in the next section). Resonant transformer technology needs to be advanced especially in the area of leakage inductance control during or after manufacturing. Operation of the resonant transformer technique relies on precise control of the transformer leakage inductance. High frequency, high power ac sources are needed to power the magnetic pulse compressor directly. (Remember, one of the techniques for compensating for voltage variation is to use ac charging of the first stage.)

Component Limitations

Virtually any component of the power conditioning system (PCS), active (prime power, switches) or passive (capacitors, inductors, resistors), can limit the system performance. In this summary, the capabilities of a subgroup of PCS components will be compared with sample parameters (Table 1) for high average power modulators.

We examined the limitations of prime power generators (rotating machines), switches (solid-state and gaseous), and capacitors in topologies that might be capable of operating in the above parameter regimes. Device limitations were examined both in terms of the present level of development and potential future development.

Although this comparison is limited in scope, it demonstrates the manner in which component limitations can affect the optimal topology of a power conditioning system for a magnetic pulse compressor.

Prime Power: Rotating Machines

The prime power delivered to the PCS can either be dc (e.g., dc high voltage power supply) or modulated (e.g. rotating machines). The latter approach may be advantageous when the PCS is driving a magnetic pulse compressor (e.g., reduced voltage regulation sensitivity). Three

classes of rotating machines were examined: high frequency alternators, compensated alternators, and compensated pulsed alternators. Alternators are commercially available and have demonstrated lifetimes of several years. Parameters for several of these alternators are listed in Table 2.

Table 2. Sample alternator specifications.

Frequency, kHz	Power, kW	Voltage, kV	Efficiency, %	Reference
9.6	375	0.8	73	1,2
3.0	500	0.8	85	1,2
3.0	3,000	NA	NA	1,2
0.96	500	1.2	96	1,2
0.96	5,000	NA	NA	1,2
0.30	40,000	70	NA	3

Many of the machines listed in Table 2 meet some of the parameters, but none meet many of them. Additional stages of power conditioning can be added to step up voltages or decrease pulse length, etc., at the cost of introducing additional components and their limitations. One unfortunate trend is the decrease in efficiency with increasing frequency.

Compensated alternators operate in about the same parameter regimes as uncompensated devices, but because of lower internal inductance they offer the promise of higher efficiency.

With the addition of a rotating flux-compression winding to an alternator, compressed monopolar output pulses can be produced. This class of machines is referred to as compulsators.[4–11] Experimental machines have achieved pulse widths of 10 to 30 μs, voltages of 50 kV, rep rates of 1 to 10 Hz, and output powers of 0.5 to 5 MW. However, not all of the above have been obtained simultaneously.

The primary limitations for all rotating machines are similar. Armature tip speeds limit the maximum output frequency. Lightweight composite materials may lead to higher velocity devices. Electrical insulation breakdown limits the output voltage. The maximum power output is primarily limited by the ability to remove internally dissipated energy from the device. Increases in efficiency and cooling system capacity are required to move to higher power levels.

Switches

Magnetic switches are considered when conventional switches fail to meet the load requirements. However, a subset of those requirements (e.g., rep rate and average power but not voltage) must be met by switches in the PCS. Switches are examined in four categories: thyratrons, spark-gaps, and both bulk and junction solid-state switches. Thyratrons are the most familiar switches in high-average-power high-voltage modulators.

Table 3 lists typical operating parameters where thyratrons have a track record which is well established and well documented. Although not all the parameters of Table 1 fall within the limits for a single device, extrapolations to multiparallel device operation can be made.

Table 3. Sample thyratron parameters.

Duty	Voltage, kV	I(peak), kA	I(ave.) A	Power, kW	Reference
Continuous	50	6	6	150	12
Continuous	35	10	low	<20	13
Continuous	60	20	low	<20	14
Continuous	20	1–2	1–3	10–30	15
Burst	100	4	8	400	16
Burst	25	5	55	600	17
Burst	40	3	30	600	18
Continuous	50	50	9	225	19

To date, thyratron development has been driven by application requirements because thyratrons are developed commercially, whereas internal funding for research and development (R&D) has to be begged, stolen, or borrowed. Recent funding by external agents has changed this situation for the better. For example, EEV is currently developing a range of 8-in.-diameter tubes for very high-average-power and peak-power applications.[20] One goal is the development of a 75-kV thyratron to operate at 5–10 kHz at average powers in the range of 1–5 MW.

In conclusion, it can be said that despite being a "mature" technology, the thyratron has by no means reached its pinnacle of achievement and as new and exciting applications arise, new and exciting devices and techniques will emerge to fulfill these applications.

Spark-gap switches are the most versatile of the available devices. A review of any of the IEEE Pulse Power Conference Proceedings will locate a number of papers on spark-gaps.

The peak voltage, current, and per-pulse energy requirements of the PCS for MPC networks can be easily met by spark-gap switches. The primary limitations are repetition rate and lifetime. Repetition rate is limited by recovery of the gas. The lifetime is typically limited by erosion of the electrodes.

Two approaches have been adopted to minimize the gas recovery time. The Advanced Test Accelerator (ATA) program at LLNL investigated the use of high gas flow rate though the switch, thereby replacing the ionized gas rather than waiting for it to recover. A repetition rate of 1 kHz was achieved at 250 kV, 40 kA, and 80-ns pulse length with ±1-ns jitter.[21–22] An alternative approach adopted at NSWC is to use a high pressure fill of hydrogen gas. The combination of hydrogen's high thermal diffusivity and the large heat capacitance (due to high pressure) leads to rapid recovery times in unblown switches. This type of switch has been tested to 50 kV, 170 kA and 15-μs pulse length (12.25 kJ) in a 2-pulse system with a delay time of 100 μs (corresponds to 10 kHz operation).[23]

Lifetime limitations due to the erosion of electrode material may be minimized by judicious choice of materials and clever design. Present limitations are on the order of 10^6 shots. It may prove difficult to substantially extend electrode life beyond this level for systems with high coulombic transfer.

Of the two classes of solid-state switches, junction devices are commercially available. Although the range of semiconductor power devices is expanding rapidly, the fact remains that individual device capabilities lie well below the levels of power and frequency that the working group was concerned with. The key question then becomes the extent to which it may be practical to build series/parallel device arrays. One point that was made in the group meeting was that power semiconductors are usually not well packaged for pulse modulator applications.

Six device families may be identified: Power MOSFETs, BJTs, IGBTs, GTOs, GCTs, and SCRs. All, except the last, act as both opening and closing switches. In all, except the first, the ON-state conductivity is modulated by minority carriers, with the result that the ON-state voltage drop is reduced, but the switching times and the switching losses are increased.

Each family encompasses a wide range of devices so that the specification of generalized performance limitations is difficult. Nevertheless, we have tried to identify those that are most relevant to the production of pulses of high peak and mean power, and tabulate them for individual devices or modules currently available in Table 4.

Table 4. Parameter limitation for junction semiconductor switches.[24]

	V[max], kV	Average Imax, A	V(on), V	at	J, A/cm^2	dI/dt, A/ns
MOS	1.0	10	2		10	10
BJT	1.5	1000	1		50	1
IGBT	1.5	400	0-5-20		50	10
GTO	4.0	3000	3		100	0.3
MCT	1.5	200	1		200	4
SCR	5.0	5000	1.5		200	1

Table 4 does, of course, represent a considerable oversimplification of some complex parameter interactions. Two features that require more detailed analysis than is possible here are the mean current and the permitted maximum peak current for low duty cycle operation, and the relationship between V(on) and current density. In SCRs an I^2*t value is often quoted, based on a 10-ms, half sine wave. This does not apply with short pulse lengths. As far as V(on) is concerned, it would probably be best to choose an acceptable value and compare the current densities at that value for all devices. Enough information to do this probably is not available to us at this time.

The MOS, IGBT, and MCT families are each based on a cellular structure, and so are available only on square dice. With the others (BJT, GTO, and SCR), a single device can occupy a whole wafer, so that edge beveling and passivation permit the higher voltage ratings quoted in Table 4.

Series and parallel arrays introduce problems of voltage sharing (transient and steady-state), current sharing (transient and steady-state), and insulated drive circuitry. Power MOSFETs with avalanche capability offer the fewest sharing difficulties, but the bipolar devices would all require current-sharing inductances and voltage-sharing capacitances, with their attendant circuit implications and losses. Such arrays of SCRs (usually series arrays only) are used in HVDC transmission systems. The 60-Hz rectifier and inverter sets handle more than 2000 MW, e.g., 2 kA at ±500 kV. Optical fibers insulate and power the gate-driven circuits. To attempt to use this approach in a pulse modulator with a much more demanding transient and recovery specification would present very severe problems.

A newer and potentially more promising approach to solid-state pulse-power switching is known as the bulk solid-state switch; it is typically based on highly resistive silicon or gallium arsenide (GaAs) wafers in which metal contacts (for connection to the external circuit) are formed. In the case of bulk GaAs, the switch can theoretically withstand electric fields greater than 200 kV/cm.[25] For standard wafer sizes this could mean a single solid-state switch operating at hundreds of kilovolts, far in excess of present or expected single device thyristor

performance.[26] Unfortunately, bulk switch voltage hold off is usually limited by surface flashover. The current state of the art for GaAs is 100 kV,[27–28] while for silicon it is more than 120 kV.[29]

Because bulk switches avoid thyristor or MOSFET device topologies, they must be driven into conduction by different means. Typically, either light-activation or electron-beam (e-beam) activation is used. For the former case, a laser pulse either generates all of the switch conductivity (linear photoconductivity) or the laser pulse triggers some gain mechanism.[30–31] An e-beam irradiating the region between the contacts also can generate electron-hole pairs, and thus close the switch. E-beam irradiation is often considered to be more efficient for activating large-volume, high-power switches than laser irradiation; therefore, high gain can be achieved[32] (gain is defined as the ratio of switched electrical energy to required activation energy). However, nanosecond switching is difficult with e-beams. Laser activation, even in the linear photoconductive mode, can have substantial gain if the photogenerated carriers have long enough lifetimes. In fact, microsecond electrical pulses can be generated by irradiating silicon[33] or copper-compensated GaAs[34–35] with nanosecond laser pulses. "Lock on" is another mechanism observed in GaAS and InP bulk switches that allows high gain to be achieved with light activation[27–28]. Like MOSFETs and some thyristors, some bulk switches can be turned off without commutation. In the case of copper-compensated GaAS, a second fast laser pulse of a different wavelength can drive the switch into the off-state against an increasing electric field.[36–37] Bulk switches have been operated at current densities exceeding 10 kA/cm^2[34] and currents exceeding 4 kA.[29] In the case of optical control, current rise and fall times can be nanoseconds or less.

Power conditioning for future magnetic pulse compressors will require high average power operation (e.g., greater than 500 kW CW for a 1000 hours or more). Using bulk solid-state switches in this operating regime has not been investigated and would probably pose quite a challenge. Bulk switches typically have an on-state resistance greater than 1 ohm[38] and ,therefore, would dissipate too much power in the switch. The on-state resistance must be trimmed probably to the 100-milliohm range or less to be competitive with low-loss solid-state switches such as the thyristor. Even at these low resistances, careful design of the switch package would be necessary to dissipate an average switch power on the order of 1 kW for a 50-kV, 1-kA, 10-kHz switch assuming a 1-μs pulse width. Unfortunately, a high-average power data base for bulk switches has not been developed; therefore, questions concerning maximum switch dissipation and lifetime are still unanswered. However, improvements in bulk switch design are still occurring, and the concurrent improvement in high peak power semiconductor laser diodes could provide an efficient light source for future bulk switch applications. In this case, the natural optical isolation and low cost of bulk devices could result in vastly improved and less expensive solid-state switch banks that would replace much larger stacks of thyristors in high-repetition-rate power conditioning modulators.

Capacitors

The limitations of capacitors in the PCS for high-average-power MPC networks is briefly examined to illustrate that passive component limitations can be as substantial as those of the active components.

It should first be noted that the high repetition rate, average current, and shot life of the sample parameters prohibits the use of many of the pulse discharge capacitors familiar to the pulse power community. The available rep-rated capacitors are lower in energy density by 1 to 2 orders of magnitude than single-shot pulse discharge cans. As a result, modulators are larger, power leads longer, and inductances higher which limits the minimum pulse length.

Even within the category of high repetition capacitors it may be difficult to find devices with shot lifetimes in excess of

10^{20} shots. Of the 12 capacitors examined by McDuff[39] only three survived beyond 5×10^9 shots.

Another important factor is capacitor losses which are lumped into the capacitor equivalent series resistance (ESR).[40] For a 1-MW system operating at 20 kV, the average current is 50 A. At 1-milliohm ESR the capacitor loss is 2.5 kW. Substantial heating of capacitors degrades dielectric performance and substantially reduces capacitor life.

Conclusions

Although this summary does not exhaustively examine the limitations of PCS components, it does introduce the reader to a number of the most substantial limitations. More importantly, it demonstrates that in designing a PCS for a MPC network, the designer must be judicious in the choice of topologies and the components to fulfill the design. Further, this is an iterative process that directly affects what the optimum magnetic pulse compressor is for a given load.

Any future research in the area of components should address the limitations defined above.

Magnetic Pulse Compressor—The Power Conditioner Load

The Need for New Approaches

A magnetic pulse compressor is needed, basically, because the power conditioner is not the ideal. The ideal power conditioner would produce a pulse of energy with parameters that are perfectly matched to the load requirements. Since power conditions are not ideal, we need magnetic pulse compressors to properly condition the electrical energy before it gets to the load. The purpose of this workshop was to address problems within magnetic pulse compressors. It should be remembered that magnetic pulse compressors are used to solve problems within the power conditioner. It may be that magnetic pulse compressors are not the ideal fix for power conditioning technology. Magnetic pulse compressors increase the complexity of the system which results in decreased reliability of the system, increased system cost, and reduced system maintainability. Magnetic pulse compressors also reduce the efficiency of the system. Reduced efficiency results in a greater heat load on the thermal management subsystem (requiring a larger thermal management system) and an increase in the prime power requirements which leads to increased capital costs and operation costs. Magnetic pulse compressors increase the system weight and size which reduces the system portability and has a negative impact on maintenance. Surely, we must look for other fixes to power conditioner technology that do not have the negative impact of magnetic pulse compressors.

Sources of MPC Problems

Before we try to look for other approaches to replace magnetic pulse compressors, we should spent a few moments reviewing the sources of problems within magnetic pulse compressors.

Magnetic pulse compressors have a critical problem in the area of switching gain. For example, this low gain results in a requirement for multiple stages to achieve a suitable power gain. In magnetic pulse compressors, the delivered energy must be completely transferred from one stage to another in a sequential process. All the energy must be stored in each stage resulting in significant system growth with the addition of stages. Typical power gains for magnetic switches are on the order of 5 to 10.

Another critical source of magnetic pulse compressor problems is in the area of materials. Magnetic materials have limitations in magnetic flux density, efficiency, mechanical strength (ferrites), thermal properties, and dielectric limitations.

Because magnetic switches are constant energy-density devices, the size and the weight of the switches scale linearly with the energy transferred by the switch. To double the energy that is transferred by the switch, the size and weight of the switch must be doubled. Furthermore, since the efficiency of a magnetic switch is fixed by

the switching time and the applied voltage, doubling the energy also results in twice the energy that is dissipated by the switch.

Because magnetic materials are either dense metals or ferrites, they are heavy replacements for plasma-based switches or solid-state devices. Also, because the timing of the switch depends on the magnitude of the voltage, magnetic pulse compressors are sensitive to voltage variations as discussed earlier.

Technical Approaches for Magnetic Pulse Compressor Alternatives

We considered four basic areas as possible alternatives to the use of magnetic pulse compressor: advanced switches, stacked circuits, transformer-based combining techniques, and cumulative wave circuits.

Switch improvements were discussed in an earlier section. Advanced switches should be designed to have higher gains than magnetic pulse compressor so that only one stage of compression is needed. Possible alternatives include larger thyratrons, hollow cathode devices (BLT, pseudosparks, etc.), crossatrons, tacitrons, and even advanced solid-state devices.

Stacked circuit alternatives are circuits that consist of discrete circuit elements (capacitors, inductors, etc.) and are arranged such that no set of components is subjected to the combined effects of all other components. Marx banks are an example of one type of stacked circuit. Low voltage capacitors are combined to generate high voltages. Such stacked circuits allow the use of low to medium technology components for a high technology application. Darlington circuits and switched capacitor circuits are examples of stacked lines.

Another alternative to magnetic pulse compressor is to use a fraction turn transformer to combine multiple circuits. Fractional-turn transformers are made similar to induction accelerators except that the e-beam is replaced by a metal conductor. The outputs of many low voltage circuits can be combined in a fractical-turn transformer (one circuit per induction stage) to generate very high voltages. Because of the design of a fractional turn transformer, leakage inductance can be on the order of picohenries, giving very good coupling between the multiple circuits and the load.

Finally, stacked lines can be extended into distributed component circuits and become cumulative wave circuits. Cumulative wave circuits use transmission lines to combine the electrical waves from multiple sources into one wave. These circuits use the time delay features of transmission lines to isolate the load from the sources. Examples of cumulative wave devices include stacked transmission line circuits and spiral lines.

Future Directions for Research

Additional work should be pursued in advanced switching, new circuit topologies, and new materials. Magnetic pulse compressors are used to make up for switching limitations in power conditioner technology. Advanced switches can replace magnetic pulse compressor and result in a significant improvement in the overall system performance and characteristics. New circuit topologies are needed to reduce the switching requirements, including alternate pulse-forming and network-generation techniques, fault isolation circuitry for stacked systems, and electric pulse compression techniques (as opposed to MPC techniques). Finally, new materials are needed to pave the way to new device technology and use. New materials are needed for switches, capacitors, nonlinear components, and basic high voltage insulation.

Summary

The power conditioning working group identified and addressed three critical issues associated with power conditioner technology for magnetic pulse compressor: voltage regulation, power conditioner components, and magnetic pulse compressors as a load. These issues were identified, their effects were surveyed, sources of problems were discussed, technical approaches were suggested, and, finally, possible research directions were defined.

References

1. P. G. Simpson, *Induction Heating, Coil and System Design*, (New York, Toronto, London; McGraw-Hill Book Company Inc., 1960).
2. "TOCCO-High Frequency Motor Generators," Catalog published by Ohio Crankshaft Co.
3. Personal Communication with Dennis Pavlik, 501-3E21, Westinghouse Sciences Technology Center, Pittsburgh, PA 15235.
4. W. F. Weldon, H. H. Woodson, M. D. Driga, U.S. Patent 4,200,831, April 29, 1980.
5. B. M. Carder, B. T. Merritt, and W. L. Gagnon (LLNL), W. L. Bird, W. F. Weldon, and R. C. Zowarka, "Driving Parallel Flashlamps with a Compensated Pulsed Alternator," presented at the *14th Pulsed Power Modulation Symposium*, Orlando, FL, June 6, 1980.
6. C. A. Morgan, W. L. Bird, and W. F. Weldon, "A 10 MJ Active Rotary Flux Compressor for Driving Xenon Flashlamps," presented at the *4th IEEE International Pulsed Power Conference*, Albuquerque, NM, June 6–8, 1983.
7. W. F. Weldon, W. L. Bird, M. D. Driga, K. M. Tolk, H. H. Woodson, and H. G. Rylander, "Fundamental Limitations and Design Considerations for Compensated Pulsed Alternators," *Proceedings of the 2nd IEEE Pulsed Power Conference*, June 12–14, 1979, Lubbock, TX.
8. M. L. Spann, S. B. Pratap, M. D. Werst, W. A. Walls, and W. G. Fulcher, "Compulsator Research at the University of Texas at Austin—an Overview," *IEEE Transactions on Magnetics*, **25**(1), Jan. 1989, pp. 529–537.
9. S. B. Pratap, M. L. Spann, and W. A. Walls, "Air-Core Compensated Pulsed Alternators," presented at the *7th IEEE Pulsed Power Conference*, Monterey, CA, June 11–14, 1989.
10. M. L. Spann, W. L. Bird, W. F. Weldon, and H. H. Woodson, "The Design, Assembly, and Testing of an Active Rotary Flux Compressor," presented at the *3rd IEEE International Pulsed Power Conference*, Albuquerque, NM, June 1–3, 1981.
11. S. B. Pratap, W. L. Bird, G. L. Godwin, and W. F. Weldon, "A Compulsator Driven Rapid-Fire EM Gun," presented at the *2nd IEEE Symposium on Electromagnetic Launch Technology*, Boston, MA, October 11–14, 1983.
12. A. R. Donaldson, J. C. Cron, R. R. Hanselman, "The Second Generation SLAC Modulator," Conference Record of the *IEEE 17th Power Modulator Symposium*, 1986, p. 230.
13. C. McDuff, K. Rust, H. Menown, C. Neale, "Evaluation of Bi-directionally Conducting Thyratrons for Pulsed Excimer Lasers," Conference Record of the *IEEE 16th Power Modulator Symposium*, 1984, p. 288.
14. H. Menown, C. A. Pirrie, N. S. Nicholls, "Advanced Thyratrons as Switches for the Nineties," Conference Record of the *17th IEEE Power Modulator Symposium*, 1986, p. 69.
15. Typical conditions of operation in commercial and scientific copper vapor lasers.
16. R. B. Molyneux-Berry, "Double-ended Thyratrons in High Power Burst Mode Pulse Modulator Applications," Conference Record of the *13th IEEE Power Modulator Symposium*, 1978, p. 44.
17. J. McGowan, J. Creedon, "High Average Current—High Repetition Thyratron Testing at ETDL," Conference Record of the *18th IEEE Power Modulator Symposium*, 1988, p. 156.
18. T. Cavazos, to be published, 1990.
19. G. McDuff, T. R. Burkes, W. M. Portnoy, "Switching Devices for High Average Power Magnetic Pulse Compressors," to be published.
20. K. Rust, "1 MV Repetition-Rated Modulator," Conference Record of the *18th IEEE Power Modulator Symposium*, 1988, p. 52.
21. A. Faltens, et. al., "High Repetition Rate Burst-Mode Spark Gap," *13th Pulse Power Symposium*, Buffalo, NY, 1978, p. 98. (UCRL-80934).

22. L. Reginato, et. al., "Advanced Test Accelerator (ATA) Pulse Power Technology Development," *1981 Particle Accelerator Conference.* (UCRL-85037), Lawrence Livermore National Laboratory, Livermore, CA.
23. Hutcherson, Moran and Ball, "Triggered Spark Gap Recovery," *6th IEEE Pulsed Power Conference,* Arlington, VA 1987.
24. Adapted from T. Van de Wouw and J. Holdsworth, *Proceedings of the PCI Conference,* June 1989.
25. W. T. White, III, C. G. Dease, and G. H. Khanaka, "Analysis of the Performance of the Gallium Arsenide Photoavalanche Switches," in *Proceedings of 7th IEEE Pulsed Power Conference,* B. H. Bernstein and J. P. Shannon, Ed., New York, IEEEE, 1989, pp. 422–425.
26. H. Mehta, "Power electronics," *Electric Power Research Inst. J.,* **13**(8), pp. 44–47, 1988.
27. G. M. Loubriel, F. J. Zutavern, J. P. Hjalmarson, and M. W. O'Malley, "Closing Photoconductive and Semiconductor Switches," in *Proceedings of 7th IEEE Pulsed Power Conference,* B. H. Bernstein and J. P. Shannon, Ed., New York, IEEE, 1989, pp. 365–367.
28. F. J. Zutavern, G. M. Loubriel, B. B. McKenzie, W. M. O'Malley, R. A. Hamil, L. P. Schanwald, and H. P. Hjalmarson, "Photoconductive Semiconductor Switch (PCSS) Recovery," in *Proceedings of 7th IEEE Pulsed Power Conference,* B. H. Bernstein and J. P. Shannon, Ed., New York, IEEE, 1989, pp. 412–417.
29. G. M. Loubriel, M. W. O'Malley, F. J. Zutavern, B. B. McKenzie, W. R. Conley, and H. P. Hjalmarson, "High Current Photoconductive Semiconductor Switches," in *Conference Record of 18th Power Modulator Symposium,* New York, IEEE, 1988, pp. 312–317.
30. M. D. Pocha, R. L. Druce, M. J. Wilson, W. W. Hofer, "Avalanche Photoconductive Switching," in *Proceedings of 7th IEEE Pulsed Power Conference,* B. H. Bernstein and J. P. Shannon, Ed., New York, IEEE, 1989, pp. 866–868.
31. R. L. Druce, M. D. Pocha, K. L. Griffin, W. W. Hofer, "Subnanosecond Linear GaAS Photoconductive Switching," in *Proceedings of 7th IEEE Pulsed Power Conference,* B. H. Bernstein and J. P. Shannon, Ed., New York, IEEE, 1989, pp. 882–886.
32. K. H. Schoenbach, V. K. Lakdawala, D. C. Stoudt, T. F. Smith, and R. P. Brinkmann, "Electron-Beam-Controlled High-Power Semiconductor Switches," *IEEE Trans. Electron Devices,* **36**, pp. 1793–1802, 1989.
33. R. M. Coeller, M. C. Thompson, R. B. Hammond, R. A. Lemons, W. Nunnally, "Investigation of Cryogenic Photoconductive Power Switches," in *Proceedings of 6th IEEE Pulsed Power Conference,* P. J. Turchi and B. H. Bernstein, Ed., New York, IEEE, 1987, pp. 157–160.
34. M. S. Mazzola, K. H. Schoenbach, V. K. Lakdawala, R. Germer, G. M. Loubriel, and F. J. Zutavern, "GaAS Photoconductive Closing Switches with High Dark Resistance and Microsecond Conductivity Decay," *Appl. Phys. Lett.,* **54**, pp. 742–744, 1989.
35. M. S. Mazzola, K. H. Schoenbach, V. K. Lakdawala, and S. T. Ko, "Investigation of a Photoconductive Closing and Opening Bulk GaAS Semconductor Switch," in *Proceeding of 7th IEEE Pulsed Power Conference,* B. H. Bernstein and J. P. Shannon, Ed., New York, IEEE, 1989, pp. 418–421.
36. K. H. Schoenbach, V. K. Lakdawala, R. Germer, and S. T. Ko, "An Optically Controlled Closing and Opening Semiconductor Switch," *J. Appl. Phys. Lett.,* **63**, pp. 2460–2463, 1988.
37. M. S. Mazzola, K. H. Schoenbach, V. K. Lakdawala, and S. T. Ko, "Nanosecond Optical Quenching of Photoconductivity in a Bulk GaAS Switch," *J. Appl. Phys. Lett.,* **55**, pp. 2102–2104, 1989.

38. F. J. Zutavern, G. M. Loubriel, and M. W. O'Malley, "Recent Developments in Opening Photoconductive Semiconductor Switches," in *Proceedings of 6th IEEE Pulsed Power Conference*, P. J. Turchi and B. H. Bernstein, Ed., New York, IEEE, 1987, pp. 577–580.
39. G. McDuff, "Capacitors for Repetitively Pulsed Lasers," to be published.
40. K. Rust and G. McDuff, "Calorimetric Measurements of the Equivalent Series Resistance of Low-Loss, High-Repetition Rate Pulse Discharge Capacitors," *16th Power Modulator Symposium*, Seattle, WA, 1986.

Core Cooling and Dielectrics Group

Kim W. Reed, Chairman
Henry C. Harjes, Cochairman

Working Group Members

R. Adler
S. Bahowick
L. Gordon
H. C. Harjes
T. Morris
D. Pavlik
K. W. Reed
G. J. Rohwein
D. J. Sharp
G. Shneyenson
M. Thevenot

Introduction

For magnetic switches to be a viable technology for high average power pulse compression systems, they must be very efficient, very reliable, and have long lifetimes. The design of magnetic switches that meet these criteria will require significant progress in at least two technical areas: thermal management within the switch (i.e., core cooling) and electrical insulation within the switch (i.e., dielectrics). The charter of the Core Cooling and Dielectrics Group was to discuss these two areas and identify what research and development (R&D) might have the greatest impact in improving magnetic switch technology. Of the two basic types of switch cores (bulk ferrites and laminate structures) most of the discussion in the group centered on laminate structures. This focus was primarily due to a lack of group experience with ferrite cores in magnetic switches and not because ferrites were considered inherently inferior.

Ferrites are generally the best magnetic materials for very fast pulse applications (time to saturation < 50 ns) due to their lower high frequency losses. Conversely, in applications where the time to saturation is much > 50 ns, ferromagnetic materials are typically used because they have larger saturation inductions. At the electric field stresses of interest in most magnetic switch applications, insulation within ferrites does not seem to be an issue. A NiZn ferrite core, for example, can sustain bulk stresses of up to 200 kV/cm. It, thus, seemed reasonable to omit ferrites from discussions about dielectrics. In the core cooling discussions, specific ferrite core geometries were again not considered. However, many of the principles and techniques discussed can be applied to ferrite cores.

Laminate structures include all cores constructed from alternating layers of a metallic sheet or ribbon magnetic material and some type of insulating material in either a stacked or spiral wound geometry. In laminate cores, the most common fault mode is dielectric breakdown of the interlamina insulation. Reliability and lifetime requirements thus favor greater insulation thickness to reduce electric field stress in the insulation. However, since insulation reduces packing factor (PF = ratio of magnetic material cross-sectional area to total core cross-sectional area), the requirement for high efficiency favors minimum insulation thickness. Similarly, cooling schemes generally call for the insertion of cooling channels in the core to maintain reasonable operating temperatures. At a given thermal generation rate, lower operating temperatures and higher reliability is generally achieved by increasing the number of channels. This, however, reduces packing factor and efficiency. Much of the group's discussion dealt with how to best compromise these conflicting requirements;

that is, how to achieve desired reliability and lifetime performance with minimal insulation and cooling channels.

G. J. Rohwein represented the Core and Dielectrics Group in the opening plenary session with a presentation entitled "Insulation of Dense Spiral Windings." In this presentation he pointed out that polymer film and liquid insulation materials used in spiral-wound magnetic switch cores are subject to many of the life-limiting and breakdown mechanisms associated with capacitors and spiral strip transformers. Because of these similarities, one can gain considerable insight into the performance of magnetic core insulation under various service conditions be reviewing the design practices and problems associated with capacitors and spiral transformers under different operating conditions. One major similarity between all spiral-wound, high-voltage devices is the fact that maximum local stresses occur along the edges of the ribbon foils or strips regardless of the actual electric field distribution. Therefore, control of edge stresses through techniques of margin grading and edge quality control are important considerations in design and manufacture. Service conditions, also a dominant factor, have shown in separate tests on capacitors and transformers that the safe operating stress for extended-life ($\geq 10^7$ shots) high rep-rate service is approximately a factor of five less than that for limited life (~10,000 shot), single shot service. Although similar data for spiral-wound magnetic cores presently does not exist, there is a strong possibility that they will follow the same general rule because polymer-laminate, high-voltage structures are affected primarily by simple over stress in a single shot (limited life) mode, but gradual material degradation from corona, heat and high-frequency effects at high pulse repetition rates (extended life). A fourth, and less predictable damage mechanism associated with rep-rated service that occurs in liquid/film- insulated windings is charge injection, which can cause unexpected catastrophic failure of a winding from localized charge accumulation on insulating film surfaces. Techniques for controlling charge injection effects are under development but, at present, are not totally effective. Basically, they involve controlling the surface resistivity of the polymer film and the volume resistivity of the liquid impregnant to avoid charge build-up.

Future improvements in insulating materials, particularly corona resistance, will be required to increase the present limits on energy density of capacitors and transformers and the packing fraction of magnetic switch cores. However, improved dielectric materials may be slow in coming unless there is sufficient economic incentive for manufacturers to improve present product lines. Since the pulse power industry is much smaller than the commercial power industry, the necessary incentives will undoubtedly be coupled to power industry requirements.

Based on the expertise available within the group, three subgroups were formed to focus on the following subtopics:

- Core Cooling Techniques
  Headed by: Sally Bahowick, LLNL.
- Dielectrics and Impregnants
  Headed by: Don Sharp, SNL.
- Ac Power Industry Experience
  Headed by: Dennis Pavlik, Westinghouse.

Ac Power Industry Experience was added to the agenda to explore how the magnetic switch community might benefit from the many years of experience which that industry has in building efficient, reliable, long life, high average power electrical devices characterized by similar insulation and cooling problems. Although a knowledge of the power industries' experience may not yield direct solutions to magnetic switch problems, it should help to identify potential problem areas and point the way to finding solutions.

To give the subgroup discussions a small degree of structure, each subgroup attempted to accomplish the following objectives:

- Establish what the state-of-the-art is.
- Identify the key problems and issues.
- Determine what research needs to be done.

This report is a summary of the discussions which took place in each of the subgroups. It is organized into major sections that correspond to the three subtopics with subsections for each of the three objectives.

Core Cooling Techniques

State of the Art

For magnetic switches to be a viable technology for high power pulse compression applications, they must operate with efficiencies in the high 90%'s. Present trends are toward multi-megawatt, continuously operating systems for which even a small percentage of the total power deposited as heat in the switch cores can represent tens of watts per cc of volumetric thermal generation. The ability to remove this internally generated heat is therefore a pivotal factor in determining the usefulness of magnetic switches for high power pulse compression.

Core losses due to both eddy currents and magnetic domain wall movement are determined from published data that presents loss as a function of time to saturation, T_S.[1–3] Actual losses depend on the voltage waveform applied to the switch, thickness of the METGLAS ribbon and temperature. The data published in the references is for a constant voltage pulse applied to the excitation windings (constant dB/dt), using a 0.0022-cm thick ribbon at room temperature. The domain configuration that applies depends on the magnetization rate, dB/dt. In turn, the way in which losses vary with the applied voltage waveform is a function of whether the saturation wave or bar domain configuration applies. In a magnetically switched pulse compression system, the usual voltage waveform is a raised cosine:

$$V_{in}(t) = V_o(1 - \cos\{\pi t/T_s\}). \qquad (1)$$

With 2605CO METGLAS, the loss for a raised cosine input voltage is greater than that compiled for a square input voltage pulse by the following factors:

dB/dt	Loss Raised Cosine/Loss Square Pulse
< 1 Tesla/μs	1.2 x
> 1 Tesla/μs	1.8 x

For the purpose of parametric studies with $T_S \leq 10$ μs, the published data can be correlated by:

Loss per pulse[J/m^3] =

$$K \cdot \delta B_S[\text{Tesla}]^a / T_S[\mu s]^b \qquad (2)$$

where, δB_S is the flux density swing, and

	METGLAS type		
Constant	2605CO	2605S-3A	2605S-2
K	228	140	150
a	1.53	1.56	1.75
b	0.827	0.615	0.824

Thermal and fluid dynamic models for simple cooling channels are available in the literature. Data are tabulated in the form of correlations for the Nusselt Number, Nu, in terms of the Rayleigh Number, Ra, for free convection and the Reynolds Number, Re, for forced convection—for a variety of cooling channel configurations.[4–7] These correlations, however, are approximations and are sensitive to the specific experimental conditions, such as the presence and amounts of small quantities of dissolved gas in the coolant.[8] Thus, in some cases it is necessary to experimentally verify channel wall temperatures as a function of heat flux at the walls under conditions replicating those expected in the actual device. For example, channel sizes and spacings in magnetic core designs for the RHEPP project[9] will be based on wall temperatures measured in free and forced convection channel experiments conducted in fluids like Shell Diala A/AX transformer oil with various uniform heat fluxes on the walls of the channels. In the case of a core

using free convection cooling, the maximum core temperature, half way between the channels in the build, is given by:

$$T_{max} = T_{wall}\{q''\} + \frac{q'''\delta b^2}{8\, k_{\uparrow}} \qquad (3)$$

where

q'' = wall heat flux
q''' = volumetric heat generation rate
T_{wall} = maximum wall temperature
δb = build height between channels
$k_{\uparrow}$ = thermal conductivity normal to ribbon
$\{\ \}$ = "a function of"

Design curves are generated by plotting T_{max} versus q''' for a given channel geometry with fixed values of δb. These curves are based on a fixed inlet temperature, with fluid continually being removed from the top of the reservoir, passed through a heat exchanger and returned on the bottom. The required cooling channel spacing is found on the curves by drawing a horizontal line across the plot at the maximum allowable core temperature and a vertical line at the applied thermal generation rate and interpolating the value of δb at the intersection. Bulk parameter values for this calculation are obtained from the following relations:

$$g''' = g'''METGLAS \cdot SF \qquad (4)$$

$$g'' = g''' \cdot \delta b \qquad (5)$$

$$k_{\uparrow} = \frac{t_1 + t_2 + t_3}{t_1/k_1 + t_2/k_2 + t_3/k_3} \qquad (6)$$

$$k_{\equiv} = \frac{k_1/A_1 + k_2/A_2 + k_3/A_3}{A_1 + A_2 + A_3} \qquad (7)$$

where, the subscript, i, indicates the material region and

t_i = thickness of region, i
A_i = cross sectional area of region, i
$k_{\uparrow}$ = thermal conductivity normal to ribbon
$k_{\equiv}$ = thermal conductivity in plane of winding
SF = core stacking factor

As an example, the multiturn second stage RHEPP switch described in Ref. 10 has a core bulk thermal generation rate of 0.025 W/cc. By holding the oil reservoir at 37°C via a passive outdoor heat exchanger, the core can be cooled by inserting 0.5-cm wide free convection channels, spaced radially in the build at 5-cm intervals. This would hold the maximum core temperature below 100°C at steady state. The electrical windings of this switch consist of wide copper ribbon and polycarbonate film which is wound onto the core in a tape wound geometry to form a laminate structure similar to that of the core. The volumetric thermal generation rate in the windings is 0.014 W/cc and at that level 0.5-cm cooling channels must be located in the build at intervals of no more than about 8 cm to limit T_{max} to 100°C. Since the total build is only 3.8 cm, cooling channels are not required in the electrical windings of this switch. Had it been necessary to put cooling channels in both the magnetic and electrical builds of the switch, the need for buoyancy driven convection would have required that both the electrical and core windings be tilted 45 degrees off vertical—which would reduce the cooling film coefficient in the channels by only about 10%.[11] In applications like this, free convection cooling is useful for volumetric thermal generation rates up to about 0.5 W/cc. The maximum allowable build between channels at this heat rate would be about 1.25 cm with a channel height of 0.16 cm.

A typical high power magnetic switch is represented by the MAG-1-D output switch at Lawrence Livermore National Laboratory (LLNL), Figure 1. This switch is impregnated with and immersed in Freon-113. A single turn coaxial geometry is used for minimum saturated inductance, L_S.

Table 1 summarizes the switch dimensions and operational parameters.

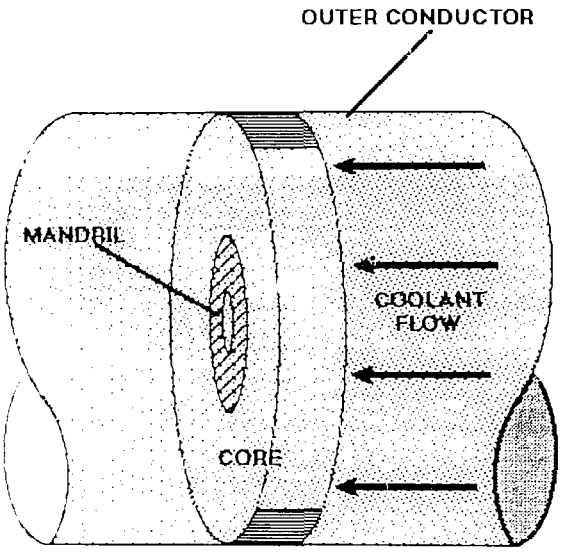

Figure 1. Representation of the MAG-1-D output magnetic switch core in its coaxial housing.

Table 1. MAG-1-D output magnetic switch magnetic core data.

METGLAS type	=	2605CO
METGLAS thickness	=	0.00152 cm
Insulator type	=	Mylar
Insulator thickness	=	0.00064 cm
Packing factor (P.F.)	=	0.62
Number of turns (NL)	=	4687
Core diameter	=	38.1 cm
Mandril diameter	=	22.9 cm
Margin width	=	0.22 cm
Loss per pulse	=	85 joules/pulse
Pulses per second	=	5000 pps
Mode of operation	=	50 pulse burst, >50 Hz average
Time to saturation (T_S)	=	235 ns
Bulk thermal Generation rate	=	16 W/cc
Freon layer thickness	=	0.00038 cm
$k_{\uparrow}$	=	0.0017 W/cm-°C
$k_{=}$	=	0.0457 W/cm-°C
$k_{\uparrow margin}$	=	0.00075 W/cm-°C
$k_{=margin}$	=	0.00084 W/cm-°C

In the MAG-1-D output switch, forced convection cooling channels must be used in order to keep the temperature rise in the coolant from becoming too large as it traverses the channel. An acceptable temperature rise in the channel is taken to be about 22°C. The same relation can be used here to calculate maximum core temperature with forced convection as was used earlier for free convection, with the following relation substituted for T_{wall}:

$$T_{wall} = T_{in} + \frac{q'''\delta b\, L}{2\,\phi v\, c_p H} + \frac{q'''\delta b}{2\,h} \qquad (8)$$

where

T_{in} = coolant inlet temperature
L = cooling channel length
ϕ = coolant density
v = coolant velocity in channel
c_p = coolant specific heat
H = channel height
h = convective film coefficient on channel wall

In this calculation, the film coefficient that applies to fully developed laminar flow between isoflux plates is used:[12]

$$h = \frac{Nu \cdot k}{H} \qquad (9)$$

where

k = coolant thermal conductivity
Nu = Nusselt Number (= 4.36 laminar, isoflux).

This simple analysis predicts that to maintain a maximum core temperature between channels of 100°C with a coolant temperature rise of 22°C (Freon would have to be pressurized to prevent boiling) would require 0.025-cm high channels to be placed every 0.19 cm in the magnetic build. The usual energy balance:

$$Q = c_p \cdot \frac{dm}{dt} \cdot (T_o - T_i) \qquad (10)$$

where

Q = total heat power being cooled
c_p = fluid specific heat
dm/dt = mass flow rate
T_o = channel outlet temperature
T_i = channel inlet temperature

yields a required coolant flow rate of 7 liters/sec, resulting in a pressure drop across the core of 0.49 psi, based on the following relation for an annular channel:[13]

$$\delta P = \frac{12 f L \mu}{H^3} \qquad (11)$$

where

δP = pressure drop across core
L = channel length
μ = coolant dynamic viscosity
f = volumetric flow rate/unit width
H = channel height (plate-to-plate)

Other relations for forced convection pressure drops in ducts of various cross sections are given in Ref. 6.

Problem Areas

Magnetic switches must be well insulated electrically, making them intrinsically well insulated thermally. In a wound magnetic switch, the serial arrangement of high thermal conductivity METGLAS with poor thermal conductivity insulation (e.g., Mylar-Type C, Polycarbonate, Kapton) and liquid dielectric (e.g., transformer oil, Freon, Fluorinert), yields a composite thermal conductivity normal to the plane of the winding ($k_\perp \simeq 0.003$ W/cm-°K) that is typically more than an order of magnitude lower than the thermal conductivity in the plane of the winding ($k_\equiv \simeq 0.05$ W/cm-°K), where the highly conducting METGLAS is in parallel with the poorly conducting dielectric. It is very important to completely impregnate both the core and electrical windings with dielectric fluid, since $k_\perp$ is about four times smaller ($k_\perp \simeq 0.00063$ W/cm-°K) if there is air in the windings instead of fluid. The margin consists of alternate layers of poorly conducting dielectric sheet and poorly conducting dielectric liquid, resulting in a nearly isotropic thermal conductivity of about 0.0013 W/cm-°K. Thus, even though heat can be readily conducted along the METGLAS to the core margins, it is prevented from rapidly escaping by the highly insulating margins. In multiturn magnetic switches with tape-wound type electrical windings, the windings have essentially the same thermal properties as the core, with good thermal conduction in the plane of the winding, poor thermal conduction normal to the winding and a highly insulating margin. The coaxial electrical winding of a high speed switch, however, does not pose a cooling problem since it has a high surface to volume ratio and good thermal conductivity in all directions.

In switches using free convection cooling, the core must be tilted requiring that the lower margin have a structural support to prevent the windings from telescoping. This core support must be designed so as not to cause surface flashover on the margin that it is against. Due to limitations on standard METGLAS widths, cores are often wound with several tandem subcores on the same mandril. The gaps between these subcores in a compound core result from practical limitations in the winding process. Tilting such a switch could be a problem since it would be difficult to prevent or control the collapse of the gaps between the subcores. The gaps between subcores have the same thermal characteristics as the margins and seriously impede axial heat flow. Thus, it is generally preferable to wind cores from a single ribbon, unless radial coolant flow is provided between the subcores.

In free convection channels, provisions must be made to maintain the coolant bath at a constant temperature. Rep-rated pulse compression systems of current interest must

continuously process several to tens of megawatts (e.g., RHEPP is 5 MW). If the compressor is operating at 95% efficiency, several hundred kilowatts of heat must be removed. The cost per kilowatt of cooling capacity for evaporative cooling is about $35/kW, while refrigeration cooling costs about $100/kW. So for economic reasons, a passive heat removal system (cooling tower) is preferable. For effective operation, evaporative heat removal systems typically operate with the hot side (switch bath) on the order of ≥ 11°C above the temperature of the medium that the heat is being exhausted to. This limits how cool the switch bath can be, which in turn, limits how far apart the cooling channels can be placed in the switches being cooled.

In all switches, it is important for the ratio of the saturated inductance (determines the minimum switching time) to the unsaturated inductance (determines the maximum allowable charging time) to be small. To accomplish this, the ratio of the core space occupied by cooling channels to the space occupied by magnetic material must be small (1/5 or less). Thus, during design calculations, the channel height should be upper bounded by a fixed fraction of the build between channels. At thermal generation rates for which free convection channels are adequate, the allowable build spacings between channels are generally large (> 1 cm) allowing channel heights to be large (0.5 cm > H > 0.1 cm). In this range of channel heights there is relatively little dependance of cooling performance on channel height, so this parameter can be selected on the basis of convenience.

At generation rates for which forced convection is necessary, the build between channels must be small (0.1 cm > H) corresponding to even smaller channel heights. Pressure drops across the core at the required flow rates are appreciable, making low viscosity coolants important. The MAG-1-D output switch is a good example of this regime and uses freon-113 as a low viscosity coolant. Axial loading impressed by the coolant requires that the core be axially supported to prevent telescoping. MAG-1-D switch with a pressure drop of only 0.49 psi across the core must withstand nearly 90 pounds of lateral force.

Areas That Need Research

Good dielectrics that are also good coolants must be identified. Factors that should be considered include:

- Price.
- Dielectric properties.
- Thermal properties.
- Material compatibility.
- Environmental and safety compatibility.

Key coolant thermal properties and desirable magnitudes are summarized in Table 2 for both free and forced convection. The question mark under free convection thermal conductivity indicates that a higher value for this parameter yields a higher convective film coefficient at the channel wall which is desirable. Conversely, a higher thermal conductivity makes the rise in coolant temperature in the channel greater. Dc volumetric resistivity should be high because it sets an upper bound on pulse length, above which losses become too large. In terms of dielectric strength and loss, the liquid dielectric is usually the weak link in a solid/liquid dielectric system. Therefore, a high ε_r is desirable because it concentrates the fields in the solid dielectric. On the other hand, the dc volumetric resistivity and loss tangents for high ε_r dielectrics tend to deteriorate more quickly, making periodic replenishment necessary. The optimum trade-off is to use low ε_r coolants in slower switches where field stresses are low and high ε_r coolants in fast switches where higher stresses make increased maintenance acceptable.

Table 2. Desirable coolant properties.

Property	Free	Forced
Density	↑High	↑High
Specific heat	↑High	↑High
Coefficient of thermal expansion	High	NA
Dynamic viscosity	NA	↓Low
boiling point	$>T_{max}$	$>T_{max}$
Thermal conductivity	?	↑High
Dc volumetric resistivity	↑High	↑High
Loss tangent	↓Low	↓Low
Dielectric strength	↑High	↑High
Dielectric constant	↑↓	↑↓

In low-power switches, cooling channels can be constructed by simply winding transverse support strips (e.g., 0.3 cm × 0.3 cm × total winding width, polycarbonate) into the core spool, spaced closely enough along the length of the ribbon to prevent the build from sagging into the channel (e.g., every 2–3 cm). Conversely, for high power switches where the channels may be only 0.025 cm high; channel designs, support materials and winding techniques must be developed. In addition to being as small as possible, these channel structures must provide good build support, good heat exchange with the wall and low impedance to flow. A variety of complex structures are being considered for this purpose at LLNL.[14] Some of these structures would create complex flow patterns, requiring that good models be developed for pressure drop as a function of flow rate and flow rate required as a function of thermal generation rate. A determination must be made of whether it is correct to model the straight through channels proposed in the LLNL work as having fully developed laminar flow throughout, since they are so small (H ≈ 0.025 cm). The concern is that tiny imperfections in the wall may dominate flow and heat transfer behavior.

For open geometry multiturn switches the effects of core saturation is another area that needs further attention. When such a switch saturates, large amounts of magnetic flux sweep through the conductors in and around the core. The resulting eddy currents introduce loss that adds to the undesirable heating of the core and windings, and reduces the overall switch efficiency. Ways to predict and model these saturation induced losses and heating effects must be developed and included in the electrical and thermal models of the switch. If the electrical model indicates that the saturation induced losses lower efficiency to an unacceptable level, then ways must be devised to reduce interaction of the saturation flux with conductors. If these losses result in unacceptable localized heating, then the cooling design (density of channels, channel design, flow regime, etc.) must be modified accordingly.

A related effect that occurs in multiturn switches with tape wound electrical windings is nonuniform current distribution across the width of the windings. When such a switch saturates and magnetic flux is no longer confined to the core, the flux interacts with current in the windings and the current distribution becomes peaked at the edges of the windings. More current flows in the imaginary filaments near the edges of the windings because they are less coupled to adjacent filaments than are filaments in the center of the winding. The electrical windings should be wound as tightly as possible, as this increases coupling among the turns and reduces current peaking on the edges of the windings. Power per unit volume varies as the square of current per unit width in the plate conductor, so that the local thermal generation rate will quadruple if local current per unit width peaks by a factor of two (Figure 2a). If the actual current is represented by uniform distributions extending a quarter of the plate width in from the edges of the plate with amplitudes twice the mean current

(Figure 2b), the overall circuit loss will double. Ways to predict this nonuniform current distribution must be either developed or gathered from existing sources,[15] so that nonuniform thermal generation can be included in the electrical and thermal models.

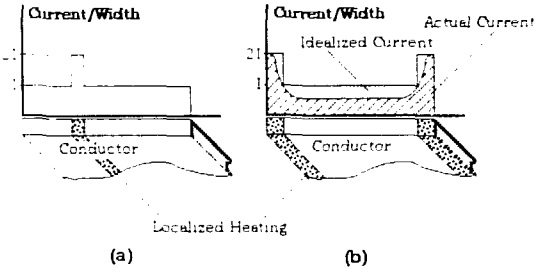

Figure 2. (a) Effect of local current peaking in a plate conductor, (b) idealized current distribution compared to actual distribution.

Very little data is currently available for METGLAS properties as a function of temperature. These switches operate over a temperature range of 25° to 120°C, so it is essential to obtain data for METGLAS loss, B_{sat}, B_{rem} and μ_r as a function of temperature in this range.

Recommended Experiments

Experiments have been conducted at Sandia in which the heating that occurs during actual switch operation is experimentally simulated by passing a dc current through the magnetic ribbon of the core. Thermocouples are placed in strategic locations throughout the core. These experiments have proven to be of great help in understanding the bulk properties and thermal behavior of magnetic switches at Sandia. Direct current is used to heat the METGLAS ribbon to avoid having to compensate for the effects caused by the large inductance of the core. The current evenly heats the experimental core, limiting this type of modeling to magnetic switch cores with uniform thermal generation. Uniform loss should be a good assumption since during each cycle of the applied pulse train all parts of a real core experience the same saturating magnetic wave, albeit at different times, and therefore, experience the same magnetization, magnetization rate, and resultant volumetric loss. An experiment of this type is recommended to characterize and evaluate the cooling channel structures (meshes, etc.) being developed at LLNL. The results from such an experiment should be widely used, as eventually all high power pulse compression systems will have to cool output stages with tens of watts per cc heat generation.

Very little data are currently available for METGLAS properties as a function of temperature. Since magnetic switches operate over a range of 25° to 120°C, it is essential to obtain complete data for loss, B_{sat}, B_{rem} and μ_r in this temperature range. All this information can be extracted from a measurement of the B-H loop as a function of temperature. The B-H loop can be generated by pulsing a set of windings on a test core and measuring the current in the pulsed winding and the voltage in a separate one-turn sampling winding:

$$B = \frac{1}{A_M}\int_0^t V_s\,dt \qquad (12)$$

$$H = \frac{N_E I_p}{d_M} \qquad (13)$$

where

A_M = the effective magnetic cross section
N_E = number of electrical windings
d_M = the effective magnetic path length
V_s = voltage induced in sampling winding
I_p = current in the pulsed winding.

The voltage sampling winding must be wound tightly and directly on the core. Voltage is monitored in this separate winding to prevent the I•R drops caused by

the high pulsed currents in the multiturn excitation winding from adding to the dI/dt contribution. The electrical windings and core should be configured so that the shape of the magnetic field does not change when the core saturates. For example, if multiple turn electrical windings are required, the core should be a toroid completely covered by a closely wound, one layer solenoid wound directly on the core. Thus, whether the core is saturated or not, A_M can be taken as the cross sectional area of the solenoid and d_M can be taken as the mean length of the solenoid. If a single turn switch is required for this test, a coaxial configuration keeps the magnetic field shape fixed. The core should be heated to the desired temperature by passing a dc current through the METGLAS ribbon from which the core is wound. Since pulse shape and frequency effect both the loss and μ_r, the core should then be pulsed via the electrical windings with the exact pulse shape and duration for which data is required. Magnetic induction, B_m, as determined from the integral of voltage is plotted against magnetic field, H_m, as determined from the current.

While correlations for film coefficient in both free and forced convection channels are tabulated in the literature, these are approximations to data, that in turn is very dependant on the condition of the materials used, specific geometries, and the way in which the measurements are taken. *While this data is useful for ballpark* calculations, it is recommended that for final design purposes, simple resistively heated experiments be conducted using typical magnetic switch dielectrics that have been exposed to representative conditions and treatment, to verify the channel wall temperatures as a function of position and heat flux. In addition, geometries that more closely represent magnetic switch applications can be used. One recommended experimental setup consists of two parallel mounted plates of aluminum with an adjustable channel spacing in between (Figure 3). A uniformly distributed array of power resistors mounted on the back surface of each plate provides a calibrated source of heat flux into the channel. The backs of the plates and the resistors are completely covered with closed cell polyurethane foam insulation to force all of the heat generated by the resistors into the channel. Thermocouples are imbedded in holes bored into the back side of the aluminum plates to within 0.05 cm of the channel surface. A sufficient array of thermocouples is installed to measure temperature variations both along and transverse to the flow direction. In the free convection experiments, temperatures at the inlet and outlet of the channel should be measured in addition to those in the wall. The inlet end of the channel must be fitted with a manifold for the forced convection experiments, and coolant flow rate and pressure must be monitored in the inlet manifold.

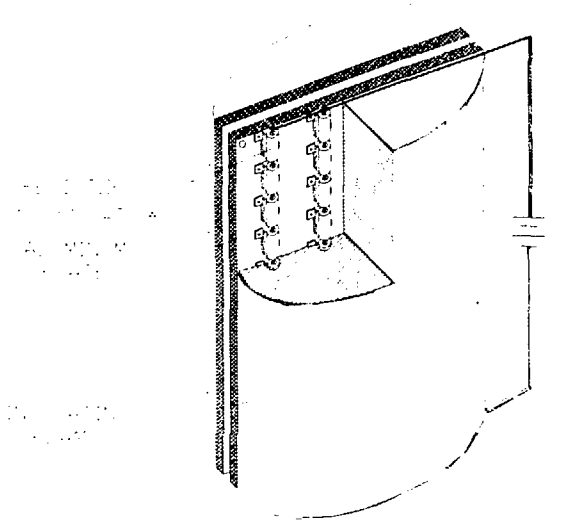

Figure 3. Experimental setup for measuring cooling channel performance.

Dielectrics and Impregnants

State of the Art

Insulation is required in the core of a magnetic switch to limit the eddy currents that are generated when an externally applied magnetic field begins to diffuse into an electrically conductive magnetic

material. Without insulation, a magnetic core would be rendered useless by the high losses and interior shielding that would result from the eddy currents. This phenomenon is described in more detail in the literature,[16-17] but, basically must be controlled by electrically segmenting the core, with insulation, to increase the surface area to volume ratio of the magnetic material. Since most magnetic material is manufactured in either thin sheet (for stampings) or thin ribbon form, magnetic cores are most often built as laminate structures (i.e., stackings of individually insulated stampings, Figure 4a, or spiral windings of ribbon with some type of insulation, Figure 4b). For such magnetic switches with the common raised cosine applied voltage, the eddy-current energy loss (W_e) and the peak inter-lamina electric field (E_L) can be estimated with the following equations from Ref. 16:

$$W_e = \frac{1.8\ \text{vol}\ (x_L B_{sat})^2}{\rho\ T_c} \qquad (14)$$

$$E_L = \frac{8\ B_{sat}\ w_L}{T_c}\ \frac{SF}{1 - SF} \qquad (15)$$

By using the formulations of Ref. 16, an expression for volume of magnetic material can be found which when substituted into the first equation yields an estimate of the ratio of eddy-current energy loss to total pulse energy:

$$\frac{W_e}{W} = \frac{1.1\ \mu_r \mu_o PC^2 x_L^2}{\rho\ SF\ T_c} \qquad (16)$$

where

V_{app} = applied voltage = $V_{peak}[1 - \cos(2\pi t/T_c)]/2$
t = time
T_c = period of the applied voltage waveform
vol = volume of magnetic material
x_L = thickness of magnetic lamination
B_{sat} = saturation magnetic flux density = $\Delta B/2$
ρ = electrical resistivity of the magnetic material
w_L = width of the laminations
SF = stacking factor = $N_L\ x_L$ / total core stacking height
N_L = number of laminations
W = total pulse energy = $0.5\ C\ V_{peak}^2$
C = stage capacitance
PC = stage pulse compression factor = $T_c/2\tau$
τ = stage discharge time = $\pi\sqrt{L_{sat}C/2}$
L_{sat} = saturated inductance of the switch = $N_E^2\ A/l_{mag}$
N_E = number of electrical coil turns,
A = cross sectional area of the coil
l_{mag} = average magnetic path length of the coil.

It is important to note that many simplifying assumptions, including the expression for the inductance of an ideal solenoid for L_{sat}, are used in the derivation of these equations; consequently, in practical situations values obtained with them must generally be considered estimates. The equations do, however, demonstrate how W_e and E_L tend to vary with material constants and design parameters. As the frequency of the applied voltage increases both W_e and E_L tend to increase which is why thermal management of dissipated energy and insulation dielectric strength are the two of the most critical issues in high speed magnetic switches. For a given magnetic material, losses are generally controlled by decreasing the magnetic lamination thickness as the switching frequency increases (Eq. 14). This approach is useful until the material's practical lower thickness limit is reached. At higher frequencies, higher losses must be tolerated and managed or another material must be selected (ferrites perhaps). Similarly, the interlamina electric field is generally controlled by increasing the insulation thickness (i.e., reducing SF, Eq. 15). This, nowever, lowers the switch's efficiency (Eq. 16), and forces a design compromise

between efficiency and the higher reliability/lifetime that would be achieved by operating at lower fields. Since electrical breakdown of the interlamina insulation is the principal failure mode of magnetic switches, one of the primary challenges in switch design is minimizing insulation thickness while maintaining high reliability.

In applications where interlaminar voltages are less than a few volts, there are several dielectric coatings available that have been used for insulation in conventional magnetic cores for years. These coatings (lacquers, MgO, SiO_2, etc.) can be applied in thin layers and packing factors in excess of 0.9 can easily be achieved. However, in most applications where magnetic switches are presently used, interlaminar voltages exceed a few volts. For these applications, coatings of sufficient quality and dielectric strength are not available so an insulation system similar to that used in high voltage capacitors is typically employed. This system, depicted in Figure 4b, consists of one or more layers of a thin dielectric film (Mylar, polycarbonate, Kapton, Kraft paper, etc.) and a dielectric fluid impregnant (Freon, Fluorinert, oil, etc.). The film typically extends an eighth to a quarter of an inch beyond the edges of the magnetic material to form margins on the sides of the core and the fluid is usually vacuum impregnated into the core.

In Table 3, data on some recent magnetic switches that have been designed in this manner are summarized. The switches of Table 3 are fairly representative of the state of the art in magnetic switch design. Each of the switches was designed for a high peak power application where the time to saturation was on the order of 100 ns. For such applications, METGLAS is the magnetic material of choice because it has the best high frequency characteristics (lowest losses) of the high saturation induction magnetic materials ($\Delta B > 3$). The cores are all fabricated in the same basic manner (i.e., wound on specialized winding machines like those used in constructing tape wound capacitors) and, in most cases, good performance has been demonstrated by the switches. However, all applications to date have been at relatively low average power levels. Consequently, it has not been necessary to put much effort into dealing with thermal management issues or optimizing switch designs to achieve maximum efficiency. In addition, the number of shots that have been accumulated is relatively small so the data base on long-term effects and lifetime is limited.

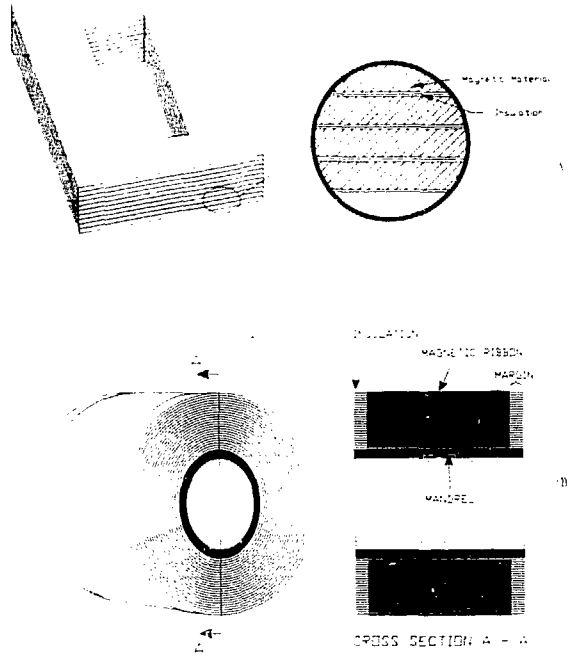

Figure 4. Typical laminate structures used in magnetic switches: (a) stacked stampings; (b) tape wound ribbon.

Table 3. Data on recent magnetic switches.

Switches Data	MAG-1-D/OUT LLNL	FEL/SW2 CESTA	COMET/MS2A SNL
Magnetic material	2605CO METGLAS	2605CO METGLAS	2605SC METGLAS
Insulation	Mylar, 2x6.4 μm	Mylar, 1x6 μm	Mylar, 2x6 μm
Impregnant	Freon-113	Freon	Fluorinert
Packing factor	0.62	0.65	0.6
~ Mass (kg)	50	200	800
~ E_L (kV/cm)	80	100	230
Energy/pulse (kJ)	0.45	0.7	115
Time to sat. (ns)	235	360	100
Risetime V_{out} (ns)	15	30	30
Contin. rep-rate demonstrated	>50 Hz	Single shot	Single shot
Avg. power out demonstrated	>20 kW	–	–
Shots accumulated approx.	10^8	10^2	Failed after 25
References	34–36	37	38–39

Problem Areas

The insulation scheme of Figure 4b is generally adequate in low average power applications, but it has some shortcomings. The required fabrication technique is a minor shortcoming because it is difficult and somewhat tricky to wind a core with multiple layers of material, especially if some of the layers are very thin (< 10 μm thick) dielectric films. Another minor shortcoming is that the packing factor of these types of cores is typically low (0.5–0.7). This is due in part to the margins, to the imperfect stacking of the multiple layers of material, and, in some cases, to excess insulation that is required to achieve necessary interlaminar holdoff voltages. The last item, when it occurs, is a major shortcoming of this insulation system and is prevalent in METGLAS cores.

Since METGLAS is a cast material, it has a significantly rougher surface quality than conventional rolled magnetic materials. The stacking factor of METGLAS on itself is typically between 0.75 and 0.85 and this is part of the reason that switches wound with METGLAS have poor packing factors. However, the most serious problem with the surface

morphology of METGLAS is the existence of relatively large surface protuberances called Pips. Pips typically occur at a rate of a few per linear foot of ribbon and are the result of craters that develop on the surface of the wheel on which METGLAS is cast. During the casting process, the craters erode and the mirror image Pips continue to grow in size through the process. Near the end of a run, Pips can be as tall as the ribbon is thick (i.e., ~ 25 μm). Consequently, when METGLAS and a thin (< 25 μm thick) dielectric film are wound together to form a magnetic switch, the film is degraded during the winding process and the resulting electric field strength of the film is significantly reduced.[18] The COMET switch (of Table 3) was designed to operate with an interlaminar electric field an order of magnitude below the expected breakdown level of its insulation (as demonstrated in wound capacitors). The most probable explanation of the low level failure of this switch is that the insulation was degraded during the winding process.[18] The other switches in Table 1 have achieved much longer lifetimes than the COMET switch but they were much smaller (i.e., they had much less insulation surface area or volume) and they operated at even lower fields. Since these switches were operated at fields far lower than the insulation should have been capable of withstanding, in effect, excess (i.e., thicker than necessary) insulation was used and low packing factors were the consequence.

Another major shortcoming of METGLAS switches is the impracticality of annealing the core after winding. To optimize the magnetic properties of a METGLAS core, it must be properly annealed to relieve residual winding stresses.[19] The best way to achieve this is to anneal the magnetic material in its final position (i.e., after the core is wound). Unfortunately, most dielectric films with the exception of the polyimides (Kapton) cannot endure the temperatures of the METGLAS anneal cycle. In the case of Kapton insulated cores, annealing can be done but the effect is useless because of the difference in thermal expansion rates between Kapton and METGLAS. When such a core returns to room temperature after annealing, the Kapton puts so much stress on the METGLAS that magnetic properties can be worse than they were before annealing.[20] METGLAS can be annealed prior to winding the core and for alloys with high anisotropy energy (2605CO) much of the benefit can be retained in the wound core. However, for the other alloys, the stresses that remain in the core after winding are sufficient to eliminate much of the benefit gained from preannealing.

In addition to the problems that have been observed in low average power switches, there is another class of problems that will probably only become important in high average power applications. In such applications, efficiency is much more important and in general lifetimes must be extended by several orders of magnitude up to 10^9 or 10^{10} pulses. Consequently, it is more important to optimize switch designs. Optimization usually requires that the insulation operate at the maximum electric field that allows lifetime requirements to be met. To satisfy this design criteria, knowledge is required in two areas: (1) what the local time dependent interlaminar voltages are in a switch and (2) how insulation lifetime varies with electric field stress. Information in the first area is definitely inadequate. Local interlaminar voltages have never been measured and detailed calculations have not been done (computer codes that adequately model the nonlinear behavior of the magnetic material are not available). At present, interlaminar voltages can only be crudely estimated by making the following assumptions: (1) the voltage is the same in all laminations and does not depend on the position of the lamination in the structure and (2) the voltage is simply related to and has the same time dependence as the waveform that is applied to the terminals of the switch. These assumptions may be reasonable while a switch is unsaturated and still in the relatively linear portion of the B-H curve, but, they do not seem

reasonable in the final phase of saturation when the switch is beginning to make the rapid transition from the open to the closed state. During this time, the voltage applied to the switch is typically at its peak and, consequently, interlaminar stresses are likely at their peaks. Without better information about interlaminar stresses during this critical time, optimal switch designs, which only use the necessary quantity of insulation in each lamination, may not be realizable.

Information in the second area, how insulation lifetime varies with electric field stress, E, is also inadequate. A review of data on conventional dielectric films indicates that in general:[21]

$$\text{Lifetime } \alpha 1/(E^n) \qquad (17)$$

where (n = 4 to 8) for most materials. In capacitors, transformers, and coils, the electric field stress levels that can be tolerated in single shot applications are considerably higher than those that can be tolerated in continuous or repetitive applications. For example, Table 4 lists typical operating stress levels for these devices in three modes of operation; single shot, burst, and continuous. In each case, the operating stress level is significantly derated as the duty on the device is increased. A similar relationship should be expected in magnetic switches and it needs to be determined.

Table 4. Approximate stress ranges for capacitors, transformers, and coils in three modes of bipolar operation.[22]

Device mode	Capacitors, kV/mil	Transformers, kV/mil	Coils, kV/mil
Single shot (to ~ 10,000 shots)	3-5	1-1.5	1-1.5
Burst rep-rate 6 (>10 shots, no heating)	1.5-3	0.5-1	0.5-1
Continuous rep-rate 7 (>10 shots to 20 yr. ac)	1-1.5	0.1-0.3	0.1-0.3

Although the local electric field is one of the most important factors effecting insulation lifetime, there are many others that must be considered. In Table 5, a number of factors that are known to effect insulation lifetime are listed. At their extremes, some of these factors (such as excessive electric field, excessive temperature, etc.) have dramatic effects on the insulation which are immediately apparent. However, in the regimes of interest in high average power switches, these factors generally effect the insulation in a subtle manner so that it takes a very long time for damage to become apparent. It is the long-term nature of these effects that makes them so difficult to quantify, and, consequently, the data base on them is limited. The situation is further complicated by the fact that in any practical switch many of the effects will be occurring simultaneously and there are likely complex interdependencies between effects. This group of effects, because they are not very well understood, will likely present a major obstacle in the development of high average power magnetic switches. In the following paragraph, some of these effects are discussed.

Table 5. Factors which effect breakdown.[22]

Electric stress
Total voltage
Pulse duration
Electrode material and surface conditions
Dielectric flaws
Fabrication and processing
Moisture
Impurities - chemical, particle
Voltage reversals, high frequency ringing
Corona and partial discharge
Pulse shape (dV/dt)
Pulse repetition rate
Temperature
Charge injection
Surface tracking
Electromechanical forces
Stress aging

Partial discharges and corona are electric field driven processes whose effects are well documented in the literature.[23–25] These processes slowly erode solid insulations and in some cases cause undesirable changes in the chemical composition of impregnants. Since the data needed to establish safe long-term operating levels in magnetic switches is generally unavailable, a reasonable approach is to use the limited data available on partial discharge and corona inception levels and design so that the peak expected electric field is below those levels. Test data on many materials demonstrate, that when this is done, insulation lifetime increases dramatically. However, in a large magnetic switch structure, a number of factors will have a significant, if not dominant, effect on what the inception levels are. These factors include such things as magnetic ribbon surface condition; presence of moisture, bubbles, or contaminates in the impregnant; and presence of flaws or voids in the dielectric. More data is needed on how inception levels vary with such factors so that they can be properly considered in switch designs and adequately controlled during the fabrication and operation of a switch. Insulation lifetime also will depend on temperature. Thermal aging has an adverse effect on mechanical properties and a relationship between breakdown strength and temperature has been observed in some materials.[26] The breakdown strength of 2-mil thick Mylar decreases by ~20% when the temperature increases from 25° to 125°C. The frequency content of the applied pulse can also effect insulation lifetime. In Ref. 26, data is presented which shows how the breakdown strength of some materials decreases significantly as the frequency of the applied waveform increases. Electromechanical forces (due to magnetostriction, Lorentz forces, etc.) may also impact lifetime by inducing stress aging or fatigue in switch materials. Interestingly, there is also some evidence that suggests pulse repetition rate may effect lifetime. In Ref. 27, the lifetime of capacitors was observed to decrease by more than an order of magnitude when the pulse repetition rate was increased from 250–1000 Hz.

Another shortcoming of the present insulation system that will probably only become important in future high average power applications is the impregnant. The number of dielectric fluids that have been used in magnetic switches is very limited (Freon, Fluorinert, or oil). Transformer oil has been used extensively in the ac power industry for years and is the lowest cost dielectric fluid that is compatible with iron. It has a good operating temperature range and a reasonable breakdown strength. Its disadvantages are low thermal conductivity and relatively high viscosity. Consequently, it does not impregnate non-paper insulated switches very well and is not the best choice for thermal management schemes. Freon has been used most often in recent switches. However, because of environmental concerns over the use of Clorofluorocarbons it will probably be de-emphasized in future designs. Its advantages are reasonable cost, very low viscosity, and reasonable breakdown strength. Its disadvantages are low boiling point and low thermal conductivity. In the Meg-1-D switch, the chemical composition of the Freon was observed to change during the coarse of operation and it was becoming chemically active (i.e., attacking other

switch components). Fluorinert has not been used in very many applications because its cost is two orders of magnitude higher than that of oil. Its advantages include low viscosity, good temperature range, and high breakdown strength. Its disadvantages are low thermal conductivity and high cost. For high average power applications these fluids do not seem to be the optimal choices for satisfying electrical, thermal, and economic requirements. Other dielectric fluids with interesting properties exist, but there is no data base for accessing their long term compatibility with magnetic switch materials in the operational environment.

Research Areas

Since the local, time dependent, interlaminar, electric field is one of the primary factors that effects insulation lifetime in a magnetic switch, it should be better known than it presently is. An experiment similar to the one depicted in Figure 5 would for the first time provide data on what the time dependent electric fields are at several locations in a saturating magnetic switch. By varying the charging inductance, L_0, and voltage, V_0, appropriately, data could be obtained over an interesting range of saturation times (from several 100 s of ns down to <20 ns for instance). The interlaminar field probes shown in the figure should be very thin (on the order of 25 μm thick or less) and preferably nonconductive so that they do not significantly perturb the field distribution in the switch. Electro-optical crystals, which use the Kerr effect to rotate the polarization of laser light transmitted through them in response to an applied electric field, seem to be well suited for this application. Minor improvements in the present state of the art (to make thinner crystals and perform efficient optical coupling to them) would be required, but, little difficulty is anticipated in accomplishing this.[28] The data from such an experiment could be used to assess the accuracy of the present method of estimating the local electric fields. If there are significant discrepancies (i.e., unexpected magnitudes, variation in field strength with location, unexpected time dependent behavior, etc.), a computer code capable of accurately calculating the local fields should be developed using data from the experiment as a benchmark. In the Network and System Modeling Group of this workshop, the development of codes for use in circuit simulations or system analysis were discussed. These codes would likely be considerably different from the one proposed here because in circuit simulations only the terminal voltage and current of the switch need be predicted.

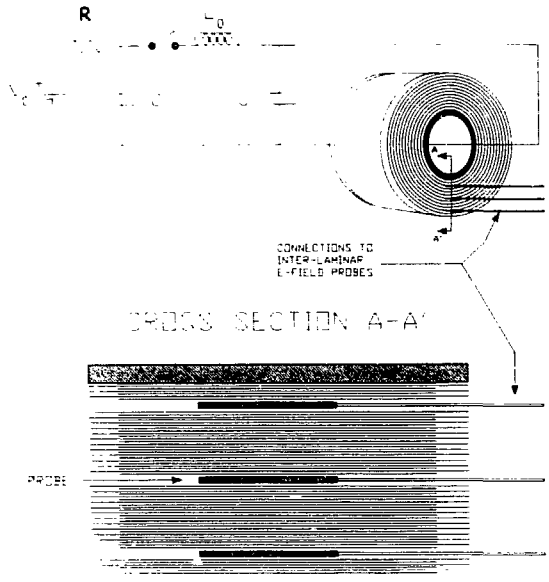

Figure 5. Concept of an experiment in which the time dependent inter-laminar electric fields in a saturating magnetic switch could be measured.

Whereas, a code that calculates local electric fields would have to predict the behavior of the core on a more microscopic level. In both cases, however, the principle challenge in code development is in modeling the behavior of the nonlinear magnetic material. This topic has been studied for many years and was discussed in more detail by the Network and System Modeling Group. The development of a code for calculating electric fields would take considerable effort, but, it would be a valuable tool to use in optimizing switch designs.

Since METGLAS is used in most magnetic switches, it would be useful to determine what improvements could reasonably be made to METGLAS ribbon to address the problems the ribbon causes for the insulation system. The surface morphology of METGLAS has improved over the years due to improvements in the casting process. Further work in this area might be the best way to attack this problem. Improvement in the stacking factor of METGLAS would be useful, but it is more important that Pips be eliminated or controlled so that their size is limited to something near that of normal surface protuberances. If Pips cannot be adequately controlled in the casting process, the feasibility of post processing techniques (such acid dips, electropolishing, etc.) should be explored. Improvements in the METGLAS anneal cycle, so that common insulations could endure it, would also be of value. If this is not feasible, then work should be done to find ways to wind cores so that the benefits of annealing before winding are better persevered.

The insulation systems that are presently used in high speed magnetic switches could be improved if better insulating materials were used. For high average power applications, a list of characteristics that would be desirable in solid dielectrics and fluid impregnants is given in Table 6. Most of these characteristics are desirable in many applications (capacitors, transformers, etc.) and research efforts directed at developing such materials already exist. The magnetic switch community should keep abreast of developments in this area and promising new materials should be investigated in small scale magnetic switch experiments to form a data base for use in large scale switch designs. At present, there are several commercially available, dielectric films that come closer to the characteristics of Table 6 than Mylar does. For example, polycarbonate and Danar have higher temperature capabilities and are much more resistant to long term damage mechanisms like partial discharges and charge trapping.[29] Similarly, new impregnants which have better characteristics than those that have been used in the past should be investigated. Some properties of oil, Freon, Fluorinert, and a few interesting new impregnants, that are commercially available, are compared in Table 7. Fluids such as Baylectrol 4900 and Sure-sol 250 seem to offer some advantages.

Table 6. Desirable characteristics for solid dielectrics and liquid impregnants.

Characteristics	Solid Dielectrics	Liquid Impregnants
Dielectric strength lg. area	High	High
Thermal conductivity	High	High
Max. operating temperature	High	High
Specific heat	High	High
Loss tangent	Low	Low
Dc volumetric resistivity	High	High
Density	High	High
Coeff. thermal expansion	Match to mag. mat.	High
Dynamic viscosity	—	Low
Stability and lifetime	Long	Long
Resistance to corona and PD	High	High

Table 7. Properties of potential fluid.

Property Fluid	Kin. visc. (cSt)	Spec. grav.	C P J/kg-K	Flash point (C)	Thermal cond. (W/m-K)	Dielec. stren. (kV)	Loss tan (at 100°C)	ε r	Cost $/gal
DIALA AX	9.37	0.886	1861	145	0.126	35 *	7E-4	2.25	2.12
Shell Oil	(at 40°C)	(at 15°C)	(at 20°C)			(at 60 Hz)	(at 60 Hz)	(at 25°C)	
561 SILICONE	32.0	0.96	1506	300	0.151	40 *	15E-4	2.70	18.5
Dow Corning	(at 50°C)	(at 25°C)	(at 25°C)					(at 25°C)	
SCF-150	7.65	0.98	_	150	_	75 ***	1E-4	2.60	8.17
Sybron	(at 25°C)	(at 25°C)							
TANACOL CG	4.85	0.98	1966	146	0.38	51 ***	19E-4	2.55	6.56
Sybron	(at 38°C)	(at 25°C)					(at 60 Hz)	(at 100C)	
BAYLECTROL 4900	3.50	1.035	1580	146	0.13	70 **	30E-4	3.50	_
Bayer/Mobay	(at 40°C)	(at 20°C)					(at 50 Hz)	(at 20°C)	
WEMCOL	5.00	0.988	1966	155	0.12	60 *	2E-4	2.83	_
ABB	(at 38°C)					typical		(at 25°C)	
SURE-SOL 250	5.00	0.99	2021	145	0.132	45 *	200E-4	2.77	6.49
Koch Chem	(at 40°C)	(at 20°C)	(at 57°C)	min	(at 204°C)	min	(at 60 Hz)	(at 25°C)	
HATCOL PXE	5.20	0.985	1924	145	0.117	60 *	5E-4	2.50	7.70
Hatco Chem	(at 38°C)	(at 20°C)	(at 20°C)		(at 40°C)		(at 100 Hz)	(at 100C)	
PROPYLENE CARB	1.67	1.206	2853	132	0.200	_	_	69.0	3.65
Kodak	(at 25°C)		(at 100°C)						
FREON-TF	0.43	1.564	891	48	0.485	35 *	1E-4	2.41	41.66
Fisher Scientif	(at 25°C)	(at 25°C)	(at 20°C)	BP			(at 100 Hz)	(at 24°C)	
FLUORINERT FC-72	0.40	1.681	1046	56	0.057	38 ***	3E-4	1.76	301.1
3-M				BP					
FLUORINERT FC-77	0.80	1.777	1046	97	0.063	40 ***	3E-4	1.86	306.4
3-M				BP					
FLUORINERT FC-40	2.20	1.873	1046	155	0.066	46 ***	3E-4	1.89	404.3
3-M				BP					
FLUORINERT FC-43	2.80	1.873	1046	174	0.066	42 ***	1E-4	1.90	601.4
3-M				BP					

BP = Boiling point
* = Test method (D-877)
** = Test method(IEC-156)
*** = Information on test method not found

By improving materials, the conventional magnetic switch insulation system will certainly be advanced. However, there are several shortcomings that are inherent in the system that will not be improved by material changes. A much larger benefit might be realized by making a fundamental change to the system. For instance, by developing higher voltage coatings to eliminate the need for using dielectric films, the system would benefit from the advantages that coatings provide. These include (1) elimination of edge margins which would significantly improve the thermal characteristics of the core, (2) improvement in the core packing factor, and, (3) simplification of the core fabrication process by eliminating the need to co-wind multiple layers of material. To be useful, any candidate coating would have to satisfy the following requirements. It would have to be applicable in thicknesses between 2–15 μm. It would have to be of very high quality so that there would be a very low probability in a large switch of any coating flaws in adjacent layers overlaying. It would have to be conformal and provide excellent edge coverage. Its dielectric strength needs to be reasonably high (on the order of a few 100 kV/cm) and the coating process must be cost effective (i.e., a few $/kg of magnetic material). The coating also must be compatible with the magnetic material it covers so that magnetic properties are not adversely affected. These requirements are demanding and cannot be satisfied by most conventional coating techniques. For example, dip type coatings are cost effective but in very thin layers their quality is typically insufficient and surface tension effects prevent them from being conformal (i.e., edges and surface protrusions are not well covered). Similarly, vapor and chemical-vapor deposited coatings can be conformal, but their quality is also insufficient and they are not cost effective (they must be done in a vacuum or low pressure environment and throughput rates are limited). On the otherhand, electrophoretically deposited coatings do seem to offer the potential of satisfying these requirements.

The electrophoretic (EP) coating technique has been used in industry for many years in a variety of coating applications and is described extensively in the literature.[31–32] Basically, this technique is analogous to electroplating except that a plastic, instead of a metallic, material is deposited on an electrically conductive substrate. A schematic illustration of a typical electrophoresis cell in which the coating is applied to the cathode is shown in Figure 6. The primary advantage that the EP process has over other coating processes is that it is electric field driven. This causes the coating to deposit in a conformal manner on the surface of the substrate with a thickness that is slightly dependent on the magnitude of the surface electric field. In areas where the surface electric field is higher (i.e., on the edges and over sharp surface protrusions) the coating has the desirable feature that it tends to be thicker. In addition, the electric field driven nature of the process yields another important attribute. When the coating is initially applied to a substrate, a relatively low dc voltage is required (50-100 V). Once cured, the coating quality is typically very good, but as in any process, there is a small probability that the coating will contain a flaw (i.e., a bubble, contaminate, etc.). In a large magnetic switch which would require miles of coated material, a very low flaw rate is required to have reasonable assurance that flaws in adjacent layers will not align. With the EP process, flaws can be detected and repaired by subjecting coated material to a second coating step. In the second step, the cell voltage is increased to several 100 V so that any flawed areas can be exposed (broken down) and then recoated. This feature of the EP process enhances its chances of satisfying the coating quality requirement.

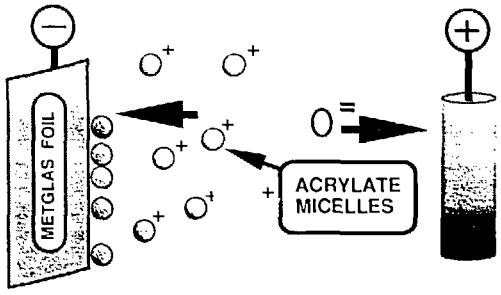

Figure 6. In a typical electrophoresis cell the coating is formed by charged particles in solution that are attracted to and coalesce on the substrate which is one of the electrodes in the cell (in this case the cathode).

Initial results from experiments using this technique to coat METGLAS were reported to the Core Cooling and Dielectrics group in a paper presented by Don Sharp.[32] At Sandia National Laboratories, a machine capable of applying a coating in thicknesses from 2–24 μm to METGLAS ribbon at a rate of a few feet/minute has been constructed. The machine uses a unique coating solution which consists of an electrophoretically active, aqueous dispersed, acrylic polymer (methyl methacrylate) that can be rapidly cured by ultraviolet irradiation. The ability to use a UV cure in stead of the thermal cure that is used with most EP solutions is important because during a thermal cure the coating tends to soften and flow. Consequently, surface tension effects can cause the coating to lose some of its conformal nature. With the UV cure this problem is avoided and as shown in the scanning electron micrograph of Figure 7, excellent edge coverage is achieved. Breakdown tests on reasonable quantities of coated material in wound geometries have not yet been done but preliminary tests in a point to plane geometry on ~ 2-in. × 6 in.-samples with a 12-μm thick coating have been. This initial breakdown distribution consisted of 15 data points and was relatively broad. It had a breakdown threshold of 0.4 MV/cm, a mean dc breakdown strength of ~ 1.4 MV/cm, a maximum breakdown level of 2.1 MV/cm, and a standard deviation of 39%. This is expected to improve as the coating process is refined. As an initial demonstration of the effect of the second coating step, similar coated samples were recoated with a greatly increased coating cell voltage of 450 V. When tested these samples had a breakdown threshold of 1 MV/cm, an average breakdown level of 1.8 MV/cm, a maximum breakdown level of 2.2 MV/cm, and a standard deviation of 20%. This result demonstrates that the primary effect of the second coating step is to increase the breakdown threshold and reduce the low level tail of the breakdown distribution. In a large structure like a magnetic switch, this effect is very important because this part of the distribution will dominate in determining the breakdown characteristics of switch. The magnetic properties of the methyl methacrylate coated METGLAS have also not yet been measured. However, in earlier work with an EP applied, thermally cured, styrene-acrylate coating, the magnetic properties of field annealed 2605CO METGLAS were not significantly degraded.[33]

Figure 7. SEM micrograph showing a cross sectional view of a coated METGLAS ribbon near its edge. The coating on this sample is ~ 10 μm thick.

Since the early results from experiments with EP coatings have been encouraging, research in this area should certainly be continued and possibly expanded. The raw materials in EP solutions are typically inexpensive so the coating process, once perfected, should be cost effective. In addition, consultations with the EP community would yield valuable information and possibly ideas for new solutions better suited to our application. A large number EP solutions have been developed over the years for a variety of applications. Some of these would be worthy of investigating, and, since the properties of EP solutions can be tailored to some extent with the use of additives, it should be possible to produce coatings with properties better suited to magnetic switch applications.

Work in the areas discussed above will certainly be of value in the development of high average power magnetic switches, but, probably the most important work required is in the area of long term effects. An extensive research effort to look at these effects must be supported. The first step in such an effort should be a literature search to gather any useful data on long-term effects. The ac power industry routinely produces components (capacitors, transformers, etc.) which use similar insulation systems and operate continuously for many years, so much valuable data should be available. However, data on newer materials and data in the regimes of interest for most parameters will not be found. Thus, small and medium scale experiments must be done to complete the data base and to define scaling laws. Included should be; experiments to measure partial discharge and corona inception levels, and, experiments to determine the lifetime of various insulating materials as a function of electric field, temperature, pulse frequency content, pulse rep-rate, etc. Small scale pulse compressors also should be constructed to test switch designs in a working system. Such systems would offer the only practical way in terms of time, hardware cost, and power cost to acquire component lifetime data. In addition, it should be possible to determine if there are any significant interdependencies between effects in this way. Such test beds are also the ideal place to develop solutions to problems once they are identified. For example, ideas such as putting additives in impregnants to improve long term stability could easily be tried in such test beds. Without the information that an effort like this would provide, it will not be possible to design high average power magnetic pulse compression systems for commercial applications.

Ac Power Industry Experience

State of the Art

The ac power industry has been producing long lifetime, continuously operating, high average power electrical equipment for many years. Much of this equipment (capacitors, transformers, etc.) is similar in many ways to a magnetic switch. Each device is a laminate structure of metal and insulation which must be designed to operate reliably and efficiently. The insulation in each device must withstand similar electric field stresses and thermal management of losses is a key design issue for each. In the case of magnetic cores for power transformers, both tape wound and stacked stamping geometries are used. The magnetic material of choice is typically a grain oriented silicon steel such as Silectron while other alloys like 50-50 NiFe, Deltamax, Square Permalloy, or Supermendur, to name a few, are sometimes selected. In recent years, amorphous metal alloys (METGLAS 2605S-2) have also been used in some applications. The insulation in cores for typical applications where interlaminar voltages are around 1 V or less is provided by coatings such as alkoxide, magnesium methylate, monoaluminum phosphate, magnesium oxide/silicate (Westinghouse Corp. proprietary), or Sol-Gel glass. There has also been some effort in the industry exploring electrophoretic coating processes. In specialized applications where interlaminar voltages are higher, insulation is provided by films

such as electrical grade papers, Mylar, polycarbonate, or Kapton. The thermal loading in power transformers, because they operate at low frequencies (60-400 Hz) and because they normally have efficiencies above 99%, is much lower than that expected in high average power magnetic switches. Loss densities are typically on the order of 0.006 W/cc in the cores and 0.07 W/cc in the electrical windings. The cores generally do not require internal cooling passages and are solid while the windings often require passively cooled channels.

The industry has accumulated a great deal of practical experience in a number of important areas. Analytical methods have been developed to model the magnetic, electrical, and thermal characteristics of power transformers.[40-42] Codes like WEMAP,[43] ANSYS,[44] and PE2D[45] are commonly used. These tools are valuable in applying information from past experience to the design of new devices. In building an extensive data base, procedures and practices have been established on how to do effective lifetime testing of high power devices. Considerable information on the long term effects of electrical stress on core insulations has been acquired.[40,46-47] This includes information on how the effects tend to interact and how they must be considered collectively in predicting device lifetimes.[48-49] Much work has also been done to acquire data on and model thermal aging effects in dielectrics.[40,50-52] Many cooling techniques have been evaluated and the most practical approaches have been identified.[40-41,53-55] Information concerning the effects of mechanical stresses (due to magnetostriction in cores, shock wave effects, $J \times B$ forces in windings, etc.) is also available.[40,56] In addition, techniques which are vitally important during the fabrication and operation of devices (such as dielectric fluid impregnation, moisture absorption control, gas bubble control, etc.) have been established.

Problem Areas

Although there are many similarities there are also some important differences between magnetic switches and the devices common in the ac power industry. One of the more important of these is that the frequency content of pulses typically applied to magnetic switches is far higher than the frequencies at which power devices operate. Consequently, the loss densities in high average power magnetic switches will be much higher and the cooling techniques of the power industry may not be extendable to this regime. In addition, since many long-term effects are sensitive to the frequency of the applied electrical stress, much of the available information on them will not be directly applicable to magnetic switch designs. Another significant difference is that the materials that are likely to be used in magnetic switches are not the same as those that are most commonly used in power devices. Consequently, the bulk of available data will be on materials of little interest and little or no information may exist on specific materials of interest.

The quantity of information that has been generated by the ac power industry is enormous. Only a fraction of this will be useful to the magnetic switch community and it may not be trivial to dig this out. In addition, some of the more useful information will likely be unpublished because there was no desire to do so or because it was considered proprietary. Without good contacts in the industry, this information may never be obtained. The option, however, is to unnecessarily repeat some of the mistakes that were made years ago in the power industry as they were developing long lifetime devices.

Research Areas

Most of the problems that will be encountered in the development of high average power magnetic switches will be similar in nature to those that have been overcome in the development of many ac power devices. A study of power industry experience should, thus, be done. Such a study is not likely to yield direct solutions to most of the problems, but, should be useful in minimizing the number of

iterations it takes to overcome them. For example, much could be learned about how to do effective small scale lifetime testing to establish acceptable stress levels. Similarly, a better knowledge of what kinds of long term effects are likely to be important would be very useful in designing these experiments. The study should include a thorough literature search resulting in a complete bibliography and the establishment of several good contacts within the industry. Contacts should be able to suggest sources of pertinent information for the study and, when problems are encountered in switches, they might be able to recognize them as manifestations of an old problems that have already been solved.

Conclusions

Most of the experience with magnetic switches, to date, has been at relatively low average power levels. Consequently, there has been little need to worry about thermal management, long term effects in insulation, or the optimization of switch designs to improve reliability and efficiency. In high average power applications, these issues will dominate and much research will have to be done before acceptable switch designs are realized.

Magnetic switches operate with volumetric thermal generation rates that span three orders of magnitude. Free convection channels are effective for heat rates up to about 0.5 W/cc. Above this rate, excessive temperature rise in the channels makes it necessary to use forced convection. In multiturn magnetic switches, nonuniform current distributions in the plate type conductors and effects of eddy currents caused by flux that escapes the core on saturation should be included in both electrical and cooling design considerations. Lots of data for cooling channel performance is available in the literature, but it is recommended that final cooling channel designs be based on measurements with materials and under conditions that occur in actual devices.

The need for high reliability and high efficiency imposes conflicting requirements that must be successfully compromised in the design optimization process. In order to make optimal use of the insulation in a core (i.e., operate it at the highest stress that allows lifetime requirements to be met), it is essential that the time dependent interlaminar electric fields in a saturating core be measured. If measurements do not agree well with the conventional estimates, then a design tool (i.e., computer code) should be developed to accurately calculate interlaminar fields. With better materials, higher stresses will be acceptable in cores. Some commercially available insulating films (such as polycarbonate, Danar, etc.) and impregnants (such as Baylectrol 4900, Suresol 250, etc.) may have better electrical or thermal properties than materials used in previous switches and should be investigated. Similarly, the community should keep abreast of new material developments and be prepared to test those that are most interesting when they become available. In order to get top performance from thin insulations in METGLAS cores, the surface morphology of METGLAS (especially the control of PIPs) needs to be improved either by advances in the casting process or by post processing. In cores where thin dielectric films are used as the primary insulation, thermal management is made more difficult by the insulation margins which are considerable thermal barriers. This situation could be improved if viable, high quality coating options were available to serve as the primary insulation. Early work directed at developing electrophoretically applied conformal plastic coatings to METGLAS has been encouraging and continued support is recommended. Since the EP process is electric field driven, it offers advantages over other coating processes. The coating is conformal with a thickness that is slightly dependent on the electric field on the surface of the substrate. Near the edges and over surface protuberances where the surface field is higher the coating tends to

be thicker. In addition, by subjecting coated ribbon to a second coating step, rare flaws can be exposed and recoated. This dramatically improves the overall quality of the coating and enhances its chances of satisfying the quality requirements of a large magnetic switch application.

The ac power industry has learned to deal with long term effects in their average power electrical devices. Thus, valuable information could be acquired by doing a good literature search and establishing more contacts in that industry. However, since this will not provide all the necessary data and information, it is essential that an extensive research effort on long term effects be supported. The research effort should include small scale experiments designed to measure things like partial discharge and corona inception levels and study insulation lifetime as a function of many parameters (such as electric field stress, temperature, pulse frequency content, pulse rep-rate, etc.). Fully operational small scale modulators should also be constructed to study system effects, acquire component lifetime data, and serve as test beds where new ideas can be tried. In the coarse of these tests, good fabrication and operational techniques and procedures also need to be established.

Glossary of Terms

a	=	r/R, inner channel radius over outer channel radius
A_i	=	cross sectional area of region, i.
A_M	=	effective magnetic cross section
B_m	=	measured magnetic induction
B_{rem}	=	remnant magnetic flux density
B_{sat}	=	flux density swing, $B_{final} - B_{initial}$
δB_s	=	METGLAS saturation induction
δb	=	build height between channels
c_p	=	coolant specific heat
d_M	=	effective magnetic path length
E_L	=	interlaminar electric field
ε_r	=	relative dielectric constant
f	=	volumetric flow rate per unit width
H	=	channel height
h	=	convective film coefficient on channel wall
H_m	=	measured magnetic field
k	=	coolant thermal conductivity
$k\uparrow$	=	thermal conductivity normal to ribbon.
$k_{\equiv}$	=	thermal conductivity in the plane of core winding
$k\uparrow_{margin}$	=	thermal conductivity in margin normal to winding
$k_{\equiv\ margin}$	=	thermal conductivity in margin in plane of winding
L	=	cooling channel length
μ	=	coolant dynamic viscosity
μ_r	=	relative magnetic permeability
N_L	=	Number of laminations in the core
N_E	=	Number of Electrical Turns.
Nu	=	Nusselt Number
δP	=	pressure drop across core
P.F.	=	packing factor (A_M/total core cross sectional area)
SF	=	stacking factor ($N_L\ x_L$/total build height of core)
q''	=	wall heat flux
q'''	=	volumetric heat generation rate
ϕ	=	coolant density
R	=	outer channel radius
r	=	inner channel radius
Ra	=	Rayleigh Number
Re	=	Reynolds Number
t_i	=	thickness of region, i
T_{in}	=	coolant inlet temperature
T_{max}	=	maximum temperature in the core
T_s	=	time to saturation
T_{wall}	=	maximum wall temperature
V_{in}	=	voltage applied to input winding
V_L	=	interlamination voltage
v	=	coolant velocity in channel
W_e	=	eddy current energy loss
w_L	=	magnetic lamination width
x_L	=	magnetic lamination thickness
$\{\ \}$	=	"a function of"

References

1. C.H. Smith, "Permeabilities of Metallic Glasses at High Magnetization Rates," *Proceedings of IEEE 18th Power Modulator Symposium*, pp. 336-339, 1988.
2. C.H. Smith, "Magnetic Pulse Compression by Metallic Glasses," *J. Appl. Phys.*, **64**(10), Nov. 15, 1988.
3. "Improved Amorphous Metal Materials for Magnetic Pulse Compression," by Allied Signal Inc., Corp. Tech., P.O. Box 1021R, Morristown, NJ 07960, Sandia Report No. SAND89-7095, 1989.
4. *Heat Transfer Data Book*, Section 504.3, Genium Publishing Co., Schenectady, NY 12301, Updated 1989.
5. B. Gebhart, Y. Jaluria, R.L. Mahajan, and B. Sammakia, *Buoyancy Induced Flows and Transport*, Section 10.6, Hemisphere Pub. Co., NY, 1988.
6. W.M. Rohsenow, J.P. Hartnett, and E.N. Ganic, *Handbook of Heat Transfer Fundamentals*, 2nd Ed., pp. 6-33 to 6-41, McGraw-Hill, 1985.
7. Frank Kreith, *Principles of Heat Transfer*, 3rd Ed., Intext Press, Inc., 1973.
8. D. Dropkin and E. Somerscales, "Convective Heat Transfer in Liquids Confined by Two Parallel Plates Which are Inclined at Various Angles with Respect to the Horizontal," *Journal of Heat Transfer, Transactions of the ASME*, pp. 77-84, February 1965.
9. "Channel Cooling Techniques for Repetitively Pulsed Magnetic Switches," to be published in the 1990-*19th Power Modulator Symposium*, June 26-28, 1990.
10. "The Repetitive High Energy Pulsed Power Module," to be published in the 1990-*19th Power Modulator Symposium*, June 26-28, 1990.
11. Saduk Kakac, Ramesh K. Shah, and Win Aung, *Handbook of Single-Phase Convective Heat Transfer*, Ch. 12, John Wiley & Sons, 1987.
12. W.M. Rohsenow, J.P. Hartnett and E.N. Ganic, *Handbook of Heat Transfer Fundamentals*, 2nd Ed., p. 7-17, McGraw-Hill, 1985.
13. I.H. Shames, *Mechanics of Fluids*, pg. 290, McGraw-Hill, 1962.
14. Roger Stone, et.al., "Core Cooling Studies at LLNL and Sandia," *Proceeding of 1990 International Magnetic Pulse Compression Workshop.*
15. R. W. Reynolds, "Numerical Predictions of the Magnetic Field Distribution, Current Density, and Temperature Distribution in Magnetically Accelerated Flyer Plates," Sandia Internal Report No. SCL-TM-70-213, April 1970.
16. W. C. Nunnally, "Magnetic Switches and Circuits," Los Alamos National Laboratory Report No. LA-8862-MS, Rev. 2, May 1984.
17. S. Chikazumi, *Physics of Magnetism*, English Edition, John Wiley & Sons Inc., 1964.
18. H. C. Harjes, G. A. Mann, and E. L. Neau, "Improved Insulation Schemes for Multi-Terawatt Magnetic Switches," *Proceedings of 7th IEEE Pulsed Power Conference*, Monterey, Ca, June 1989, p. 684.
19. A. Datta, et.al., "Saturation and Engineering Magnetostriction of Iron-Base Amorphous Alloy for Power Application," *J. Appl. Phys.*, **55**(6), 1984, p. 1784.
20. C. H. Smith, and D. M. Nathasingh, "Magnetic Properties of Metallic Glasses Under Fast Pulse Excitation," *Proceedings of IEEE 16th Power Modulator Symposium*, Arlington, Va, June, 1984, p. 240.
21. "Multifactor Stress Aging of Electrical Insulation," *Applied Physics Communications*, 7(1,2), 1987, pp. 19-55.
22. G. J. Rohwein, "Insulation of Dense Spiral Windings," invited talk for Core Cooling and Dielectrics Group, *Proceedings of 1990 International Magnetic Pulse Compression Workshop.*
23. F. M. Clark, *Insulating Material for Design and Engineering Practice*, John Wiley and Sons Inc., New York, 1962.
24. K. J. Bickford, G. H. Mauldin, and W. J. Sarjent, "Partial Discharge Characteristics of Liquid Impregnated, Laminate Dielectric Structures," *Proceedings of 1981 IEEE Conference on Electrical Insulation and Dielectric*

Phenomenon, Whitehaven, Pa, 1981, p. 177.
25. W. J. Sarjent, J. R. Laghari, and K. J. Bickford, "Charge Injection Effects upon Partial Discharges in a DC and DC plus AC Laminate Insulation Environment," *Proceedings of the ASOSR Special Conference on Prime Power for High Energy Space Systems*, Norfolk, Va, 1982, p. VII-8-1.
26. J. J. Chapman and L. J. Frisco, "A Practical Interpretation of Dielectric Measurements to 100-MC," Dielectrics Laboratory, Johns Hopkins University, Baltimore, Md, 1958.
27. G. McDuff, W. C. Nunnally, K. Rust, and W. J. Sarjent, "Diagnostics and Performance Evaluation Multi Kilohertz Capacitors," *Proceedings of the Special Symposium on High Energy Density Capacitors and Dielectric Materials*, 1980 NAS Conference on Electrical Insulation and Dielectric Phenomena, Boston, Ma, 1980, p. 270.
28. B. Nelson, Geo-Centers, Inc., private communication.
29. G. J. Rohwein, Results of Oil-Film Flashover Tests, unpublished research.
30. *Handbook of Electro-Plating Technology*, Electro-Chemical Publications Ltd., Bell and Bain Ltd., Glasgow, Scottland, Great Britain, 1978.
31. Milan Bier, editor, *Electrophoresis Theory, Methods, and Applications*, Academic Press, New York, NY, Vol. I, 1959, and Vol. II, 1967.
32. D. J. Sharp, H. C. Harjes, G. A. Mann, and F. A. Morgan, "Coating Possibilities for Magnetic Switches," *Proceedings of 1990 International Magnetic Pulse Compression Workshop.*
33. C. H. Smith, B. N. Turman, and H. C. Harjes, "Insulations for Metallic Glasses in Pulse Power Systems," *Proceedings of IEEE 1990 19th Power Modulator Symposium*, San Diego, Ca, 1990, p. 174.
34. D. Birx, et.al., "The Application of Magnetic Switches as Pulse Sources for Induction Linacs," *IEEE Transactions on Nuclear Science*, NS-30(4), 1983, p. 2763.
35. D. Birx, et.al., "A Multipurpose 5-MeV Linear Induction Accelerator," *Proceedings of IEEE 1984 16th Power Modulator Symposium*, p. 186.
36. D. M. Barrett, S. E. Sampayan and W. C. Turner, "Critical System Issues and Modeling Requirements - the Problem of Beam Energy Sweep in an Electron Linear Induction Accelerator," *Proceedings of the International Magnetic Pulse Compression Workshop*, Granlibakken, Lake Tahoe, CA, February 12-14, 1990.
37. M. Thevenot, P. Eyl, and P. Anthouard, "Magnetic Compressor Studies for FEL Applications at the Centre D'Etudes Dcientifiques et Techniiques D'Aquitaine," *Proceedings of 1990 International Magnetic Pulse Compression Workshop.*
38. E. L. Neau, "COMET: A 6 MV, 400 kJ. Magnetically-Switched Pulse-Power Module," *Proceedings of 4th IEEE Pulsed Power Conference*, Albuquerque, NM, 1983, p. 246.
39. E. L. Neau, T. L. Woolston, and K. J. Penn, "COMET-II, a Two-Stage, Magnetically Switched Pulsed-Power Module," *Proceedings of IEEE 1984 16th Power Modulator Symposium*, p. 292.
40. Richard L. Bean, et. al., *Transformers for the Electric Power Industry*, Library of Congress No. 58-14344, McGraw Hill, 1959.
41. Emil Stenkrist, "Temperatures and Conditions of Oil Flow in Large Oil-Immersed Transformers," *ASEA Journal*, 1949.
42. W.H. McAdams, *Heat Transmission*, 3rd Ed., McGraw Hill Book Co., 1954.
43. Westinghouse Electric Corporation
Engineering Services Bureau
Bldg 701 Science and Technology Center
Pittsburgh, Pa. 15235
Attn: J. Lipniskis
44. Swanson Analysis Systems
P.O. Box 65 Johnson Road
Houston, Pa. 15342
45. Rutherford Appleton Laboratories
46. W.G. Stranding and R.C. Hughes, "Breakdown Under Impulse Voltages of Solid and Liquid Dielectrics in

Combination," *Proceedings of Inst. Electrical Engineers*, Paper 2050 S, April, 1956.
47. C.M.L. Sommermann, et. al., "Impulse Ionization Breakdown in Liquid Dielectrics," *Trans. AIEE*, **73**, part I, pp. 147-153, 1954.
48. J. R. Laghari, "Multifactor Stress Aging of Electrical Insulation," *Applied Physics Communications*, **7**(1&2), 19-55 (1987).
49. J. R. Laghari, "A Review of AC and Pulse Capacitor Technology," *Applied Physics Communications*, **6**(2&3), 213-251 (1986).
50. T.W. Dakin, H. Philofsky and W.C. Divens, "Significant Factors in Thermal Aging Tests of Flexible Sheet Insulation," *Trans AIEE*, **74**, part I, pg. 289, 1955.
51. R.M. Plettner and G.C. Currin, "A Method of Evaluation of the Thermal Aging Stability of Flexible Sheet Insulation," *ASTM Special Tech. Pub.* **161**, pg. 111, 1954.
52. F.M. Clark, "Factors Affecting the Mechanical Deterioration of Cellulose Insulation," *Trans. AIEE*, **61**, pp. 742-749, 1942.
53. *Design Manual Featuring Tape Wound Cores*, Magnetics, Inc., Spang Co., 1962.
54. J.R. Meador, "Temperature Rise of Water Cooled Power Transformers," *Trans. AIEE*, **65**, pg. 19, 1946.
55. S.W. Chi, *Heat Pipe Theory and Practice: A Sourcebook*, Hemisphere Publishing Co., Copyright 1967.
56. "Bibliography on Transformer Noise," AIEE Committee, *Trans. AIEE*, pp. 1760-1762, 1955.

Circuits and Applications Group

James Swingle, Chairman
Ken Whitham, Cochairman

Working Group Members

S. Eckhouse
E. Chu
D. Loree
G. Morris, Jr.
V. A. Vizar
K. Whitham
M. Honig
S. Ashby
W. Nunnally
G. Neau
L. Schlitt
R. Kuenning
M. Sheaffer
R. Stone

Introduction

The Circuits and Applications Working Group was assigned the task of surveying the range of potential applications for magnetic switch technology. By providing information to the workshop on typical sets of requirements for magnetic switch networks and identifying technical issues that need to be resolved in each topical area, it was intended that the group's work would assist specialists in materials and components in identifying important future research and development (R&D). The group felt that it was also important to identify areas where magnetic switches may not be useful and, therefore, serve to assist researchers in avoiding unproductive work.

The group convened during the first session to hear three invited papers and to begin devising an approach for the treatment of a large number of potential applications. Shimon Eckhouse (Maxwell) presented a summary of work being performed on induction linac technology for driving high gradient rf accelerators for x-ray lithography and linear colliders. Bob Kuenning (PSI) presented a methodology for scaling magnetic switch networks, taking into account thermal management issues and materials behavior. Buddy Swingle (LLNL) presented information surveying induction linac applications as the power source for microwave and mm-wave free electron lasers (FELs), relativistic klystrons (RK), optical FELs, heavy ion accelerators, and e-beam machines for industrial use. In subsequent sessions, talks by Dr. Vizar from the Institute of High Current Electronics (Tomsk, U.S.S.R.) were presented on the subject of magnetic pulse compressors for excimer lasers and on saturable-inductor assisted thryatrons.

General Considerations for Magnetic Switch Applications

Magnetic switching networks have been brought out of the closet during the past 10 years because some of their performance characteristics were not available using other technology. Specifically, the advantageous characteristics of magnetic switches are: (1) high average power due to simultaneous capabilities for high voltage, current, and pulse repetition frequency (PRF), (2) high peak power, (3) low conduction losses limited only by the size of the conductors used, and (4) very good reliability and lifetime. These characteristics can be put to practical use in several ways:

- Magnetic compression of a pulse generated using conventional technology.
- Use of magnetic switch in series with conventional switches to reduce their switching losses during turn-on (by delaying their current risetime) and assist their turn off (by delaying the reapplication of voltage after a current zero).

• Isolation of pulse circuits and/or summation of pulses at a common node to increase the effective pulse rate.

Although magnetic switches have definite advantages in some applications, they also have practical limits as follows:

• Core size, proportional to the pulse energy, is limited by fabrication considerations.

• Average power is limited by thermal management considerations.

• The pulse risetime is limited by the ratio of the saturated inductance to the system impedance.

• The compression gain per stage is limited by material parameters, especially at short saturation times.

• High performance magnetic materials are expensive.

It is essential that the circuit designer remember that other technologies can fulfill system requirements within their own particular parameter regime. These alternatives can often fulfill requirements at lower cost and at reduced volume and weight when compared with magnetic switch networks. Therefore, it is important to identify system needs that motivate the designer to consider magnetic switches due to the extension of requirements beyond the regime that can be satisfied by conventional technology. "Will we know a useful magnetic switch when we see one?" A useful rule-of-thumb is proposed as follows:

"If I cannot amplify or augment conventional technology by significantly reducing overall switching losses, increasing lifetime or extending system parameters through pulse compression or switching delay, then I probably should not go to the trouble of using magnetic switches."

With this background, the reasons for using magnetic switches were compared with the specifications of many types of applications while considering the practical limitations of their use.

Potential Applications

The assessment process started with an attempt to assemble a reasonably complete list of possible applications. The topics were put into the following groups based on similarity of requirements:

- **Conventional lasers and radar:**
  - — Electrical discharge devices for excimer, carbon dioxide, and metal vapor lasers.
  - — E-beam driven gas lasers.
  - — Radar modulators.

- **Ultra-high current applications:**
  - — Electromagnetic launchers.
  - — Bremsstrahlung and EMP simulators.
  - — Light ion accelerators.

- **Induction accelerators:**
  - — Microwave and mm-wave FELs.
  - — Relativistic klystrons and high gradient rf accelerators.
  - — Optical FELs for inertial fusion.
  - — Industrial e-beam sources for processing of food, municipal waste, and stack gases.
  - — Heavy ion accelerators.

Assessment of Applications

Conventional Lasers and Radar

There have been a large number of open literature references on the use of saturable inductors in pulse power networks driving electrical discharge lasers, including UV or x-ray preionized excimer and CO_2 lasers, and metal vapor devices (e.g. Cu vapor). Research and commercial applications of these lasers have increasingly required high repetition rate operation (100–1000 s of Hz). Many of the devices operate in the pulse-length regime of 10–100 s of ns, requiring significant amounts of pulse compression after the primary commutator. Reliability and component lifetime also are significant concerns for devices that are approaching commercial application. The combination of high average and peak power, pulse compression, and long lifetime make investigation of the use of magnetic switches compelling for this range of applications. Similar applications exist in pulse power networks for driving e-beam diodes used in pumping gas lasers. Finally,

the original proposed use of magnetic modulators, radar, was listed. The magnetics are used to deliver pulse power to microwave converter devices.

Ultra-High Peak Current Applications

Several applications were listed that were distinguishable as a group because of the high peak current required (100–1000 s of kA). Electromagnetic launchers require delivery of extremely high peak current pulses that electromagnetically couple energy to a projectile. Railguns and coaxial induction launchers are examples. Pulse lengths tend to be fairly large even for multistage designs. Switching and energy recovery requirements become quite stressing. Pulse power driven e-beam diode machines for electromagnetic pulse (EMP) and radiation effects simulation require very high peak current and were added to the list of topics for this group. Finally, in the event that requirements for light ion accelerators move into the high repetition rate regime, magnetic networks may become useful for switching the high current needed for this application.

Induction Accelerators

Microwave and mm-wave FELs operating at high average power for tokamak heating or linear collider applications appear to be viable technical options. Alternatives in the waveform of these devices and excursions in core materials and design are needed. The group studied a 1-ms, 10-MeV, 3-kA, 1-kHz linear induction accelerator (LIA) for tokamak applications, and compared the potential benefits and technical issues with conventional approaches. The prime power source was a turbine driving a rotary flux compressor. The magnetic modulator and induction cores were assumed to be METGLAS. This concept appears to warrant further study. The large range of other potential applications were given only preliminary assessments. The induction accelerator can also be the power source for relativistic klystrons used to drive high-gradient rf linacs in linear colliders or x-ray lithography systems. The use of an optical FEL for pumping solid-state laser media for inertial fusion appeared to be a very challenging problem. The concept requires the long-pulse induction core technology mentioned above. Some of the pulse power elements of the tokamak concept also may be important for this application; however, the financially-driven need to reuse the induction cores by recirculating the beam implies the invention of MHz-regime burst mode pulse power units. Multiplexing and reset issues also require significant study to develop a viable concept suitable for more detailed engineering analysis. Furthermore, the inertial fusion problem cannot be productively addressed without early commitment to detailed cost modeling, allowing for the simultaneous optimization of many system parameters. This assessment also holds for heavy ion accelerators based on induction technology. All the induction accelerator concepts would benefit from higher performance materials at lower costs. Decisions about how far to push a particular parameter await detailed trades on cost and performance for any particular application in order to identify how much improvement and investment in development is warranted.

Conventional Lasers and Radar

This subgroup addressed the application of magnetic switches to several discharge pumped lasers, to e-beam pumped lasers, and to RF modulators. In general, all these applications were placed in this group because they relate to fairly well established devices that have been studied in the R&D community for 10–20 years and because they require moderate single pulse energy (1–10,000 J), moderate energy and peak current (100–1000 kV and 0.1100 kA), and high PRF (0.1–20 kHz). In most cases, magnetic switch technology can potentially fill the role of augmenting and extending the utility of conventional pulse power technology into regimes of interest for industrial and energy applications.

Electric Discharge Lasers

The conventional lasers that could benefit from the introduction of magnetic switch technology include excimers, CO_2, and metal vapor lasers (e.g. Cu vapor). The networks of saturable inductors can be used for pulse compression of the output of conventional switches (thyratrons or SCRs) or for isolation of the conventional pulse power networks from the nonlinear load of the electrical discharge. This discharge is often prepared by a preionization pulse from flashboards or x-ray sources. The characteristics of the load for these applications are shown in Table 1.

Schematic representations of the Melville line, the voltage doubling circuit, and the saturable transformer circuit for pulse compression are shown in Figure 1.

Assessment. Many of the applications of these discharge lasers, including cutting and welding, lithography, laser radar, and energy applications require that the technology prevail after aggressive competitions on cost and performance from alterative schemes. The components comprising the networks used in these applications must excel in lifetime and reliability. The cost, size, and weight of

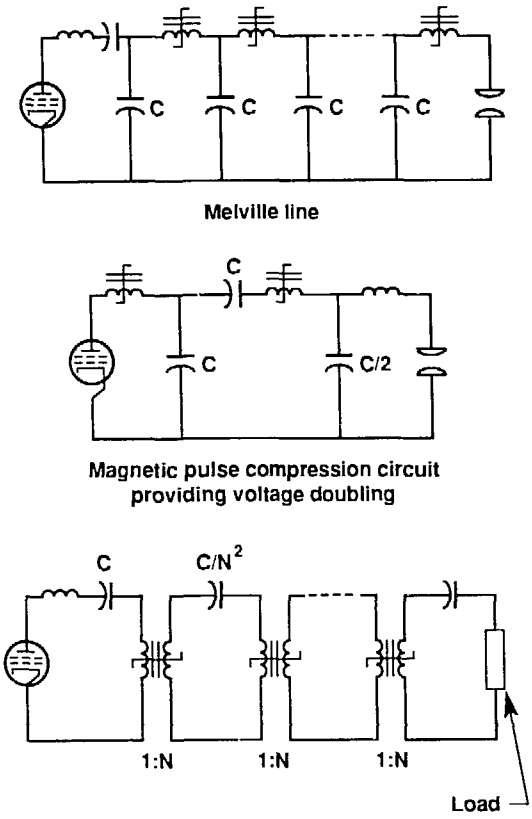

Figure 1. Pulse compression circuits.

Table 1. Characteristics of electric discharge lasers with possible applications for magnetic switch networks.

Parameter	Excimer	Cu Vapor	CO_2
Voltage	20–150 kV	20–50 kV	10–200 kV
Peak current	10–200 kA	1–100 kA	1–300 kA
Pulse length	50–200 ns	<1 μs	0.1–10 μs
Risetime	10–50 ns	10–30 ns	30–300 ns
Voltage regulation	±20%	NA	±20%
PRF	20–2000 Hz	0.3–20 kHz	10–1000 Hz
Mag efficiency	>50%	>50%	>50%
MTBF (shots)	10^8–10^{10}	$>10^{10}$	10^8–10^{10}
Load impedance	High impedance initially, near constant voltage during the rest of the pulse.		
Applicable circuits	Melville line, voltage doubling circuit, saturable transformers		

magnetic core materials must be reduced in order to qualify magnetic switch technology. This is particularly important for the high-performance magnetic materials that are currently of interest in the R&D environment. Commercial applications await significant improvements.

E-Beam Pumped Gas Lasers

Excimer and CO_2 lasers have been operated as atmospheric-pressure, large volume devices when pumped by e-beam diodes. Magnetic fields have been applied typically to concentrate the deposited electron energy in the excited volume. Upon extension of the application of these devices to the high repetition rate regime, conventional switch technology is often inadequate. Typical parameters for commercial and energy applications of e-beam driven laser devices are given in Table 2.

Table 2. Characteristics of e-beam pumped gas lasers for commercial and energy applications.

Parameter	e-beam pumped gas laser
Voltage	100–1000 kV
Peak current	1–100 kA
Pulse length	0.1–10 μs
Risetime	<200 ns
Voltage regulation	±10%
PRF	1–1000 Hz
Mag efficiency	>75%
Lifetime (shots)	$>10^6$
Load characteristics	Hot cathode for high power, cold cathode for low power.
Applicable circuits	Melville line with or without pulse transformer.

Assessment. Magnetic switches can potentially be useful in this class of applications if costs and performance of magnetic materials can be improved. The precise amount of improvement, in the sense of a cost-effective commitment of resources, remains to be determined from detailed cost studies, which were not possible on the timescale of the workshop.

Radar Modulators

Pulse compression for radar applications was the motivation for Melville to originally propose the magnetic modulator. The general requirements are listed in Table 3.

Table 3. Radar modulator requirements.

Parameter	Requirements
Voltage	10–350 kV
Peak current	1–1000 A
Pulse length	0.5–10 μs
Risetime	<10% of pulse length
Voltage regulation	<1%
PRF	0.001–10 kHz
Efficiency	>80%
Lifetime (shots)	$>10^{10}$

The loads for these modulators typically have a well-defined impedance, behaving according to Child's law. Circuits making use of saturable transformers or Melville lines with output pulse transformers are appropriate for this application.

Assessment. Since the first proposal for the magnetic modulator, other conventional approaches have experienced improvements in the capabilities of components. Both vacuum and solid-state electronics have produced many design options for pulse modulation. In most cases, these conventional solutions meet the

requirements with reduced size, weight, and cost compared with the magnetic designs. This situation will change only if drastic increases in the requirements develop in the future.

Technical Issues

All the networks discussed in this section must operate at high repetition rate with long component lifetime. Several technical issues for magnetic switch concepts must be resolved in meeting the requirements:

- For high repetition rate systems, internal energy reflections can last longer than the interpulse period. Energy reflections can be suppressed through damping; however, this results in a loss of efficiency. Careful matching of circuits can be done over a limited operating range.
- Magnetic switch cores present difficult problems for thermal management. Variation of properties with temperature can contribute to the problem noted above. Selection of cooling fluids must account for compatibility with the rest of the system.
- Interactions of reset circuits with the main circuit at high PRF lead to pulse-to-pulse variations. Damping in reset circuits may be required for some applications.
- Mechanical connections must minimize inductance and resistance to eliminate contact arcing for long life applications. Contact arcing leads to erosion, dielectric fluid deterioration, and corrosion.
- Magnetic switch core winding insulation could be improved to obtain a thinner, more reliable dielectric medium capable of withstanding higher fields. Higher working temperature also is desirable.

Ultra-High Current Applications

These topics were collected together because of the requirements for 100–1000 s of kiloamperes in peak current. The list includes electromagnetic launchers, bremsstrahlung and EMP simulators, light ion accelerators, and imploding plasma sources. Research activity has been pursued in all of these areas for decades without the introduction of magnetic switch technology. In general, their use in the future depends on changes in the requirements for these applications so that the high reliability and high repetition rate capability of the technology will justify the cost and size of the new components. Advances in the materials technology, once again, could encourage introduction of the magnetic switch concepts much sooner than will be the case under existing constraints.

Electromagnetic Launchers

Significant R&D efforts have been invested in the problem of converting electrical power to kinetic energy of a projectile or plasma mass. Velocities in the range 1–10 km/s have been observed in early prototypes involving small projectiles. For practical electric gun applications, the power must be applied over timescales of milliseconds and the peak current must be in the range 0.1–10 MA, depending on the particular concept. The railgun concept requires peak current in the upper end of this range. The circuit concept is shown in Figure 2. Upon charging of the inductive energy store and introduction of the projectile into the barrel, the switch opens. Current then is delivered to the gun barrel.

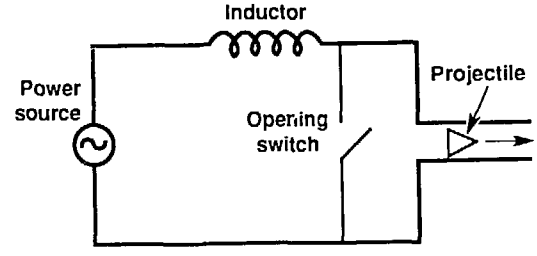

Figure 2. Railgun circuit concept.

Multistage coaxial induction launchers also have been proposed. A schematic of the circuit concept is shown in Figure 3, where each induction stage is driven by a capacitor. For the multistage launcher, timescales for the pulse power network are somewhat lower than for the railgun, but still of order 100 μs for moderate velocity. It is possible to employ a cascaded magnetic switch network, similar to the Melville line, to move stored energy not transferred to the projectile in each stage down the device to subsequent stages.

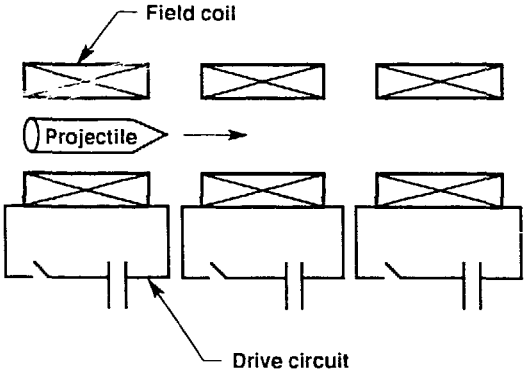

Figure 3. Multistage coax induction launches.

Assessment. Electromagnetic launcher power systems, in general, require the delivery of enormous amounts of energy to the projectile. For example, the kinetic energy in a 2 kg projectile moving at 10 km/s is 100 MJ. Furthermore, minimizing the launcher length to make it practical requires maximizing the acceleration force. To provide a sustained acceleration of 10^5 g, a general limit due to strength of materials, requires the delivery of 1 MJ per kg of projectile mass for each meter of launcher travel. In addition, the energy is usually delivered over timescales ranging from milliseconds to tens of microseconds at voltages on the order of several tens of kilovolts. The energy requirements in concert with the high currents favor large conductor cross sections and a minimum number of turns. This results in large core volumes and weights that rival that of the energy storage systems. The large core volume, based on overall energy requirements, is consistent with the volt-second rating based on millisecond to microsecond saturation times at tens of kilovolts. For comparison, the present range of magnetic switch applications (4 MV–125 ns to 50 kV–10 μs) represents about 0.5 volt-seconds of equivalent core cross section, while the electromagnetic launchers require several tens of volt-seconds, even when multiple turns are used, making magnetic switches clearly impractical for this application.

Bremsstrahlung/EMP Simulators and Light Ion Accelerators

In this group of applications, the pulse power system may be expected to deliver 10–30-MV, 1-MA, 50-ns pulses. The energy in the pulse, from each module, may be 1 MJ and the PRF may be in the range 10 pulses per day to 10 pulses per second. Magnetic blocking cores, based on amorphous alloys, are used in the linear induction voltage adder section of these accelerators to increase the voltage from the conventional pulse forming network to that required in the electron or ion beam diodes.

Assessment. The switching used in these pulse forming networks can be conventional self-closing water switches, but may require saturable magnetic switches for the next generation of accelerators. Available material loss data and design techniques appear adequate for this type of application; however, development of accurate thermal models is needed. Special techniques may be required to form the ramped voltage waveforms from the Melville lines for the light ion accelerator. Low module jitter and matched module throughput times will be required, as will some form of active timing compensation. The driving factors in selecting magnetic switching over conventional technologies, particularly for accelerators with a number of parallel modules and a large component count, is the combined need for moderate PRF with high reliability and component lifetime. Much work needs to be done on the

characterization of failure mechanisms and lifetime scaling relationships for the magnetic switches, similar to that available for capacitors and cables.

Imploding Plasma Sources

High power generators for driving imploding plasma loads use a succession of pulse compression stages not unlike those found in a magnetic modulator. A capacitor, usually water insulated, is charged from a Marx generator. This capacitor either acts as a pulse forming line when discharged or, if more pulse compression is needed, it powers additional switched stages charging the PFL. Presently, these generators use either water switches or gas switches to transfer energy between capacitors. These switches perform reasonably well, but have some disadvantages. Water switches are lossy, especially at high voltages (large gaps). They also have problems with jitter and generation of large shock waves in the water. Gas switches almost always require triggering and the problem of routing the trigger signals across the high voltage interelectrode gap. They also have current and voltage limits, can be expensive, and can require excessive maintenance if charge transfer is high. Magnetic switches have no intrinsic coulomb transfer limits and their voltage is limited only by the cross-sectional area of the core. They require no trigger pulse (although they might require an external reset connection). Within these generators, there are two regions of switch operation. Switches for the capacitors near the Marx generator have large volt-second requirements because of the slow discharge, but inductance is not usually a concern because of the long timescales. Switches located nearer to the load end of the machine have a lower volt-second requirement, but the switch size may need to be increased due to the need to keep inductance low for the fast pulse. This is similar to the change in the switching requirement that occurs in a magnetic pulse compressor.

The size of the magnetic switches in such a generator becomes the major issue. For example, consider a magnetic switch intended to replace a 3-MV gas switch used to discharge a transfer capacitor in one of these generators. The gas switch is not a simple switch, but is by no means beyond the state of the art. If the transfer capacitor has a 1.3-μs charge time, the volt-second requirement for the magnetic switch is 1.95 volt-seconds. Choosing a 0.6-m length and 0.3-m inner diameter gives a design using 20,000 kg of magnetic material for this one switch. A similar amount of material would be required for other switches in the generator. The cost of the switches would approach the cost of the remainder of the generator.

Assessment. Due to the high costs of magnetic switching in this application and the fact that other technologies have been well developed, generators are often designed around the capabilities of existing switches. Demands are reduced on individual switches by breaking the generator into smaller modules. While magnetic switches can certainly be used in these generators, in most cases other approaches can be implemented at lower cost. If the cost per volt-second could be reduced by a factor of 2–3, this technology might begin to look attractive.

Induction Accelerators

The range of induction accelerator applications that may require the use of magnetic switches is shown in Table 4. Details on the requirements for these applications were given in one of the invited papers. From a technical feasibility standpoint, the microwave and mm-wave FELs appear to be viable technical options that will require engineering development of magnetic switch networks for high reliability and good waveform control. The group focused its work on an assessment of alternative waveform options for tokamak ECRH applications. In particular, a conceptual design for a microsecond pulse induction accelerator was developed so that its technical issues could be assessed relative to the current designs based on ETA II technology. There was no time to address the space-power beaming application,

while the high gradient accelerator drive sources (FEL or relativistic klystron) were addressed in invited papers. An alterative microwave source for this application was suggested by Gordon Bowden (SLAC). Cross-field amplifiers, if arrayed in sufficient numbers in parallel, could be driven by magnetic modulators in the class of the MAG-1D at LLNL. The industrial applications for low energy induction accelerators were reviewed in an invited paper. The group felt that alterative sources are perhaps better candidates for these applications. The technical issues associated with the inertial fusion drivers (optical FEL pump source and heavy ion accelerator) are enormous, and it was felt that insufficient time was available in the workshop to do a worthwhile assessment of them. Furthermore, the issue of cost and its relationship to design choices is central to such an assessment. Therefore, design trades cannot be performed without first developing comprehensive models of performance and cost that can be subjected to nonlinear optimization studies.

The remainder of the available time was used to study the tokamak heating application because it represents an area that clearly needs magnetic switch technology, and it offers an opportunity to study excursions from existing technology.

Table 4. Survey of induction accelerator applications.

General Category	Possible Applications	Comments
Microwave/mm-wave FELs	ECRH in tokamaks space power beaming linear collider	Long-pulse assessed Not examined Invited paper (Swingle)
Relativistic klystron driven high gradient rf	VUV and x-ray sources linear collider	Invited papers (Eckhouse, Swingle) same linacs
Cross-field amplifier	Linear collider	Suggested by G. Bowden (SLAC)
E-beam sources	Food irradiation, municipal waste decontamination, stack gas processing	Other sources perhaps better
Optical FEL	Optical pump for solid state media driving inertial fusion	Not examined
Heavy ion accelerator	Inertial fusion	Not examined

The top-level parameters describing the induction accelerators that would be suitable for these applications are shown in Table 5. The values shown are those that have received significant attention within the R&D community and do not include important excursions that may be possible based on new materials and component technology. An example of such an excursion is the long-pulse accelerator concept that was studied during the workshop for the tokamak heating application.

Table 5. Top-level parameters for induction accelerators.

Application	E-beam energy, MeV	Peak current, kA	Pulse length, μs	Energy regulation, %	PRF, kHz
ECRH (tokamak)	8–13	1–3	0.04–0.1	<1	3–20
Linear collider (FEL)	1–10	1–3	0.04–0.1	<1	1–10
Linear collider, VUV, x-ray lithography (RK)	1–10	1–3	0.04–0.1	<5	1–10
E-beam processing	1–3	1–3	0.04–0.1	<10	1–10
Laser fusion (optical FEL)	200–400	0.1–1	1–5	<0.4	0.001–0.01
Heavy ion fusion	10^4	0.006–2.6 (pulse compression)	50–0.115 (pulse compression)	shaped	0.01

MM-wave FELs for ECRH Heating in Tokamaks

The capability to produce high average power in the mm-wave regime makes the induction FEL an attractive option for supplying power for electron cyclotron heating of tokamaks. The top-level requirements for the mm-wave source are listed in Table 6.

Table 6. Top-level requirements for mm-wave source for ECRH in tokamaks.

Parameter	Requirement
Frequency	280 and 560 GHz
Average power	40 MW
Tunability	
over ms	6–8%
over long timescales	20%

These requirements are those specified for the Compact Ignition Tokamak (CIT) and the International Thermonuclear Engineering Tokamak (ITER).

A long-pulse configuration (>1 μs) was investigated and compared with the present short-pulse (<100 ns) concepts. To obtain the 40 MW of 280 GHz radiation, three FELs per tokamak were specified. This provides some flexibility in operation and allows a design that has some specific advantages that will be discussed later. Table 7 lists the parameters of the two alterative accelerator schemes.

Table 7. Parameters of two accelerators.

Parameter	Short-pulse	Long-pulse
Peak current	3 kA	3 kA
E-beam energy	15 MeV	10 MeV
Pulse width	50 ns	1 μs
PRF	13 kHz	1 kHz

Figure 4 shows the long-pulse configuration studied. The overall system consists of a single prime power source (based on rotating machinery) driving a single power conditioning system. The

power conditioning system drives 50 magnetic pulse compressors in parallel. Each magnetic pulse compressor drives a single accelerator cell. This architecture alleviates the module synchronization problem since all of the magnetic pulse compressors are charged from a common source. By driving a single cell with each magnetic pulse compressor, the single pulse energy is 800 J.

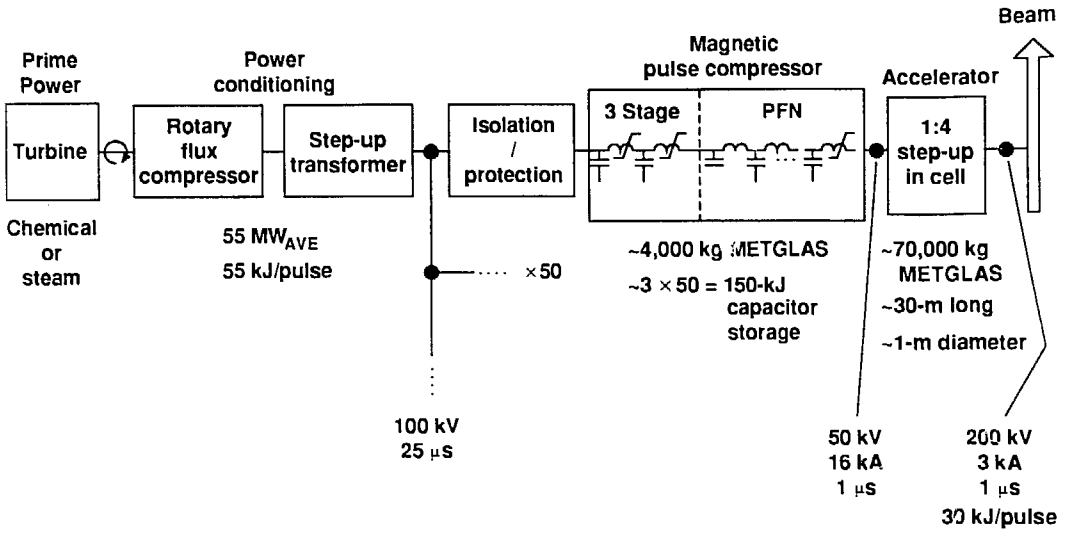

Figure 4. Long pulse configuration accelerator.

Accelerator. The accelerator consists of 50 induction cells which contain 2605CO METGLAS cores. The cores are separated radially into four segments which are driven in parallel by the magnetic pulse compressor. The configuration is shown in Figure 5. This flux strapping concept distributes the flux evenly throughout the core, precluding premature saturation in local regions, and provides a fourfold voltage increase at the cell. Thus, the 200-kV accelerating voltage requires a 50-kV pulse from the magnetic pulse compressor. The estimated magnetization current of each core group is 1 kA, which must be driven in parallel with the 3-kA beam current. Each magnetic pulse compressor must deliver 16 kA. Channels can be incorporated into the cores for forced convection cooling, but the heat load is low due to the long pulse length and moderate PRF.

Magnetic Pulse Compressor. The magnetic pulse compressor contains three stages of compression with compression ratios from input-to-output of 3, 3, and 2.5, respectively. The output stage is configured as a multisection pulse forming network using discrete capacitors which are repetitively charged to 100 kV. The charge time for the PFN is 2.5 μs, and the e-folding time for the discharge of the PFN is 80 ns. A design for this reactor which includes early switchout of the pulse uses 10 turns on a 5×8 cm^2 cross section core with a mean radius of 25 cm. With a packing fraction of 0.5, the core contains about 3000 cm^3 of METGLAS. The layer-to-layer voltage is approximately 5 V which may permit the use of insulating coatings and higher packing fractions. The remaining cores were assumed to require comparable volumes of material. The long pulse lengths used in this design should permit the construction of a relatively high efficiency magnetic pulse compressor. No attempt was made to estimate actual losses. The efficiency of the magnetic pulse compressor was assumed to be 75%.

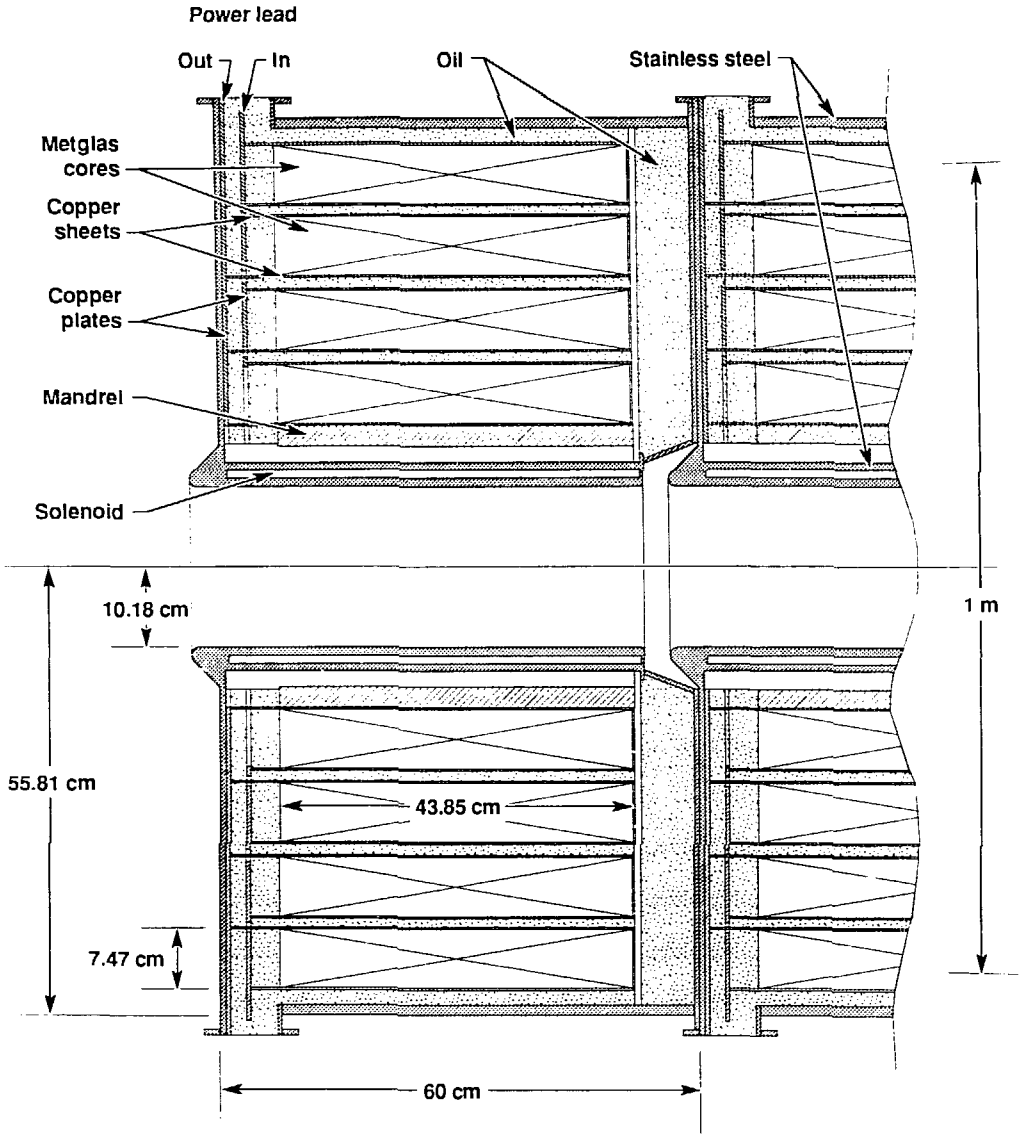

Figure 5. Long pulse accelerator induction cell.

The total mass of the METGLAS used in the 50 magnetic pulse compressors is estimated to be 4000 kg. The total mass of METGLAS in the accelerator cores was estimated to be 70,000 kg per beamline. Each of the three compression stages in each magnetic pulse compressor must store ~1 kJ. Therefore, a total capacitor energy storage requirement for the accelerator is in the regime (1 kJ) × (3 stages per magnetic pulse compressor) × (50 magnetic pulse compressors per beamline) = 150 kJ per beamline. The capacitors need to be able to withstand 100 kV at high repetition rate.

Power Conditioning. The power conditioning system consists of a single rotary flux compressor with associated stepup transformer, fault protection, and drive circuitry. The system delivers a continuous train of 55-kJ, 25-μs, 100-kV pulses to the input of the 50 magnetic pulse compressors at a 1-kHz PRF. The average power delivered by the unit is 55 MW. The voltage at the output of the rotary flux compressor is 25 kV and the stepup transformer has a voltage ratio of 4:1. The rotary flux compressor is driven by a turbine which could be driven by steam from the power plant which the system services.

Assessment of Long-Pulse Induction Linac. An initial assessment of the long-pulse induction linac option identified several significant advantages over the short-pulse concept that had been proposed in earlier work. Although no obvious disadvantages were found for the long-pulse system, key issues that need to be studied in further detail were highlighted. Whether these issues will eventually become irrelevant, disadvantageous, or even show-stoppers was beyond our capability to assess during the workshop.

As mentioned above, one of the major motivations of the long-pulse option was to reduce the PRF from a rather uncomfortable value of ~13 kHz to a rate that essentially eliminated PRF as a risk issue. A conservative value of 1 kHz was selected, although one could increase that by probably a factor of 2–3 without causing large concerns. In addition to the lower PRF, the longer pulse enabled us to reduce the electron energy to 10 MeV, which is below the threshold for neutron-induced activation for the facility. Consequently, not only will less shielding be required for the bremsstrahlung produced during operation, but the area should be accessible for maintenance immediately after shutdown of a beamline.

The longer pulse length increases the wall plug efficiency of the induction accelerator since a small fraction of the pulse is taken up in the rise and fall time. Pulse compression requirements also are reduced which will further enhance efficiency. One of the key requirements on the electron beam imposed by the FEL is pulse flatness (<1%). The longer pulse will reduce the dV/dt across the accelerator gap, enable us to avoid the ringing at the head and tail of the voltage pulse, and in general facilitate correcting for factors that could produce voltage sweep during the pulse.

Despite our inability to identify clear-cut disadvantages of the longer-pulse option, several areas need to be examined in more depth. Although rf breakdown in mm-wave transport to the tokamak is not expected, the effect of the longer pulse on the design margin of previous concepts was not studied. Brightness requirements for the FEL have been readily achieved for the short-pulse concept. Increasing the pulse length of the injector may require reducing the field stresses which may produce brightness degradation. Resolution of this issue requires a detailed design of the injector. Our quick look at e-beam transport did not reveal any significant differences with the short-pulse regime; however, detailed simulations are clearly required.

The accelerator and magnetic pulse compressors require about 10 times the amount of METGLAS as for the short pulse concept. Reductions in cost and improvements in the performance and reliability of this material could significantly enhance the usefulness of the long-pulse concept. The use of the rotary flux compressor for long-pulse devices needs to be further developed and assessed for technical issues that are specific to the mm-wave FEL application. It is suspected that requirements are significantly reduced compared with those for laser fusion.

'90

Invited Poster Presentation

AMORPHOUS MAGNETIC MATERIALS FOR EFFICIENT PULSE COMPRESSION

M.GREENWOOD, UNIVERSITY OF BRISTOL, U.K.

SUMMARY

Loss data for a range of magnetic materials suitable for magnetic pulse compression are presented. The data has been measured under pulse compressor conditions and a significant increase in losses has been recorded over those measured under constant voltage magnetisation. These data are then analysed using a previously derived loss factor and other techniques, to compare material suitability for high repetition rate pulse compressor applications. This analysis shows the likely advantage of certain cobalt based amorphous alloys. Finally a practical pulse compressor is described which uses these high efficiency magnetic materials, and although unoptimised, is greater than 70% efficient.

INTRODUCTION

As the requirement for pulse power systems to operate at higher and higher repetition rates increases, so does the importance of accurate prediction of component behaviour. In magnetic pulse compression the efficiency of the magnetic switches affects not only the pulse energy delivered to the load but also the maximum repetition rate at which the system will operate. The subsequent core heating leads to both short and long term degradation of core material properties, affects core insulation and construction, and also other components within the system.

The materials most commonly used for pulse compressor cores are Allied Metals' 2605SC and 2605CO. These are high flux density iron-based amorphous magnetic materials, which have relatively low losses compared to silicon-iron and nickel-iron materials. However these materials do have several drawbacks, especially when used for high repetition rate applications. The range of amorphous magnetic materials includes cobalt based alloys having lower available flux densities. These materials also exhibit much lower loss densities. This allows a tradeoff to be made between core loss density, core volume and total core loss.

This paper analyses this tradeoff, with experimental data recorded specifically for pulse compressor operation. A previously derived loss factor[1] is used to assess material suitability, along with core volume predictions and loss density data. This analysis is then tested using a low energy pulse compressor suitable for high repetition rate operation.

THEORY

To assess magnetic alloys for suitability as core materials for pulse compressors it is important not only to know the loss densities of the materials used, but the absolute loss for a given core design. Because of variations in core flux density the required core volume varies greatly between materials. In the past it has been usual to use a high flux density material to minimise the core volume, however this does not necessarily minimise core loss.

Definition of a loss factor[1] which gives a figure proportional to the absolute losses, enables different materials to be compared. The loss factor (LF) is defined as:-

$$LF = E_v / \Delta B^2 \qquad (1)$$

where E_v is the magnetisation energy loss per unit volume, and ΔB is the available flux swing of the core material.

This loss factor enables all non-material dependent parameters to be removed from the core loss equation, these being either design parameters or functions of core construction.

The values of the two parameters that make up LF must be those found under pulse compressor conditions. Although there have been extensive studies of losses in ferromagnetic materials under pulsed conditions[2,3], neither these nor theoretical models accurately predict the losses for pulse compression applications. Therefore, measurements have been taken under compressor conditions, with a rate of magnetisation (dB/dt) proportional to ($1-\cos\omega t$) over a range of saturation times.

EXPERIMENTAL DATA

The materials used in the experimental work are listed in Table 1. All of the amorphous alloys were in the form of standard 25mm (1") wide, 25μm thick ribbon, with 5 or 6μm Mylar as the interlaminar insulation.

Suitable pre-winding annealing of the amorphous alloys was carried out by the manufacturers, except in the case of the 2605SC material. This is both difficult to wind after annealing due to brittleness, and suffers from a degradation of the annealed properties during the re-winding as a result of stress sensitivity. This material was used unannealed, which is relatively common[4,5].

	ΔBm * (T)	-Br + Bs (T)	-Bs + Bs (T)	MAJOR CONSTITUENT ELEMENT
ALLIED 2605CO	3.6	3.20	3.40	Fe
ALLIED 2605SC-UN	3.2	1.90	3.00	Fe
TELCON HCR NiFe	3.0	3.00	3.00	NiFe
ALLIED 2705MN	2.4	2.20	2.20	Co
VAC 6150z	2.0	2.00	2.00	Co
VAC 6030z	1.6	1.55	1.60	Co
VAC 6025z	1.1	1.10	1.10	Co
MULLARD 3C8 FERRITE	0.9	0.45	0.85	MnZn

* Manufacturers maximum available flux swing

TABLE.1 Summary of materials properties

The nickel-iron alloy was chosen from a standard set of cores from the manufacturer, this used 13μm ribbon, and as only deposition layer interlaminar insulation was available it was precluded from use in experiments with magnetisation times below a few microseconds. A ferrite core, in the form of an E-core was also chosen, this core has been used successfully in the past for pulse compression[6].

Material properties are summarised in Table 1. The maximum available flux swing quoted by the manufacturers is given in the first Column. This can be compared to the measured flux swing (confirmed for both low frequency and pulsed magnetisation) from negative remanance and from negative saturation, given in Columns two and three respectively.

The cores were designed to be part of a small 1 Joule pulse compressor. This generated core designs of a reasonable size and cost, and which would perform a dual function, as they could be used initially for loss measurements and later in the pulse compressor.

The pulse system used for the magnetisation experiments is shown in Fig.1. This circuit represents a single stage compression line, and generates a voltage waveform, and hence a rate of change of flux in the magnetic switch, which is proportional to (1-cosωt). In the past, researchers have carried measurements under conditions of constant dB/dt (i.e. constant voltage) but these are not representative of compressor conditions. In order to make a direct comparison with this other work we also carried out experiments using constant voltage excitation, and these measurements confirmed those published previously. From pulsed magnetisation waveforms and measured core parameters B-H loops were constructed, and the

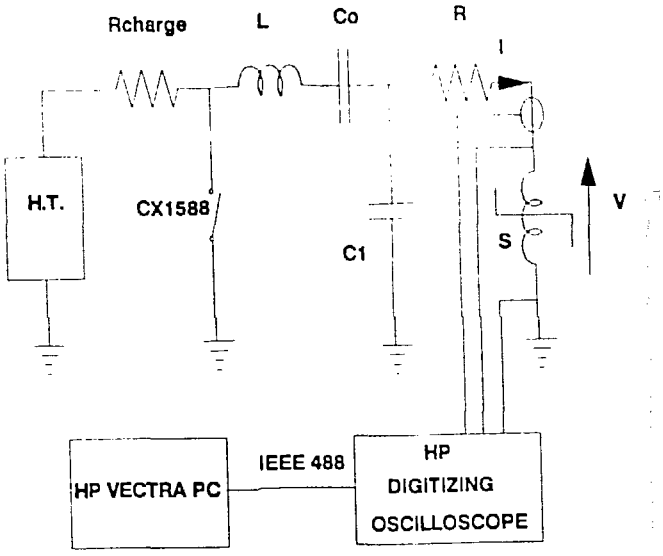

FIG.1 Experimental setup

relevant loss density and other information was extracted. Loss measurements were made for a range of magnetisation times between 10μs and 250ns.

The volume of magnetic material required for a given core design varies as the inverse square of the available flux swing. If we take the flux swing as being from negative remanance to positive saturation ($-B_r+B_s$) then the relative volume requirements of the materials tested are as shown in Fig.2.

The loss characteristics for the materials are shown in Fig.3. These are for $dB/dt \propto$ (1-cosωt) and show increases of up to 70% in the worst case compared with constant dB/dt.

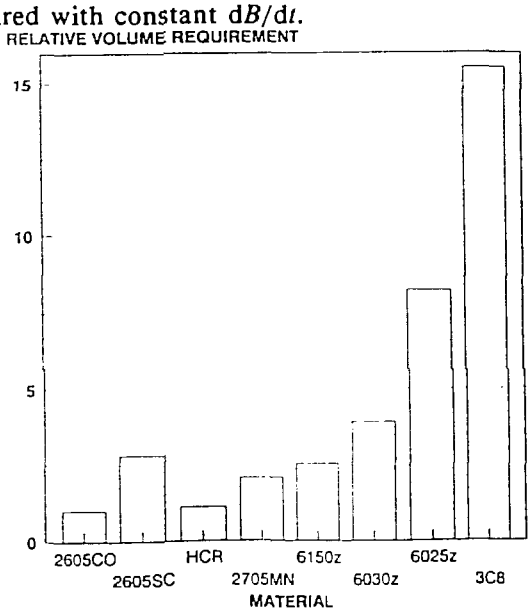

FIG.2 Relative core volume requirements for materials under test

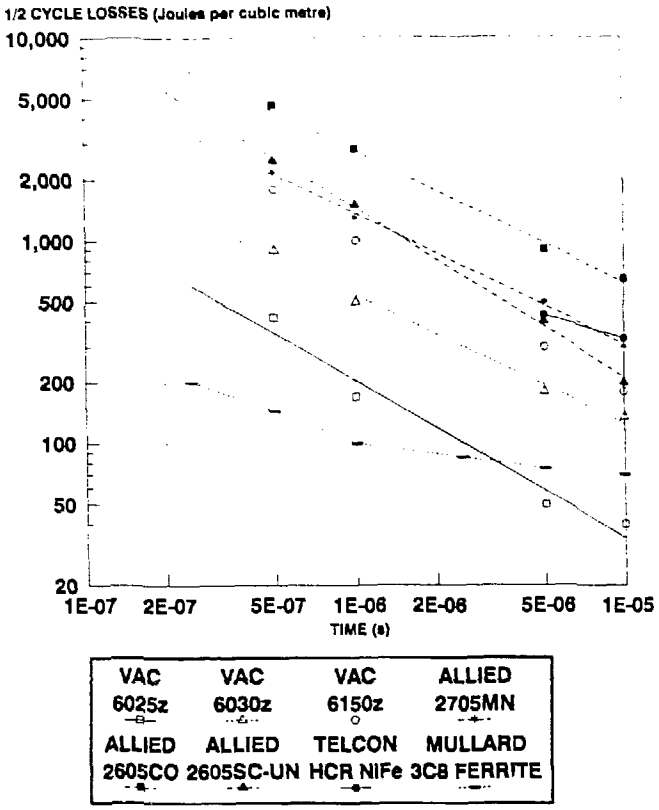

FIG.3 Material loss characteristics under (1-cosωt) dB/dt magnetisation

ANALYSIS

The measured loss densities show a dependence between $\tau_{sat}^{-0.55}$ and $\tau_{sat}^{-0.75}$ for the amorphous materials. This indicates a magnetisation process which lies somewhere inbetween bar domain and saturation wave behaviour[2]. The highest loss densities occurred in the iron-based amorphous alloys. These loss densities decrease with decreasing ΔB through the range of cobalt based alloys. The ferrite shows the lowest loss density across the full range of magnetisation times, except for the lowest ΔB cobalt alloy at the lowest rate of magnetisation.

The relative volume requirements shown in Fig.2, indicate that the iron-based amorphous alloys and the NiFe alloys have the lowest volume requirements, and the ferrite the highest, requiring some 15 times the volume of the lowest volume amorphous alloy. The cobalt alloys fill the region of volume requirements between the highest and lowest volume materials.

The loss factor(LF) defined in Equation 1, is illustrated in Fig.4. At the lower magnetisation rates the highest LF materials are the iron based amorphous materials and the ferrite. Core losses in this part of a compressor are low, of the order of 1-2%, and winding losses tend to assume equal importance. The lowest loss materials are the NiFe alloy and the lowest ΔB cobalt alloy, 6025z. However the volume requirement of the NiFe material is much lower than that of 6025z, which may also lead to lower winding losses.

As magnetisation rate increases the ferrite becomes the most efficient material, and the iron-based amorphous alloys remain the least efficient. The cobalt alloys again bridge the gap between the two.

In high repetition rate systems the core losses, especially in the later stages of compression, are significant. The high power loss densities generated in the low volume requirement materials such as 2605CO means that core heating becomes a problem. Use of higher volume, high efficiency materials relieves this problem without increasing the total losses. If suitable cobalt based amorphous alloys are chosen the power loss density can be significantly reduced. The total losses are also lower, and yet the massive volume increase encountered when using ferrite material is avoided.

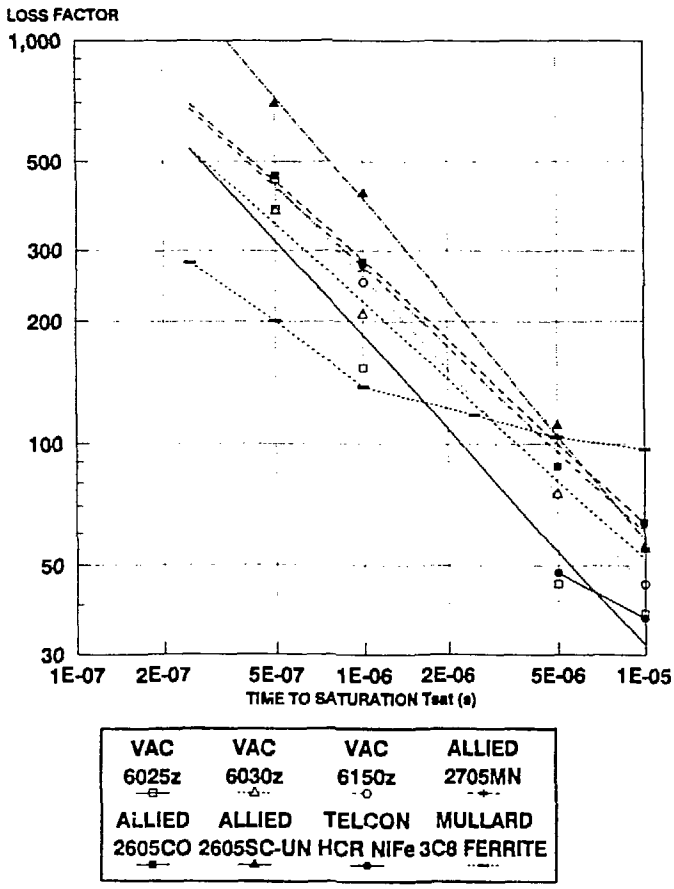

FIG.4 Loss Factor

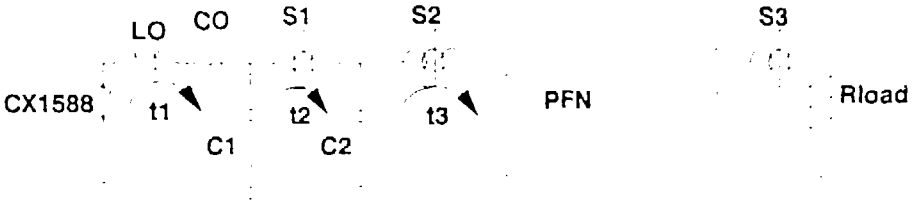

CO,1,2,PFN = 20nF t1=6us t2=1.3us t3=250ns
Vcharge = 10kV PFN = EITHER 120ns 3ohm OR 60ns 1.5ohm line

FIG.5 Experimental 3-stage pulse compressor

PULSE COMPRESSOR

In order to demonstrate that the experimental data could be used to design a high efficiency system, a low energy (1 Joule) three stage pulse compressor was used as a test bed. Core design was based upon manufacturers' data for flux swing and packing fraction, and estimated values for parameters such as saturated permeability and winding factor. Actual values varied considerably from those assumed, so the effective core gains were also very different. The result of this is a pulse system that is unoptimised, but one which does give a good indication of the validity of the predictions.

The compressor (Fig.5) uses the CX1588 hydrogen thyratron, used in the pulse magnetisation experiments, as an initiating switch. The charging voltage is 10kV, and the first stage capacitor is charged in 6μs. Two different PFN's were used, the first was an 8-stage, 3Ω, 120ns line, which was used in conjunction with a multiturn toroidal magnetic switch. This generated a 45ns risetime, 120ns pulse (Fig.6) into a 3Ω matched copper sulphate load. The overall efficiency of this system was greater than 70%. A very low inductance, multiturn geometry is difficult to achieve, and with small numbers of turns the effective inductance factor increases considerably. Therefore to achieve very fast risetimes a transmission line geometry must be adopted. The second PFN used was a 4-stage 60ns 1.5Ω transmission line, with a racetrack geometry final stage magnetic switch. This produced a 20ns risetime pulse into a matched load (Fig.7), with a total compressor efficiency of greater than 65%. The transmission line and load section are shown in Fig.8.

The choice of cores was based on the previous analysis. Increased volume was offset against a reduction in losses. The first stage core was VAC 6150z, the second VAC 6030z, the multiturn final stage core was VAC 6025z and the transmission line core VAC 6030z. The performance of the cores is

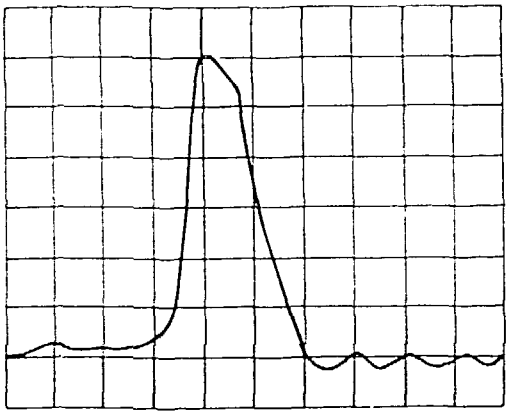

FIG.6 Load voltage waveform (100ns/div→, 700V/div↑) for multiturn toroidal switch.

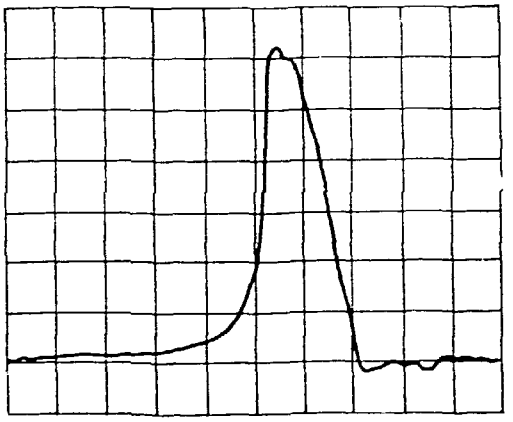

FIG.7 Load voltage waveform (50ns/div→, 500V/div↑) for racetrack core

summarised in Table 2. The total core losses are somewhat high, this is due to the high gain per stage that resulted from variation of the core parameters from the designed values. As core volume, and therefore core loss, is proportional to the square of the core gain then an small increase in core gain significantly affects the total core loss.

Other advantages of these cobalt based materials are their near zero magnetostriction and relative ease of handling, this means they are easily wound

into toroids, and more importantly transmission line geometries, without losing their favourable properties. This is much more difficult to achieve with some of the iron based alloys. Another advantage is their high squareness ($B_r/B_s \rightarrow 1$) and low coercive force, this means that only a small reset field need be applied to achieve the maximum flux swing, and high squareness also helps reduce pulse to pulse jitter.

CONCLUSIONS

By making use of the full range of available amorphous magnetic materials it is possible to optimise a pulse compressor design with respect to core losses and volume.

	Core Gain	% Loss
1st stage - 6150z	4.6	1.9
2nd stage - 6030z	5.2	4.9
3Ω line - 6025z	2.1	7.4
1.5Ω line - 6030z	4.2	12.0

TABLE.2 Core performance data

REFERENCES

[1] M.Greenwood, J.Gowar and B.M.Bird, "A Comparability Parameter for Amorphous Magnetic Materials," *7th I.E.E.E. Pulsed Power Conference*, 11-14 June 1989.

[2] C.H.Smith and L.Barberi,"Dynamic Magnetisation of Metallic Glasses", *Proc. 5th I.E.E.E. Pulsed Power Conf.*, Crystal City, VA. June 10-12, 1985.

[3] R.M.Jones,"Step dB/dt Magnetisation Losses in Toroidal Amorphous Ribbon and Polycrystalline Cores", *I.E.E.E. Trans. Magnetics*, MAG-18, 1559-61, 1982.

[4] T.J.Pacala, et al.,"Magnetic Modulator for a Repetitively Pulsed Xenon Chloride Laser System", *Proc. 16th Power Modulator Symposium*, June 1984.

[5] J.E.Dolan, et al.,"Investigation of the Magnetic Switching Properties of Unannealed Metglas 2605SC Tape, *7th I.E.E.E. Pulsed Power Conf.*, June 11-14, 1989.

[6] H.J.Baker, et al.,"An Efficient Laser Pulser using Ferrite Magnetic Switches", *J.Phys.E:Sci.Instrum.* 21, 218-224, 1988.

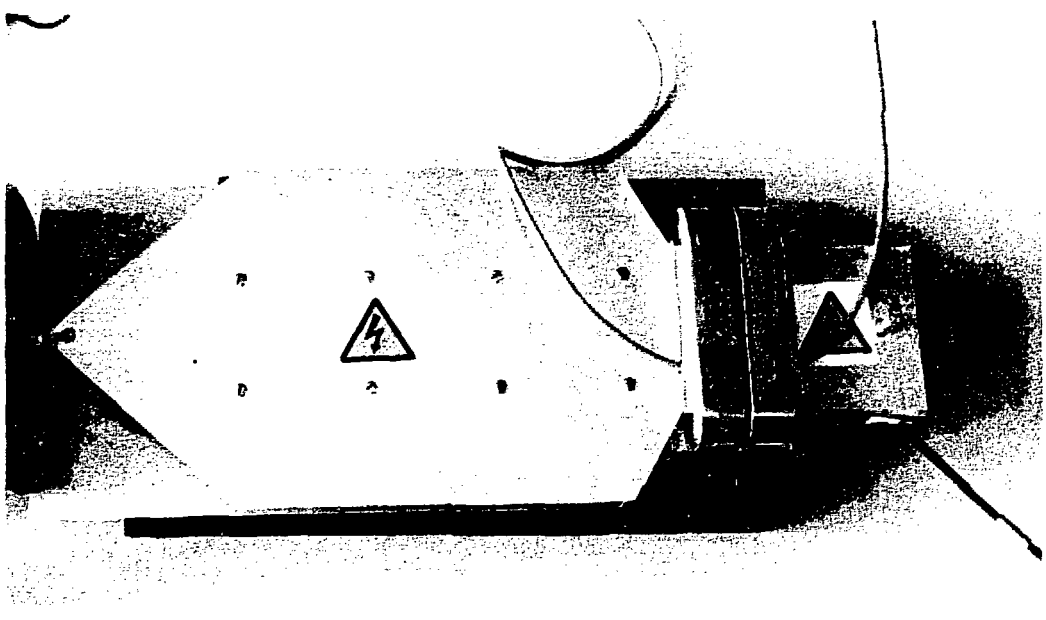

FIG.8 Transmission line geometry final stage switch

HIGH CURRENT BACK LIGHTED THYRATRON SWITCHES*

G. Kirkman-Amemiya*, T.Y. Hsu,
R.L. Liou and M. A. Gundersen

University of Southern California
Department of Electrical Engineering
Los Angeles, California 90089-0484

ABSTRACT

High power operation of the BLT switch is described. This paper includes a description of the switch structure and several optical triggering methods. Result of experimental observations of high current operation are reported including measurements of 100kV DC holdoff, peak currents >80kA and rates of current rise $>10^{11}$A/sec.

INTRODUCTION

The Back of the cathode Light activated Thyratron or BLT switch[1,2] is an optically triggered version of the Pseudospark switch[2]. The BLT operates with peak currents and current rates of rise comparable to high pressure spark gaps but with the repetition rates and low electrode erosion characteristic of hydrogen thyratrons. Unlike the hydrogen thyratron the switch requires no cathode heater power and has a much simpler gridless structure, also the symmetric structure of the BLT allows it to conduct reverse currents without electrode damage. Unlike the Pseudospark switch the BLT is optically triggered allowing for complete electrical isolation of the triggering circuit. In this paper we discuss the BLT switch, several optical triggering methods, and the electrical characteristics (peak current and rate of current rise) of several versions of the switch.

SWITCH STRUCTURE AND OPERATION

The switch structure is cylindrically symmetric consisting of two cup shaped electrodes with flat bottoms that face each other and are separated by about 3-5mm, each electrode has an aperture on the cylinder central axis of 3-5mm diameter. The electrodes are positioned within a cylindrical ceramic or glass insulator and the structure is filled with a low pressure gas usually hydrogen at about 0.2 torr. For this pressure and electrode separation the switch has a high breakdown voltage by operating on the left side of Paschen minimum[3]. The central apertures perturb the field giving a longer effective path for breakdown with a lower breakdown voltage. When electrons are added to the region of the cathode aperture an ionization avalanche can occur producing a homogeneous discharge plasma confined to this central region of the electrodes. A hollow cathode type discharge is formed that gives a rapid rise in ionization and current through the switch. The ions produced during these transient phases bombarb the cathode producing secondary electron emission and heating the cathode surface to a temperature where thermionic emission is possible. The discharge continues in a high current dense glow discharge phase using the thermionic cathode produced at the front surface of the cathode electrode. The switch conducts at a current density of $\approx$10kA/cm^2 that continues for a time determined by the external circuit.

The operating voltage is similar to that of hydrogen thyratrons up to about 35kV for typical single gap devices however the peak currents and rate of current rise are significantly higher than thyratrons. The switch has operated at peak currents over 80kA with pulse lengths from 50nsec to several μsec. The rate of current rise is usually limited by the external circuit except if the switch is operated at a decreased gas pressure. The high peak currents and rise rates are important to several pulsed power applications such as lasers and modulators for accelerators that typically require magnetic pulse sharpening and compression to obtain the required pulse shape, in some applications replacing the thyratron by a BLT switch may eliminate the need for magnetic circuitry[4]. Also circuits that have poorly matched loads, such as the excimer laser discharge can produce reverse currents that are damaging to thyratrons due to arcing that can occur on reverse conduction, the symmetric structure of the BLT allows it to handle nearly 100% reverse currents without damage.

OPTICAL TRIGGERING

We have investigated several optical triggering methods including laser[1], flashlamp[4] and light guided by an optical fiber[5]. In each case a small amount of unfocused light is incident on the back surface of the cathode near the central aperture. The required starting electrons are produced by photoemission from the metal surface typically molybdenum, tungsten or nickel. Through photoemission 1mJ of photons each having an energy about equal to the cathode work function can produce a number of starting electrons sufficient to initiate the discharge with a delay of ~100ns and jitter <1ns.

HIGH POWER OPERATION

Recent experiments have shown that even for peak currents as high as 82 kA and dI/dt of 4×10^{11} A/sec the performance is not limited by the BLT switch. In these tests a flashlamp triggered switch was tested in a circuit whose load resistance could be changed to produce different peak currents. The circuit consisted of two 0.4μF capacitors in parallel, a

1mΩ current viewing resistor , the flashlamp triggered switch and a carbon block load resistor of 1Ω to produce an overdamped discharge or 0.25Ω to give a near critical damping and for the highest currents the load resistors were replaced by copper conductors to produce a ringing discharge. The peak current and dI/dt show a linear dependence on initial voltage indicating that the current is determined by constant circuit parameters and not a switch discharge limit that would be indicated by a nonlinear behavior.

In nearly all cases the current is circuit limited and the switch operates in a diffuse discharge. Occasionally at high currents arc like behavior is observed. These arcs or sparks can be observed by eye or with camera as bright spots in the discharge plasma and at the cathode surfaces and are sometimes observed as dips in the current waveform or spikes on the voltage waveform. These defects however occur only for very short times compared to the total pulse length and the remainder of the current pulse shows a circuit dependent waveform. The reason for arc like behavior has not been carefully characterized and requires further study. The number of arc type events increases with increasing current however even at 82kA the current and voltage waveforms normally show show no symptoms of the arc like behavior.

Higher voltage holdoff can be obtained by multigap BLT switches. We have tested several versions of multigap BLT switches[6] the first consisted simply of two BLT switches in series resulting in twice the DC holdoff of a single switch. Next several variations of baffled and open structured stacked BLT switches were fabricated and tested. The highest voltage and currents have been obtained with a tightly baffled 3-gap flashlamp triggered switch. This switch had a DC holdoff of 100kV, 70kA peak current and $3x10^{11}$A/sec rate of current rise switching 630J/pulse in single shot operation.

Testing of a sealed ceramic BLT switch[7] designed for high power operation is in a preliminary stage. The sealed switch shows more stable operation due to high temperature vacuum processing and a reservoir to maintain the hydrogen pressure within the tube. Using a 1.25ohm, 100nsec pulse forming line the switch has been operated at 22.5kV, 8kA, >2x1011A/sec dI/dt and 10Hz limited by the triggering light source.

CONCLUSION

In conclusion the BLT switch is a candidate to replace thyratrons in applications requiring high peak currents and rates of current rise. The BLT conducts currents characteristic of high pressure spark gaps with electrode erosion rates comparable to thyratrons. Optical triggering allows for electrical isolation simplifying multiple gap (series) switch operation. Optimization of the sealed ceramic version of this switch should result in a high power switch suitable for a variety of pulsed power applications.

REFERENCES

1) G. F. Kirkman and M. A. Gundersen, "A low pressure light initiated glow discharge switch for high power applications," Appl. Phys. Lett. 49, 494 (1986).

2) K. Frank, E. Boggasch, J. Christiansen, A. Goertler, W. Hartmann, C. Kozlik, G. Kirkman, C. G. Braun, V. Dominic, M.A. Gundersen, H. Riege and G. Mechtersheimer, "High power pseudospark and BLT switches," IEEE Trans.Plasma Science, Vol. **16** (2), 317 (1988).

3) M. J. Shonhuber , "Breakdown of gases below Paschen minimum: basic design data of high voltage equipment," IEEE Trans. Power Appar. Syst. **PAS-88**, 100 (1969)

4) G. Kirkman, W. Hartmann, and M.A. Gundersen, "A flashlamp triggered high power thyratron type switch," App. Phys. Lett. **52**, 613 (1988).

5) C.G. Braun, W. Hartmann, V. Dominic, G. Kirkman, M. Gundersen and G.McDuff, "Fiber optic triggered high-power low-pressure glow discharge switches,"IEEE Trans. Electron Devices, Vol. **35**, (4), 559 (1988).

6) T. Y. Hsu, G. Kirkman, and M. A. Gundersen, "Multiple-gap Back-Lighted thyratrons for high power applications," to be published.

7) The sealed ceramic BLT switch was provided for testing by Integrated Applied Physics Inc. Arcadia, California.

* This work was supported by ARO, AFOSR and SDIO.

** G. Kirkman-Amemiya is also with Integrated Applied Physics, 140 E. Santa Clara St., Arcadia, California 91006

Ignitron Research at Texas Tech University

D. Loree
under the supervision of: M. Giesselmann, and M. Kristiansen
Department of Electrical Engineering
Pulsed Power Laboratory
Texas Tech University
Lubbock, Texas 79406

INTRODUCTION

The ignitron project at Texas Tech University is a joint research effort between Lawrence Livermore National Laboratory, Richardson Electronics/ Division of National Electronics, and the University. The goal of the collective efforts of all participants is the development, testing, and manufacturing of a new generation of high current, high coulomb ignitron switches for pulsed power applications. Part of this goal has been attained with the manufacturing of a restructured pulsed power ignitron, the NL-9000. Research at LLNL has involved high current testing of prototype ignitron designs (~800 kA, 100's C levels). Research at the University has involved studying axial magnetic field effects on ignitron behavior as well as the effects on ignitron performance of wall composition, tube geometry, anode geometry, alternate triggering mechanisms and conduction plasma phenomena.

TEST CIRCUITS AND SYSTEM DESCRIPTIONS

There have been three test stands and three test ignitrons utilized in the three years of ignitron research at Texas Tech University. The three test ignitrons are: (1) the NL-2909, a modified size D ignitron which has all internal components removed except the ignitors, the mercury, and the anode, (2) a glass-walled ignitron which allows the optical study of the conduction plasma at high current, and (3) a full size, fully demountable ignitron (called the DIG) which has limited visual access to the discharge volume via four viewports and which allows the alteration of many internal structures and materials. The first two test stands were configured in such a way as to allow water-cooled electromagnets to apply a DC axial magnetic field to the test ignitron. For this testing, all ignitrons were run in a critically damped circuit configuration with a 2.56 mF, 10 kV capacitor bank but for the holdoff voltage tests, a 1.89 μF, 60 kV capacitor was utilized instead of the bank. Interferometric research on the DIG at higher currents involved the construction of a 1 μH test stand with the DIG acting as a crowbar switch for increased coulomb capability, and the capacitor bank being utilized as the drive source. The series switch in this configuration is a commercial size E ignitron (the

size D ignitrons did not stand up to the testing levels). The Mach-Zehnder interferometer consists of a block C-shaped chamber of square cross-section with the open area used to insert the test stand, various minors and beam splitters with alignment motors, either cascaded Uniblitz shutters or a ferroelectric shutter, and a 2 watt argon laser as the light source. To record all optical results (either fringe patterns from the interferometer or visual plasma features), a Dynafax mechanical rotating camera with an interframe time of 45 μs and an exposure time of 3 μs was utilized.

SUMMARY OF RESULTS

This paper touches on some of the past and present results of the ignitron tests performed at Texas Tech University and displays the directions for future work. Profound effects on hold-off voltage, very similar in nature to a Paschen curve, were found for all three test tubes when placed in an axial magnetic field. The magnetic field effect was found to be very dependent upon wall material and through it field distribution. Optical studies of the effect of the axial magnetic field on the discharge plasma of the glass-walled ignitron revealed structure and intensity differences at the same values of peak current [1]. When trying to compare values of arc resistances for the test ignitrons to other references, a profound difference in values could be seen [2]. We therefore investigated the effect of current risetime on arc resistance and found a correlation. Slower current rise allows more time for plasma formation and thus the formation of a more conductive plasma channel. In looking at other switches, it was found that sculptured contacts in vacuum arc interrupters enhanced arc motion during current conduction. The investigations of anode geometry were designed to show the positive effects of a sculptured anode on anode erosion and overall tube lifetime. Numerical data displays a lower arc voltage at various peak current levels for the slit-cup anode as compared to the solid anode and the cup anode [3]. Interferometry was utilized in conjunction with this phase of the research in order to begin a study of an ignitron plasma during high current conduction periods. Future knowledge of the discharge plasma charged particle density and other plasma behavior will help in the optimizing the ignitron for high peak power applications[4].

Recent research in this laboratory has concentrated on replacing the conventional ignitron ignitor with a spark gap ignitor. It is thought that this will remove a major mechanism of ignitron failure at high currents. Conventional ignitors break off or become shorted and/or untriggerable in the high current, high coulomb regimes interesting to the pulsed power community. Using existing ignitor trigger circuitry with the addition of a step-up transformer, we have shown the practicality of the spark gap ignitor.

REFERENCES

(1) D.L. Adkins-Loree, M. Giesselmann, and M. Kristiansen, "Axial Magnetic Field Effects on Redesigned Ignitrons Utilizing Glass Walls and Cylindrical Dielectric Inserts", Proc. of the 18th Power Modulator Symposium, Hilton Head, South Carolina, June 1988.

(2) D.B. Cummings, R. Kihara, and K.S. Leighton, "High Current Ignitron Development", Proc. of the 18th Power Modulator Symposium, Hilton Head, South Carolina, June 1988.

(3) J.E. Burke, D.L. Loree, M. Giesselmann, and M. Kristiansen, "Optical Study Of The Effects Of Anode Geometry On The Performance Of An Ignitron", Proc. of the 7th Pulsed Power Conference, Monterey, California, June 1989.

(4) D.L. Loree, J.E. Burke, M. Giesselmann, and M. Kristiansen, "Preliminary Interferometric Investigations Of A Demountable Ignitron", Proc. of the 7th Pulsed Power Conference, Monterey, California, June 1989.

Ignitron Research at Texas Tech University

Sponsored by: Lawrence Livermore National Laboratory and Richardson Electronics

Research conducted by : D.L. Loree, J. E. Burke, M. Giesselmann, and M. Kristiansen

Areas of Research:

- Optical Plasma Studies
- Axial Magnetic Field Effects
- Holdoff Voltage Comparisons
- Risetime vs. Arc Voltage Tests
- Anode Geometry Comparisons
- Mach-Zehnder Interferometry
- Spark Gap Ignitor Testing

Test Ignitrons Utilized at Texas Tech University

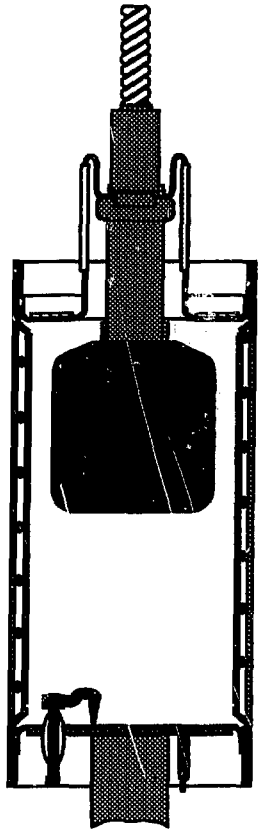

NL-2909

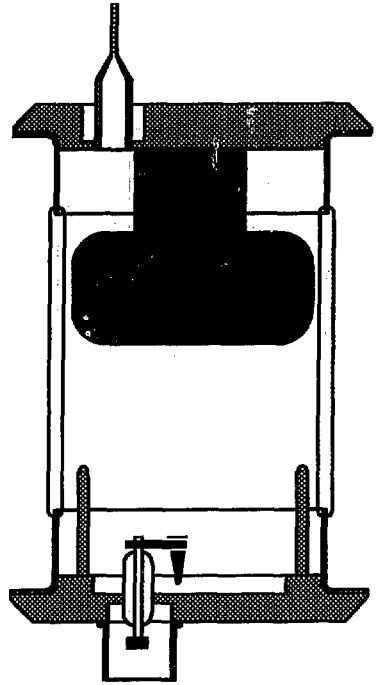

Glass-Walled Ignitron

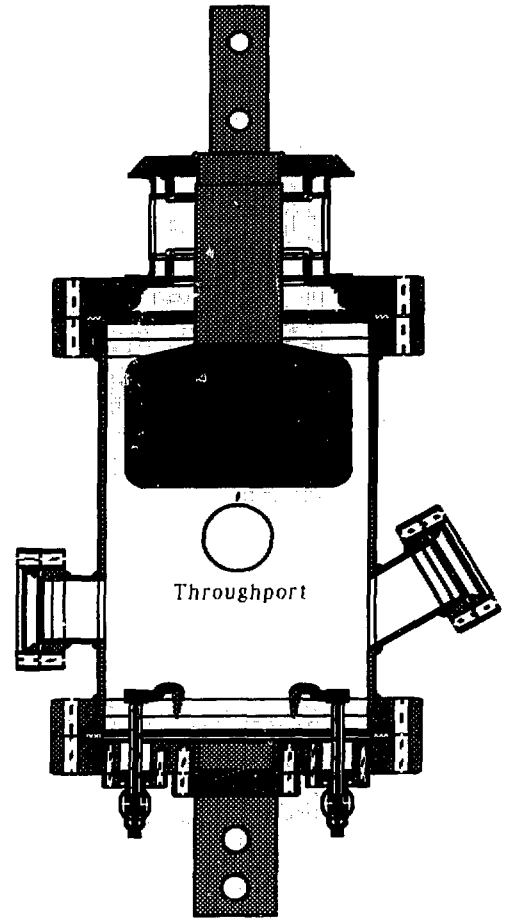

Demountable Ignitron (DIG)

Glass-Walled Ignitron Time Lapse Photographs

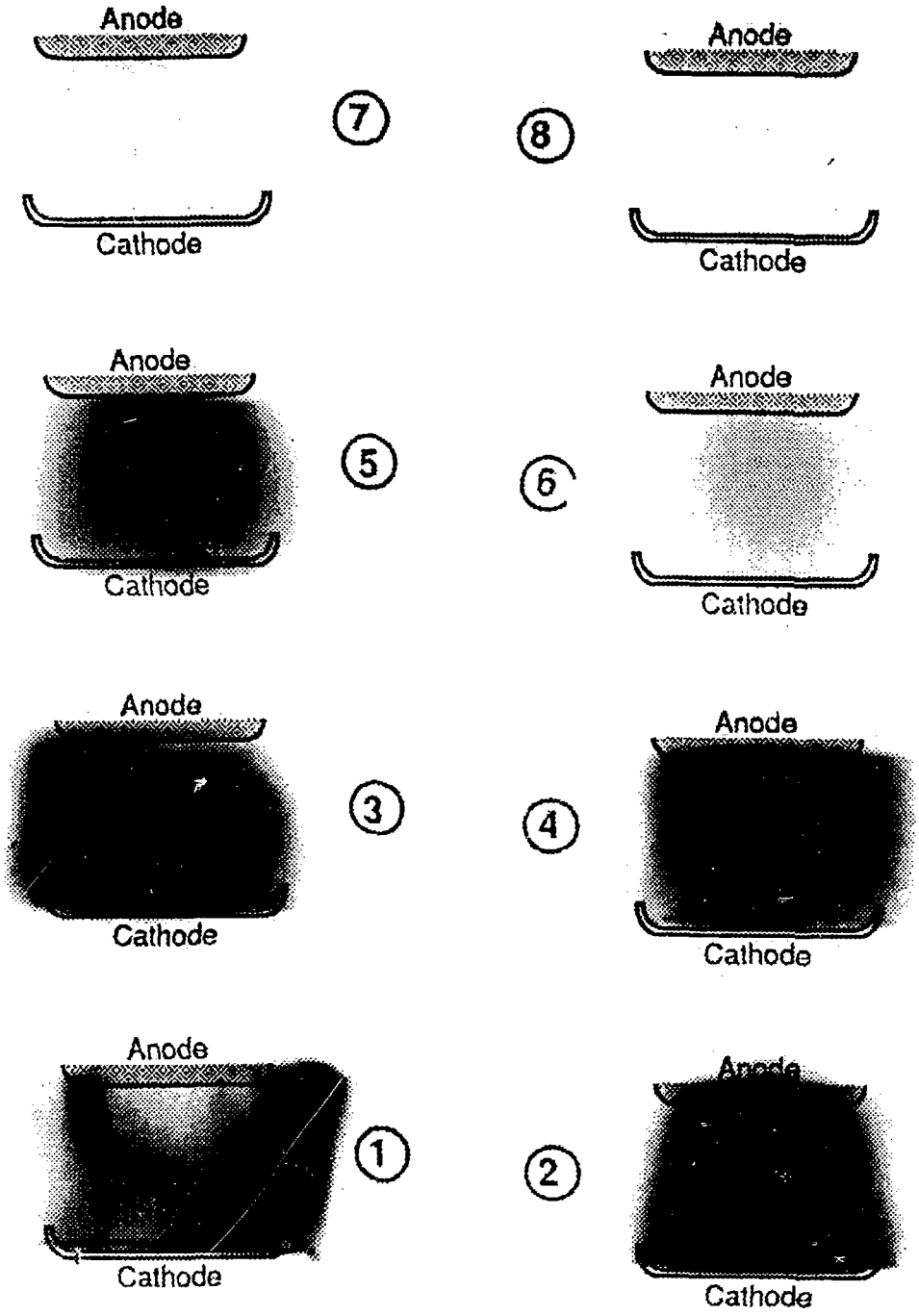

Ip=40 kA, Axial Magnetic Field=0 T

Equipotential Plots and Graphs of the Effects of Axial Magnetic Field on Holdoff Voltage for Different Test Ignitrons

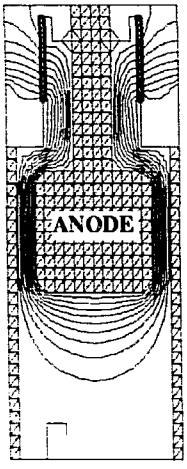

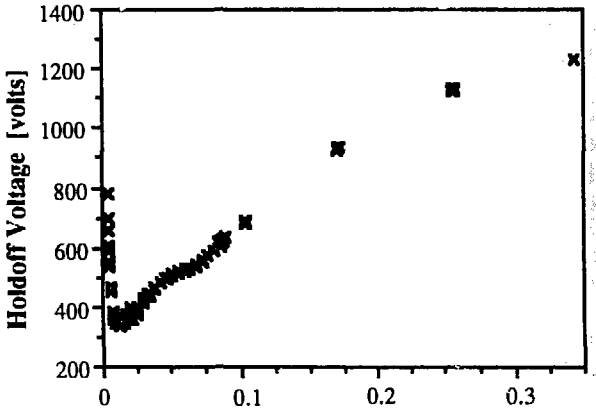

NL-2909 Ignitron

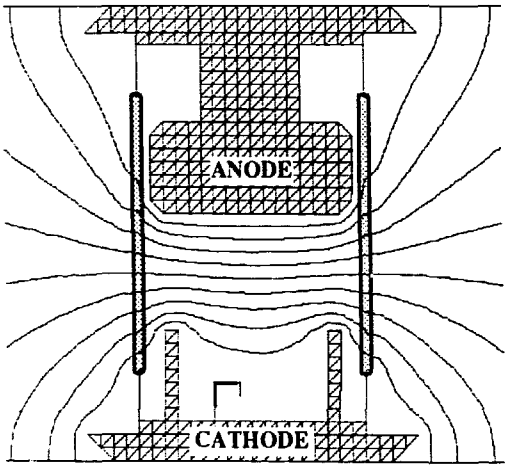

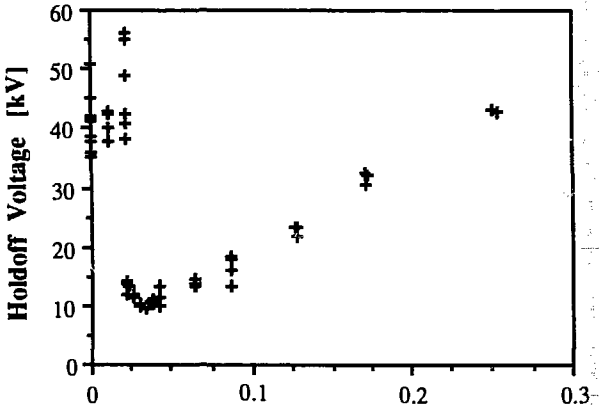

Glass-walled Ignitron

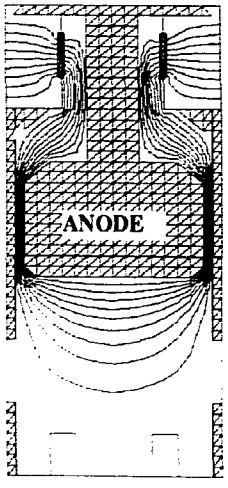

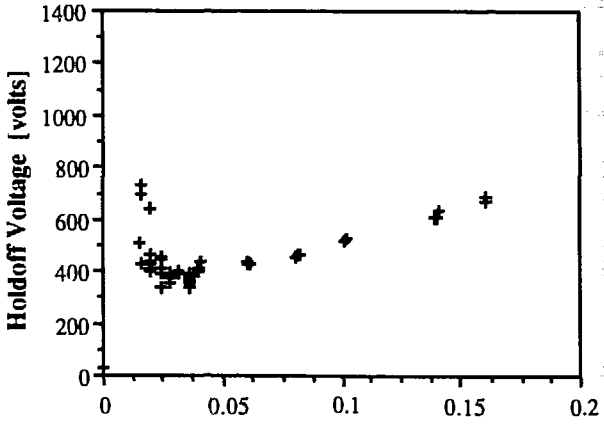

Demountable Ignitron

Effects of Current Risetime on Arc Resistance

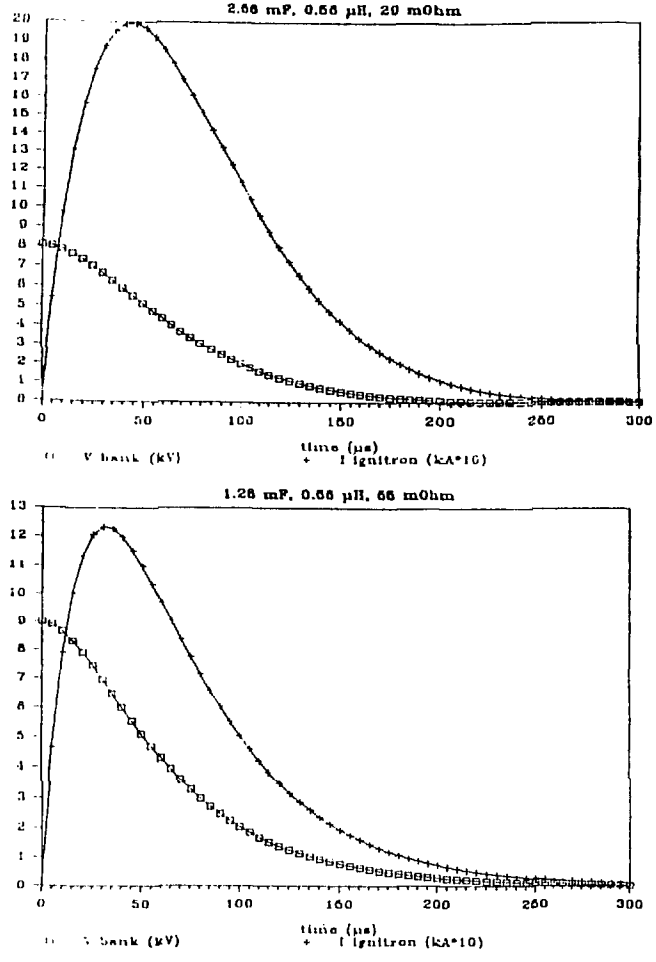

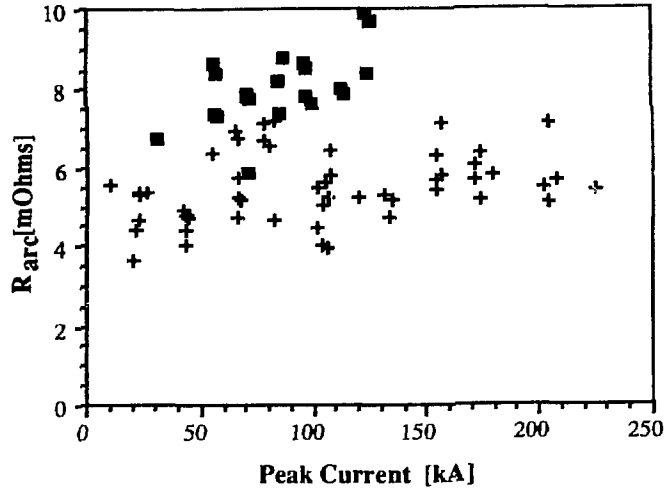

+ = shots with 4 banks
■ = shots with 2 banks

(Rarc measured at peak current and done with DIG.)

Summary: The faster the current risetime, the higher the arc resistance. This is probably due to the plasma formation time.

Effects of Anode Geometry on Arc Voltage

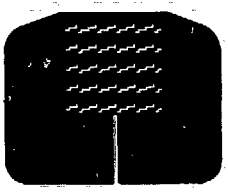

Graphite Anode
(Cross-section)

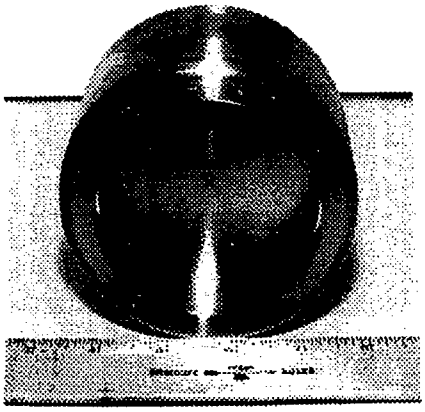

Cup Anode
(Stainless Steel)

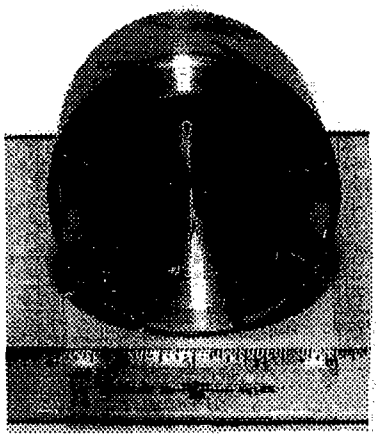

Slit-cup Anode
(Stainless Steel)

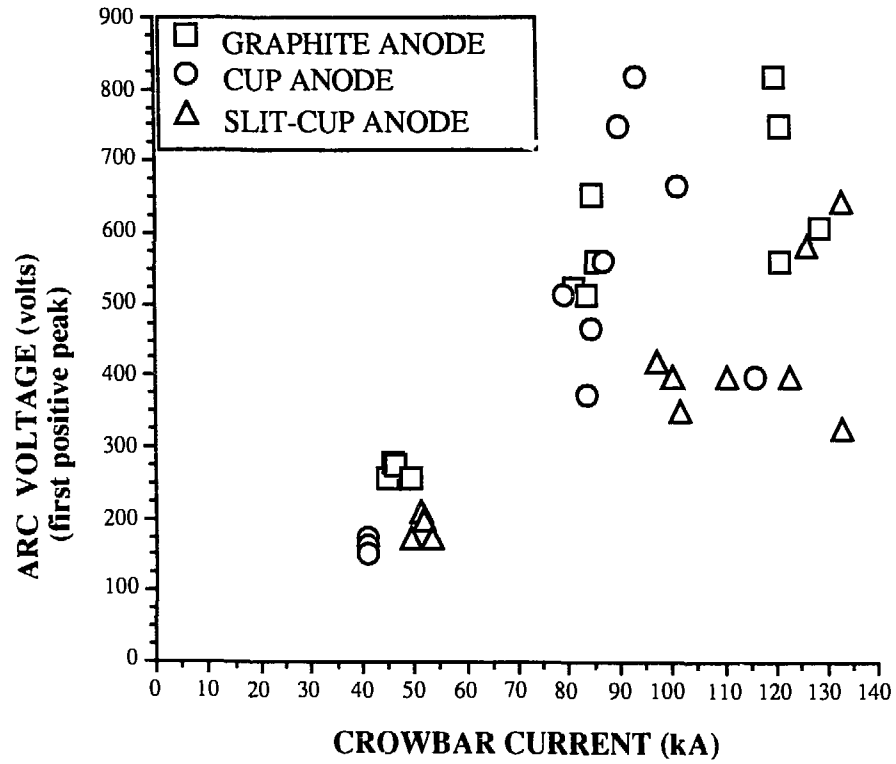

Mach-Zehnder Interferometry System

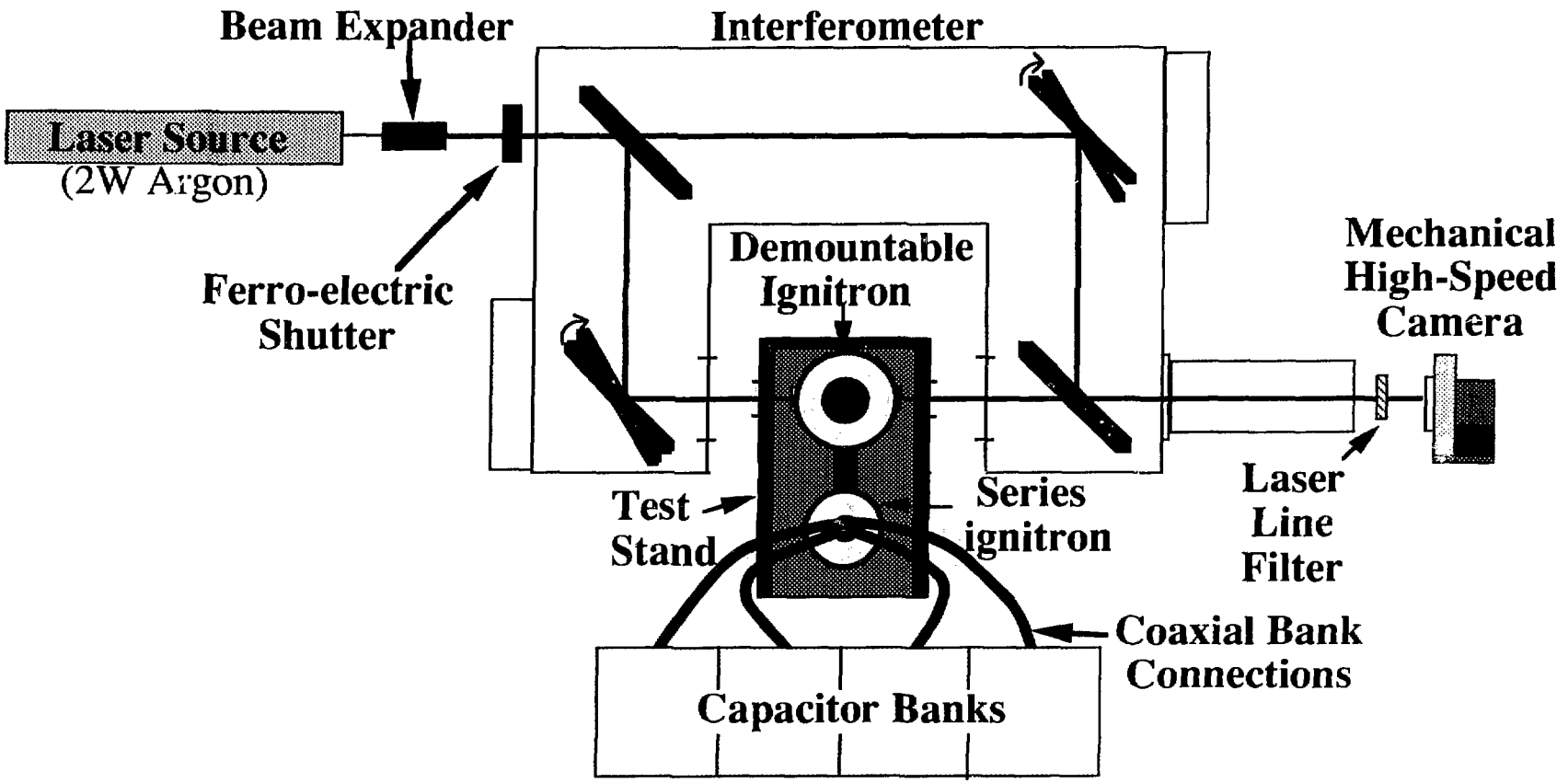

Spark Gap Ignitor Testing

The major failure mechanism for ignitrons under heavy use (high current, high coulomb, or both) is **ignitor failure**. Either the ignitor "shorts" to the mercury cathode and is non-triggerable or it breaks off entirely. Improving the performance of this small feature of the conventional ignitron could improve the device lifetime considerably.

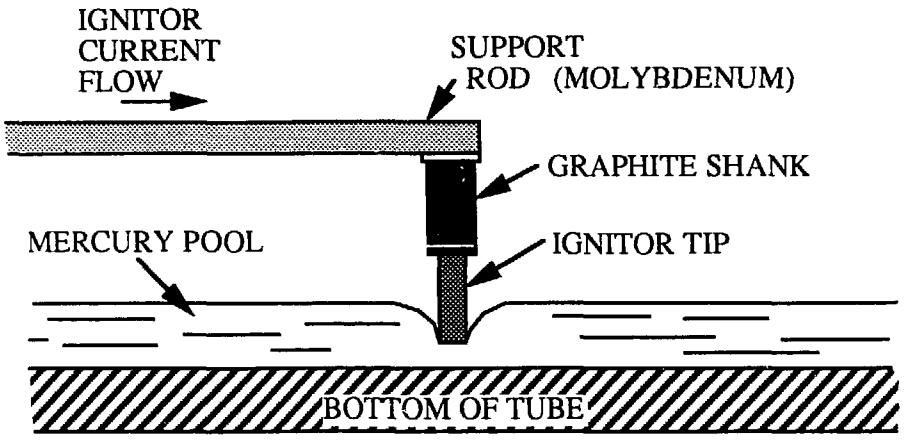

* tip is of a boron carbide compound

CONVENTIONAL IGNITOR DESIGN

We hope to alter the design of the conventional ignitor into a spark gap design which is triggerable by the same type of circuits used to trigger conventional ignitors with only a higher turns ratio on the output transformer. This design will not have the same "shorting" capability and can be made of stronger materials than the conventional ignitor.

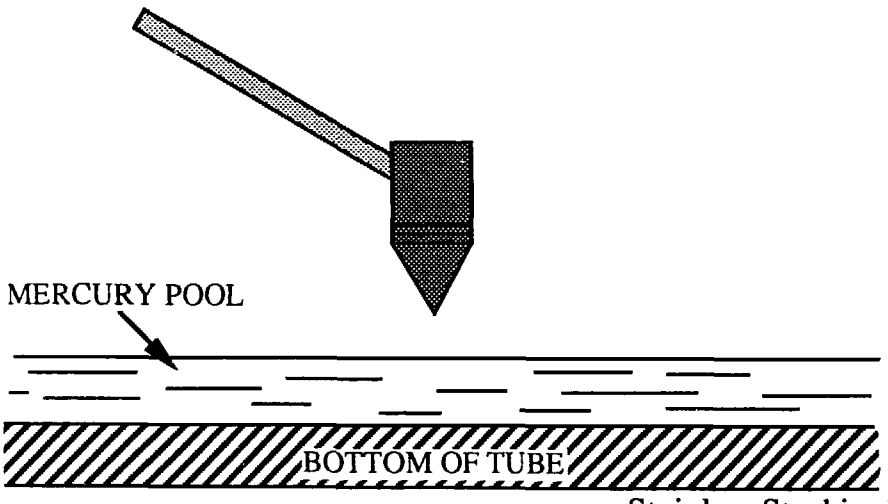

Stainless Steel ignitor

SPARK GAP IGNITOR DESIGN

Voltage Trace of Spark Gap Ignitor

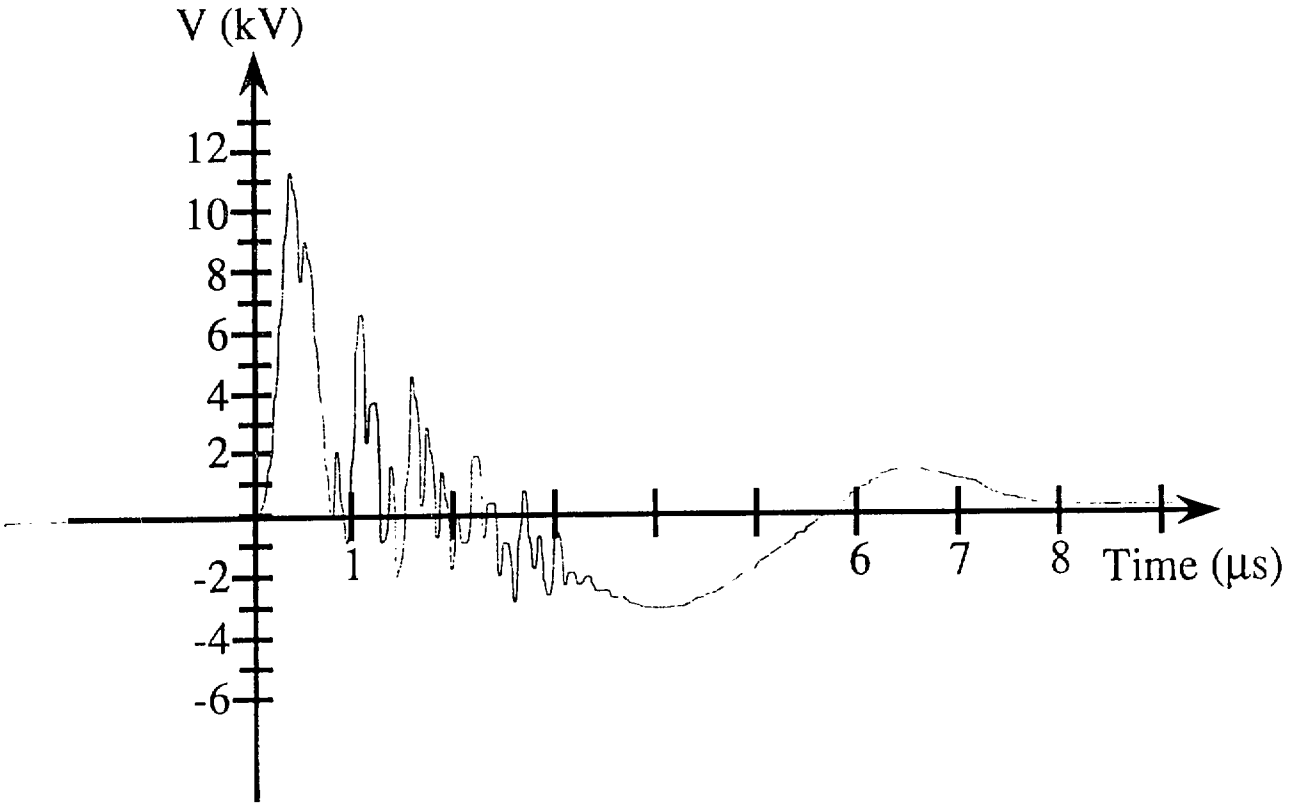

Manufacturer's Changes in Ignitrons Designed for Pulsed Power Applications

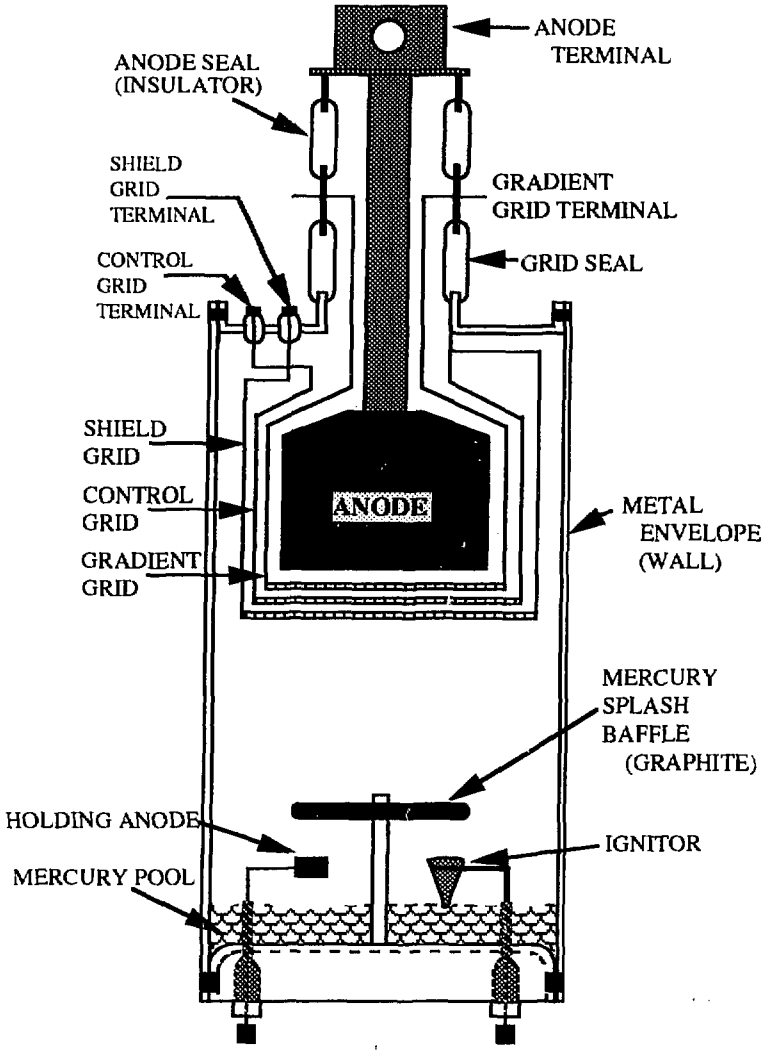

Welding Ignitron

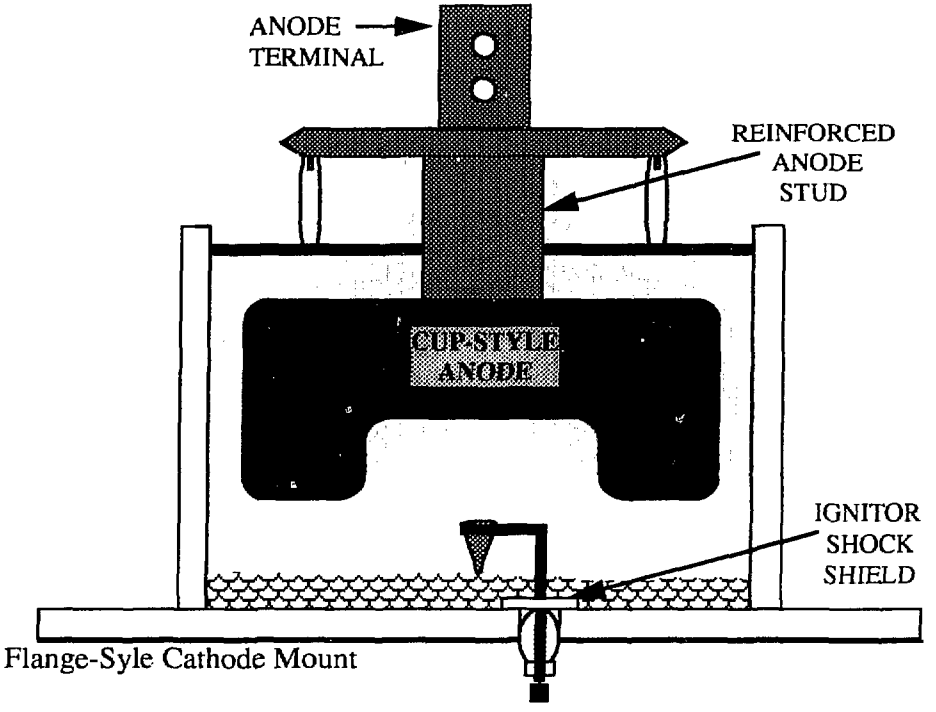

Pulsed Power Ignitron

PRACTICAL ISSUES FOR USING BULK SOLID STATE SWITCHES IN HIGH-REP-RATE MODULATORS

Michael S. Mazzola*, David C. Stoudt*, and
Karl H. Schoenbach

Department of Electrical and Computer Engineering
Old Dominion University
Norfolk, Virginia 23529

* The authors are currently with Naval Surface Warfare Center, Directed Energy Weapons Branch, Dahlgren, Virginia 22448.

What is a Bulk Solid-State Switch?

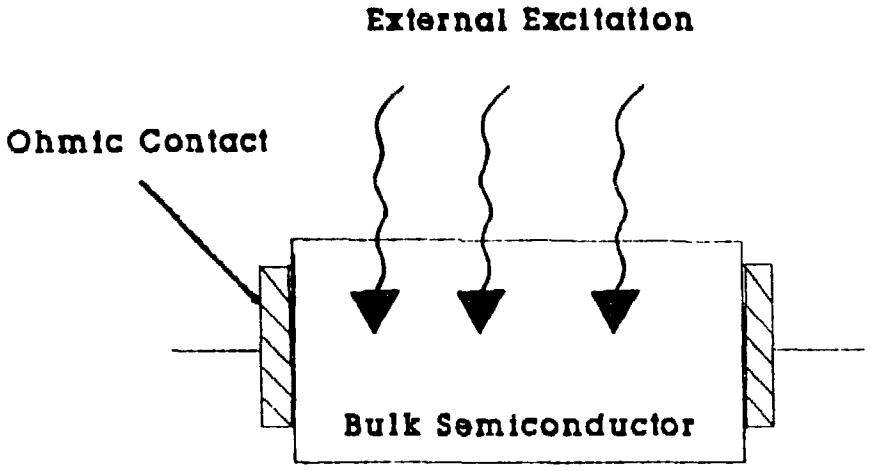

- A large volume semiconductor slab made of some high-resistivity semiconductor such as Silicon, Gallium Arsenide, or Indium Phosphide.
- External radiation (optical or electron-beam) triggers or sustains the conductivity.
- Large volume device structures (p-i-n or n-i-n) are sometimes used.

How are BSS Switches different from other devices (i.e., MOSFET, BJT, SCR, GTO)?

- Short electon-hole pair lifetime in typical semi-insulating GaAs, gold-doped Si, and iron-doped InP can result in sub-nanosecond switch opening for high repetition rate switching.

- Scalability to tens of kV and kA demonstrated, can replace MOSFET and SCR stacks with a single BSSS.

- True optical isolation allows further scaling by stacking BSS Switches, thus eliminating cumbersome gate isolation circuits.

- Radiation absorption processes are so fast (fs) that jitter is limited by excitation source (laser or e-beam)

Types of High-Repetition-Rate BSSS Applications.

- Ultra-wide-bandwidth (UWB) sources (ps switching required)
  - High power microwave generators
  - UWB radar
- Charged particle beam accelerators (ns switching required)
  - RF cavity drivers
  - Auxiliary power conditioning
- Auxiliary power conditioning for magnetic modulators (ps switching required?)

Issues Limiting High-Rep-Rate BSSS Applications:

- Efficiency of light-sustained opening switches typically is very low, thus requiring impractical, large lasers.

- Voltage scaling has been limited by:
  - Surface flashover (typically limited to about 100 kv/cm)
  - Charge injection which limits useful dc voltage hold-off to a few kV/cm.

- Fast opening effect observed at low fields (< 10 kV/cm) fails at high fields due to lock-on effect.

Two concepts are offered to substantially improve BSS opening switch efficiency.

- A 'light-toggled' closing/opening GaAs switch: the Bulk Optically Controlled Semiconductor Switch (BOSS).

- An electron-beam sustained closing/opening GaAs switch: the Electron-Beam Controlled Semiconductor Switch (EBCS).

A Bulk Optically Controlled Opening Switch

- The BOSS concept involves the optical excitation of trapped electrons from deep copper centers in copper-compensated, silicon-doped, semi-insulating GaAs.

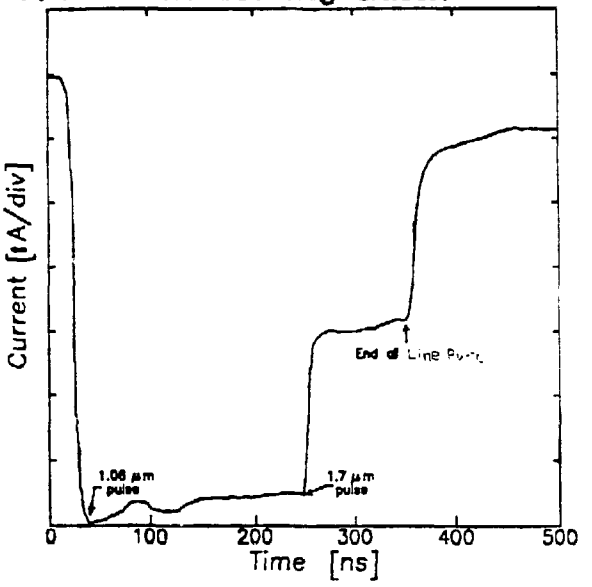

- Photoconductivity with up to μs lifetime can be excited by ns or ps 1064 nm laser pulses.

- Exciting long-life photoconductivity eliminates need for sustaining conductivity with a laser as in conventional GaAs opening switches.

- Photoconductivity can be quenched on command over ns or less with a second~1800 nm laser pulse.

- Reference: M.S. Mazzola, K.H. Schoenbach, V.K. Lakdawala, and S.T. Ko, Appl. Phys. Lett., vol. 55, 2102, (1989).

An Electron-Beam Controlled Closing/Opening Switch

- The EBCS concept involves the bulk excitation of conductivity in a p-i-n GaAs diode through a two-step process. First, an e-beam excites a thin plasma layer which in turn generates volume photoconductivity through the deep penetration of recombination radiation.

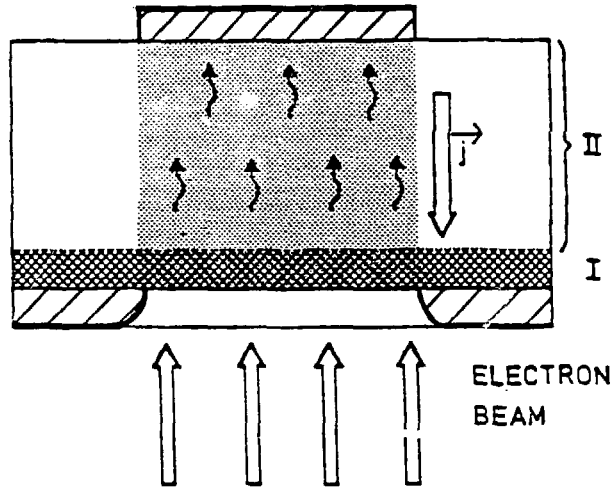

- Sustaining conduction against fast recombination with an e-beam instead of a laser dramatically improves opening switch efficiency.

- Modulation of EBC switch conductivity to form complex waveforms can be achieved with simple e-beam intensity control.

- Reference: K.H. Schoenbach, V.K. Lakdawala, D.C. Stoudt, T.F. Smith, and R.P. Brinkmann, IEEE Trans. Electron Devices, vol. 36, 1793, (1989).

Voltage hold-off has been improved by controling:

- Surface flashover with optomized electrical contact materials and geometries, and dielectrics so that fields)140 kV/cm have been achieved.

- Charge injection by:
  - Pulse-charging purely bulk switches, or
  - Forming large area p-i-n and n-i-n device structures to allow dc charging.

For example, a bulk semi-insulating GaAs switch with ohmic contacts exhibits the following dark I-V curve:

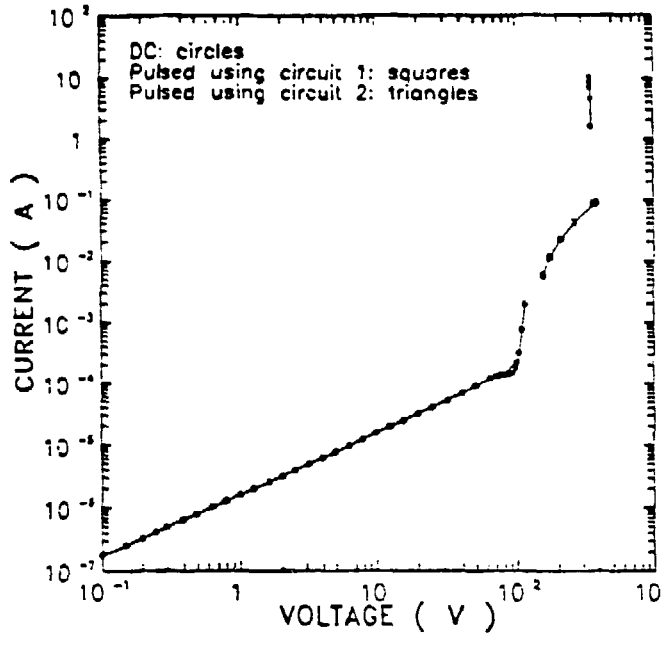

With a large area (1 cm^2) p^+-n^- GaAs switch, the vertical transition is suppressed:

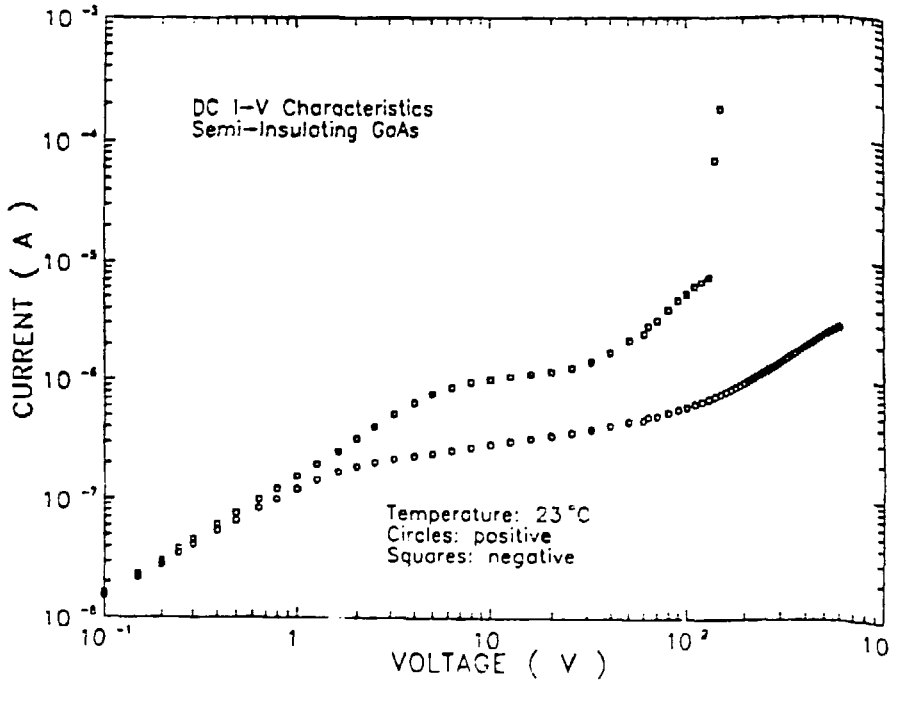

Control of lock-on will be achieved by:

- Understanding the mechanism behind lock-on so that structures can be implemented to control it.
  For example:
  - Lock-on may be related to charge injection which results in a super linear rise in dark current at fields)2 kV/cm.
  - Charge injection can be controlled by p-i-n or n-i-n device structures.
- Optical quenching (see the BOSS concept) has been shown to interrupt lock-on in Cu:Si:GaAs, at least temporarily (see the following slide).

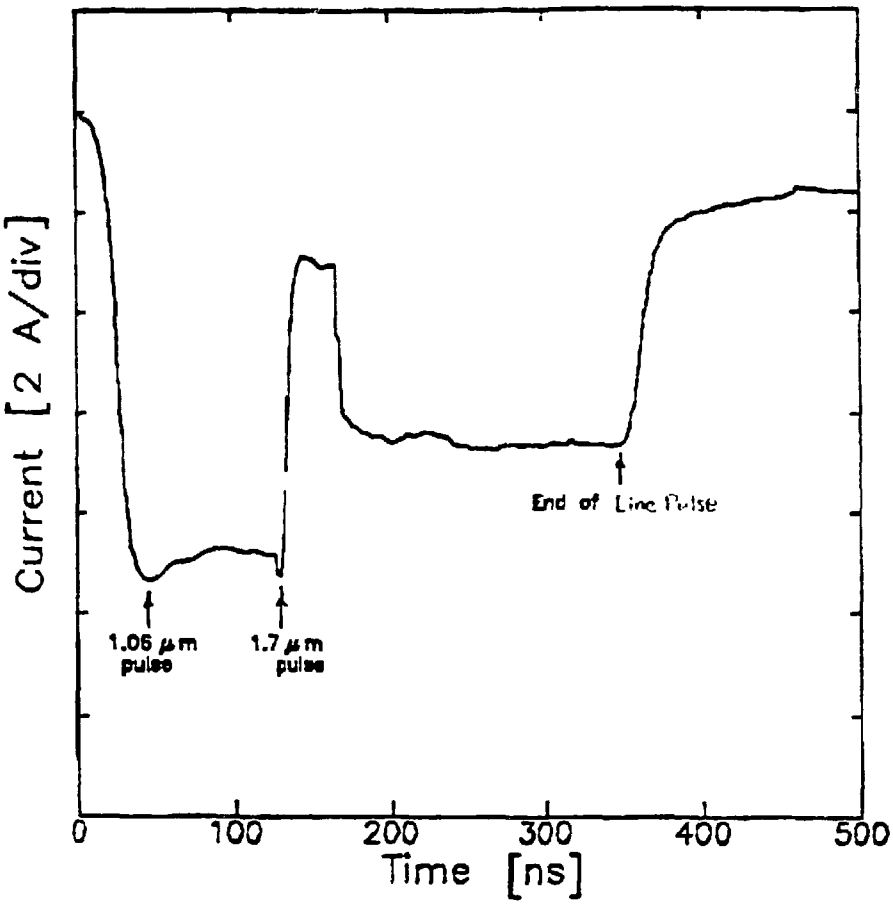
Current [2 A/div]
1.06 μm pulse
1.7 μm pulse
End of Line Pulse
0
100
200
300
400
500
Time [ns]

MCT PERFORMANCE CHARACTERIZATION

Stephen A. Merryman

Space Power Institute
Auburn University, AL

Ph. (205)844-5922
FAX (205)844-5900

International Workshop on Magnetic Pulse Compression

February 12-14, 1990

Granlibakken
Lake Tahoe, CA

MCT Performance Characterization

Stephen A. Merryman

Space Power Institute
Auburn University, AL

International Workshop on Magnetic Pulse Compression

February 12-14, 1990

Granlibakken
Lake Tahoe, CA

Abstract

MOS-controlled thyristors (MCT's) are being considered for use in power conversion systems. Because of their relatively high current densities and high frequency of operation, they present the opportunity for significant weight and volume savings, a primary consideration for space power systems. Additionally, the thermal management problem is simplified because the low forward voltage drop across the device reduces the losses substantially. However, before MCT's realize their full potential for practical applications, their performance specifications must be determined. The research at the Space Power Institute at Auburn University focuses on determining the performance characteristics (turn-on time, turn-off time, gate trigger requirements, etc.) of MCT's under severe thermal stresses (temperature range from -196 C to 250 C). Also, the maximum single-pulse (non-destructive) current level is being investigated to determine the upper current limit at which MCT's can safely operate. The current distribution between multiple MCT's connected in parallel is also being studied. Knowledge of these performance characteristics is important both for the design of space power systems with high reliability and for future device developers to improve these characteristics.

Research Objectives

Why consider MCTs?

[V. A. K. Temple, "MCTs-thyristors for the future," *Power Technics Magazine*, November 1989, pp. 21-24.]

- ability to control both **turn-on** and **turn-off** of the device
  - 200 ns turn-on time, 2 μsec turn-off time
- relative **high current densities** and **high frequency** of operation present opportunity for significant **weight and volume savings** (a primary consideration for space power applications)
- **low forward voltage drop** reduces losses substantially, thus reducing the thermal management problem
- mixes the ease and speed of MOS gate control with the high voltage and current capability of thyristors

Goals

- determine the performance characteristics of MCTs under severe thermal stresses (-196 C to 250 C)
- determine the maximum single-pulse (nondestructive) current
- characterize current sharing in multiple MCTs connected in parallel

MCT Operation

MCT Equivalent Circuit

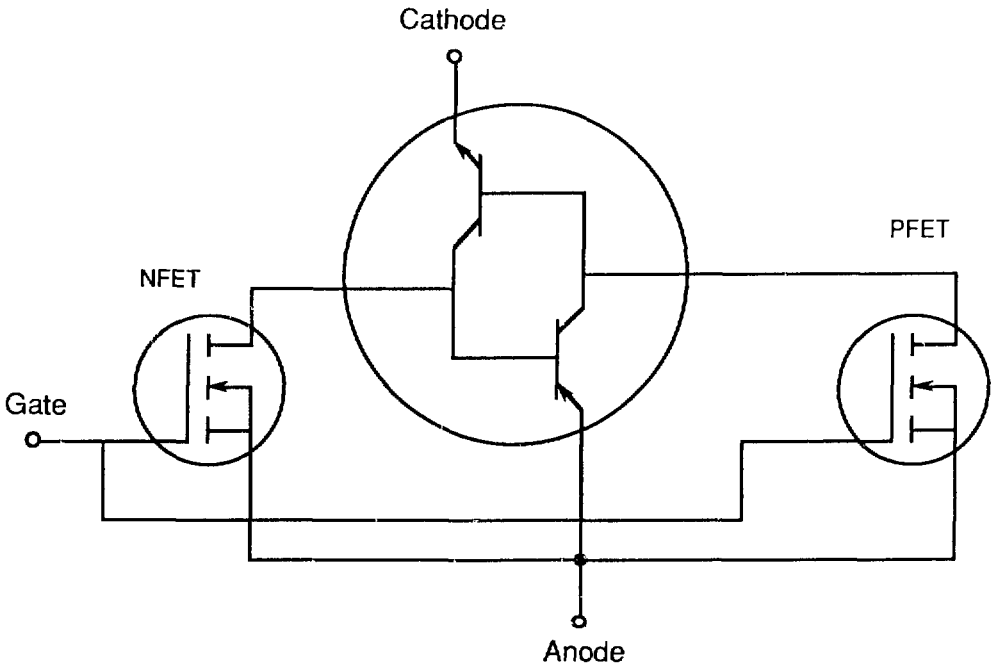

Figure 1 MCT Test Circuit

MCT operation can be described as a bipolar NPNP thyristor with opposite polarity FETs connected between its anode and the appropriate layers to turn it on and off. Since an MCT is a NPNP device, the output terminal (cathode) must be negatively biased. To turn on the MCT, a negative voltage (-5 V) with respect to the anode is applied to the gate terminal which turns the P channel FET on, firing the bipolar SCR. To turn off the MCT, a positive voltage (~14 V) with respect to the anode is applied to the gate which turns on the N channel FET; thus, the base drive to the PNP bipolar transistor making up part of the SCR is shunted, causing the SCR to turn off.

Experimental Setup

MCT Test Circuit

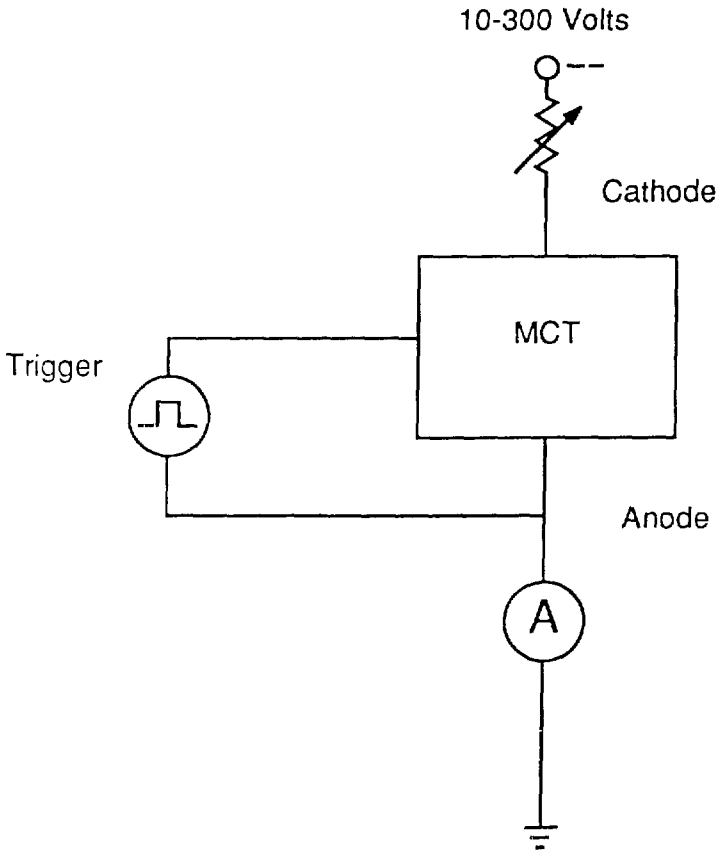

Trigger source was a function generator with ~20 V_{p-p} with a DC offset so that voltage levels of a square wave could be set at -5 V and +14 V

Temperature of MCT was controlled by heating an aluminum block (7" x 7" x 1.5") to which the MCT was mounted.

For leakage tests, the gate was held at +14 V using a DC power supply.

Experimental Tests

Parameters Tested

- Minimum controllable current, I_{on}
- Turn-on voltage (minimum MOS switch voltage necessary to control I_{on})
- Turn-off voltage (complement to turn-on voltage)
- Leakage current, I_l, during voltage standoff
- Forward voltage drop, V_{ak}, across the device
- Parameters determined from turn-off waveform
  - T_{doffi}, time from trigger point to 90% I_{max}
  - T_{fi}, time from 90% tp 10% I_{max}
  - T_{ei}, time from trigger point to I=0
  - T_{doffv}, time from trigger point to 10% V_{max}
  - E_v, integral of V*I from t_o (trigger point) to t_1 (90% V_{max})
  - E_i, integral of V*I from t_1 to t_2(I=0)
  - E_t, $E_v + E_i$

Each of the above parameters were recorded for a combination of voltages (usually 10, 50, 100, and 200 V) over a wide temperature range.

- Initial tests at higher current and power levels (with emphasis on current sharing between devices in parallel) is currently underway

Results

The following figures illustrate typical results for many of the tested parameters as a function of temperature.

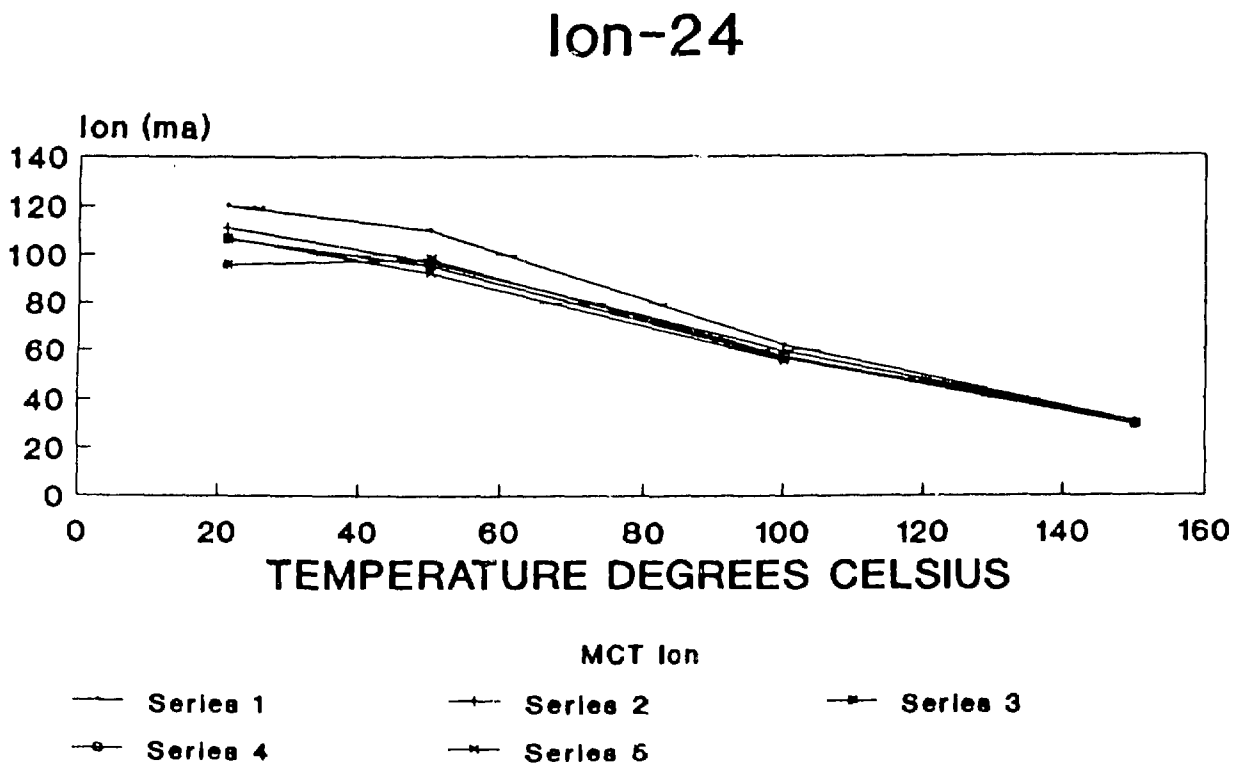

Figure 3 Minimum Controllable Current

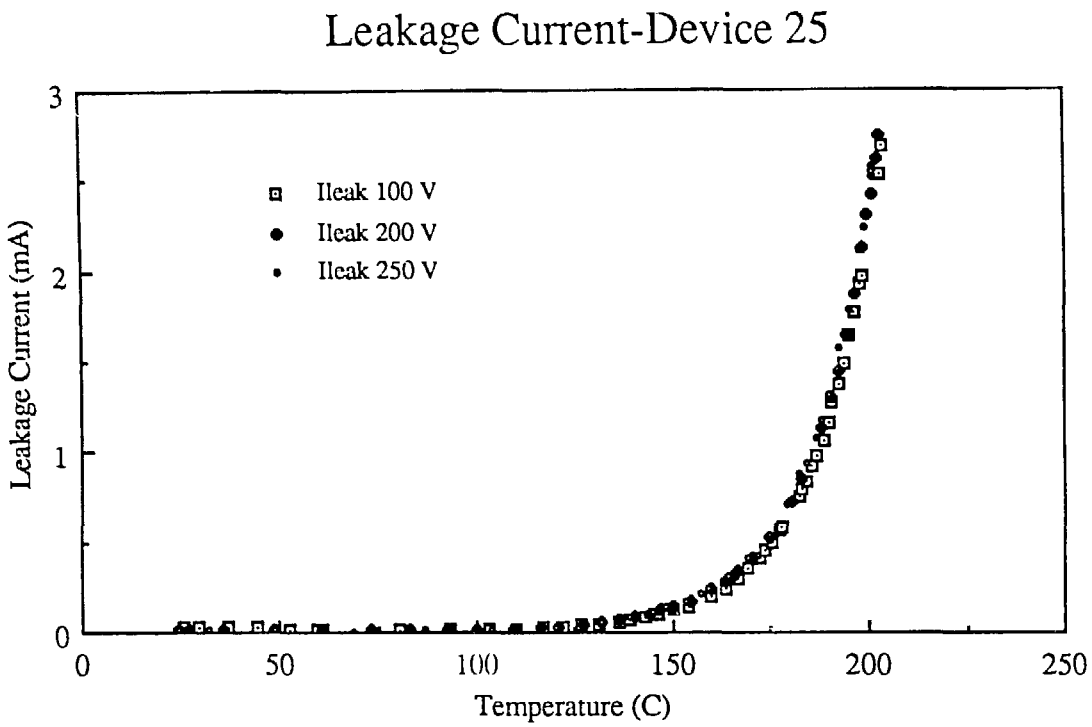

Figure 4 Leakage Current

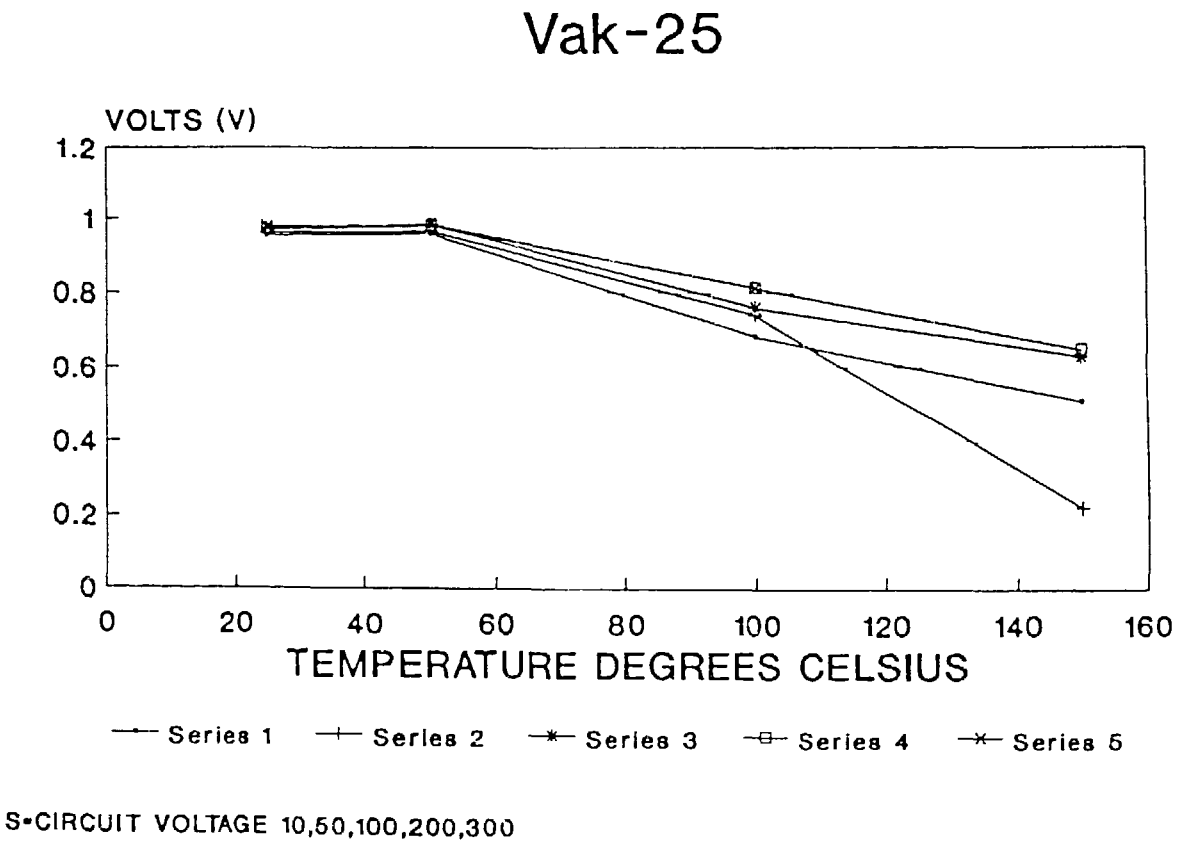

Figure 5 Voltage Drop Across the Device

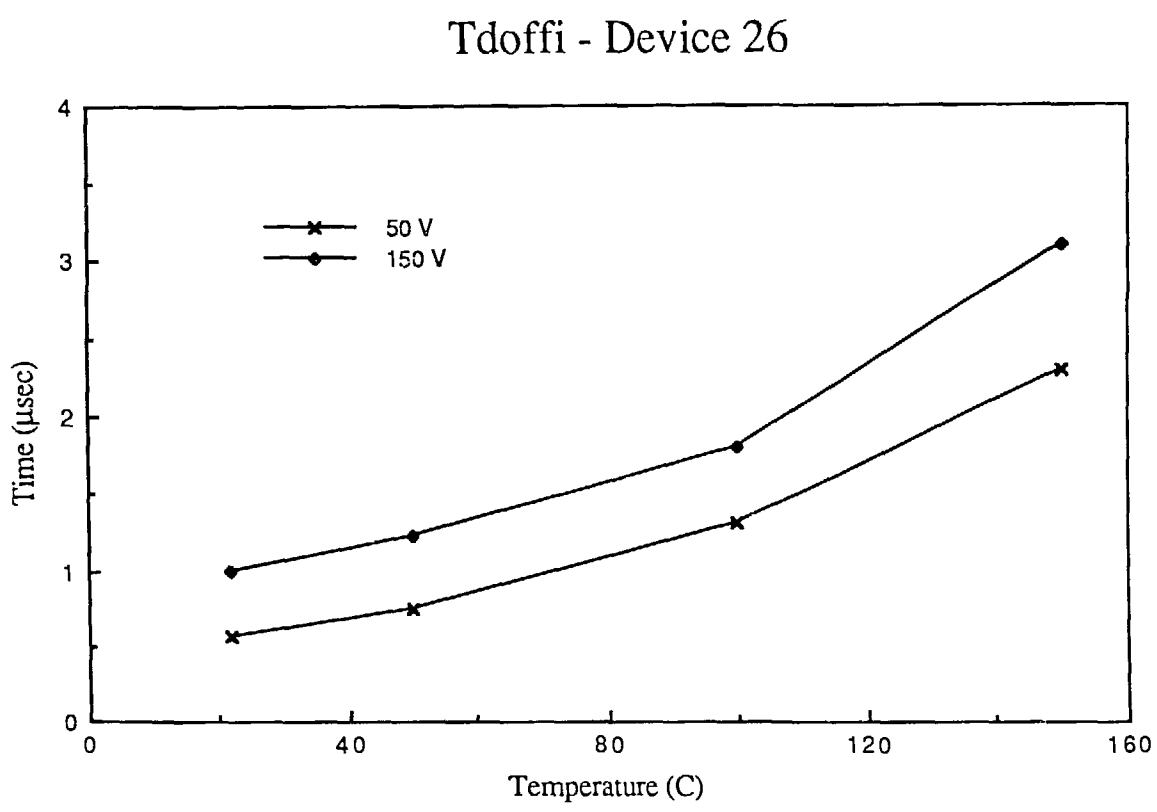

Figure 6 Time from Trigger Point to 90% I_{max}

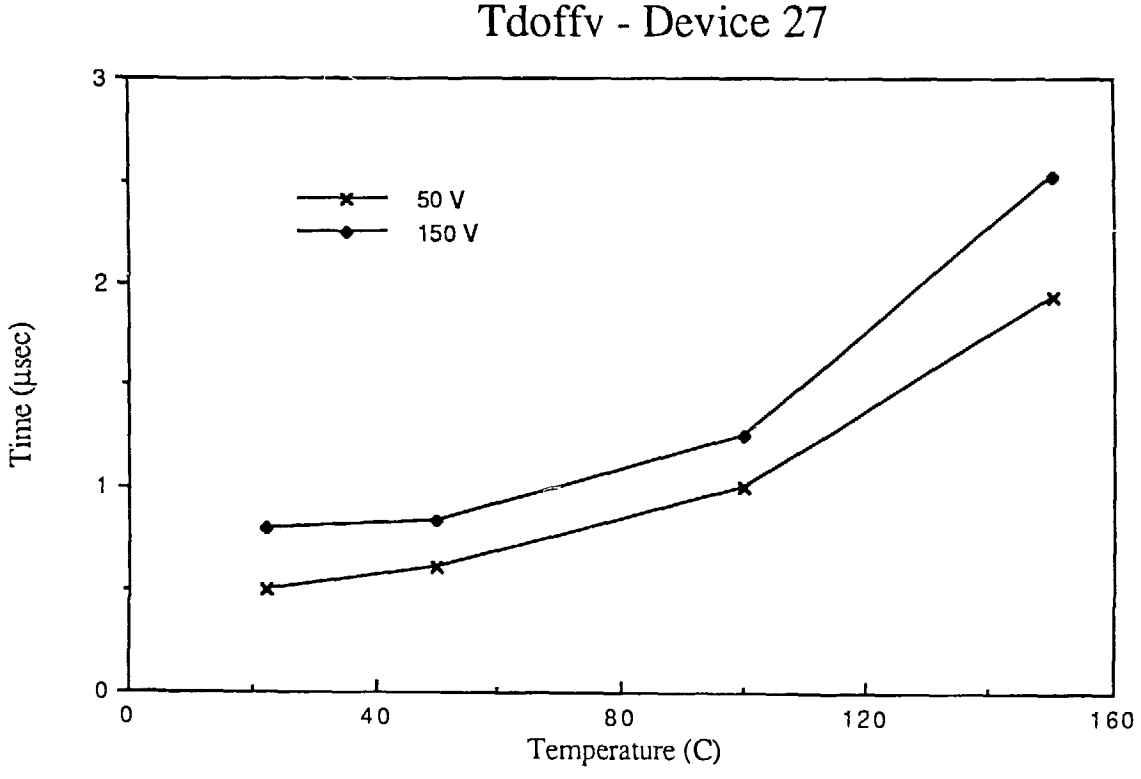

Figure 7 Time from Trigger Point to10% V_{max}

Summary and Conclusions

- Irradiated devices (4 MRAD) were unreliable at lower temperatures and difficult to turn-on
- Irradiated (4 MRAD) devices operated more reliably at elevated temperatures
- I_{on} decreases as temperature increases and shows a slight decrease with increased voltage
- I_ℓ increased rapidly for increasing temperatures above approximately 125 C
  I_ℓ was independent of device voltage and rate-of-rise temperature
- V_{ak} increases with increasing circuit voltage, but decreases with increasing temperature
- T_{doffi} and T_{doffv} increased with an increase in temperature and were slightly higher for higher voltages
- T_{fi} and E_t did not show much variation for increasing temperatures, but were higher for higher voltages

Problems Encountered

- Devices 23 and 24 (GE Lot#9789B003-13) latched into an intermediate ON condition when tested at 200 C.
- Device 23, which was used extensively during preliminary testing and equipment setup, no longer has gate control. The device is normally ON.
- Device 25 failed after testing at 200 C (no longer able to turn the device on)
- Device 28 failed during a 50 C test. Device was tested at -196 C (where a high V_{on} and I_{on} was required to turn it ON) prior to the test during which it failed.

Future Directions

- Testing of packaged, nonradiated devices at low temperatures (down to liquid nitrogen temperatures)
  - awaiting delivery of devices
- Testing of unpackaged, radiated devices at elevated temperatures, looking at junction temperature with IR thermography using Mikron Thermal Tracer
  - awaiting delivery of devices
- Determine maximum single-pulse current limit (non-destructive)
- Continue to characterize operation of devices connected in parallel

TRIGGERED CONDUCTION CHARACTERISTICS OF THE MAGNETICALLY DELAYED VACUUM SWITCH

Gibson Morris, R. A. Dougal
Dept. of Electrical and Computer Engineering
University of South Carolina
Columbus, S.C. 29208

Abstract

Utilization of a saturable inductor to delay the onset of current through a vacuum gap alleviates the poor turn-on performance (large jitter, high power dissipation, long current risetime) inherent in vacuum switches, thus allowing the advantages (high voltage holdoff, fast recovery, high repetition rate) to be realized. The concept is to hold off the main current with the saturable inductor until a sufficiently dense plasma channel exists in the vacuum gap to conduct the main current. In this way electrical stress on the switch is minimized; however, failure to inject sufficient plasma into the vacuum gap during the trigger activation period results in degraded switch performance. Recent investigations indicate that insufficient plasma injection manifests itself as a transient interruption of the main current. The nature of this phenomenon and its causes, in terms of switch and plasma dynamics, is the focus of current research.

Introduction

Many of the requirements demanded of a high performance switch (fast recovery, high voltage hold-off, and wide triggering range) are satisfied by the vacuum gap switch. However, these switches exhibit slow current risetime and excessive power dissipation during the turn-on phase[2][3]. These poor turn-on characteristics are a result of the requirement to generate a conducting medium of sufficient density to support a high discharge current. Therefore if a sufficient conducting medium is injected into the vacuum gap during a period when current is suppressed by a saturable inductor, significant improvement in switch operation is observed. This improvement manifests itself in lower jitter, improved turn-on performance, and less electrode erosion. The problem of establishing a sufficiently dense conducting channel during the inductor holdoff period is complex and depends on gap spacing, electrode and trigger insulator material, plasma dynamics, as well as inductor core characteristics. Reduction in electrode erosion, while significantly increasing switch lifetime, also reduces the plasma density that contributes to the conduction channel. Therefore, the beneficial aspects of closely coupling a saturable inductor and a vacuum gap to optimize switch performance are partially offset by the requirement to generate additional plasma at the outset to compensate for the shortfall created by reduced electrode erosion. This balance between erosion, trigger plasma injection, and overall switch performance is a main component of our current research.

Operation

Successful operation of the Magnetically Delayed Vacuum Switch (MDVS) requires that the saturable inductor prohibit current conduction until the vacuum gap becomes filled with a sufficiently dense conducting medium to sustain the main discharge current. Therefore, injection of sufficient conducting plasma during the inductor hold-off period is a critical design parameter. A vacuum switch operates in a current limited mode instantaneously upon injection of a trigger plasma. This current limitation results from a lack of sufficient ion density to neutralize negative space charge beyond the expanding boundary of the trigger plasma. Onset of higher currents cannot occur until the relatively slowly expanding plasma traverses the gap. The high voltage normally appearing across the gap during this phase accelerates electrons to high energies causing significant impact damage to the electrodes and coupling large amounts of energy into material ejection processes[4]. Voltage stress in the MDVS on the other hand, is transferred from the vacuum gap to the magnetic switching element during the period the trigger plasma traverses the gap. The magnetic switch saturates only after the plasma propagation interval, then transfers voltage stress to the load. The plasma filled gap immediately achieves conduction in a diffuse mode and the current risetime is limited only by the saturated inductance of the magnetic switch. The net result of this process is a reduction in electrode erosion, faster current rise time, and improved turn-on performance of the switch.

Experimental

The MDVS (fig.1) test assembly consists of a vacuum gap with two main electrodes, the anode of which is coupled directly to a saturable inductor. The trigger assembly is housed in the cathode and consists of a barium titanate insulator and a thoriated tungsten trigger pin. Firm contact at the triple junctions is maintained by a counterpoised spring arrangement in the trigger assembly. The energy store consists of a variable number of 25-ohm, 250-ns transit time coaxial cables that can be charged to voltages as high as 50-kv. Energy is switched into a matching resistor assembly for which the total impedance is variable between 10 and 50 ohms.

In previous investigations, a krytron based trigger circuit that generated a 100-amp, 200-ns pulse resulted in reliable triggering of main current discharges to 600-amps. Also previously observed was a substantial reduction in switch losses when using magnetic assistance (figs. 3,4). Visual observation of electrodes during these investigations confirmed a significant reduction in electrode erosion in the MDVS[1]. However, the krytron trigger circuit was not capable of operation at high repetition rates.

Recent investigations indicate that insufficient trigger energy results in a transient interruption in the main discharge current as illustrated in fig. 5. Preliminary results indicate that a direct relationship exists between the trigger current amplitude and turn-on performance of the vacuum gap. Current investigations are focused on reducing MDVS jitter and eliminating the interruption processes. This current interruption behavior has been studied as a function of several gap parameters: anode material, gap distance, main current, and trigger current were each varied. Preliminary results indicate that for a given anode material, gap spacing, and main current, a minimum trigger current is required for good switch performance. For larger gap separations, higher main currents, or harder anode materials, larger trigger currents are required. For example, using aluminum main electrodes and a gap spacing of 2mm, a trigger current of 80-amp resulted in good conduction of a 500-amp discharge. When the main

discharge current was increased to 1000 amps, a transient current interruption similiar to that shown in fig. 5 resulted. Increasing the trigger current to 125-amp resulted again in good conduction performance. However, for a 125-amp trigger current, when the gap spacing was increased to 5mm or the aluminum electrode replaced with stainless steel, poor performance was once again exhibited. These observations support the proposition that injection of sufficient trigger plasma is essential to good switch performance. Insufficient plasma injection results in poor turn-on performance and increased losses in the main switch, which in turn translate to increased electrode erosion and a reduction in switch lifetime.

Since one of the desired characteristics of a good switch is low jitter, a series of preliminary experiments were conducted to ascertain the MDVS jitter. Jitter is defined as the deviation in delay between the onset of 10% of trigger current and 10% of main current. Initial results indicate that a jitter<5-ns (fig.7) is possible, providing the trigger current rising edge is uniform, i.e., a fast trigger current risetime is important in minimizing jitter.

Most of the power dissipation depicted in fig. 4(a) is due to the discharge of the stray capacitance of the vacuum gap. The current associated with this discharge facilitates the generation of trigger plasma. Enhancing this process should lead to increased plasma density for a given trigger energy thereby reducing/eliminating the unwanted transient current interruption.

To achieve the desired repetitive triggering capability, a solid state trigger circuit was designed using an insulated gate bipolar transistor (IGBT)(fig.6). The IGBT can operate at high current densities but requires very low gate drive power because of its mos gate. While the IGBT circuit can reliably trigger the MDVS at the required repetition rate, trigger current rise time and amplitude are insufficient to obtain the desired jitter and turn-on performance of the MDVS. Therefore we are currently designing a magnetic pulse compression circuit that will modify the IGBT trigger circuit output to produce the desired trigger pulse, i.e., 200-amp, 30-ns rise time, 20khz pulse.

Summary

The advantages of the MDVS over the vacuum gap switch have been demonstrated. Further work is required to optimize the triggering system to reduce/eliminate effects caused by insufficient plasma injection. Understanding the current interruption processes depicted in fig. 5 should ultimately result in prevention of this phenomenon, thereby significantly reducing power dissipation in the switch and improving electrode lifetime. Additionally, reduction in power dissipation should enhance switch recovery, since fewer discharge byproducts will remain in the gap after current cessation. Finally, improving risetime of the trigger pulse with a magnetic pulse compressor should reduce switch jitter.

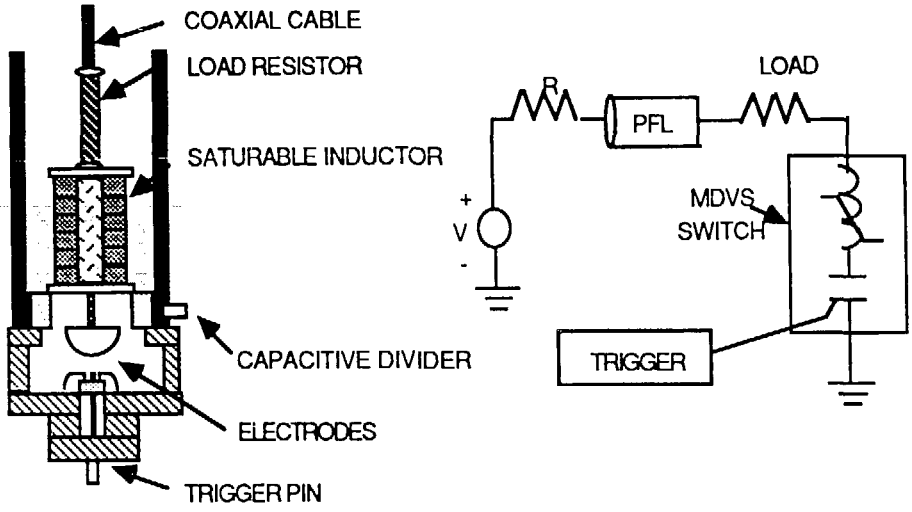

Fig. 1 Magnetically Delayed Vacuum Switch

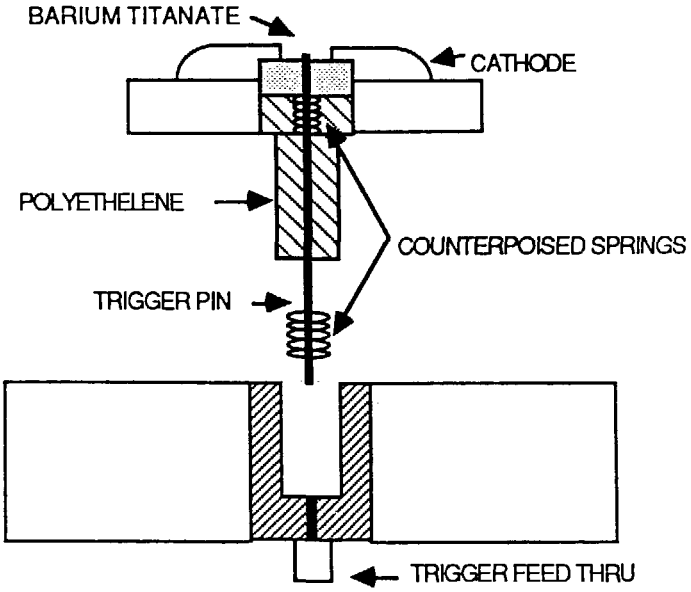

Fig. 2 Trigger Assembly

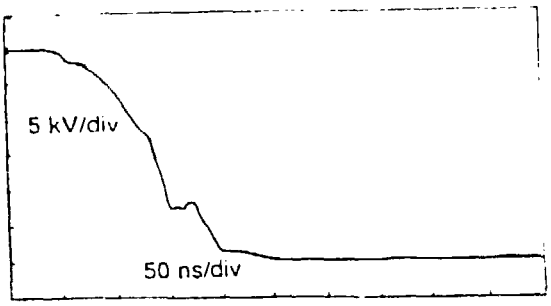

(a)

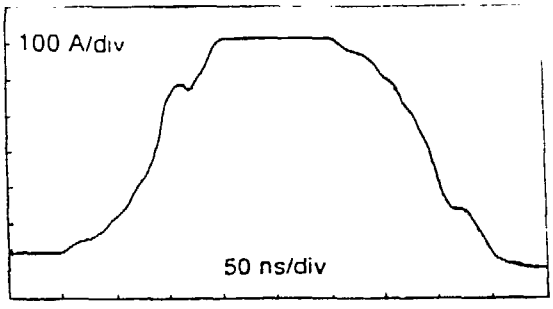

(b)

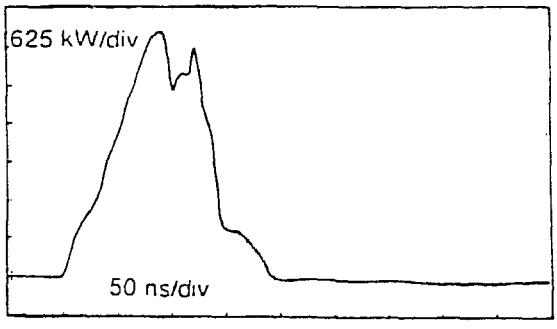

(c)

Fig. 3 Unassisted Vacuum Switch. (a) Load voltage (b) Load current (c) power loss Note large power loss.

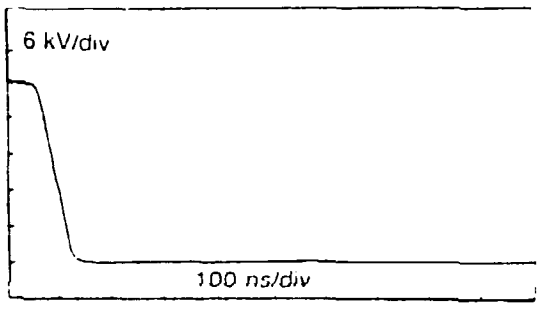

(a)

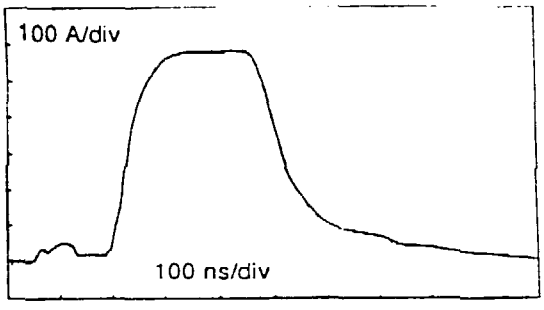

(b)

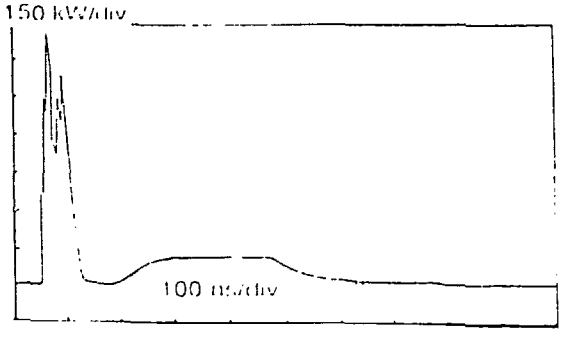

(c)

Fig. 4 MDVS . (a) Load voltage (b) Load current (c) Power loss
Note reduction in power loss, mainly confined to the period during switch capacitance discharge.

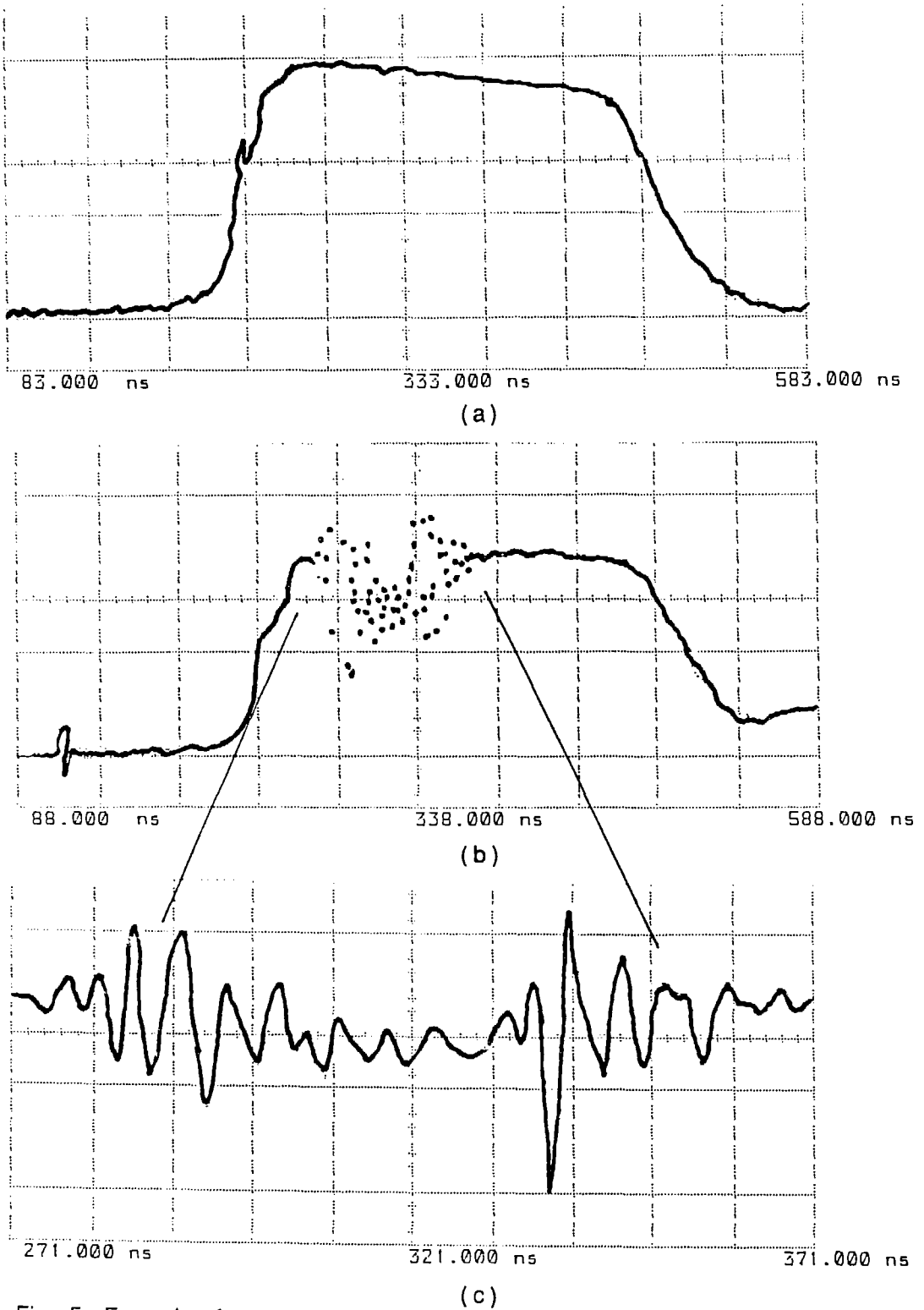

Fig 5 Example of current interruption phenomena. Main current-500amps (aluminum anode, gap-2mm). (a) Trigger current 76 amps, 50-ns/div. No current interruption. (b) Trigger current 38 amps, 50-ns/div. Current interruption occurred. (c) Same as (a) expanded to 10-ns/div.

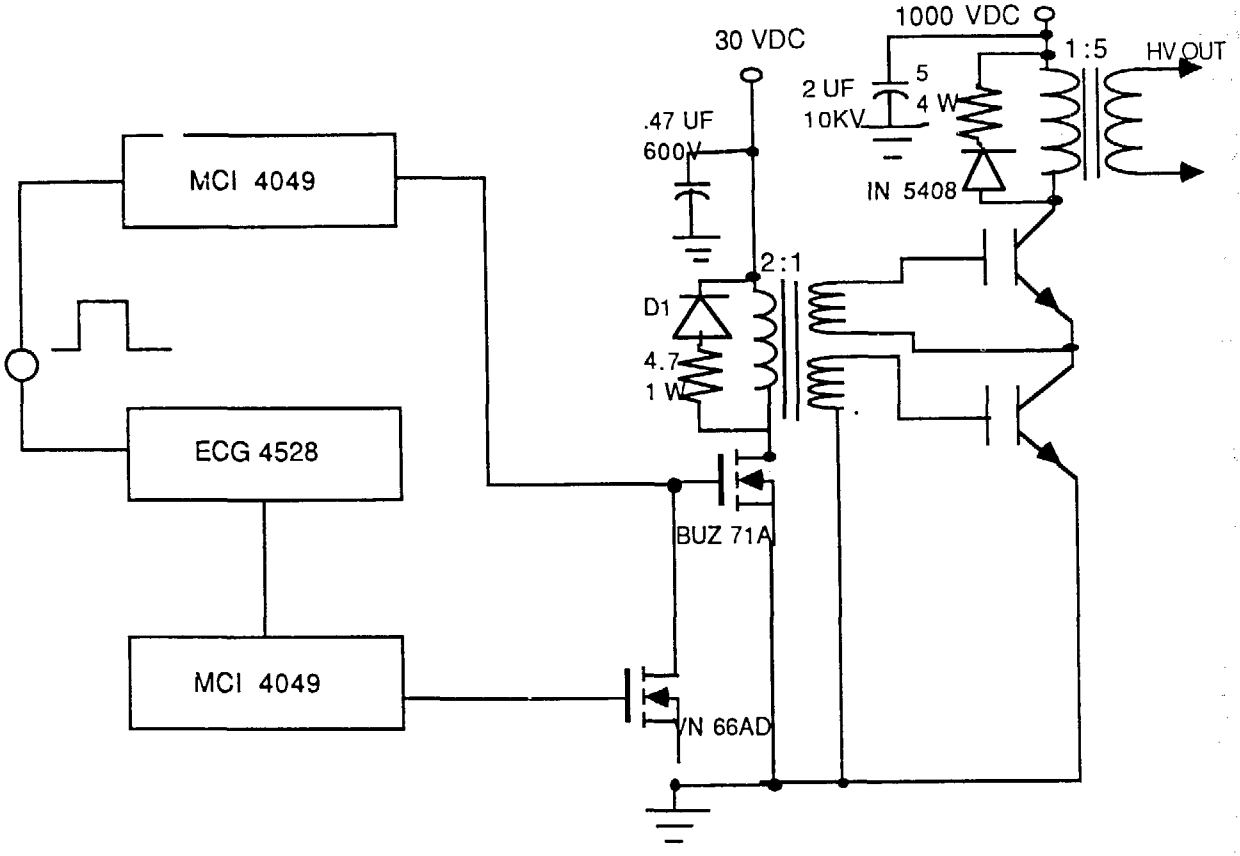

Fig. 6 5-kv, 80-amp, 20-khz pulse generator

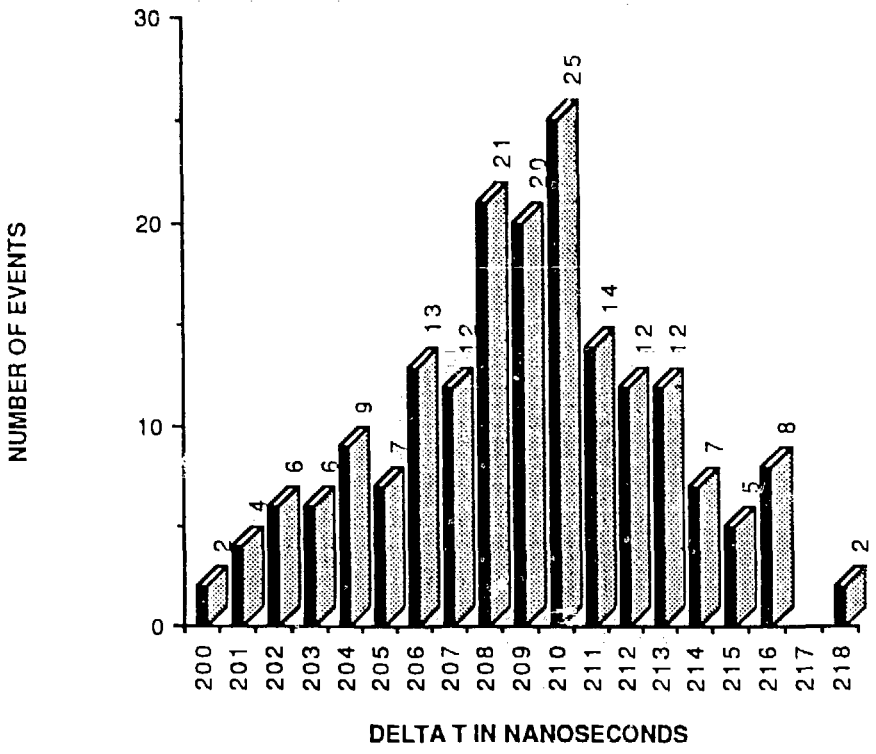

Fig. 7 Variation in delay between trigger and main current(std. dev.=5.63-ns)

Acknowledgement

This research is supported by The Center for the Commercial Development of Space Power funds from NASA Grant NAGW-1192-CCDS-AL, Auburn University, and the Center's Industrial Partners.

References

[1] George D. Volakakis, Magnetically delayed vacuum switch, M.S. Thesis, University of South Carolina, 1989.

[2] C. L. McDonald, Recovery time of a vacuum switch, M.S. Thesis, University of South Carolina, 1985.

[3] F. T. Warren, R. A. Dougal, T. S. Sudarshan, and J. E. Thompson, "A model for highly overstressed vacuum breakdown", *Proc. of the 5th IEEE Pulsed Power Conference*, pp 327-330, 1985.

[4] R. A. Dougal, G. D. Volakakis, M. D. Abdalla, "Magnetically delayed vacuum switching", *Proc. of the 6th Pulsed Power Conference*, pp. 21-24, 1987.

V. A. Vizir
High Current Electronics Institute, Tomsk

Power Characteristics of Magnetic Switches in High Current Nanosecond Regime

February 12-14, 1990

POWER CHARACTERISTICS OF MAGNETIC SWITCH IN HIGH CURRENT NANOSECOND REGIME

Vizir' V.A., *Mesyats G.A.

Institute of High Current Electronics, 634055, Tomsk, USSR

*Institute of Electrophysics, 620219, Sverdlovsk, USSR

Introduction

Magnetic switches are saturable chokes with magnetic core which are being widely used in the pulsed technique [1] . The general analysis of the operation of such switches in low level power generators are given elswhere [2] . In the recent years the magnetic switches are being used in high power, high voltage generator of nanosecond range applied for lasers and charged particles accelerators [3,4]

These papers give simple relations and graphs which provide the estimation of realization probability and calculation of the main dimensions of magnetic switch v.s.energy, voltage and pulse duration. To know these relations is of major importance for designing of magnetic compressors for laser and particles accelerators, where the switch dimensions need to be matched with load dimensions, specially with the laser's discharge electrodes. The parameters of magnetic generator used for pulsed excimer laser pumping with the radiation power of 1 kW are also given in this report.

Analysis of magnetic switch operation

The typical scheme of a series magnetic generator circuitry is given in the Fig.1. The generator consists of several LC compression stages coupled in cascade, based on cores of ferromagnetic material

with sharply nonlinear characteristics, The transfer of energy from one stage to another is accompanied by pulse compression in time and power enhancement due to the fulfilment of the condition; $L_{n-1} \gg L_n \gg L_{n+1}$. The power pulse compression is defined by a pulse compression coefficient:

$$K_c = \frac{\tau_{n-1}}{\tau_n} \qquad (1)$$

where τ_{n-1} and τ_n - the duration of pulses in the upstream and downstream stages respectively. The energy of the pulse, neglecting the losses, is defined by the expressions:

$$W = \frac{C U_m^2}{2} \quad ; \quad W = \frac{U_m J_{mn} \tau_n}{\pi} \qquad (2)$$

Here Um - the amplitude of pulsed voltage; Jmn - the pulsed current amplitude of - n -th stage;

The time duration of energy transfer through the stage is defined by the inductance of the saturable stage choke - L_n and of the capacitor inductance- L_c :

$$\tau_n = \pi \sqrt{(L_n + 2L_c)C/2} \qquad (3)$$

Inductivity of the saturated choke is:

$$L_n = \frac{\mu_0 \mu_n S_c N^2}{l_c} \qquad (4)$$

Here: μ_0 - the magnetic constant, S_c - the area of choke core cross-section, N - the number of winding coils, l_c - the average length of the magnetic force line of the core, μ_n - the seeming magnetic permeability of the inductor.

$$\mu_n = \mu_S - 1 + A/S_c$$

where: μ_S - the relative magnetic permeability of the saturated core, A - the area of the winding cross-section.

It is clear from the formulae (3) and (4) that the minimum duration and respectively the maximum power of the pulse is reached for

N=1. Due to it for nanosecond range the one-turn inductors are used. So, it is reduced to coaxial. For coaxial inductor:

$$L_n = \frac{\mu_0 \mu_c l}{2\pi} \ln \frac{D}{d} \qquad (5)$$

where: D and d - the outer and inner diameter of coaxial respectively, l - length of coaxial. The calculations show that formulae (4) and (5) give practically the same results for $D/d < 2{,}3$.

The area of core cross section is determined by a volt-second characteristic of the input pulse of the stage:

$$S_c = \frac{\int_0^{\tau_{n-1}} u\,dt}{\Delta B} \qquad (6)$$

where ΔB - the flux swing of magnetic induction in the core. For typical cosinus voltage pulse form:

$$S_c = \frac{U_m \tau_{n-1}}{2\Delta B} \qquad (7)$$

Substituting (7) in (4) , and (4) in (3), and using (1) and (2), after transformation, we'll get:

$$W = \left(\frac{2\Delta B}{\pi^2 \mu_0 \mu_n a} \right) \cdot \frac{U_m \tau_n l_c}{K_c} \qquad (8)$$

Here $a = (1 + 2 L_c / L_n)$.

The expression in the brackets has the dimension $A/\sqrt{m}$

Let us define:

$$H_p = \frac{2\Delta B}{\pi^2 \mu_0 \mu_n a} \qquad (9)$$

And finally we'll get:

$$W = \frac{H_p \cdot U_m \cdot \tau_n \cdot l_c}{K_c} \qquad (10)$$

Equating (2) and (10), we'll get:

$$H_p = \frac{K_c \cdot J_{mn}}{\pi \cdot l_c} = \frac{K_c}{\pi} H_{mn} \qquad (11)$$

So, H_p - some calculated magnetic field strength, which is equal to the strength in the core for $K_c = \pi$.

So, from (10) it is clear that for given voltage and pulse duration at the input and at the exit, the energy of the pulse translated by the compression stage is defined only by the magnetic field path length of the inductor. The coefficient of the proportionality characterizes the quality of the magnetic material and the skill of the designer. The pulse energy is higher for larger H_p.

Let us determine the specific volumetric energy of switch - $W_v = W/V_c$ (V_c - the core volume). Introducing (1) and (7) in the (10) and transforming it, we'll get:

$$W_v = \frac{2\Delta B \cdot H_p}{K_c^2} \qquad (12)$$

As it is seen it does not depend on the pulse duration and its voltage, but is only a function of electromagnetic and constructive parameters. Let us determine from (10) the specific linear energy of switch - $W_e = W/\ell_c$:

$$W_\ell = \frac{H_p U_m \tau_n}{K_c} \qquad (13)$$

It is clear that W_e is defined by voltsecond characteristic of the pulse. The W_v and W_e are dependent on the compression coefficient. The limits of this coefficient variation can be determined from the following considerations. The minimum of the compression stage at all is approximately $K_c = (1,5 \div 2)$. The maximum value is limited by the rise of the energy losses for remagnetization and due to it - by the decrease of energy transfer, and at last - by the pulse form distortions due to prepulse appearance of nonpermitted by the work conditions value.

The energy losses in the core at total magnetic swing ($\Delta B = 2B_s$) could be approximately defined formulae [2] :

$$W_m \simeq \frac{3.3\, B_s\, S_w\, V_c}{\tau_{n-1}} \qquad (14)$$

Here B_s - the saturated magnetic flux density, S_w - the swithing coefficient which was found experimentally, which is equal to the quantity of electricity needed for remagnetization of the core. S_w has two additive components: the first one S_{wo} is pertinent to the magnetic viscozity, the second S_{we} takes care of the inductive current in the ferromagnetic strip ($S_{we} = \frac{B_s d^2}{4\rho}$, where d - the strip thickness, ρ - special resistance).

In case of ferrites with partial remagnetization the coefficient 3,3 in formula (14) is substituted for 1,7.

Dividing (14) over (10) and taking care of (7), we'll get:

$$\frac{W_m}{W} \simeq 0{,}8\, \frac{S_w\, K_c}{H_p\, \tau_n} \qquad (15)$$

The value $\frac{S_w}{H_p}$ has dimentions of time and it is equal to time of core remagnetization due to the jump of the calculated field strength H_p. Let us call it the calculated time constant - $\tau_p = S_w / H_p$

So, the maximum attainable compression coefficient will be defined from (15)

$$K_{c.max} \simeq \frac{1{,}25\, \tau_n}{\tau_p} \cdot \frac{W_m}{W} \qquad (16)$$

Let us assume the level of permissible losses - (W_m/W) $\leq 0{,}05$. For this value the prepulse is still not high $\Delta U \leq 0{,}15\, U_m$, and with proper cooling of the core the high frequency of pulses can be realized. In certain cases even $\frac{W_m}{W} \leq 0{,}1$ could be permited, but the pulse distortion and core heating are too high.

So, finally:

$$K_{c.max} \leq \frac{0{,}06\, \tau_n}{\tau_p} \qquad (17)$$

For the ferrite core the coefficient 0,06 is substituted for 0,1. It is clear that the lesser is the calculated time constant the higher the compression coefficient value can be attained.

Now, we got the calculated parameters - H_p, τ_p, W_v, W_e, $K_{c\ max}$, which characterize magnetic switch in all details.

The initial and calculated dates for magnetic switches designed from widely used ferromagnetics: metall -amorphous alloy 2 НСР, permalloy 5 СНП and ferrit 200 ВНП are given in Table 1. The inductance difference was assumed to be equal to $\Delta B = 2B_s$ for alloyes and $\Delta B = 1{,}5B_s$ for ferrit. The values of μ_n and α depend in general on K_c. They are assumed to be minimum found from experiment for K_c= 3-4. The switching coefficients for permalloy and ferrit are given in Literature, for the metallo-amorphous alloy it was found in our experiments. The volumetric and linear specific energies and compression coefficients are given in relative units.

Table 1

Material	ΔB T	μ_n	α	S_w mcC/m	H_p кА/m	τ_p ns	W_v	W_e	$K_{c.max}$
Metallo-amorphous alloy 2НСР-20 mcm	3.0	2.0	1.8	230	135	1.7	1.0	1.0	1.0
Permalloy 50НП-10mcm	3.0	2.5	1.7	160	115	1.4	0.8	0.85	1.2
Ferrit 200 ВНП	0.7	2.0	1.3	40	44	0.9	0.08	0.33	3.0

One can see from the Table that the largest W_v specific energy has the magnetic switch made from metall -amorphous alloy. The W_v energy of the permalloy switch is slightly smaller, W_v energy of the ferrit switch is smaller by an order of magnitude. The absolute value of the W_v energy for the metall -amorphous alloy switch equal

to $W_v \simeq 200$ kJ/m^3 at the compression coefficient of $K_c=2$. The W_l specific linear energy of the switches does not differ in such degree as the volumetric one. The largest compression coefficient has the ferrit switch. It allowes to reach the minimum pulse length of $\tau_{n.min} \simeq 15$ ns at $K_c = 2$, compared to $\tau_{n\,min} \simeq 55$ ns for the alloy switch.

The W_v specific energy versus compression coefficient and the maximum compression coefficient versus pulse length for the alloy switch are given in Fig.2.

Fig. 3 gives the dependence of the W_e specific energy on the pulse length for a number of the compression coefficients at the pulse voltage of 1 MV. The dotted traces below the line $K_c=K_{c\,max}$ represent the values of W_e in restricted area $W_m/W > 0.05$. Figs.2 and 3 may be used for the permalloy switch as well using the scale coefficients given in Table 1.

The above mentioned dependencies allow to estimate the possibility of realization and to calculate the main switch dimensions. Usually the values W, U_m, τ_n and K_c are known. Fig, 2 gives W_v for given K_c. If $K_c > K_{c\,max}$ the two-stage circuit should be chooseh what also allowes to save the ferromagnetic. Fig.3 gives W_e for given τ_n. The core crossection S_c and length are determined by equations:

$$S_c = \frac{W_e \cdot U_m}{W} \qquad (18)$$

$$l_c = \frac{W}{W_e \cdot U_m} \qquad \text{in another way} \qquad l_c = \frac{K_c \cdot W}{H_\rho U_m \tau_n} \qquad (19)$$

Here the voltage in MV must be used. Becouse the values of μ_n and α were assumed to be minimal possible, the values of W_v and W_e determined from Figs.2 and 3 may be obtained in carefull desigr only. The abovementioned method [5] consisting in the~20% deminishing of S_c and l_c with corresponding ~10% voltage increase allowes

to exceed the calculated values of W_v and W_e by a factor of 1.5.

Practical realization

Such calculations were used to construct a number of one-stage magnetic pulse generators to pump excimer discharge lasers with the output radiation pulse energy of (0.2-10)J and repetition rate of (50-200) Hz. Table 2 gives the basic parameters of the most powerfull generator.

Table 2

	W kJ	U_m kV	τ ns	C nF	K_c	f Hz
Project (January,89)	1.0	125	200	120	3.5	100
State on 1.02.90	0.4	80	200	120	3.5	200

The magnetic switch was designed from six oval cores made from the tape 2 HCP-20 mcm. The S_c crossection of the core was of 125 cm^2, the ℓ_c length - 1,6 m. The initial pulse generator is assambled out of 4 thyratrons ТГИ - 2500/50, switching the LC -circuit used to double the voltage. The traces of tyratron current pulse and generator output voltage when coupled to the resistive load 2 Ohm and to the laser discharge gap are given in Fig.4. Today the peak XeCl-laser radiation power equals to 500 W at the repetition rate 200 Hz.

References

1. W.S.Melvill. Proceedings JEE, London, Vol.98, Pt.3,P.185(1951).
2. L.A.Meyerovich, et al. Magnetic pulse generators.Sov.Radio,M.,1968
3. D.L.Birx et al. IEEE Trans. on NS, Vol.NS-30, P.2763(1983).
4. E.Y.Chu et al. 15th Power modulator Symposium, IEEE Conf.P.32,1982.
5. E.Y.Chu. 4th IEEE Pulsed Power Conference,Albuquerque,P.252(1983).

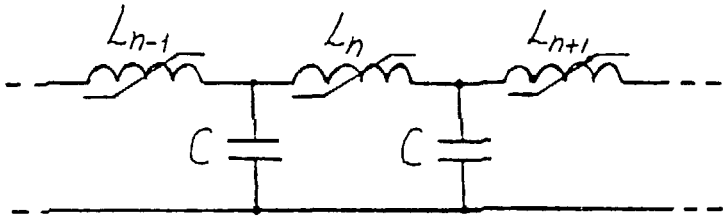

Figure 1. Circuit of series magnetic compressor pulses

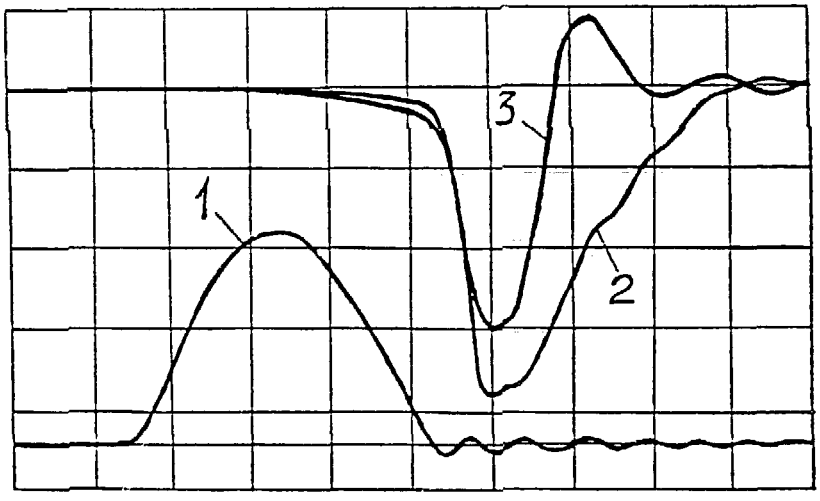

Figure 4. Oscillograms of magnetic compressor pulses

1 - thyratron current (3 kA/div)
2 - voltage on active load (16 kV/div)
3 - voltage on laser discharge electrodes (16 kV/div)
Time scale - 200 ns/div

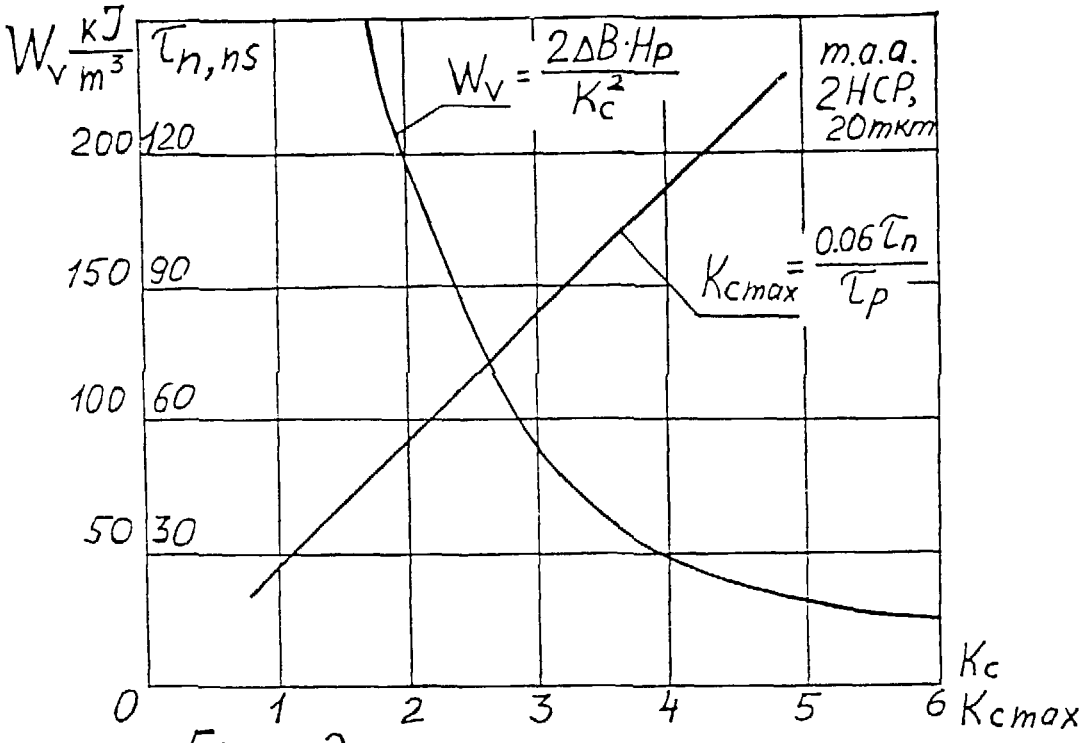

Figure 2. Specific volumetric energy of magnetic switch and maximum compression coefficient

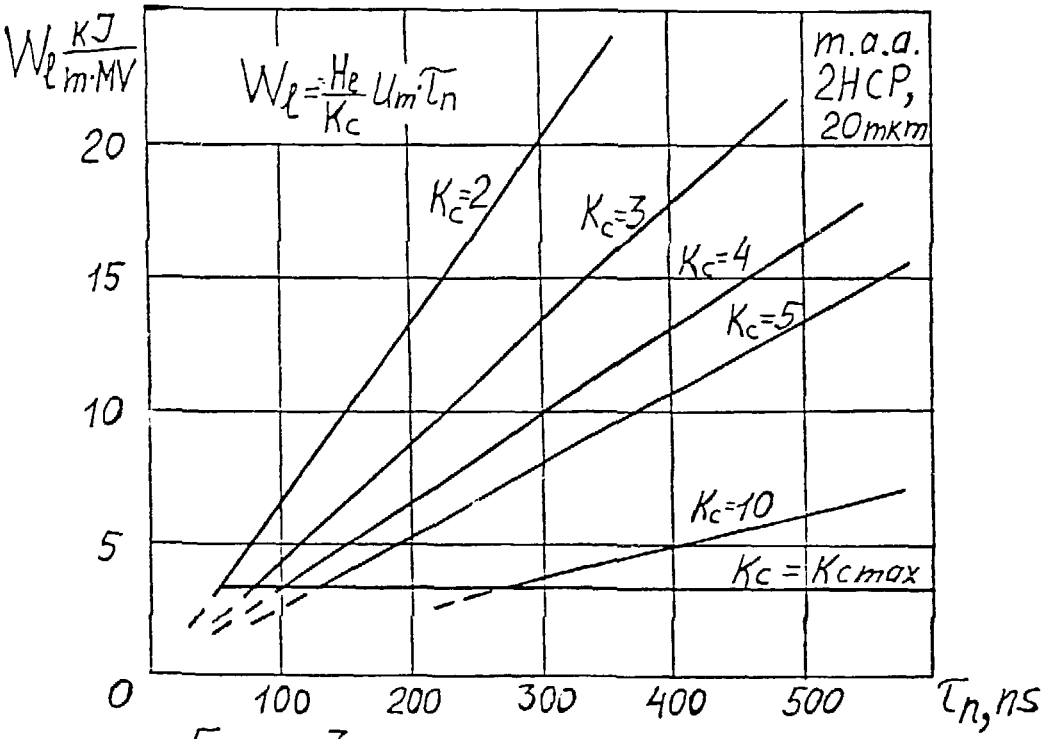

Figure 3. Specific lineas energy of magnetic switch

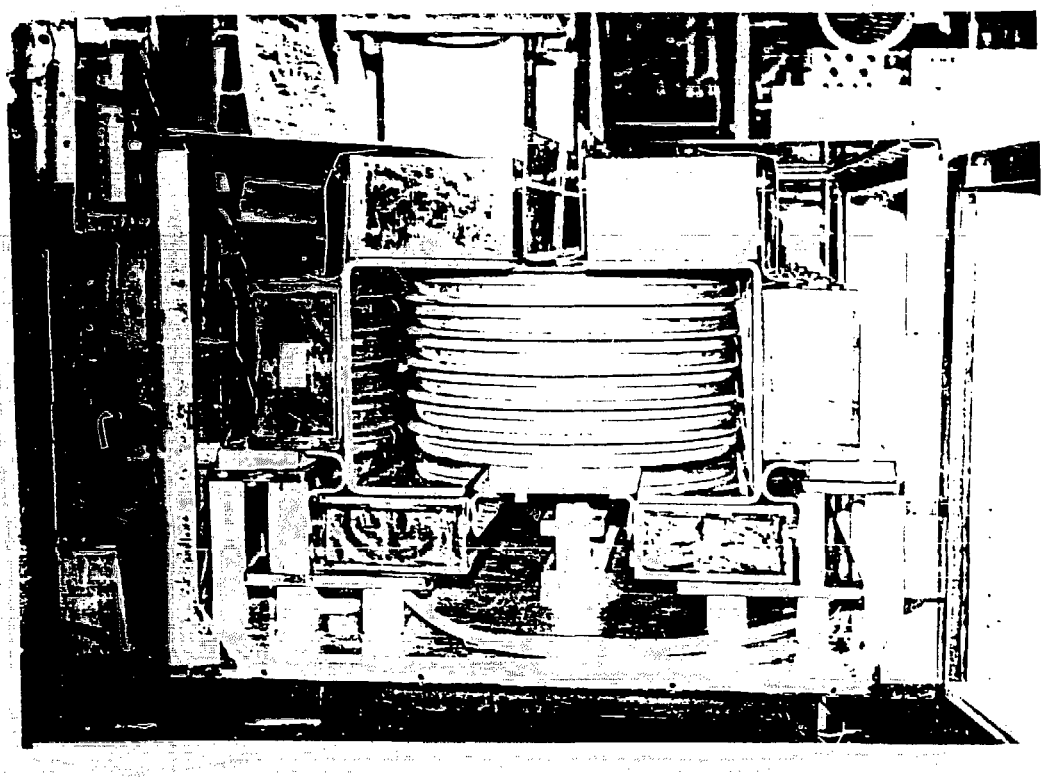

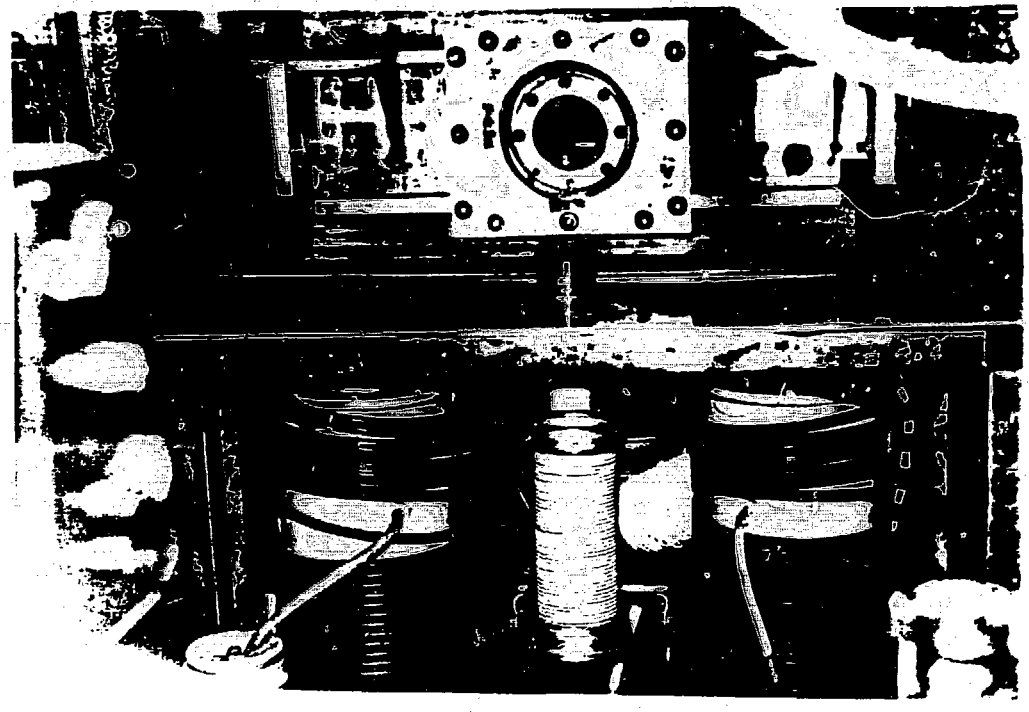

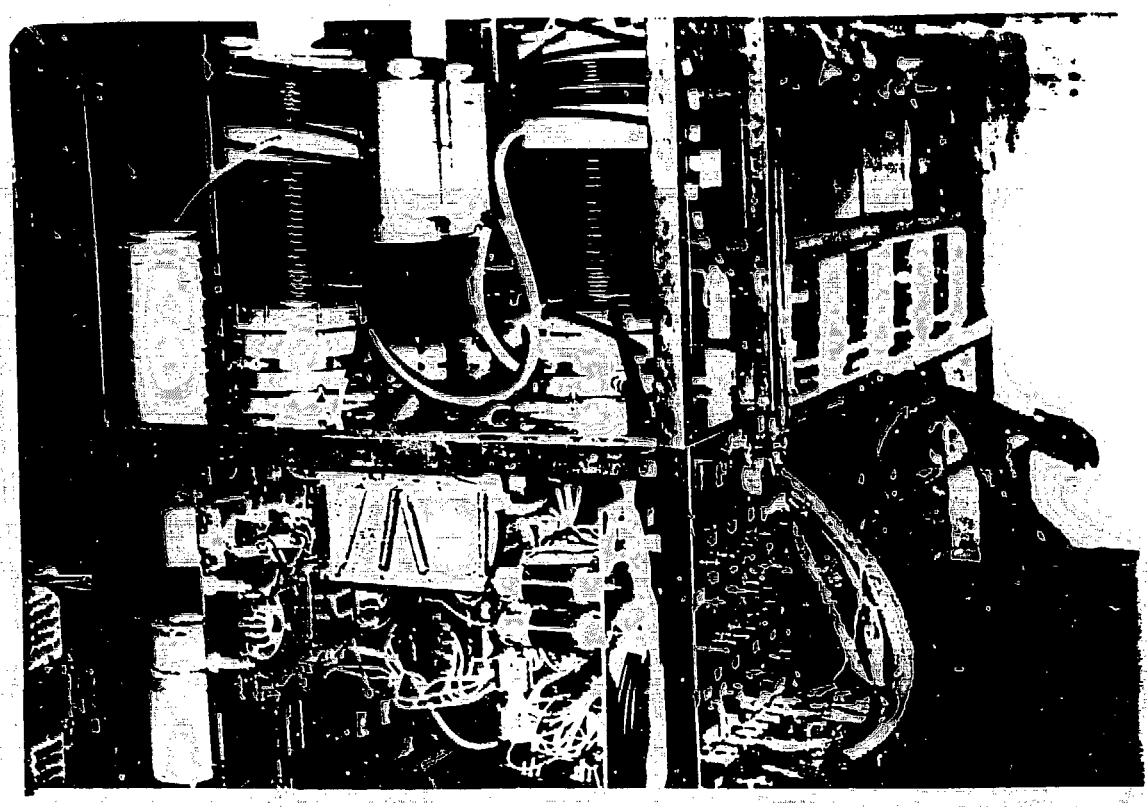

V. M. Bystritskii
High Current Electronics Institute

Pulse Sharpening Using the Magnetic Core and Plasma Opening

POSTER

February 12-14, 1990

PULSE SHARPENING USING THE MAGNETIC CORE AND PLASMA OPENING SWITCH

*Bystritskii V.M., Krasik Ya.E., Ivanov I.B.,
*Mesyats G.A., Ryzhakin N.N., Usov Yu.P.

Institute of Nuclear Physics, Tomsk, 634050, USSR
*Institute of Electrophysics, Sverdlovsk, 620219, USSR

Introduction

The application of Inductor Cores (IC) in pulsed power circuitry could improve the functional range of the high current accelerator due to realizing of the possibility to tranzit from high impedance mode of operation to low one and visa versa. The application of current enhancing Inductor Cores Section (ICS) in conjunction with inductive storage and Plasma Opening Switch (POS) could result also in power enhancement and compression of the output pulse [1-3].

The example of the simple voltage enhancing scheme with ICS installed between the generator and the diode load is given at the Fig. 1a. The model circuitry of this scheme (Fig. 1b) shows that it

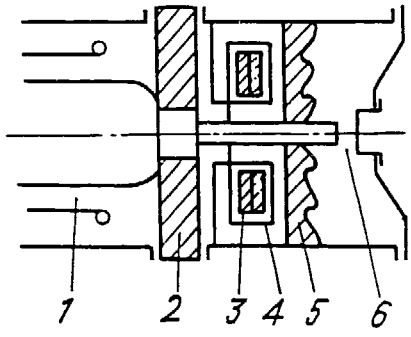

Fig. 1a. Experimental scheme for voltage enhamcement. Symbols are the same as in the Fig. 2a.

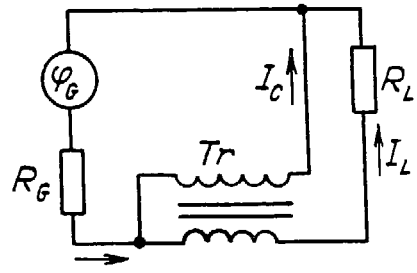

Fig. 1b. The model circuit. φ_G - generator, R_G - generator impedance, Tr - core transformer, I_c - current in the coils of inductor, R_L, L_L - impedance and current of the load.

operates in the regime of autotransformer with voltage transformation coefficient K_v equal to 2 in ideal case without energy losses in the

cores and scattered magnetic flux [2]. As it follows from simple analysis of this scheme the matched value of the load impedance equals to $K_v^2 \cdot R_G$, where R_G - is the generator impedance.

The current enhancing scheme with ICS placed between the generator and the load is given in the Fig. 2a. The respective current

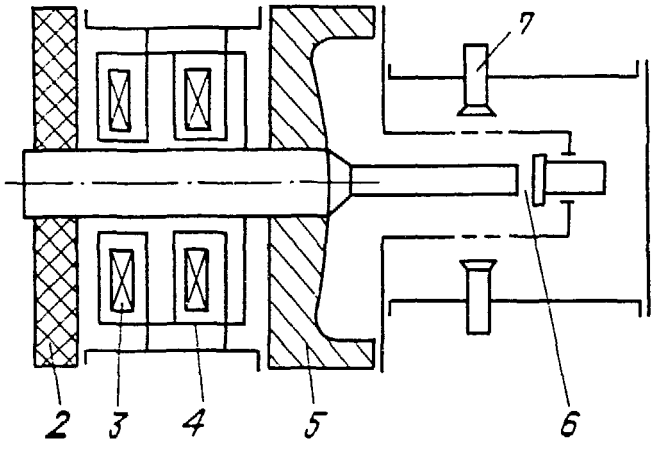

Fig. 2a. Experimental scheme for current enhancement: 1-Double forming line, 2-insulating interface, 3-inductor cores, 4-coils of the cores, 5-vacuum-oil interface, 6-electron diode (or magnetically insulated ion diode), 7-plasma opening switch (POS).

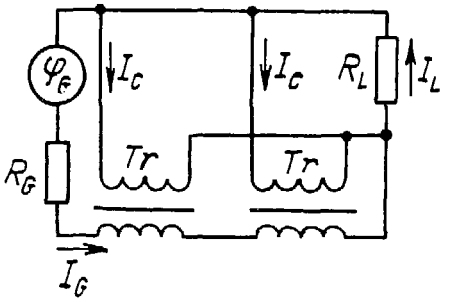

Fig. 2b. The model circuit. Symbols are the same as in Fig. 1b.

enhancement coefficient K_c in this scheme is equal to 3 in ideal case without losses. The Fig. 2b gives the model scheme of the circuitry. In this case the matched impedance load is equal to R_G/K_c^2.

Modifying this scheme by plasma opening switch, placed after the ICS, could result in considerable increase of the output power due to the compression of the time needed to extract the energy stored in the circuitry inductance. This idea is valid in the assumption that intrinsic POS impedance behaviour is almost independent on the current amplitude, stored in the inductance of the circuitry. Analyzing the simple model circuitry with the POS and without the ICS we could use the expressions for the characteristics of switching obtained in [3] (Fig. 2c). In assumption of the $L_2 \ll L_1$, $R_G < R_1 \ll R_S$ and ideal POS operation (POS impedance before the switching is equal to zero, after the switching - it is constant R_S), this characteristics are following:

$$t_- = (L_1+L_2)/(R_G+R_L); \qquad t_+ = L_2/R_S \tag{1}$$

where t_+ - is the switching time, t_- - is the time of current decaying in the store inductance (the total width of the output pulse).

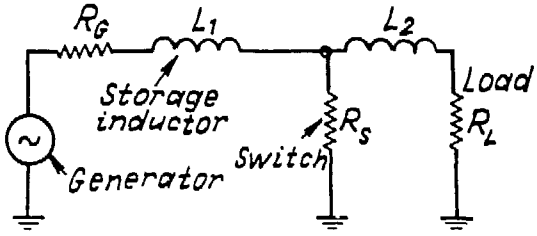

Fig. 2c. The model circuit for POS application in inductive storage system.

In the modified scheme with the ICS placed between the POS and the generator the respective values are equal to:

$$t^*_- \cong (L_1/K_c^2+L_2)/(R_G/K_c^2+R_L); \qquad t^*_+ \cong t_+/(1 + K_c^2L_2/L_1) \tag{2}$$

It is clear that the values of t^*_-, t^*_+ in comparison with (1) are considerably lower in the scope of our assumptions. The respective expressions for load power in the [3] is following:

$$P_L = R_L L_1^2 I_0^2 \cdot \{1-2\cdot[\ln(x)+1]/x\} /(L_1+L_2)^2; \tag{3}$$

where: $x = R_S L_1/L_2(R_G+R_L) >> 1$.
In modified scheme with ICS installed, as it was said before, the respective P value is following:

$$P^*_L = R_L L_1^2 I_0^2 \cdot \{ 1-2\cdot[1+\ln(x^*)]/x^* \ /[(L_1/K_c^2)+L_2]^2; \tag{4}$$

where the I_0 - is the current amplitude in the storing inductance during the conduction phase of the POS; $x^* = x(R_G+R_L)/(R_G+R_L K_c^2)$.

The analysis of the expression (4) shows that in the range of interest for the characteristics R and L the value of the P^*_L would be also higher in comparison with P_L without ICS application. Two extreme cases could be considered relevant to discussed scheme: without saturation and with it. In the first case all energy stored in L_1 during POS switching will be transmitted to the secondary circuitry, i.e. in the load. In the second case, when the saturation of the cores are being reached near the maximum of the stored current, the switching of the POS will result in the cut off the residual energy stored in the primary circuitry. To minimize its value the

inductance L_1 ought to be low, in the same time fulfilling the following condition:

$$L_1 \approx t_p R_G / 1.25 \qquad (5)$$

More clearly the advantages of ICS application can be demonstrated in the simple scheme, where the POS plays the role of the load (plasma filled diode), and for additional simplicity we will assume that L_2 and R_G could be neglected; the POS impedance has the time dependence of the linear character: $R_S = at$. In these approximations the voltage and power transmitted to the load and front duration of the pulse in the case of the scheme without the ICS will be respectively equal to:

$$\varphi_{max} = 0.6 \cdot I_0 (aL_1)^{1/2}; \quad P_{max} = 0.43 \cdot I_0^2 (aL_1)^{1/2};$$
$$t_v = (L_1/a)^{1/2}; \quad I = I_0 \cdot \exp(-at^2/L_1). \qquad (6)$$

In the scheme with ICS, installed between the generator and the POS, retaining the same characteristics of the POS and the generator, we will get the following expressions:

$$\varphi^*_{max} = 0.6 \cdot I_0 (aL_1)^{1/2}; \quad P^*_{max} = 0.43 \cdot I_0^2 K_v (aL_1)^{1/2}.$$
$$t^*_v = (L_1/a)^{1/2}/K_c \qquad (7)$$

Summarizing the said above: it is clear that application of the ICS in current enhancing mode between the generator and the POS results in the rise of the load power and the output pulse compression, transmitted to the load.

Experimental set up and diagnostics

To check the idea of considered above approach we made several experiments on the nanosecond high power generator with following parameters [4]: $\tau_p = 80$ ns, $R_G = 8$ Ohm, $\varphi = 300 - 350$ kV.

The scheme of the experimental set-ups are given in the Fig. 1a and 2a. In both cases the cores were fabricated from 10 mkm laminates. Magnetic flux swing was equal to $1.6 \cdot 10^{-2}$ Vs during the operation in

the voltage enhancing regime, and $9 \cdot 10^{-3}$ Vs in the current enhancing regime. The four plasma guns were used for the POS, which were placed 65 mm from the surface of the inner high voltage electrode. The diameter of the anode electrode made in form of "squirrel cage" was equal to 50 mm in the POS. The cathode electrode diameter there was equal to 30 mm. The POS plasma flow velocity was measured as $3 \cdot 10^{6}$ cm/s. The planar and plasma filled diodes were used for the load alternatively. The inductance between the POS and the diode was not more than 5 nH. The inductance of the section between the ICS and POS varied in the range of 55 nH - 70 nH. In the experiments with the enhancing voltage ICS the electron and magnetically insulated ion diodes were used [5]. The diagnostics included Rogovsky coils, voltage dividers, dI/dt loops, collimated Faraday cup to measure the ion flow.

Experimental results

The Fig. 3 demonstrates the typical waveforms of the currents and voltages in the ICS regimes of voltage enhancement. The coefficient of this enhancement made up 1.8 and was almost constant for all diode impedances used, which made up to 90 % of the theoretical value. For this regime the compression of effective energy transition time was pertinent to the cores saturation (Fig. 4). The current of magnetization was not more than 5 kA (Fig. 5).

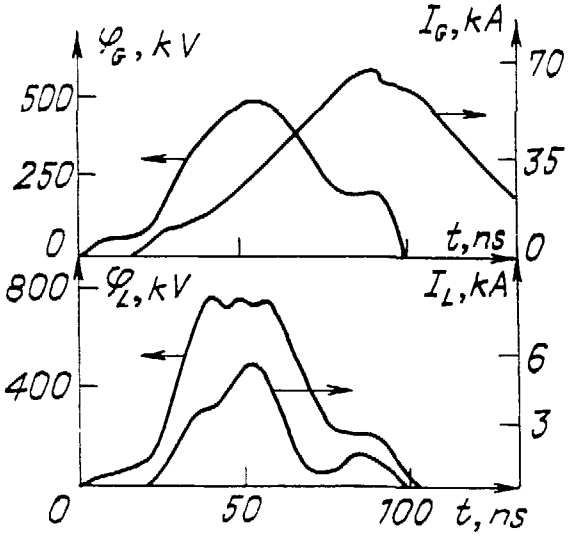

Fig. 3. Pulses waveforms for the scheme 1a: I_G - generator current, I_L - load current for the load - magnetically insulated ion diode, φ_G - exit voltage of the generator, φ_L - exit voltage of the load.

The respective losses in the cores were not more than 30 J. The total magnetic flux swing in the cores was equal to 1.2 - 1.5 10^{-2} Vs, which was less than our previous estimates. The energy transmission efficiency to the matched load reached 80 % at the level of 10^{10} W and it

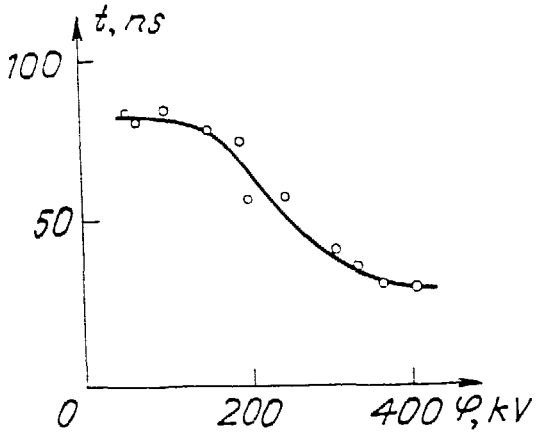

Fig. 4. Volt-seconds characteristics of the cores.

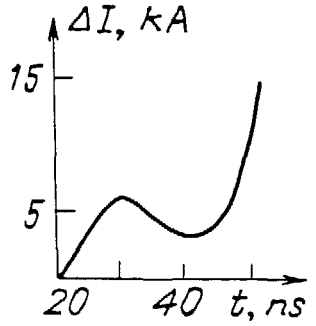

Fig. 5. The time dependence of the magnetizing current of the cores.

decreased to 40-50 % for highly mismatched load. Using for a load a magnetically insulated diode with cathode transparency of 40 % we got the proton beam extracted from the diode of 750 keV of energy and 5 kA amplitude of current. The main losses in the regime of voltage enhancement were coupled with the surface current along the insulator, which made up more than 5 kA, and also with the remagnetization of the cores. During the operation with the ICS in the regime of current enhancement the power reached $1.1 \cdot 10^{10}$ W for 100 kA of the electron beam current, the efficiency of energy transmission to the diode reached 60 %. Such limitation of the efficiency was due to the big inductance of the load, which reached 45 nH. In the experiments with the inductive load of 50 nH, the load current amplitude was equal to 185 kA, the cores saturation took place at 70 ns in the pulse. For inductive load of 70 nH the load current reached only 170 kA.

In experiments with the ICS and the POS the amplitude of the stored current through the last was not more than 135 kA. From the Fig. 6 it is clear that the current deviation from the short circuit case value began simultaneously with the voltage appearance at the load. In the beginning of the switching the voltage reached 100 kV. During the switching the voltage amplitude reached 500 kV, load

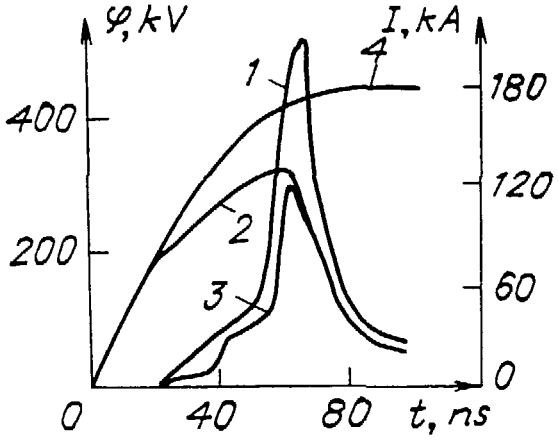

Fig. 6. The waveforms for operation of the scheme 2a:
1 - the voltage at the load,
2 - the current through POS,
3 - the current through the load (plasma filled diode) L_L= 55 nH,
4 - short circuit current.

current - 90 kA. The power amplitude attained $4.5 \cdot 10^{10}$ W, the voltage pulse duration - 8 - 10 ns, the POS impedance in the maximum of voltage - 20 Ohm.

The best switching of the POS were realized in the cases when the current break up took the place 5 - 10 ns before the cores saturation. When this happened after the cores saturation the efficiency sharply dropped. In optimized firings of the accelerator the factor of power enhancement in comparison with matched regular regime (without ICS and POS) made up factor of 3 - 3.5.

Summary

1. The application of additional induction cores section in various regimes of operation (voltage or current enhancement) ensure the profileration of functional abilities of the pulse generator in wide range of operational impedance.
2. The application of ICS, operating in the current enhancing mode in conjunction with POS installed after the ICS, provide considerable power increase and time compression of the output pulse.

References

1. Anazkii A.I., Vakhrushin Yu.M. Linear Inductive Accelerators, Moscow, Atomenergoizdat, 1978.
2. Pantyushin V.S. Elektrotekhnika, Moscow, Vysshaya Shkola, 1976.
3. Ottinger P.F., Goldstein S.A., Meger R.A. Theoretical modeling

of plasma erosion opening switch for inductive store application, J. Appl. Phys., v. 56, pp.774-784, 1984.
4. Akerman D.R., Volkov S.N., Krasik Ya.E. Pribory i Tekhnika Experimenta (Sov), n. 4, p.34-36, 1983.
5. Sudan R.N. Proceedings of 3-rd Intern. Conf. on High Power Part. Beams, Novosibirsk, v. 1, 1979.

'90

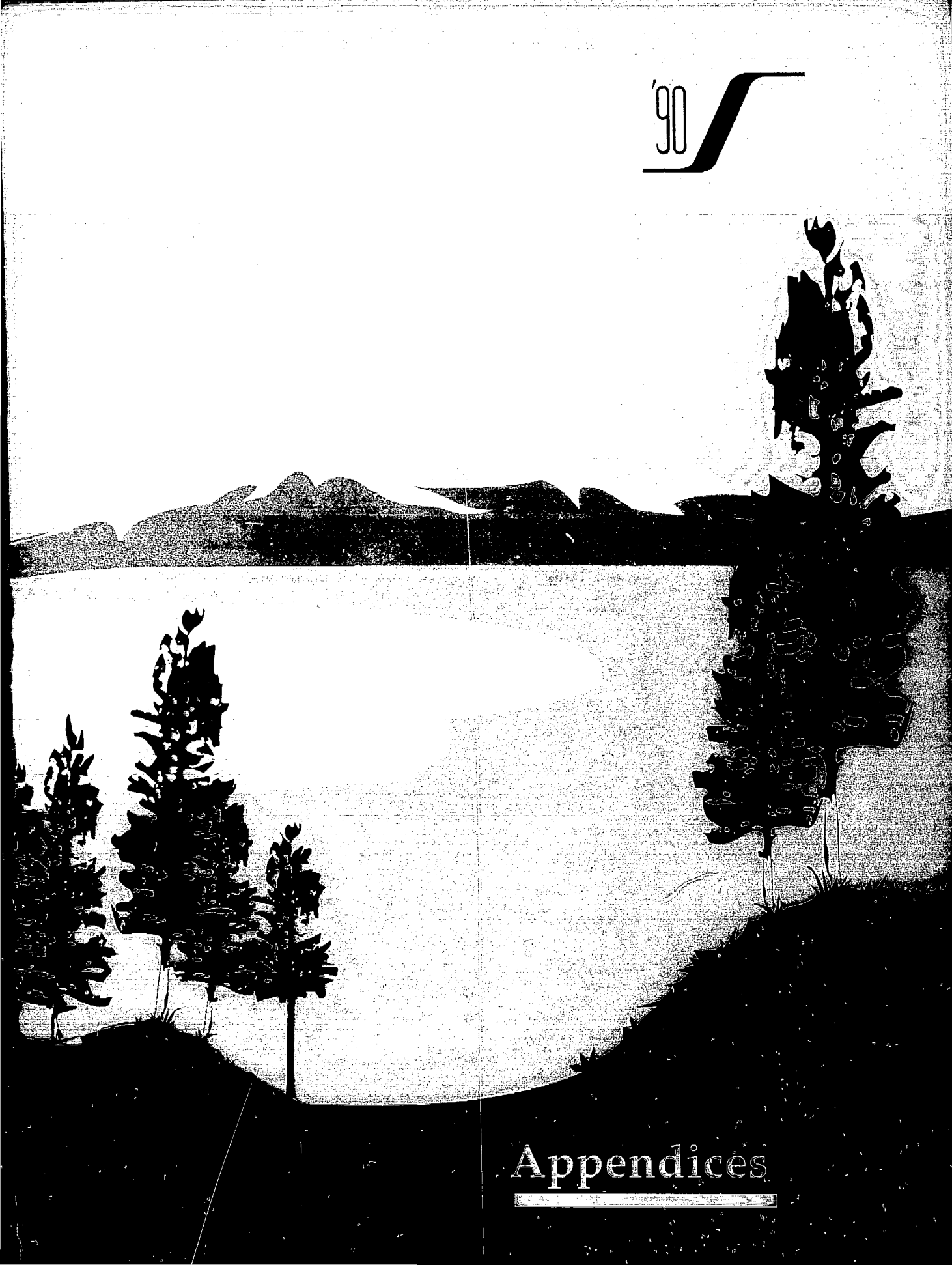

Appendices

Appendix A

Bibliography

Appendix A
Bibliography

Introduction

The books and articles listed in this bibliography are favorite references from the various personal libraries of those serving on the organizing committee. Copies of every article were collected, filed, and brought to Granlibakken as an on-site reference library for all the working group members. The bibliography listing is included as a proceedings appendix to assist other researchers in finding books and articles that directly apply to magnetic pulse compression technology.

The bibliography is divided into six sections:

1. Theory and Modeling of Magnetic Pulse Compression Networks and Systems
2. Magnetic Material Modeling, Theory, and Data
3. Magnetic Pulse Compressor Designs, Concepts, Evaluations, and Theory
4. Magnetic Pulse Compression System Applications
5. Switching Applications
5. Switching and Power Conditioning Systems
6. Miscellaneous Topics

We on the editorial staff hope that this bibliography will serve as a long-lasting guide through the diverse history of magnetic pulse compression technology and related fields.

1. Theory and Modeling of Magnetic Pulse Compression Networks and Systems

This section includes the papers that describe appropriate modeling methods for systems and networks that use magnetic pulse compression. Also included are papers that explore the theoretical concepts generally used to describe networks and systems.

1.1 D.M. Barrett, "Modeling the Characteristics of a Magnetically Switched Pulse-Forming Line," *Digest of Technical Papers Seventh IEEE Pulsed Power Conference*, pp. 1–4, Monterey, CA (June 1989).

1.2 L. Chua, *Introduction to Nonlinear Network Theory* (McGraw-Hill, New York, 1969).

1.3 P. Corcoran, I. Smith, and D. Wake, "Three 'Reverse Engineering' Codes for Pulse Power System Design," *Digest of Technical Papers Seventh IEEE Pulsed Power Conference*, pp. 465–467, Monterey, CA (June 1989).

1.4 W. Hochwald and C.T. Kleiner, "Digital Simulation of Nonlinear Electromagnetic Circuits," *IEEE Transactions on Magnetics*, **MAG-2**, pp. 532–539 (Sept. 1966).

1.5 G.A. Huttlin and A.J. Lells, *TLINES: A Computer Program for Circuits of Transmission Lines*, Harry Diamond Laboratory, (Dec. 1983).

1.6 M.L. Kiefer and M.M. Wigner, "SCREAMER - A Single-Line Pulsed-Power Design Tool," *Digest of Technical Papers 5th IEEE Pulse Power Conference*, pp. 685–688, Arlington, VA (June 1985).

1.7 C.T. Kleiner, "Application of a Phenomenological Core Model in the SYSCAP 2.5 Circuit Analysis Program," *IEEE Transactions on Magnetics*, **MAG-19**(5), pp. 2186–188 (Sept. 1983).

1.8 D.A. Lowther and P.P. Silvester, *Computer-Aided Design in Magnetics* (Springer-Verlag, New York, 1986).

1.9 D. Nitzan, "Computation of Flux-Switching in Magnetic Circuits," *IEEE Transactions on Magnetics*, **MAG-1**, pp. 222–233 (Sept 1965).

1.10 D. Nitzan, "Computer Program for Transient Analysis of Circuits Including Magnetic Cores," *IEEE Transactions on Magnetics*, **MAG-5**, pp. 524–533 (Sept. 1969).

1.11 D. Nitzan, "Engineering Flux-Switching Models for Toroidal and Mulitipath Cores," *IEEE Transactions Communications and Electronics*, **CE-83**, pp. 309–314 (May 1964).

1.12 D. Nitzan and J.R. Herndon, *Modeling of Magnetic Cores for Computer Circuit Analysis*, Harry Diamond Lab, Washington, D.C., Technical Report AD 864 933 (Sept. 1969).

1.13 D. Nitzan, "Models for Elastic and Inelastic Flux Switching," *IEEE Transactions on Magnetics*, **MAG-2**, pp. 751–760 (Dec. 1966).

1.14 D. Pei and P.O. Lauritzen, "Computer Model of Magnetic Saturation and Hysteresis for Use on SPICE2," *IEEE Transactions on Power Electronics*, **PE-1**(2), pp. 101–110 (April 1986).

1.15 A.J. Power, J.E. Dolan, and H.R. Bolton, "Simulation of a Pulse Compression Circuit Incorporating a Realistic Magnetic Switch Model," *Digest of Technical Papers Seventh IEEE Pulsed Power Conference*, pp. 663–666, Monterey, CA (June 1989).

1.16 J.A. Resh, "Towards General Simulation of Ferromagnetic Devices," *Proceedings 12th Midwest Symposium on Circuit Theory*, Austin, TX, V.2.1 to V.2.7 (April 1969).

1.17 H.E. Rhinehart and R.A. Dougal, "Computer Simulation of Magnetic Switching Circuits," *Digest of Technical Papers Seventh IEEE Pulsed Power Conference*, pp. 163–166, Monterey, CA (June 1989).

1.18 H. Rhinehart, *Computer Simulation of Magnetic Switching Circuits and Magnetic Energy Losses* (University of So. Carolina, SC, Ph.D. Thesis, 1989).

1.19 W.N. Weseloh, "TLCODE- A Transmission Line Code for Pulsed Power Design," *Digest of Technical Papers Seventh IEEE Pulsed Power Conference*, pp. 989–982, Monterey, CA (June 1989).

2. Magnetic Materials Modeling, Theory, and Data

This section includes papers that describe modeling techniques that apply to magnetic materials. Also included are articles covering theoretical concepts for material modeling as well as experimental data for magnetic materials.

Subsections 2a through 2d contain papers which describe suitable magnetic materials for switch contstruction and give experimental data on material behavior. Sections 2e through 2f concentrate on modeling the the magnetic behavior of these materials, and provide supportive theory and data for such models. In this bibliography, models are categorized as *Megascopic, Domain Wall Motion, or Micromagnetic. Megascopic models* simulate bulk material behavior and are classified as either static or dynamic. Most such models are empirical, but some do have physical bases. The so called "static models" function independent of magnetization rate

and are best used over a restricted frequency range. *Domain Wall Motion models* attempt to simulate the movement of magnetic domain walls within a material during magnetization. *Micromagnetic models* describe magnetic behavior at the molecular level.

2a. Materials-Polycrystalline

2.a.1 G.G. Berg, *Study of Magnetic Cores*, Lawrence Livermore National Laboratory, Livermore, CA, UCID-15028 (Sept. 1966).

2.a.2 R.M. Brownell, "Direct Observation of Outward-Progressing Flux Change in Tape-Wound Cores at Power Frequencies," *Journal of Applied Physics*, 33(1), p. 118 (May 22, 1961).

2.a.3 W. Schlosser and I. Bady, "Materials For Magnetic Assist," *Proceedings of the Fifth Symposium on Hydrogen Thyratrons and Modulators*, pp. 159–170, Fort Monmouth, NJ (May 1958).

2.a.4 John Wallace, "Microlaminated Ferromagnetic Composites for Magnetic Switching," *Digest of Technical Papers Sixth IEEE Pulsed Power Conference*, pp. 17–20, Arlington, VA (June 1987).

2b. Materials-Amorphous

2.b.1 J.J. Becker, "Magnetization Reversal Behavior in an Amorphous Alloy," *IEEE Transactions on Magnetics*, **MAG-11**(5), pp. 1326–1328 (Sept. 1975).

2.b.2 R. Boll and H.R. Hilzinger, "Comparison of Amorphous Materials, Ferrites, and Permalloys," *IEEE Transactions on Magnetics*, **MAG-19**(5), pp. 1946–1951 (Sept. 1983).

2.b.3 P. Chaudhari, B. Giessen, and D, Turnbull, "Metallic Glasses," *Scientific American*, **242**(4), pp. 98–117 (April 1980).

2.b.4 A. Datta and C.H. Smith, "Fe-Co-B-Si Amorphous Alloy with Maximum Saturation Induction," *Proceedings 5th International Conference on Rapidly Quenched Metals*, pp. 1315–1318 (Sept. 1984).

2.b.5 J.E. Dolan, H.R. Bolton, and A.J. Power, "Investigation of Magnetic Switching Properties of Unannealed METGLAS 2605SC Tape," *Digest of Technical Papers Seventh IEEE Pulsed Power Conference*, pp. 688–691, Monterey, CA (June 1989).

2.b.6 J. Gilman, "Ferrous Metallic Glasses," *Metal Progress*, pp. 1–6 (Aug. 1979).

2.b.7 John J. Gilman, "Metallic Glasses," *Physics Today*, pp. 46–53 (May 1975).

2.b.8 A.A. Glazer and R.I Tagirov, "Amorphous Metallic Materials," *Bulletin of Academy of Sciences of USSR, Physical Series* (Izvestiya Akademii Nauk SSSR, Seriya Fizicheskaya) 42-8, p. 1600 (1978).

2.b.9 R.M. Jones, A.J. Collins, and N.G. Cleaver, "A Comparison of the Step dB/dt Pulse Magnetization Losses in Some Amorphous Ribbon and Conventional Toroids," *IEEE Transactions on Magnetics*, **MAG-17**(6), pp. 2707–2709 (Nov. 1981).

2.b.10 R.M. Jones, "Step dB/dt Magnetization Losses in Toroidal Amorphous Ribbon and Polycrystalline Cores," *IEEE Transactions on Magnetics*, **MAG-18**(6), pp. 1559–1561 (Nov. 1982).

2.b.11 R.M. Jones, "Step dB/dt Switching Characteristics of Square Loop, Strip Wound Ni-Fe Toroids," *IEEE Transactions on Magnetics*, **MAG-19**(5), pp. 2024–2026 (Sept. 1983).

2.b.12 R.M. Jones, *A Study of Pulse Magnetization and Pulse Transformers* (University of Wales, Ph.D. Thesis, May 1979).

2.b.13 H. Kronmüller, "Micromagnetism in Amorphous Alloys," *IEEE Transactions on Magnetics*, **MAG-15**(5), pp. 1218–1225 (Sept. 1979).

2.b.14 R.A. Levy and R. Hasegawa, *Amorphous Magnetism II* (1976).

2.b.15 J.D. Livingston and W.G. Morris, "SEM Studies of Magnetic Domains in Amorphous Ribbons," *IEEE Transactions on Magnetics*, **MAG-17**(6), pp. 2624–2626 (Nov. 1981).

2.b.16 K. Matsubara, T. Nakata, and M. Nakano, "Study on Building Factor of Stacked Core Made of Amorphous Sheets," *Journal of Applied Physics*, **64**(10), part 2, pp. 5707 (Nov. 1988).

2.b.17 C. Modzelewski, H.T. Savage, L.T. Kabacoff, et al., "Magnetomechanical Coupling and Permeability in Transversely Annealed Metglas 2605 Alloys," *IEEE Transactions on Magnetics*, **MAG-17**(6), pp. 2837–2839 (Nov. 1981).

2.b.18 D.M. Nathasingh, C. Smith, and A. Datta, "Effects of Coatings on the Soft Magnetic Properties of An Iron-Based Amorphous Alloy," *IEEE Transactions on Magnetics*, **MAG-20**(5), pp. 1332–1334 (Sept. 1984).

2.b.19 D. Nathasingh and C. Smith, "A New High-Flux, Low-Loss Magnetic Material for High Frequency Applications," *Proceedings Powercon 7*, **B2**(1-12) (March 1980).

2.b.20 R.C. O'Handley, "Domain Wall Kinetics in Soft Ferromagnetic Metallic Glasses," *Journal of Applied Physics*, **46**(11), pp. 4996–5001 (Nov. 1975).

2.b.21 R.C. O'Handley, L.I. Mendelsohn, R. Hasagawa, et al., "Low-Field Magnetic Properties of Fe80-B20 Glass," *Journal of Applied Physics*, **47**(10), pp. 4660–4662 (Oct. 1976).

2.b.22 V.R.V. Ramanan, C.H. Smith, and G.E. Fish, "Metallic Glasses in Magnetic Applications," *Key Engineering Materials*, **13–15**, pp. 849–861 (1987).

2.b.23 D. Raskin and L.A. Davis, "Metallic Glasses: A Magnetic Alternative," *IEEE Spectrum*, **18**(11), pp. 28–33 (Nov. 1981).

2.b.24 S.M. Sheard, M.R.J. Gibbs, and R.K. Avery, "Characterization of Co-Based Metallic Glasses for Saturable Inductor Cores," *Journal of Magnetism and Magnetic Materials*, **75**, pp. 397–406 (1988).

2.b.25 S.M. Sheard, *Metallic Glasses for Pulse Compression* (University of Bath, U.K., Ph.D. Thesis, 1989).

2.b.26 H. Shishido, T. Kan, and Y. Ito, "The Magnetic Domain and Properties of Amorphous Ribbons," *IEEE Transactions on Magnetics*, **MAG-21**(1), pp. 49–52 (Jan. 1985).

2.b.27 C.H. Smith and L. Barberi, "Dynamic Magnetization of Metallic Glasses," *Digest of Technical Papers 5th IEEE Pulsed Power Conference*, pp. 664–667, Arlington, VA (June 1985).

2.b.28 C.H. Smith and L. Barberi, "Fast Magnetization Reversals in Tape-Wound, Square-Loop Amorphous Alloy Cores," *Proceedings Soft Magnetic Materials 7 Conference, European Physics Society*, pp. 329–331, Blackpool U.K. (Aug. 1985).

2.b.29 C.H. Smith, "Magnetic Losses in Metallic Glasses Under Pulsed Excitation," *IEEE Transactions Nuclear Science*, **NS-30**(4), p. 2918 (Aug. 1983).

2.b.30 C. Smith and D. Nathasingh, "Magnetic Properties of Metallic Glasses Under Fast Pulse Excitation," *IEEE Conference Record of 1984 Sixteenth Power Modulator Symposium*, pp. 240–244, City, State (June 1984).

2.b.31 C.H. Smith, "Magnetic Pulse Compression by Metallic Glasses,"

Journal of Applied Physics, **64**(10), part 2, pp. 6032–6034 (Nov. 1988).

2.b.32 C. Smith, "Metallic Glasses for Magnetic Switches," *IEEE Conference Record of 1982 Fifteenth Power Modulator Symposium*, pp. 22–27, Baltimore, MD (June 1982).

2.b.33 C.H. Smith, "Metallic Glasses in High-Energy Pulsed Power Systems," *Glass...Current Issues*, A.F. Wright and J. Dupuy, editors, pp. 188–199 (Martinus Nijhoff Publishers, 1985).

2.b.34 C.H. Smith, "Permeabilities of Metallic Glasses at High Magnetization Rates," *IEEE Conference Record of the 1988 Eighteenth Power Modulator Symposium*, pp. 336–339, Hilton Head, SC (June 1988).

2.b.35 C.H. Smith, D. Nathasingh, and R.H. Liebermann, "Thickness Dependence of Magnetic Losses in Amorphous FeBSiC Ribbon Under Step dB/dt Magnetization," *IEEE Transactions on Magnetics*, **MAG-20**(5), p. 1320 (Sept. 1984).

2.b.36 M.L. Spano, K.B. Hathaway, and H.T Savage, "Magnetostriction and Magnetic Anisotropy of Field Annealed Metglas 2605 Alloys via DC M-H Loop Measurement Under Stress," *Journal of Applied Physics*, **53**(3), p. 2667 (March 1982).

2.b.37 V.J. Thottuvelil, T.G. Wilson, and H.A. Owen Jr., "Unusual High-Frequency Behavior of Some Amorphous Metallic-Alloy Tape-Wound Magnetic Cores," *IEEE Transactions on Magnetics*, **MAG-20**(4), pp. 570–578 (July 1984).

2.b.38 B.N. Turman, *Improved Amorphous Metal Materials for Magnetic Pulse Compression*, Pulsed Power Research and Engineering Division, Sandia National Lab./Allied Signal UC-404 (Aug. 1989).

2.b.39 S.V. Vonsovskii and E.A. Turov, "Metallic Glasses and Amorphous Magnetism," *Bulletin of Academy of Sciences of USSR, Physical Series* (Izvestiya Akademii Nauk SSSR, Seriya Fizicheskaya) 42-8, p. 1570 (1978).

2c. Materials-Ferrites

2.c.1 M. Belling, S. Cygan, M. Rickley, et al., "Dynamic B-H Curves of Magnetic Materials under Magnetic Switching Transients," *Digest of Technical Papers 5th IEEE Pulsed Power Conference*, pp. 668–671, Arlington, VA (June 1985).

2.c.2 E. Roess, "Soft Magnetic Ferrites and Applications in Telecommunication and Power Converters," *IEEE Transactions on Magnetics*, **MAG-18**(6), p. 1529 (Nov. 1982).

2.c.3 E.C. Snelling, *Soft Ferrites, Properties and Applications* (Butterworths and Co., 1988).

2.c.4 R. Soohoo, *Theory and Application of Ferrites* (Prentice-Hall, 1960).

2d. Materials-General

2.d.1 R.M. Bozorth, *Ferromagnetism* (Van Nostrand Co., Princeton, 1951).

2.d.2 W. Brown, Jr., *Magnetostatic Principles in Ferromagnetism* (North-Holland, New York, 1962).

2.d.3 C.-W. Chen, *Magnetism and Metallurgy of Soft Magnetic Materials* (North-Holland, also Dover, City 1977).

2.d.4 S. Chikazumi and S.H. Charap, *Physics of Magnetism* (John Wiley and Sons, New York, 1964).

2.d.5 B.D. Cullity, *Introduction to Magnetic Materials* (Addison-Wesley, Reading, Mass., 1972).

2.d.6 D.A. Lowther and P.P. Silvester, *Computer-Aided Design in Magnetics* (Springer-Verlag, New York, 1986).

2.d.7 K.H. Stewart, *Ferromagnetic Domains* (Cambridge University Press, Cambridge, 1954).

2.d.8 R.S. Tebble and D.J. Craik, *Magnetic Materials* (Wiley-Interscience, New York, 1969).

2e. Models-Megascopic, Static

2.e.1 D. Abe, et al., Use of Metallic Glasses in Magnetic Switching, Engineering Clinic Report, Harvey-Mudd College, Claremont, CA (July 1981).

2.e.2 D.L. Atherton and D.C. Jiles, "Effects of Stress on the Magnetization of Steel," IEEE Transactions on Magnetics, **MAG-19**(5), pp. 2021–2023 (Sept. 1983).

2.e.3 R.C. Barker, "Magnetization in Tape-Wound Cores," AIEE Transactions, part 1 (Communications and Electronics), **79**, pp. 482–503 (Nov. 1960).

2.e.4 D.M. Barrett, "Modeling the Characteristics of a Magnetically Switched Pulse-Forming Line," Digest of Technical Papers Seventh IEEE Pulsed Power Conference, pp. 1–4, Monterey, CA (June 1989).

2.e.5 W. Baran, "Core Magnet Assembly with Anisotropic Permanent Magnets," IEEE Transactions on Magnetics, **MAG-19**, p. 2498 (1983).

2.e.6 G. Biorci and A. Ferro, "Hysteresis Losses Along Open Transformations," Le Journal de Physique et le Radium, Torino, Italy, pp. 237–240 (Feb. 1959).

2.e.7 G. Biorci and D. Pescetti, "Some Consequences of the Analytical Theory of the Ferromagnetic Hysteresis," Le Journal de Physique et le Radium, Torino, Italy, pp. 233–236 (Feb. 1959).

2.e.8 R. Bouc, "Modèle Mathématique d'Hystérésis (A Mathematical Model for Hysteresis)" (translation: UCRL-TRANS-12239, Lawrence Livermore National Laboratory, Livermore, CA), Acustica, **24**, pp. 16–25 (1971).

2.e.9 D. Briansky, "Single Analytical Formula for the Entire B/H Curve," International Journal Elect. Engineering Education, **5**(2), pp. 199–201 (1967).

2.e.10 B.D. Coleman and M.L. Hodgdon, "On A Class of Constitutive Relations for Ferromagnetic Hysteresis," Archive for Rational Mechanics and Analysis, **99**(4), pp. 375–396 (1987).

2.e.11 B.D. Coleman and M.L. Hodgdon, "A Constitutive Relation for Rate Independent Hysteresis in Ferromagnetically Soft Materials," International Journal Engineering Science, **24**(6), pp. 897–919 (1986).

2.e.12 J.L. Coulson, R.D. Slater, and R.R.S. Simpson, "Representation of Magnetic Characteristic Including Hysteresis Using Preisach's Theory," Proceedings IEE, **124**, pp. 895–898 (Oct. 1977).

2.e.13 N. Curland and D.E. Speliotis, "A Theoretical Study of an Isolated Transition Using an Iterative Hysteresis Model," IEEE Transactions on Magnetics, **MAG-6**, pp. 640–646 (Sept. 1970).

2.e.14 R.M. Del Vecchio, "An Efficient Procedure for Modeling Complex Hysteresis Processes in Ferromagnetic Materials," IEEE Transactions on Magnetics, **MAG-16** (1980).

2.e.15 A. di Napoli, R. Paggi, "A Model of Anisotropic Grain-Oriented Steel," IEEE Transactions on Magnetics, **MAG-19**, pp. 1557–1561 (1983).

2.e.16 T. Doong and I.D. Mayergoyz, "On Numerical Implementation of Hysteresis Models," IEEE Transactions on Magnetics, **MAG-21**(5), pp. 1853–1855 (1985).

2.e.17 M.K. El-Sherbiny, "Representation of the Magnetization Characteristic by a Sum of Exponentials," IEEE Transactions on Magnetics, **MAG-9**, pp. 60–61 (1973).

2.e.18 J.S. Everatt, "Computer Simulation of Nonlinear Inductors with Hysteresis," Electronics Letters, **6**(26), pp. 833–834 (Dec. 1970).

2.e.19 D.H. Everett, "A General Approach to Hysteresis," Transactions Faraday Society, **51**, pp. 1551–1557 (1955).

2.e.20 M. Gabler, "Analysis of Minor Loop Behavior During Alternating Flux Reversal in Rectangular-Loop Toroidal Cores," IEEE Transactions on Magnetics, **MAG-3**(2) (March 1967).

2.e.21 D.H. Gillott and M.D. Agrams, "Determination of Minor Hysteresis Loops of Isotropic Ferromagnetic Materials," IEEE Transactions on Magnetics, pp. 235–236 (Sept. 1965).

2.e.22 A.Y. Hannalla and D.C. MacDonald, "Representation of Soft Magnetic Materials," Proceedings IEE, 127, part A, pp. 386–391 (Aug. 1980).

2.e.23 W. Hochwald and C.T. Kleiner, "Digital Simulation of Nonlinear Electromagnetic Circuits," IEEE Transactions on Magnetics, **MAG-2**, pp. 532–539 (Sept. 1966).

2.e.24 N. Janssens, "Static Models of Magnetic Hysteresis," IEEE Transactions on Magnetics, **MAG-13**(5), pp. 1379–1381 (Sept. 1977).

2.e.25 D.C. Jiles and D.L. Atherton, "Ferromagnetic Hysteresis," IEEE Transactions on Magnetics, **MAG-19**(5), p. 2183 (Sept. 1983).

2.e.26 D.C. Jiles and D.L. Atherton, "Theory of Ferromagnetic Hysteresis," Journal of Applied Physics, 55(6), pp. 2115–2120 (March 1984).

2.e.27 D.C. Jiles and D.L. Atherton, "Theory of Ferromagnetic Hysteresis," Journal of Magnetism and Magnetic Materials, **61**, pp. 48–60 (1986).

2.e.28 D.C. Jiles and D.L. Atherton, "Theory of the Magnetisation Process in Ferromagnets and its Application to the Magnetomechanical Effect," Journal of Physics D: Applied Physics, **17**, pp. 1265–1281 (1984).

2.e.29 M. Jufer and A. Apostolides, "An Analysis of Eddy Current and Hysteresis Losses in Solid Iron Based on Simulation of Saturation and Hysteresis Characteristics," IEEE Transactions Power Applied and Systems, **PAS-95**, pp. 1786–1794 (Nov. 1976).

2.e.30 W.K. Macfadyen, R.R.S. Simpson, R.D. Slater, et al., "Representation of Magnetization Curves by Exponential Series," Proceedings Institute Elec. Engineering, **120**, pp. 902–904 (1973).

2.e.31 W. Manly Jr., "An Appraisal of Several Nonlinear Hysteresis Loop Models," IEEE Transactions on Magnetics, pp. 256–260 (Sept. 1973).

2.e.32 I. Mayergoyz, "Mathematical Models of Hysteresis," IEEE Transactions on Magnetics, **MAG-22**(5), pp. 603–608 (Sept. 86).

2.e.33 F.H. Middleton, "Analytic Hysteresis Function," Journal of Applied Physics, **325**, p. 251S (1961).

2.e.34 S. Ohteru, "On Expressions of Magnetic Hysteresis Characteristics," AIEE Transactions Power Applied and Systems, **PAS-78**, pp. 1809–1815 (Feb. 1960).

2.e.35 D.L. Portigal, "A Magnetic Recording Simulation Program Having an Improved Fit to Actual Hysteresis Loops," IEEE Transactions on Magnetics, **MAG-11**, pp. 934–941 (May 1975).

2.e.36 R. Potter and R. Schmulian, "Self-Consistantly Computed Magnetization Patterns in Thin Magnetic Recording Media," IEEE Transactions on Magnetics, **MAG-7**, pp. 873–880 (Dec. 1971).

2.e.37 M.A. Rahman, M. Poloujadoff, R.D. Jackson, et al., "Improved Algorithms for Digital Simulation of Hysteresis Processes in Semi Hard Magnetic Materials," IEEE Transactions on Magnetics, **MAG-17**(6), pp. 3253–3255 (Nov. 1981).

2.e.38 J.A. Resh, "Towards General Simulation of Ferromagnetic Devices," Proceedings 12th Midwest Symposium on Circuit Theory, Austin, TX, V.2.1 to V.2.7 (April 1969).

2.e.39 J. Rivas, J.M. Zamarro, E. Martin, and C. Pereira, "Simple Approximation for Magnetization Curves and Hysteresis Loops," IEEE Transactions on Magnetics, **MAG-17** (July 1981).

2.e.40 R.W. Roberts and R.I. Van Nice, "Influence of ID/OD Ratio on Static and Dynamic Magnetic Properties of Toroidal Cores," AIEE Transactions Communications and Electronics, **74**, pp. 599–607 (Nov. 1955).

2.e.41 M.J. Sablik, G.L. Burkhardt, H. Kwun, and D.C. Jiles, "A Model for the Effect of Stress on the Low-Frequency Harmonic Content of the Magnetic Induction in Ferromagnetic Materials," Journal of Applied Physics, **63**, pp. 3930–3932 (April 1988).

2.e.42 M.J. Sablik, H. Kwun, G.L. Burkhardt, and D.C. Jiles, "Model for the Effect of Tensile and Compressive Stress on Ferromagnetic Hysteresis," Journal of Applied Physics, **61**, pp. 3799–3801 (April 1987).

2.e.43 M.J. Sablik and D.C. Jiles, "A Model for Hysteresis in Magnetostriction," Journal of Applied Physics, **64**(10), part. 2, pp. 5402–5404 (Nov. 1988).

2.e.44 S.N. Talukdar and J.R. Bailey, "Hysteresis Models for System Studies," IEEE Transactions Pow. Applied and Systems, **PAS-95**, pp. 1429–1434 (July 1976).

2.e.45 J.W. Teape, R.R.S. Simpson, R.D. Slater, and W.S. Wood, "Representation of Magnetic Characteristic Including Hysteresis by Exponential Series," Proceedings IEE, **121**, pp. 1019–1020 (1974).

2.e.46 W. Thompson, "Mathematical Model for Nonlinear Magnetic Cores at Low Frequency," IEEE Transactions on Magnetics, **MAG-10** (June 1974).

2.e.47 F. Trutt, E. Erdelyi, and R. Hopkins, "Representation of the Magnetization Characteristic of DC Machines for Computer Use," IEEE Transactions Power Apparatus and Systems, **PAS-87**(3), pp. 665–669 (March 1968).

2.e.48 S.S. Udpa and W. Lord, "A Fourier Descriptor Model of Hysteresis Loop Phenomena," IEEE Transactions on Magnetics, **MAG-21**(6), pp. 2370–2373 (Nov. 1985).

2.e.49 S. Ueno and K. Harada, "Hysteresis Model of Partial Flux Reversal in Ferrite Cores," IEEE Transactions on Magnetics, **MAG-7**, pp. 550–553 (Sept. 1971).

2.e.50 S. Ueno and K. Harada, "Complete and Partial Flux Switching in Ferrite Cores," IEEE Transactions on Magnetics, **MAG-8**, pp. 657–659 (Sept. 1972).

2.e.51 R.H. Van der Helden, J.R. Brauer, J.J. Ruehl, et al., "Utilizing Permanent Magnets in Nonlinear

Three-Dimensional Finite Element Models," IEEE Transactions on Magnetics, **MAG-24**(6), pp. 2931–2933 (Nov. 1988).

2.e.52 W.N. Weseloh, "Representation of Magnetization Curves Over Extended Range by Rational-Fraction Approximation," Proceedings IEE, **116**(1), pp. 156–60 (1969).

2.e.53 K. Wiesen and S. H. Charap, "A Better Scalar Preisach Algorithm," IEEE Transactions on Magnetics, **24**(6), pp. 2491–2493 (Nov. 1988).

2f. Models-Megascopic, Dynamic

2.f.1 S. Bass, *A Generalized Hysteresis Model* (Purdue University, West Lafayette, IN, 1971).

2.f.2 C.D. Boley and M.L. Hodgdon, "Model and Simulations of Hysteresis in Magnetic Cores," in *Intermag Conference*, pp. 1–17 (March 1989).

2.f.3 D.A.H. Brown, "Behavior of Square Loop Cores in Circuits," *Electronic Engineering*, **31**, pp. 408–412 (July 1959).

2.f.4 S.H. Charap, "Magnetic Hysteresis Model," *IEEE Transactions on Magnetics*, **MAG-10**, 1091–1096 (1974).

2.f.5 T.C. Chen and A. Papoulis, "Terminal Properties of Magnetic Cores," *Proceedings IRE*, **46**, pp. 839–849 (May 1958).

2.f.6 L.O. Chua and S.C. Bass, "A Generalized Hysteresis Model," *IEEE Transactions on Circuit Theory*, **CT-19**(1), pp. 36–48 (Jan. 1972).

2.f.7 L.O. Chua and K.A. Stromsmoe, "Lumped Circuit Models for Non-Linear Inductors Exhibiting Hysteresis Loops," *IEEE Transactions on Circuit Theory*, **CT-17**(4), pp. 564–574 (Nov. 1970).

2.f.8 L.O. Chua and K.A. Stromsmoe, "Mathematical Model for Dynamic Hysteresis Loops," *International Journal Engineering Science*, **9**, pp. 435–450 (1971).

2.f.9 W. Dierking and C.T. Kleiner, "Phenomenological Magnetic Core Model for Circuit Analysis Programs," *IEEE Transactions on Magnetics*, pp. 594–596 (Sept. 1972).

2.f.10 B.N. Filippov, S.V. Zhakov, and Yu.G. Lebedev, "Influence of Domain Structure on Some Dynamic Properties of Ferromagnets," *IEEE Transactions on Magnetics*, **MAG-15**(6), pp. 1849–1854 (Nov. 1979).

2.f.11 L. Gilli and A.R. Meo, "The Behavior of Rectangular Hysteresis Cores in Every Application," *Proceedings IEEE*, **51**, pp. 1578–1585 (Nov. 1963).

2.f.12 V. Hesterman, "Evaluation of Flux-Switching Models for Magnetic Devices," *Proceedings Special Technical Conference on Non-Linear Magnetics*, Los Angeles, CA, pp. 265–292 (Nov. 1961).

2.f.13 V.W. Hesterman, *Flux-Switching Properties of a Partially Set Core Stanford Research Institute*, Stanford, CA, SRI Technical Report (Nov. 1963).

2.f.14 V.W. Hesterman, "Switching Properties of a Partially Set Square-Loop Ferrite Core," *IEEE Transactions on Magnetics*, **MAG-1**, pp. 309–314 (Dec. 1965).

2.f.15 M.L. Hodgdon, "Applications of a Theory of Ferromagnetic Hysteresis," *IEEE Transactions on Magnetics*, **MAG-24**(1), pp. 218–221 (Jan. 1988).

2.f.16 M.L. Hodgdon, "Mathematical Theory and Calculations of Magnetic Hysteresis Curves," *IEEE Transactions on Magnetics*, **MAG-24**(6), pp. 3120–2 (Nov. 1988).

2.f.17 C.T. Kleiner, "Application of a Phenomenological Core Model in the SYSCAP 2.5 Circuit Analysis Program,"

IEEE Transactions on Magnetics, **MAG-19**(5), pp. 2186–2188 (Sept. 1983).

2.f.18 N. Menyuk and J.B. Goodenough, "Magnetic Materials for Digital-Computer Components. I. A Theory of Flux Reversal in Polycrystalline Ferromagnetics," *Journal of Applied Physics*, **26**(1), pp. 8–18 (Jan. 1955).

2.f.19 D. Nitzan, "Computation of Flux-Switching in Magnetic Circuits," *IEEE Transactions on Magnetics*, **MAG-1**, pp. 222–233 (Sept 1965).

2.f.20 D. Nitzan, "Computation and Modeling of Eddy Currents in Tape-Wound Square-Loop Cores," *IEEE Transactions on Magnetics*, **MAG-7**(1), pp. 185–197 (March 1971).

2.f.21 D. Nitzan, "Computer Program for Transient Analysis of Circuits Including Magnetic Cores," *IEEE Transactions on Magnetics*, **MAG-5**, pp. 524–533 (Sept. 1969).

2.f.22 D. Nitzan, "Engineering Flux-Switching Models for Toroidal and Mulitipath Cores," *IEEE Transactions Communications and Electronics*, **CE-83**, pp. 309–314 (May 1964).

2.f.23 D. Nitzan and J.R. Herndon, *Modeling of Magnetic Cores for Computer Circuit Analysis*, Harry Diamond Lab, Washington, D.C., Technical Report AD 864 933 (Sept. 1969).

2.f.24 D. Nitzan, "Models for Elastic and Inelastic Flux Switching," *IEEE Transactions on Magnetics*, **MAG-2**, pp. 751–760 (Dec. 1966).

2.f.25 S. Prusty and M.V.S. Rao, "A Direct Piecewise Linearized Approach to Convert RMS Saturation Characteristic to Instantaneous Saturation Curve," *IEEE Transactions on Magnetics*, **MAG-16**, pp. 156–160 (1980).

2.f.26 S. Prusty and M.V.S. Rao, "A Novel Approach for Predetermination of Magnetization Characteristics of Transformers Including Hysteresis," *IEEE Transactions on Magnetics*, **MAG-20**(4), pp. 607–612 (July 1984).

2.f.27 R.H. Pry and C.P. Bean, "Calculation of the Energy Loss in Magnetic Sheet Using a Domain Model," *Journal of Applied Physics*, **29**, pp. 532–533 (March 1958).

2.f.28 Y. Saito, K. Fukushima, S. Hayano, and N. Tsuya, "Application of a Chua Type Model to the Loss and Skin Effect Calculations," *IEEE Transactions on Magnetics*, **MAG-23**(5), pp. 2227–2229 (Sept. 1987).

2.f.29 Y. Saito, M. Namiki, S. Hayano, and N. Tsuya, *Experimental Verification of Modified Chua Type Magnetization Model* (College of Engineering, Hosei University, Tokyo, Japan, 1984).

2.f.30 Y. Saito, S. Hayano, T. Yamamura, and H. Saotome, "Hysteretic Fields in a Toroidal Reactor," *IEEE Transactions on Magnetics*, **MAG-20**(5), pp. 1965–1967 (Sept. 1984).

2.f.31 Y. Saito, H. Saotome, S. Hayano, and T. Yamamura, "Modeling of Hysteretic and Anisotropic Magnetic Field Problems," *IEEE Transactions on Magnetics*, **MAG-19**(6), pp. 2510–2512 (Nov. 1983).

2.f.32 Y. Saito, H. Saotome, S. Hayano, and T. Yamamura, "Modeling of Nonlinear Inductor Exhibiting Hysteresis Loops and its Application to the Single Phase Parallel Inverters," *IEEE Transactions on Magnetics*, **MAG-19**(5), pp. 2189-11 (Sept. 1983).

2.f.33 Y. Saito, S. Hayano, and Y. Sakaki, "A Parameter Representing Eddy Current Loss of Soft Magnetic Materials and its Constitutive Equation," *Journal of Applied Physics*, **64**, pp. 5684–5686 (Nov. 1988).

2.f.34 Y. Saito, S. Hayano, T. Yamamura, and N. Tsuya, "A Representation of Magnetic Hysteresis," *IEEE*

Transactions on Magnetics, **MAG-20**(5), pp. 1434–1436 (Sept. 1984).

2.f.35 Y. Saito, S. Hayano, H. Nakamura, and Y. Kishino, et al., "A Representation of Magnetic Hysteresis by Fourier Series," *Journal of Magnetism and Magnetic Materials*, **(54–57)**, pp. 1613–1614 (1986).

2.f.36 Y. Saito, S. Hayano, Y. Kishino, K. Fukushima, et al., "A Representation of Magnetic Aftereffect," *IEEE Transactions on Magnetics*, **MAG-22**(5), pp. 647–649 (Sept. 1986).

2.f.37 Y. Saito, "3D Analysis of Magnetodynamic Fields in Electromagnetic Devices Taking Into Account the Dynamic Hysteresis Loops," *IEEE Transactions on Magnetics*, **MAG-18**, pp. 546–551 (March 1982).

2.f.38 E.A. Sands, "The Behavior of Rectangular Hysteresis Loop Magnetic Materials Under Current Pulse Conditions," *IRE Proceedings*, **40**, pp. 1246–1250 (Oct. 1952).

2.f.39 J.G. Santesmases, J. Ayala, and A.H. Cachero, "Analytical Approximation of Dynamic Hysteresis Loop and its Application to a Series Ferroresonant Circuit," *Proceedings IEE*, **117**(1), pp. 234–240 (Jan. 1970).

2.f.40 M. Stockton, E.L. Neau, and J.P. VanDevender, "Pulsed Power Switching Using Saturable Core Inductors," *Journal of Applied Physics*, **53**, pp. 2765–2767 (March 1982).

2.f.41 Keith Stromsmoe, *Modeling of Dynamic Hysteresis Loops* (Purdue University, West Lafayette, IN, Ph.D. Thesis, 1970)

2.f.42 W.J. Thompson and P.R. Munk, "Mathematical Model of Nonlinear Magnetic Cores," *IEEE Transactions on Magnetics*, **MAG-6**(3), p. 523 (Sept. 1970).

2.f.43 J.M. Zentler, *NET2 Magnetic Core Model*, Lawrence Livermore National Laboratory, Livermore, CA, Technical letter WSG 84-54, Electronics Engineering, pp. 1–13 (May 1984).

2g. Models-Domain Wall Motion

2.g.1 J.E.L. Bishop, "Understanding Magnetization Losses in Terms of Eddy Current Dominated Domain Wall Dynamics," *Journal of Magnetism and Magnetic Materials*, **19**, pp. 336–344 (1980).

2.g.2 L. Alberts, J.E.L. Bishop, and E.W. Lee, "The Behavior of Ferromagnetic Sheets in Alternating Electric and Magnetic Fields. II. Measurement of the Electrical Resistance...," *Proceedings of the Royal Society of London, Series A: Mathematical and Physical Sciences*, **276**, pp. 112–124 (1963).

2.g.3 C.P. Bean and D.S. Rodbell, "Kinetics of Magnetization in Some Square-Loop Magnetic Tapes," *Journal of Applied Physics*, **26**, pp. 124–125 (Jan. 1955).

2.g.4 J.J. Becker, "Domain Boundary Configuration During Magnetization Reversals," *Journal of Applied Physics*, **30**, pp. 387–390 (March 1959).

2.g.5 G. G. Berg, "Experimental Study of 50-50 Ni-Fe Tape-Wound Magnetic Cores for the ASTRON Accelerator," *Proceedings of Symposium on Engineering Problems of Fusion Research*, pp. CI-7-1 to CI-7-4, Los Alamos National Laboratory, Los Alamos, NM (April 1969).

2.g.6 J.E.L. Bishop and E.W. Lee, "The Behavior of Ferromagnetic Sheets in Alternating Electric and Magnetic Fields, I. A Domain Theory of the Skin Effect," *Proceedings of the Royal Society of London, Series A: Mathematical and Physical Sciences*, **276**, pp. 96–111 (1963).

2.g.7 J.E.L. Bishop, "Magnetic Domain Structure, Eddy Currents and Permeability Spectra," *British Journal of Applied Physics*, **17**, pp. 1451–1460 (1966).

2.g.8 J.E.L. Bishop, "The Influence of Domain Wall Bowing on Eddy Current Drag," *Physica Status Solidi A: Applied Research*, **7**, pp. 117–124 (1971).

2.g.9 J.E.L. Bishop, "Tables of the Frequency Dependence of Permeability for the Polivanov Domain Model," *Journal of Physics D: Applied Physics*, **4**, pp. 1235–1238 (1971).

2.g.10 J.E.L. Bishop and P.M. Clay, "The Dependence of Permeability and Losses on Direction of Magnetization in Anisotropic Ferromagnetic Laminations," *Journal of Physics D: Applied Physics*, **4**, pp. 1797–1811 (1971).

2.g.11 J.E.L. Bishop and P.M. Clay, "Magnetic Domain Interpretation of the Angle and Field Dependence of Permeability and Loss in (110)[001] Si-Fe," *Journal of Physics D: Applied Physics*, **5**, pp. 1720–1726 (1972).

2.g.12 J.E.L. Bishop, "The Analysis of Eddy-Current-Limited Magnetic Domain Wall Motion, Including Severe Bowing and Merging," *Journal of Physics D: Applied Physics*, **6**, pp. 97–115 (1973).

2.g.13 J.E.L. Bishop, "Dependence of Initial Drive Field on Switching Rate in 50-50 Ni-Fe Tape Cores," *IEEE Transactions on Magnetics*, **MAG-10**, pp. 1132–1133 (Dec. 1974).

2.g.14 J.E.L. Bishop, "Domain Wall Bowing Interpretation of Eddy Current Loss Measurements in a (110)[001] Si-Fe Monocrystal," *IEEE Transactions on Magnetics*, **MAG-12**(1), pp. 21–27 (Jan. 1976).

2.g.15 J.E.L. Bishop, "Dynamic Ferromagnetic Domain Wall Response to Incremental AF Fields and Becker Wall Area Measurement Technique," *Physica Status Solidi A: Applied Research*, **11**, pp. K75-78 (1972).

2.g.16 J.E.L. Bishop, "The Influence of a Random Domain Size Distribution on the Eddy-Current Contribution to Hysteresis in Transformer Steel," *Journal of Physics D: Applied Physics*, **9**, pp. 1367–1377 (1976).

2.g.17 J.E.L. Bishop, "Eddy-Current-Limited Growth of Ferromagnetic Domains on the Surface of Square-Loop Alloy Tapes," *Journal of Physics D: Applied Physics*, **9**, pp. 2095–2110 (1976).

2.g.18 J.E.L. Bishop, "Ruckling: A Novel Low-Loss Domain Wall Motion for (110)[001] SiFe," *IEEE Transactions on Magnetics*, **MAG-12**(3), pp. 248–255 (May 1976).

2.g.19 J.E.L. Bishop and P. Williams, "A Comparison of Rapid Surface and Volume Magnetization Measurements on 50% NiFe Tape with Models of Eddy-Current-Limited Domain," *Journal of Physics D: Applied Physics*, **10**, pp. 225–241 (1977).

2.g.20 J.E.L. Bishop, "A Simple Approximate Analytic Treatment of Extreme Domain Wall Bowing," *Journal of Physics D: Applied Physics*, **10**, pp. L67-72 (1977).

2.g.21 J.L. Bishop, "The Shape, Energy, Eddy Current Loss, and Relaxation Damping of Magnetic Domain Walls in Glassy Iron Wire," *IEEE Transactions on Magnetics*, **MAG-13**(5), pp. 1638–1645 (Sept. 1977).

2.g.22 J.E.L. Bishop, "Improved Simulation of Domain Wall Bowing in Metallic Laminations Using a New Spline Model," *Journal Magnetism and Magnetic Materials*, **10**, pp. 75–83 (1979).

2.g.23 J.E.L. Bishop, "Steady-State Eddy-Current Dominated Magnetic Domain Wall Motion with Severe Bowing and

Necking," *Journal of Magnetism and Magnetic Materials*, **12**, pp. 102–107 (1979).

2.g.24 J.E.L. Bishop, "The Contribution Made by Eddy Currents to the Effective Mass of a Magnetic Domain Wall," *Journal of Physics D: Applied Physics*, **13**, pp. L15–19 (1980).

2.g.25 J.E.L. Bishop, "Asymmetric Domain Wall Bowing and Tilting Motions in Materials with Orientations Between (100) [001] and (110) [001]," *Journal of Magnetism and Magnetic Materials*, **26**, pp. 247–251 (1982).

2.g.26 J.E.L. Bishop, "Modeling Domain Wall Motion in Soft Magnetic Alloys," *Journal of Magnetism and Magnetic Materials*, **41**, pp. 261–271 (1984).

2.g.27 J.E.L. Bishop, "Enhanced Eddy Current Loss Due to Domain Displacement," *Journal of Magnetism and Magnetic Materials*, **49**, pp. 241–249 (1985).

2.g.28 T. Bonnema, F. Friedlaender, and L. Silva, "Magnetic Domain Observations in 50 Percent Ni-Fe Tapes," *IEEE Transactions on Magnetics*, **MAG-4**(3), pp. 431–434 (Sept. 1968).

2.g.29 H. Bourne, Jr. and D. Bartran, "A Transient Solution for Domain Wall Motion," *IEEE Transactions on Magnetics*, **MAG-8**(4), pp. 741–743 (Dec. 1972).

2.g.30 H. Bourne, Jr. and D. Bartran, "Transient and Steady-State Velocity of Domain Walls for a Complete Range of Drive Fields," *IEEE Transactions on Magnetics*, **MAG-10**(4), pp. 1081–1084 (Dec. 1974).

2.g.31 N. Burais and G. Grellet, "Numerical Modeling of Iron Losses in Ferromagnetic Steel Plate," *IEEE Transactions on Magnetics*, **MAG-17**(2), pp. 558–562 (March 1982).

2.g.32 S.H. Charap, "Eddy Current Losses in Magnetic Sheet with Simple Bar-like 180 Domain Structures," *Journal of Applied Physics*, **50**, pp. 7701–7703 (Nov. 1979).

2.g.33 P.G. Collar, E.W. Lee, and J.E.L. Bishop, "Magnetic Domain Studies Using Permeability Spectra I," *Journal of Physics D: Applied Physics*, **2**, pp. 1353–1365 (1969).

2.g.34 R.W. DeBlois, "Domain Wall Motion in Metals," *Journal of Applied Physics*, **29**, pp. 459–467 (March 1958).

2.g.35 F.J. Friedlaender, *The Process of Flux Reversal in Grain-Oriented 50% Nickel-Iron Tape Cores, Magnetic Amplifier*, Technical Report no. 21, (Carnegie Institute of Technology PhD Thesis, 1955).

2.g.36 F.J. Friedlaender, "Flux Reversal in Magnetic Amplifier Cores," *AIEE Transactions part I*, **75**, pp. 268–278 (1956).

2.g.37 F.J. Friedlaender and I.P. Leliakov, "Initiation of Flux Reversal in Magnetic Amplifier Cores," *AIEE Transactions part I*, **80**, pp. 269–272 (1961).

2.g.38 F.J. Friedlaender and L.L. Ogborn, "Small-Signal Behavior of 50% Ni-Fe Tape Cores," *IEEE Transactions Communications and Electronics, part I*, **82**, pp. 372–375 (1963).

2.g.39 F.J. Friedlaender and J.D. Gassaway, "Cross-Field Effects in Tape Cores," *IEEE International Conference on Nonlinear Magnetics*, Washington, D.C., pp. 833–834 (April 1964).

2.g.40 F.J. Friedlaender and J. D. McMillen, "Anhysteretic Magnetization of Ni-Fe Tape Cores," *Journal Applied Physics*, **38**(3), pp. 1188–1190 (March 1967).

2.g.41 F. Friedlaender and J. McMillen, "A Magnetic Core Analog Memory," *IEEE*

Transactions on Magnetics, **MAG-3**(3), pp. 463–466 (Sept. 1967).

2.g.42 A.G. Ganz, "Materials: Models; Empirical, Static.Applications of Thin Permalloy Tapes in Wide-Band Telephone and Pulse Transformers," *AIEE Transactions*, **65**, pp. 177–83 (March 1946).

2.g.43 V. Ginzburg, "The Calculation of Magnetization Curves and Magnetic Hysteresis Loops for a Simplified Model of a Ferromagnetic Body," *IEEE Transactions on Magnetics*, **MAG-12**(2), pp. 119–126 (March 1976).

2.g.44 J. Goodenough, "A Theory of Domain Creation and Coercive Force in Polycrystalline Ferromagnetics," *Physical Review*, **95**(4), pp. 917–932 (Aug. 1954).

2.g.45 T.R. Haller and J.J. Kramer, "Model for Reverse-Domain Nucleation in Ferromagnetic Conductors," *Journal of Applied Physics*, **41**(3), pp. 1036–1037 (March 1970).

2.g.46 H.K. Haynes, "Model for Nonlinear Flux Reversals of Square-Loop Polycrystalline Magnetic Cores," *Journal of Applied Physics*, **29**, pp. 472-4 (March 1958).

2.g.47 F.C. Hewett and W.M. Ovem, "History Effect of Time-limited Excitation," *Journal of Applied Physics*, **34**, p. 111 (April 1963).

2.g.48 S. Hill and K.J. Overshott, "The Dependence of Power Loss on Domain Wall Bowing in Single Crystals of 3% Grain-Oriented Silicon-Iron," *IEEE Transactions on Magnetics*, **MAG-14**(5), pp. 773–775 (Sept. 1978).

2.g.49 C. Kittel and J.K. Galt, "Ferromagnetic Domain Theory," *Solid State Physics*, **3**, pp. 437–564, Edited by Frederick Seitz, David Turnbull (Academic Press, 1956).

2.g.50 J.E. Knowles, "Some Observations of Bitter Patterns on Polycrystalline 'Square-Loop' Ferrites, and a Theoretical Explanation of the Loop Shape and Pulse," *Proceedings of the Physical Society, London*, **75**, pp. 885–897 (June 1960).

2.g.51 J.E. Knowles, "A Further Explanation of the Shape of the Hysteresis Loop of 'Square-Loop' Ferrites," *Proceedings of the Physical Society, London*, **77**, pp. 225–229 (Feb. 1961).

2.g.52 J.E. Knowles, "The Irreversible Change of Magnetization produced in 'Square-Loop' Ferrite by Pulsed Magnetic Fields," *Proceedings of the Physical Society, London*, **77**, pp. 576–586 (March 1961).

2.g.53 S. Konishi, S. Hara, S. Sugatani, and Y. Sakurai, "Domains and Domain-Wall Motion in Grain-Oriented 50-Percent Ni-Fe Tapes," *IEEE Transactions on Magnetics*, **MAG-6**(1), pp. 105–110 (March 1970).

2.g.54 R.W. Kuenning, *Eddy Current Analysis Extended for Times After the Inner Wrap Completely Saturates with Non-Constant Applied Voltage*, Lawrence Livermore National Laboratory, Livermore, CA, UCID-15031 (Sept. 1966).

2.g.55 R.W. Kuenning, *Saturation Wave Analysis for Eddy Currents Entirely within the Magnetic Strip*, Lawrence Livermore National Laboratory, Livermore, CA, UCID-15029 (Sept. 1966).

2.g.56 R.W. Kuenning, *Eddy Current Analysis Extended for Non-Constant Applied Voltage*, Lawrence Livermore National Laboratory, Livermore, CA, UCID-15030 (Sept. 1966).

2.g.57 I. Leliakov and F.J. Friedlaender, "An Improved Model for Flux Reversal in Ni-Fe Cores," *AIEE Transactions (Communications and Electronics)*, **80**, pp. 23–26 (March 1961).

2.g.58 C.H. Lindsey, "The Square Loop Ferrite Core as a Circuit Element," *Proceedings IEE*, **106**, part C, pp. 117–124 (Sept. 1959).

2.g.59 W.C. Nunnally, J. Pover, T.E. Springer, A. Litton, et al., "Development of Stripline Magnetic Modulators," *IEEE Conference Record of 1982 Fifteenth Power Modulator Symposium*, pp. 23–31, Baltimore, MD (June 1982).

2.g.60 D.S. Rodbell and C.P. Bean, "Influence of Pulsed Magnetic Fields on the Reversal of Magnetization in Square-Loop Metallic Tapes," *Journal of Applied Physics*, **26**, pp. 1318–1323 (Nov. 1955).

2.g.61 Y. Sakaki, "An Approach Estimating the Number of Domain Walls and Eddy Current Losses in Grain-Oriented 3% Si-Fe Tape Wound Cores," *IEEE Transactions on Magnetics*, **MAG-16**(4), pp. 569–571 (July 1980).

2.g.62 Y. Sakaki and S.-I. Imagi, "Relationship Among Eddy Current Loss, Frequency, Maximum Flux Density and a New Parameter Concerning the Number of Domain Walls," *IEEE Transactions on Magnetics*, **MAG-17**(4), pp. 1478–1480 (July 1981).

2.g.63 Y. Sakaki and S.-I. Imagi, "Losses and Equivalent Number of Domain Walls in Polycrystalline and Amorphous Soft Magnetic Mater," *IEEE Transactions on Magnetics*, **MAG-18**(6), pp. 1840–1842 (Nov. 1982).

2.g.64 T. Sato and Y. Sakaki, "Discussion on Eddy Current Loss Under Square Wave Voltage Excitation," *IEEE Transactions on Magnetics*, **MAG-24**(6), pp. 2904–2906 (Nov. 1988).

2.g.65 N. Smith, "Domain Theory Model for Magnetic Thin Films," *IEEE Transactions on Magnetics*, **MAG-24**(6), pp. 2380–2382 (Nov. 1988).

2.g.66 P. Williams and J.E..L.Bishop, "Magnetic Domain Walls and Pulsed Magnetization Reversal in Amorphous Fe40-Ni40-P14-B6 Ribbon Under Tension," *Journal Magnetism and Magnetic Materials*, **20**, pp. 245–257 (1980).

2.g.67 H.J. Williams, W. Shockley, and C. Kittel, "Studies of the Propagation Velocity of a Ferromagnetic Domain Boundary," *Physical Review*, **80**, pp. 1090–1094 (Dec. 1950).

2.g.68 S.D. Winter, *Initial Current Response of a Tape Wound Core to an Applied Voltage Pulse*, Lawrence Livermore National Laboratory, Livermore, CA, UCID-15041 (Oct. 1966).

2.g.69 S.D. Winter, *Magnetization of Tape Assuming Uniform Distribution of Nucleating Centers Throughout the Tape*, Lawrence Livermore National Laboratory, Livermore, CA, UCID-15042 (Nov. 1966).

2.g.70 S.D. Winter and R.W. Kuenning, "Analysis of Flux Reversal in Tape Cores," *Symposium on Engineering Problems of Fusion Research*, pp. CI-6-1 to CI-6-3, Los Alamos National Laboratory, Los Alamos, NM (April 1969).

2.g.71 Stewart D. Winter, Robert Kuenning, and Gary Berg, "Pulse Properties of Large 50-50 NiFe Tape Cores," *IEEE Transactions on Magnetics*, **MAG-6**(1), pp. 41–45 (March 1970).

2.g.72 F.J. Young, S.K. Bhate, and W.M. Swift, "Theory of Eddy Current Losses in Finite Width Sheet Exhibiting Simple Bar-Like Domain Structures," *IEEE Transactions on Magnetics*, **MAG-10**, pp. 814–816 (1974).

2h. Models-Micromagnetic

2.h.1 E. Della Torre, "Numerical Micromagnetic Calculations," *IEEE Transactions on Magnetics*, **MAG-15**(5), pp. 1225–1228 (Sept. 1979).

2.h.2 R. Kikuchi, "On the Minimum of Magnetization Reversal Time," *Journal of Applied Physics*, **27**(11), pp. 1352–1357 (Nov. 1956).

2.h.3 L. Landau and E. Lifshitz, "On the Theory of the Dispersion of Magnetic Permeability in Ferromagnetic Bodies," *Physikalische Zeitschrift der Sowjetunion*, **8**, 153 (1935).

2.h.4 J. Mallinson, "On Damped Gyromagnetic Precession," *IEEE Transactions on Magnetics*, **MAG-23**(4), pp. 2003–2004 (July 1987).

2.h.5 Y. Nakatani and N. Hayashi, "Computer Simulation of Two-Dimensional Vertical Bloch Lines by Direct Integration of Gilbert Equation," *IEEE Transactions on Magnetics*, **MAG-23**(5), pp. 2179–2181 (Sept. 1987).

3. Magnetic Pulse Compressor Designs, Concepts, Evaluations, and Theory

This section includes papers that present specific magnetic pulse compressor designs, design concepts or evaluations of existing designs or concepts.

3.1 K. Aaland and G. A. Pence, *Magnetic Pulser for PAM Multiplexed Instrumentation Powered and Timed from 10 kHz 3 Phase AC*, prepared for the *The Workshop on Applied Magnetics*, Washington, D.C., May 1969, Lawrence Livermore National Laboratory, Livermore, CA, UCRL-71574, Rev. 1 (Dec. 1969).

3.2 S.E. Ball, "Optimum Switching Time for Magnetic Switches," *IEEE Conference Record of the 1988 Eighteenth Power Modulator Symposium*, pp. 86–89, Hilton Head, SC (June 1988).

3.3 S.E. Ball and H.G. Hammon III, "A High-Voltage Trigger Generator Using Magnetic Switches," *IEEE Conference Record of 1984 Sixteenth Power Modulator Symposium*, pp. 245–249 (June 1984).

3.4 S.E. Ball and T.R. Burkes, "Saturable Inductors as High Power Switches," *Digest of Technical Papers 3rd IEEE International Pulsed Power Conference*, pp. 269–272, Albuquerque, NM (June 1981).

3.5 S.E. Ball, D. Drury; R.N. Hitchcock, et al., "Laser Modulator Utilizing a Resonant Transformer with an Output Magnetic Switch," *Digest of Technical Papers Sixth IEEE Pulsed Power Conference*, pp. 256–258, Arlington, VA (June 1987).

3.6 W. Baran, "Core Magnet Assembly with Anisotropic Permanent Magnets," *IEEE Transactions on Magnetics*, **MAG-19**, p. 2498 (1983).

3.7 D. Birx, E. Cook, S. Hawkins, S. Poor, et al., "Magnetic Switching," *Digest of Technical Papers 4th IEEE Pulsed Power Conference*, pp. 231–235, Albuquerque, NM (June 1983).

3.8 D.L. Birx, E.G. Cook, L.L. Reginato, J.A. Schmidt, et al., "The Application of Magnetic Pulse Compression to the Grid System of the ETA / ATA

Accelerator," *IEEE Conference Record of 1982 Fifteenth IEEE Power Modulator Symposium*, pp. 10–13, Baltimore, MD (June 1982).

3.9 D.L. Birx, E.J. Lauer, L.L. Reginato, D. Rogers Jr., et al., "Experiments in Magnetic Switching," *Digest of Technical Papers 3rd IEEE International Pulsed Power Conference*, pp. 262–268, Albuquerque, NM (June 1981).

3.10 D. Birx, E. Cook, S. Poor, L. Reginato, J. Schmidt, et al., *Magnetic Switching, Final Chapter Book I: The ATA Upgrade Prototype*, Lawrence Livermore National Laboratory, Livermore, CA, UCID-89128 (May 1983).

3.11 D.L. Birx, E.J. Lauer, L.L. Reginato, J. Schmidt, et al., *Basic Principles Governing the Design of Magnetic Switches*, Lawrence Livermore National Laboratory, Livermore, CA, UCID-18831 (Nov. 1980).

3.12 C.R. Blaine, "Hybrid Magnetic Pulser," *Proceedings of the Fifth Symposium on Hydrogen Thyratrons and Modulators*, pp. 135–134, Fort Monmouth, NJ (May 1958).

3.13 E.E. Bowles, B.L. Burley, D.M. Barrett, H.C. Kirbie, et al., "Battery-Powered, Solid State Magnetic Compressor with Applications for High PRF Accelerators and Lasers," *Digest of Technical Papers Seventh IEEE Pulsed Power Conference*, pp. 681–683, Monterey, CA (June 1989).

3.14 G. Bredenkamp and J. Nel, "A Simultaneous Transfer Electromagnetic Pulse Compressor with Reduced Core Volume," *Digest of Technical Papers Seventh IEEE Pulsed Power Conference*, pp. 182–185, Monterey CA (June 1989).

3.15 G. Bredenkamp and P. Swart, "A Theoretical Basis for the Optimization of Electromagnetic Pulse Compressors Using Saturable Ferromagnetic Cores," *IEEE Conference Record of the 1988 Eighteenth Power Modulator Symposium*, pp. 90–94, Hilton Head, SC (June 1988).

3.16 E. Chu, "Design Considerations of Magnetic Switching Modulator," *Digest of Technical Papers 4th IEEE Pulsed Power Conference*, pp. 242–245, Albuquerque, NM (June 1983).

3.17 E.Y. Chu, G. Hofmann, H. Kent, and T. Bernhardt, "Magnetic Modulator for Low-Impedance Discharge Lasers," *IEEE Conference Record of 1982 Fifteenth IEEE Power Modulator Symposium*, pp. 32–36, Baltimore, MD (June 1982).

3.18 R.A. Dougal, G.D. Volakakis, and M.D. Abdalla, "Magnetically Delayed Vacuum Switching," *Digest of Technical Papers Sixth IEEE Pulsed Power Conference*, pp. 21–24, Arlington, VA (June 1987).

3.19 B.H. Fishbine, K.W. Zieher, S. Humphries Jr. , et al., "Operating Characteristics of a Magnetically-Switched Electron Injector," *Digest of Technical Papers, 5th IEEE Pulsed Power Conference*, pp. 677–678, Arlington, VA (June 1985).

3.20 R.J. Froelich and J.V. Stover, "A Long Pulse Magnetic Modulator," *Proceedings of the Seventh Symposium on Hydrogen Thyratrons and Modulators*, pp. 290–311, Fort Monmouth, NJ (May 1962).

3.21 I.S. Garber, *Magnetic Pulse Modulators* (U.S. Army Foreign Science and Technology Center, Charlottesville, Aug. 1983).

3.22 E. Goldfarb, "Performance of 9.6 MW Magnetic Pulse Modulator Prototype," *Proceedings of the Sixth Symposium on Hydrogen Thyratrons and Modulators*, pp. 235–249, Fort Monmouth, NJ (May 1960).

3.23 H.C. Harjes, K.J. Penn, G.A. Mann, and E.L. Neau, "Investigations Into the Design of 3 TW Magnetic Switches," *Digest of Technical Papers Sixth IEEE Pulsed Power Conference*, pp. 540–543, Arlington, VA (June 1987).

3.24 H. Hatanaka and M. Obara, "High Efficiency Operation of the High Repetition Rate Magnetic Pulse Compressor for KrF Excimer Lasers," *Digest of Technical Papers Seventh IEEE Pulsed Power Conference*, pp. 671–674, Monterey, CA (June 1989).

3.25 R.M. Jones, *A Study of Pulse Magnetization and Pulse Transformers* (University of Wales, Ph.D. Thesis, May 1979).

3.26 R. Jordan, C. Price, and L. Swain, "Two Experimental Semiconductor-Magnetic Pulse Modulators," *Proceedings of the Seventh Symposium on Hydrogen Thyratrons and Modulators*, pp. 240–259, Fort Monmouth, NJ (May 1962).

3.27 F. Kannari, M.J. Shaw, F. O'Neill, and H.T. Medhurst, "A Magnetic Switch Driven High Voltage Trigger Generator," *Digest of Technical Papers 5th IEEE Pulse Power Conference*, pp. 672–676, Arlington, VA (June 1985).

3.28 I.G. Katayev, *Electromagnetic Shock Waves* (Sovetskoye Radio, Iliffe Books Ltd, London, 1963).

3.29 I.G. Katayev and I.I. Rozhov, "Generator Producing Nanosecond Pulses With an Increased Repetition Frequency," *Instruments and Experimental Techniques* (Pribory i Teknika Eksperimenta) (4), p. 88 (1974).

3.30 L.G. Kersta, "The Nonlinear-Inductance Circuit," *Pulse Generators*, edited by G.N. Glasoe, J.V. Lebacz, pp. 471–476 (McGraw Hill, 1948).

3.31 R. Kihara and H.C. Kirbie, "An Alternator-Driven Magnetically Switched Modulator," *IEEE Conference Record of the 1986 Seventeenth Power Modulator Symposium*, pp. 246–251, Seattle, WA (June 1986).

3.32 H.C. Kirbie, *Magnetic Switching*, Lawrence Livermore National Laboratory, Livermore, CA, UCRL-100910 (April 1989).

3.33 H.C. Kirbie, G.Y. Otani, G.M. Hughes, "A Magnetically Switched Trigger Source for FXR," *Digest of Technical Papers Seventh IEEE Pulsed Power Conference*, pp. xx–xx (June 1989).

3.34 E. Lassiter, P. Johannessen, and R. Spencer, "High-Power Pulse Generation Using Semiconductors and Magnetic Cores," *Proceedings Special Technical Conference on Nonlinear Magnetics and Magnetic Amplifiers*, pp. 215–233, Washington, D.C. (Sept. 1959).

3.35 R.C. Le Craw and H.B. Bruns, "Time Delay in High Speed Ferrite Microwave Switches," *Journal Applied Physics*, **26**(1), pp. 124–125 (Jan. 1955).

3.36 Bernard Loth, "Development of a 50-Megawatt Magnetic Modulator to Simultaneously Trigger 500 Thyratrons," *Proceedings of the Seventh Symposium on Hydrogen Thyratrons and Modulators*, pp. 260–289, Fort Monmouth, NJ (May 1962).

3.37 E.W. Manteuffel and R.E. Cooper, "Direct Current Charged Magnetic Pulse Modulator," *Proceedings Special Technical Conference on Nonlinear Magnetics and Magnetic Amplifiers*, pp. 234–255, Washington, D.C. (Sept. 1959).

3.38 R.A. Mathias and E.M. Williams, "Economic Design of Saturating Reactor Magnetic Pulsers," *AIEE Transactions*, **74**, pt 1, pp. 169–171 (May 1955).

3.39 K. Matsubara, T. Nakata, and M. Nakano, "Study on Building Factor of Stacked Core made of Amorphous Sheets," *Journal of Applied Physics*, 64(10), part 2, pp. 5707 (Nov. 1988).

3.40 W.S. Melville, "The Use of Saturable Reactors as Discharge Devices for Pulse Generators," *Proceedings IEEE*, **98**, part 3, Radio and Communications, (53), pp. 185–207 (1951).

3.41 E.L. Neau, "COMET: A 6 MV, 400 KJ Magnetically-Switched Pulse-Power Module," *Digest of Technical Papers 4th IEEE Pulsed Power Conference*, pp. 246–250, Albuquerque, NM (June 1983).

3.42 E.L. Neau, T.L. Woolston, and K.J. Penn, "COMET-II A Two-Stage Magnetically Switched Pulsed Power Module," *IEEE Conference Record of 1984 Sixteenth Power Modulator Symposium*, pp. 292–294 (June 1984).

3.43 E.L. Neau, C.H. Harjes, T.L. Woolston, K.J. Penn, et al., "Recent Experiments on the 200 kJ Magnetically-Switched Comet Module," *Digest of Technical Papers 5th IEEE Pulsed Power Conference*, Arlington, VA (June 1985).

3.44 W.C. Nunnally, "Stripline Magnetic Modulators for Lasers and Accelerators," *Digest of Technical Papers 3rd IEEE International Pulsed Power Conference*, pp. 210–213, Albuquerque, NM (June 1981).

3.45 W.C. Nunnally, J. Pover, T.E. Springer, A. Litton, et al., "Development of Stripline Magnetic Modulators," *IEEE Conference Record of 1982 Fifteenth Power Modulator Symposium*, pp. 23–31, Baltimore, MD (June 1982).

3.46 W.C. Nunnally, *Magnetic Switches and Circuits*, Los Alamos National Laboratory, Los Alamos, NM, LA-8862-MS (Sept. 1982).

3.47 J.A. Oicles and E.S. Fulkerson, "An Improved 50 KV Pulser Design," *IEEE Conference Record of 1982 Fifteenth Power Modulator Symposium*, pp. 51–54, Baltimore, MD (June 1982).

3.48 R.I. Okunev, L.N. Pakhomov, V.Yu. Petrun'kin, et al., "Magnetothyristror Pulse Generator for Pumping Copper-Vapor Lasers," *Soviet Technical Physics Letters* (Pis'ma v Zhurnal Tekhnicheskoi Fiziki) **9**, pp. 670–673 (June 1983).

3.49 T. Pacala, I. S. McDonald, et al., "Magnetic Modulator for a Repetitively Pulsed Xenon Chloride Laser System," *IEEE Conference Record of 1984 Sixteenth Power Modulator Symposium*, pp. 250–254 (June 1984).

3.50 R.A. Petr, J.P. Zumdiek, J. Demboski, I. Smilanski, et al., "Magnetic Pulse Compression for Copper-Vapor Lasers," *Digest of Technical Papers 4th IEEE Pulsed Power Conference*, pp. 236–41, Albuquerque, NM (June 1983).

3.51 V.A. Petrov and U. Eberl, "High Voltage Magnetic Generator of Nanosecond Pulses," *Instruments and Experimental Techniques* (Pribory i Teknika Eksperimenta) (1) **90** (1977).

3.52 N.P Polyakov and Yu.P. Yarushkin, "Optimization of Magnetic Reversal Modes in Magnetic Pulse Generators," *Elektrishetsvo* **11**, 73 (Nov 1978).

3.53 N.P. Polyakov, P.P Rumyantsev, V.V. Sinenko, et al., "Use of Saturable Reactors to Switch High Energies," *Instruments and Experimental Techniques* (Pribory i Teknika Eksperimenta) 5, 129 (1978).

3.54 H. Rhinehart, R. Dougal, and W.C. Nunnally, "Design and Analysis of a High Power 1 kHz Magnetic Modulator,"

Digest of Technical Papers 5th IEEE Pulsed Power Conference, pp. 660–663, Arlington, VA (June 1985).

3.55 R.W. Roberts and R.I. Van Nice, "Influence of ID/OD Ratio on Static and Dynamic Magnetic Properties of Toroidal Cores," *AIEE Transactions Communications and Electronics*, **74**, pp. 599–607 (Nov. 1955).

3.56 Y. Saito, M. Namiki, S. Hayano, and N. Tsuya, *Experimental Verification of Modified Chua Type Magnetization Model* (College of Engineering, Hosei University, Tokyo, Japan, 1984).

3.57 D.L. Birx, L.L. Reginato, and J.A. Schmidt, "An Investigation Into the Repetition Rate Limitations of Magnetic Switches," *IEEE Conference Record of 1982 Fifteenth Power Modulator Symposium*, pp. 4–9, Baltimore, MD (June 1982).

3.58 S. Schneider, "Pulse Sharpening with a Series Ferrite Magnetic Switch in Line-Type and Blumlein Modulators," *IEEE Conference Record of 1982 Fifteenth Power Modulator Symposium*, pp. 37–46, Baltimore, MD (June 1982).

3.59 T. Shimada and M. Obura, "Semiconductor Switched Magnetic Modulator for Rep-Rate Lasers," *Digest of Technical Papers 5th IEEE Pulsed Power Conference*, pp. 656–659, Arlington, VA (June 1985).

3.60 T. Shimada, M. Obura, and T. Fujioka, "Development of a Magnetic Switching Modulator for High Rep-Rated Lasers," *IEEE Conference Record of 1984 Sixteenth Power Modulator Symposium*, pp. 255–258 (June 1984).

3.61 V.A. Shvets, "Nonlinear Multichannel Pulse-Sharpening Line Containing Ferrite Rings With Nonrectangular Hysteresis Loop," *Instruments and Experimental Techniques* (Pribory i Teknika Eksperimenta) (4), p. 116 (1982).

3.62 I. Smilanski, "Advances in Magnetic Pulse Compression for Copper Vapor Lasers," *IEEE Conference Record of the 1988 Eighteenth Power Modulator Symposium*, pp. 84–85, Hilton Head, SC (June 1988).

3.63 E.J. Smith, "Design and Performance of Magnetic Pulse Modulators," *Proceedings of the Fifth Symposium on Hydrogen Thyratrons and Modulators*, pp. 112–134, Fort Monmouth, NJ (May 1958).

3.64 C. Smith, "Magnetic Shielding to Multi-Gigawatt Switches: Ten Years of Amorphous Magnetic Applications," *IEEE Transactions on Magnetics*, **MAG-18**(6), p. 1376 (Nov. 1982).

3.65 M. Stockton, E.L. Neau, and J.P. VanDevender, "Pulsed Power Switching Using Saturable Core Inductors," *Journal of Applied Physics*, **53**, pp. 2765–2767 (March 1982).

3.66 P. Swart, G. Bredenkamp, and H. Von Bergmann, "Computer Spreadsheet Design, Numerical Simulation and Practical Evaluation of a Lossy Series Pulse Compressor," *Digest of Technical Papers Sixth IEEE Pulsed Power Conference*, pp. 680–683, Arlington, VA (June 1987).

3.67 J.P. VanDevender and R.A. Reber, "High Voltage Magnetically Switched Pulsed Power Systems," *Digest of Technical Papers 3rd IEEE International Pulsed Power Conference*, pp. 256–261, Albuquerque, NM (June 1981).

3.68 M. Weiner, "Pulse Sharpening in Ferrite Transmission Lines," *Digest of Technical Papers 2nd IEEE International Pulsed Power Conference*, pp. 91–95, Lubbock, Texas (June 1979).

3.69 M. Weiner, S. Schneider, and F. Dollak, "Lumped Circuit Ferrite Pulse Sharpener," *Digest of Technical Papers 4th IEEE Pulsed Power Conference*, pp. 150–154, Albuquerque, NM (June 1983).

3.70 B.M. Wolframm, "Magnetic Pulse Modulator for a Missile Guidance System (MP 505)," *Proceedings of the Sixth Symposium on Hydrogen Thyratrons and Modulators*, pp. 312–320, Fort Monmouth, NJ (May 1960).

3.71 B.M. Wolframm, "Solid State Pulse Modulator for a Two-Repetition Rate, Two-Pulse-Width Surveillance Radar," *Proceedings of the Sixth Symposium on Hydrogen Thyratrons and Modulators*, pp. 221–234, Fort Monmouth, NJ (May 1960).

4. Magnetic Pulse Compression System Applications

This section includes papers that describe or propose systems that could utilize magnetic pulse compression techniques.

4.1 S.B. Ahlstrom, "Irradiation of Municipal Sludge for Pathogen Control, Why or Why not?" *Radiation Physics and Chemistry*, **31**(1–3), pp. 131–138 (1988).

4.2 J.P. Barber and D.P. Bauer, "Switching for Electric Rail Guns," *IEEE Transactions on Magnetics*, **MAG-20**(2), pp. 304–307 (March 1984).

4.3 W.A. Barletta, *An Injection System for a PEP-Based Asymmetric Storage Ring Collider for the Copious Production of B Mesons*, Lawrence Livermore National Laboratory, Livermore, CA, UCID-21819 (Aug. 1989).

4.4 W.A. Barletta, *High Gradient Accelerators for Linear Light Sources*, Lawrence Livermore National Laboratory, Livermore, CA, UCRL-99268, Rev. 1 (Sept. 1988).

4.5 W.A. Barletta, *Compact X-ray Laser in the Laboratory*, Lawrence Livermore National Laboratory, Livermore, CA, UCRL-99661 (Oct. 1988).

4.6 W.A. Barletta and A.M. Sessler, *Radiation from Fine, Intense, Self-focused Beams at High Energy*, Lawrence Livermore National Laboratory, Livermore, CA, UCRL-98767, Rev. 1 (Oct. 1988).

4.7 J.R. Bayless and R.J. Adler, "Linear Induction Accelerators for Radiation Processing," *Radiation Physics and Chemistry*, **31**(1–3), pp. 327–331 (1988).

4.8 P. Bhartia and I.J. Bahl, *Millimeter Wave Engineering and Applications* (Wiley-Interscience Publications).

4.9 D.L. Birx, *Induction Linacs as Radiation Processors*, Lawrence Livermore National Laboratory, Livermore, CA, UCID-20785 (Feb. 1986).

4.10 D.L. Birx, S. A. Hawkins, S.E. Poor, L.L. Reginato, et al., "Multipurpose 5-MeV Linear Induction Accelerator," *IEEE Conference Record of 1984 Sixteenth Power Modulator Symposium*, pp. 186–190 (June 1984).

4.11 R.J. Briggs, *Linear Induction Accelerators*, Lawrence Livermore National Laboratory, Livermore, CA, M01-2

4.12 T.J. Burgess and M. Cowan, "Multistage Induction Mass Accelerator," *IEEE Transactions on Magnetics*, **MAG-20**(2), pp. 235–238 (March 1984).

4.13 M.R. Cleland, R.A. Fernald, and S.R. Maloof, "Electron Beam Process Design for the Treatment of Wastes and Economic Feasibility of the Process," *Radiation Physics and Chemistry*, **24**(1), 179–190 (1984).

4.14 M. Crawford, "Silicon Chip Race Advances Into X-Rays," *Science*, **246**, pp. 1382–1383 (Dec. 1989).

4.15 M.D. Driga, W.F. Weldon, and H.H. Woodson, "Electromagnetic Induction Launchers," *IEEE Transactions on Magnetics*, **MAG-22**(6), pp. 1453–1475 (Nov. 1986).

4.16 C.M. Fowler, E.L. Zimmermann, C.E. Cummings, et al., "Magnetic Switching, Accelerators Railguns Powered by Explosive driven Flux Compression Generators," *IEEE Transactions on Magnetics*, **MAG-22**(6), pp. 1475–1480 (Nov. 1986).

4.17 P. Fuchs, B. Roth, U. Schwing, H. Angele, et al., "Removal of NOx and SO2 By the Electron Beam Process," *Radiation Physics and Chemistry*, **31**(1–3), pp. 45–56 (1988).

4.18 V.L. Granatstein and I. Alexeff, *High-Power Microwave Sources* (Artech House, Inc., 1987).

4.19 S. Hashimoto, K. Nishimura, and S. Machi, "Economic Feasibility of Irradiation-Composting Plant of Sewage Sludge," *Radiation Physics and Chemistry*, **31**(1–3), pp. 109–114 (1988).

4.20 J. He, E. Levi, Z. Zabar, and L. Birenbaum, "Concerning the Design of Capacitively Driven Induction Coil Guns," *IEEE Transactions on Plasma Science*, **17**(3), pp. 429–438 (June 1989).

4.21 S. Hiramatsu, K. Ebihara, Y. Kimura, J. Kishiro, et al., "Proposal for an X-Band Single-Stage FEL," *Nuclear Instruments and Methods in Physics Research*, A285, pp. 83–91 (1989).

4.22 E.M. Honig, "Switching Considerations and New Transfer Circuits for Electromagnetic Launch Systems," *IEEE Transactions on Magnetics*, **MAG-20**(2), pp. 312–315 (March 1984).

4.23 D.B. Hopkins, E.H. Hoyer, K. Halbach, et al., *An FEL Power Source for a TeV Linear Collider*, Lawrence Berkeley Laboratory, Berkeley, CA, LBL-25936 (Oct. 1988).

4.24 D.W. Ignat, D.R. Cohn, and P.P. Woskov, "The CIT and Electron Cyclotron Heating: Description of Need, Assessment of Prospects," Compact Ignition Tokamak AA-881018-PPL-05 (Oct. 1988).

4.25 P. Jackson, "Eureka Project develops 1-kW Excimer Laser," *Lasers and Optronics*, pp. 28–30 (Dec. 1989).

4.26 W.A. Barletta, "Economics of Induction Linac Drivers for Radiation Sources," *Adriatic Conference on Undulator Magnets for Synchrotron Radiation and Free Electron Lasers*, pp. 1–18 (June 1987).

4.27 R.A. Jong and R.R. Stone, *Preliminary Design of an Induction-Linac Based Free-Electron Laser Amplifier for Plasma Heating in CIT/ITER*, Lawrence Livermore National Laboratory, Livermore, CA, UCRL-99595 (Sept. 1988).

4.28 R.A. Jong and R.R. Stone, *Induction-Linac Based Free-Electron Laser Amplifier for Fusion Applications*, Lawrence Livermore National Laboratory, Livermore, CA, UCRL-98675 (Aug. 1988).

4.29 R.A. Jong, D.P. Atkinson, J.A. Byers, F.E. Coffield, et al., *IMP, a Free-Electron Laser Amplifier for Plasma Heating in the Microwave Tokamak Experiment*, Lawrence Livermore National Laboratory, Livermore, CA, UCRL-99368 (Aug. 1988).

4.30 S. Jordan, "Progress in the Electron Beam Treatment of Stack Gases," *Radiation Physics and Chemistry*, **31**(1–3), pp. 21–28 (1988).

4.31 J. Kishiro, K. Ebihara, S. Hiramatsu, Y. Kimura, et al., "The Microwave Free Electron Laser Test Stand at KEK," Pages, *XIV International Conference on High Energy Accelerators*, Tsukuba, Japan (Sept. 1989).

4.32 H. Kolm and P. Mongeau, "Basic Principles of Coaxial Launch Technology," *IEEE Transactions on Magnetics*, **MAG-20**(2), pp. 227–230 (March 1984).

4.33 J.E. Leiss, N.J. Norris, and M.A. Wilson, "Design and Performance of a Long-Pulse High-Current Linear Induction Accelerator at the National Bureau of Standards," *Particle Accelerators*, **10**, pp. 223–234 (1980).

4.34 C. Levaillant and C.L. Gallien, "Sanitation Methods using High Energy Electron Beams," *Radiation Physics and Chemistry*, **14**, pp. 309–316 (1979).

4.35 R.A. Marshall, "A Reusable Inverse Railgun Magnetic Flux Compression Generator to Suit the Earth-to-Space-Rail Launcher," *IEEE Transactions on Magnetics*, **MAG-20**(2), pp. 223–226 (March 1984).

4.36 K. McKinney and P. Mongeau, "Multiple Stage Pulsed Induction Acceleration," *IEEE Transactions on Magnetics*, **MAG-20**(2), 239–242 (March 1984).

4.37 W.E. Nexsen, D.P. Atkinson, D.M. Barrett, et al , "The ETA-II Induction Linac as a High Average Power FEL Driver," *11th International Conference on Free Electron Lasers*, Naples, FL., p. 235 (Aug. 1989).

4.38 W.C. Nunnally and E.M. Honig, "Resonant Rail Gun Concept," *Digest of Technical Papers 5th IEEE Pulsed Power Conference*, pp. 559–565, Arlington, Va. (June 1985).

4.39 J.E. Osher and J.V. Parker, "Guest Editorial - Introduction to this Special Issue on Electromagnetic Launchers," *IEEE Transactions on Plasma Science*, **17**(3), pp. 349–352 (June 1989).

4.40 A.J. Power, H.R. Bolton, and W. Bessel, "Simulation of a Pulsed Power Scheme Feeding a Dense Z-Pinch Plasma Load," *Digest of Technical Papers Sixth IEEE Pulsed Power Conference*, pp. 696–699, Arlington, VA (June 1987).

4.41 D. Prosnitz, "The Physics of Free Electron Lasers and Applications to Electron Cyclotron Heating," *15th European Conference on Controlled Fusion*, pp. 1–12 (July 1988).

4.42 H.D. Shay, W.A. Barletta, S.S. Yu, R. Schlueter, et al., *Prospects for a Soft X-Ray FEL Powered by a Relativistic-Klystron High-Gradient Accelerator (RK-HGA)*, Lawrence Livermore National Laboratory, Livermore, CA, UCRL-100891 (Sept. 1989).

4.43 T. Shidara, M. Akemoto, M. Yoshida, S. Takeda et al., "Design Study of an X-Band Klystron Modulator using Magnetic-Pulse-Compression Techniques," *7th Symposium on Accelerator Science and Technology*, Osaka, Japan (Dec. 1989).

4.44 I. Smilanksi, S.R. Byron, and T.R. Burkes, "Electrical Exicitation of an XeCl Laser Using Magnetic Pulse Compression," *Applied Physics Letters*, **40**(7), pp. 547–548 (April 1982).

4.45 R. Stone, *IFEL Options for 40-MW, 280-GHz Output*, Lawrence Livermore National Laboratory, Livermore, CA, UCID-21705 (May 1989).

4.46 J.G. Trump, E.W. Merrill, and K.A. Wright, "Disinfection of Sewage

Wastewater and Sludge by Electron Treatment," *Radiation Physics and Chemistry*, **24**(1), pp. 55–66 (1984).

4.47 W.F. Weldon and H.H. Woodson, "Pulsed Power Requirements for Electromagnetic Launchers," *IEEE Transactions on Magnetics*, **Mag-20**(2), pp 200–202 (March 1984).

4.48 K. Williams, W.A. Frutiger, J. Hiley, and S.V. Nablo, "Requirements for Very High Power Electron Beam Systems for Utility Stack Gas Treatment," *Radiation Physics and Chemistry*, **31**(1–3), pp. 29–44 (1988).

4.49 M.A. Wilson, "Recirculation Acceleration of High Current Relativistic Electron Beams, A Feasibility Study," *IEEE Transactions on Nuclear Science*, **NS-28**(3), pp. 3375–3377 (June 1981).

5. Switching and Power Conditioning Systems

This section includes papers that describe, evaluate or propose primary switching devices and/or power conditioning systems.

5.1 H.J. Baker, P.A. Ellsmore, and E.C. Sille, "Thyristor/Pulse Transformer Design for Magnetic Pulse Compressor Circuits," *IEEE Conference Record of the 1986 Seventeenth Power Modulator Symposium*, pp. 260–263, Seattle, WA (June 1986).

5.2 D.L. Birx, E.G. Cook, S. Hawkins, A. Meyers, et al., "Regulation and Drive System for High Rep-Rate Magnetic Pulse Compressors," *IEEE Conference Record of 1982 Fifteenth IEEE Power Modulator Symposium*, pp. 15–21, Baltimore, MD (June 1982).

5.3 S. Black and T.R. Burkes, "Command Charge Using Saturable Inductors," *Digest of Technical Papers 2nd IEEE International Pulsed Power Conference*, pp. 102–105, Lubbock, Texas (June 1979).

5.4 T.R. Burkes, *Critical Analysis and Assessment of High Power Switches*, Lubbock, TX: Texas Tech University (Sept. 1978).

5.5 E.G. Cook and L.L. Reginato, "Off-Resonance Transformer Charging for 250 kV Water Blumlein," *IEEE Transactions on Electron Devices*, ed. 26(10), pp. 1512 (Oct 1979).

5.6 J.E. Creedon and S. Schneider, "A Magnetic Assist for High-Power Hydrogen Thyratrons," *Proceedings of the Fifth Symposium on Hydrogen Thyratrons and Modulators*, pp. 145–148, Fort Monmouth, NJ (May 1958).

5.7 R.A. Dougal, G.D. Volakakis, and M.D. Abdalla, "Magnetically Delayed Vacuum Switching," *Digest of Technical Papers Sixth IEEE Pulsed Power Conference*, pp. 21–24, Arlington, VA (June 1987).

5.8 R.L. Haumesser, Dr. D.L. Lockwood, et al., "High Voltage High Power Pulse Transformer," *IEEE Conference Record of 1982 Fifteenth Power Modulator Symposium*, pp. 55–66, Baltimore, MD (June 1982).

5.9 E.M. Honig, "Generation of a 75-MW 5-kHz Pulse Train From an Inductive Energy Store," *IEEE Transactions on Plasma Science*, **PS-12**(1), pp. 24–28 (March 1984).

5.10 L.G. Kersta, "The Nonlinear-inductance Circuit," *Pulse Generators*, edited by G.N. Glasoe, J.V. Lebacqz, pp. 471–476 (McGraw Hill, 1948).

5.11 E. Lassiter, P. Johannessen, and R. Spencer, "High-Power Pulse Generation Using Semiconductors and Magnetic Cores," *Proceedings Special Technical Conference on Nonlinear Magnetics and Magnetic Amplifiers*, pp. 215–233, Washington, D.C. (Sept. 1959).

5.12 E.J. Lauer and D.L. Birx, "Tests of a Low-Pressure Switch Protected by a Saturating Inductor," *IEEE Conference Record of 1982 Fifteenth Power Modulator Symposium*, pp. 47–50, Baltimore, MD (June 1982).

5.13 D.L. Lockwood, R.I. McNall, and R.L. Haumesser, *Development of Lightweight Transformers for Airborne High Power Supplies*, Thermal Technical Laboratory report AFAPL-TR-76-102, pp. 48–59 (1976).

5.14 C.W. Reed, *Proceedings of a Symposium on High-Energy-Density Capacitors and Dielectric Materials* (National Academy Press, Washington, D.C., 1981).

5.15 T. Shimada and M. Obura, "Semiconductor Switched Magnetic Modulator for Rep-Rate Lasers," *Digest of Technical Papers 5th IEEE Pulsed Power Conference*, pp. 656–659, Arlington, VA (June 1985).

5.16 T.F. Turner, "Modulator Design Problems in the Proposed Stanford Two-Mile Linear Electron Accelerator," *Proceedings of the Sixth Symposium on Hydrogen Thyratrons and Modulators*, pp. 139–157, Fort Monmouth, NJ (May 1960).

5.17 W.C. Turner, G.L. Caporaso, G.D. Craig, et al., *Impedance Characteristics of Induction Accelerator Cells*, Lawrence Livermore National Laboratory, Livermore, CA, UCRL-97738 (July 1988).

5.18 J.P. VanDevender and R.A. Reber, "High Voltage Magnetically Switched Pulsed Power Systems," *Digest of Technical Papers 3rd IEEE International Pulsed Power Conference*, pp. 256–261, Albuquerque, NM (June 1981).

6. Miscellaneous Topics

This section includes books and papers that are of general reference interest, but do not fit into any of the previous categories.

6.1 Baumeister and Marks, *Standard Handbook for Mechanical Engineers*, 8th Edition (McGraw-Hill, New York, 1978).

6.2 J. Bemesderfer, R.L. Druce, B. Frantz, et al., *Pulsed Power Bibliography vols I and II, Final Report*, AFWL-TR-83-74, Vol. I and II, Air Force Weapons Laboratory, Kirtland AFB, NM (Aug. 1983).

6.3 Bolz and Tuve, *Handbook of Tables for Applied Engineering Science*, 2nd Edition (CRC Press, Cleveland, 1976).

6.4 R.L. Druce and A.H. Guenther, "Computerized Bibliography of Pulsed Power," *IEEE Conference Record of 1982 Fifteenth Power Modulator Symposium*, pp. 1–3, Baltimore, MD (June 1982).

6.5 W. A. Geyger, *Magnetic Amplifier Circuits, Basic Principles, Characteristics and Applications* (McGraw-Hill Book Company, Inc., New York, 1957).

6.6 J.P. Holman, *Heat Transfer* (McGraw-Hill Book Co., 1963).

6.7 J.D. Jackson, *Classical Electrodynamics* (John Wiley and Sons, New York, 1975).

6.8 D.L. Lafuze, *Magnetic Amplifier Analysis* (John Wiley and Sons, Inc., New York, 1962).

6.9 M.J. Mulcahy, *High Voltage Technology Seminar*, (Ion Physics Corporation, Sept. 1969).

6.10 Martin Plonus, *Applied Electromagnetics* (McGraw-Hill, New York, 1978).

6.11 Rohsenow and Hartnett, *Handbook of Heat Transfer* (McGraw-Hill Book Co., New York, 1973).

6.12 W.J. Sarjeant, Editor, *Polymer Laminate Structures* (Dept. of Electrical and Computer Engineering, State University of New York at Buffalo, March 1982).

6.13 F.A. Sattler, L.C. Scala, "Pigmented Polyester Magnet Wire for High Temperature Operation," *AIEE*, pp. 503–504 (Nov. 1960).

6.14 JP.G. Simpson, *Induction Heating Coil and System Design* (McGraw-Hill Book Company, Inc., New York, 1960).

6.15 H.F. Storm, *Magnetic Amplifiers* (John Wiley and Sons, Inc., New York, 1955).

Appendix B

Attendee List

Appendix B
Attendee List

Bill Abraham
Lawrence Livermore National Laboratory
P. O. Box 808, L-405
Livermore, CA
USA 94550

Richard Adler
North Star Research Corporation
5555 Zuni S.E., Suite 345
Albuquerque, NM
USA 87108

Steven Ashby
Physics International Company
2700 Merced Street
San Leandro, CA
USA 94577

Ken Avery
McDonald Douglas Space Systems Co.
5301 Bolsa Ave, M/S 11-3
Huntington Beach, CA
USA 92647-2048

Sally Bahowick
Lawrence Livermore National Laboratory
P.O. Box 808, L-285
Livermore, CA
USA 94550

Dave Barrett
Lawrence Livermore National Laboratory
P.O. Box 808, L-464
Livermore, CA
USA 94550

Gordon Bowden
Stanford Linear Accelerator Center
P.O. Box 4349
Stanford, CA
USA 94309

Otto Buchert
Vacuumschmelze gmbh
186 Wood Ave S.
Iselin, NY
USA 08830

Craig Burkhart
Pulse Sciences, Inc.
5330 Derry Avenue, Suite J
Agoura Hills, CA
USA 91301

V. Bystriskii
High Current Institute - Tomsk
Academicheski Prospect 4
Tomsk 55
USSR 634055

Edmond Chu
Maxwell Laboratories, Inc.
8888 Balboa Avenue
San Diego, CA
USA 92123

Randy Curry
Pulse Sciences Inc.
600 McCormick Street
San Leandro, CA
USA 94577

Gloria Davalos
Lawrence Livermore National Laboratory
P.O. Box 808, L-637
Livermore, CA
USA 94550

John DeFord
Lawrence Livermore National Laboratory
P.O. Box 808, L-626
Livermore, CA
USA 94550

Roger Dougal
University of South Carolina
Dept. of Electrical Engineering
Columbia, SC
USA 29208

Shimon Eckhouse
Maxwell Laboratories
8888 Balboa Avenue
San Diego, CA
USA 92123

Gordon Fish
Allied Signal Inc.
Box 1021R
Morristown, NJ
USA 07962

Craig Fong
Lawrence Berkeley Laboratory
1 Cyclotron Road, Bldg. 47 R-112
Berkeley, CA
USA 94720

Donald Gonzalez
Lawrence Livermore National Laboratory
P.O. Box 808, L-662
Livermore, CA
USA 94550

Lloyd Gordon
Auburn Univ. -Space Power Institute
231 Leach Center
Auburn Univ., AL
USA 36849

John Gowar
Bristol University
Dept. of Electrical Engineering
Bristol
UK BS81TR

Mark Greenwood
c/o J. Gowar, University of Bristol
Dept. of Electrical Engineering
Bristol
UK BS81TR

Art Guenther
Los Alamos National Laboratory
P.O. Box 1663, M/S A110
Los Alamos, NM
USA 87545

Martin Gundersen
University of Southern California
Dept. of Electrical Eng.- SSC-420
Los Angeles, CA
USA 90089-0484

Henry Harjes
Sandia National Laboratories
P.O. Box 5800, Div. 1243
Albuquerque, NM
USA 87185

Marion Hodgdon
Los Alamos National Laboratory
M-6, MS-J970
Los Alamos, NM
USA 87545

Emanuel Honig
Los Alamos National Laboratory
Group CLS-7, M/S-E525
Los Alamos, NM
USA 87545

Thomas G. Innes
Lawrence Livermore National Laboratory
P.O. Box 808, L-153
Livermore, CA
USA 94550

Cheri Johnson
Lawrence Livermore National Laboratory
P.O. Box 808, L-711
Livermore, CA
USA 94550

David L. Johnson
Sandia National Laboratories
P.O. Box 5800 Div. 1238
Albuquerque, NM
USA 87185

R. J. Kares
Berkeley Research Associates
P.O. Box 241
Berkeley, CA
USA 94701

Ron Kihara
Lawrence Livermore National Laboratory
P.O. Box 808, L-153
Livermore, CA
USA 94550

Hugh C. Kirbie
Lawrence Livermore National Laboratory
P.O. Box 808, L-627
Livermore, CA
USA 94550

George Amemiya-Kirkman
Integrated Applied Physics Inc.
Arcadia, CA
USA 91006

Jun-Ichi Kishiro
National Lab for High Energy Physics, KEK
305 Tsukuba
Ibaraki
Japan

Magne Kristiansen
Texas Tech University
Dept. of Electrical Eng. - M/S 3102
Lubbock, TX
USA 79409-4439

Robert Kuenning
Pulse Sciences Inc.
600 McCormick Street
San Leandro, CA
USA 94577

Diana L. Loree
Texas Tech University
Box 4439
Lubbock, TX
USA 79409

Michael S. Mazzola
NSWC
Code F-12
Dahlgren, VA
USA 22448-5000

Glen McDuff
Idaho National Engineering Laboratory
P.O. Box 1625
Idaho Falls, ID
USA 83415

Hugh Menown
English Electric Valve
106 Waterhouse Lane
Chelmsford, Essex
UK CM12QU

G. Mesyats
USSR Academy of Sciences
GSP - 1, B-71
Moscow
USSR 117961

Gibson Morris, Jr.
University of South Carolina
1100 Wheat Street, #208
Columbia, SC
USA 29201

Thomas Morris
Allied Signal Metals
6 Eastmans Road
Parsippany, NJ
USA 07927

E. L. Neau
Sandia National Laboratories
P.O. Box 5800, Div. 1252
Albuquerque, NM
USA 87185

Mark Newton
Lawrence Livermore National Laboratory
P.O. Box 808, L-627
Livermore, CA
USA 94550

Bill Niven
Lawrence Livermore National Laboratory
P.O. Box 5511, L-469
Livermore, CA
USA 94550

W. C. Nunnally
University of Texas, Austin
Center for Energy Conversion Research, Box 19380
Arlington, TX
USA 76019

L. A. Ostrovsky
Institute of Applied Physics
Ulyanov Street, 46
Gorky
USSR 603600

Mark Parsons
Los Alamos National Laboratory
P.O. 1663, M/S P-940
Los Alamos, NM
USA 87545

Dennis Pavlik
Westinghouse Electric Science. & Technology Center
1310 Buelah Rd.
Pittsburgh, PA
USA 15235

Anthony Payne
Lawrence Livermore National Laboratory
P.O. Box 808, L-627
Livermore, CA
USA 94550

David L. Pehrson
Lawrence Livermore National Laboratory
P.O. Box 808, L-119
Livermore, CA
USA 94550

Colin Pirrie
English Electric Valve Co.
106 Waterhouse Lane
Chelmsford, Essex
UK CM12QU

Sid Pratap
University of Texas, Center for
Electromechanics
10100 Burnet Road
Austin, TX
USA 78758

Donald Prosnitz
Lawrence Livermore National Laboratory
P.O. Box 808, L-626
Livermore, CA
USA 94550

Kim Reed
Sandia National Laboratories
P.O. Box 5800, Div 1253
Albuquerque, NM
USA 87185

G. J. Rohwein
Sandia National Laboratories
P.O. Box 5800, Div. 1253
Albuquerque, NM
USA 87185

Jane Rubert
Lawrence Livermore National Laboratory
P.O. Box 808, L-641
Livermore, CA
USA 94550

Steve Sampayan
Lawrence Livermore National Laboratory
P.O. Box 808, L-627
Livermore, CA
USA 94550

Leland Schlitt
Leland Schlitt Consulting Services
2725 Briarwood Drive
Livermore, CA
USA 94550

Nigel Seddon
British Aerospace
FPC 30 Br. Aerospace Plc, P.O. Box 5
Bristol Filton
UK BS12 7QW

Donald J. Sharp
Sandia National Laboratories
P.O. Box 5800, Div. 1841
Albuquerque, NM
USA 87185

Michael K. Sheaffer
Lawrence Livermore National Laboratory
P.O. Box 808, L-626
Livermore, CA
USA 94550

Dr. Makoto Shiho
Japan Atomic Energy Research Institute
801-1 Mukaiyama
Naka-machi, Naka-gun Ibaraki-ken
Japan

G. A. Shneyerson
Leningrad Polytechnic - Leningrad
Polytechnicheskaya Street, 29
Leningrad
USSR 195251

Phil Siemens
Lawrence Livermore National Laboratory
P.O. Box 5511, L-546
Livermore, CA
USA 94550

Carl Smith
Allied-Signal Inc.
P.O. Box 1021R
Morristown, NJ
USA 07962-1021

Roger Stone
Lawrence Livermore National Laboratory
P.O. Box 808, L-641
Livermore, CA
USA 94550

James Swingle
1200 Crystal Drive
Apt. 613
Arlington, VA
USA 22202

M. Thevenot
CESTA
BP n 2 33114
Le Barp
France

Bill Turner
Lawrence Livermore National Laboratory
P.O. Box 808, L-626
Livermore, CA
USA 94550

Sally Twisselmann
Lawrence Livermore National Laboratory
P.O. Box 808, L-38
Livermore, CA
USA 94550

Fred van Haaften
Los Alamos National Laboratory
Mail Code 851
Los Alamos, NM
USA 87545

V. A. Vizar
High Current Institute-Tomsk
Academicheski Prospect 4
Tomsk 55
USSR 634055

Tom Warren
Physics International Company
2700 Merced Street
San Leandro, CA
USA 94577

Ronald Weinberg
Lawrence Livermore National Laboratory
P.O. Box 808, L-410
Livermore, CA
USA 94550

Ralf Wengerter
Vacuumschmelze gmbh
Grüner Weg 37
Hanau
Federal Republic of Germany, 6450

W. N. Weseloh
Power Spectra Inc.
42660 Christy Street
Fremont, CA
USA 94538

Glen Westenskow
Lawrence Livermore National Laboratory
P.O. Box 808, L-626
Livermore, CA
USA 94550

Ken Whitham
Beta Development Corporation
6780-R Sierra Court
Dublin, CA
USA 94568

Sue Winkler Allen
Lawrence Livermore National Laboratory
P.O. Box 808, L-546
Livermore, CA
USA 94550

Richard Wood
National Magnetics Corporation
15925 Piuma Avenue
Cerritos, CA
USA 90701

Chris Young
Tetra Corp.
4905 Hawkins Street NE
Albuquerque, NM
USA 87109-4345

Jan-Mark Zentler
Lawrence Livermore National Laboratory
P.O. Box 808, L-153
Livermore, CA
USA 94550